Spring 5-15-2017

Structural, Biophysical, and Functional Studies of TREM2 In Neurodegenerative Disease

Daniel L. Kober
Washington University in St. Louis

WASHINGTON UNIVERSITY IN ST. LOUIS

Division of Biology and Biomedical Sciences
Neurosciences

Dissertation Examination Committee:
Tom J. Brett, Chair
Carlos Cruchaga
Daved H. Fremont
Jeffrey P. Henderson
Robyn S. Klein
Thaddeus S. Stappenbeck

Structural, Biophysical, and Functional Studies of TREM2

In Neurodegenerative Disease

by
Daniel Luke Kober

A dissertation presented to
The Graduate School
of Washington University in
partial fulfillment of the
requirements for the degree
of Doctor of Philosophy

May 2017
St. Louis, Missouri

Table of Contents

List of Figures

Chapter 6

List of Tables

List of Abbreviations

1,2-dimyristoyl-sn-glycero-3-phosphocholine, DMPC
1,2-dipalmitoyl-sn-glycero-3-phosphocholine, DPPC
amyloid beta, Aβ
apolipoprotein E, ApoE
asymmetric unit, ASU
beta-mercaptoethanol, β-ME
bone marrow-derived macrophages, BMDM
chondroitin sulfate, CS
circular dichroism, CD
co-immunoprecipitation, co-IP
differential scanning fluorimetry, DSF
ethylenediaminetetraacetic acid, EDTA
glycosaminoglycan, GAG
guanidine hydrochloride, GuHCl
heparan sulfate, HS
immunoglobulin, Ig
Immuno-tyrosine activation motif, ITAM
Immuno-tyrosine inhibitory motif, ITIM
isopropyl β-D-1-thiogalactopyranoside, IPTG
luria Broth, LB
milligram, mg
Molecular Weight, MW
N-acetylglucosamine, NAG
paraformaldehyde, PFA
non-crystallographic symmetry, NCS
room temperature, RT
size-exclusion chromatography, SEC
small-angle X-ray scattering, SAXS
sodium dodecyl sulfate – polyacrylamide gel electrophoresis, SDS-PAGE

Acknowledgments

When presenting my work, I have often been asked how a pulmonary lab ended up researching Alzheimer's disease. This is all a credit to my thesis advisor, Tom Brett, who gave me an incredible amount of freedom to take this project in directions I thought were exciting, even if they were new to the lab. Therefore, first and foremost, I would like to thank Tom for his mentorship, which helped me become a better scientist. Without his guidance, this project would not have had the success that it did. I would also like to thank the Brett (and Alexander-Brett!) lab members for making my time in the Brett lab so enjoyable and stimulating.

I would like to acknowledge the American Heart Association for providing funding for this work through two pre-doctoral fellowships.

I would also like to thank Michael Holtzman, David Holtzman, Carlos Cruchaga, Celeste Karch, Laura Piccio, Michael Gross, Marco Colonna, Carl Frieden, Jeff Henderson, Daved Fremont, and their labs for reagents, collaborations, and discussions. The number of people who contributed reagents and/or expertise speaks volumes for the culture at Washington University.

I would especially like to thank my thesis committee for all of their advice and guidance, which shaped this project. I am further indebted for their support towards obtaining the next stages of my career.

Finally, I would like to thank Jennifer for being so loving and supportive through the long and stressful days, and for always believing it would all be worth it.

Dan Kober

Washington University in St. Louis

May 2017

Dedicated to my parents.

ABSTRACT OF THE DISSERTATION

Structural, Biophysical, and Functional Studies of TREM2

In Neurodegenerative Disease

by

Daniel Luke Kober

Doctor of Philosophy in Biology and Biomedical Sciences

Molecular Microbiology and Microbial Pathogenesis

Washington University in St. Louis, 2017

Tom J. Brett, Thesis Advisor

Alzheimer's disease (AD) and other neurodegenerative diseases present a large and growing challenge to global health. The immune system, particularly the innate immune system, is increasingly recognized as having a major role in these pathologies. The innate immune system is responsible to contain disease and promote healing. However, immune misregulation exacerbates disease. The innate immunomodulatory receptor Triggering receptor expressed on myeloid cells-2 (TREM2) is expressed on myeloid cells such as dendritic cells, macrophages, and in the brain, on microglia. TREM2 is a single-pass transmembrane receptor with an extracellular Ig domain that mediates ligand binding. This protein regulates inflammation *in vitro* and is required *in vivo* to sustain the microglia response during neurodegenerative diseases. Additionally, genetic studies have identified rare coding variants that increase risk for AD and separate variants that cause the severe, early fatal dementia known as Nasu-Hakola Disease (NHD). Combined, these animal and genetic studies have described a crucial role for TREM2

and identified variants that contribute disease risk. However, a full understanding of TREM2 function has been lacking due to a dearth of information regarding its structure and ligands.

The goal of this study was to determine the TREM2 structure and understand how the disease variants alter structure and function. The TREM2 Ig domain was expressed, purified, and crystallized using a novel mammalian expression system. The TREM2 crystal structure and subsequent biophysical and functional assays revealed that NHD variants reduce protein stability and cause protein misfolding while the AD variants have minimal structural changes and instead impact ligand binding. TREM2 bound cell-surface sulfated proteoglycans on mammalian cells. AD-risk variants decreased binding while another variant, which is possibly protective, increased binding. These variants mapped a functional ligand-binding surface on the TREM2 protein. Functionally, chemical inhibition of nascent proteoglycan sulfation impaired TREM2 signaling, suggesting a ligand that acts *in cis* to position TREM2 for signaling. Additionally, TREM2 interacts with the soluble lipoprotein apolipoprotein E (ApoE) and with amyloid beta (Aβ) peptides. Intriguingly, AD-risk variants impair both of these interactions, suggesting a physiological relevance during AD. These experiments offer the first structural and mechanistic studies of TREM2 function and will engender targeted molecular therapies to restore or enhance TREM2 function during neurodegenerative disease.

Chapter 1: TREM2 in health and disease

This section is modified from a submitted manuscript titled "TREM2-ligand interactions in health and disease." Submitted to J. Mol Biol.

1.1 TREM2 is a poorly understood innate immune receptor

Triggering receptor expression on myeloid cells-2 (TREM2) is an extracellular innate immune receptor expressed on myeloid cells such as dendritic cells and resident tissue macrophages including osteoclasts and microglia. The protein consists of an extracellular V-type immunoglobulin (Ig) domain followed by a short stalk leading to a single transmembrane pass which interacts with DNAX-activation protein 12 (DAP12, also known as TYROBP) to mediate downstream signaling. TREM2 terminates with a short cytosolic tail lacking known signaling motifs (1). In addition to the membrane-bound form, soluble TREM2 ectodomains (sTREM2) can be generated by proteolytic processing (2, 3) or by alternative splice sites (4). The importance of TREM2 is highlighted by genetic studies linking TREM2 variants to various neurodegenerative diseases, including Alzheimer's disease (AD) (5, 6). TREM2 has been implicated in a wide array of functions including cell maturation, survival, proliferation, activation, phagocytosis, and the regulation of inflammation. Accompanying this diverse set of functions is an even longer list of potential TREM2 ligands (see **Table 4**). Indeed, since its discovery, the identification of bona fide endogenous TREM2 ligands has proven difficult, although there is an emerging pattern of ligands that are anionic and/or lipidic in nature. It unclear if the true TREM2 ligand is among the suggested ligands or whether TREM2 is simply a highly promiscuous receptor that can engage a wide array of ligands. A full understanding of

TREM2 function is not possible without complete information regarding its structure and ligands.

1.2 The role of TREM2 in disease

1.2.1 TREM2 variants are associated with neurodegenerative diseases

The importance of TREM2 in neuronal health was first demonstrated by genetic studies that identified *TREM2* variants in families with Nasu-Hakola disease (NHD, also known as Polycystic lipomembranous osteodysplasia with sclerosing leukoencephalopathy, or PLOSL) a fatal disease characterized by presenile dementia and bone cysts (7-9). NHD patients are homozygous for loss-of-function *DAP12* or *TREM2* variants. In some cases, *TREM2* mutant carriers present a fronto-temporal lobar degenerative form of dementia lacking the bone phenotype. These *TREM2* mutations include splice site (8, 10), early stop sites (8, 11-13), and ectodomain coding variants (7, 8, 14-16). These mutations are all believed to produce nonfunctional proteins. More recently, separate coding variants in the Ig domain of TREM2 were linked to an increase risk for AD (5, 6). The link between *TREM2* variants, particularly the R47H and R62H variants and AD is now well-established (4, 17-19). *TREM2* AD risk variants carry roughly the same risk as a copy of the apolipoprotein E ε4 (*APOE4*) allele and clearly link the innate immune system to neurodegenerative disease (20). Beyond AD, *TREM2* variants have been linked to other neurodegenerative diseases, including Parkinson's disease (21, 22), and sporadic amyotrophic lateral sclerosis (23), and fronto-temporal dementia (24, 25), though these non-AD associations have not been as widely reproduced (19). The association of distinct variants with different diseases is born out on the functional level. Initial cellular studies suggested the NHD coding mutants impair surface trafficking and glycan maturation, while the

AD variants are surface-expressed and have mature glycosylations (3, 26). However, a structural understanding for these phenotypes were lacking.

1.2.2 Animal models of CNS disease highlight a role for TREM2 in microglia.

Most studies of TREM2 in neurodegenerative diseases have used mouse models of AD. Here, I highlight key findings from those models and draw connections between the AD phenotypes and those observed in other neurodegenerative models such as stroke and MS to identify functions TREM2 may be carrying out during disease (**Table 1**).

TREM2 is expressed on microglia during neurodegenerative disease

Animal studies by several groups have consistently found *Trem2* expression in the CNS restricted to microglia and increasing with age and disease progression (5, 27-30). Within the normal human brain, *TREM2* is expressed most highly in white matter, with transcripts detected in all major areas (31). Pathway analysis identified the TREM2 co-receptor DAP12 as a key regulator of expression changes in late-onset AD (LOAD) disease (32). Although there have been reports of TREM2 detection on non-myeloid cells in the CNS (5, 33), these cases used immunostaining methods to identify neuronal expression of TREM2, which may identify soluble TREM2 (sTREM2) produced in microglia that is released and bound to neurons which express a TREM2 ligand (34-36). RNA expression analyses have confirmed *Trem2* is expressed selectively in microglia in the brain (37, 38), and parabiosis experiments show these microglia are most likely resident microglia and not derived from infiltrating monocytes (39), although this is still controversial (40). Within the AD brain, laser microdissection (41) and high-resolution microscopy (42) showed *Trem2* is highly expressed on plaque-associated microglia and localized on microglia processes that are in contact with Aβ plaques. Thus, *TREM2* is expressed on

microglia in the brain and its expression increases both with aging and in response to disease. Consistent with its expression on microglia, studies using *Trem2*-deficient animal models of AD have shown a role for TREM2 in microglial survival and activation (**Table 1**).

TREM2 in models of Aβ pathology

The amyloid cascade hypothesis posits that Aβ is cause of AD, whether directly by mediating neurotoxicity or indirectly by triggering other neurotoxic events, such as tau aggregation (43). It is based on the observation that autosomal dominant mutations causative for AD are found in proteins responsible for the production and maturation of the Aβ peptide. Common animal models of AD are genetically engineered to carry these mutant proteins and/or overexpress Aβ. To date, all AD studies involving *Trem2* knockout mice have utilized such models. However, the Aβ phenotypes have been inconsistent in these studies. Some studies using *Trem2*$^{-/-}$ mice found no change in the overall plaque load (39, 44), while other studies found increased (27, 40) or even decreased burden (28, 40). Some of these differences are perhaps explained by the timing of data collection (40), although they could suggest Aβ clearance is not the primary role for TREM2.

While there have been mixed results on the accumulation of Aβ, all *Trem2*$^{-/-}$ studies have found decreased clustering of myeloid or microglial cells around plaques, suggesting a defect in microgliosis, or microglia activation (27, 28, 39, 40, 42, 44). These studies have also found that *Trem2*$^{-/-}$ mice have fewer microglia and increased microglia apoptosis. Importantly, samples from human R47H carriers recapitulate the microglia-Aβ plaque phenotype observed in *Trem2* haploinsufficient mice, with fewer microglia clustering around the plaques, and the plaques acquire a more toxic, diffuse morphology (42). Therefore, although TREM2 may not have a

dramatic effect on the overall Aβ content of the diseased brain, it strongly affects the ability of microglia to respond to and contain the plaques.

TREM2 in models of Tau pathology

Besides Aβ, intracellular tangles of hyperphosphorylated tau proteins are the other major pathological component of AD (45). While no studies using *Trem2*$^{-/-}$ mice have been published in tau models, studies altering *Trem2* expression *in vivo* by lentiviral overexpression (under a Cd11b promoter) or shRNA knockdown in the P301S tau transgenic model found that TREM2 reduces inflammation, decreases tau kinase activity, and improves cognitive function (46, 47). Future studies should utilize *Trem2* knockout and mutant *Trem2* knock-in models on this background to understand the role of TREM2 in tau-mediate neuropathies.

TREM2 in other neurodegenerative diseases

Similar to what has been observed in AD models, mouse models of aging, prion pathogenesis and the cuprizone model of multiple sclerosis (MS) have fewer activated microglia in the course of the disease (48-50). In MS, there was less myelin clearance by *Trem2*-deficient microglia (48, 49) and although there was no obvious deficiency in myelin uptake *in vitro*, *Trem2* deficiency was associated with decreased expression of lipid metabolism enzymes and a failure to degrade myelin debris and (48, 49). These findings suggest a more general defect in activation (48-50). Other studies examining the role of TREM2 in stroke have found increased expression following ischemic attack (36, 51, 52). As in the other cases, these studies have found that *Trem2* deficiency decreased inflammation, impaired microglial activation, and resulted in a failure of microglia to cluster at scar tissue (36, 51).

Summary TREM2 in of neurodegenerative disease

The consensus from the neurodegenerative disease studies is that TREM2 is important for enabling the response of myeloid cells (primarily microglia in the CNS) to disease. Mice lacking TREM2 have fewer microglia, and these microglia fail to activate and respond to damage during disease. These observations suggest a general deficit in microgliosis. Additionally, sTREM2 in the CSF seems to be a general feature of inflammatory neurodegenerative disease. Soluble TREM2 was first identified in the CSF of MS patients and neuroinflammatory patients (53), and has since been identified in a number of AD cohorts (54-57).

1.2.3 Non-CNS diseases: TREM2 in COPD, gut injury, and infection

Because of the genetic link between TREM2 and neurodegenerative disease, the majority of TREM2 research in the last few years has focused its role in the CNS. However, TREM2 has important roles outside the CNS, particularly in models where the activation and phenotype of myeloid/macrophage cells is important for disease outcome. In a model of viral-induced chronic obstructive pulmonary disease (COPD), TREM2 is required for survival and proliferation of alternatively activated (M2) macrophages (58). Unlike the healthy microglial response in AD, these macrophages foster a COPD-like disease. However, the role of TREM2 in preventing macrophage apoptosis and permitting macrophage proliferation bears a striking similarity to the TREM2 phenotype in CNS diseases. This study also identified a potential role for sTREM2 as a signaling molecule, as application of recombinant sTREM2 prevented macrophage apoptosis following M-CSF withdrawal.

In a gut injury model, TREM2 also promoted an M2 macrophage phenotype, which was important for promoting for wound healing (59). TREM2-expressing macrophages infiltrated the wound area, inhibited the expression of inflammatory cytokines, and promoted the expression of

Th2 cytokines IL-4 and IL-13. However, in a chemical injury model of inflammatory bowel disorder (IBD), TREM2 promoted an inflammatory phenotype that was detrimental to healing (60). The differences in these studies may be due to the environment. In the biopsy injury model, the first step in healing was for epithelial cells to form a layer over the wound, which the authors hypothesized reduced exposure to bacteria and therefore reduced strong TLR signals that are known to down-regulate TREM2 (59). The healing response may be different in the chemical model, and the interaction between TREM2 and TLR pathways may result in the increased inflammation observed in that model (60).

While the initial characterizations of NHD patients with DAP12 and TREM2 mutants did not report immune deficiencies (8, 61, 62), the role of TREM2 in infections has been studied in various models of bacterial infection. In general, these models are more acute than those discussed above, and therefore may highlight different roles for TREM2 in the rapid response to bacteria. These studies have mostly found TREM2 to be phagocytic and anti-inflammatory, although there are some exceptions (**Table 1**). Cell-level studies have shown that TREM2 regulates the response to bacteria, in two examples by promoting the bacteria killing through production of reactive oxygen species (ROS) (63, 64) – even against bacteria that were not directly bound by TREM2 (63). The role of TREM2 may vary with different pathogens, as it did not promote killing of *B. abortus*, (65) a pathogen that specializes in invading and surviving in macrophages.

Conclusions from disease models of TREM2.

Recent years have seen substantial progress in identifying an important role for TREM2 at the animal level. These studies using *Trem2*-deficient mice are highlighting its role in sustaining the microglial response to disease. However, important questions remain about what

precise functions TREM2 is performing, how different ligands may stimulate these functions, and how disease variants mutations affect function. Mechanistically, there are several possibilities for TREM2 functions, and the answers to these questions depend on understanding the interaction between TREM2, its signaling mechanisms, and its ligands.

Table 1 – Summary of TREM2 observations in disease models				
Disease	Observation or model	Phenotype	Possible role of TREM2	Reference:
Neurodegenerative disease				
Nasu-Hakola Disease	Osteopenic mice	Reduced proliferation of osteoclast precursors, accelerated osteoclast maturation and apoptosis.	Myeloid proliferation and survival	(66)
Alzheimer's disease Aβ Models	APPPS1 mice	Decreased number and size of plaque-associated microglia in *Trem2* heterozygotes. No change in total Aβ.	Microgliosis	(44)
	5XFAD mice	*Trem2*$^{-/-}$ mice have Increased Aβ and impaired microglial response at 8mo. Decreased microglial survival.	Microglia survival, microgliosis. Protective in Aβ	(27)
	5XFAD, APPPS1 mice	5XFAD *Trem2*$^{-/-}$ mice have fewer microglia (8mo) and less plaque clustering (4,8mo), producing diffuse plaque morphology and increased neuronal pathology. No change in total Aβ.	Microgliosis, microglial proliferaction. Protective in Aβ	(39)
	APPPS1 mice	*Trem2*$^{-/-}$ mice have reduced Aβ plaque burden at 4mo. Decreased plaque clustering of Iba1+ cells.	Plaque response. Possible role in proliferation, survival, and/or trafficking Detrimental in Aβ	(28)
	5XFAD, CRND8, PS/APP Human R47H carrier samples	TREM2 is required for microglial barrier function around Aβ plaques. Human R47H carriers mirror *Trem2* haploinsufficient mice.	Microgliosis and protective plaque response	(42)
	APPPS1 mice	TREM2 increases Aβ burden early, but reduces Aβ burden late in disease.	Microglial/myeloid proliferation, inflammation, and plaque response	(40)
	APPswe/PS1dE9 mice	*In vivo* overexpression reduced plaque load and inflammation.	Anti-inflammatory Phagocytosis of Aβ	(29)
	APPswe/PS1dE9 mice	Overexpressing *Trem2* in old mice (18mo) had no effect on AD pathology.	Age-restricted protective role	(67)
Alzheimer's disease Tau models	P301S mice	*Trem2* overexpression ameliorated tau pathology.	Protective, anti-inflammatory	(46)
	P301S mice	Lentiviral knockdown increased tau pathology.	Protective, anti-inflammatory	(47)
Multiple Sclerosis	Cuprizone	TREM2 sustains microglia during aging and cuprizone challenge. Reduces myelin debris.	Microglial survival and proliferation during aging myelin response	(49)
	Cuprizone	*Trem2*$^{-/-}$ mice have increased myelin debris, decreased microglial proliferation and activation.	Microgliosis and proliferation	(48)
	EAE	Antibody blockade of TREM2 signaling exacerbates symptoms.	Beneficial in MS	(68)
	EAE	EAE symptoms were reduced by *Trem2*-transduced macrophages.	Anti-inflammatory, protective	(69)
Prion Pathogenesis	Prion infection	No effect on prion	Microgliosis and	(50)

		pathogenesis, but reduced microlial activation.	proliferation	
Cardiovascular disease				
Stroke	Experimental Ischemia	*Trem2*$^{-/-}$ mice had increased infarction, decreased microglia activation, and fewer phagocytic microglia.	Microgliosis and phagocytosis Protective following stoke	(36)
	Experimental Ischemia	*Trem2*$^{-/-}$ mice have fewer microglia at glial scars and decreased microglial activation. No change in scar size.	Microgliosis	(51)
Chronic pulmonary disease				
Viral-induced COPD	SeV-induced chronic airway disease	*Trem2*$^{-/-}$ mice have reduced macrophage expansion which reduced chronic disease. IL-13 stimulation produces sTREM2 which prevents macrophage apoptosis.	Survival and proliferation. sTREM2 prevents macrophage apoptosis.	(58)
Wound Healing				
Colon injury	Chemical colon injury	*Trem2*$^{-/-}$ mice had reduced inflammation and wound damage.	Inflammatory, bacterial killing.	(60)
	Biopsy injury	TREM2 required for wound healing and promotes M2 phenotype	Promote anti-inflammatory M2 phenotype	(59)
Infection				
Animal infection	*E. coli* endotoximia.	TREM2 was protective in sepsis infection.	Phagocytic, anti-inflammatory	(70)
	LPS and *E. coli* endotoximia.	Trem2$^{-/-}$ mice had increased early inflammation and faster resolution.	Phagocytic. Anti-inflammatory.	(71)
	P. aeruginosa	TREM2 activated PI3K/Akt pathway to control inflammation.	Anti-inflammatory	(72)
	S. pneumoniae	TREM2 decreased C1q expression in alveolar macrophages and TREM2 was detrimental to survival in intranasal challenge.	Anti-phagocytotic, pro-inflammatory in AMs. Opposite results in BMDMs	(73)
In vitro cellular infection	*P. aeruginosa*	TREM2 increased ROS production through Akt/PI3K pathway. No change in phagocytosis.	Bacterial killing	(64)
	S. Typhimurium	TREM2/DAP12 required for ROS response following Salmonella infection.	Bacterial killing	(63)
	B. abortus	TREM2 inhibited NO production and increased bacterial load.	Promotes bacterial growth	(65)

Table 1 is modified from Kober and Brett, 2017. J Mol Biol. Submitted

1.3 Mechanisms of TREM2 Signaling

1.3.1 DAP12 mediates multiple intracellular responses

DAP12 is the co-receptor for TREM2 and a number of other single-pass transmembrane receptors. DAP12 contains an Immuno-Tyrosine Activation Motif (ITAM, consensus sequence: YxxI/Lx(6–12)YxxI/L) Broadly, TREM2 signaling through DAP12 results in ITAM phosphorylation which leads to Ca^{2+} mobilization, ERK (MAPK) phosphorylation, and Actin remodeling (1). However, TREM2 also negatively regulates TLR signaling and has roles in signaling pathways for other receptors (74). Altogether, TREM2 is intimately involved with regulating cellular homeostasis, survival, and proliferation. Here I review the TREM2 signaling pathway and highlight areas where TREM2 signaling may have results outside canonical ITAM activation. This develops a framework for incorporating the results of this research into TREM2 biology.

DAP12 associates with receptors through transmembrane interactions

Upon translation into the ER, DAP12 forms a disulfide-bonded homodimer with two intermolecular disulfide bonds forming in the ER lumen. Within the transmembrane domain, an electronegative Asp from each DAP12 monomer forms a 2:1 interaction with a Lys from the receptor. A Thr four residues below the Asp is also involved in the electrostatic network (75-77). The interaction with the receptor is important to shield the polar residues and allow trafficking to the cell surface. (Reviewed in (78)). While it is established that DAP12 requires complexing with a receptor for trafficking to the cell surface, there have been reports of TREM2 surface expression in *Dap12* and *Dap12/Dap10*-deficient cells (58, 79, 80). Other DAP12-coupled

receptors do require DAP12 for surface expression (80), so it is possible that DAP12 could traffic to the surface with another receptor and there engage with TREM2.

The DAP12 signaling pathway

The standard DAP12-receptor signaling pathway was delineated using Ly49D as a model DAP12-coupled receptor on NK cells (81). First, the DAP12 ITAM is phosphorylated by Src kinases. The two phosphorylated Tyr residue in the ITAM create a binding site for the SH2 domain of the kinase Syk. Activation of Syk lead to the phosphorylation of ERK1/2, PLCγ1, and Cbl. These same features are observed with TREM2: Stimulation with an anti-TREM2 antibody induced calcium flux and ERK phosphorylation, while monovalent stimulation by anti-TREM2 Fab did not result in calcium flux (82). Functionally, TREM2 stimulation prolonged DC survival following withdrawal of GM-CSF and IL-4. TREM2 has also been implicated in actin mobilization (11, 83). Monocytes from TREM2-null NHD patients had defective actin rearrangement following RANKL/MCSF stimulation. These initial studies linked TREM2 to the hallmark ITAM signaling events: Ca^{2+} mobilization, ERK phosphorylation, and actin remodeling (**Fig 1.1A**). Subsequent studies have further elucidated the TREM2 signaling pathway, and began to identify nuances that are key to fully understanding TREM2 function.

Although DAP12 is the primary adaptor for TREM2, DAP10 also interacts with DAP12-TREM2 complex, possibly through the formation of DAP12-DAP10 heterodimers. DAP10 contains a YINM motif that can recruit PI3K. Accordingly, DAP10 was required for effective activation of PI3K, Grb2, and therefore Akt and ERK signaling. However, calcium mobilization was surprisingly unchanged in $DAP10^{-/-}$ bone marrow derived macrophages (BMDMs) (84). Beyond DAP12, signaling cascades in hematopoietic cells that begin with ITAM

phosphorylation use scaffolding proteins to recruit downstream effector proteins such as Grb2, Cbl, PI3K, and Vav. Two such proteins are the Linkers for the Activation of T and B cells (LAT and LAB, LAB is also known as LAT2 and NTAL) (85). While they share most functions, a key difference is that LAT stimulates calcium mobilization more efficiently than LAB. DAP12 can signal using either LAT or LAB, however TREM2 signaling through DAP12 signaling utilizes LAB in osteoclasts and BMDMs (86).

TREM2-DAP12 signaling is inhibited by phosphatases and ubiquitin ligases

Once activated, how is TREM2 signaling terminated? Following TREM2 stimulation by anti-TREM2 antibodies, the phosphatidylinositol phosphatase SHIP-1 binds the phosphorylated membrane-proximal tyrosine, pY65, within the ITAM motif of DAP12 to inhibit DAP12 signaling and TREM2-dependent osteoclast multinucleation (84). This tyrosine is part of a "closet ITIM" sequence which was previously hypothesized to mediate inhibitory signals (SPYQEL, canonical ITIM is S/I/V/LxYxxI/V/L) (87). Furthermore, as noted above, the E3 ubiquitin ligase Cbl is recruited to LAB and forms a complex with LAB and PI3K (86) to target Src and Syk for ubiquitination and degradation (88). This activity requires LAB, as *LAB*$^{-/-}$ cells have increased Syk activation but decreased ERK activation (86). Finally, TREM-like transcript 1, (TREML1, also TLT-1), an ITIM-containing member of the TREM family is expressed in bone tissue (89) and associates with the tyrosine phosphatase SHP-1 upon phosphorylation. An alternatively-spliced transcript lacking much of the ectodomain (TREML1s) is also expressed in osteoclast precursors and macrophages. TREML1s co-immunoprecipitates (co-IPs) with TREM2, SHP-1, and SHIP-1 and decreases ERK, Akt, and calcium signals following RANKL stimulation (90). Accordingly, TREML1 (or 1s) may inhibit TREM2 signaling (**Fig 1.1B**).

Therefore, DAP12 signaling directly leads to its own inhibition by recruiting inhibitory phosphatases and ubiquitin ligases.

TREM2 regulates inflammation through tonic signaling and inhibitory adaptors.

While TREM1 uses DAP12 to enhance inflammatory TLR signals (62), TREM2 decreases TLR signals in cultured bone-marrow derived macrophages and dendritic cells (91-93). TREM2-dependent modulation of cytokine production did not require exogenous stimulation of TREM2, suggesting TREM2 is recognizing endogenous ligands to produce an inhibitory signal. There is precedence for inhibitory ITAM signaling in a similar system (94). In this example, IgA binds its receptor FcαRI, which signals through the ITAM-containing co-receptor FcRγ to produce either inhibitory (SHP-1 recruiting) or activating ITAM signals based on whether IgA is monomeric or aggregated by antigens. The transient monomeric interaction produces inefficient ITAM phosphorylation, leading the recruitment of the inhibitory tyrosine phosphatase SHP-1. This IgA-FcαRI-FcRγ system is analogous to ligand-TREM2-DAP12 and previous commentaries have suggested TREM2 could mediate tonic signals through such a mechanism (95-97) **(Fig 1.1C).** However, the endogenous, inhibitory TREM2 ligand has not been identified. Along these lines, it was recently observed that expression of DAP12 with a C-terminal fragment of TREM2 lacking the ectodomain but containing the DAP12-interacting transmembrane domain is sufficient to inhibit cytokine production following LPS stimulation (98). The C-terminal fragment may occupy DAP12 similarly to TREM2 with a monovalent ligand.

TREM2 also uses adaptor proteins to influence the inflammatory environment. *LAB*$^{-/-}$ macrophages have increased ERK phosphorylation following TLR stimulation (86). It could be

that TREM2 signaling through LAB restricts ERK or other signaling molecules needed for TLR signaling, or that LAB-dependent Cbl-mediated ubiquitination reduces the level of kinases needed to activate TLR pathways (85). Another pathway for inhibiting TLR signals is the recruitment of the anti-inflammatory adaptor protein DOK3 to DAP12 following TLR stimulation with LPS. Following LPS stimulation, DOK3 becomes phosphorylated, associates with DAP12, and interacts with Grb2 and Sos1 to inhibit the TLR response. In this system, SHIP-1 was not required to inhibit TLR signals, demonstrating that the inhibition of ITAM signaling by SHIP-1 is separate from the inhibition of TLR signaling by DAP12 (99) (**FIG 1.2A**).

1.3.2 Soluble TREM2 as a signaling molecule

TREM2 has been predominantly thought to signal through DAP12. However, the production of soluble TREM ectodomains appears to be a general feature of the TREM family as soluble forms of TREM1 (100) TREML1 (101) have been detected. While sTREM1 is thought to be a decoy receptor (102), application of sTREM2 (residues 19-136) to cultured BMDMs resulted in ERK and MAPK14 activation that persisted several hours and prevented apoptosis following M-CSF withdrawal (**Fig 1.1D)**. A similar finding in primary mouse microglia was reported very recently (103). It is interesting that cell survival has been attributed to both soluble TREM2 and membrane-bound TREM2. These findings suggest that sTREM2 signals through a separate pathway to reinforce the results of membrane-bound TREM2 and highlights the importance of TREM2 in myeloid cell homeostasis.

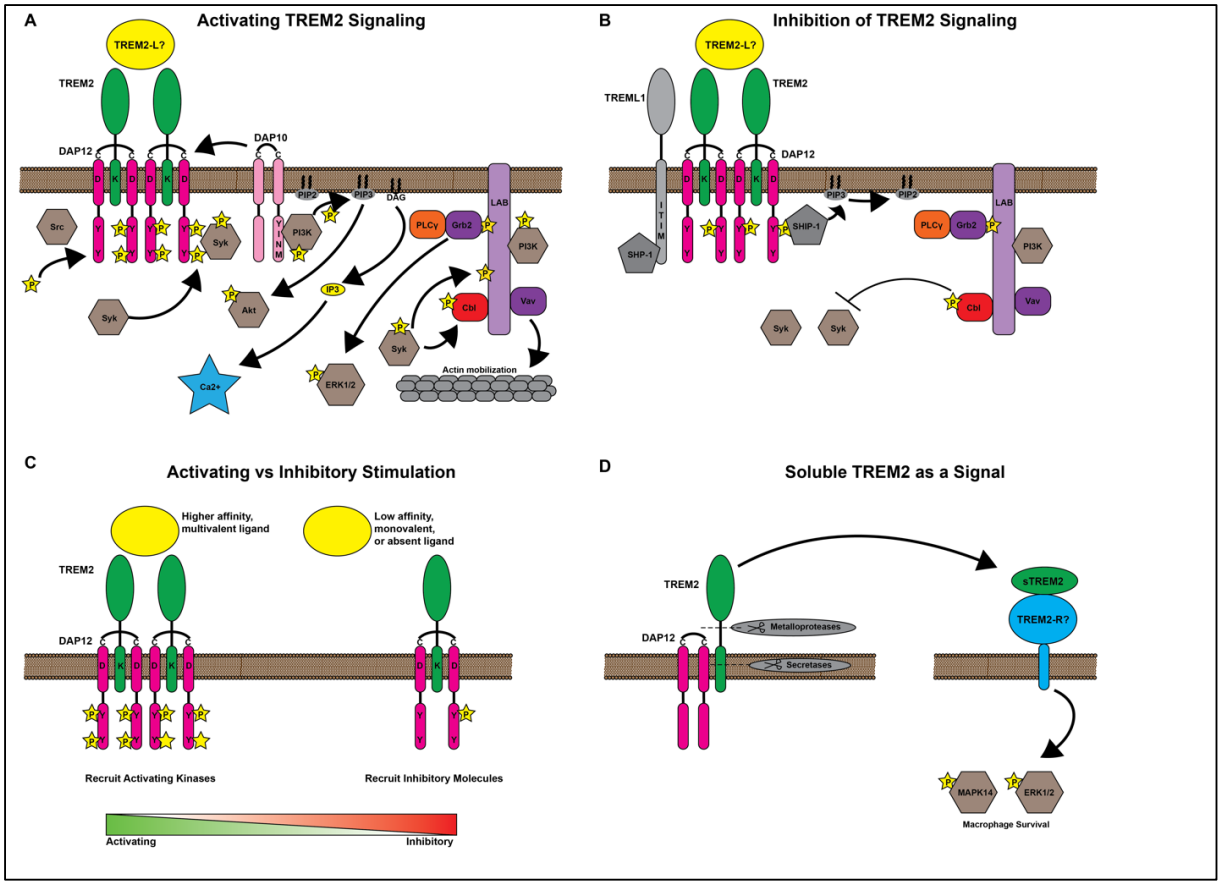

Figure 1.1. TREM2 Signaling mechanisms. A) Canonical TREM2 signaling occurs following cross-linking of TREM2. Src phosphorylates the DAP12 ITAM. This recruits and activates Syk. Syk activity leads the phosphorylation and activation of downstream effectors including PI3K, PLCγ, LAB or LAT, Cbl, Grb2, and Vav. DAP10 also recruits PI3K. The end result of these pathways is Akt activation, calcium flux, ERK/MAPK activity, and actin mobilization. **B)** TREM2 signaling is inhibited through multiple mechanisms. TREML1 associates with TREM2 signaling complexes and recruits SHP-1 through its ITIM. The scaffolding protein LAB recruits the E3 ubiquitin ligase Cbl, which downregulates Src and Syk. Incomplete DAP12 phosphorylation results in a "hidden ITIM" which can recruit SHIP-1. **C)** The most prevalent model for multifaceted TREM2 signaling is activating vs tonic receptor engagement by multivalent, high-affinity ligands vs low affinity, monovalent ligands. **D)** Soluble TREM2 is produced by proteolytic cleavage and may have signaling functions separate from transmembrane TREM2.

Figure 1.1 modified from Kober and Brett 2017, J Mol Biol. *submitted*.

1.3.3 TREM2 regulates signaling by other receptors

Plexin-A1 is expressed in a number of tissues including DCs and osteoclasts and is a receptor for two separate Semaphorin proteins. When expressed on osteoclast precursors, Plexin-A1 constitutively interacts with Neuropilin-1 (Nrp1) to mediate Semaphorin-3A (Sema3A) signaling, which prevents osteoclast maturation (104). However, when osteoclast precursors are stimulated with RANKL, Nrp1 is downregulated and Plexin-A1 can by bound by Sema6D to drive osteoclast maturation (105). Unexpectedly, this Sema6D signaling required TREM2 and DAP12 (106). Stimulation of BMDCs with a soluble form of Sema6D resulted in DAP12 phosphorylation. An interaction between TREM2 and Plexin-A1 was identified using co-IP and intracellular FRET, suggesting TREM2 connects DAP12 to Plexin-A1 (106). This Plexin-A1/TREM2 interaction is specific for Sema6D signaling, because the Nrp1-Plexin-A1 interaction displaces TREM2 in co-IP experiments (104, 107) (**Fig 1.2B**).

TREM2 is also involved in M-CSF-mediated survival and proliferation in macrophages and osteoclast precursors. M-CSF signaling through its receptor CSF-1R activates β-catenin and this requires phosphorylation of β-catenin by calmodulin-dependent kinases downstream of DAP12 (66, 108). In mice, the β-catenin deficit in osteoclast precursors reduces proliferation and prematurely accelerates osteoclast maturation. The increase in osteoclasts produces an osteopenic phenotype in the *Trem2*$^{-/-}$ mice, similar to NHD patients (66). A separate study showed M-CSF stimulation resulted in DAP12 phosphorylation by Src kinases activated by CSF-1R (109). This mechanism suggests these receptor pairs are in close physical proximity; however, a direct interaction between TREM2 and CSF-1R has not been reported (**Fig 1.2C**).

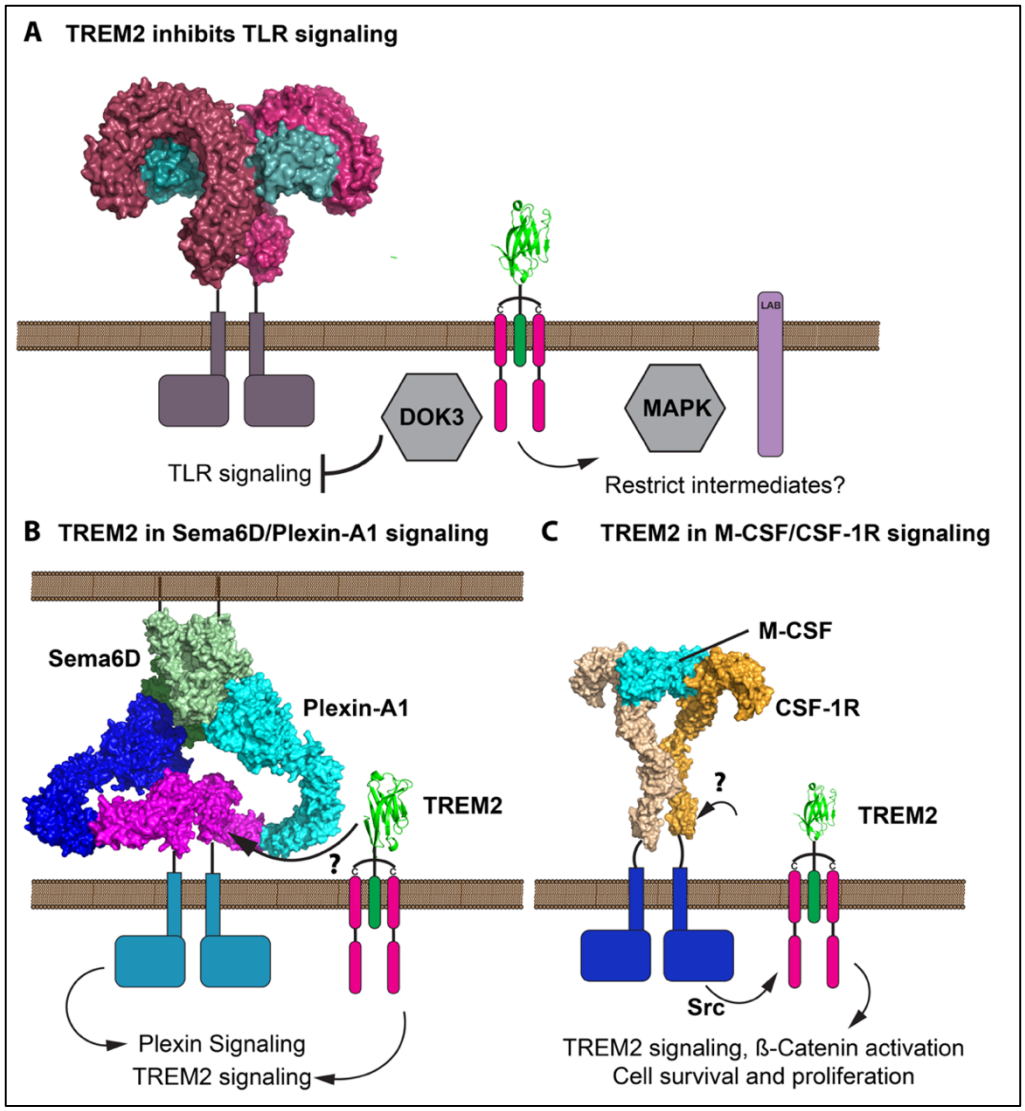

Figure 1.2. Role for TREM2 in regulating other signal pathways. A) TREM2 inhibits TLR responses through the recruitment of DOK3 to the DAP12 ITAM at the plasma membrane and potentially by sequestering signaling intermediates such as ERK or creating a less activating environment with scaffolding proteins such as LAB. (Structures PDBs: TREM2 5ELI and 3FXI - signaling complex of TLR4 (dark and light red), MD2 (cyans) complexed with LPS). **B)** TREM2 is required for the Plexin-A1 response to Sema6D. Two molecules of Plexin-A1 dimerize upon binding to a dimer of Sema6D. The Ig-like domains of Plexin-A1 colored in magenta were required for the interaction with TREM2. Structure PDBs: TREM2 5ELI, Plexin-A4 dimer 5L5K - (Blue and cyan with magenta highlights) superimposed on Sema6D (greens, 3OKY,). **C)** TREM2 signaling is required for β-catenin activation during M-CSF/CSF-1R signaling. (Structure PDB: 4WRM - CSF-1R orange and M-CSF cyan with signaling dimer shown in lighter shading).

Figure 1.2 modified from Kober and Brett 2017, J Mol Biol. *Submitted.*

PDB references: 5ELI (110), 3FXI (111), 5L5K (112), 3OKY (113), and 4WRM (114)

1.4 Summary of the literature and goals of this project

Genetic studies have linked TREM2 to various neurodegenerative diseases. Within the Ig domain of TREM2, distinct coding variants are associated with either AD or NHD. Cellular studies suggested these variants may have discrete effects on the protein. However, at the start of this work, the structure of TREM2 was unknown. TREM2 is expressed on myeloid cells including microglia. Animal models published prior and throughout the course of this work revealed a role for TREM2 in myeloid cell homeostasis and survival. TREM2 signals through the DAP12 ITAM pathway to promote cell survival, maturation, and proliferation. These functions may include interactions other receptor pathways. TREM2 regulates inflammation, and is generally considered to facilitate an anti-inflammatory environment. Microglia lacking TREM2 are unable to mount a vigorous defense against disease features such as Aβ plaques. There may also be a role for TREM2 as a soluble receptor signaling to inhibit apoptosis and reinforcing the effects of membrane-bound TREM2.

The goal of this project was to determine the TREM2 structure and to understand how disease variants affect function by testing their role in expression, folding, stability, and ligand binding. In chapters 2 and 3, I developed methods to express, purify, crystallize, and characterize the hTREM2 Ig domain. The structure suggests different loss-of-function mechanisms for TREM2 variants through altered stability (NHD) or ligand binding (AD). NDH variants, but not AD variants, are grossly misfolded and unstable. In chapter 4, I sought to provide fresh insight about the TREM2 ligand by determining the biochemical requirements for the engagement of TREM2 with a cell-surface ligand and showed that AD variants disrupt binding to this ligand. In chapter 5, I provide the first quantitative characterization of the newly discovered TREM2-ApoE interaction and demonstrate for the first time that TREM2 directly interacts with Aβ. Finally, in

chapter 6, I develop a model for TREM2 function through interaction with the various ligands examined in this work and in the literature. These findings are relevant for future studies of TREM2 in microglia, neurodegenerative disease, and other inflammatory disorders. Additionally, these findings will provide a structural framework for the rational design of molecular therapeutics directed at rescuing or enhancing TREM2 function.

1.5 References:

1. Colonna M, Wang Y. TREM2 variants: new keys to decipher Alzheimer disease pathogenesis. Nat Rev Neurosci. 2016;17(4):201-7. doi: 10.1038/nrn.2016.7. PubMed PMID: 26911435.
2. Wunderlich P, Glebov K, Kemmerling N, Tien NT, Neumann H, Walter J. Sequential proteolytic processing of the triggering receptor expressed on myeloid cells-2 (TREM2) protein by ectodomain shedding and gamma-secretase-dependent intramembranous cleavage. J Biol Chem. 2013;288(46):33027-36. doi: 10.1074/jbc.M113.517540. PubMed PMID: 24078628; PMCID: PMC3829152.
3. Kleinberger G, Yamanishi Y, Suarez-Calvet M, Czirr E, Lohmann E, Cuyvers E, Struyfs H, Pettkus N, Wenninger-Weinzierl A, Mazaheri F, Tahirovic S, Lleo A, Alcolea D, Fortea J, Willem M, Lammich S, Molinuevo JL, Sanchez-Valle R, Antonell A, Ramirez A, Heneka MT, Sleegers K, van der Zee J, Martin JJ, Engelborghs S, Demirtas-Tatlidede A, Zetterberg H, Van Broeckhoven C, Gurvit H, Wyss-Coray T, Hardy J, Colonna M, Haass C. TREM2 mutations implicated in neurodegeneration impair cell surface transport and phagocytosis. Sci Transl Med. 2014;6(243):243ra86. doi: 10.1126/scitranslmed.3009093. PubMed PMID: 24990881.
4. Jin SC, Benitez BA, Karch CM, Cooper B, Skorupa T, Carrell D, Norton JB, Hsu S, Harari O, Cai Y, Bertelsen S, Goate AM, Cruchaga C. Coding variants in TREM2 increase risk for Alzheimer's disease. Hum Mol Genet. 2014;23(21):5838-46. doi: 10.1093/hmg/ddu277. PubMed PMID: 24899047; PMCID: PMC4189899.
5. Guerreiro R, Wojtas A, Bras J, Carrasquillo M, Rogaeva E, Majounie E, Cruchaga C, Sassi C, Kauwe JS, Younkin S, Hazrati L, Collinge J, Pocock J, Lashley T, Williams J, Lambert JC, Amouyel P, Goate A, Rademakers R, Morgan K, Powell J, St George-Hyslop P, Singleton A, Hardy J, Alzheimer Genetic Analysis G. TREM2 variants in Alzheimer's disease. N Engl J Med. 2013;368(2):117-27. doi: 10.1056/NEJMoa1211851. PubMed PMID: 23150934; PMCID: PMC3631573.
6. Jonsson T, Stefansson H, Steinberg S, Jonsdottir I, Jonsson PV, Snaedal J, Bjornsson S, Huttenlocher J, Levey AI, Lah JJ, Rujescu D, Hampel H, Giegling I, Andreassen OA, Engedal K, Ulstein I, Djurovic S, Ibrahim-Verbaas C, Hofman A, Ikram MA, van Duijn CM, Thorsteinsdottir U, Kong A, Stefansson K. Variant of TREM2 associated with the risk of Alzheimer's disease. N Engl J Med. 2013;368(2):107-16. doi: 10.1056/NEJMoa1211103. PubMed PMID: 23150908; PMCID: PMC3677583.

7. Klunemann HH, Ridha BH, Magy L, Wherrett JR, Hemelsoet DM, Keen RW, De Bleecker JL, Rossor MN, Marienhagen J, Klein HE, Peltonen L, Paloneva J. The genetic causes of basal ganglia calcification, dementia, and bone cysts: DAP12 and TREM2. Neurology. 2005;64(9):1502-7. doi: 10.1212/01.WNL.0000160304.00003.CA. PubMed PMID: 15883308.
8. Paloneva J, Manninen T, Christman G, Hovanes K, Mandelin J, Adolfsson R, Bianchin M, Bird T, Miranda R, Salmaggi A, Tranebjaerg L, Konttinen Y, Peltonen L. Mutations in two genes encoding different subunits of a receptor signaling complex result in an identical disease phenotype. Am J Hum Genet. 2002;71(3):656-62. doi: 10.1086/342259. PubMed PMID: 12080485; PMCID: PMC379202.
9. Paloneva Bm J, Autti T, Raininko R, Partanen J, Salonen O, Puranen M, Hakola P, Haltia M. CNS manifestations of Nasu-Hakola disease: A frontal dementia with bone cysts. Neurology. 2001;56(11):1552-8. doi: 10.1212/wnl.56.11.1552.
10. Chouery E, Delague V, Bergougnoux A, Koussa S, Serre JL, Megarbane A. Mutations in TREM2 lead to pure early-onset dementia without bone cysts. Human mutation. 2008;29(9):E194-204. doi: 10.1002/humu.20836. PubMed PMID: 18546367.
11. Paloneva J, Mandelin J, Kiialainen A, Bohling T, Prudlo J, Hakola P, Haltia M, Konttinen YT, Peltonen L. DAP12/TREM2 deficiency results in impaired osteoclast differentiation and osteoporotic features. J Exp Med. 2003;198(4):669-75. doi: 10.1084/jem.20030027. PubMed PMID: 12925681; PMCID: PMC2194176.
12. Soragna D, Papi L, Ratti MT, Sestini R, Tupler R, Montalbetti L. An Italian family affected by Nasu-Hakola disease with a novel genetic mutation in the TREM2 gene. J Neurol Neurosurg Psychiatry. 2003;74(6):825-6. doi: 10.1136/jnnp.74.6.825-a. PubMed PMID: 12754369; PMCID: PMC1738498.
13. Giraldo M, Lopera F, Siniard AL, Corneveaux JJ, Schrauwen I, Carvajal J, Munoz C, Ramirez-Restrepo M, Gaiteri C, Myers AJ, Caselli RJ, Kosik KS, Reiman EM, Huentelman MJ. Variants in triggering receptor expressed on myeloid cells 2 are associated with both behavioral variant frontotemporal lobar degeneration and Alzheimer's disease. Neurobiol Aging. 2013;34(8):2077 e11-8. doi: 10.1016/j.neurobiolaging.2013.02.016. PubMed PMID: 23582655; PMCID: PMC3830921.
14. Guerreiro R, Bilgic B, Guven G, Bras J, Rohrer J, Lohmann E, Hanagasi H, Gurvit H, Emre M. Novel compound heterozygous mutation in TREM2 found in a Turkish frontotemporal dementia-like family. Neurobiol Aging. 2013;34(12):2890 e1-5. doi: 10.1016/j.neurobiolaging.2013.06.005. PubMed PMID: 23870839; PMCID: PMC3898264.
15. Guerreiro RJ, Lohmann E, Bras JM, Gibbs JR, Rohrer JD, Gurunlian N, Dursun B, Bilgic B, Hanagasi H, Gurvit H, Emre M, Singleton A, Hardy J. Using exome sequencing to reveal mutations in TREM2 presenting as a frontotemporal dementia-like syndrome without bone involvement. JAMA Neurol. 2013;70(1):78-84. doi: 10.1001/jamaneurol.2013.579. PubMed PMID: 23318515; PMCID: PMC4001789.
16. Le Ber I, De Septenville A, Guerreiro R, Bras J, Camuzat A, Caroppo P, Lattante S, Couarch P, Kabashi E, Bouya-Ahmed K, Dubois B, Brice A. Homozygous TREM2 mutation in a family with atypical frontotemporal dementia. Neurobiol Aging. 2014;35(10):2419 e23-5. doi: 10.1016/j.neurobiolaging.2014.04.010. PubMed PMID: 24910390; PMCID: PMC4208293.
17. Jin SC, Carrasquillo MM, Benitez BA, Skorupa T, Carrell D, Patel D, Lincoln S, Krishnan S, Kachadoorian M, Reitz C, Mayeux R, Wingo TS, Lah JJ, Levey AI, Murrell J, Hendrie H, Foroud T, Graff-Radford NR, Goate AM, Cruchaga C, Ertekin-Taner N. TREM2 is associated with increased risk for Alzheimer's disease in African Americans. Mol Neurodegener.

2015;10(1):19. doi: 10.1186/s13024-015-0016-9. PubMed PMID: 25886450; PMCID: PMC4426167.
18. Cruchaga C, Kauwe JSK, Harari O, Jin SC, Cai Y, Karch CM, Benitez Ba, Jeng AT, Skorupa T, Carrell D, Bertelsen S, Bailey M, McKean D, Shulman JM, De Jager PL, Chibnik L, Bennett Da, Arnold SE, Harold D, Sims R, Gerrish A, Williams J, Van Deerlin VM, Lee VMY, Shaw LM, Trojanowski JQ, Haines JL, Mayeux R, Pericak-Vance Ma, Farrer La, Schellenberg GD, Peskind ER, Galasko D, Fagan AM, Holtzman DM, Morris JC, Goate AM. GWAS of cerebrospinal fluid tau levels identifies risk variants for Alzheimer's disease. Neuron. 2013;78(2):256-68. doi: 10.1016/j.neuron.2013.02.026.
19. Lill CM, Rengmark A, Pihlstrom L, Fogh I, Shatunov A, Sleiman PM, Wang LS, Liu T, Lassen CF, Meissner E, Alexopoulos P, Calvo A, Chio A, Dizdar N, Faltraco F, Forsgren L, Kirchheiner J, Kurz A, Larsen JP, Liebsch M, Linder J, Morrison KE, Nissbrandt H, Otto M, Pahnke J, Partch A, Restagno G, Rujescu D, Schnack C, Shaw CE, Shaw PJ, Tumani H, Tysnes OB, Valladares O, Silani V, van den Berg LH, van Rheenen W, Veldink JH, Lindenberger U, Steinhagen-Thiessen E, Consortium S, Teipel S, Perneczky R, Hakonarson H, Hampel H, von Arnim CA, Olsen JH, Van Deerlin VM, Al-Chalabi A, Toft M, Ritz B, Bertram L. The role of TREM2 R47H as a risk factor for Alzheimer's disease, frontotemporal lobar degeneration, amyotrophic lateral sclerosis, and Parkinson's disease. Alzheimer's & dementia : the journal of the Alzheimer's Association. 2015;11(12):1407-16. doi: 10.1016/j.jalz.2014.12.009. PubMed PMID: 25936935; PMCID: PMC4627856.
20. Golde TE, Streit WJ, Chakrabarty P. Alzheimer's disease risk alleles in TREM2 illuminate innate immunity in Alzheimer's disease. Alzheimers Res Ther. 2013;5(3):24. doi: 10.1186/alzrt178. PubMed PMID: 23692967; PMCID: PMC3706774.
21. Rayaprolu S, Mullen B, Baker M, Lynch T, Finger E, Seeley WW, Hatanpaa KJ, Lomen-Hoerth C, Kertesz A, Bigio EH, Lippa C, Josephs Ka, Knopman DS, White CL, Caselli R, Mackenzie IR, Miller BL, Boczarska-Jedynak M, Opala G, Krygowska-Wajs A, Barcikowska M, Younkin SG, Petersen RC, Ertekin-Taner N, Uitti RJ, Meschia JF, Boylan KB, Boeve BF, Graff-Radford NR, Wszolek ZK, Dickson DW, Rademakers R, Ross Oa. TREM2 in neurodegeneration: evidence for association of the p.R47H variant with frontotemporal dementia and Parkinson's disease. Molecular neurodegeneration. 2013;8:19-. doi: 10.1186/1750-1326-8-19.
22. Liu G, Liu Y, Jiang Q, Jiang Y, Feng R, Zhang L, Chen Z, Li K, Liu J. Convergent Genetic and Expression Datasets Highlight TREM2 in Parkinson's Disease Susceptibility. Mol Neurobiol. 2016;53(7):4931-8. doi: 10.1007/s12035-015-9416-7. PubMed PMID: 26365049.
23. Cady J, Koval ED, Benitez Ba, Zaidman C, Jockel-Balsarotti J, Allred P, Baloh RH, Ravits J, Simpson E, Appel SH, Pestronk A, Goate AM, Miller TM, Cruchaga C, Harms MB. TREM2 variant p.R47H as a risk factor for sporadic amyotrophic lateral sclerosis. JAMA neurology. 2014;71(4):449-53. doi: 10.1001/jamaneurol.2013.6237.
24. Borroni B, Ferrari F, Galimberti D, Nacmias B, Barone C, Bagnoli S, Fenoglio C, Piaceri I, Archetti S, Bonvicini C, Gennarelli M, Turla M, Scarpini E, Sorbi S, Padovani A. Heterozygous TREM2 mutations in frontotemporal dementia. Neurobiol Aging. 2014;35(4):934 e7-10. doi: 10.1016/j.neurobiolaging.2013.09.017. PubMed PMID: 24139279.
25. Cuyvers E, Bettens K, Philtjens S, Van Langenhove T, Gijselinck I, van der Zee J, Engelborghs S, Vandenbulcke M, Van Dongen J, Geerts N, Maes G, Mattheijssens M, Peeters K, Cras P, Vandenberghe R, De Deyn PP, Van Broeckhoven C, Cruts M, Sleegers K, consortium B. Investigating the role of rare heterozygous TREM2 variants in Alzheimer's disease and

frontotemporal dementia. Neurobiol Aging. 2014;35(3):726 e11-9. doi: 10.1016/j.neurobiolaging.2013.09.009. PubMed PMID: 24119542.
26. Park JS, Ji IJ, An HJ, Kang MJ, Kang SW, Kim DH, Yoon SY. Disease-Associated Mutations of TREM2 Alter the Processing of N-Linked Oligosaccharides in the Golgi Apparatus. Traffic. 2015;16(5):510-8. doi: 10.1111/tra.12264. PubMed PMID: 25615530.
27. Wang Y, Cella M, Mallinson K, Ulrich JD, Young KL, Robinette ML, Gilfillan S, Krishnan GM, Sudhakar S, Zinselmeyer BH, Holtzman DM, Cirrito JR, Colonna M. TREM2 lipid sensing sustains the microglial response in an Alzheimer's disease model. Cell. 2015;160(6):1061-71. doi: 10.1016/j.cell.2015.01.049. PubMed PMID: 25728668; PMCID: PMC4477963.
28. Jay TR, Miller CM, Cheng PJ, Graham LC, Bemiller S, Broihier ML, Xu G, Margevicius D, Karlo JC, Sousa GL, Cotleur AC, Butovsky O, Bekris L, Staugaitis SM, Leverenz JB, Pimplikar SW, Landreth GE, Howell GR, Ransohoff RM, Lamb BT. TREM2 deficiency eliminates TREM2+ inflammatory macrophages and ameliorates pathology in Alzheimer's disease mouse models. J Exp Med. 2015;212(3):287-95. doi: 10.1084/jem.20142322. PubMed PMID: 25732305; PMCID: PMC4354365.
29. Jiang T, Tan L, Zhu XC, Zhang QQ, Cao L, Tan MS, Gu LZ, Wang HF, Ding ZZ, Zhang YD, Yu JT. Upregulation of TREM2 ameliorates neuropathology and rescues spatial cognitive impairment in a transgenic mouse model of Alzheimer's disease. Neuropsychopharmacology. 2014;39(13):2949-62. doi: 10.1038/npp.2014.164. PubMed PMID: 25047746; PMCID: PMC4229581.
30. Jiang T, Yu JT, Zhu XC, Tan MS, Gu LZ, Zhang YD, Tan L. Triggering receptor expressed on myeloid cells 2 knockdown exacerbates aging-related neuroinflammation and cognitive deficiency in senescence-accelerated mouse prone 8 mice. Neurobiol Aging. 2014;35(6):1243-51. doi: 10.1016/j.neurobiolaging.2013.11.026. PubMed PMID: 24368090.
31. Forabosco P, Ramasamy A, Trabzuni D, Walker R, Smith C, Bras J, Levine AP, Hardy J, Pocock JM, Guerreiro R, Weale ME, Ryten M. Insights into TREM2 biology by network analysis of human brain gene expression data. Neurobiol Aging. 2013;34(12):2699-714. doi: 10.1016/j.neurobiolaging.2013.05.001. PubMed PMID: 23855984; PMCID: PMC3988951.
32. Zhang B, Gaiteri C, Bodea LG, Wang Z, McElwee J, Podtelezhnikov AA, Zhang C, Xie T, Tran L, Dobrin R, Fluder E, Clurman B, Melquist S, Narayanan M, Suver C, Shah H, Mahajan M, Gillis T, Mysore J, MacDonald ME, Lamb JR, Bennett DA, Molony C, Stone DJ, Gudnason V, Myers AJ, Schadt EE, Neumann H, Zhu J, Emilsson V. Integrated systems approach identifies genetic nodes and networks in late-onset Alzheimer's disease. Cell. 2013;153(3):707-20. doi: 10.1016/j.cell.2013.03.030. PubMed PMID: 23622250; PMCID: PMC3677161.
33. Sessa G, Podini P, Mariani M, Meroni A, Spreafico R, Sinigaglia F, Colonna M, Panina P, Meldolesi J. Distribution and signaling of TREM2/DAP12, the receptor system mutated in human polycystic lipomembraneous osteodysplasia with sclerosing leukoencephalopathy dementia. Eur J Neurosci. 2004;20(10):2617-28. doi: 10.1111/j.1460-9568.2004.03729.x. PubMed PMID: 15548205.
34. Hsieh CL, Koike M, Spusta SC, Niemi EC, Yenari M, Nakamura MC, Seaman WE. A role for TREM2 ligands in the phagocytosis of apoptotic neuronal cells by microglia. J Neurochem. 2009;109(4):1144-56. doi: 10.1111/j.1471-4159.2009.06042.x. PubMed PMID: 19302484; PMCID: PMC3087597.

35. Stefano L, Racchetti G, Bianco F, Passini N, Gupta RS, Panina Bordignon P, Meldolesi J. The surface-exposed chaperone, Hsp60, is an agonist of the microglial TREM2 receptor. J Neurochem. 2009;110(1):284-94. doi: 10.1111/j.1471-4159.2009.06130.x. PubMed PMID: 19457124.
36. Kawabori M, Kacimi R, Kauppinen T, Calosing C, Kim JY, Hsieh CL, Nakamura MC, Yenari MA. Triggering receptor expressed on myeloid cells 2 (TREM2) deficiency attenuates phagocytic activities of microglia and exacerbates ischemic damage in experimental stroke. J Neurosci. 2015;35(8):3384-96. doi: 10.1523/JNEUROSCI.2620-14.2015. PubMed PMID: 25716838; PMCID: PMC4339351.
37. Hickman SE, Kingery ND, Ohsumi TK, Borowsky ML, Wang LC, Means TK, El Khoury J. The microglial sensome revealed by direct RNA sequencing. Nature neuroscience. 2013;16(12):1896-905. doi: 10.1038/nn.3554. PubMed PMID: 24162652; PMCID: PMC3840123.
38. Butovsky O, Jedrychowski MP, Moore CS, Cialic R, Lanser AJ, Gabriely G, Koeglsperger T, Dake B, Wu PM, Doykan CE, Fanek Z, Liu L, Chen Z, Rothstein JD, Ransohoff RM, Gygi SP, Antel JP, Weiner HL. Identification of a unique TGF-beta-dependent molecular and functional signature in microglia. Nature neuroscience. 2014;17(1):131-43. doi: 10.1038/nn.3599. PubMed PMID: 24316888; PMCID: PMC4066672.
39. Wang Y, Ulland TK, Ulrich JD, Song W, Tzaferis JA, Hole JT, Yuan P, Mahan TE, Shi Y, Gilfillan S, Cella M, Grutzendler J, DeMattos RB, Cirrito JR, Holtzman DM, Colonna M. TREM2-mediated early microglial response limits diffusion and toxicity of amyloid plaques. J Exp Med. 2016;213(5):667-75. doi: 10.1084/jem.20151948. PubMed PMID: 27091843; PMCID: PMC4854736.
40. Jay TR, Hirsch AM, Broihier ML, Miller CM, Neilson LE, Ransohoff RM, Lamb BT, Landreth GE. Disease Progression-Dependent Effects of TREM2 Deficiency in a Mouse Model of Alzheimer's Disease. J Neurosci. 2017;37(3):637-47. doi: 10.1523/JNEUROSCI.2110-16.2017. PubMed PMID: 28100745.
41. Frank S, Burbach GJ, Bonin M, Walter M, Streit W, Bechmann I, Deller T. TREM2 is upregulated in amyloid plaque-associated microglia in aged APP23 transgenic mice. Glia. 2008;56(13):1438-47. doi: 10.1002/glia.20710. PubMed PMID: 18551625.
42. Yuan P, Condello C, Keene CD, Wang Y, Bird TD, Paul SM, Luo W, Colonna M, Baddeley D, Grutzendler J. TREM2 Haplodeficiency in Mice and Humans Impairs the Microglia Barrier Function Leading to Decreased Amyloid Compaction and Severe Axonal Dystrophy. Neuron. 2016;90(4):724-39. doi: 10.1016/j.neuron.2016.05.003. PubMed PMID: 27196974; PMCID: PMC4898967.
43. Musiek ES, Holtzman DM. Three dimensions of the amyloid hypothesis: time, space and 'wingmen'. Nature neuroscience. 2015;18(6):800-6. doi: 10.1038/nn.4018. PubMed PMID: 26007213; PMCID: PMC4445458.
44. Ulrich JD, Finn MB, Wang Y, Shen A, Mahan TE, Jiang H, Stewart FR, Piccio L, Colonna M, Holtzmann DM. Altered microglial repsonse to AB plaques in APPPS1-21 mice heterozygous for TREM2. Molecular Neurodegeneration. 2014;9(20).
45. Pimplikar SW. Neuroinflammation in Alzheimer's disease: from pathogenesis to a therapeutic target. J Clin Immunol. 2014;34 Suppl 1(1):S64-9. doi: 10.1007/s10875-014-0032-5. PubMed PMID: 24711006.
46. Jiang T, Zhang YD, Chen Q, Gao Q, Zhu XC, Zhou JS, Shi JQ, Lu H, Tan L, Yu JT. TREM2 modifies microglial phenotype and provides neuroprotection in P301S tau transgenic

mice. Neuropharmacology. 2016;105:196-206. doi: 10.1016/j.neuropharm.2016.01.028. PubMed PMID: 26802771.
47. Jiang T, Tan L, Zhu XC, Zhou JS, Cao L, Tan MS, Wang HF, Chen Q, Zhang YD, Yu JT. Silencing of TREM2 exacerbates tau pathology, neurodegenerative changes, and spatial learning deficits in P301S tau transgenic mice. Neurobiol Aging. 2015;36(12):3176-86. doi: 10.1016/j.neurobiolaging.2015.08.019. PubMed PMID: 26364736.
48. Cantoni C, Bollman B, Licastro D, Xie M, Mikesell R, Schmidt R, Yuede CM, Galimberti D, Olivecrona G, Klein RS, Cross AH, Otero K, Piccio L. TREM2 regulates microglial cell activation in response to demyelination in vivo. Acta Neuropathol. 2015;129(3):429-47. doi: 10.1007/s00401-015-1388-1. PubMed PMID: 25631124; PMCID: PMC4667728.
49. Poliani PL, Wang Y, Fontana E, Robinette ML, Yamanishi Y, Gilfillan S, Colonna M. TREM2 sustains microglial expansion during aging and response to demyelination. J Clin Invest. 2015;125(5):2161-70. doi: 10.1172/JCI77983. PubMed PMID: 25893602; PMCID: PMC4463196.
50. Zhu C, Herrmann US, Li B, Abakumova I, Moos R, Schwarz P, Rushing EJ, Colonna M, Aguzzi A. Triggering receptor expressed on myeloid cells-2 is involved in prion-induced microglial activation but does not contribute to prion pathogenesis in mouse brains. Neurobiol Aging. 2015;36(5):1994-2003. doi: 10.1016/j.neurobiolaging.2015.02.019. PubMed PMID: 25816748.
51. Sieber MW, Jaenisch N, Brehm M, Guenther M, Linnartz-Gerlach B, Neumann H, Witte OW, Frahm C. Attenuated inflammatory response in triggering receptor expressed on myeloid cells 2 (TREM2) knock-out mice following stroke. PLoS One. 2013;8(1):e52982. doi: 10.1371/journal.pone.0052982. PubMed PMID: 23301011; PMCID: PMC3536811.
52. Kawabori M, Hokari M, Zheng Z, Kim JY, Calosing C, Hsieh CL, Nakamura MC, Yenari MA. Triggering Receptor Expressed on Myeloid Cells-2 Correlates to Hypothermic Neuroprotection in Ischemic Stroke. Ther Hypothermia Temp Manag. 2013;3(4):189-98. doi: 10.1089/ther.2013.0020. PubMed PMID: 24380032; PMCID: PMC3868297.
53. Piccio L, Buonsanti C, Cella M, Tassi I, Schmidt RE, Fenoglio C, Rinker J, 2nd, Naismith RT, Panina-Bordignon P, Passini N, Galimberti D, Scarpini E, Colonna M, Cross AH. Identification of soluble TREM-2 in the cerebrospinal fluid and its association with multiple sclerosis and CNS inflammation. Brain. 2008;131(Pt 11):3081-91. doi: 10.1093/brain/awn217. PubMed PMID: 18790823; PMCID: PMC2577803.
54. Heslegrave A, Heywood W, Paterson R, Magdalinou N, Svensson J, Johansson P, Ohrfelt A, Blennow K, Hardy J, Schott J, Mills K, Zetterberg H. Increased cerebrospinal fluid soluble TREM2 concentration in Alzheimer's disease. Mol Neurodegener. 2016;11:3. doi: 10.1186/s13024-016-0071-x. PubMed PMID: 26754172; PMCID: PMC4709982.
55. Suarez-Calvet M, Kleinberger G, Araque Caballero MA, Brendel M, Rominger A, Alcolea D, Fortea J, Lleo A, Blesa R, Gispert JD, Sanchez-Valle R, Antonell A, Rami L, Molinuevo JL, Brosseron F, Traschutz A, Heneka MT, Struyfs H, Engelborghs S, Sleegers K, Van Broeckhoven C, Zetterberg H, Nellgard B, Blennow K, Crispin A, Ewers M, Haass C. sTREM2 cerebrospinal fluid levels are a potential biomarker for microglia activity in early-stage Alzheimer's disease and associate with neuronal injury markers. EMBO Mol Med. 2016;8(5):466-76. doi: 10.15252/emmm.201506123. PubMed PMID: 26941262; PMCID: PMC5120370.

56. Henjum K, Almdahl IS, Arskog V, Minthon L, Hansson O, Fladby T, Nilsson LN. Cerebrospinal fluid soluble TREM2 in aging and Alzheimer's disease. Alzheimers Res Ther. 2016;8(1):17. doi: 10.1186/s13195-016-0182-1. PubMed PMID: 27121148; PMCID: PMC4848774.
57. Gispert JD, Suarez-Calvet M, Monte GC, Tucholka A, Falcon C, Rojas S, Rami L, Sanchez-Valle R, Llado A, Kleinberger G, Haass C, Molinuevo JL. Cerebrospinal fluid sTREM2 levels are associated with gray matter volume increases and reduced diffusivity in early Alzheimer's disease. Alzheimer's & dementia : the journal of the Alzheimer's Association. 2016;12(12):1259-72. doi: 10.1016/j.jalz.2016.06.005. PubMed PMID: 27423963.
58. Wu K, Byers DE, Jin X, Agapov E, Alexander-Brett J, Patel AC, Cella M, Gilfilan S, Colonna M, Kober DL, Brett TJ, Holtzman MJ. TREM-2 promotes macrophage survival and lung disease after respiratory viral infection. J Exp Med. 2015;212(5):681-97. doi: 10.1084/jem.20141732. PubMed PMID: 25897174; PMCID: PMC4419356.
59. Seno H, Miyoshi H, Brown SL, Geske MJ, Colonna M, Stappenbeck TS. Efficient colonic mucosal wound repair requires Trem2 signaling. Proc Natl Acad Sci U S A. 2009;106(1):256-61. doi: 10.1073/pnas.0803343106. PubMed PMID: 19109436; PMCID: PMC2629230.
60. Correale C, Genua M, Vetrano S, Mazzini E, Martinoli C, Spinelli A, Arena V, Peyrin-Biroulet L, Caprioli F, Passini N, Panina-Bordignon P, Repici A, Malesci A, Rutella S, Rescigno M, Danese S. Bacterial sensor triggering receptor expressed on myeloid cells-2 regulates the mucosal inflammatory response. Gastroenterology. 2013;144(2):346-56 e3. doi: 10.1053/j.gastro.2012.10.040. PubMed PMID: 23108068.
61. Paloneva J, Kestila M, Wu J, Salminen A, Bohling T, Ruotsalainen V, Hakola P, Bakker AB, Phillips JH, Pekkarinen P, Lanier LL, Timonen T, Peltonen L. Loss-of-function mutations in TYROBP (DAP12) result in a presenile dementia with bone cysts. Nat Genet. 2000;25(3):357-61. doi: 10.1038/77153. PubMed PMID: 10888890.
62. Colonna M. TREMs in the immune system and beyond. Nat Rev Immunol. 2003;3(6):445-53. doi: 10.1038/nri1106. PubMed PMID: 12776204.
63. Charles JF, Humphrey MB, Zhao X, Quarles E, Nakamura MC, Aderem A, Seaman WE, Smith KD. The innate immune response to Salmonella enterica serovar Typhimurium by macrophages is dependent on TREM2-DAP12. Infect Immun. 2008;76(6):2439-47. doi: 10.1128/IAI.00115-08. PubMed PMID: 18391000; PMCID: PMC2423085.
64. Zhu M, Li D, Wu Y, Huang X, Wu M. TREM-2 promotes macrophage-mediated eradication of Pseudomonas aeruginosa via a PI3K/Akt pathway. Scand J Immunol. 2014;79(3):187-96. doi: 10.1111/sji.12148. PubMed PMID: 24383713.
65. Wei P, Lu Q, Cui G, Guan Z, Yang L, Sun C, Sun W, Peng Q. The role of TREM-2 in internalization and intracellular survival of Brucella abortus in murine macrophages. Vet Immunol Immunopathol. 2015;163(3-4):194-201. doi: 10.1016/j.vetimm.2014.12.007. PubMed PMID: 25563793.
66. Otero K, Shinohara M, Zhao H, Cella M, Gilfillan S, Colucci A, Faccio R, Ross FP, Teitelbaum SL, Takayanagi H, Colonna M. TREM2 and beta-catenin regulate bone homeostasis by controlling the rate of osteoclastogenesis. J Immunol. 2012;188(6):2612-21. doi: 10.4049/jimmunol.1102836. PubMed PMID: 22312126; PMCID: PMC3732181.
67. Jiang T, Wan Y, Zhang YD, Zhou JS, Gao Q, Zhu XC, Shi JQ, Lu H, Tan L, Yu JT. TREM2 Overexpression has No Improvement on Neuropathology and Cognitive Impairment in

Aging APPswe/PS1dE9 Mice. Mol Neurobiol. 2017;54(2):855-65. doi: 10.1007/s12035-016-9704-x. PubMed PMID: 26780455.
68. Piccio L, Buonsanti C, Mariani M, Cella M, Gilfillan S, Cross AH, Colonna M, Panina-Bordignon P. Blockade of TREM-2 exacerbates experimental autoimmune encephalomyelitis. Eur J Immunol. 2007;37(5):1290-301. doi: 10.1002/eji.200636837. PubMed PMID: 17407101.
69. Takahashi K, Prinz M, Stagi M, Chechneva O, Neumann H. TREM2-transduced myeloid precursors mediate nervous tissue debris clearance and facilitate recovery in an animal model of multiple sclerosis. PLoS Med. 2007;4(4):e124. doi: 10.1371/journal.pmed.0040124. PubMed PMID: 17425404; PMCID: PMC1851623.
70. Chen Q, Zhang K, Jin Y, Zhu T, Cheng B, Shu Q, Fang X. Triggering receptor expressed on myeloid cells-2 protects against polymicrobial sepsis by enhancing bacterial clearance. Am J Respir Crit Care Med. 2013;188(2):201-12. doi: 10.1164/rccm.201211-1967OC. PubMed PMID: 23721075.
71. Gawish R, Martins R, Bohm B, Wimberger T, Sharif O, Lakovits K, Schmidt M, Knapp S. Triggering receptor expressed on myeloid cells-2 fine-tunes inflammatory responses in murine Gram-negative sepsis. FASEB J. 2015;29(4):1247-57. doi: 10.1096/fj.14-260067. PubMed PMID: 25477281.
72. Sun M, Zhu M, Chen K, Nie X, Deng Q, Hazlett LD, Wu Y, Li M, Wu M, Huang X. TREM-2 promotes host resistance against Pseudomonas aeruginosa infection by suppressing corneal inflammation via a PI3K/Akt signaling pathway. Invest Ophthalmol Vis Sci. 2013;54(5):3451-62. doi: 10.1167/iovs.12-10938. PubMed PMID: 23611998; PMCID: PMC3658264.
73. Sharif O, Gawish R, Warszawska JM, Martins R, Lakovits K, Hladik A, Doninger B, Brunner J, Korosec A, Schwarzenbacher RE, Berg T, Kralovics R, Colinge J, Mesteri I, Gilfillan S, Salmaggi A, Verschoor A, Colonna M, Knapp S. The triggering receptor expressed on myeloid cells 2 inhibits complement component 1q effector mechanisms and exerts detrimental effects during pneumococcal pneumonia. PLoS Pathog. 2014;10(6):e1004167. doi: 10.1371/journal.ppat.1004167. PubMed PMID: 24945405; PMCID: PMC4055749.
74. Ford JW, McVicar DW. TREM and TREM-like receptors in inflammation and disease. Curr Opin Immunol. 2009;21(1):38-46. doi: 10.1016/j.coi.2009.01.009. PubMed PMID: 19230638; PMCID: PMC2723941.
75. Wei P, Zheng BK, Guo PR, Kawakami T, Luo SZ. The association of polar residues in the DAP12 homodimer: TOXCAT and molecular dynamics simulation studies. Biophys J. 2013;104(7):1435-44. doi: 10.1016/j.bpj.2013.01.054. PubMed PMID: 23561520; PMCID: PMC3617422.
76. Cheng X, Im W. NMR observable-based structure refinement of DAP12-NKG2C activating immunoreceptor complex in explicit membranes. Biophys J. 2012;102(7):L27-9. doi: 10.1016/j.bpj.2012.03.002. PubMed PMID: 22500771; PMCID: PMC3318141.
77. Call ME, Wucherpfennig KW, Chou JJ. The structural basis for intramembrane assembly of an activating immunoreceptor complex. Nat Immunol. 2010;11(11):1023-9. doi: 10.1038/ni.1943. PubMed PMID: 20890284; PMCID: PMC3215083.
78. Call ME, Wucherpfennig KW. Common themes in the assembly and architecture of activating immune receptors. Nat Rev Immunol. 2007;7(11):841-50. doi: 10.1038/nri2186. PubMed PMID: 17960150.
79. Humphrey MB, Daws MR, Spusta SC, Niemi EC, Torchia JA, Lanier LL, Seaman WE, Nakamura MC. TREM2, a DAP12-associated receptor, regulates osteoclast differentiation and

function. J Bone Miner Res. 2006;21(2):237-45. doi: 10.1359/JBMR.051016. PubMed PMID: 16418779.
80. Inui M, Kikuchi Y, Aoki N, Endo S, Maeda T, Sugahara-Tobinai A, Fujimura S, Nakamura A, Kumanogoh A, Colonna M, Takai T. Signal adaptor DAP10 associates with MDL-1 and triggers osteoclastogenesis in cooperation with DAP12. Proc Natl Acad Sci U S A. 2009;106(12):4816-21. doi: 10.1073/pnas.0900463106. PubMed PMID: 19251634; PMCID: PMC2660769.
81. McVicar DW, Taylor LS, Gosselin P, Willette-Brown J, Mikhael AI, Geahlen RL, Nakamura MC, Linnemeyer P, Seaman WE, Anderson SK, Ortaldo JR, Mason LH. DAP12-mediated signal transduction in natural killer cells. A dominant role for the Syk protein-tyrosine kinase. J Biol Chem. 1998;273(49):32934-42. doi: 10.1074/jbc.273.49.32934. PubMed PMID: 9830044.
82. Bouchon A, Hernandez-Munain C, Cella M, Colonna M. A DAP12-mediated pathway regulates expression of CC chemokine receptor 7 and maturation of human dendritic cells. J Exp Med. 2001;194(8):1111-22. PubMed PMID: 11602640; PMCID: PMC2193511.
83. Cella M, Buonsanti C, Strader C, Kondo T, Salmaggi A, Colonna M. Impaired differentiation of osteoclasts in TREM-2-deficient individuals. J Exp Med. 2003;198(4):645-51. doi: 10.1084/jem.20022220. PubMed PMID: 12913093; PMCID: PMC2194167.
84. Peng Q, Malhotra S, Torchia JA, Kerr WG, Coggeshall KM, Humphrey MB. TREM2- and DAP12-dependent activation of PI3K requires DAP10 and is inhibited by SHIP1. Sci Signal. 2010;3(122):ra38. doi: 10.1126/scisignal.2000500. PubMed PMID: 20484116; PMCID: PMC2900152.
85. Orr SJ, McVicar DW. LAB/NTAL/Lat2: a force to be reckoned with in all leukocytes? J Leukoc Biol. 2011;89(1):11-9. doi: 10.1189/jlb.0410221. PubMed PMID: 20643813; PMCID: PMC3004523.
86. Whittaker GC, Orr SJ, Quigley L, Hughes L, Francischetti IM, Zhang W, McVicar DW. The linker for activation of B cells (LAB)/non-T cell activation linker (NTAL) regulates triggering receptor expressed on myeloid cells (TREM)-2 signaling and macrophage inflammatory responses independently of the linker for activation of T cells. J Biol Chem. 2010;285(5):2976-85. doi: 10.1074/jbc.M109.038398. PubMed PMID: 19948717; PMCID: PMC2823438.
87. Barrow AD, Trowsdale J. You say ITAM and I say ITIM, let's call the whole thing off: the ambiguity of immunoreceptor signalling. Eur J Immunol. 2006;36(7):1646-53. doi: 10.1002/eji.200636195. PubMed PMID: 16783855.
88. Rao N, Dodge I, Band H. The Cbl family of ubiquitin ligases: critical negative regulators of tyrosine kinase signaling in the immune system. J Leukoc Biol. 2002;71(5):753-63. PubMed PMID: 11994499.
89. Washington AV, Quigley L, McVicar DW. Initial characterization of TREM-like transcript (TLT)-1: a putative inhibitory receptor within the TREM cluster. Blood. 2002;100(10):3822-4. doi: 10.1182/blood-2002-02-0523. PubMed PMID: 12393607.
90. Yoon SH, Lee YD, Ha J, Lee Y, Kim HH. TLT-1s, alternative transcripts of triggering receptor expressed on myeloid cell-like transcript-1 (TLT-1), Inhibits the triggering receptor expressed on myeloid cell-2 (TREM-2)-mediated signaling pathway during osteoclastogenesis. J Biol Chem. 2012;287(35):29620-6. doi: 10.1074/jbc.M112.351239. PubMed PMID: 22761415; PMCID: PMC3436187.

91. Hamerman JA, Jarjoura JR, Humphrey MB, Nakamura MC, Seaman WE, Lanier LL. Cutting edge: inhibition of TLR and FcR responses in macrophages by triggering receptor expressed on myeloid cells (TREM)-2 and DAP12. J Immunol. 2006;177(4):2051-5. PubMed PMID: 16887962.
92. Turnbull IR, Gilfillan S, Cella M, Aoshi T, Miller M, Piccio L, Hernandez M, Colonna M. Cutting edge: TREM-2 attenuates macrophage activation. J Immunol. 2006;177(6):3520-4. PubMed PMID: 16951310.
93. Ito H, Hamerman JA. TREM-2, triggering receptor expressed on myeloid cell-2, negatively regulates TLR responses in dendritic cells. Eur J Immunol. 2012;42(1):176-85. doi: 10.1002/eji.201141679. PubMed PMID: 21956652; PMCID: PMC3444819.
94. Pasquier B, Launay P, Kanamaru Y, Moura IC, Pfirsch S, Ruffie C, Henin D, Benhamou M, Pretolani M, Blank U, Monteiro RC. Identification of FcalphaRI as an inhibitory receptor that controls inflammation: dual role of FcRgamma ITAM. Immunity. 2005;22(1):31-42. doi: 10.1016/j.immuni.2004.11.017. PubMed PMID: 15664157.
95. Hamerman JA, Lanier LL. Inhibition of immune responses by ITAM-bearing receptors. Sci STKE. 2006;2006(320):re1. doi: 10.1126/stke.3202006re1. PubMed PMID: 16449667.
96. Xing J, Titus AR, Humphrey MB. The TREM2-DAP12 signaling pathway in Nasu-Hakola disease: a molecular genetics perspective. Res Rep Biochem. 2015;5:89-100. doi: 10.2147/RRBC.S58057. PubMed PMID: 26478868; PMCID: PMC4605443.
97. Turnbull IR, Colonna M. Activating and inhibitory functions of DAP12. Nat Rev Immunol. 2007;7(2):155-61. doi: 10.1038/nri2014. PubMed PMID: 17220916.
98. Zhong L, Chen XF, Zhang ZL, Wang Z, Shi XZ, Xu K, Zhang YW, Xu H, Bu G. DAP12 Stabilizes the C-terminal Fragment of the Triggering Receptor Expressed on Myeloid Cells-2 (TREM2) and Protects against LPS-induced Pro-inflammatory Response. J Biol Chem. 2015;290(25):15866-77. doi: 10.1074/jbc.M115.645986. PubMed PMID: 25957402; PMCID: PMC4505493.
99. Peng Q, Long CL, Malhotra S, Humphrey MB. A physical interaction between the adaptor proteins DOK3 and DAP12 is required to inhibit lipopolysaccharide signaling in macrophages. Sci Signal. 2013;6(289):ra72. doi: 10.1126/scisignal.2003801. PubMed PMID: 23962980; PMCID: PMC3923308.
100. Gomez-Pina V, Soares-Schanoski A, Rodriguez-Rojas A, Del Fresno C, Garcia F, Vallejo-Cremades MT, Fernandez-Ruiz I, Arnalich F, Fuentes-Prior P, Lopez-Collazo E. Metalloproteinases shed TREM-1 ectodomain from lipopolysaccharide-stimulated human monocytes. J Immunol. 2007;179(6):4065-73. doi: 10.4049/jimmunol.179.6.4065. PubMed PMID: 17785845.
101. Gattis JL, Washington AV, Chisholm MM, Quigley L, Szyk A, McVicar DW, Lubkowski J. The structure of the extracellular domain of triggering receptor expressed on myeloid cells like transcript-1 and evidence for a naturally occurring soluble fragment. J Biol Chem. 2006;281(19):13396-403. doi: 10.1074/jbc.M600489200. PubMed PMID: 16505478.
102. Haselmayer P, Grosse-Hovest L, von Landenberg P, Schild H, Radsak MP. TREM-1 ligand expression on platelets enhances neutrophil activation. Blood. 2007;110(3):1029-35. doi: 10.1182/blood-2007-01-069195. PubMed PMID: 17452516.
103. Zhong L, Chen XF, Wang T, Wang Z, Liao C, Wang Z, Huang R, Wang D, Li X, Wu L, Jia L, Zheng H, Painter M, Atagi Y, Liu CC, Zhang YW, Fryer JD, Xu H, Bu G. Soluble TREM2 induces inflammatory responses and enhances microglial survival. J Exp Med. 2017. doi: 10.1084/jem.20160844. PubMed PMID: 28209725.

104. Hayashi M, Nakashima T, Taniguchi M, Kodama T, Kumanogoh A, Takayanagi H. Osteoprotection by semaphorin 3A. Nature. 2012;485(7396):69-74. doi: 10.1038/nature11000. PubMed PMID: 22522930.
105. Kumanogoh A, Kikutani H. Immunological functions of the neuropilins and plexins as receptors for semaphorins. Nature Reviews Immunology. 2013;13(11):802-14. doi: 10.1038/nri3545. PubMed PMID: WOS:000326158400010.
106. Takegahara N, Takamatsu H, Toyofuku T, Tsujimura T, Okuno T, Yukawa K, Mizui M, Yamamoto M, Prasad DV, Suzuki K, Ishii M, Terai K, Moriya M, Nakatsuji Y, Sakoda S, Sato S, Akira S, Takeda K, Inui M, Takai T, Ikawa M, Okabe M, Kumanogoh A, Kikutani H. Plexin-A1 and its interaction with DAP12 in immune responses and bone homeostasis. Nat Cell Biol. 2006;8(6):615-22. doi: 10.1038/ncb1416. PubMed PMID: 16715077.
107. Zhang Y, Su J, Wu S, Teng Y, Yin Z, Guo Y, Li J, Li K, Yao L, Li X. DDR2 (discoidin domain receptor 2) suppresses osteoclastogenesis and is a potential therapeutic target in osteoporosis. Sci Signal. 2015;8(369):ra31. doi: 10.1126/scisignal.2005835. PubMed PMID: 25805889.
108. Otero K, Turnbull IR, Poliani PL, Vermi W, Cerutti E, Aoshi T, Tassi I, Takai T, Stanley SL, Miller M, Shaw AS, Colonna M. Macrophage colony-stimulating factor induces the proliferation and survival of macrophages via a pathway involving DAP12 and beta-catenin. Nat Immunol. 2009;10(7):734-43. doi: 10.1038/ni.1744. PubMed PMID: 19503107; PMCID: PMC4004764.
109. Zou W, Reeve JL, Liu Y, Teitelbaum SL, Ross FP. DAP12 couples c-Fms activation to the osteoclast cytoskeleton by recruitment of Syk. Mol Cell. 2008;31(3):422-31. doi: 10.1016/j.molcel.2008.06.023. PubMed PMID: 18691974; PMCID: PMC2584874.
110. Kober DL, Alexander-Brett JM, Karch CM, Cruchaga C, Colonna M, Holtzman MJ, Brett TJ. Neurodegenerative disease mutations in TREM2 reveal a functional surface and distinct loss-of-function mechanisms. Elife. 2016;5:e20391. doi: 10.7554/eLife.20391. PubMed PMID: 27995897; PMCID: PMC5173322.
111. Park BS, Song DH, Kim HM, Choi BS, Lee H, Lee JO. The structural basis of lipopolysaccharide recognition by the TLR4-MD-2 complex. Nature. 2009;458(7242):1191-5. doi: 10.1038/nature07830. PubMed PMID: 19252480.
112. Kong Y, Janssen BJ, Malinauskas T, Vangoor VR, Coles CH, Kaufmann R, Ni T, Gilbert RJ, Padilla-Parra S, Pasterkamp RJ, Jones EY. Structural Basis for Plexin Activation and Regulation. Neuron. 2016;91(3):548-60. doi: 10.1016/j.neuron.2016.06.018. PubMed PMID: 27397516; PMCID: PMC4980550.
113. Janssen BJ, Robinson RA, Perez-Branguli F, Bell CH, Mitchell KJ, Siebold C, Jones EY. Structural basis of semaphorin-plexin signalling. Nature. 2010;467(7319):1118-22. doi: 10.1038/nature09468. PubMed PMID: 20877282; PMCID: PMC3587840.
114. Felix J, De Munck S, Verstraete K, Meuris L, Callewaert N, Elegheert J, Savvides SN. Structure and Assembly Mechanism of the Signaling Complex Mediated by Human CSF-1. Structure. 2015;23(9):1621-31. doi: 10.1016/j.str.2015.06.019. PubMed PMID: 26235028.

Chapter 2: Expression, purification, and crystallization of TREM2

2.1 Expression systems

Structural studies require the ability to produce milligram (mg) amounts of properly folded protein that is stable and well-behaved. In the course of these studies, TREM2 was expressed from bother bacterial and mammalian systems. Mammalian expression and purification yielded protein in the range of 1-5 mg/L culture, while bacterial systems do not produce stable protein.

2.1.1 Bioinformatic features of the TREM2 ectodomain

The *TREM2* gene encodes a 230 amino acid transcript. Domain boundaries are annotated in **Figure 2.1a**. Upon translation in the ER, the N-terminal signal peptide is removed. The TREM2 ectodomain is residues 19-172, with 19-132 annotated as a V-type Ig domain. Following the protein stalk, TREM2 has a single-pass transmembrane helix and a short intracellular tail lacking any recognized signaling motifs (1). This study focused on characterizing the Ig domain, which is predicted to have two N-linked glycosylation sites at residues N20 and N79 (2).

2.1.2 Expression of TREM2 in bacterial systems

Cloning TREM2 Ig domains

The human *TREM2* Ig domain (19-134) was cloned from a pMX-3p lentiviral construct containing the full *TREM2* gene kindly provided by Marco Colonna. Mouse *Trem2* cDNA, a gift from Michael Holtzman, was similarly used as a template for PCR (Ig domain = 19-136). The predicted molecular weight (MW) of these domains were 14.387 kDa (human) and 14.440 kDa

(mouse). For bacterial expression, the Ig domains were amplified by PCR and ligated into pET23b as tagless constructs.

Expressing and purification of TREM2 Ig domains from bacteria

Tagless hTREM2 and mTREM2 Ig domains were expressed as inclusion bodies in Rosetta2 (DE3) cells. After transformation, single colonies were selected and starter cultures grown overnight under double antibiotic selection. The starter culture was used as inoculum for 2-4L of Luria Broth (LB) media, and cultures were grown to an OD_{600} of ~ 1.0. Cultures were induced with 500mM Isopropyl β-D-1-thiogalactopyranoside (IPTG) at 37°C for 5 hours.

After pelleting the cultures, insoluble inclusion bodies were harvested as follows (and as described in (2)) Cell pellets were resuspended in Lysis Buffer containing 50 mM Tris pH 8.0, 12.5% sucrose, 50 mM NaCl, 0.5 mM ethylenediaminetetraacetic acid (EDTA), 0.5% Triton X-100, freshly added 10 mM DTT, 0.5 mg/mL lysozyme and DNAse. Cells were lysed by sonication, centrifuged, and inclusion bodies were subjected to three washes in 50 mM Tris pH 8.0, 100 mM NaCl, 1mM EDTA, and 0.5% Triton X-100 before a final wash in the aforementioned buffer lacking Triton X-100. Extensive sonication was used in each step to break up the inclusion body pellet in order to obtain pure TREM2 proteins (**Fig 2.1b**).

Refolding TREM2 from inclusion bodies

For refolding attempts, inclusion bodies were solubilized in 6 M guanidine hydrochloride (GuHCl), 20 mM β-mercaptoethanol (β-ME), and 50 mM Tris pH 8.0. Because several TREM and related Ig domain proteins had been successfully refolded and crystallized (3-7), TREM2 Ig domains were subjected to refolding trials. Initial attempts utilized conditions from a commercial

refolding screen (Athena Enzyme Systems) as well as a standard refolding condition: 100 mM Tris pH 8.5, 400 mM Arginine, 2 mM EDTA, 5 mM reduced glutathione and 0.5 mM oxidized glutathione. Inclusion bodies were added to filtered, pre-chilled buffer and allowed to refold overnight at 4°C. After refolding, insoluble aggregates were pelleted and soluble TREM2 analyzed by sodium dodecyl sulfate – polyacrylamide gel electrophoresis (SDS-PAGE) (**Fig 2.1c, d**). Although TREM2 proteins were detected, attempts to further purify protein by size-exclusion chromatography (SEC) were unsuccessful.

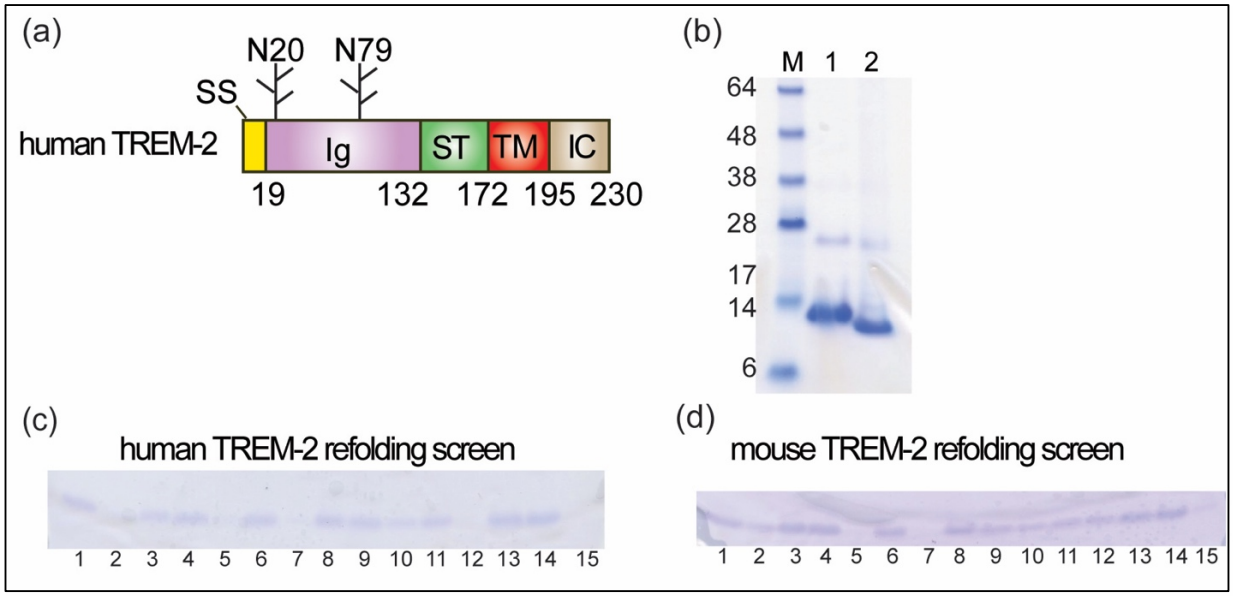

Figure 2.1 Bacteria-expressed TREM2 a) Schematic for TREM2 protein domain and features. N-linked glycan sites shown with sticks. Domains: SS = signal sequence, Ig = immunoglobulin, ST = stalk, TM = transmembrane, and IC = intracellular. **b)** Human (1) and mouse (2) inclusion bodies analyzed by reducing SDS-PAGE. **c)** human and **d)** mouse TREM2 soluble after refolding screen.

Figure 2.1 reprinted from Kober et al 2014 (2) with permission by Elsevier

In 2016, a report demonstrated the use of differential scanning fluorimetry (DSF) to screen refolding conditions (8). This experiment uses a dye that is quenched in an aqueous environment. As the protein in the experiment unfolds, the dye binds the exposed hydrophobic residues and fluoresces. This progression can by monitored using a real-time PCR machine. Separately, in the process of purifying mammalian-expressed TREM2 (discussed below), it was discovered that TREM2 interacted with the matrix of the SEC columns. Additionally, NDSB molecules were found to improve crystal quality. A DSF screen (created by Chris Nelson and Rick Stegemen) was used to screen refolding conditions. Four potential conditions were identified: 1) 0.5 M NDSB-201, 100 mM Tris pH 9.5, and 5/0.5 mM reduced/oxidized glutathione, 2) 0.5 M Arginine, 100 mM Bis-tris phosphate pH 9.0 with 5/0.5 mM reduced/oxidized glutathione, and 3) condition #2 with 10% Glycerol, and 4) 0.5 M Arginine, 100 mM Tris pH 7.5, 0.2 M sucrose and 5/0.5 mM reduced/oxidized glutathione. These conditions were scaled up to 250 mL refoldings, concentrated, and the product protein analyzed with an analytical s200 column (GE) in 150 mM NaCl, 20 mM Tris pH 8.5, and 20 mM NDSB-201. In these conditions, refolded TREM2 was observed, and the protein appeared at the expected monomer size by non-reducing SDS-PAGE (**Fig 2.2A, B**). DSF was used to validate this finding, and a reduced Tm was observed when the protein was denatured in the presence 1 mM DTT (**Fig 2.2C**), confirming the presence of disulfide bonds. In additional optimization, addition of 500 mM GuHCl to the NDSB condition reduced aggregation and further improved yields. However, the refolded protein behaved poorly when concentrated and has not yet been amenable to crystallization trials.

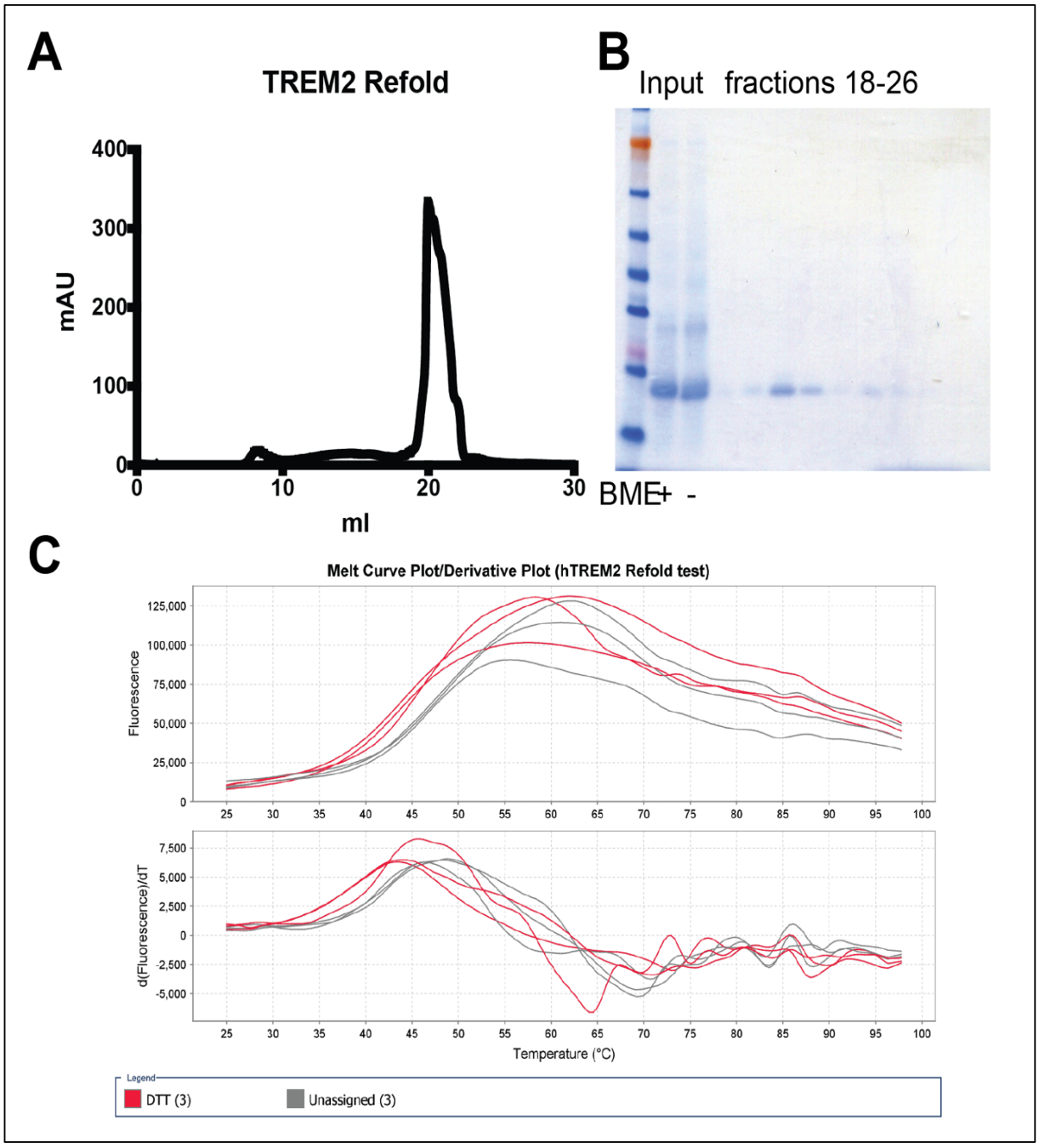

Figure 2.2 hTREM2 can be refolded. A) SEC profile of TREM2 refolded in 0.5 M NDSB-201 and run in Tris pH 8 sizing buffer containing 20 mM NDSB-201. **B)** Concentrated SEC input shown ±β–ME confirms refolded TREM2 lacks intermolecular disulfide bonds. Fractions from SEC peak run without reducing agent confirm the eluted peak is properly folded protein. **C)** DSF profiles of refolded TREM2 analyzed ± 1 mM DTT. Tm = 46.7 and 44.5 without and with DTT. Analyzed with Life Technologies Protein Thermal Shift software v1.1.

2.1.3 Expression and purification of TREM2 from a mammalian system

Cloning TREM2 in pHLSEC

To produce TREM2 from mammalian cells, TREM2 Ig domains were cloned into the pHLSEC vector using PCR amplification and AgeI-KpnI restriction enzyme digestion. PCR templates were as described above. TREM2 variants were produced as detailed in (9), generally through site-guided mutagenesis, although in later studies some variants were introduced by Gibson block assembly. The pHLSEC vector contains an optimized secretion signal and C-terminal 6-His tag for facile purification (10).

Expression in 293F cells

TREM2 expression in mammalian cells was conducted as described in these publications (2, 9, 11). Transient transfection of HEK 293F cells was accomplished by diluting DNA (1μg/ million cells) and either a chemically modified PEI (PEI-TMC-25, synthesized by Artie Romero, 2 μg/ μg DNA) or Hype-5 transfection reagent (OZ Biosciences, 1.5 μg/ μg DNA) separately into Opti-MEM media and then combining for 30 min to form complexes before addition to 293F cells. 293F cells were grown on shaking, baffled flasks in 8% CO_2 in 293 freestyle media (Invitrogen) supplemented with Pen/Strep. After 72 hours, cells were pelleted and the supernatants filtered using 0.2 micron filters (Nalgene). The supernatants were passed over nickel chelated on nitrilotriacetic acid-agarose beads (NiNTA), which binds the 6-His purification tag. Supernatants were supplemented with 10% (v/v) of 1.5 M NaCl, 0.1 M Tris pH 8.5, 0.5 M K_2HPO_4, and 50 mM imidazole, which adjusts the pH and reduces background binding and enhances binding. For optimal binding, supernatant was concentrated ten-fold using an Amicon concentration cell (76 mm, 10 MWKO membrane). Proteins were bound to NiNTA

using a gravity column, washed in 300 mM NaCl, 20 mM imidazole, and 50 mM K_2HPO_4 pH 8.0, and then eluted in 300 mM NaCl, 250 mM imidazole, and 50 mM K_2HPO_4, pH 8.0 (2, 11).

Tools to control TREM2 glycosylation

Mammalian glycosylations are both chemically and structurally heterogeneous and therefore detrimental to crystallization (12, 13). Because TREM2 has two N-linked glycosylations, TREM2 was expressed in the presence of 1 μg/mL kifunensine, an inhibitor of glycan maturation for structural studies. The immature glycans are specifically recognized and cleaved after the first N-acetylglucosamine (NAG) by EndoH. Following NiNTA purification of TREM2, an amylose-binding version of EndH, EndoHf, was added to the protein overnight at room temperature (RT) and then removed by incubation with amylose resin.

Expression of TREM2 in HEK 293s GnTI$^{-/-}$ cells

As an alternative to the kifunensine/EndoHf processing, HEK 293s GnTI$^{-/-}$ cells (14) were used to produce proteins with uniform, truncated glycosylations. These have been useful in small-angle X-ray scattering (SAXS) studies (15) and even crystallization (16). This protocol was developed because it was observed that the R47H variant protein was more prone to proteolytic degradation when deglycosylated compared to WT or glycosylated variant protein. It was envisioned that this system could facilitate crystallization of the R47H variant. HEK 293s GnTI$^{-/-}$ cells are typically grown in DMEM media with 10% FBS. To facilitate structural studies, I adapted them to serum-free growth conditions through lifting cells using trypsin and resuspending them in serum-free freestyle media. In some cases, I grew them in a 1:1 mix of freestyle and EX-CELL 293 serum-free media (Sigma). This protocol was suggested for adaption. However, EX-CELL media is reported to inhibit transfection, so on the day of

transfection, cells would be resuspended in 50% volume 293 freestyle media for transfection. Following transfection the 50% volume EX-CELL media was added. The cells would tolerate either adaption protocol for the short-term, but with time (~1 month or so) I would observe fully-glycosylated protein by SEC and SDS-PAGE. This happened several times, even when grown and maintained completely separate from potentially contaminating 293F cells. The GnTI$^{-/-}$ cells seem to be capable of escape mutations in the glycosylation machinery, with may help them cope with the stress of serum-free adaption. Despite these setbacks, potential crystal hits of GnTI$^{-/-}$-derived hTREM2 R47H, although they were not reproducible and unfortunately decayed before harvesting (**Fig 2.3C**).

Purification of hTREM2 from mammalian cells

TREM2 proteins were purified by SEC in 150 mM NaCl and 20 mM Tris pH 8.5 on an analytical s200 column (GE). Initial attempts using 150 mM NaCl and 20 mM HEPES pH 7.5 (sizing buffer) were unsuccessful and the increased pH was necessary to obtain protein, probably through reducing interactions with the column matrix (TREM2 pI_{calc} = 8.5). Consistent with an interaction between TREM2 and the matrix, the glycosylation status of TREM2 greatly affected the elution volume (**Fig 2.3A, B**). Deglycosylated protein elutes well past one CV, suggesting an interaction with the column that is reduced by the glycosylation.

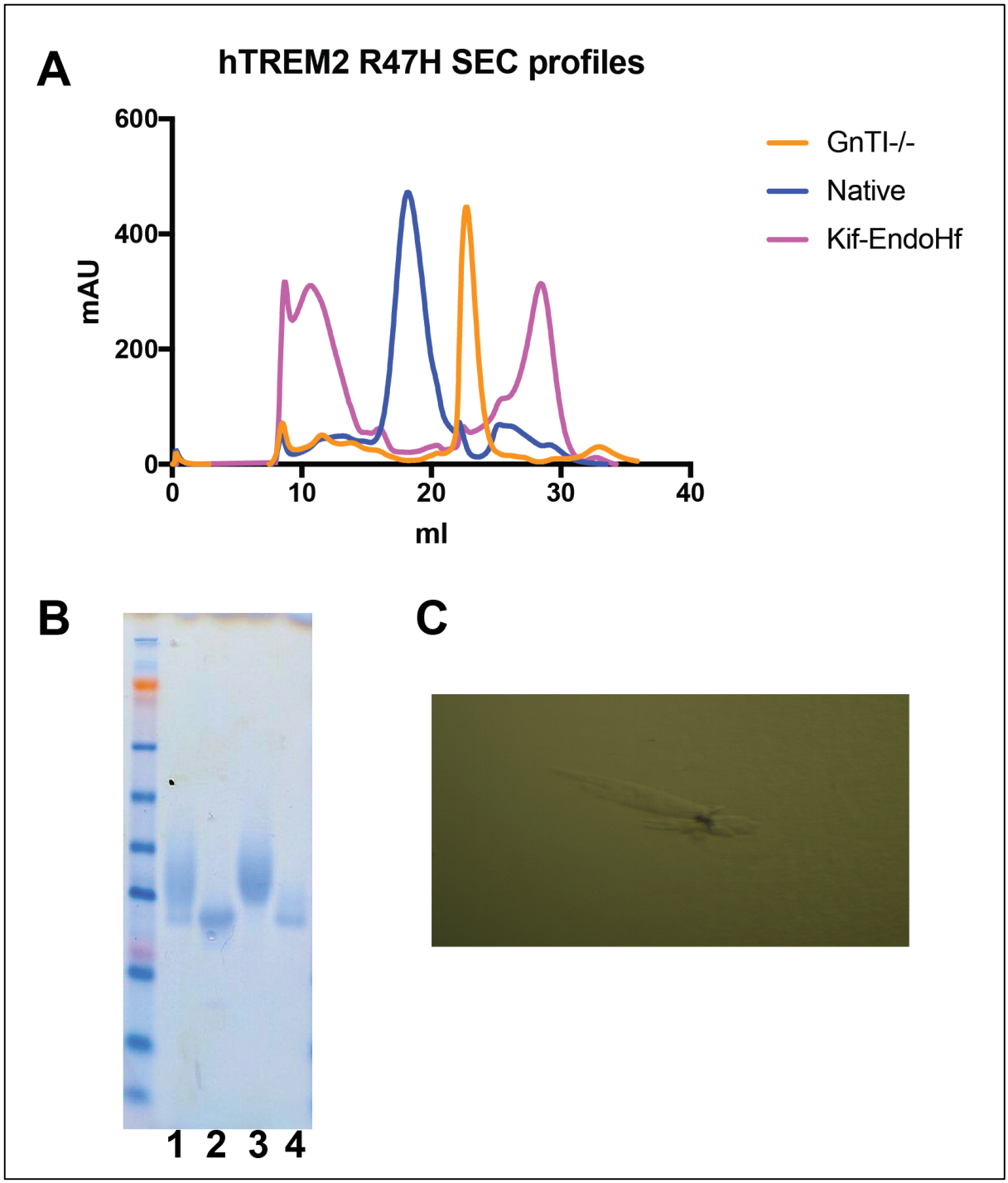

Figure 2.3. Chromatographic characterization of TREM2 in different states of glycosylation and preliminary R47H crystals. A) SEC profiles of R47H purified from native 293F, 293s GnTI-/-, or kifunensine-treated and EndoHf-deglycosylated 293F cells. **B)** SEC-purified WT (1,2) and R47H (3,4) proteins from native and GnTI cells. **C)** Initial R47H crystals in 0.1 M Tris pH 7.0, 0.2 M NaCl, and 35% MPD.

2.2 Crystallization of TREM2

2.2.1 Obtaining and optimizing TREM2 crystals

Tom Brett and David Randolf obtained initial crystal hits of TREM2 using mammalian-expressed hTREM2 purified by NiNTA without subsequent purification by SEC. NiNTA-purified proteins were deglycosylated with EndoHf, and concentrated to 10 mg/mL (**Fig 2.4a,b**). Crystallization screens (JCSG I-IV, Qiagen) were set by hanging drop using a TTP Mosquito robot. These crystals (condition 2.5 M NaCl, 0.2 M MgCl2, and 0.1 M Tris pH 8.0) diffracted poorly. Using the Hampton additive screen, 0.2 M of NDSB-201, NDSB-211, or $BaCl_2$ were found to improve crystal size and diffraction (**Fig 2.4c**). Conditions were further refined so that optimal crystals grew in 2.0 to 2.5 M NaCl, 0.1 M HEPES pH 7.0-7.5, 0.2 M MgCl2, and 0.2 of the additive. Crystals were harvested in mother liquor with 25% ethylene glycol. Data was collected at APS, ID-19. The best-diffracting crystal was grown with NDSB-201 (2).

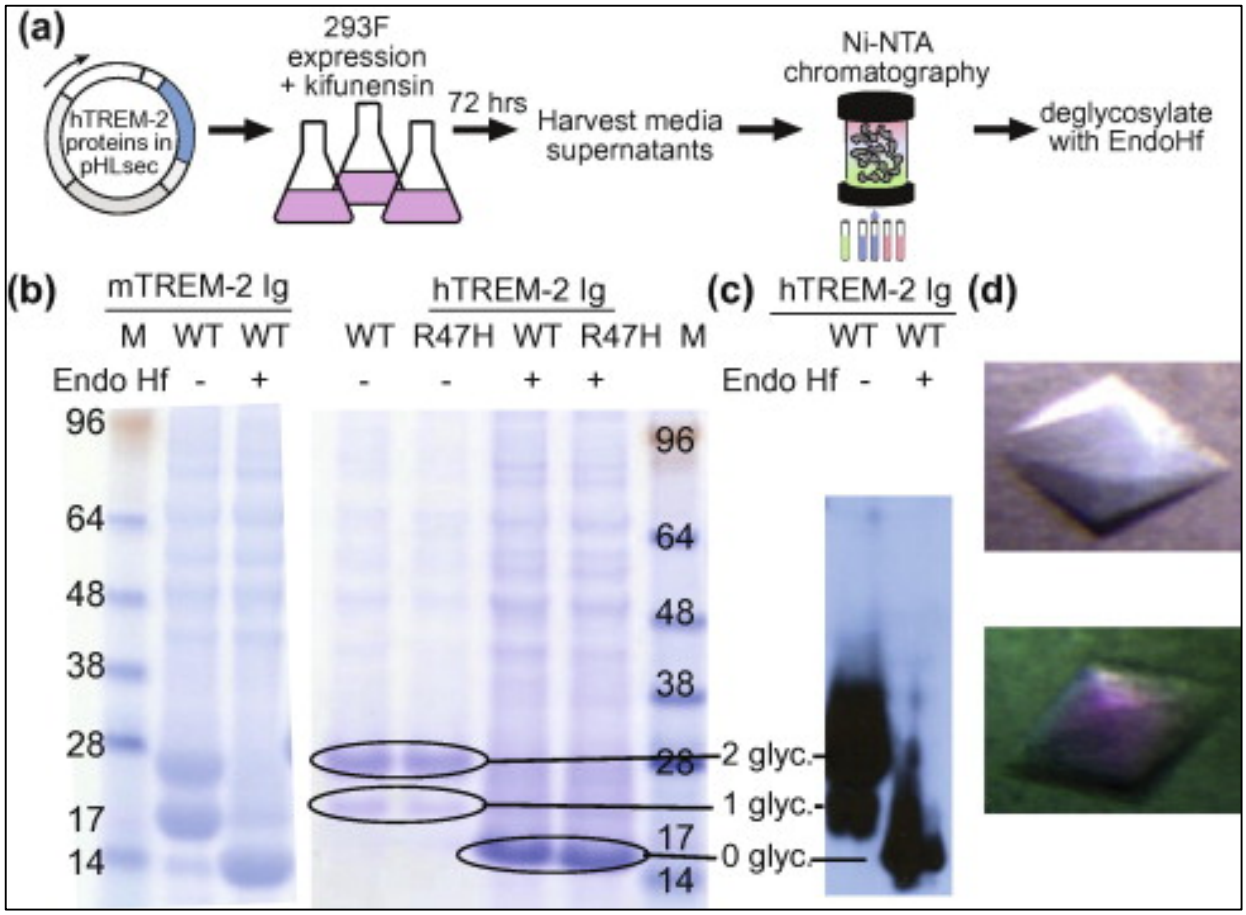

Figure 2.4. Expression, purification, and crystallization of mammalian-expressed hTREM2. a) schematic for expression and purification of hTREM2 Ig domains. **b)** NiNTA-purified TREM2 Ig domains from kifunensine-treated cells before (-) or after (+) deglycosylation by EndoHf. WT mouse and human proteins and human R47H shown. **c)** Immunoblot for 6-His tag confirms the major species as TREM2. **d)** TREM2 crystals grown as described with NDSB-201 additive.

Figure 2.4 modified from Kober et al 2014 (2), reprinted with permission from Elsevier.

2.2.2 Determining the TREM2 structure

Molecular replacement.

Diffraction data was processed and scaled with HKL-2000 (17). The space group was found to be either $P6_222$ or $P6_422$. Distinguishing between these groups requires a phasing solution. Molecular replacement was conducted using PHASER (18). A number of probes were

tried, including mTREM1 (1U9K), hTREM1 (1SMO), hNKp44 (1HKF), hTREML1 (2FRG), mCLM1 (1ZOX). The CCP4 programs Chainsaw and Ensembler were used to create side-chain truncated and/or ensemble models. Ultimately, mTREM1 provided the best solution in the space group $P6_422$ (TFZ = 13.8, Rigid body R_{work} and R_{free} of 0.3909 and 0.4602). Surprisingly, only two copies of the protein were found, which indicates a solvent content of 83% within the Asymmetric unit (ASU) (**Fig 2.5A**).

Validating the molecular replacement solution

The high solvent volume suggested the possibility that another protein had co-crystallized with TREM2. This was especially a concern given that purification was only done with NiNTA. However, the solution does have continuous lattice contacts (**Fig 2.5B**) (2), showing that TREM2 could be forming crystal contacts without another protein. To address whether TREM2 was the only protein in the crystal, crystals were harvested, washed in mother liquor, separated by SDS-PAGE and analyzed by silver stain (**Fig 2.5C**). These crystals only contained a single band, which was confirmed by immunoblot to have the 6-His purification tag. Furthermore, Patterson self-rotation analysis confirmed the expected peaks for the space group at kappa = 60°, 120°, and 180°. An additional peak was observed at kappa = 90°, likely due to two-fold non-crystallographic symmetry (NCS) created by the two copies of TREM2 in the ASU (**Fig 2.5D**). Patterson self-rotation analysis was performed with the program GLRF (19) with a 25 Å radius (2).

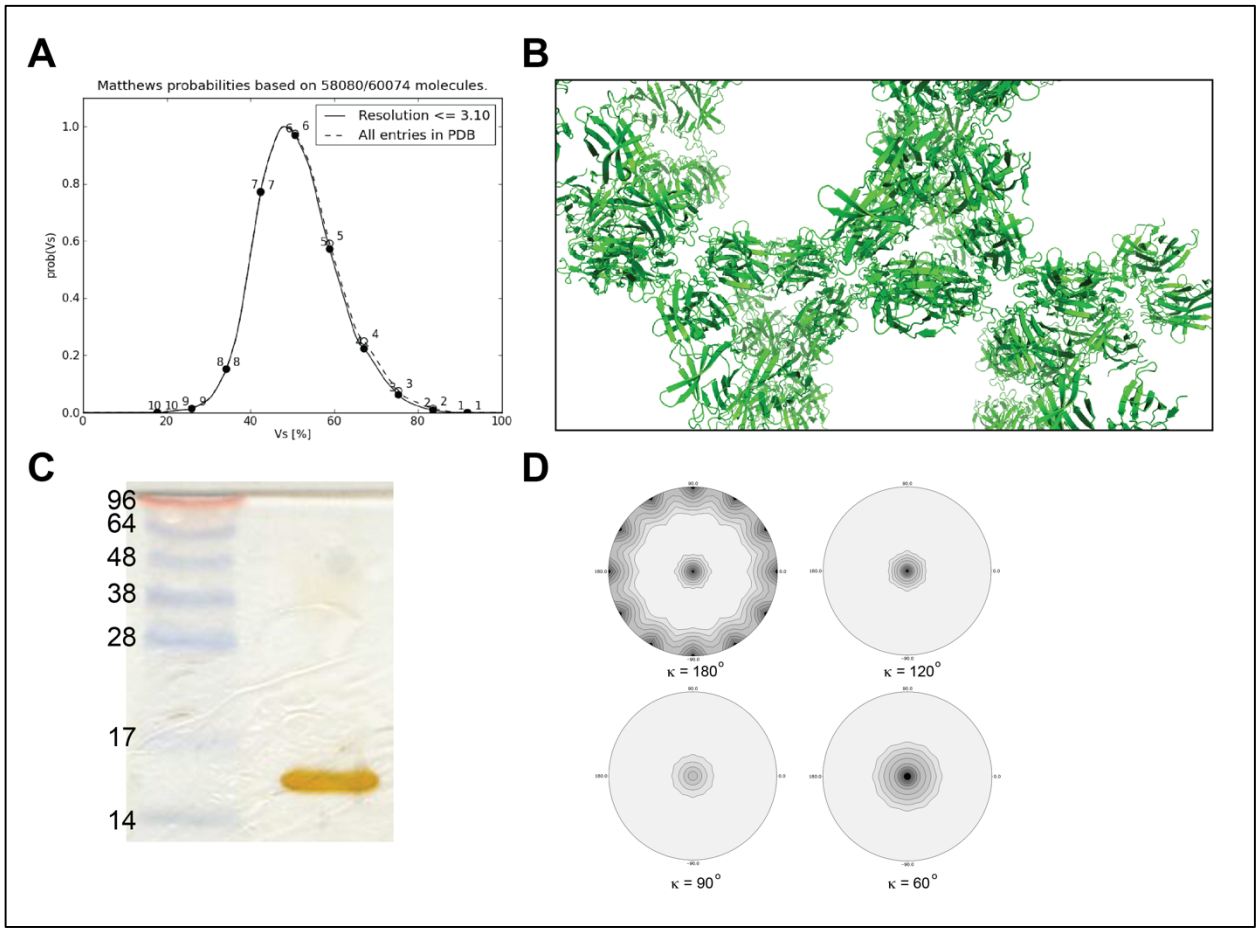

Figure 2.5. Initial analysis of the TREM2 molecular replacement solution. A) Matthews probability for protein copy number in the ASU. Generated at http://www.ruppweb.org/mattprob/default.html. **B)** TREM2 proteins form a continuous lattice. TREM2 structure with symmetry mates generated using the symexp command in Pymol. **C)** Silver stain of harvested TREM2 crystals shows TREM2 is the only protein present in the crystal. **D)** Patterson self-rotation analysis at selected kappa angles.

Panels C and D are reproduced from Kober et al 2014 (2) with permission from Elsevier

2.2.3 Refining the TREM2 structure

Determining the resolution cut-off

Traditionally, the resolution for diffraction data analysis is determined by where the I/sigma of the diffraction spots is 2. However, Karplus and Diederichs demonstrated that data past this threshold can be useful and developed the CC* statistic to interpret where data quality decreases (20). This is partially enabled by the multiplicity of data collection, which can be high in crystallographic experiments, especially in certain crystal lattices. In practice, it can be demonstrated whether increasing resolution improves the model. This is done by scaling the data to a certain resolution, for example 3.3 Å and building a model. Similarly, data is scaled to 3.2 Å and a model built using that data. The model from the 3.2 Å data is then tested against the 3.3 Å data. If the 3.2 Å model gives a lower R_{free} value at 3.3 Å than the 3.3 Å model, the 3.2 Å data, even if weak, is improving the model quality. In this manner, as shown in Table 2, the initial TREM2 solution was manually refined at 3.3 Å until the R_{free} was around 31%. Then, this solution was tested on data reprocessed and scaled to further resolutions and the final TREM2 dataset was extended to 3.1 Å.

Table 2. Determining Resolution cut-off		**Refine at:**			
		3.3	3.2	3.1	3.0
Calculate at:	3.3	26.26/31.66	25.30/31.47		
	3.2		26.75/31.88	26.79/31.80	
	3.1			27.71/32.47	27.64/32.87
	3.0				28.30/32.52

Table 2. is modified from Kober et al. 2016 (9)

Refinement strategies

Once the resolution was determined, refinement proceeded through iteratively manual building in Coot (21) followed by refinement in PHENIX (22). Conservative strategies such as secondary structure restraints, group B factors, NCS restraints, and TLS refinements were employed. Final statistics are shown in **Table 3**. The model was of high-quality, with an overall Molprobity score of 1.66 (100^{th} percentile), clash score of 9.62 (96th percentile), and the Ramachandran statistics were 97.7% favored, 0% outliers, and 2.3% allowed. The model and data were deposited in the protein data bank (PDB, accession code 5ELI).

Table 3. Data collection and refinement statistics

	Human TREM2 Ectodomain
Data collection	
Space group	P 6_4 2 2
Cell dimensions	
a, *b*, *c* (Å)	125.76, 125.76, 183.70
α, β, γ (°)	90, 90, 120
Resolution (Å)	50.00-3.10 (3.21-3.10) *
R_{sym}	0.11 (1.00)
Mean $I / \sigma I$	21.0 (1.76)
Completeness (%)	99.88 (99.75)
Redundancy	12.9 (13.4)
Refinement	
Resolution (Å)	50.00-3.10
No. reflections	16285
R_{work} / R_{free}	0.2605 / 0.2736
No. atoms	1784
Protein	1756
Carbohydrate	28
B-factors	93.48
Protein	92.39
Carbohydrate	162.1
R.m.s. deviations	
Bond lengths (Å)	0.006
Bond angles (°)	1.18

*Values in parentheses are for highest-resolution shell.

Table modified from Kober et al, 2016. (9)

2.3 Results of the TREM2 structure

2.3.1 Interesting features of the TREM2 structure

TREM2 has unexplained density on a hydrophobic surface

The top surface of TREM2 is highly hydrophobic. When refining the structure, a blob of strong density above this surface was observed that was not explained by the protein chain (**Fig 2.6**). Given the limited resolution, it was not possible to identify the ligand from the electron density. Attempts were made to model a ligand, using codes for NDSB-201 (1PS), HEPES (EPE), and phosphocholine (CH5). None were able to improve the R_{free}, even with allowing partial occupancies. The blob seems to be on a special position with the molecule, with symmetry mates sitting above it. Modeling a ligand on one end of the blob places a ligand on the other end. For molecules like NDSB, which seem to fit best running through the blob, this meant the two molecules would be placed on top of each other in the same density. Because TREM2 was expressed in mammalian cells and could have bound an endogenous ligand, attempts were made to determine if TREM2 had co-purified with a lipid cofactor. To do this, a number of lipid extraction techniques were performed and samples analyzed by HPLC with the help of Artie Romero. Three different extraction methods were attempted. All extractions were performed in new glass centrifuge tubes that were solvent-washed before exposure to samples.

1. **Bligh and Dyer** (23). To a 200 µL sample, 0.750 mL of 1:2 chloroform:methanol mixture is added in a glass tube and vortexed. Then another 0.250 mL of chloroform is added and mixed. Finally, 0.250 mL of H_2O is added. The sample is gently centrifuged to separate the aqueous and organic layers. A glass capillary tip is used to remove the

organic lower phase. The sample was dried under vacuum and resuspended in MeOH for HPLC analysis.

2. **MTBE extraction** (24). To a 200 µL samples,1.5 mL of methyl tert-butyl ether (MTBE) is added and placed on shaker for 1 hr with periodic vortexing. Then, 1.25 mL of H_2O is added for 10 min. The sample is spun and the upper organic phase is collected, dried, and resuspended for analysis.
3. **Acetonitrile-methanol** (25). To the 200 µL samples, 1400 µL of 25:40:35 acetonitrile: methanol: H_2O were added on ice for 10 min. Then the sample was spun at 14,000 rpm in the cold room for 20 min. Supernatant was removed, dried, and subjected to HPLC analysis.

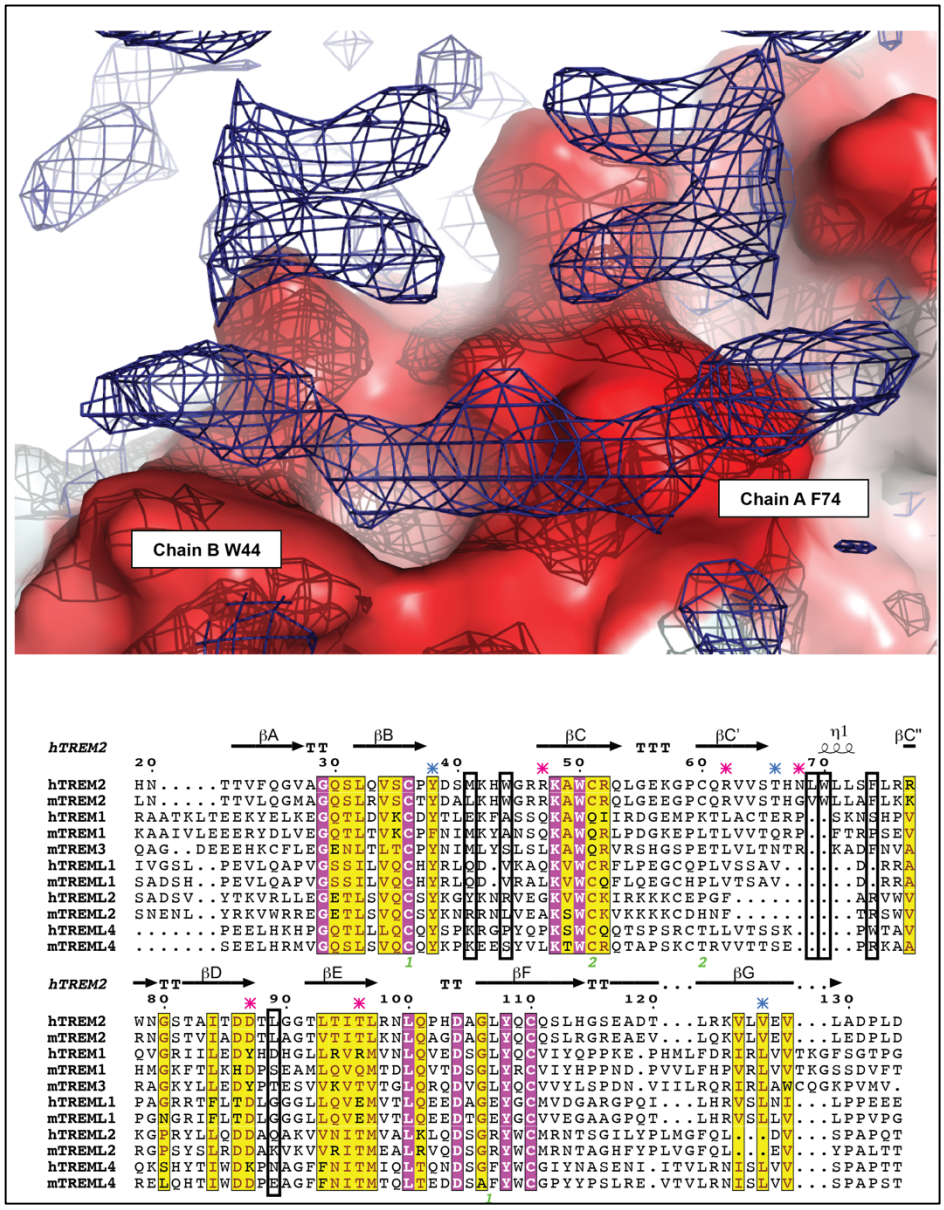

Figure 2.6. Unexplained density – a co-crystallized ligand? Top - Fo-Fc density contoured at 2s in blue. TREM2 ASU colored by hydrophobicity using the color_h script was used to generate a protein surface colored by hydrophobicity. **Bottom** – alignment of TREM family Ig domains with conserved residues identified using the espript server. Invariant residues are yellow and conserved residues in magenta. Residues in the hydrophobic surface labeled with black boxes. AD-linked residues with magenta asterisks. Secondary structure from DSSP server.

Despite these efforts, there was no conclusive evidence for an organic particle enriched in the purified TREM2 samples over unrelated controls. In one experiment, harvested crystals were analyzed and NDSB was detected (a standard of NDSB was run for comparison), but the crystals were not extensively washed and therefore I could not exclude detecting NSDB from the crystallization liquid. Relatedly, one crystal dataset was collected where $BaCl_2$ was used as an additive instead of NDSB, and lysophosphocholine was soaked into the crystal to see if it could be bound. This crystal diffracted to about 3.4 Å and the tubular density was not present. However, the PC could have partially displaced a bound ligand and disrupted the density in that manner. Altogether, it has not been possible to conclusively identify whether the density blob is due to NDSB-201, although that is the most conservative interpretation.

Comparison of TREM2 monomers in the ASU

There are two copies of TREM2 in the ASU. The only obvious difference is the shifting of a loop, which makes lattice contacts in the B molecule (Cα RMSD < 1Å between the two chains). Moreover, the AD residues are not impacted by this small alteration (**Fig 2.7a, b**). For clarity, chain A is shown whenever a single monomer is depicted. Could the two copies represent a biological dimer? While tempting, it should be noted that the N79-NAG glycan is participant in the dimer interface and presumably the full-length glycan would disrupt this interaction. The PISA server was used to examine symmetry-related molecules as possible interfaces. No interactions were predicted to be stable, and the largest surface buried between proteins is between the B chains related by the x,x-y+1,-z-1/3 symmetry operation (~680 $Å^2$ buried surface). The complex significance score was 0.0 for all interfaces, showing they are unlikely to be stable in solution (**Fig 2.7c**). This is consistent with reports of human and mouse TREM1 behaving as

monomers in solution (3, 4). So, while this data does not rule out that TREM2 is oligomeric in solution, it is unlikely that the interfaces observed in the crystal structure represent biological interactions. Therefore, all analyses will consider TREM2 as a monomer.

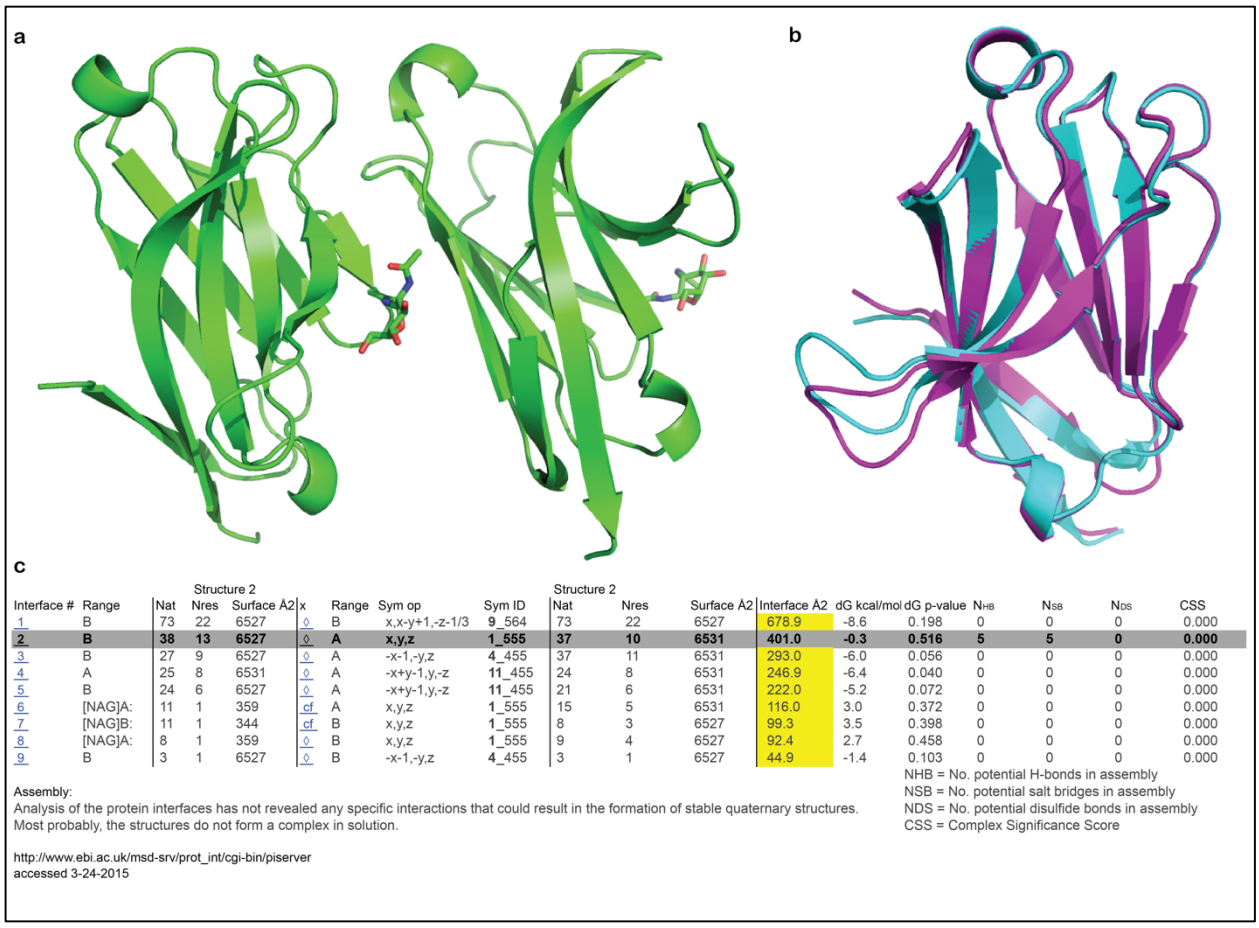

Figure 2.7. TREM2 interactions in the crystal structure. a) the TREM2 ASU has two copies arranged in similar orientation. **b)** TREM2 monomers superposed on one another. Chain A in magenta and B in cyan. **c)** PISA analysis table, showing that the interfaces are not predicted to result in complex formation.

Figure 2.7 reused from Kober et al, 2016 (9)

2.3.2 The TREM2 structure suggests distinct loss-of-function mechanisms

With the TREM2 structure determined, the next objective was to use the structure to generate hypotheses for the role of disease-linked variants. The structure lacks density only one

C-terminal and four N-terminal residues. Density for the N79-NAG, but not the N20-NAG is present. All disease-associated residues within the Ig domain were present in the structure. The residues linked to disease were mapped on the TREM2 structure (**Fig 2.8b**). A pattern emerged where the NHD-causing residues all face inward, towards the protein core. In contrast, the AD-associated variants are all on the protein surface. This qualitative observation was quantified with Naccess (26) (**Fig 2.8c**). Analysis of packing contacts further confirmed the NHD residues make extensive Van der Waals contacts within the protein core (9). This observation inspired the hypothesis that the NHD variants impact protein function by disrupting protein folding or stability while the AD variants likely do not impair protein folding or stability but may disrupt ligand binding. Strong density was observed for all the surface AD variants and the N79-NAG (**Fig 2.8 d-g**). Overall, the AD-linked residues have only minor interactions with other residues. Potential structural interactions with these residues are polar interactions between D87 and the βD-E loop, and those between the R47 side change and the carbonyl oxygen on the T66 backbone. The other residues (R62, N68, T96) make no obvious polar contacts. Overall, these minimal interactions suggest the AD-linked variants would most likely impact function through altered ligand binding and not through destabilizing the protein.

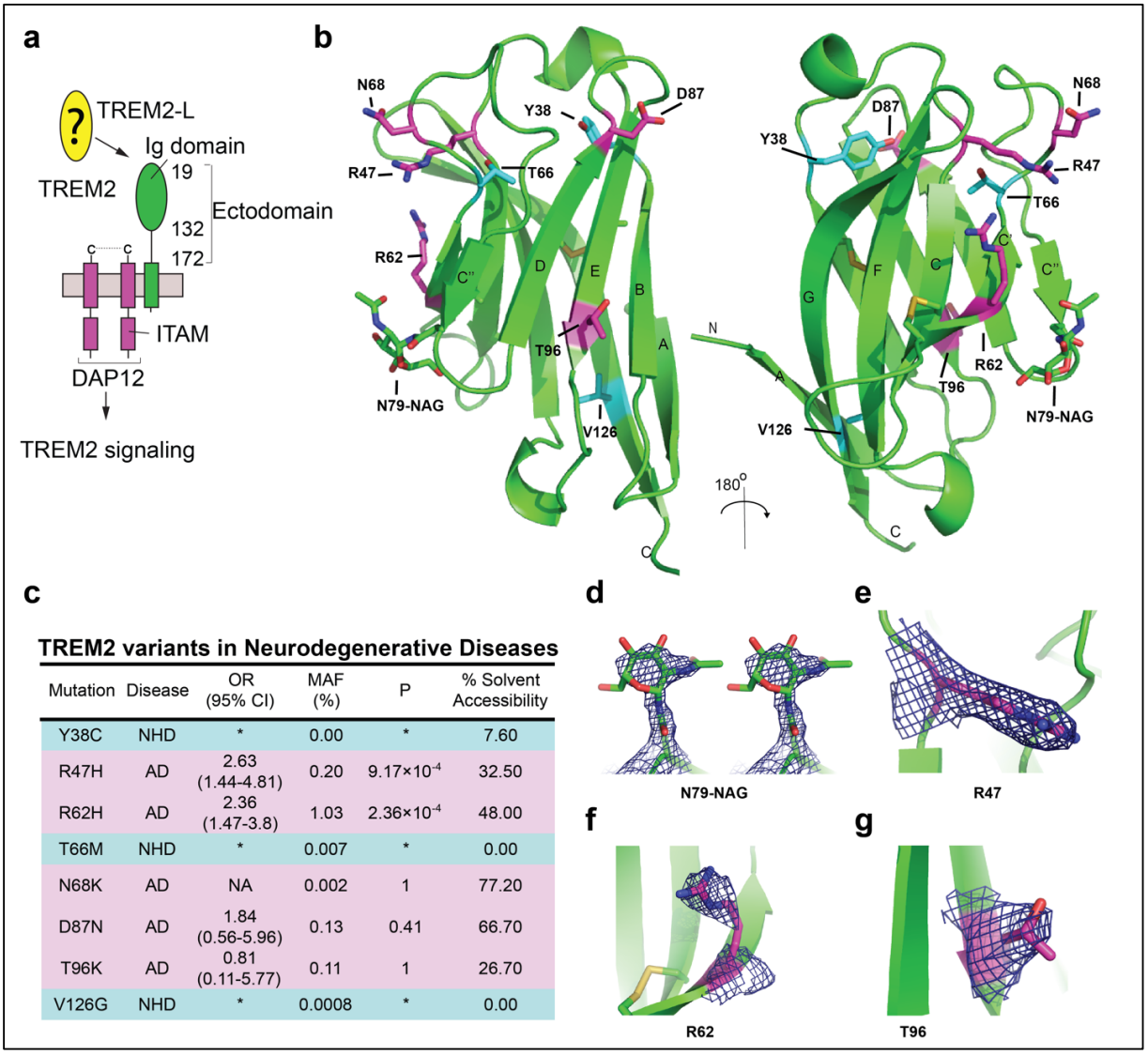

Mutation	Disease	OR (95% CI)	MAF (%)	P	% Solvent Accessibility
Y38C	NHD	*	0.00	*	7.60
R47H	AD	2.63 (1.44-4.81)	0.20	9.17×10^{-4}	32.50
R62H	AD	2.36 (1.47-3.8)	1.03	2.36×10^{-4}	48.00
T66M	NHD	*	0.007	*	0.00
N68K	AD	NA	0.002	1	77.20
D87N	AD	1.84 (0.56-5.96)	0.13	0.41	66.70
T96K	AD	0.81 (0.11-5.77)	0.11	1	26.70
V126G	NHD	*	0.0008	*	0.00

Figure 2.8. TREM2 structure and location of disease-linked residues. **a)** Schematic for TREM2 strucutre. The Ig domain portion of the ectodomain was crystallized. **b)** The TREM2 structure in two different orientations. AD-associated residues are shown in magenta, NHD in cyan. N79-NAG shown in green sticks. **c)** Table of disease variants showing disease, odds ratio (OR), mean allelic frequency (MAF), p-value, and % solvent accessibility, calculated by Naccess. **d-g**, Density for N79-NAG (**d**, shown in stereo), R47 **(e)**, R62 **(f)** and T96 **(g)**. Density is 2mFo-DFc contoured at 2σ.

Figure re-used from Kober et al, 2016 (9) and genetic data in the table from (27).

2.4 References:

1. Colonna M. TREMs in the immune system and beyond. Nat Rev Immunol. 2003;3(6):445-53. doi: 10.1038/nri1106. PubMed PMID: 12776204.
2. Kober DL, Wanhainen KM, Johnson BM, Randolph DT, Holtzman MJ, Brett TJ. Preparation, crystallization, and preliminary crystallographic analysis of wild-type and mutant human TREM-2 ectodomains linked to neurodegenerative and inflammatory diseases. Protein expression and purification. 2014;96:32-8. doi: 10.1016/j.pep.2014.01.015.
3. Kelker MS, Foss TR, Peti W, Teyton L, Kelly JW, Wüthrich K, Wilson Ia. Crystal structure of human triggering receptor expressed on myeloid cells 1 (TREM-1) at 1.47 A. Journal of molecular biology. 2004;342(4):1237-48. doi: 10.1016/j.jmb.2004.07.089.
4. Kelker MS, Debler EW, Wilson IA. Crystal Structure of Mouse Triggering Receptor Expressed on Myeloid Cells 1 (TREM-1) at 1.76 Å. Journal of molecular biology. 2004;344(5):1175-81. doi: http://dx.doi.org/10.1016/j.jmb.2004.10.009.
5. Márquez JA, Galfré E, Dupeux F, Flot D, Moran O, Dimasi N. The Crystal Structure of the Extracellular Domain of the Inhibitor Receptor Expressed on Myeloid Cells IREM-1. Journal of Molecular Biology. 2007;367(2):310-8. doi: http://dx.doi.org/10.1016/j.jmb.2007.01.011.
6. Gattis JL, Washington AV, Chisholm MM, Quigley L, Szyk A, McVicar DW, Lubkowski J. The structure of the extracellular domain of triggering receptor expressed on myeloid cells like transcript-1 and evidence for a naturally occurring soluble fragment. J Biol Chem. 2006;281(19):13396-403. doi: 10.1074/jbc.M600489200. PubMed PMID: 16505478.
7. Cantoni C, Ponassi M, Biassoni R, Conte R, Spallarossa A, Moretta A, Moretta L, Bolognesi M, Bordo D. The Three-Dimensional Structure of the Human NK Cell Receptor NKp44, a Triggering Partner in Natural Cytotoxicity. Structure. 2003;11(6):725-34. doi: http://dx.doi.org/10.1016/S0969-2126(03)00095-9.
8. Biter AB, de la Peña AH, Thapar R, Lin JZ, Phillips KJ. DSF Guided Refolding As A Novel Method Of Protein Production. Scientific Reports. 2016;6:18906. doi: 10.1038/srep18906

http://www.nature.com/articles/srep18906 - supplementary-information.
9. Kober DL, Alexander-Brett JM, Karch CM, Cruchaga C, Colonna M, Holtzman MJ, Brett TJ. Neurodegenerative disease mutations in TREM2 reveal a functional surface and distinct loss-of-function mechanisms. Elife. 2016;5:e20391. doi: 10.7554/eLife.20391. PubMed PMID: 27995897; PMCID: PMC5173322.
10. Aricescu aR, Lu W, Jones EY. A time- and cost-efficient system for high-level protein production in mammalian cells. Acta crystallographica Section D, Biological crystallography. 2006;62(Pt 10):1243-50. doi: 10.1107/S0907444906029799.
11. Kober DL, Yurtsever Z, Brett TJ. Efficient mammalian cell expression and single-step purification of extracellular glycoproteins for crystallization. J Vis Exp. 2015;106:53445.
12. Aricescu AR, Owens RJ. Expression of recombinant glycoproteins in mammalian cells: towards an integrative approach to structural biology. Current Opinion in Structural Biology. 2013;23(3):345-56. doi: http://dx.doi.org/10.1016/j.sbi.2013.04.003.
13. Rich JR, Withers SG. Emerging methods for the production of homogeneous human glycoproteins. Nat Chem Biol. 2009;5(4):206-15.
14. Reeves PJ, Callewaert N, Contreras R, Khorana HG. Structure and function in rhodopsin: High-level expression of rhodopsin with restricted and homogeneous N-glycosylation by a tetracycline-inducible N-acetylglucosaminyltransferase I-negative HEK293S stable mammalian

cell line. Proceedings of the National Academy of Sciences. 2002;99(21):13419-24. doi: 10.1073/pnas.212519299.
15. Felix J, Elegheert J, Gutsche I, Shkumatov Alexander V, Wen Y, Bracke N, Pannecoucke E, Vandenberghe I, Devreese B, Svergun Dmitri I, Pauwels E, Vergauwen B, Savvides Savvas N. Human IL-34 and CSF-1 Establish Structurally Similar Extracellular Assemblies with Their Common Hematopoietic Receptor. Structure. 2013;21(4):528-39. doi: http://dx.doi.org/10.1016/j.str.2013.01.018.
16. Pronker MF, Lemstra S, Snijder J, Heck AJR, Thies-Weesie DME, Pasterkamp RJ, Janssen BJC. Structural basis of myelin-associated glycoprotein adhesion and signalling. Nature Communications. 2016;7:13584. doi: 10.1038/ncomms13584

http://www.nature.com/articles/ncomms13584 - supplementary-information.
17. Otwinowski Z, Minor W. Processing of X-ray Diffraction Data Collected in Oscillation Mode. 1st ed. C.W. Carter JRMS, editor. New York: Academic Press; 1997. 700 p.
18. McCoy AJ, Grosse-Kunstleve RW, Adams PD, Winn MD, Storoni LC, Read RJ. Phaser crystallographic software. Journal of Applied Crystallography. 2007;40(4):658-74. doi: doi:10.1107/S0021889807021206.
19. Tong L, Rossmann MG. [34] Rotation function calculations with GLRF program. Methods in Enzymology: Academic Press; 1997. p. 594-611.
20. Karplus PA, Diederichs K. Linking crystallographic model and data quality. Science (New York, NY). 2012;336(6084):1030-3. doi: 10.1126/science.1218231.
21. Emsley P, Lohkamp B, Scott WG, Cowtan K. Features and development of Coot. Acta Crystallographica Section D. 2010;66(4):486-501. doi: doi:10.1107/S0907444910007493.
22. Adams PD, Afonine PV, Bunkoczi G, Chen VB, Davis IW, Echols N, Headd JJ, Hung L-W, Kapral GJ, Grosse-Kunstleve RW, McCoy AJ, Moriarty NW, Oeffner R, Read RJ, Richardson DC, Richardson JS, Terwilliger TC, Zwart PH. PHENIX: a comprehensive Python-based system for macromolecular structure solution. Acta Crystallographica Section D. 2010;66(2):213-21. doi: doi:10.1107/S0907444909052925.
23. Bligh EG, Dyer EG. A rapid method of total lipid extraction and purification. Can J Biochem Physiol. 1959;37(8):911-7.
24. Matyash V, Liebisch G, Kurzchalia TV, Shevchenko A, Schwudke D. Lipid extraction by methyl-tert-butyl ether for high-throughput lipidomics. Journal of lipid research. 2008;49(5):1137-46. doi: 10.1194/jlr.D700041-JLR200.
25. Mapstone M, Cheema AK, Fiandaca MS, Zhong X, Mhyre TR, MacArthur LH, Hall WJ, Fisher SG, Peterson DR, Haley JM, Nazar MD, Rich SA, Berlau DJ, Peltz CB, Tan MT, Kawas CH, Federoff HJ. Plasma phospholipids identify antecedent memory impairment in older adults. Nat Med. 2014;20(4):415-8. doi: 10.1038/nm.3466. PubMed PMID: 24608097.
26. Hubbard S, Thornton J. NACCESS, Computer Program. 1993.
27. Jin SC, Benitez BA, Karch CM, Cooper B, Skorupa T, Carrell D, Norton JB, Hsu S, Harari O, Cai Y, Bertelsen S, Goate AM, Cruchaga C. Coding variants in TREM2 increase risk for Alzheimer's disease. Hum Mol Genet. 2014;23(21):5838-46. doi: 10.1093/hmg/ddu277. PubMed PMID: 24899047; PMCID: PMC4189899.

Chapter 3: Biophysical impact of neurodegenerative variants on TREM2

3.1 Solution behavior of WT and variant TREM2 proteins

The TREM2 structure suggested that AD-linked variants would be properly folded and stable while the NHD variants would be misfolded. These misfolded variants might be expected to be cleared by ERAD quality control machinery in the ER and not secreted (if expressed as soluble Ig domain) or reach the cell surface (if expressed in full-length proteins). To test the former possibility, disease variants were introduced into the hTREM2 Ig domain within the pHLSEC vector. Large-scale expressions of WT and mutants would be purified by NiNTA and then purified by SEC using a superdex 200 10/300 GL analytical column in 150 mM NaCl with 20 mM Tris pH 8.5 with a flow rate of 0.5 mL/min. If the proteins eluted as WT, they would then be concentrated and re-run on the column to establish that they remained monodisperse.

3.1.1 Expression and solution behavior of NHD variants.

Although it was hypothesized that the NHD variants would not be secreted, immunoblot analysis of supernatant from transfected 293F cells surprisingly showed significant amounts of these proteins. However, analysis by reducing/non-reducing SDS-PAGE followed by immunoblot for the 6-His tag demonstrated these proteins have aberrant intermolecular disulfide bonds. In fact, no properly-migrating monomeric species were observed in these experiments (**Fig 3.1a**). Because these proteins were secreted, they were purified by NiNTA and analyzed by SEC. In contrast to WT, which elutes at a volume corresponding to the predicted MW (**Fig 3.1b, c**). the NHD variants elute early, in fractions that correspond to aggregated or oligomeric

proteins (**Fig 3.d-i**). NHD proteins were not efficiently recovered after concentrating the fractions, and were therefore not tested in further biophysical assays (such as DSF).

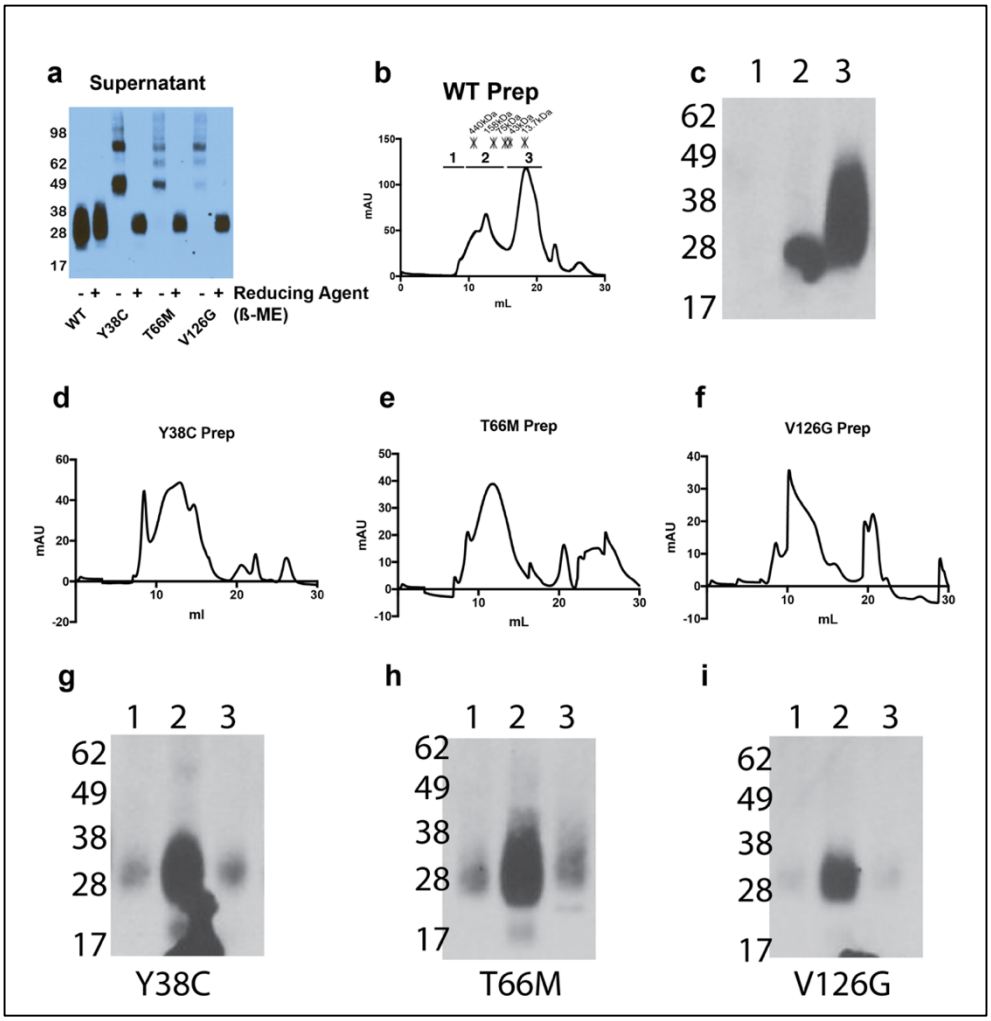

Figure 3.1 Solution behavior of NDH TREM2 Ig domains. a) anti-6-His immunoblot analysis of supernatant from 293F cells transfected with WT or NHD variant proteins. + or – indicates presence of β–ME in the loading buffer. NHD domains run as higher molecular weights, indicated intermolecular disulfide bonding. **b)** SEC purification of WT TREM2. WT protein elutes in fraction 3, which corresponds to about 14kDa. Elution volumes of MW standards shown with *. **c)** Immunoblot of pooled fractions from WT TREM2 SEC run. **d-f)** SEC profiles of NHD variants. **g-i)** Anti-6 his immunoblot of pooled fractions from SEC runs. NHD proteins elute as aggregates, with minimal monomeric protein detected.

Figure 3.1 modified from Kober et al, 2016 (1)

3.1.2 Expression and solution behavior of surface variants.

The crystal structure suggests the surface variants should behave like WT. As with the NHD variants, these were expressed in 293F cells and analyzed by SEC. As an additional check, the purified fractions were again run on the column to see if they remained monodisperse. In these experiments, all surface variants (R47H, R62H, N68K, D87N, T96K) all elute at the same volume as WT and with similar profiles. All proteins could be re-run on the column with minimal aggregation or shouldering (**Fig 3.2**). Upon purification, WT and mutant Ig domains were analyzed by reducing/non-reducing SDS-PAGE to see if they had aberrant disulfide bonding. No improper oligomers were detected.

Concerning the glycosylation status of the surface variants

In these studies, differential glycosylations have not been observed. One group expressed full-length WT or R47H in HeLa cells, analyzed glycosylations using immunoblots and mass spectroscopy, and reported that the R47H has slightly altered glycosylation patterns (2, 3). Importantly, these reports do not show that R47H is under-glycosylated or lacks mature glycans, rather, they report that the mature glycans have slightly altered modifications compared to WT. My studies used HEK293 cells and predominantly expressed just the Ig domain. It is possible that the different cell lines or different domains could produce different glycosylation. However, over the course of this work the AD disease variants were expressed numerous times and there was not obviously detectible impairment of glycan maturation or changes in the appearance by SDS-PAGE (**Fig 3.2 m,n**).

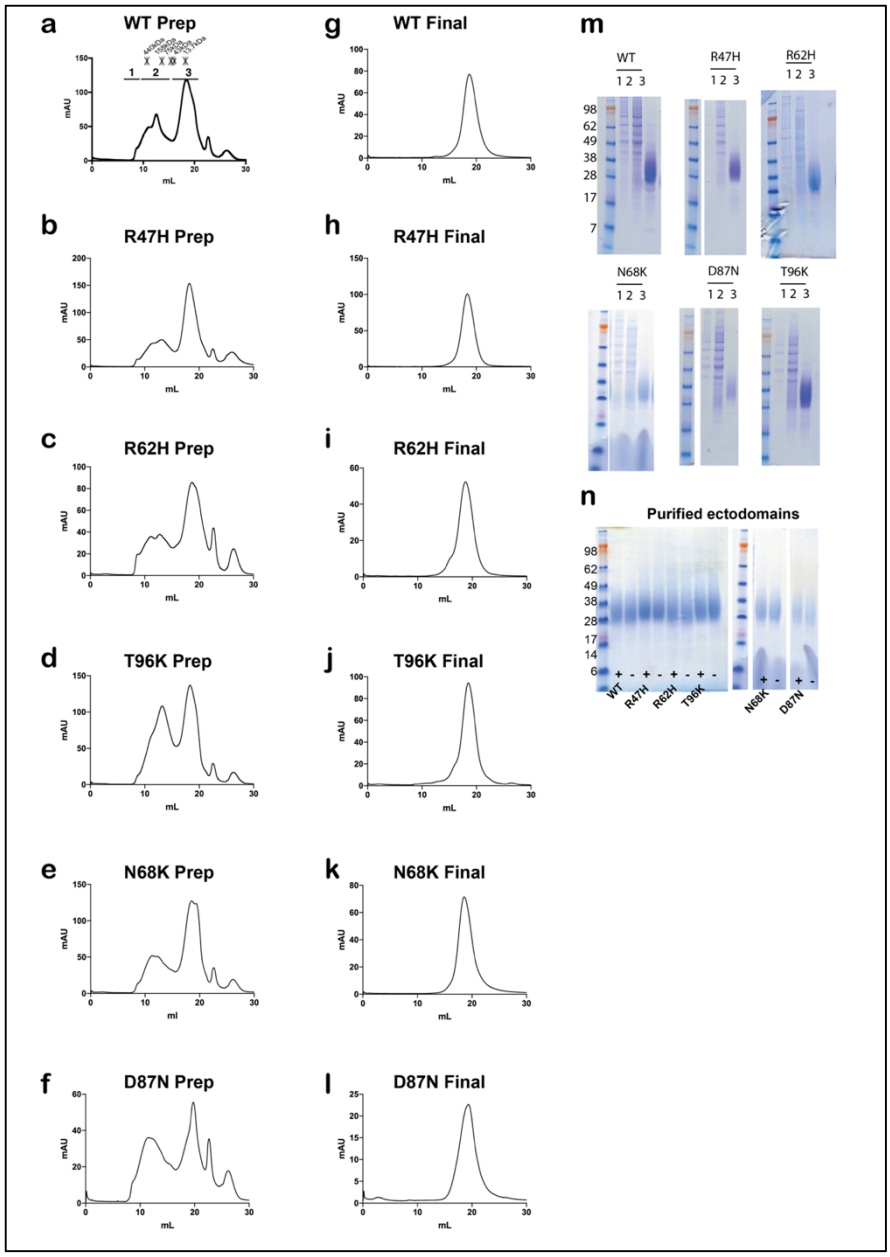

Figure 3.2. Purification and SEC analysis of WT and surface AD variants. **a-f)** Preparative SEC of WT or surface variant proteins. Fractions were collected as depicted in panel **a** and analyzed by SDS PAGE (m). g-l) Fraction 3, which is the purified protein, was concentrated and run again. All proteins re-run as monodisperse peaks, with minimal aggregation. **m)** Protein fractions were pooled and concentrated. TREM2 proteins elute in the third peak, which corresponds to a monomeric MW. **n)** purified proteins were run ± β–ME to test for improper disulfides.

Figure 3.2 modified from Kober et al, 2016 (1)

3.2 Cell surface expression of WT and variant TREM2

3.2.1 Rationale and experimental design for cell surface expression

That the NHD variants could be secreted and detected was surprising, as it was hypothesized they would be retained in the ER. Indeed, two separate studies had reported the Y38C and T66M variant were not expressed on the cell surface (2, 4). To see if the buried and surface variants could achieve cell surface expression, full-length TREM2 constructs with an N-terminal FLAG tag were introduced into the pHLSEC vector. These constructs express the full transmembrane TREM2 gene with an extracellular N-terminal FLAG tag. The FLAG peptide, DYKDDDDK, is a linear motif recognized by anti-FLAG antibodies (Sigma, M2 clone) independently of conformation. This antibody would detect surface-expressed TREM2 even if misfolded. Separately, through the Hydriboma center at Washington University, two hamsters were immunized with mammalian expressed hTREM2 Ig domain and the full mTREM2 ectodomain. Immune reactivity was confirmed by ELISA to biotinylated human and mouse proteins. These antibodies were raised against folded epitopes and should recognize TREM2 in its native state. Polyclonal sera from these animals were produced as part of an effort to produce monoclonal anti-TREM2 antibodies (Antibody characterization is detailed in section 5.5). Finally, a commercial mTREM2 antibody (R&D, provided by the Michael Holtzman lab) was used to confirm the observations made with the hamster sera. In these experiments, 293F cells were co-transfected with full-length FLAG-TREM2 and mDAP12 in a pcDNA3.1 vector (cDNA provided by M. Holtzman). Transfection was accomplished with by mixing equal amounts of TREM2 and DAP12 DNA with 293fectin. Cells were collected after 24 hours, placed on ice, washed in chilled FACS buffer (PBS with 1% FBS), and stained with anti-FLAG-FITC (1:50) or anti-TREM2 sera (1:1000, followed by anti-hamster secondary-PE, 1:200, eBioscience). Cells

were not permeabilized, and were on ice for the entire process. Flow cytometry data was collected on a BD FACscan and data was analyzed using FlowJo (Treestar). Background in staining experiments was very minimal, and was defined by the staining to 293F cells transfected with DAP12-only.

In addition to the flow cytometry experiments, confocal experiments were conducted to evaluate surface expression in an independent system. 293T cells were plated on glass coverslips and co-transfected with FLAG-TREM2 and DAP12 as described above. Cells were washed in cold PBS, fixed in 4% paraformaldehyde (PFA) in PBS, and then were either left unpermeabilized or were permeabilized with 0.1% triton X-100. Cells were blocked in animal-free blocker (Vector laboratories) and then stained with mouse anti-FLAG overnight at 4° C (1:1000). In the morning, cells were washed, stained with Alexa Fluor 555-conjugated secondary (1:200) for one hour before being washed and mounted with VECTASHEILD mounting medium containing DAPI, which stain nuclei. Finally, total TREM2 was evaluated by anti-FLAG immunoblot of cell lysates. Cells were collected, washed into PBS with 0.1% triton X-100, and left rotating at 4° C for 15 min to lyse cells. Insoluble debris (nuclei, membranous organelles) were pelleted by centrifugation and the supernatant added to 2x SDS buffer with β-ME, boiled for 10 min, and analyzed by SDS-PAGE.

3.2.2 AD and NHD TREM2 variants are surface-expressed

TREM2 surface expression was measured by flow cytometry in two different formats – by detecting the linear FLAG epitope or the folded TREM2 protein. Expression was evaluated by quantifying the percentage of cells that were TREM2+ by FLAG or hamster sera after subtracting the percent positive in DAP12-only cells, and then normalizing this value to WT.

Contrary to the initial hypothesis, but consistent with their secretion by 293F cells, all the variants were detectable using anti-FLAG immunostaining (**Fig 3.3a**). In contrast, there was a significant reduction in the number of TREM2+ cells using the polyclonal sera (**Fig 3.3b**). This difference was even more pronounced using the commercial monoclonal (**Fig 3.3c**). The decreased detection with the polyclonal sera is especially significant because the polyclonal should not be sensitive to a single epitope, whereas the monoclonal might be impacted by certain variant sequences.

In the confocal experiments, the FLAG antibody confirmed surface expression of WT, Y38C, and R47H – representative members of the buried and surface disease-risk variants (**Fig 3.3d**). If anything, expression was higher in the NHD variant. This increased intensity could be due to decreased proteolytic processing of this variant. Anti-FLAG immunoblot of the whole cell lysate also confirmed equivalent or even increased expression for the NHD variants (**Fig 3.3e**).

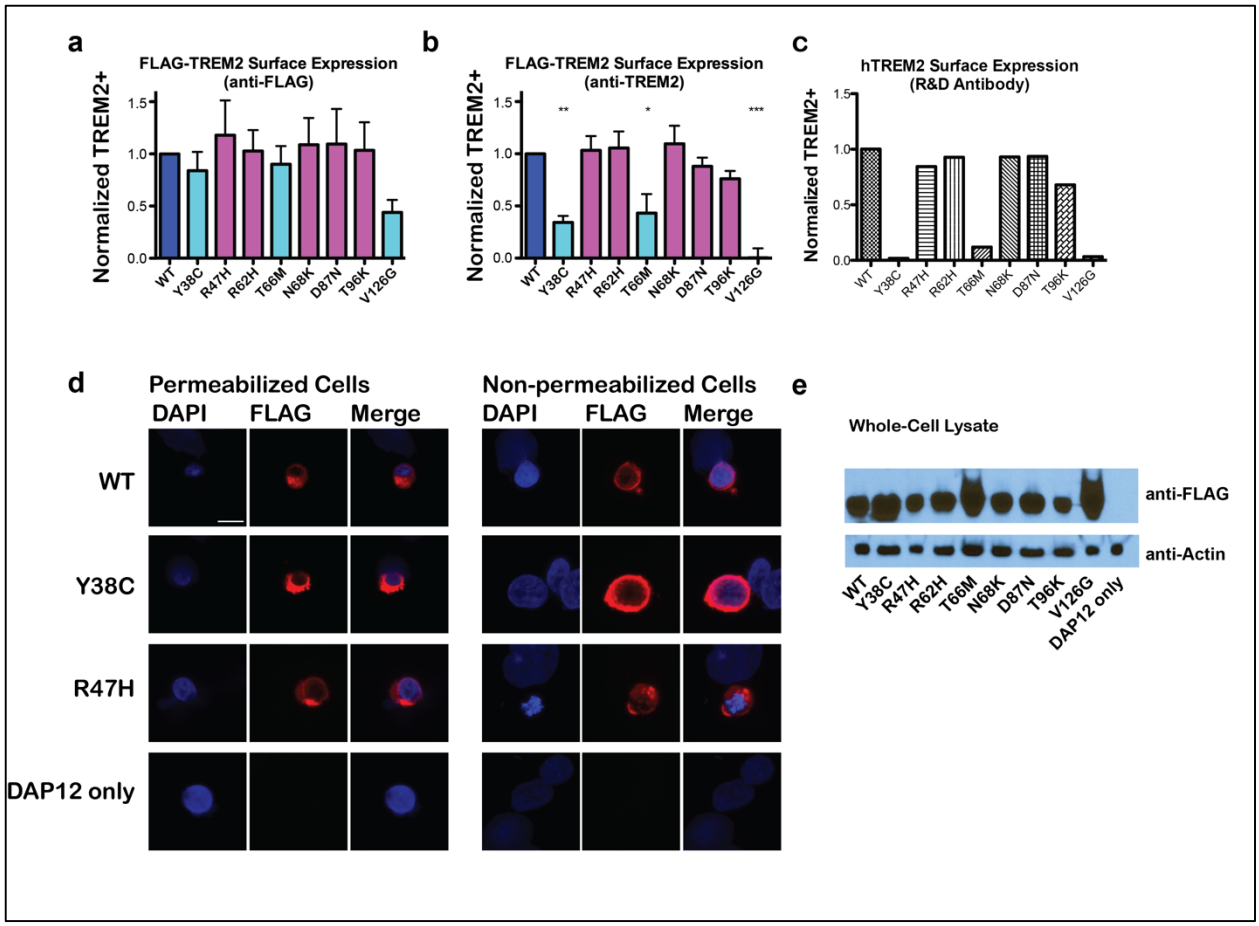

Figure 3.3 Surface expression studies of WT and variant TREM2. a) Normalized TREM2 surface expression by anti-FLAG measured by flow cytometry. **b)** Normalized TREM2 surface expression by anti-TREM2 polyclonal sera measured by flow cytometry **c)** Normalized TREM2 surface expression by a commercial monoclonal measured by flow cytometry. **d)** Confocal microscopy of FLAG-TREM2 expressed in permeabilized on non-permeabilized 293T cells confirms surface expression of AD and NHD variants. **e)** Anti-FLAG immunoblot of full-length TREM2 proteins expressed in 293T cells.

Figure 3.3 modified from Kober et al, 2016. (1)

Taken together, data using both the Ig and full-length variant TREM2 support the prediction from the crystal structure that the NHD residues cause protein misfolding, as they have intermolecular disulfide bonds and have decreased detection by conformation-sensitive antibodies. Despite being misfolded, these variants are surface expressed. It is possible that this

is be an artifact of protein construction or overexpression. However, given that secretion was observed with a C-terminal 6-His tag and surface expression was observed with an N-terminal FLAG tag, it is unlikely that the secretion or expression is an artifact of the protein construct. This finding will need to be confirmed with *in vivo* animal knock-ins or human samples. If these variants are surface-expressed, they may present a therapeutic target. In contrast to the NHD variants, the AD-risk and other surface variants do not cause folding defects on a gross scale. They behave comparably to WT by SEC and are recognized both by a commercial monoclonal and novel polyclonal that are sensitive to TREM2 misfolding.

3.3 Using CD spectroscopy to evaluate TREM2 folding

The secretion and expression studies showed that the AD variants and other possible AD variants which are on the protein surface probably do not cause disease by loss of structural integrity. However, detailed studies of solution structure and stability might reveal nuances associated with risk variants. In these experiments, the NHD variants were not used because they resisted SEC purification. The surface variants R47H, R62H and T96K were used for all experiments because the R to H variants have the strongest genetic link to disease while the T96K variant showed increased binding in cell-binding assays and may be protective (discussed later). The N68K and D87N variants were only used in initial circular dichroism spectroscopy (CD) analysis to confirm folding as predicted by structural and solution studies.

3.3.1 CD spectroscopy reveals a subtle change in the R47H variant

CD spectroscopy is a spectroscopic technique that measures the difference between the left and right circularly polarized light absorbed by a sample. This value is reported as the mean residue molar ellipticity. CD experiments were conducted in a JASCO J-815 machine in the laboratory of Daved Fremont. Because chloride absorbs strongly in the far-UV range, proteins

were exchanged into sterile-filtered 150 mM NaF and 10 mM phosphate pH 7.0. This buffer was also used as the dilution agent. An equal volume of concentrator flow-through was used for buffer subtraction. Experiments were either conducted at 3 μM in a 10 mm cuvette or at 30 μM in a 1 mm cuvette. All thermal denaturations were conducted in the 10 mm cuvette placed in a Peltier temperature controller with a small stir bar to ensure mixing. In all CD experiments, proteins were expressed in mammalian cells and purified by SEC as described above. Experiments were always conducted within one week of purification, and generally on the same day as purification. With melting experiments, the data was smoothed using the JASCO software. All CD curves, except for N68K and D87N were replicated on at least three individual expressions. WT and R47H were analyzed on at least five individual expressions.

Ig domains have a typical β-sheet minima around 218 nm, but also have a characteristic secondary minima around 233 nm, which is thought to be due to canonical tryptophan residues within the Ig fold (5). These features were observed with WT and all surface variants (**Fig 3.4a**). This analysis showed that the surface variants do not grossly alter the fold. In initial experiments, it was noted that the R47H variant has a slightly altered CD profile. To quantify this, the ratio of the two minima were evaluated. R47H was the only variant with an altered profile by this analysis, and this was statistically significant (**Fig 3.4b**) (1). Therefore, this analysis shows that the surface variants retain a characteristic Ig fold, although the R47H variant has a slight, but measurable conformational change.

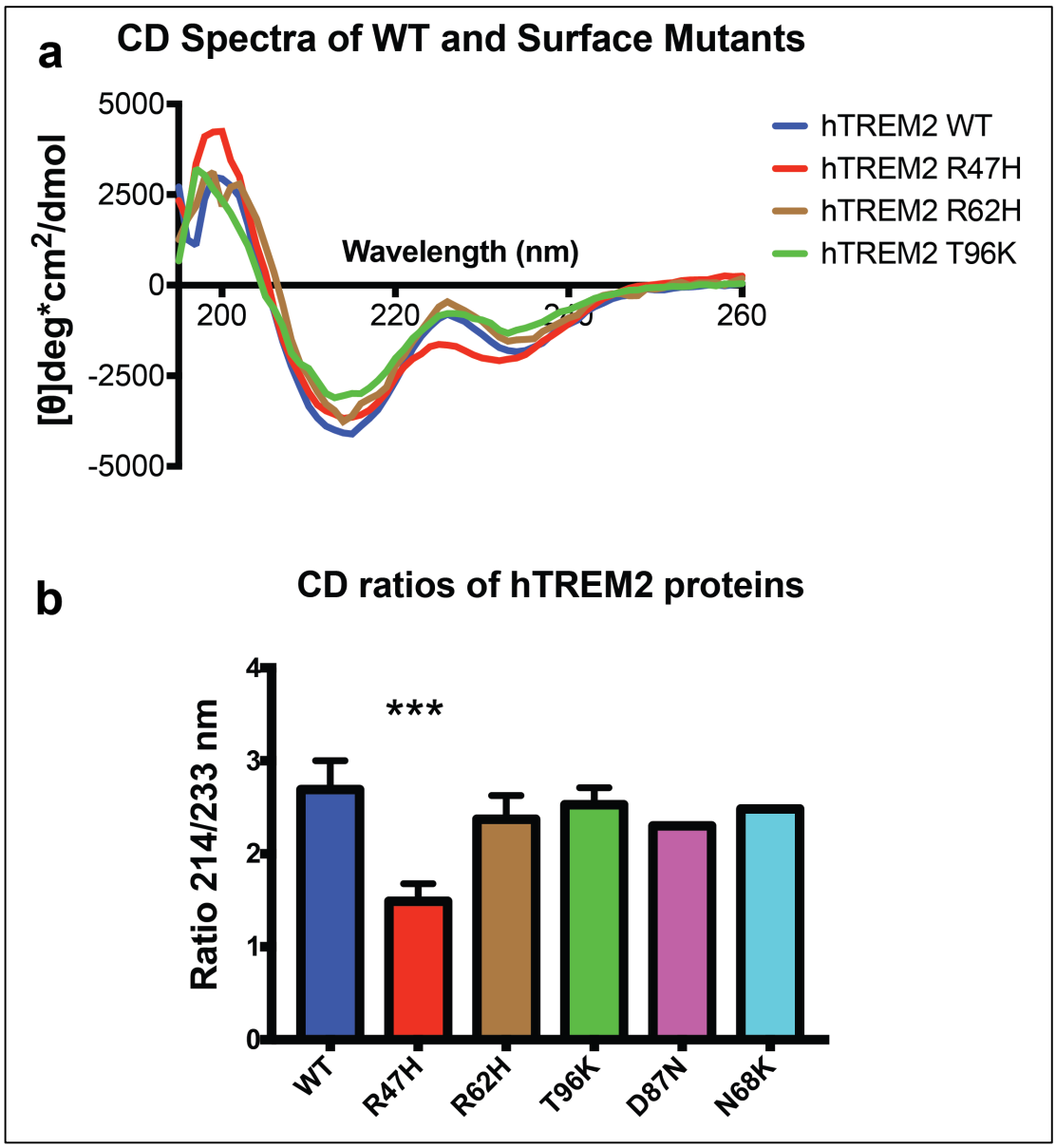

Figure 3.4 CD characterization of WT and surface variant TREM2 proteins. a) CD profiles of WT, R47H, R62H, and T96K. b) Ratio of minima at 214 to 233 nm in WT and all surface variant proteins. *** = $p<0.001$ by ANOVA with Bonferroni post-test correction. Note: D87N and N68K were not included in statistical test as their N = 1. All others $N \geq 3$.

Figure 3.4 modified from Kober et al, 2016 (1)

3.4 Thermal and chemical stability of WT and variant TREM2 Ig domains

To assess whether TREM2 variants impact protein stability of the surface variants, a number of assays were performed. In all cases, SEC-purified protein was used. The SEC experiments where purified protein was re-run on the column confirmed that protein remains monodisperse, free from aggregates, and is therefore suitable for denaturation experiments.

3.4.1 Thermal stability by CD spectroscopy

To determine suitable wavelengths to monitor TREM2 unfolded by CD, an interval scan experiment was conducted where WT TREM2 was heated from 20° C to 90° C and full CD scans taken every 5° C. This experiment revealed a transition at 225 nm that was suitable for monitoring (**Fig 3.5a**). (The larger transition around 205 is noisier and usually beyond the voltage limit when DTT is in the buffer). While this transition is different than the classical flattening loss of CD signal, it is typical of Ig domains (5). TREM2 thermal denaturation in CD experiments was reversible (**Fig 3.5b**) with the native CD spectra restored after returning to 20° C. All surface variants were capable of refolding, while refolding was ablated for WT and all variants in the presence of 1 mM DTT (not shown). Therefore, WT and variant TREM2 proteins were melted from 20° C to 90° C with continuous monitoring at 225 nm (**Fig 3.5c**). In these experiments, R47H and R62H were indistinguishable from WT, while the T96K variant had a slightly lower transition. All proteins had reduced transitions in the presence of 1 mM DTT, confirming the presence of disulfide bonds that were enhancing protein stability.

3.4.2 Thermal stability by differential scanning fluorimetry

Thermal stability was also assessed by DSF. These assays were performed using an ABI Fast7500 qPCR machine according to the manufacturer's protocol. Data were analyzed using the Protein Thermal Shift software (ABI). Melting temperatures were calculated by Boltzman curve fitting. Protein was exchanged into PBS, the concentration was adjusted to 0.5 mg/mL and 12.5 µL of this was added to the reaction mix with a total volume of 20 µL. In early experiments, it was noted that there is a small concentration-dependence to the Tm, so all experiments were done at this same concentration. Samples were run with or without 1 mM DTT. All proteins had reduced Tm with DTT. There was a statistically significant pattern where WT melted later than R47H and R62H, which melted after T96K. With DTT, all proteins again had a reduced melting point. While these measurements were statistically significant, within the DSF literature and previous experiments in our lab, a melting point change of ≤ 5° C is very modest and unlikely to be biologically significant (**Fig 3.5d**).

3.4.3 Chemical stability by CD spectroscopy

In addition to thermal melting experiments, chemical stability was tested through CD experiments conducted where TREM2 WT or variants were incubated in increasing concentrations of GuHCl. In these experiments, proteins were incubated with GuHCl for at least an hour before measuring and at least one partially denatured sample was measured a second time an hour later to confirm equilibrium had been reached. It was hoped that these measurements could assess the ΔG of protein folding (6). However, this method requires a linear transition. For TREM2, the curve would shift as in the thermal melting conditions, and then reverse and slowly flatten. For this analysis, the melting concentration was recorded as the GuHCl concentration of the transition point. Consistent with the DSF and CD data, WT TREM2

denatured slightly later than R47H and R62H, which were slightly more stable than T96K (**Fig 3.5e**).

Taken together, these analyses (expression, SEC, surface expression by flow cytometry and confocal microscopy, CD scans, thermal and chemical denaturation by CD and DSF) support the primary interpretation of the crystal structure – that the NHD variants are misfolded and suffer reduced stability, while the surface variants, which include the primary AD-risk variants, are largely intact. These proteins are folded and behave like WT by course solution methods. Finer analysis detailed subtle but measurable alterations; however, these are unlikely to be pathological.

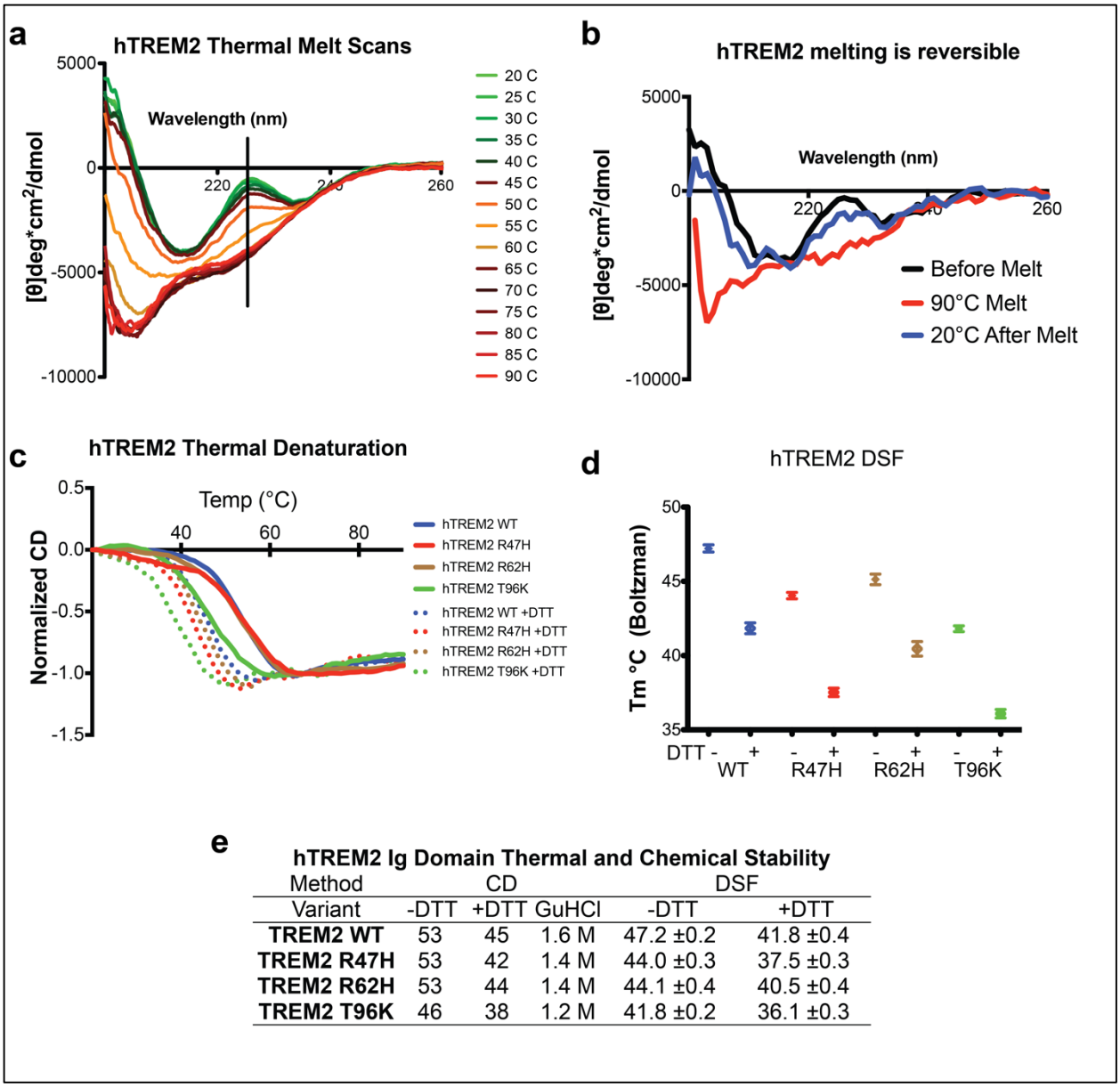

e

hTREM2 Ig Domain Thermal and Chemical Stability

Method	CD			DSF	
Variant	-DTT	+DTT	GuHCl	-DTT	+DTT
TREM2 WT	53	45	1.6 M	47.2 ±0.2	41.8 ±0.4
TREM2 R47H	53	42	1.4 M	44.0 ±0.3	37.5 ±0.3
TREM2 R62H	53	44	1.4 M	44.1 ±0.4	40.5 ±0.4
TREM2 T96K	46	38	1.2 M	41.8 ±0.2	36.1 ±0.3

Figure 3.5. Thermal and chemical denaturation experiments. **a)** Interval scan of WT TREM2 at 5° C increments from 20-90° C. TREM2 has a transition at 225 nm that was monitored in subsequent melting experiments **b)** WT TREM2 CD scans before thermal denaturation, at 90° C, and after returning to 20° C for 30 min. TREM2 largely regains folding, and this was observed for all surface variants. Refolding was ablated in the presence of 1 mM DTT. **c)** Thermal denaturation of WT or variant TREM2 measured at 225 nm in the absence or presence of 1 mM DTT. DTT results in a reduced melting for all variants. **d)** Melting temperatures from DSF experiments in the presence or absence of DTT. Mean and SEM of at least three independent experiments. **e)** Table of thermal and chemical denaturation values.

Figure 3.5 panels a, c, d, and e are modified from Kober et al, 2016 (1).

3.5 References:

1. Kober DL, Alexander-Brett JM, Karch CM, Cruchaga C, Colonna M, Holtzman MJ, Brett TJ. Neurodegenerative disease mutations in TREM2 reveal a functional surface and distinct loss-of-function mechanisms. Elife. 2016;5:e20391. doi: 10.7554/eLife.20391. PubMed PMID: 27995897; PMCID: PMC5173322.
2. Park JS, Ji IJ, An HJ, Kang MJ, Kang SW, Kim DH, Yoon SY. Disease-Associated Mutations of TREM2 Alter the Processing of N-Linked Oligosaccharides in the Golgi Apparatus. Traffic. 2015;16(5):510-8. doi: 10.1111/tra.12264. PubMed PMID: 25615530.
3. Park JS, Ji IJ, Kim DH, An HJ, Yoon SY. The Alzheimer's Disease-Associated R47H Variant of TREM2 Has an Altered Glycosylation Pattern and Protein Stability. Front Neurosci. 2016;10(618):618. doi: 10.3389/fnins.2016.00618. PubMed PMID: 28149270; PMCID: PMC5241589.
4. Kleinberger G, Yamanishi Y, Suarez-Calvet M, Czirr E, Lohmann E, Cuyvers E, Struyfs H, Pettkus N, Wenninger-Weinzierl A, Mazaheri F, Tahirovic S, Lleo A, Alcolea D, Fortea J, Willem M, Lammich S, Molinuevo JL, Sanchez-Valle R, Antonell A, Ramirez A, Heneka MT, Sleegers K, van der Zee J, Martin JJ, Engelborghs S, Demirtas-Tatlidede A, Zetterberg H, Van Broeckhoven C, Gurvit H, Wyss-Coray T, Hardy J, Colonna M, Haass C. TREM2 mutations implicated in neurodegeneration impair cell surface transport and phagocytosis. Sci Transl Med. 2014;6(243):243ra86. doi: 10.1126/scitranslmed.3009093. PubMed PMID: 24990881.
5. Sikkink L, Ramirez-Alvarado M. Salts enhance both protein stability and amyloid formation of an immunoglobulin light chain. Biophysical chemistry. 2008;135(1-3):25-31. doi: 10.1016/j.bpc.2008.02.019.
6. Greenfield NJ. Using circular dichroism collected as a function of temperature to determine the thermodynamics of protein unfolding and binding interactions. Nat Protocols. 2007;1(6):2527-35. doi: http://www.nature.com/nprot/journal/v1/n6/suppinfo/nprot.2006.204_S1.html.

Chapter 4: Impact of neurodegenerative variants on TREM2-ligand binding

4.1 TREM2 ligands in the literature

Because the AD variants did not grossly affect TREM2 structure or stability, it was hypothesized that they might alter ligand binding. Although the endogenous TREM2 ligand is unresolved, a long list of potential TREM2 ligands or interacting partners has been proposed in the literature. These are summarized in **Table 4**, which lists the ligands, techniques used to demonstrate an interaction, the K_D if reported, and the role of disease-risk variants if tested. Briefly, prior to this work, TREM2 had been shown to bind a variety of mammalian cells, including myeloid cells (1, 2) and non-myeloid CNS cells such as astrocytes (3-5) and neurons (4, 6-8). These data suggested potential ligands for TREM2 that could exist *in cis* or *in trans* relative to the TREM2-expressing myeloid cell. Additionally, TREM2 was shown to recognize a wide range of anionic bacterial ligands (5) and directly binds bacteria (5, 9, 10). TREM2 had also been shown to bind the chaperone protein HSP60, which may be surface-expressed on apoptotic neurons (4) and TREM2 co-IPs with potential co-receptor proteins, most notably Plexin-A1 (11) and TREML1s, a short transcript of TREML1, which contains an inhibitory ITIM motif (12). In 2012, TREM2 was shown to bind a wide range of phospholipids (13). This phospholipid interaction gained considerable interest during the course of this work and is discussed at length below. Finally, during the course of this work, multiple groups reported an interaction with soluble lipoproteins, including ApoE, one of the major risk factors for AD (14-17).

Table 4. Reported TREM2 ligands

Ligand	Techniques	K_D	Variants	Ref
Bacteria/bacterial components				
Whole Bacteria	CS, P, FC, RC, CB, E			(5, 9, 10)
C. jejuni lysate	E, RC			(18)
N. gonococcus lipooligosaccharides	E, SPR, RC	350nM		(19)
Anionic Bacterial Carbohydrates	CB			(5)
Cholera toxin B	E, RC			(20)
Mammalian Cells				
THP-1 monocytes	FC			(7)
BMDMs	FC			(1)
BMDCs	FC			(2)
Astrocytes	RC, CS			(3-5)
Neuronal Cells	CS, RC, FC			(4, 6-8)
Apoptotic cells	FC, RC, P			(6, 21)
Anionic molecules				
Phospholipids & Sulfolipids	E, DB, RC, LB		R47H, R62H ↓ D87N, T96K ↑	(7, 13, 15, 17, 21-23)
DNA	IP, RC			(8)
Sulfated proteoglycans	FC			(7)
Mammalian proteins				
HSP60	E, CS.	3.8μM		(4)
Plexin-A1	FRET, IP			(11)
TREML1 (short transcript)	IP			(12)
Apolipoproteins (A,B,E,J)	DB, P, IP, E, BLI, PM	6.7nM (14)	R47H ↓(14, 15) R47H, R62H, D87N↓(16)	(14-16)
Lipoparticles	BLI, RC, PM		R47H, R62H ↓ D87N↑↓, T96K ↑	(16, 17)
Negative results				
Certain Mammalian Cells	CS			(5)
Apoptotic Jurkat cells	FC			(15)

Key: E = ELISA, RC = reporter cell, FC = flow cytometry, P = phagocytosis/cellular uptake, IP = Co-immunoprecipitation, CB = competitive binding, CS = cell staining, LB = liposome binding, BLI = Biolayer Interferometry, PM = protein microarray, SPR = surface plasmon resonance, DB = dot blot.

4.2 TREM2 variants minimally impact phospholipid binding

4.2.1 TREM2 and Ig domain-phospholipid binding in the literature

Cannon et al first reported that TREM2 (produced as a Fc-fusion protein) bound to phospholipids (13). They used a solid-state ELISA system and found that TREM2 and CD300 family members bound plated phospholipids. Similar findings were reported by Bailey et al (15), who used a dot blotting system. More recently, the Colonna lab reported that both mouse (22) and human (21) TREM2 signaled when incubated overnight on plated phospholipids. This was measured by GFP expression under the control of a NFAT reporter, which is activated by calcium flux as a result of TREM2 signaling. Interestingly, the pattern is different for these systems **(Fig 4.1)**. The signaling assays respond to lower concentrations of plated phosphatidylcholine (PC). In contrast, PC binding was barely detected in the solid-state assays. Wang et al also showed that the R47H variant has decreased signaling to phospholipids (21). This was the first time a TREM2 variant had been shown to alter signaling. Therefore, this study sought to answer whether the TREM2 variants altered direct binding to phospholipids.

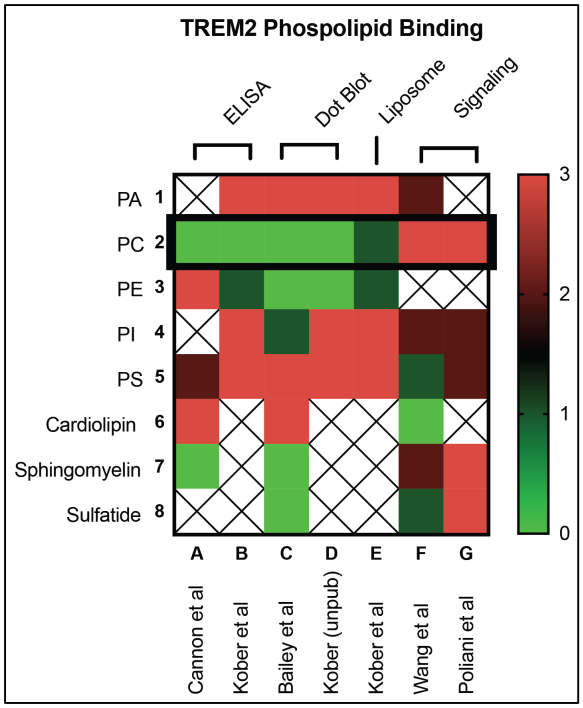

Figure 4.1 Heat map of phospholipid interactions from the literature and this study. Binding to or signaling from selective lipids in each study was qualitatively scaled from 0-3 for none, weak, moderate, and strong binding or signaling. The lipid species is listed on the Y-axis and the study is listed on the lower X-axis with the type of assay listed on the top X-axis. Empty boxes indicate the lipid was not evaluated in that study. Black box highlights PC as an example where binding and signaling studies produce different results,

4.2.2 TREM2 binds phospholipids differently than other Ig domains

There is precedent for similar Ig domains selectively binding phospholipids. Members of the CD300 and TIM family proteins selectively bind PS and sometimes PE and the binding determinants are well-understood (24-30). (The CD300 proteins are also known as CMRF35-like (CLM), IREM, or LMIR). Lipid binding by this family of proteins is highly dependent on a divalent metal (usually Ca^{2+}) coordinated within the lipid-binding pocket. The acyl chains of the lipid are coordinated by hydrophobic residues on the C-C' and FG loops. The FG loop in particular contain a canonical "WFND" motif that is thought to insert into the plasma membrane to help the protein search for a binding lipid (30). Importantly, these lipid binding mechanisms have been shown to require divalent cations, are sensitive to EDTA and EGTA, and are highly specific for PS (sometimes PS and PE) (24-30). As noted above, TREM2 differed from these

other proteins with the reports of binding fairly non-selectively to phospholipids. Additionally, Cannon et al showed that Ca^{2+} or Mg^{2+} did not enhance TREM2 lipid binding (13).

To test whether purified TREM2 directly bound phospholipids with selectivity or in a cation-dependent manner, a number of experiments were conducted. For solid-state ELISAs, lipids were solubilized in methanol or methanol chloroform as needed. Solubilized lipids were diluted in methanol and 100 μL of lipids at 5 μg/mL were plated on ELISA plates and allowed to air dry. Wells were blocked in 3% BSA in PBS and then 100 μL of biotinylated protein (usually diluted 1:1000) was added at overnight at 4°C and then washed in BSA/PBS with 0.05% Tween-20. Biotinylated protein was detected by streptavidin-HRP and a colorimetric peroxidase substrate (TMB microwell peroxidate substrate, KPL) (Biotinylation protocol is described in section 4.3). **Fig 4.2a** shows the binding of mTREM2 to plated phospholipids in the presence of 5 mM EDTA, Ca^{2+}, or Mg^{2+}. Binding was not affected by any of the treatments. Similar results were obtained with hTREM2. Additionally, the binding to phosphatidic acid (PA) shows that the head group is not required, arguing against selective binding. In contrast to the signaling assays, but consistent with the initial report by Cannon et al, PC was bound only at background level.

The TREM2 sequence and structure provide clues as to why the binding mechanism is different. Most notably, the hydrophobic residues of the "WFND" motif in the FG loop are absent in TREM2 (**Fig 4.2b**). The residues in this loop from the TREM2 and TIM4-PS crystal structures are shown in **Fig 4.2c**. In addition to the absent hydrophobic residues, the Asp which coordinates the Ca^{2+} in the TIM4 structure is facing away from the canonical lipid binding pocket in TREM2. It is possible that this residue could be rotated towards the groove during lipid binding, but the lack of sensitivity to divalent metals or chelators suggests that this mechanism is not how TREM2 binds phospholipids.

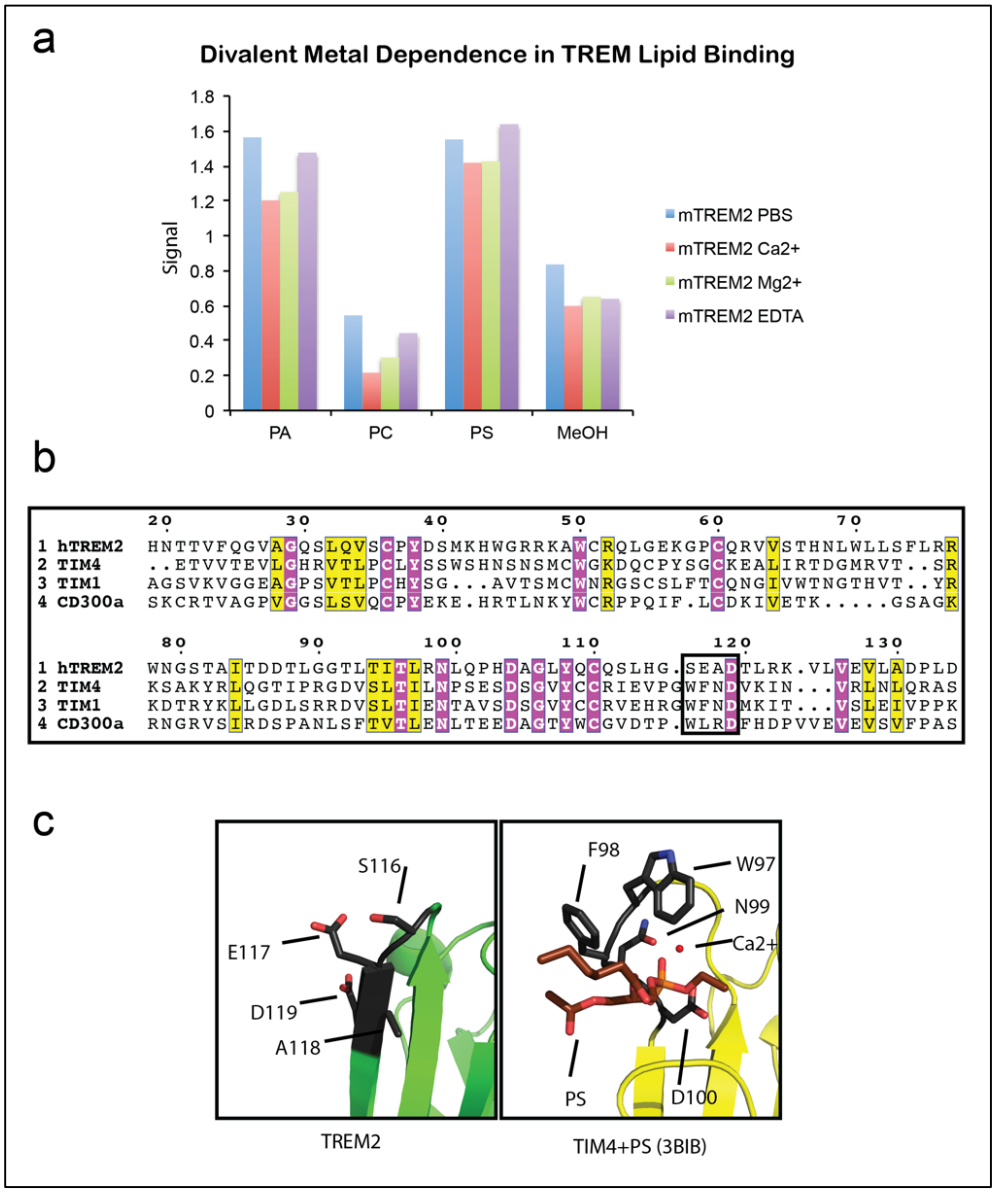

Figure 4.2 TREM2 binds phospholipids differently than other Ig domains with selective binding. a) TREM2 binding does not require divalent metals to bind phospholipids. TREM2 prefers anionic species, but does not require a headgroup to coordinate binding. Solid-state ELISAs were conducted in the presence of 5 mM EDTA, calcium, or magnesium. Representative of two independent experiments with both human and mouse TREM2. **b)** Sequence alignment of the Ig domains of TREM2, CD300a, TIM1 and TIM4 shows TREM2 does not have canonical lipid-binding motifs. **c)** hTREM2 and TIM4 (3BIB) aligned showing the hydrophobic residues that interact with PS are not present in TREM2 and the D required to coordinate Ca^{2+} in 3BIB.

Figure 4.2 is modified from Kober et al, 2016 (7)

4.2.3 TREM2 AD variants do not lose phospholipid binding

Having established that TREM2 binds phospholipids, the role of TREM2 variants in phospholipid binding was examined. Phospholipid binding was tested using solid-state ELISA, liposome sedimentation, and direct binding by BLI. ELISAs were performed as described above. TREM2-avitag proteins were purified by NiNTA, concentrated, biotinylated, and used to probe plated lipids. To control for differences in biotinylation efficiency, the signal for each protein was normalized to its background signal on MeOH coated plates. All overall protein signals were comparable, especially compared to TREML2 or TREML4, which had extremely minor binding to phospholipids and required much lower dilutions for appreciable signal (not shown). The ELISA assays showed that the overall level of binding between the mutants was comparable and that the discrimination between different phospholipids was unchanged (**Fig 4.3a, b**). This is completely different from the signaling assays, where R47H loses almost all signal to most phospholipids but retains signaling to PC and Sphingomyelin (21).

Liposome sedimentation was also performed to assess binding to a more physiological form of lipid presentation. Crude liposomes were made as previously described (31). Liposomes were made by reconstituting PC, PE, and cholesterol in PBS (35:35:10 w/w/w) after vacuum-drying to remove organic solvent, and then subjecting them to three freeze-thaw cycles at 37° C and in liquid N_2 followed by vortexing to achieve a uniform liposome suspension. To measure specific binding to individual lipids, 20% w/w of the indicated phospholipids were added to the base liposome. Liposomes were mixed with SEC-purified TREM2 and the concentration quantified by BCA. 100 μg liposomes were mixed with 10 μg TREM2 proteins for one hour at RT and then pelleted by centrifugation (16,800xg). The supernatant was removed, SDS-PAGE loading buffer was added to the pellet, which was then analyzed by anti-6-His immunoblot.

Similar to the ELISA assays, preferential binding to anionic lipids (PA, PG, PI, PS) but not more neutral lipids (PC, PE) was observed. Most notably, the R47H and other variants had similar levels of overall binding and there was no change in the lipid preference (**Fig 4.3c**).

Finally, to assess direct binding and kinetics, liposomes were immobilized using aminopropylsaline (APS) pins in the BLI system and used to measure binding to SEC-purified WT or R47H proteins. Minimal binding was observed to base liposomes (not shown), while both WT and R47H bound PS liposomes comparably (Steady-state response K_D's of 1.4 and $2.5*10^{-5}$ M, with R^2 of 0.997 and 0991, respectively) **(Fig 4.3d)**. Nearly identical values were also determined by kinetic fits, but not reported here because of the need to optimize dissociation conditions.

In three different assays, the R47H and R62H variants do not appear to have a large effect on binding to phospholipids. It remains possible that subtle change in affinity is missed in these assays. Another important consideration is the manner of phospholipid presentation. Towards that end, a recent report demonstrated TREM2 binding to phospholipids on a strip dot blot assay but failed to detect TREM2 binding to apoptotic Jurkat cells, which expressed PS on the cell surface as assessed by TIM1 and Annexin V binding (15). This suggests phospholipid exposure is not sufficient for TREM2 cell binding. While phospholipids stimulate TREM2 signaling, they are unlikely to be the full TREM2 ligand.

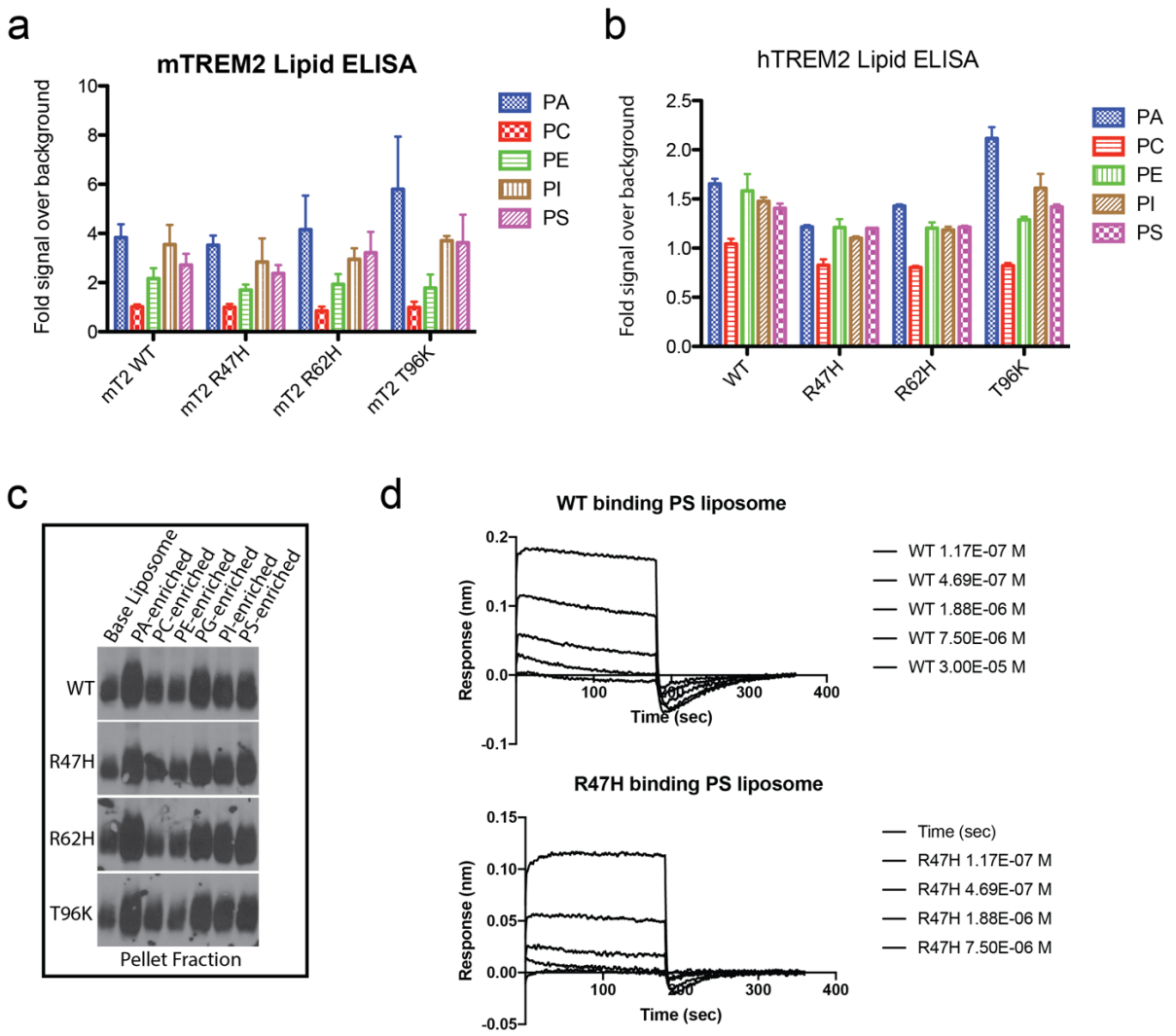

Figure 4.3 TREM2 variants do not grossly impact phospholipid binding. a) Mouse TREM2 and **b)** Human TREM2 phospholipid ELISAs. **c)** hTREM2 liposome sedimentation assays. **d)** BLI analysis of WT or R47H hTREM2 binding to PS-enriched liposomes from **(c)** immobilized onto aminopropylsilane (APS) pins and dipped into purified TREM2 proteins. Background binding to uncoated pins was subtracted. Minimal binding was observed to base liposomes in the same experiment.

Figure 4.3 a-c are modified from Kober et al, 2016 (7)

4.3 TREM2 binds a cell-surface ligand

4.3.1 TREM2 binds a GAG-dependent cell-surface ligand

TREM2 had been previously shown to bind various mammalian cells (**Table 4**). However, with the exception of increased staining when apoptosis was induced (6), no demonstration of specific or selective binding had been made. In contrast, the only report examining TREM2 binding to viable cells stimulated with different conditions found no change in TREM2 binding to DCs pretreated with LPS, CpG DNA, or Zymosan (2).

To investigate whether TREM2 could bind a specific cell-surface ligand, a staining reagent was produced by expressing TREM2 in the pHL-Avitag construct which encodes a C-terminal BirA biotinylation tag. The protein is purified by NiNTA chromatography and then exchanged into biotinylation buffer (100 mM Tris pH 7.5, 5 mM $MgCl_2$, and 200 mM NaCl*), *In some experiments, NaCl was replaced with 200 mM K-Glutamate for 4°C biotinylation. biotinylated *in vitro* by addition of 10 µL BirA enzyme at 1 mg/mL, 1/10 vol buffer A (0.5 M bicine pH 8.3), 1/10 buffer B (100mM ATP, 100uM MgOAc) and 50 µM final concentration of free biotin. Excess biotin was removed using a desalting column and biotinylation verified by immunoblot with streptavidin-HRP. For cell staining, biotinylated TREM2 proteins were diluted in FACS buffer (PBS with 1% FBS) and then complexed with phycoerythrin-conjugated streptavidin (SAPE) for at least 30 min on ice. 100 µL aliquots of staining solution would be added to cells that were harvested and washed into FACS buffer. Culturing conditions for cells in this study are listed in **Table 5**.

Table 5. Cell culture conditions in this study					
Cell	Media Base	Serum	Additives	$\%CO_2$	ATCC #
THP-1	RPMI	10%	P/S, 10 mM HEPES, 50 μM β–ME, L-glut	5%	TIB-202
N2A	MEM	10%	P/S, L-glut, MEM NEAA	5%	CCL-131
CHO (K1 or 745)	F12	10%	P/S, L-glut	5%	CCL-61
293T	DMEM	10%	P/S, L-glut	5%	CRL-3216
293F	Freestyle	None	P/S	8%	
Expi293	Expi293 Medium	None	Anti-Anti	8%	
RAW 264.7	DMEM	10%	P/S, L-glut	5%	TIB-71
BV2	DMEM	5%	P/S, L-glut	5%	

Several cell lines were screened for TREM2 binding, and cells were treated with various stimuli to test whether binding was to a specific ligand. TREM2 bound THP-1 cells, and staining could be ablated by treating the cells overnight with 20 ng/μL PMA and 500 μg/mL ionomycin. Staining was not decreased by treatment with LPS (1 μg/mL), polyIC (1 μg/mL), M-CSF (20 ng/μL) or IL-13 (50 ng/mL) (**Fig 4.4a, b).** This was the first time a treatment had been shown to decrease TREM2 staining and showed that TREM2 stained a specific ligand on these cells.

Next, proteases were used to see whether the cell-surface ligand had a proteinaceous component. 50 μg/mL of the indicated proteases were added to cells on ice for 30 min. Protease-treated cells were washed four times with FACS buffer supplemented with PMSF before staining with SAPE-TREM2 complexes, also in the presence of PMSF and HALT protease inhibitor cocktail. Proteinase K completely abolished staining to THP-1, and N2A and 293F cells (**Fig 4.4 c,d,e**). Other proteases (chymotrypsin, trypsin, elastase) had intermittent effects (**Fig 4.4 c,e**). These experiments demonstrated a protein-component to the cell-surface ligand. They also confirmed that membrane phospholipids are not sufficient for cellular binding by TREM2.

Because TREM2 has a high pI and binding was observed to a number of different cells, both myeloid and non-myeloid, proteoglycans were considered as possible ligand. To test whether TREM2 bound cells in a glycosaminoglycan (GAG)-dependent manner, CHO cells that do (CHO-K1) or do not (CHO-745) express heparan sulfates (HS) or chondroitin sulfates (CS) (32) were tested for TREM2 binding. TREM2 bound CHO-K1 robustly, but not CHO-745 cells (**Fig 4.4f**). To answer whether TREM2 selectively bound either HS or CS, cells were pre-treated with enzymes that selectively cleave HS or CS. Heparinases and chondroitinase ABC were purchased from Sigma and reconstituted according to the manufacturer's protocol. Heparinases I, II, and III (which also cleave HS) were combined into a cocktail to remove HS, and chrondroitinase ABC was used to cleave CS. Final enzyme concentrations were 0.1 U/mL. Cells in PBS supplemented with 0.1% BSA were treated for 1 hr at 37° C while shaking and then washed three times in cold FACs buffer. TREM2 staining of CHO cells, THP-1 cells, and N2A cells was greatly diminished following treatment with heparinases, but not with chrondroitinase, although N2A did show some reduction with chrondrotinase (**Fig 4.4 f, g, h**). These experiments demonstrated that TREM2 bound a cell-surface ligand in a protein and GAG-dependent manner, and suggest that HS is the dominant ligand on these cells. Importantly, this is observed on myeloid cells (THP-1 are human monocytic), suggesting that HS may interact with TREM2 *in cis* to mediate function.

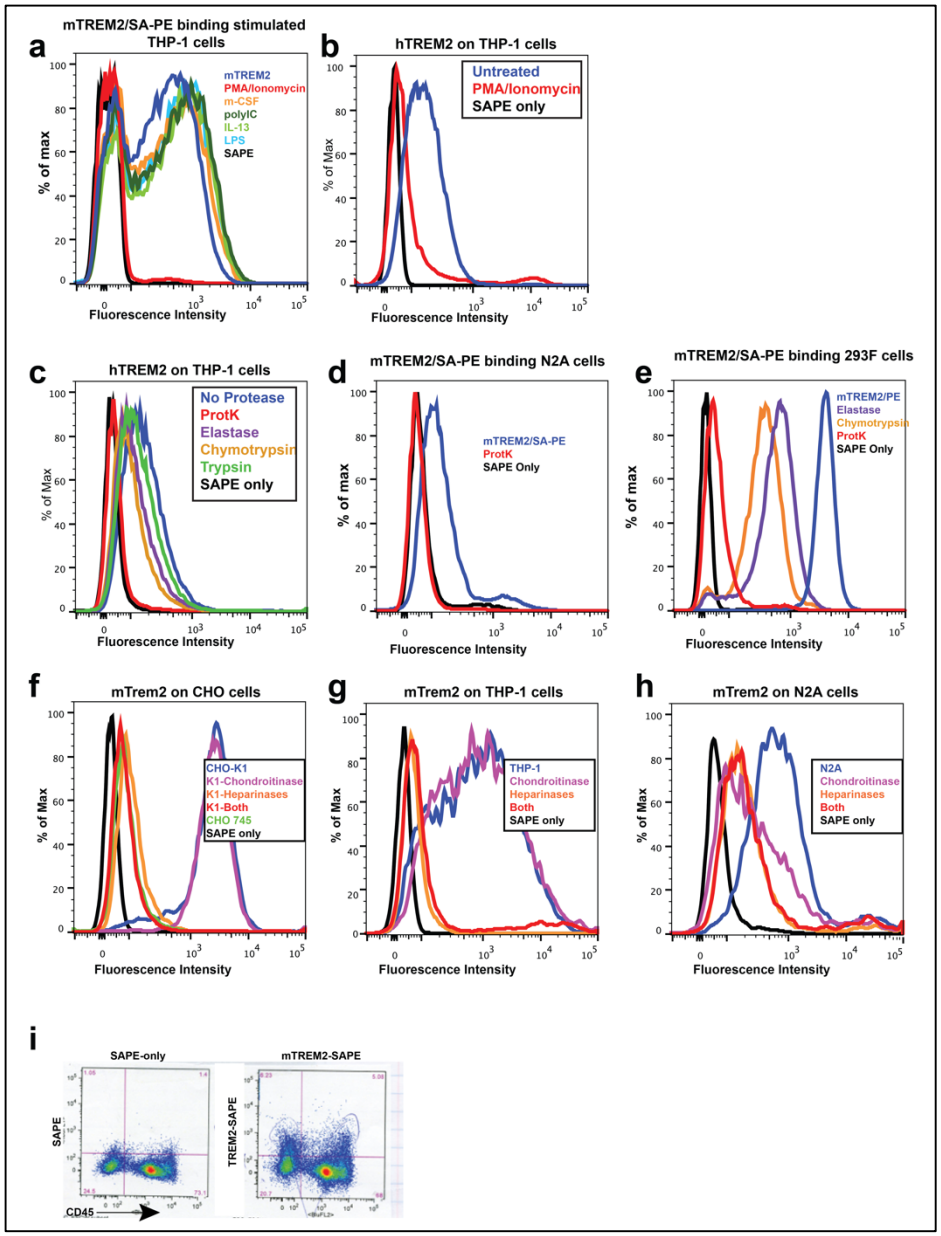

Figure 4.4 TREM2 binds a specific cell-surface ligand. **a)** mTREM2 binding THP-1 cells stimulated as with the indicated conditions. **b)** hTREM2 binding THP-1 ± PMA/ionomycin **c)** hTREM2 binding THP-1 cells pre-treated with indicated proteases **d)** mTREM2 binding N2A cells and **e)** 293F cells pre-treated with indicated proteases. **f-h)** mTREM2 binding **f)** CHO-K1 or CHO-745 cells **g)** THP-1 cells, or **h)** N2A cells pre-treated with heparinases or chondroitinase **i)** mTREM2 binding to mouse whole-lung digest cells co-stained with CD45 shows that TREM2 stains CD45 + and - subsets.

Figure 4.4 a-h are modified from Kober et al, 2016 (7)

4.3.2 Other TREM proteins with high pIs do not bind the same ligand

Because TREM2 has a pI, it was possible that binding sulfated proteoglycans is an artifact of surface charge, not a specifically recognized ligand. To address this, the Ig domains of human and mouse TREML2 and TREML4 were cloned into pHLSEC vectors using Gibson block assembly and then introduced into the pHL-Avitag vector through EcoI-KpnI restriction enzyme digests. These proteins have similarly high pIs, **Figure 4.5a** shows the pI_{calc} for these Ig domains. Unlike TREM2, these proteins did not robustly bind N2A cells (**Fig 4.5b**) or THP-1 cells (not shown) as assessed by flow cytometry. This finding argues that the cell-surface ligand recognition by TREM2 is not an artifact of charge but has at least some level of specificity. This is also consistent with the observation TREM2 is selective for HS over CS.

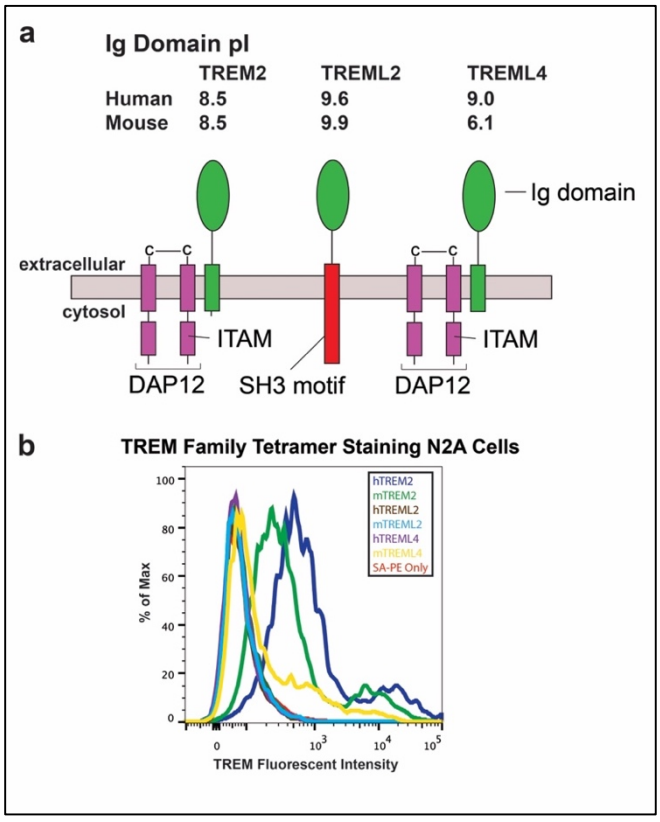

Figure 4.5 TREM-like proteins with similar basic pI do not bind the same cells as TREM2. **a)** Schematic and pI_{calc} for human and mouse TREML2 and TREML4 Ig domains. **b)** Biotinylated Ig domains were complexed with streptavidin-PE and used in binding experiments. TREML2 and TREML4 had very little binding to N2A cells (similar results with THP-1 cells).

Figure 4.5 is modified from Kober et al, 2016 (7)

4.4 TREM2 variants alter ligand binding

Satisfied that TREM2 binds a selective ligand, the next question was whether the surface variants altered binding to this ligand. This was tested in a variety of assays, monomer binding, tetramer binding, and competition assays.

4.4.1 TREM2 variants have altered cell binding

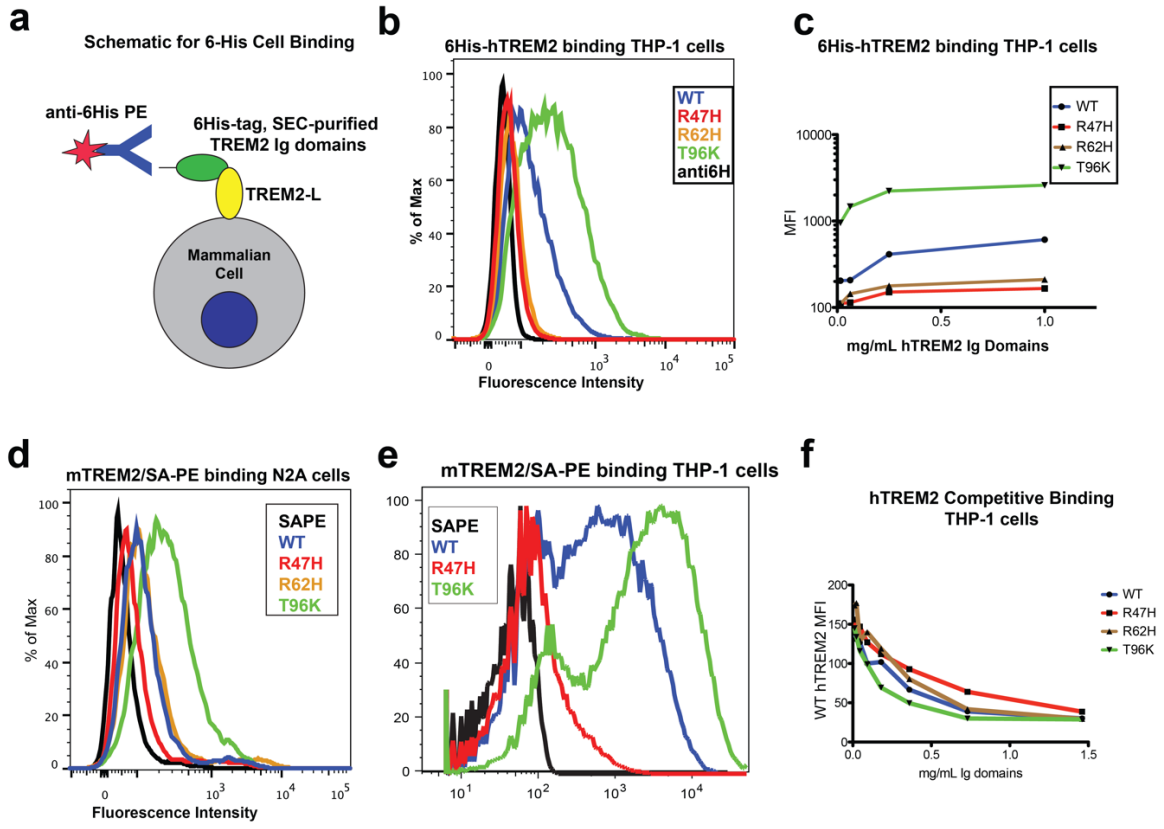

Figure 4.6. TREM2 surface variants alter ligand binding. a) Schematic for detection of SEC-purified 6-His TREM2 proteins by flow cytometry **b)** SEC-purified 6-His hTREM2 proteins binding THP-1 cells. **c)** Dose-dependent binding of 6-His proteins to THP-1 cells. **d)** mTREM2-SAPE tetramer staining N2A and **e)** THP-1 cells **f)** hTREM2 competitive binding where purified Ig domains compete with SAPE-WT tetramers for binding THP-1 cells.

Figure 4.6 is modified from Kober et al, 2016 (7)

Monomeric variant TREM2 proteins have altered binding

To test whether the purified, monomeric mutants would alter binding to THP-1 cells, hTREM2 WT, R47H, R62H, and T96K were purified by NiNTA using their 6-His tag and then purified by SEC to obtain monomeric proteins. Proteins concentrations were carefully matched by UV_{280} and BCA analysis. Washed THP-1 cells were incubated with increasing concentrations of TREM2 proteins for 1 hour before being washed and incubated with a PE-conjugated anti-6-His antibody for 30 min. Cells were analyzed by flow cytometry (**Fig 4.6a**). In each data point, 20,000 cells were counted. This assay was repeated three times with two independent protein expressions. The disease-risk variants R47H and R62H had reduced binding that never matched WT MFI at any concentration. In contrast, the T96K variant had more staining at all concentrations (representative plot shown in **Fig 4.6b** and MFI plotted against concentration in **Fig 4.6c**).

Tetramer staining shows altered binding

Similar results were observed in staining experiments with mTREM2 tetramers. R47H had decreased binding while T96K has increased binding. The effect of R62H was less pronounced and not as reproducible. Staining is shown to N2A (**Fig 4.6d)** and THP-1 **(Fig 4.6e).**

Competition assays show altered binding

Finally, binding was evaluated in a competition format. In these experiments, the amount of WT tetramers needed for binding was first titrated so that there would be as little excess tetramer as possible. Separately, WT or variant hTREM2 proteins were incubated with THP-1 cells for one hour. Then, TREM2-SAPE was added for 20-30 min. Cells were then washed and analyzed by flow cytometry. The T96K competed more effectively than WT, as shown by

reduced MFI at the same concentrations. The R47H variant was less effective, and had higher MFIs. The R62H variant had a modest effect.

Collectively, these experiments show that the R47H variant, and perhaps the R62H variant to a lesser extent, lose binding compared to WT. This trend was observed in multiple formats and on multiple cells lines. In contrast, the T96K variant robustly increased binding in all formats. Notably, in some genetic analyses, this variant has been associated with decreased risk for AD (**Fig 2.9)**. Complicating the genetic analysis is the observation that this variant is also commonly found in linkage disequilibrium with another variant, L211P (33). L211P is in the cytosolic tail and it is unclear whether it impacts TREM2 function. In a preliminary experiments this variant did not decrease surface expression (not shown).

4.5 TREM2 variants identify a functional binding surface

4.5.1 TREM2 has a basic surface not conserved on other TREM proteins

To interpret the results of the gain and loss of function variants, the protein electrostatic solvent-accessible surface was examined. A prominent basic patch was found on the protein (**Fig 4.7a, b**) that includes the R47 and R62 residues. The T96 residue is on the other side of this patch. The R to H mutations would decrease the basic potential, while the T to K change would increase the basic surface. This surface is absent on the other TREM family proteins that have been crystallized (**Fig 4.7 d-f**) **d)**mTREM1 pdb 1U9K (34), **e)** hTREM1 pdb 1SMO (35), and **f)** hTREML1 pdb 2FRG (36). Additionally, alignment of the Ig domains of the TREM family proteins shows that the residues in the basic surface, while conserved in TREM2, are not conserved within the larger TREM family (**Fig 4.7c**). In contrast, the NHD residues are more conserved, which attests to their structural role.

4.5.2 Structure-guided mutations alter binding

To test whether this surface is a functional ligand binding site, mutations to two prominent arginine residues within this surface were introduced and tested in binding experiments. As predicted, these mutations resulted in loss of binding to THP-1 cells (**Fig 4.7g**). These findings support the hypothesis that the AD-disease risk residues impair binding to a cell-surface ligand that is primarily HS proteoglycans.

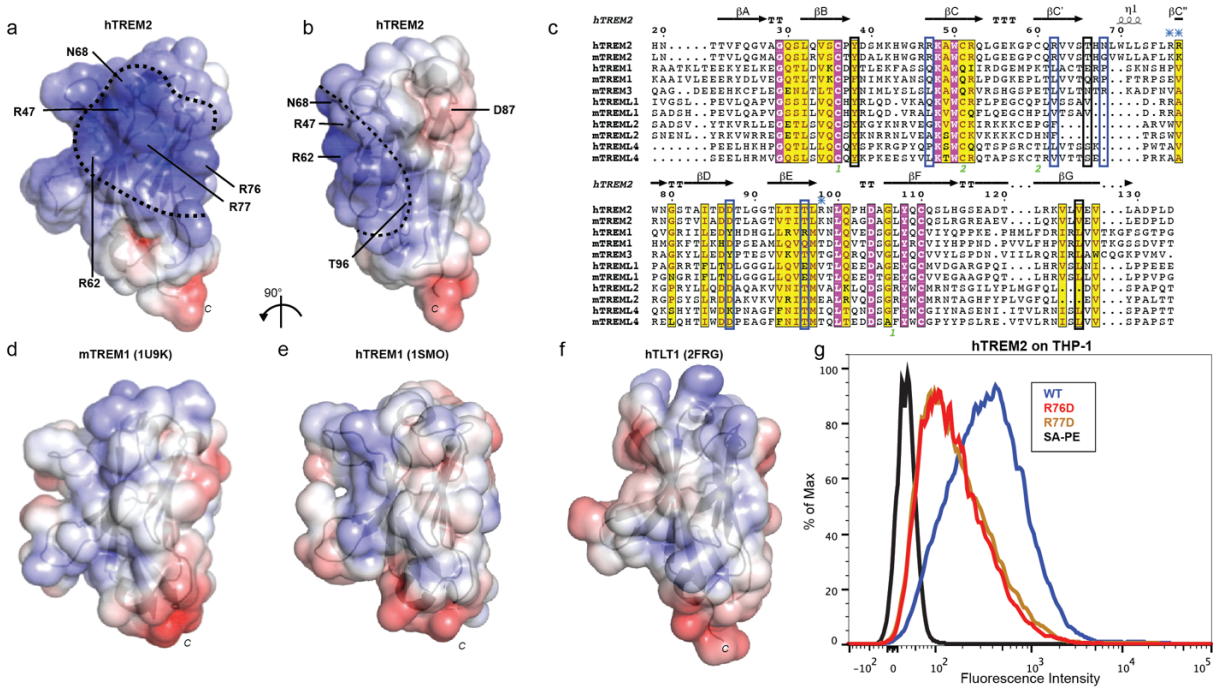

Figure 4.7. Disease variants reveal a functional ligand-binding surface. a) hTREM2 solvent-accessible surface electrostatics generated by APBS, scaled from 6.0 kT/e (blue) to +6 kT/e (red). Dotted line outlines the basic patch. **b)** TREM2 rotated to show the patch extending to T96 residue. The lysine variant adds to this surface. **c)** sequence alignment of human and mouse TREM family members. TREM2 structure assigned by DSSP server shown on top. Disulfide bonds labeled in green. NHD residues highlighted with black boxes, AD residues with blue boxes. Residues contributing to the basic patch marked with blue asterisks. Conserved residues in yellow and invariant residues in magenta. **d)** mTREM1, **e)** hTREM1, and f) hTREML1 aligned to TREM2 in **(a)** and solvent-accessible electrostatics colored on the same scale. **g)** TREM2 basic-patch mutants R76D and R77D have reduced binding to THP-1 cells.

Figure 4.7 is re-used from Kober et al, 2016 (7)

4.6 TREM2 directly binds heparin

To test whether TREM2 could directly bind heparan sulfate, a BLI experiment was devised where biotinylated heparin was immobilized on a streptavidin pin and dipped into wells containing purified hTREM2. The BLI assay buffer was PBS with 0.1% BSA and 0.005% Tween-20. Heparin was placed on the pin because it is polymeric would complicate the interpretation of binding if it was the analyte (By BLI convention, the ligand is immobilized on the pin and the analyte is in the well). Heparin is a commonly used surrogate for HS in binding studies. Both heparin and HS are polymers of a disaccharide unit and differ in the degree of sulfation. Heparin is readily available commercially and is has been used in many structural studies for HS-binding proteins (i.e. (37)).

To load heparin, 10 µL of 1 mg/mL heparin was diluted into 500 mM NaCl in a phosphate buffer. This was to reduce the charge-repulsion in order to get more heparin loaded on the pin. This process still needs optimization, as heparin loading has been variable pin-to-pin and in different experiments. Additionally, in the course of these experiments, it was noticed that TREM2 has a high amount of non-specific binding to the streptavidin pins. Therefore, it is necessary to do a double-reference experiment where a blank pin is run through the same wells as the heparin-loaded pin. Missing this control confounded early experiments. However, I was able to get one experiment where biotinylated heparin was loaded and bound to WT-TREM2 in a double-reference format (**Fig 4.8**). This experiment needs to be optimized and performed with the variants, but it does show that TREM2 can directly bind heparin, and presumably HS. This is consistent with the cell-staining and suggests that TREM2 is directly binding HS on the cell surface.

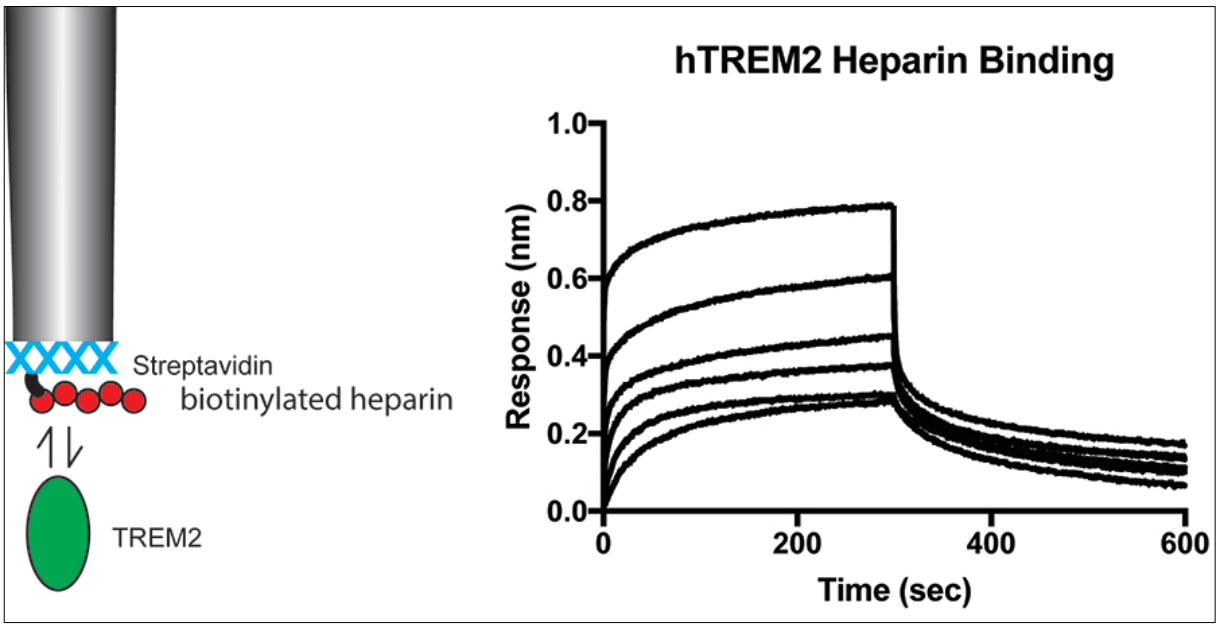

Figure 4.8. Human TREM2 binding to immobilized heparin by BLI. WT TREM2 was titrated in the range of 0.035 – 35.0 μM. Data is double reference-subtracted.

4.7 Impact of variants and GAGs on TREM2 signaling

4.7.1 Disease variants have altered signaling

Because surface expression of the misfolded proteins was observed, I wanted to test whether these variants could produce intracellular signals. In these experiments, phosphor-ERK immunoblotting was used to assess TREM2 signaling. ERK phosphorylation and activation is one of the hallmarks of ITAM signaling, and was one of the first features described for TREM2 signaling (38).

In these experiments, RAW 264.7 (mouse macrophage) cells were seeded in a 24-well plate (300 µL media/well) and transfected with full-length FLAG-TREM2 (0.25 µg/well) complexed 1:2 with Lipofectamine 2000. Cells expressed TREM2 for 24 hours and before being stimulated with anti-FLAG at 1:100 dilution from a 1 mg/mL stock (Sigma, M2 clone). Cells were returned to the 37° C incubator for the indicated amount of time and then placed on ice to quench signaling. The media was immediately aspirated and replaced with ice-cold PBS with EDTA to lift the cells. Cells were lifted, centrifuged at 1000 x g for 5 min, and then 50 µL of ice-cold PBS with 0.1% triton X-100 was added. Cells were rotated for 15 min at 4° C to undergo lysis and then insoluble debris was pelleted by centrifugation for 5 min at 16,800 x g. 30 µL of supernatant was removed and mixed with 30 µL 2x SDS loading dye, boiled 5 min, and analyzed by SDS-PAGE and immunoblot for the indicated proteins. Immunoblots were performed with anti-ERK and anti-p-ERK from Cell Signaling and were used at 1:2000 dilutions. Anti-ERK was diluted in PBS with 0.1% Tween-20 supplemented with 0.5% milk while anti-p-ERK was diluted in PBS with 0.1% Tween-20 supplemented with 1% BSA. These diluents were suggested by the manufacturer. The primary antibodies were incubated for 30-60 min in trays while shaking at RT. Secondary antibodies (mouse for ERK and rabbit for p-ERK) were from Santa-Cruz and

were used 1:2000 in the same buffer as the primaries. Secondary antibodies were incubated for 20 min.

In addition to RAW 264.7, Cos-7 cells (a gift from Colin Nichols) were also used in stimulation experiments. HEK293T cells were also attempted, but in these cells ERK was not reliably detected. Cos-7 cells were treated in the same way as RAW 264.7 cells, except that DAP12 was co-transfected with TREM2.

Consistent with the surface expression experiments, p-ERK levels above background could be detected for the proteins. Using time courses, WT proteins appeared to have signaling that persisted for longer than Y38C (NHD) or R47H (AD) (**Fig 4.9**). This effect was perhaps subtle, but it was reproducible in two different cell lines. One possibility is that, whether by misfolding or reduced recognition of a signaling co-factor, the disease variants result in reduced signaling. Another possibility is altered trafficking, and it was recently reported that the R47H protein has reduced interactions with trafficking complexes (39). These possibilities still need to be tested further, perhaps using a more robust system of measurement.

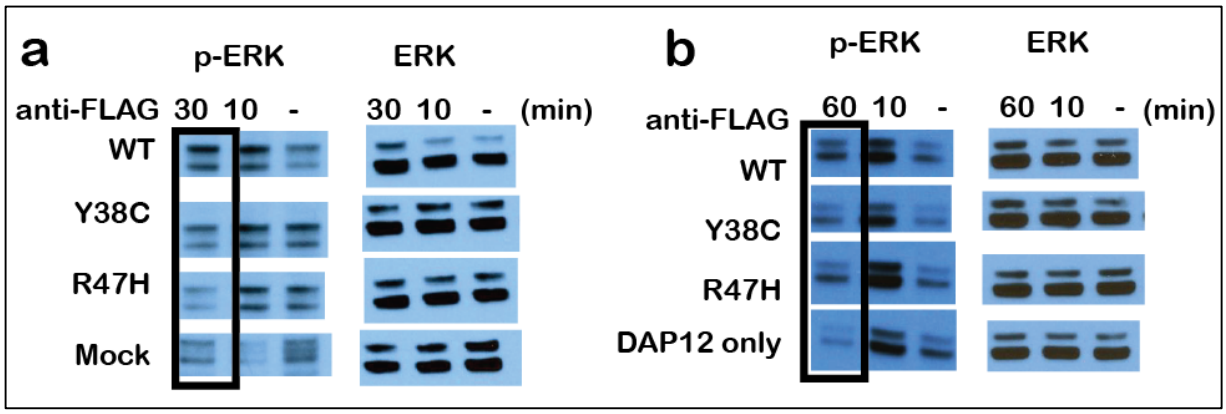

Figure 4.9. Disease variants alter TREM2 signaling. a) Full-length FLAG-tagged TREM2 was transfected in RAW264.7 cells and stimulated with anti-FLAG antibody. Left: Signaling was assessed by phosphor-ERK immunoblot. Right: loading control (ERK). **b)** Signaling assay performed in Cos-7 cells. Cos-7 cells were co-transfected with DAP12 for signaling experiments.

Figure 4.9 is modified from Kober et al, 2016 (7)

4.7.2 Inhibiting GAG sulfation impairs TREM2 signaling

Because TREM2 interacts with HS proteoglycans on the cell surface of myeloid, I wanted to test whether these have a functional role in TREM2 signaling. Sodium chlorate is an inhibitor of sulfation on nascent GAG chains, and has been used with RAW 264.7 cells (40) and does not appear to inhibit ERK phosphorylation (41, 42). RAW264.7 cells were grown in 20 mM sodium chlorate for 24 hours before transfection with FLAG-TREM2 constructs. WT TREM2 was then expressed for 24 hours and stimulation experiments were conducted as described above. In these experiments, TREM2 signaling was inhibited in chlorate-treated cells, suggesting that the TREM2-HS interaction could be important for TREM2 signaling (**Fig 4.10**).

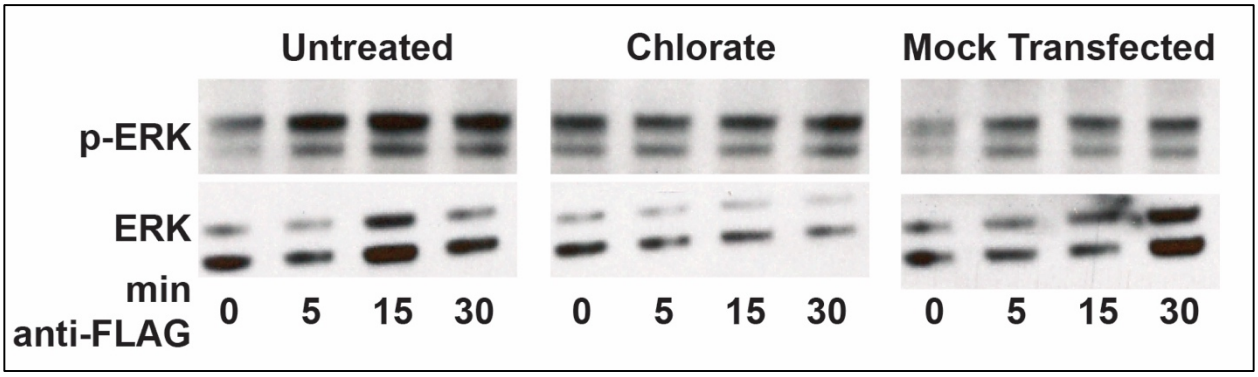

Figure 4.10. Inhibiting GAG sulfation impairs TREM2 signaling. RAW 264.7 cells were untreated or treated with 20 mM chlorate before being transfected with TREM2. Cells were stimulated with anti-FLAG and TREM2 signaling assessed by pERK immunoblot. Chlorate-treated cells have an impaired signaling response. Representative of two independent experiments.

4.7.3 Inhibiting GAG sulfation does not impair TREM2 surface expression

One possibility for impaired signaling during GAG inhibition is that HS is necessary for cell-surface expression or that chlorate inhibits TREM2 trafficking as an off-target effect. To test this possibility, immunostaining experiments were conducted on RAW 264.7 plated on glass coverslips that were pre-treated with poly-lysine and then treated and transfected in parallel with the cells used in signaling experiments. Immunostaining was done as described above, with the modification that anti-FLAG antibodies were incubated for at 1:1000 for 2 hours at RT and then secondary antibodies for 1 hr at RT. Cells were not permeabilized, so that surface expression could be determined. In this initial experiment, comparable levels of surface expression were detected on both treated and untreated cells. Interestingly, chlorate treatment resulted in more diffuse TREM2 staining, whereas untreated cells were more clustered and punctate (**Fig 4.11**).

These experiments need to be reproduced and a scoring system developed. Experiments should also be conducted with the TREM2 variants. However, one possibility from these results is that HS chains cluster or orient TREM2 on the cell surface to receive stimulating signals from external ligands.

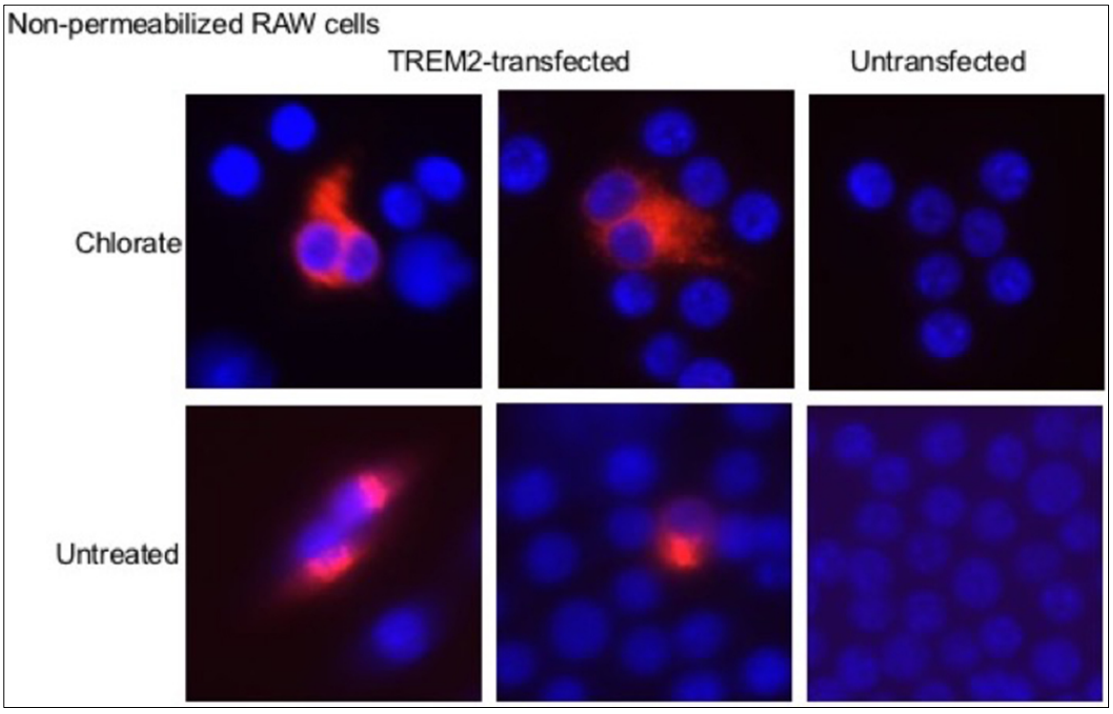

Figure 4.11. Inhibiting GAG sulfation alters TREM2 surface expression patterns. RAW cells transfected with FLAG-TREM2 in presence (upper) or absence (lower) of 20 mM chlorate. Fixed, non-permeabilized and stained with anti-FLAG.

4.8 References:

1. Hamerman JA, Jarjoura JR, Humphrey MB, Nakamura MC, Seaman WE, Lanier LL. Cutting edge: inhibition of TLR and FcR responses in macrophages by triggering receptor expressed on myeloid cells (TREM)-2 and DAP12. J Immunol. 2006;177(4):2051-5. PubMed PMID: 16887962.
2. Ito H, Hamerman JA. TREM-2, triggering receptor expressed on myeloid cell-2, negatively regulates TLR responses in dendritic cells. Eur J Immunol. 2012;42(1):176-85. doi: 10.1002/eji.201141679. PubMed PMID: 21956652; PMCID: PMC3444819.
3. Piccio L, Buonsanti C, Mariani M, Cella M, Gilfillan S, Cross AH, Colonna M, Panina-Bordignon P. Blockade of TREM-2 exacerbates experimental autoimmune encephalomyelitis. Eur J Immunol. 2007;37(5):1290-301. doi: 10.1002/eji.200636837. PubMed PMID: 17407101.
4. Stefano L, Racchetti G, Bianco F, Passini N, Gupta RS, Panina Bordignon P, Meldolesi J. The surface-exposed chaperone, Hsp60, is an agonist of the microglial TREM2 receptor. J Neurochem. 2009;110(1):284-94. doi: 10.1111/j.1471-4159.2009.06130.x. PubMed PMID: 19457124.
5. Daws MR, Sullam PM, Niemi EC, Chen TT, Tchao NK, Seaman WE. Pattern recognition by TREM-2: binding of anionic ligands. J Immunol. 2003;171(2):594-9. PubMed PMID: 12847223.
6. Hsieh CL, Koike M, Spusta SC, Niemi EC, Yenari M, Nakamura MC, Seaman WE. A role for TREM2 ligands in the phagocytosis of apoptotic neuronal cells by microglia. J Neurochem. 2009;109(4):1144-56. doi: 10.1111/j.1471-4159.2009.06042.x. PubMed PMID: 19302484; PMCID: PMC3087597.
7. Kober DL, Alexander-Brett JM, Karch CM, Cruchaga C, Colonna M, Holtzman MJ, Brett TJ. Neurodegenerative disease mutations in TREM2 reveal a functional surface and distinct loss-of-function mechanisms. Elife. 2016;5:e20391. doi: 10.7554/eLife.20391. PubMed PMID: 27995897; PMCID: PMC5173322.
8. Kawabori M, Kacimi R, Kauppinen T, Calosing C, Kim JY, Hsieh CL, Nakamura MC, Yenari MA. Triggering receptor expressed on myeloid cells 2 (TREM2) deficiency attenuates phagocytic activities of microglia and exacerbates ischemic damage in experimental stroke. J Neurosci. 2015;35(8):3384-96. doi: 10.1523/JNEUROSCI.2620-14.2015. PubMed PMID: 25716838; PMCID: PMC4339351.
9. N'Diaye EN, Branda CS, Branda SS, Nevarez L, Colonna M, Lowell C, Hamerman JA, Seaman WE. TREM-2 (triggering receptor expressed on myeloid cells 2) is a phagocytic receptor for bacteria. J Cell Biol. 2009;184(2):215-23. doi: 10.1083/jcb.200808080. PubMed PMID: 19171755; PMCID: PMC2654305.
10. Charles JF, Humphrey MB, Zhao X, Quarles E, Nakamura MC, Aderem A, Seaman WE, Smith KD. The innate immune response to Salmonella enterica serovar Typhimurium by macrophages is dependent on TREM2-DAP12. Infect Immun. 2008;76(6):2439-47. doi: 10.1128/IAI.00115-08. PubMed PMID: 18391000; PMCID: PMC2423085.
11. Takegahara N, Takamatsu H, Toyofuku T, Tsujimura T, Okuno T, Yukawa K, Mizui M, Yamamoto M, Prasad DV, Suzuki K, Ishii M, Terai K, Moriya M, Nakatsuji Y, Sakoda S, Sato S, Akira S, Takeda K, Inui M, Takai T, Ikawa M, Okabe M, Kumanogoh A, Kikutani H. Plexin-A1 and its interaction with DAP12 in immune responses and bone homeostasis. Nat Cell Biol. 2006;8(6):615-22. doi: 10.1038/ncb1416. PubMed PMID: 16715077.

12. Yoon SH, Lee YD, Ha J, Lee Y, Kim HH. TLT-1s, alternative transcripts of triggering receptor expressed on myeloid cell-like transcript-1 (TLT-1), Inhibits the triggering receptor expressed on myeloid cell-2 (TREM-2)-mediated signaling pathway during osteoclastogenesis. J Biol Chem. 2012;287(35):29620-6. doi: 10.1074/jbc.M112.351239. PubMed PMID: 22761415; PMCID: PMC3436187.
13. Cannon JP, O'Driscoll M, Litman GW. Specific lipid recognition is a general feature of CD300 and TREM molecules. Immunogenetics. 2012;64(1):39-47. doi: 10.1007/s00251-011-0562-4. PubMed PMID: 21800138.
14. Atagi Y, Liu CC, Painter MM, Chen XF, Verbeeck C, Zheng H, Li X, Rademakers R, Kang SS, Xu H, Younkin S, Das P, Fryer JD, Bu G. Apolipoprotein E Is a Ligand for Triggering Receptor Expressed on Myeloid Cells 2 (TREM2). J Biol Chem. 2015;290(43):26043-50. doi: 10.1074/jbc.M115.679043. PubMed PMID: 26374899; PMCID: PMC4646257.
15. Bailey CC, DeVaux LB, Farzan M. The Triggering Receptor Expressed on Myeloid Cells 2 Binds Apolipoprotein E. J Biol Chem. 2015;290(43):26033-42. doi: 10.1074/jbc.M115.677286. PubMed PMID: 26374897; PMCID: PMC4646256.
16. Yeh FL, Wang Y, Tom I, Gonzalez LC, Sheng M. TREM2 Binds to Apolipoproteins, Including APOE and CLU/APOJ, and Thereby Facilitates Uptake of Amyloid-Beta by Microglia. Neuron. 2016;91(2):328-40. doi: 10.1016/j.neuron.2016.06.015. PubMed PMID: 27477018.
17. Song W, Hooli B, Mullin K, Jin SC, Cella M, Ulland TK, Wang Y, Tanzi RE, Colonna M. Alzheimer's disease-associated TREM2 variants exhibit either decreased or increased ligand-dependent activation. Alzheimer's & dementia : the journal of the Alzheimer's Association. 2016. doi: 10.1016/j.jalz.2016.07.004. PubMed PMID: 27520774; PMCID: PMC5299056.
18. Phongsisay V. Campylobacter jejuni targets immunoglobulin-like receptor LMIR5. Mol Immunol. 2015;63(2):574-8. doi: 10.1016/j.molimm.2014.07.024. PubMed PMID: 25172092.
19. Quan DN, Cooper MD, Potter JL, Roberts MH, Cheng H, Jarvis GA. TREM-2 binds to lipooligosaccharides of Neisseria gonorrhoeae and is expressed on reproductive tract epithelial cells. Mucosal Immunology. 2008;1(3):229-38. doi: 10.1038/mi.2008.1. PubMed PMID: WOS:000260470800007.
20. Phongsisay V, Iizasa E, Hara H, Yoshida H. Evidence for TLR4 and FcRgamma-CARD9 activation by cholera toxin B subunit and its direct bindings to TREM2 and LMIR5 receptors. Mol Immunol. 2015;66(2):463-71. doi: 10.1016/j.molimm.2015.05.008. PubMed PMID: 26021803.
21. Wang Y, Cella M, Mallinson K, Ulrich JD, Young KL, Robinette ML, Gilfillan S, Krishnan GM, Sudhakar S, Zinselmeyer BH, Holtzman DM, Cirrito JR, Colonna M. TREM2 lipid sensing sustains the microglial response in an Alzheimer's disease model. Cell. 2015;160(6):1061-71. doi: 10.1016/j.cell.2015.01.049. PubMed PMID: 25728668; PMCID: PMC4477963.
22. Poliani PL, Wang Y, Fontana E, Robinette ML, Yamanishi Y, Gilfillan S, Colonna M. TREM2 sustains microglial expansion during aging and response to demyelination. J Clin Invest. 2015;125(5):2161-70. doi: 10.1172/JCI77983. PubMed PMID: 25893602; PMCID: PMC4463196.
23. Phongsisay V, Iizasa E, Hara H, Yamasaki S. 3-O-sulfo-beta-D-galactose moiety of endogenous sulfoglycolipids is a potential ligand for immunoglobulin-like receptor LMIR5. Mol Immunol. 2015;63(2):595-9. doi: 10.1016/j.molimm.2014.07.023. PubMed PMID: 25172093.

24. Nakahashi-Oda C, Tahara-Hanaoka S, Honda S-i, Shibuya K, Shibuya A. Identification of phosphatidylserine as a ligand for the CD300a immunoreceptor. Biochemical and Biophysical Research Communications. 2012;417(1):646-50. doi: http://dx.doi.org/10.1016/j.bbrc.2011.12.025.
25. Murakami Y, Tian L, Voss OH, Margulies DH, Krzewski K, Coligan JE. CD300b regulates the phagocytosis of apoptotic cells via phosphatidylserine recognition. Cell Death Differ. 2014;21(11):1746-57. doi: 10.1038/cdd.2014.86.
26. Simhadri VR, Andersen JF, Calvo E, Choi SC, Coligan JE, Borrego F. Human CD300a binds to phosphatidylethanolamine and phosphatidylserine, and modulates the phagocytosis of dead cells. Blood. 2012;119(12):2799-809. doi: 10.1182/blood-2011-08-372425. PubMed PMID: 22302738; PMCID: PMC3327458.
27. Santiago C, Ballesteros A, Martínez-Muñoz L, Mellado M, Kaplan GG, Freeman GJ, Casasnovas JM. Structures of T Cell Immunoglobulin Mucin Protein 4 Show a Metal-Ion-Dependent Ligand Binding Site where Phosphatidylserine Binds. Immunity. 2007;27(6):941-51. doi: http://dx.doi.org/10.1016/j.immuni.2007.11.008.
28. Miyanishi M, Tada K, Koike M, Uchiyama Y, Kitamura T, Nagata S. Identification of Tim4 as a phosphatidylserine receptor. Nature. 2007;450(7168):435-9. doi: http://www.nature.com/nature/journal/v450/n7168/suppinfo/nature06307_S1.html.
29. Kobayashi N, Karisola P, Pena-Cruz V, Dorfman DM, Jinushi M, Umetsu SE, Butte MJ, Nagumo H, Chernova I, Zhu B, Sharpe AH, Ito S, Dranoff G, Kaplan GG, Casasnovas JM, Umetsu DT, Dekruyff RH, Freeman GJ. TIM-1 and TIM-4 glycoproteins bind phosphatidylserine and mediate uptake of apoptotic cells. Immunity. 2007;27(6):927-40. doi: 10.1016/j.immuni.2007.11.011. PubMed PMID: 18082433; PMCID: PMC2757006.
30. Tietjen GT, Gong Z, Chen CH, Vargas E, Crooks JE, Cao KD, Heffern CT, Henderson JM, Meron M, Lin B, Roux B, Schlossman ML, Steck TL, Lee KY, Adams EJ. Molecular mechanism for differential recognition of membrane phosphatidylserine by the immune regulatory receptor Tim4. Proc Natl Acad Sci U S A. 2014;111(15):E1463-72. doi: 10.1073/pnas.1320174111. PubMed PMID: 24706780; PMCID: PMC3992656.
31. Edeling MA, Sanker S, Shima T, Umasankar PK, Höning S, Kim HY, Davidson LA, Watkins SC, Tsang M, Owen DJ, Traub LM. Structural Requirements for PACSIN/Syndapin Operation during Zebrafish Embryonic Notochord Development. PLoS ONE. 2009;4(12):e8150. doi: 10.1371/journal.pone.0008150.
32. Esko JD, Stewart TE, Taylor WH. Animal cell mutants defective in glycosaminoglycan biosynthesis. Proceedings of the National Academy of Sciences of the United States of America. 1985;82(10):3197-201. PubMed PMID: PMC397742.
33. Thelen M, Razquin C, Hernandez I, Gorostidi A, Sanchez-Valle R, Ortega-Cubero S, Wolfsgruber S, Drichel D, Fliessbach K, Duenkel T, Damian M, Heilmann S, Slotosch A, Lennarz M, Seijo-Martinez M, Rene R, Kornhuber J, Peters O, Luckhaus C, Jahn H, Hull M, Ruther E, Wiltfang J, Lorenzo E, Gascon J, Lleo A, Llado A, Campdelacreu J, Moreno F, Ahmadzadehfar H, Dementia Genetics Spanish C, Fortea J, Indakoetxea B, Heneka MT, Wetter A, Pastor MA, Riverol M, Becker T, Frolich L, Tarraga L, Boada M, Wagner M, Jessen F, Maier W, Clarimon J, Lopez de Munain A, Ruiz A, Pastor P, Ramirez A. Investigation of the role of rare TREM2 variants in frontotemporal dementia subtypes. Neurobiol Aging. 2014;35(11):2657 e13-9. doi: 10.1016/j.neurobiolaging.2014.06.018. PubMed PMID: 25042114.

34. Kelker MS, Debler EW, Wilson IA. Crystal Structure of Mouse Triggering Receptor Expressed on Myeloid Cells 1 (TREM-1) at 1.76 Å. Journal of molecular biology. 2004;344(5):1175-81. doi: http://dx.doi.org/10.1016/j.jmb.2004.10.009.
35. Kelker MS, Foss TR, Peti W, Teyton L, Kelly JW, Wüthrich K, Wilson Ia. Crystal structure of human triggering receptor expressed on myeloid cells 1 (TREM-1) at 1.47 A. Journal of molecular biology. 2004;342(4):1237-48. doi: 10.1016/j.jmb.2004.07.089.
36. Gattis JL, Washington AV, Chisholm MM, Quigley L, Szyk A, McVicar DW, Lubkowski J. The structure of the extracellular domain of triggering receptor expressed on myeloid cells like transcript-1 and evidence for a naturally occurring soluble fragment. J Biol Chem. 2006;281(19):13396-403. doi: 10.1074/jbc.M600489200. PubMed PMID: 16505478.
37. Pellegrini L, Burke DF, von Delft F, Mulloy B, Blundell TL. Crystal structure of fibroblast growth factor receptor ectodomain bound to ligand and heparin. Nature. 2000;407(6807):1029-34.
38. Bouchon A, Hernandez-Munain C, Cella M, Colonna M. A DAP12-mediated pathway regulates expression of CC chemokine receptor 7 and maturation of human dendritic cells. J Exp Med. 2001;194(8):1111-22. PubMed PMID: 11602640; PMCID: PMC2193511.
39. Yin J, Liu X, He Q, Zhou L, Yuan Z, Zhao S. Vps35-dependent recycling of Trem2 regulates microglial function. Traffic. 2016;17(12):1286-96. doi: 10.1111/tra.12451.
40. Ahn HC, Kim NY, Hur GH, Yang JM, Shin S. Role of chondroitin sulfate C in the action of anthrax toxin. Toxicology. 2012;297(1–3):10-6. doi: http://dx.doi.org/10.1016/j.tox.2012.03.008.
41. Newman DR, Li C-M, Simmons R, Khosla J, Sannes PL. Heparin affects signaling pathways stimulated by fibroblast growth factor-1 and -2 in type II cells. American Journal of Physiology - Lung Cellular and Molecular Physiology. 2004;287(1):L191-L200. doi: 10.1152/ajplung.00284.2003.
42. Levallet G, Bonnamy P-J, Levallet J. Alteration of cell membrane proteoglycans impairs FSH receptor/Gs coupling and ERK activation through PP2A-dependent mechanisms in immature rat Sertoli cells. Biochimica et Biophysica Acta (BBA) - General Subjects. 2013;1830(6):3466-75. doi: http://dx.doi.org/10.1016/j.bbagen.2013.02.027.

Chapter 5: TREM2 interacts with extracellular proteins involved in Alzheimer's disease

The work described above detailed for the first time how TREM2 interacts with a GAG-dependent cell-surface ligand. However, the full set of TREM2 ligands remains to be elucidated. This section details progress towards identifying and characterizing the interactions between TREM2 and proteins involved in AD that may represent disease-relevant TREM2 interaction partners.

5.1 The role of Apolipoprotein E and amyloid beta in Alzheimer's disease

Apolipoprotein E (ApoE) is a soluble protein that associates with lipoparticles in serum and CSF. The *APOE4* variant is the strongest risk for non-familial AD, providing about 4-8 fold increased risk with a single copy and a 12-fold increased risk with homozygosity. This allele is relatively common, with a mean allelic frequency of about 14% (1). ApoE has a number of roles, and like TREM2, it has been linked to microglia functions including phagocytosis, inflammation, and cell health (2, 3). ApoE is also involved in the formation of and response to Aβ plaques, and has isoform-dependent effects on Aβ aggregation, uptake, and clearance (1).

During the course of this work, two groups first reported that TREM2 binds ApoE, both lipid-loaded and unloaded, ApoE3 and E4, and that the R47H variant decreases binding (4, 5). Both use studies used relied on indirect, non-quantitative methods such as co-IPs, dot blots, and ELISA. However, they obtained similar results. After these initial reports, another group used a

high-throughput binding screen and BLI follow-up experiments to show an interaction between TREM2, ApoE, and other lipoproteins (6). They found the R47H, R62H, and D87N variants decreased binding, but this was determined by the response signal, not by calculating kinetics or determining a dose-dependent response. In contrast to the first reports, this group did not observe binding to non-lipidated ApoE. However, they made this determination by the response signal, which may not be similar for unloaded ApoE and lipoparticles. Functionally, TREM2 facilitated uptake of ApoE when expressed in 293T cells. Therefore, I wanted to determine whether TREM2 directly bound ApoE, whether TREM2 variants or ApoE isoforms affected binding, and what is the minimal binding domain between these proteins.

In addition to ApoE, the primary driver of AD is believed to be Aβ peptides. This model is known as the amyloid cascade hypothesis (7). Indeed, most animal models of AD overexpress mutant proteins that contribute to the production and maturation of Aβ. Whether TREM2 directly interacts with Aβ is an open question. A large number of Aβ receptors have already been identified, some thought to be protective and others harmful (8).

5.2 TREM2 directly binds ApoE and disease variants alter binding

5.2.1 TREM2 directly binds ApoE3 and ApoE4

Expression and purification of ApoE

Mammalian ApoE is expressed and secreted in lipoparticles from the liver into serum and from in the CNS, primarily from astrocytes, although microglia do produce some ApoE. Some evidence suggests neurons can be induced to secrete ApoE, but astrocytes are considered the primary expressers within the brain (9). In addition to its lipidation, secreted ApoE contains an

O-linked glycosylation on T194 (10). This glycan can be matured to contain sialic acid moieties which are subject to further post-translational modifications dependent on the environment: ApoE proteins in the CNS are more highly sialylated than ApoE from serum (11).

ApoE has three major isoforms: ApoE2, E3, and E4. ApoE3 (roughly 7%, 78% and 14% allelic frequency). ApoE3 is considered the wild-type, while ApoE4 is associated with increased risk for AD and atherosclerosis. ApoE2 is actually protective against AD, although it produces other metabolic deficits. ApoE2 homozygosity is necessary, but not entirely sufficient, for developing type III hyperlipoproteinemia. These diverse effects are considerable, especially since each isoforms differs from E3 at only a single residue. ApoE3 is C112 and R158. ApoE4 is C112R, and ApoE2 is R158C. The ApoE2 isoform nearly completely abolishes binding to the LDL receptor, which decreases lipoprotein clearance (Reviewed in (2)). The R158C mutation results in changes to the LDLR-binding surface. This mechanism was elucidated from the crystal structure of the N-terminal domain of Apoe2 (12). In contrast, ApoE4 retains receptor binding, but has altered preference for VLDL over HDL lipoparticles, altered Aβ binding. The C112R variant alters the interactions between the N-terminal region and the C-terminal tail, which mediates oligomerization and lipid binding. The structural mechanisms of are still unclear. In addition to ApoE2, the N-terminal domains of ApoE3 and ApoE4 have also been determined (13-17), however the crystal structure of any full-length ApoE isoform has been elusive. An NMR structure of ApoE3 was determined, but this required making five mutations to the C-terminal tail to reduce oligomerization and aggregation during NMR experiments (18). This model showed unexpected salt-bridges, and did not agree with data collected by other methods (19), raising concerns about the effect of the introduced mutations. Despite these many considerations, *E. coli*-derived ApoE has been the primary tool for structural studies.

I obtained ApoE constructs which encode ApoE following a thioredoxin protein containing a 6-His tag and PreScission protease site (20). This protein is expressed in *E. coli* cells, purified by NiNTA, and then cleaved by PreScission protease to release ApoE. The ApoE retains a two-residue GS tail, but the thioredoxin contains the 6-His tag. This strategy is a modification of the previous standard method, which used a thrombin cut site to cleave the fusion. The challenge to that method is that ApoE is highly sensitive to thrombin cutting within its hinge region. In that approach, ApoE would be purified by NiNTA and lipidated by mixing with 1,2-dimyristoyl-sn-glycero-3-phosphocholine (DMPC) lipoparticles, which protect it from cleavage. Thrombin would be added to release thioredoxin, following which ApoE was delipidated and denatured with methanol, solubilized in 6 M GuHCl, and purified by SEC in 4M GuHCl before being dialyzed into ammonium bicarbonate where it would refold as a tetramer (21). The method used here produces unlipidated ApoE in its tetrameric form without the need for an intermediate lipidation or refolding. The oligomeric state was verified during preliminary HDX experiments with the Michael Gross lab. PreScission protease was purified as a GST-fusion protein using a construct provided by N. Tolia. GST-protease was eluted from glutathione resin in 50 mM Tris pH 8.0, 10 mM reduced glutathione, and 1 mM DTT. The yield was over 10 mg/L. PreScission protease was aliquoted and stored at -80° C. To purify ApoE, I initially used MonoQ and SEC chromatography (**Fig 5.1**) but in later experiments found that SEC alone readily purifies the ApoE proteins.

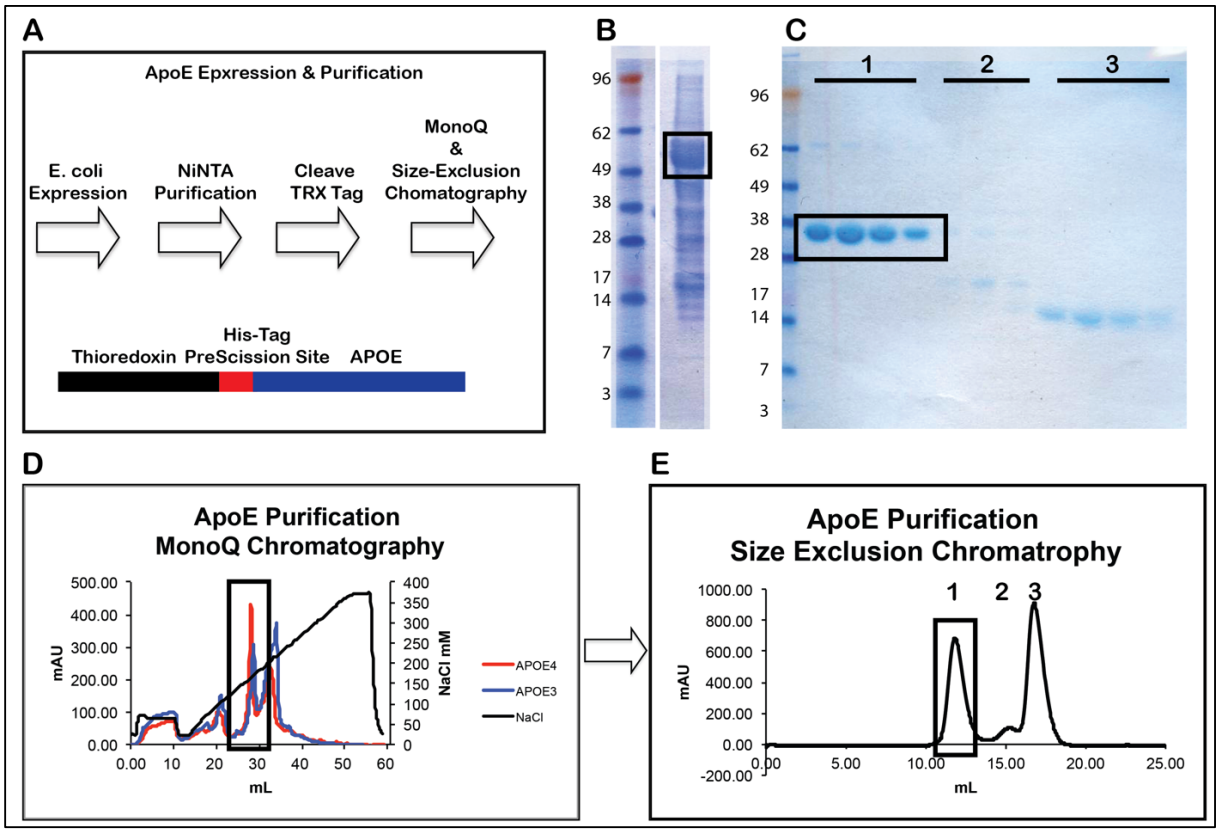

Figure 5.1 Expression and purification of ApoE3 and E4. A) Schematic for expression and purification of ApoE. **B)** ApoE3-Thioredoxin fusion from NiNTA affinity column. Box highlights uncleaved fusion protein. **C)** Purified ApoE3 from SEC chromatogram, with fractions labeled corresponding to curves in (E). Box labels cleaved, purified ApoE. ApoE presence was also verified by peptide-fragment MS and immunoblot (not shown) **D)** monoQ chromatography profile of the NiNTA elution. Box indicated fractions collected for SEC. **E)** SEC profile of ApoE3 at final purification.

TREM2 binds ApoE3 and ApoE4

To test whether TREM2 directly bound ApoE, BLI experiments were conducted where biotinylated TREM2 was immobilized on the pin and dipped into wells containing purified ApoE. The running buffer was 20 mM HEPES, 150 mM NaCl, 0.05% Tween-20, and 0.1% BSA. Both human and mouse TREM2 bound ApoE3, and human TREM2 bound both ApoE3 and ApoE4 with similar affinity (**Fig 5.2 and Table 6**). The apparent K_D of these interactions were typically in the high nanomolar range. This is considerably reduced from the single-digit nanomolar affinity reported by quantifying dot blots in the study by Atagi et al (4) (**Table 4**), but has been consistent across many experiments and these represent direct biophysical measurements. These data confirm that TREM2 can bind ApoE in the non-lipidated format and that this binding occurs with a high-nanomolar affinity. There is also no dramatic change in the affinity for ApoE3 or ApoE4, which is consistent with the previous reports.

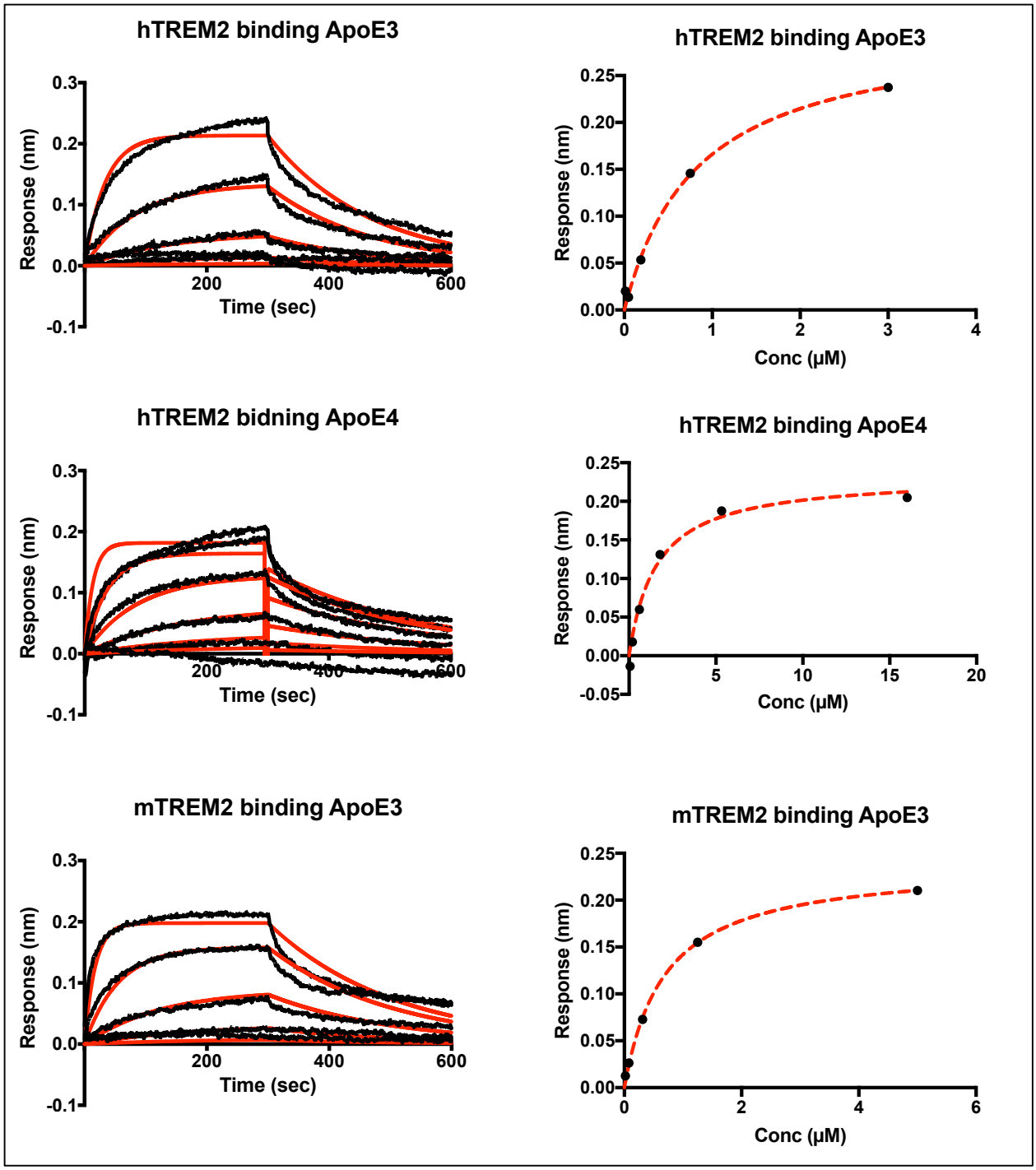

Figure 5.2 TREM2 binds full-length ApoE. Double reference-subtrated BLI data (left) and steady-state response (right) for hTREM2 binding ApoE3 (top), ApoE4 (middle) and mTREM2 binding ApoE3 (bottom). Signal is shown in black trace and fits shown in red lines or dashes.

Table 6. Affinity values from experiments in Figure 5.2

	Kinetic fits			Steady-state fits	
	K_D (M)	Error	R^2	K_D (M)	R^2
hTREM2 ApoE3	7.36E-07	9.55E-09	0.9748	8.30E-07	0.9926
hTREM2 ApoE4	8.89E-07	2.33E-08	0.9352	1.50E-06	0.9906
mTREM2 ApoE3	4.51E-07	5.92E-09	0.9685	6.90E-07	0.9984

5.2.2 Determining the minimal domain of ApoE required to bind TREM2

Expression and purification of ApoE truncation constructs

To determine the minimal domain binding site, a series of C-terminal truncations were produced and used in BLI experiments. The initial constructs were a gift from Carl Freiden and were encoded in a pet30a vector. This vector contained the full-length ApoE gene preceded by an N-terminal 8-His tag. The truncations were designed by introducing stop codons at targeted residues. These constructs were ApoE4 1-238 (stop codon inserted at 239) and ApoE3 1-169 (stop codon inserted at 170). (By convention, ApoE residues are numbered starting after the 18 residue secretion peptide). While working with these proteins, I observed the 1-238 protein suffered considerable proteolytic degradation**.** Immunoblotting revealed an intact N-terminal His tag. With the help of Hanliu Wang in the lab of Michael Gross, this proteolytic fragment was determined to be residues 1-192 (by peptide mapping and native mass). This cleavage affected about 50% of the protein within days and would be detrimental towards crystallization. Therefore, I cloned ApoE4 1-192, as well as 1-191 (PDB 1NFN) (12) and 1-183 (PDB 2KC3)

based on crystal structure and NMR PDB boundaries. PCR primers are listed in **Table 7**. Expression of some of these constructs was problematic. As part of the troubleshooting process I used restriction digests to place these constructs in pet23b vectors in addition to the pet30a vectors. **Figure 5.3** shows representative SEC traces and SDS-PAGE analyses of these proteins. Several of the proteins required overnight expression at 20° C to generate appreciable yields. All proteins were purified by NiNTA chromatography and aggregates removed by SEC in sizing buffer. All ApoE3 proteins were in buffers containing either 5 mM β–ME during NiNTA steps or 1 mM DTT during SEC. In general, the larger ApoE4 constructs and the shorter ApoE3 constructs were better behaved as assessed by their expression and SEC profiles. ApoE4 1-169 was only weakly detected by immunoblot of NiNTA eluate. All the other truncations can be expressed and readily purified.

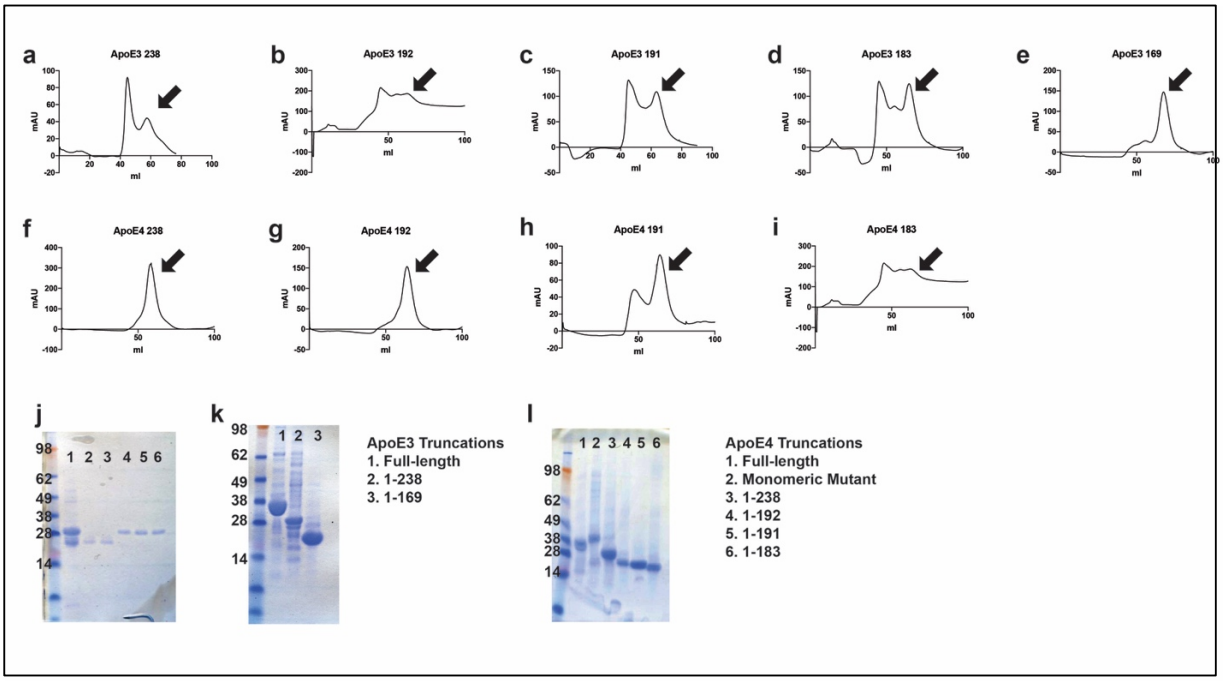

Figure 5.3 Expression and purification of ApoE truncation products. ***First row:*** ApoE3 truncation proteins. SEC profiles of **a)** ApoE3 1-238, **b)** ApoE3 1-192, **c)** ApoE3 1-191, **d)** ApoE3 1-183, **e)** ApoE3 1-169. ***Second Row:*** ApoE4 truncation protiens. SEC profiles of **f)** ApoE4 1-238, **g)** ApoE4 1-192, **h)** ApoE4 1-191, **j)** ApoE4 1-183. Black arrows mark peak containing desired protein. ***Third row:*** **j)** SDS-PAGE analysis of ApoE4 1-238 cleavage produce. #1 = 238 monoQ input after ~1 week following initial purification where the protein was a single band. 2-6 fractions in increasing NaCl concentration shows the two species cleanly separate. Immunoblot analysis was used to determine the C-terminus was intact. Peptide MS/MS and native MS was used to identify the mass and peptide content in the two species and identify the cleavage site. **k)** SDS-PAGE of ApoE3 truncation proteins used in the experiment below. **l)** purified ApoE4 proteins.

Table 7. Primers used to generate ApoE constructs	
	Sequence (5'-3')
R112C	TGGA GGACGTGTGC GGCCGCCTG
	ACCT CCTGCACACG CCGGCGGAC
A193*	AGCCCACAGTGGCCTACCGCACGCGGCCC
	GGGCCGCGTGCGGTAGGCCACTGTGGGCT
A192*	GGGAGCCCACAGTCTAGGCCCGCACGCGG
	CCGCGTGCGGGCCTAGACTGTGGGCTCCC
L184*	GCCCTGTTCCACCTAGGGCCCCAGGCGC
	GCGCCTGGGGCCCTAGGTGGAACAGGGC
NdeI-start-6H	GGGAATTCCATATGCACCATCATCACCACCATAAGGTGGAGCAAGCG GTGGAGACAGAGCCG
238-*-XhoI	CTCGAGCTACTCCGCCACCTGCTCCTTCACCTCGTCCAGGCGG
169-*-XHO	CTCGAGCTAGCCCTCGCGGGCCCCGGCCTGGTACACTGCCAG

The C-terminal domain is not required for full binding

Having cloned truncation constructs, I have begun to analyze the minimal binding domain for TREM2. In initial experiments, full-length ApoE3, a C-terminal deletion (1-238, Nterm-Hinge), or the N-terminal domain alone (1-169) were tested for binding to immobilized TREM2. Full-length and the Nterm-hinge protein bound equally, but the N-term alone had greatly reduced affinity (**Fig 5.4**). This loss of binding to the ApoE3 N-term was observed in two separate experiments. Beyond narrowing the interaction domain, these assays establish that ApoE does not have to be lipidated to interact with TREM2, as C-terminal domain is required for lipid binding (22). In future experiments, the truncations within the hinge domain (1-192, 191, and 183) will be tested to further narrow down the binding site. In initial experiments, the ApoE4 versions of these proteins seemed to be competent to bind TREM2, but the failure to produce the 1-169 construct and, until recently, not having the ApoE3 truncations cloned and expressed has prevented a final conclusion on the minimal binding interface. This determination will be

important for crystallization attempts, as the 1-238 construct of both ApoE3 and ApoE4 is very prone to proteolytic degradation. The other constructs may be more resistant and would be more suitable for co-crystal screens.

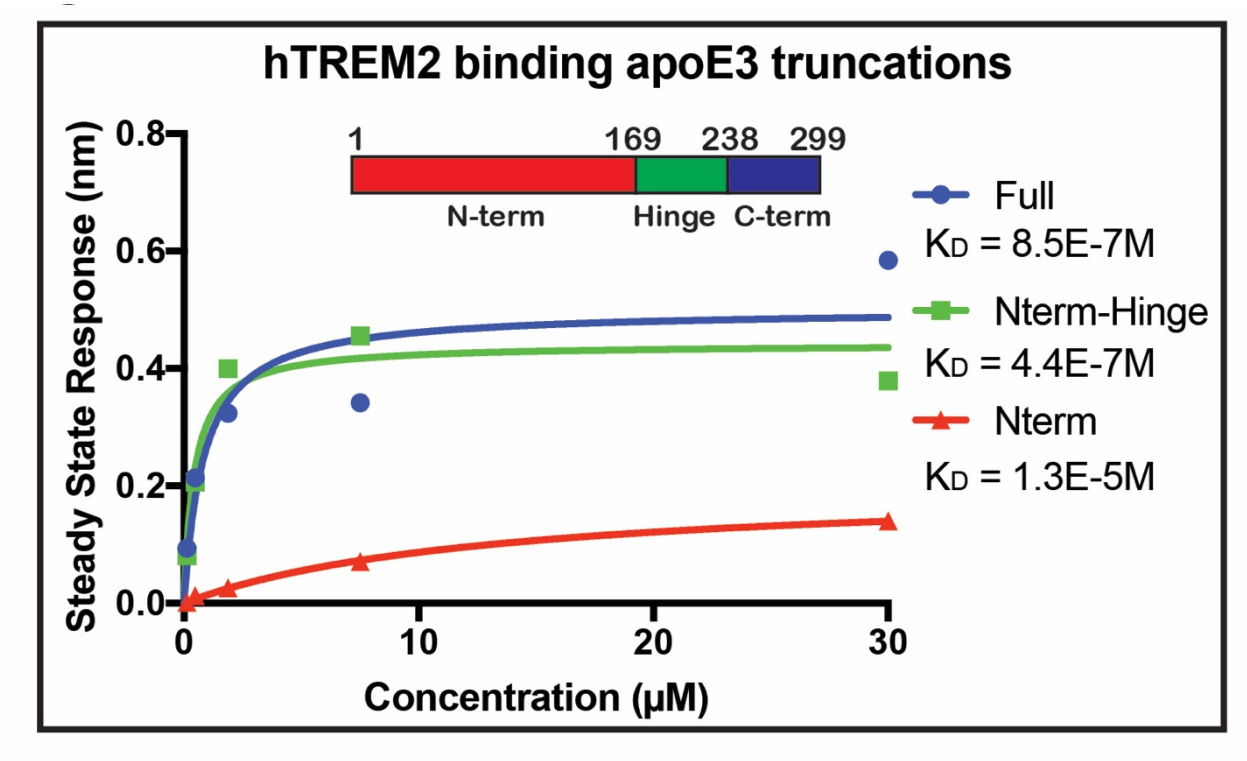

Figure 5.4. The hinge region of ApoE is required for full binding to TREM2. TREM2 was immobilized on streptavidin pins and dipped into wells containing full-length or truncated ApoE3. Steady-state response is plotted, with curve fit analysis and affinities calculated using Prism. Inset depicts domain boundaries.

5.2.3 TREM2 binds lipid-loaded ApoE

ApoE naturally occurs as a lipoprotein, so to test binding in a more physiologically relevant state, I obtained a mouse anti-ApoE antibody from the David Holtzman lab (clone HJ 15.7) for using in BLI experiments as a reagent to capture lipidated ApoE. Anti-murine-Fc BLI pins were loaded with this antibody and then dipped into lipidated supplied by Jason Ulrich of the Holtzan lab (Schematized in **Fig 5.5A**). The immobilized ApoE was then dipped into wells containing SEC-purified TREM2 in PBS buffer with 0.1% BSA (No Tween-20). Dose-dependent binding of lipidated ApoE3 by TREM2 was observed, although the kinetics of binding were appreciably different than the unlipidated experiments described above (**Fig 5.5B**). The K_D calculated in the experiment shown was about 14 µM. In the experiments with lipidated ApoE from the Holtzman lab, none of the affinities have been as high as determined by the unlipidated ApoE made in our lab.

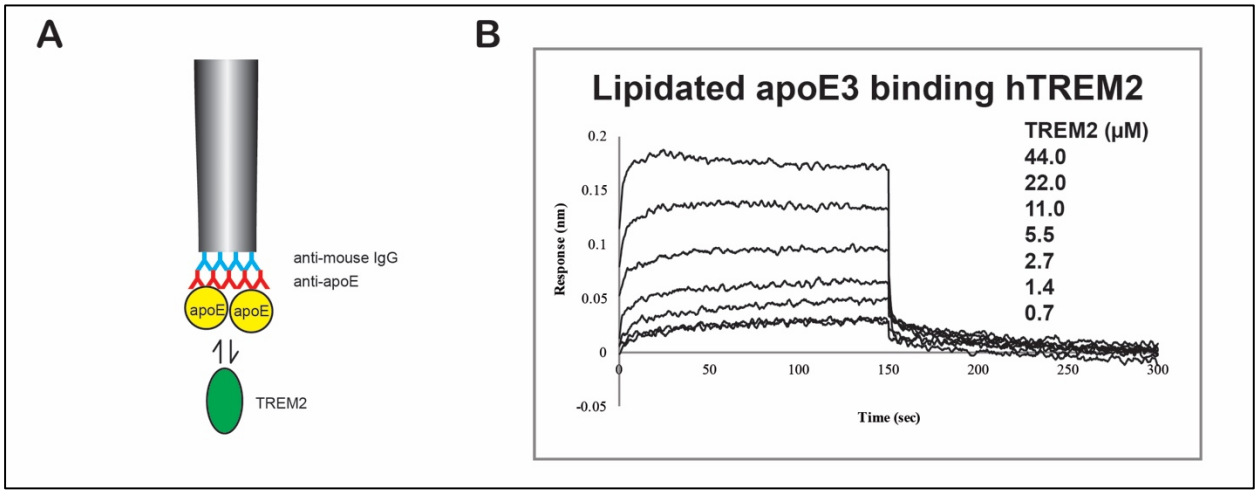

Figure 5.5. TREM2 binds lipidated ApoE3. A) Schematic for binding experiments. **B)** Double-reference subtracted curves of hTREM2 binding to immobilized ApoE3. TREM2 was titrated in a range of 44 to 0.7 µM.

5.2.4 TREM2 variants alter ApoE binding

To determine whether the basic patch is involved in binding to ApoE, I expressed and biotinylated WT, R47H, and a R47H-R76D-R77D triple mutant (HDD) which severely disrupts the basic surface. These proteins were captured on streptavidin pins and used to test binding to SEC-purified ApoE3 as described above in a double-referenced experiment. While the R47H did not completely lose binding, the both variants had reduced binding as assessed by kinetic and steady-state affinity determinations (**Table 8**). This is consistent with the initial reports of R47H losing some binding to ApoE (4-6). These differences will likely be more profound when done with ApoE immobilized on the pin to prevent complications from avidity from the tetrameric ApoE.

Table 8. Mutant TREM2 binding ApoE3.

	Kinetic fits			Steady-state fits	
	KD (M)	KD Error	Full R^2	SSG KD	SSG R^2
WT	4.11E-07	1.77E-08	0.7931	8.50E-07	0.8159
R47H	3.03E-06	1.27E-07	0.8228	6.10E-06	0.8561
HDD	6.42E-06	1.77E-07	0.968	2.20E-05	0.9917

I have also attempted to determine whether the disease variants alter binding to lipidated ApoE. These experiments used lipidated ApoE provided by Jason Ulrich. **Figure 5.6** shows the results of these experiments. In most cases, R47H appears to have reduced binding. However, in one experiment with ApoE4, there did appear to be some binding. ApoE3 was also attempted in that experiment, but there was a machine error during that part of the run. In a separate experiment not shown, I tried to reproduce the differential binding of R47H to ApoE3 and E4, but observed weak binding for both. Another concern is that I did observed quality binding in the

capture format by non-lipidated ApoE provided by Jason as a control for lipidation (not shown). Because of these inconsistencies, and because this protein was not prepared in a way where the quality can be readily assessed, I have recently begun attempting to lipidate and validate ApoE proteins made in my system (**See section 5.4.4**). Experiments with these samples will be necessary to finalize conclusion about TREM2-ApoE binding. However, in most experiments, I have observed decreased binding to the R47H variant, suggesting this surface is involved in ApoE binding.

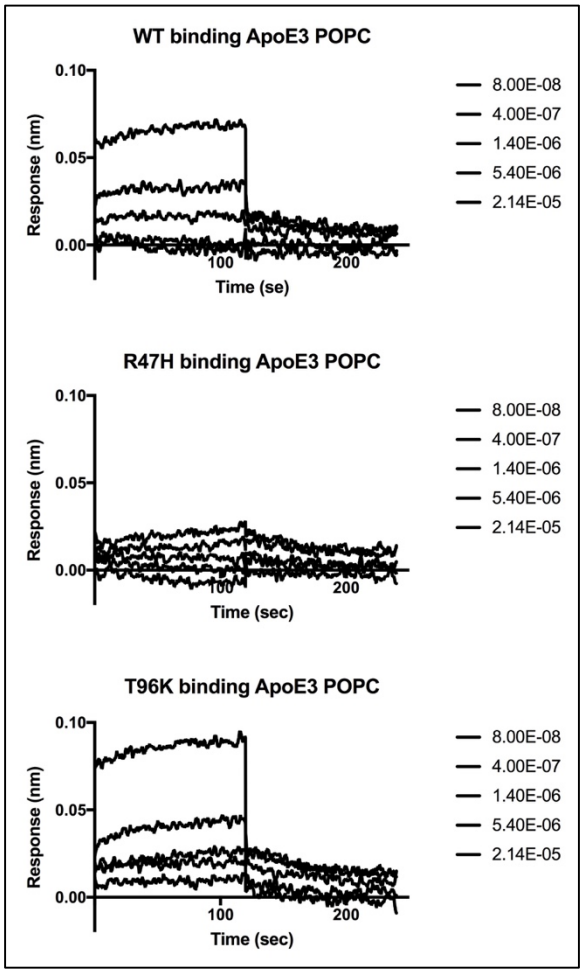

Figure 5.6. TREM2 variants alter binding to lipidated ApoE3. Lipidated ApoE3 (provided from the Holtzman lab) was immobilized on a BLI pin using a capture antibody and dipped into wells containing WT or variant TREM2 at the indicated concentrations. Curves were double-reference subtracted using a capture antibody-only loaded pin dipped into the same wells and a buffer-only control pin.

5.3 TREM2 directly binds Aβ and disease variants alter binding

There have been mixed reports on the role of TREM2 potentially interacting with (Aβ). In one report, synthetic or extracted Aβ did not induce TREM2 signaling in reporter cells (23), (This experiment is mentioned in the text but data was not shown). However, in another report, TREM2-dependent tyrosine phosphorylation was observed on microglia processes in contact with Aβ plaques, suggesting plaques, or a plaque-deposited ligand could induce TREM2 signaling (24). However, direct binding to of Aβ to TREM2 had never been demonstrated. This section details the first characterization of a TREM2-Aβ interaction.

5.3.1 Expression of a GST-Aβ fusion protein

Amyloid beta 1-42, ($A\beta_{1-42}$) is a peptide produced by the proteolytic processing of amyloid precursor protein (APP) by β-secretases and is thought to be the primary driver of AD (25). This peptide is aggregation-prone and also bactericidal (26, 27), making recombinant expression of this peptide difficult. Most studies utilize synthetic peptides; however, it is difficult to control the oligomeric state of these peptides and this complicates binding studies. One report showed that $A\beta_{1-42}$ could be expressed from *E. coli* using a GST-fusion system (28). Because FortéBio manufactures anti-GST pins for the BLI system, I cloned the $A\beta_{1-42}$ peptide onto the C-terminal end of GST expressed in the pGEX-4T1 vector through BamHI-XhoI restriction digestion using a Gibson block insert. The $A\beta_{1-42}$ sequence was optimized for expression in *E. coli*. As a control, pGEX-4T1 (which encodes GST-only) was expressed alongside the fusion protein. In the first expression, cells were induced at 30° C, but fusion protein was undetectable. To reduce potential toxicity, expression was induced at overnight at 20° C. In this case,

expression was detectable following purification with glutathione resin. To purify the protein, cells were resuspended in 30 mL PBS with 1 mM DTT /L of cells. Cells were lysed by sonication and centrifuged at 16,000 x g for 30 min to pellet debris. The supernatant was collected and incubated with 0.5 mL of glutathione resin for 1 hour at 4° C. The mixture was transferred to a gravity column. Beads were washed in 10 mL of PBS + DTT and then eluted with 50 mM Tris pH 8.0, 10 mM reduced glutathione, and 1 mM DTT in a total volume of 2 mL. Samples were analyzed by SDS-PAGE (**Fig 5.7**). Robust loading of both GST and GST-Aβ on the anti-GST pins confirmed the presence of GST.

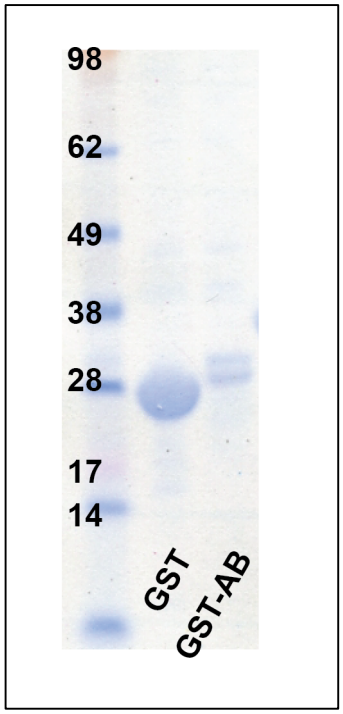

Figure 5.7. Expression and purification of GST-Aβ. GST and GST-Aβ(1-42) were expressed in E. coli. Protein purified by glutathione resin are from 1L cell pellet. Note shift in MW for GST-Abeta, and markedly reduced yield of this protein.

5.3.2 TREM2 binds Aβ

To test whether TREM2 bound the Aβ, anti-GST pins were used to capture bound GST-Aβ, and were then dipped into wells containing SEC-purified TREM2. The running buffer was PBS with 0.01% BSA and 0.005% Tween-20. To control for non-specific binding, a GST-only loaded pin was run through the same wells. To control for sensor drift, GST-only dipped into buffer was subtracted from GST-Aβ into buffer. Binding was measured to WT, R47H, and T96K TREM2 proteins. GST-Aβ bound TREM2 with an affinity in the low micromolar range (**Fig 5.8**). In one experiment, some weak binding was observed to R47H, however, the affinities were greatly reduced both as measured by kinetic fits and steady-state analysis. This assay seems to be especially sensitive to the buffer conditions. In two other experiments, one with no BSA but 0.05% Tween 20 and another with 0.1% BSA and 0.005% Tween-20, I observed no signal from R47H but similar WT signal. This micromolar affinity binding could be relevant in the context of the Aβ plaques, which are highly aggregated and fibrillated and would therefore present a high-avidity ligand. Future experiments will need to be designed to investigate binding of TREM2 to different forms of the Aβ peptides.

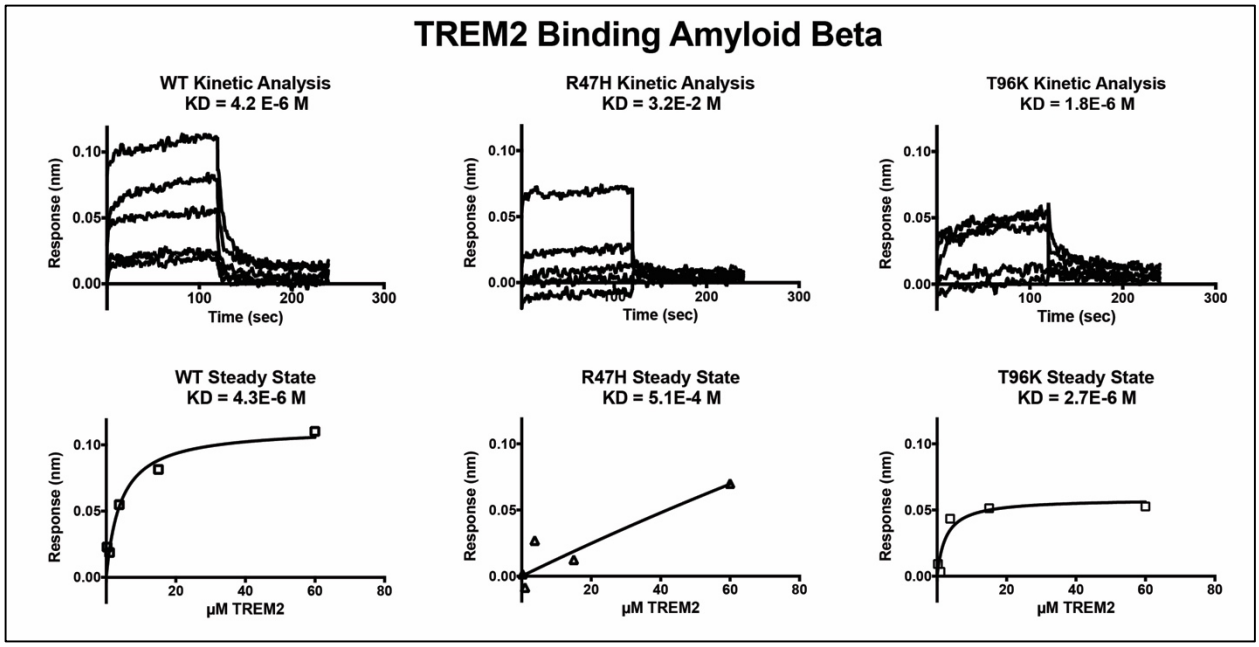

Figure 5.8. Human TREM2 Ig domain binds Aβ. BLI analysis of immobilized GST-Aβ(1-42) binding TREM2 Ig domain. Data are shown for WT TREM2 (left), AD risk variant TREM2 R47H (middle), and AD protective variant TREM2 T96K (right). Affinities shown (K_D) are derived either from kinetic analysis (upper panels) or steady state fits (lower panels).

5.4 Towards the structure of TREM2-ApoE complex

5.4.1 Attempts to crystallize the minimal TREM2-binding domain of ApoE

My preliminary experiments suggest the hinge domain of ApoE is important for TREM2 binding. This region is not observed in any of the ApoE crystal structures. In attempt to gain structural insight about this region (such as for use in docking experiments), I expressed and purified ApoE4 1-238 and attempted to crystallize this protein. Protein was purified in sizing buffer by SEC, concentrated to 8 mg/mL and crystals grew in 10% PEG3350 and 0.2 M KCl (**Fig 5.9 a,b)**. Crystals were harvested by preservation in mother liquor with 20% ethylene

glycol, frozen under a nitrogen stream, and stored in liquid N_2 until data collection. Data was collected at APS beamline 19-ID. One crystal diffracted very well, and strong data was collected out to the detector edge at 1.58 Å **(Table 9)**. The phase problem was solved by molecular replacement using PHASER and ApoE4 PDB 1B68 (29). The TFZ was 36.7, and the spacegroup was $P2_12_12_1$. All but one of the ApoE truncation crystal structures deposited in the PDB are in this space group (13 total at this writing). Unfortunately, my structure is missing the first 22 and last 73 amino acids of the ApoE4 1-238 protein. I was able to build in one of the loops not present in the search probe and to add a couple residues to the C-terminus, but was not able to observe density for the rest of the protein (**Fig 5.9c**). The crystal packing has a tight arrangement and it is difficult to see where another 70 or so residues could fit. The decent R_{free} suggests that the model could be probably be improved, but is not likely to be missing one third of the protein. It is more likely that the missing residues were cleaved to leave only the N-terminal helical bundle. Silver staining would typically be used to confirm cleavage, but these crystals were only produced in one well and were used for diffraction experiments.

Table 9. ApoE4 1-238 Data collection and refinement statistics.

	ApoE4 1-238
Data collection	
Space group	P 2_1 2_1 2_1
Cell dimensions	
a, *b*, *c* (Å)	45.38, 52.69, 72.39
α, β, γ (°)	90, 90, 90
Resolution (Å)	50.00-1.58 (1.61-1.58) *
R_{sym}	0.053 (0.494)
Mean I / σI	35.69 (2.97)
Completeness (%)	95.8 (60.4)
Redundancy	6.0 (5.6)
Refinement	
Resolution (Å)	50.00-1.58
Total reflections	148308
Unique reflections	24499 (2329)
R_{work} / R_{free}	0.1807 / 0.2102
No. atoms	1396
Protein	1172
Waters	224
B-factors	33.29
Protein	32.24
Solvent	38.81
Protein Residues	143
R.m.s. deviations	
Bond lengths (Å)	0.005
Bond angles (°)	0.75
Ramachandran statistics	
Favored	99.29%
Allowed	0.71%
Rotamer Outliers	0
Clashscore	5.08
Overall MolProbity	1.27

* Parenthesis indicate data for the highest resolution shell

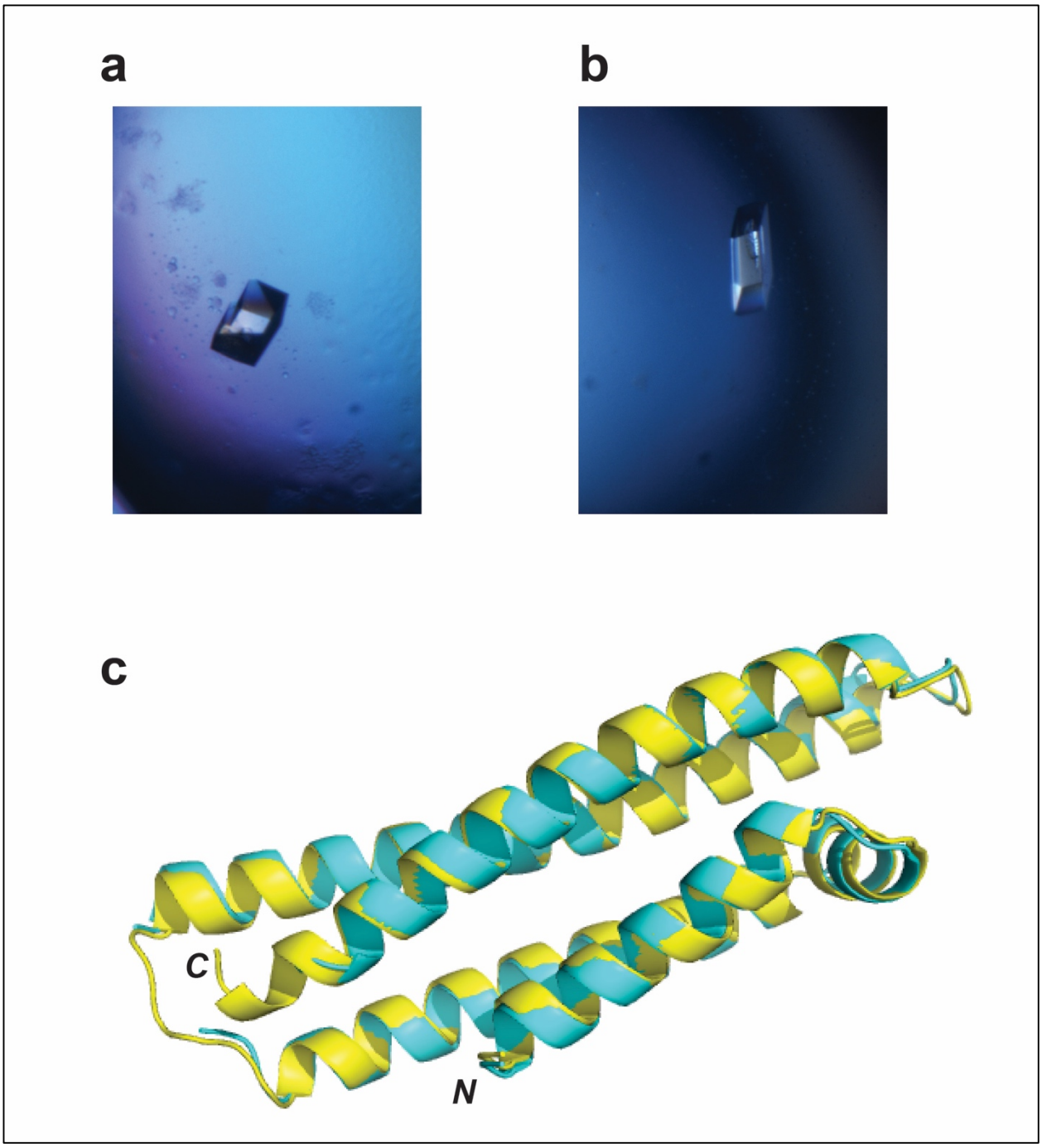

Figure 5.9. Crystal structure of N-terminal ApoE4. **a)** ApoE4 1-238 crystal grown in 10% EPG 3350 and 0.2M KCl. **b)** ApoE4 1-238 crystals grown in 0.1 M HEPES 7.0 and 10% PEG 6000. **c)** Crystal structure from crystal in a) in yellow aligned with 1B68 in cyan. N and C termini are labeled.

5.4.2 Initial attempts to crystallize the TREM2-ApoE complex

In attempt to gain a structural standing of the ApoE-TREM2 interaction, hTREM2 was expressed in mammalian cells and deglycosylated using EndoHf as before. TREM2 and ApoE4-183 were purified separately by SEC and then mixed in equimolar amounts (**Fig 5.10 a**). Small preliminary crystals were obtained after three weeks in one condition (**Fig 5.10b,c**). Unfortunately, these crystals have not been reproduced and their condition is similar to conditions for ApoE alone, so they may very well be the ApoE4 N-terminal bundle

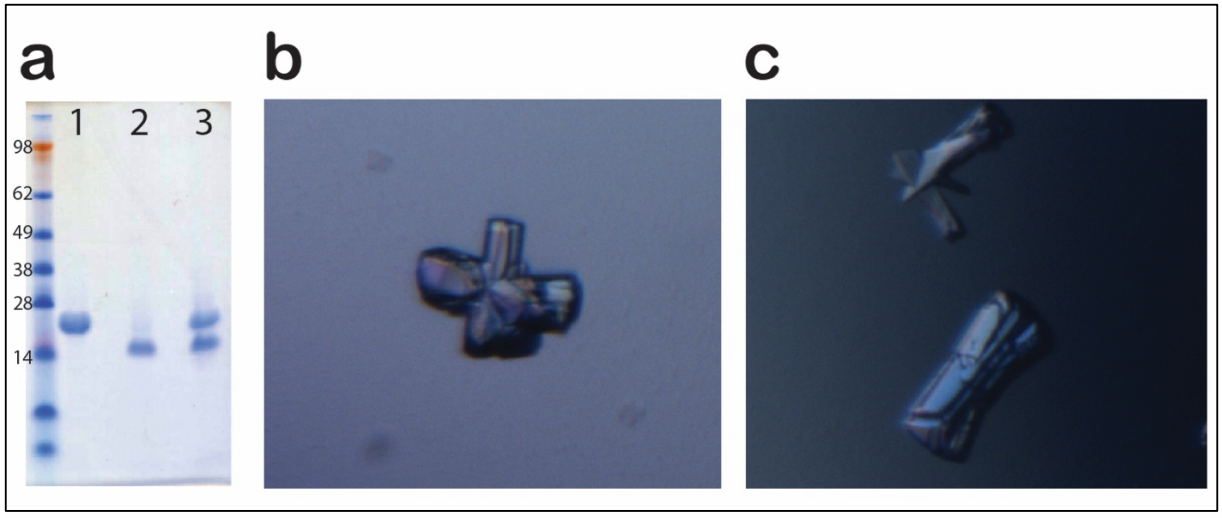

Figure 5.10. Potential crystal hit of TREM2 with ApoE4 1-183. a) SDS-PAGE gel of 1) ApoE4 1-183, 2) hTREM2, and 3) the two protein mixed at equimolar amounts (crystal input). **b-c)** preliminary crystals grown in: 10% PEG 6000 and 0.1 M MES pH 6.0

5.4.3 TREM2 SAXS Experiments

SAXS background

Small angle X-ray scattering (SAXS) is a solution technique which can be used to determine the overall shape and size of a protein. In SAXS experiments, the proteins are randomly tumbling in solution, unlike the uniform array of proteins in a crystal. Therefore, the electron scattering is a rotational average of the protein and buffer scattering. Following buffer subtraction, the scattering from the protein can be transformed and interpreted to understand the protein's behavior (30).

Sample purity and behavior is the ultimate concern with SAXS experiments. Scattering is proportional to the square of the molecular weight of a sample, so higher molecular weight contaminants will disparately affect the scattering. Likewise, protein oligomerization, whether real or artefactual, will contribute disproportionately to the scattering curve. To interpret SAXS data with confidence, one must verify that there are no concentration-dependent changes in the scattering profile. Any interpretation of oligomerization must be verified by an orthogonal method (30). Protein glycosylation is another concern. The TREM2 Ig domain contains two N-linked glycosylation sites. Carbohydrates have higher mean electron density and different hydration than protein (31), so these must be accounted for when modelling an *ab initio* structure and determining the quality of fit to the data.

Sample preparation

TREM2 proteins were purified by NiNTA and SEC. The final purity was assessed by SDS-PAGE and proteins were above 99% purity, with no visible higher molecular weight bands. Samples were concentrated to about 150 μL and buffer matching was accomplished by dialysis

using Hampton microdialysis buttons with a 50 µL sample dialyzed against 50 mL of buffer overnight at 4°C using a 3 kDa MWCO membrane. After recovery, sample concentration was measured by UV_{280}. 30 µL of sample was placed in a 96-well plate and sealed with a silicone sealing mat (both from AXYGEN) for shipment. A dilution series was done using the dialysis buffer. The dialysis buffer was 20 mM HEPES pH 7.5 with 150 mM NaCl and 2% glycerol with 200 mM NDSB-201. Glycerol is used as a scavenger to decrease radiation damage. In our trials, this was found to increase the amount of usable data. NDSB was used in the final sample to try to reduce concentration-dependent aggregation observed in preliminary experiments.

Data collection and processing

Data was collected at the SYBILS beamline at ALS. Samples were exposed at for 10.2 seconds to collect data over 33 frames of 0.3 sec/frame. In this way, the data can be monitored for damage. The wavelength was 11keV/ 1.27 Å. Data was collected at 10° C. Buffer-subtracted data files were provided by the SYBILS staff with a recommendation on frames and which buffer match to use. Data were manually inspected for radiation damage using PRIMUS, part of the ATSAS package. Curves were inspected for consistency and curves that were deemed outliers by the data comparison wizard were rejected for further analysis. After initial analysis, curves were scaled and merged to create a single file for that concentration data set. This was done for each concentration of data collected. Initial data statistics (e.g. Radius of gyration (Rg), and zero-angle scattering I(0)) were determined in PRIMUS and the interatomic distance distribution function P(r), an indirect Fourier transform of the scattering data, was done using autognom. Initial modelling was done using DAMMIF for 10 cycles and this result used as a starting model for further refinement with DAMMIN. Envelopes were visualized in Pymol.

Data interpretation and challenges

Preliminary analysis for WT and R47H proteins was performed by examining the raw data (**Fig 5.11 a,e**), comparing the data scaled by dilution factor (**Fig 5.11 b,f**), scaled Kratky plot ($I*q^2$ vs q) (**Fig 5.11 c,g**), and Guinier regions (**Fig 5.11 d,h**) and by plotting the Rg determined by Guinier fitting against protein concentration (**Fig 5.11i and Table 10**) The Kratky plot confirms that both WT and R47H are folded. However, both have some change in Rg with increasing concentrations, and this is most pronounced in with WT TREM2. These changes are most visible in the low q region of the scaled data sets (**Fig 5.11 b,f**) and the Guinier region (**Fig 5.11 d,h**). Interestingly, at all concentrations, the R47H has a lower Rg than WT. This has been observed in every SAXS experiment conducted. This could be consistent with a conformational change or a more compact protein. Interestingly, WT shows the most pronounced concentration-dependent changes. Whether this is indicative of a native ability to oligomerize or is just a SAXS artifact remains to be determined.

Table 10. Rg statistics determined from Guinier fitting in PRIMUS

Table 10		Rg	Error	Start	End	sRg limits	Fidelity
WT	Low	30.88	2.34	10	44	1.21	0.93
	Medium	32.56	0.56	3	36	1.10	0.98
	High	33.45	1.09	21	38	1.19	0.79
R47H	Low	26.31	6.5	36	58	1.26	0.76
	Medium	26.9	0.29	16	48	1.12	0.9
	High	28.4	0.26	17	43	1.10	0.87

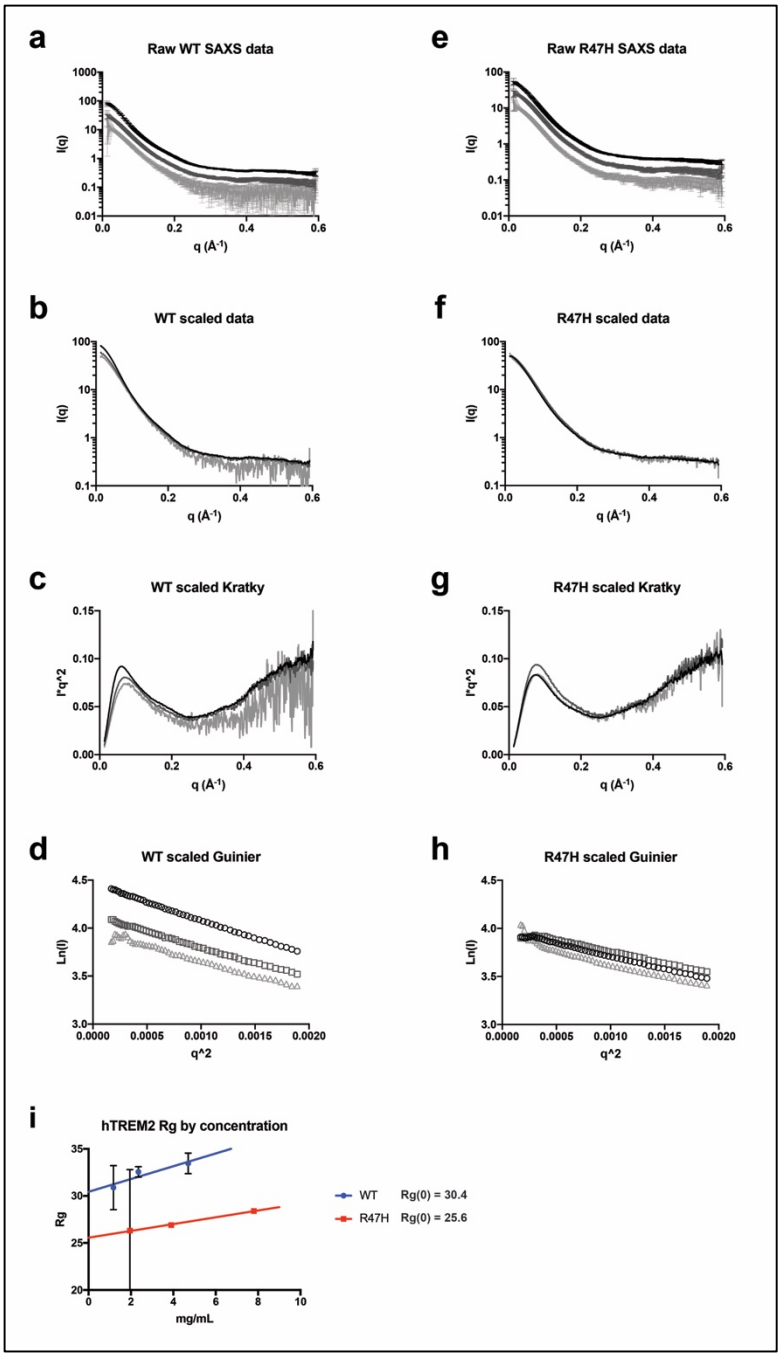

Figure 5.11 Initial SAXS analysis of WT and R47H TREM2 Ig domains. a, e) WT and R47H data at high (black) medium (dark grey) and lowest (light grey) concentrations. b, f) Data scaled by dilution factor. **c,g)** Kratky plot from scaled data. **d,h)** Guinier regions (first 50 data points) scaled by dilution factor. **i)** Rg's determined by Guinier fitting plotted against concentration show that both WT and R47H have concentration-dependent changes, although WT is much more pronounced and has a higher Rg at all concentrations.

5.4.4 Producing lipid-loaded ApoE3

For structural studies, it is important to produce protein that is well-characterized, especially with regards to being aggregate-free. I attempted to reproduce and adapt the protocols described here: (32, 33) to produce ApoE lipidated with 1,2-dipalmitoyl-sn-glycero-3-phosphocholine (DPPC). DPPC at 25 mg/mL in chloroform was purchased from Avanti. Cholate was purchased as a powder from Sigma. DPPC was dried under vacuum and cholate was reconstituted at 30 mg/mL in sizing buffer with 1 mM DTT. I calculated the volume of cholate to be used to resuspend the dried DPPC for a molar ratio of 1.4:1 cholate:DPPC. The mixture was incubated at 42° C to form a clear solution. This was cooled to RT, SEC-purified and concentrated ApoE3 was added so that the final ratio was 46:1 DPPC:ApoE3. This mixture was then placed at 42° C for 1 hr, with gentle mixing every 10 min. In the reference protocols, this is sufficient to get thorough lipidation. The protocols state that the unbound ApoE precipitates. In my hands, I did not observe much precipitation. Following incubation, two rounds of dialysis against sizing buffer with 1mM DTT were performed to remove excess cholate. The samples were then filtered and analyzed on a superpose 6 column (GE) at RT. As a control, ApoE that was not lipidated was run on the same column (**Fig 5.12 a**).

There is a slight shift towards a later retention time. In the references, it is suggested that the lipidated ApoE has two ApoE molecules per lipoparticle. The dimer plus phospholipids likely runs similarly to the tetramer created by the unlipidated protein. Therefore, SEC does not seem to be very efficient at separating lipidated and unlipidated particles. A PC detection kit (Sigma, MAK049) was used to confirm the presence of phosphotidylcholine. This assay works by hydrolizing the choline from the lipid and detecting the choline fluorometrically. The assay was conducted according to the manufacturer's specifications. Background was determined with

a no-enzyme negative control for each sample. The lipidated ApoE3 gave a strong signal, while unlipidated ApoE3 was at background level (**Fig. 5.12c).** This suggests the protein was indeed lipidated and could be used in SAXS or other structural studies. Another important experiment will be to complex ApoE3 with DPPC and DPPS to see how the lipid species influences TREM2 binding. Finally, limited proteolysis was performed to see if lipidation induced differential protection. Unlipidated ApoE3 had a slightly altered cleavage pattern with chymotrypsin (**Fig 5.12b**). This experiment should be repeated with Thrombin, as ApoE is supposed to be protected from thrombin cleavage when lipidated.

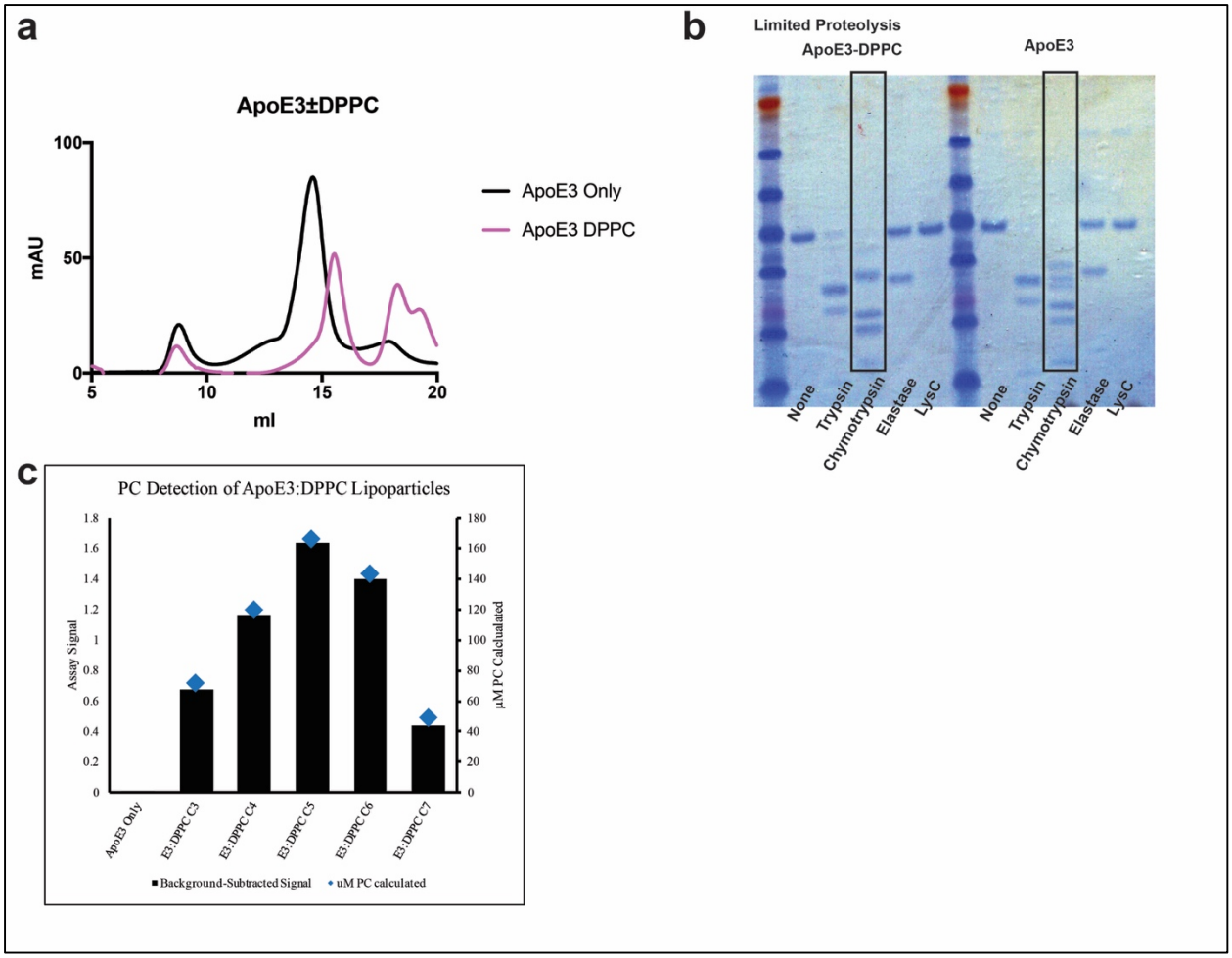

Figure 5.12. Producing lipidated ApoE3. **a)** SEC profiles of unloaded, tetrameric ApoE3 and DPPC-complexed ApoE3 analyzed by SEC on a superpose 6 column. **b)** Limited proteolysis on ApoE samples shows differential cleavage with chymotrypsin, suggesting a conformational change. **c)** Results of colormetric PC detection assay. ApoE3 complexed with DPPC had a strong signal above background that correlated with UV signature, while ApoE3 alone had no signal above background.

5.5 Generation and characterization of anti-TREM2 mAbs

To generate monoclonal anti-TREM2 antibodies, I worked with the Hybridoma center at Washington University to immunize hamsters and screen antibody clones. Two animals were immunized with human and mouse TREM2 protein expressed from 293F cells. The proteins were exchanged into PBS for immunizations. To verify an antibody response, an ELISA assay was developed. The plate was coated overnight with 100 µL of 1 µg/mL Neutravidin. In the morning, the plate was washed twice with 250 µL of PBS with 0.05% Tween-20. Wells were blocked with 100 µL of 1% BSA in PBS for 1 hr at RT. Then, 100 µL of biotinylated TREM2 was added at a 1:1000 dilution. TREM2 was captured for 30 min at RT, then washed. Wells were then exposed to 100 µL of diluted serum overnight at 4° C. The next day, unbound antibodies were washed 2x with wash buffer, and an anti-hamster-HRP secondary (Santa Cruz) was added at 1:2000 for two hours at RT. Finally, the secondary was washed and the plate developed with a chromogenic substrate (TMB peroxidase) and read on a plate reader. Immunization was considered successful when it produced a response at a serum dilution of 10^5. After validating the antibody response, the animal was sacrificed, and the splenic B cells were fused with mouse lymphoma cells to create hybridoma fusions. The cells were serially plated to isolate clonal populations to be expanded and screened for antibody responses.

With the first animal, I tried to screen antibodies by flow cytometry for cell-surface expression. This ultimately was not useful, perhaps due to the somewhat weak surface expression on 293F cells. I was able to get some clones identified and subcloned, but the final products had no reactivity. The early pooled samples of this process are saved with the hybridoma center and could be restarted if desired. For the second animal, I screened the clones by ELISA. This was very robust and strongly reactive monoclonals were generated by three

rounds of serial dilution. The final clones were amplified and stocks frozen down. Conditioned media from these clones was used in validation assays shown in **Figure 5.13**.

5.5.1 Validating monoclonal antibodies by ELISA

Human and mouse TREM2 were immobilized as described above and exposed to conditioned media from the hamster monoclonals. The signal is shown in **Fig 5.13a**. All clones were reactive against hTREM2, which is the format in which they were screened. All but two of the clones were reactive against mTREM2. These experiments were done on separate days, so the level of reactivity of human vs mouse should not be directly compared. This assay shows that most of the clones detect both human and mouse TREM2, and that two are selective for human over mouse protein.

5.5.2 Validating monoclonal antibodies by BLI

The media supernatants were also evaluated for binding to hTREM2 in BLI format. This was done at multiple dilutions of serum, and the value for 1:4 is shown. TREM2 on pins was dipped into conditioned or unconditioned media for 5 min. The response signal is shown in **Fig 5.13b**. All the antibodies tested had reactivity to hTREM2 above the unconditioned background. Note that in these assays, the antibodies are not purified, so the differences in signal could reflect different affinity, but most likely reflect different antibody concentrations. All antibody interactions had very little dissociation, indicating a high-affinity, stable interaction.

5.5.3 Validating monoclonal antibodies by cell staining

Finally, antibodies were screened for binding to hTREM2-transfected 293F cells. As a control, binding was compared to BST-2 transfected cells (unrelated protein). Four antibodies had binding in this format (**Fig 5.13c**).

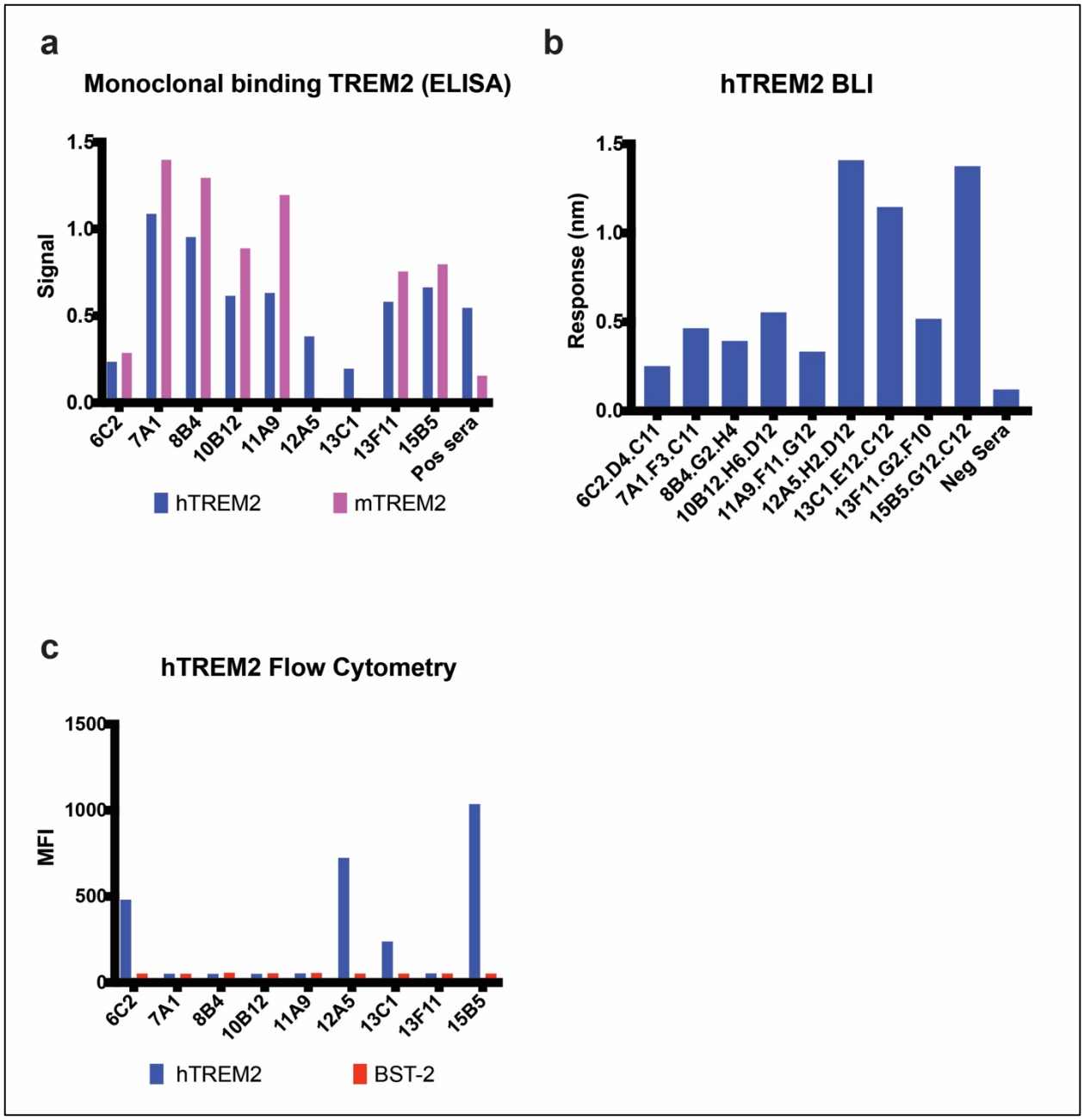

Figure 5.13 Validation of mAb TREM2 binding in different assays. a) Monoclonals binding to plated mTREM2 or hTREM2 by ELISA – note, values for hTREM2 and mTREM2 are from separate experiments. All monoclonals bound TREM2, two did not bind mTREM2. **b)** BLI response with immobilized hTREM2 dipped into wells with hybridoma-conditioned media diluted 1:4. All cultures had binding to hTREM2. **c)** MFI values for cell binding by flow cytometry. 293F cells transfected with TREM2 or BST2 (negative control). Binding observed for four monoclonals. Full clone name given in **b**, parent line names in **a** and **c**.

5.5.4 Novel antibodies block TREM2-ApoE interaction

To assess whether antibodies blocked TREM2-ApoE binding, an initial BLI experiment was performed where TREM2 was immobilized on a streptavidin pin and dipped into wells containing unconditioned hybridoma media or media conditioned with anti-TREM2 monoclonals. These were allowed to bind TREM2, which was then washed and dipped into wells containing ApoE4 1-183 (this protein had been purified for crystal trays at the time). **Figure 5.14** shows the antibody loading normalized to the highest value and the steady-state response for TREM2 into ApoE4 1-183 averaged over the last five seconds of the association stage. This experiment needs to be optimized by measuring binding to full-length ApoE, and also by increasing the antibody loading (either longer times, lower dilution of supernatant, or purified and concentration-matched monoclonals). With these caveats, the initial data suggests certain antibodies do block ApoE binding (**Fig 5.14**). Notably, the antibody with the highest loading also allowed the most ApoE binding, while other antibodies with less loading more effectively blocked ApoE binding. These tools may be useful in epitope-mapping by co-crystallization or HDX experiments with Fab fragments if an ApoE-TREM2 complex is not readily attained.

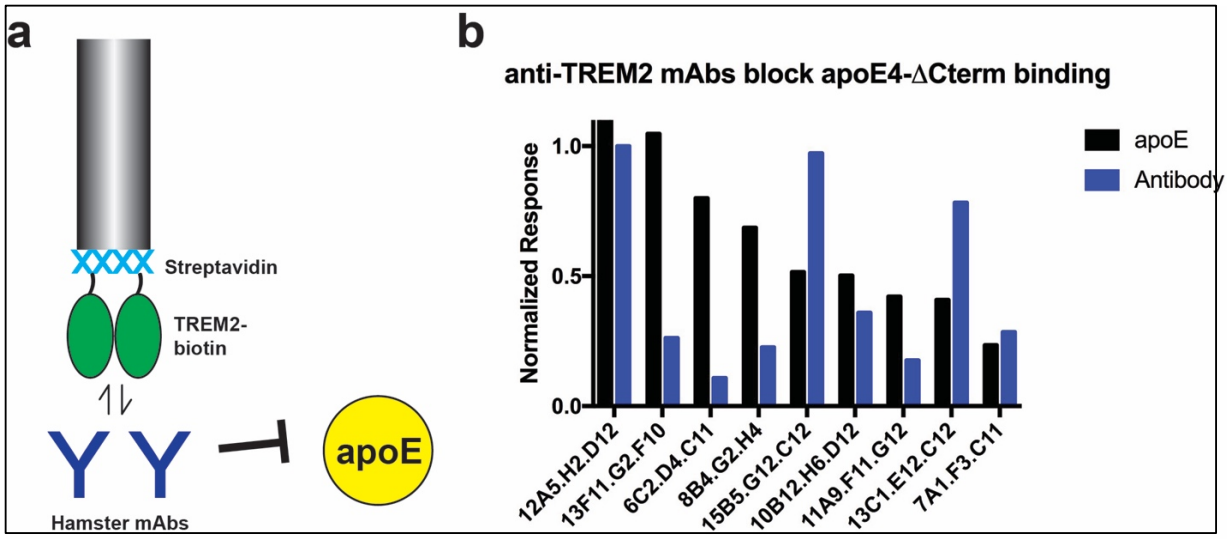

Figure 5.14 Novel anti-TREM2 antibodies block ApoE binding. a) Schematic for experiment and **b)** Antibody response normalized to the highest binder and ApoE response normalized to TREM2 dipped into unconditioned media instead of antibodies. Note that 7A1 and 11A9 block ApoE binding while having less loading than 12A5, which no reduction in ApoE binding.

5.6 References:

1. Liu C-C, Kanekiyo T, Xu H, Bu G. Apolipoprotein E and Alzheimer disease: risk, mechanisms and therapy. Nat Rev Neurol. 2013;9(2):106-18.
2. Mahley RW, Weisgraber KH, Huang Y. Apolipoprotein E: structure determines function, from atherosclerosis to Alzheimer's disease to AIDS. J Lipid Res. 2009;50 Suppl:S183-8. doi: 10.1194/jlr.R800069-JLR200. PubMed PMID: 19106071; PMCID: PMC2674716.
3. Terwel D, Steffensen KR, Verghese PB, Kummer MP, Gustafsson JA, Holtzman DM, Heneka MT. Critical role of astroglial apolipoprotein E and liver X receptor-alpha expression for microglial Abeta phagocytosis. J Neurosci. 2011;31(19):7049-59. doi: 10.1523/JNEUROSCI.6546-10.2011. PubMed PMID: 21562267.
4. Atagi Y, Liu CC, Painter MM, Chen XF, Verbeeck C, Zheng H, Li X, Rademakers R, Kang SS, Xu H, Younkin S, Das P, Fryer JD, Bu G. Apolipoprotein E Is a Ligand for Triggering Receptor Expressed on Myeloid Cells 2 (TREM2). J Biol Chem. 2015;290(43):26043-50. doi: 10.1074/jbc.M115.679043. PubMed PMID: 26374899; PMCID: PMC4646257.
5. Bailey CC, DeVaux LB, Farzan M. The Triggering Receptor Expressed on Myeloid Cells 2 Binds Apolipoprotein E. J Biol Chem. 2015;290(43):26033-42. doi: 10.1074/jbc.M115.677286. PubMed PMID: 26374897; PMCID: PMC4646256.
6. Yeh FL, Wang Y, Tom I, Gonzalez LC, Sheng M. TREM2 Binds to Apolipoproteins, Including APOE and CLU/APOJ, and Thereby Facilitates Uptake of Amyloid-Beta by Microglia. Neuron. 2016;91(2):328-40. doi: 10.1016/j.neuron.2016.06.015. PubMed PMID: 27477018.
7. Musiek ES, Holtzman DM. Three dimensions of the amyloid hypothesis: time, space and 'wingmen'. Nature neuroscience. 2015;18(6):800-6. doi: 10.1038/nn.4018. PubMed PMID: 26007213; PMCID: PMC4445458.
8. Jarosz-Griffiths HH, Noble E, Rushworth JV, Hooper NM. Amyloid-β Receptors: The Good, the Bad, and the Prion Protein. Journal of Biological Chemistry. 2016;291(7):3174-83. doi: 10.1074/jbc.R115.702704.
9. Holtzman DM, Herz J, Bu G. Apolipoprotein E and Apolipoprotein E Receptors: Normal Biology and Roles in Alzheimer Disease. Cold Spring Harbor perspectives in medicine. 2012;2(3). doi: 10.1101/cshperspect.a006312.
10. Wernette-Hammond ME, Lauer SJ, Corsini A, Walker D, Taylor JM, Rall SC. Glycosylation of human apolipoprotein E. The carbohydrate attachment site is threonine 194. Journal of Biological Chemistry. 1989;264(15):9094-101.
11. Pitas RE, Boyles JK, Lee SH, Foss D, Mahley RW. Astrocytes synthesize apolipoprotein E and metabolize apolipoprotein E-containing lipoproteins. Biochimica et Biophysica Acta (BBA) - Lipids and Lipid Metabolism. 1987;917(1):148-61. doi: http://dx.doi.org/10.1016/0005-2760(87)90295-5.
12. Dong LM, Parkin S, Trakhanov SD, Rupp B, Simmons T, Arnold KS, Newhouse YM, Innerarity TL, Weisgraber KH. Novel mechanism for defective receptor binding of apolipoprotein E2 in type III hyperlipoproteinemia. Nat Struct Biol. 1996;3(8):718-22. PubMed PMID: 8756331.
13. Wilson C, Mau T, Weisgraber KH, Wardell MR, Mahley RW, Agard DA. Salt bridge relay triggers defective LDL receptor binding by a mutant apolipoprotein. Structure. 1994;2(8):713-8. PubMed PMID: 7994571.

14. Dong J, Peters-Libeu CA, Weisgraber KH, Segelke BW, Rupp B, Capila I, Hernaiz MJ, LeBrun LA, Linhardt RJ. Interaction of the N-terminal domain of apolipoprotein E4 with heparin. Biochemistry. 2001;40(9):2826-34. PubMed PMID: 11258893.
15. Wilson C, Wardell M, Weisgraber K, Mahley R, Agard D. Three-dimensional structure of the LDL receptor-binding domain of human apolipoprotein E. Science. 1991;252(5014):1817-22. doi: 10.1126/science.2063194.
16. Dong LM, Wilson C, Wardell MR, Simmons T, Mahley RW, Weisgraber KH, Agard DA. Human apolipoprotein E. Role of arginine 61 in mediating the lipoprotein preferences of the E3 and E4 isoforms. Journal of Biological Chemistry. 1994;269(35):22358-65.
17. Segelke BW, Forstner M, Knapp M, Trakhanov SD, Parkin S, Newhouse YM, Bellamy HD, Weisgraber KH, Rupp B. Conformational flexibility in the apolipoprotein E amino-terminal domain structure determined from three new crystal forms: Implications for lipid binding. Protein Science. 2000;9(5):886-97. doi: 10.1110/ps.9.5.886.
18. Chen J, Li Q, Wang J. Topology of human apolipoprotein E3 uniquely regulates its diverse biological functions. Proceedings of the National Academy of Sciences. 2011;108(36):14813-8. doi: 10.1073/pnas.1106420108.
19. Frieden C, Garai K. Concerning the structure of apoE. Protein Science. 2013;22(12):1820-5. doi: 10.1002/pro.2379.
20. Garai K, Mustafi SM, Baban B, Frieden C. Structural differences between apolipoprotein E3 and E4 as measured by (19)F NMR. Protein Sci. 2010;19(1):66-74. doi: 10.1002/pro.283. PubMed PMID: 19904741; PMCID: PMC2817840.
21. Newhouse Y, Weisgraber KH. Apolipoprotein E Expression and Purification. In: Roberson ED, editor. Alzheimer's Disease and Frontotemporal Dementia: Methods and Protocols. Totowa, NJ: Humana Press; 2011. p. 127-40.
22. Frieden C. ApoE: the role of conserved residues in defining function. Protein Sci. 2015;24(1):138-44. doi: 10.1002/pro.2597. PubMed PMID: 25377861; PMCID: PMC4282419.
23. Wang Y, Cella M, Mallinson K, Ulrich JD, Young KL, Robinette ML, Gilfillan S, Krishnan GM, Sudhakar S, Zinselmeyer BH, Holtzman DM, Cirrito JR, Colonna M. TREM2 lipid sensing sustains the microglial response in an Alzheimer's disease model. Cell. 2015;160(6):1061-71. doi: 10.1016/j.cell.2015.01.049. PubMed PMID: 25728668; PMCID: PMC4477963.
24. Yuan P, Condello C, Keene CD, Wang Y, Bird TD, Paul SM, Luo W, Colonna M, Baddeley D, Grutzendler J. TREM2 Haplodeficiency in Mice and Humans Impairs the Microglia Barrier Function Leading to Decreased Amyloid Compaction and Severe Axonal Dystrophy. Neuron. 2016;90(4):724-39. doi: 10.1016/j.neuron.2016.05.003. PubMed PMID: 27196974; PMCID: PMC4898967.
25. Haass C, Kaether C, Thinakaran G, Sisodia S. Trafficking and Proteolytic Processing of APP. Cold Spring Harbor perspectives in medicine. 2012;2(5). doi: 10.1101/cshperspect.a006270.
26. Kumar DKV, Choi SH, Washicosky KJ, Eimer WA, Tucker S, Ghofrani J, Lefkowitz A, McColl G, Goldstein LE, Tanzi RE, Moir RD. Amyloid-β peptide protects against microbial infection in mouse and worm models of Alzheimer’s disease. Science Translational Medicine. 2016;8(340):340ra72-ra72. doi: 10.1126/scitranslmed.aaf1059.
27. Spitzer P, Condic M, Herrmann M, Oberstein TJ, Scharin-Mehlmann M, Gilbert DF, Friedrich O, Grömer T, Kornhuber J, Lang R, Maler JM. Amyloidogenic amyloid-β-peptide

variants induce microbial agglutination and exert antimicrobial activity. Scientific Reports. 2016;6:32228. doi: 10.1038/srep32228.
28. Zhang L, Yu H, Song C, Lin X, Chen B, Tan C, Cao G, Wang Z. Expression, purification, and characterization of recombinant human β-amyloid42 peptide in Escherichia coli. Protein Expression and Purification. 2009;64(1):55-62. doi: http://dx.doi.org/10.1016/j.pep.2008.10.007.
29. Dong J, Peters-Libeu CA, Weisgraber KH, Segelke BW, Rupp B, Capila I, Hernáiz MJ, LeBrun LA, Linhardt RJ. Interaction of the N-Terminal Domain of Apolipoprotein E4 with Heparin. Biochemistry. 2001;40(9):2826-34. doi: 10.1021/bi002417n.
30. Jacques DA, Trewhella J. Small-angle scattering for structural biology--expanding the frontier while avoiding the pitfalls. Protein Sci. 2010;19(4):642-57. doi: 10.1002/pro.351. PubMed PMID: 20120026; PMCID: PMC2867006.
31. Guttman M, Weinkam P, Sali A, Lee Kelly K. All-Atom Ensemble Modeling to Analyze Small-Angle X-Ray Scattering of Glycosylated Proteins. Structure. 2013;21(3):321-31. doi: http://dx.doi.org/10.1016/j.str.2013.02.004.
32. Peters-Libeu CA, Newhouse Y, Hall SC, Witkowska HE, Weisgraber KH. Apolipoprotein E*dipalmitoylphosphatidylcholine particles are ellipsoidal in solution. J Lipid Res. 2007;48(5):1035-44. doi: 10.1194/jlr.M600545-JLR200. PubMed PMID: 17308333.
33. Newhouse Y, Peters-Libeu C, Weisgraber KH. Crystallization and preliminary X-ray diffraction analysis of apolipoprotein E-containing lipoprotein particles. Acta Crystallogr Sect F Struct Biol Cryst Commun. 2005;61(Pt 11):981-4. doi: 10.1107/S1744309105032410. PubMed PMID: 16511213; PMCID: PMC1978127.

Chapter 6: Implications for TREM2 in health and disease

6.1 TREM2 functions in health and disease

This section is modified from a submitted manuscript titled "TREM2-ligand interactions in health and disease." Submitted to J. Mol Biol.

TREM2 is an immunomodulatory protein expressed on myeloid cells including microglia in the brain. Genetic studies have conclusively linked TREM2 to neurodegenerative disease and animal and cellular studies have revealed a role for TREM2 in a broad array of functions including cell survival, proliferation, activation, inflammation, and phagocytosis (1). Exactly how TREM2 functions is still not fully known, and this depends on understanding the TREM2 structure how TREM2 interacts with its ligands. The goal of this study was to help fill the gap between genetic studies that identified specific, important residues on TREM2 and the animal/cellular studies that identified the roles for TREM2. By understanding the TREM2 structure and how the different variants alter structure and function, this work further elucidates the mechanisms underpinning TREM2 in health and disease. In the first section of this chapter, I describe the different reported TREM2 functions and discuss how they could be associated with different ligands or modes of signaling. In the subsequent sections, I highlight the contributions from this study and propose a model for TREM2 function before finally suggesting future and translational directions for this work.

The reported ligands for TREM2 are broad and include ligands that could be thought to represent steady-state tonic stimuli or disease-specific stimuli. Therefore, the functions of

TREM2 signaling could range from specific responses such as phagocytosis, cell activation, or collaboration with other signaling pathways to maintain cell survival and proliferation (**Fig 6.1**). These possibilities are not mutually exclusive; on the contrary, it may be useful to conceptualize the different ligands as either tonic, homeostatic signals or damage-associated signals which produce different kinds or strengths of stimuli in order to accomplish the wide variety of functions reported for TREM2. Here, I propose where different ligands could contribute to TREM2 function. This model provides a framework to interpret the results of this study.

TREM2 functions from endogenous signals maintain myeloid cell homeostasis, regulate inflammation, and enable phagocytosis.

During development and homeostatic conditions, TREM2 is important for myeloid cell survival, proliferation, and maturation. TREM2 signals ensure myeloid cells remain ready and competent to respond to damage and disease.

1. **TREM2 responds to tonic stimuli as a receptor and/or co-receptor for myeloid survival and maturation so that myeloid cells can respond to disease stimuli.**

This is an attractive, but still unknown mechanism where TREM2 signaling sustains myeloid cell survival and proliferation in order that the myeloid cells can respond to other stimuli in a condition-specific manner. One possible mechanism is a role for TREM2 in β-catenin activation (2), which probably involves interactions with M-CSF signals (3). Another possibility is TREM2 is not engaging an activating ligand, but is preferentially associating with DAP12 to localize it at the cell surface where it can phosphorylated by Src or other kinases activated by CSF-1R or other survival pathways (4) **(Fig 6.1A).**

2. **TREM2 signals are important for myeloid cell maturation**

Studies using human monocytes from NHD patients with mutations in TREM2 observed decreased capacity to mature into osteoclasts and DCs (5, 6). Similar to collaboration with M-CSF, TREM2 connects Plexin-A1 to DAP12 for osteoclastogenesis. Plexin-A1$^{-/-}$ mice have defects in DC antigen presentation and OC maturation (7), similar to what had been reported for DAP12$^{-/-}$ mice (8). Therefore, TREM2 plays a role in the ability of myeloid cells to mature following stimulation by cytokines **(Fig 6.1B).**

3. TREM2 responds to tonic stimuli to regulate inflammation.

TREM2 and DAP12 reduce inflammatory TLR signals (9, 10) in cultured BMDMs. This role did not require stimulation with an exogenous ligand, suggesting it is mediated by a ligand on the BMDMs or perhaps from the culture media. This function likely also involves co-regulation of adaptor proteins that dampen TLR signaling such as LAB and DOK3 **(Fig 6.1C).**

Which ligands could be important for these functions? Many of these *in vitro* results did not require antibody stimulation of TREM2, suggesting a ligand present on the myeloid cells or readily available in culture. Phospholipids, proteoglycans, or lipoproteins make attractive candidates as these ligands would be ubiquitous. For example, APOE is highly abundant in serum and CSF, with concentrations in the μg/mL range (11). However, because these ligands are so ubiquitous, understanding how signaling could be regulated is a challenge.

TREM2 functions during disease

In addition to its role as a tonic receptor, TREM2 recognizes a variety of ligands associated with damage, disease, and infection. These ligands may mimic tonic stimuli or instead may produce an activating signal above the tonic threshold.

1. **TREM2 responds to damage stimuli to drive survival and activation of myeloid cells.**

During disease, TREM2 responds to DAMPs such as ligands exposed on apoptotic membranes (12), myelin lipids (13), DNA exposed by necrotic cells (14), ligands presented by Aβ plaques, or perhaps lipoparticles enriched in apoptotic phospholipids (15). TREM2 stimulation by these ligands could be important for TREM2 function under the additional stress from damage. In this scenario, TREM2 signaling licenses the response to pathogens and other damage. This cellular activation program can take a number of forms including sustaining cell survival, regulating cytokine production, and/or permitting phagocytosis by other receptor pathways. For example, TREM2 was required for full phagocytic capacity of antibody-Aβ beta complexes (which are recognized by FcR for phagocytosis), showing TREM2 enables the phagocytic functions of other receptors (16). TREM2 inhibits inflammatory cytokine production in cultured microglia following exposure to apoptotic neurons (17), and *Trem2*-deficient and haploinsufficient microglia have impaired microgliosis and don't properly respond to plaques (15, 18-21) **(Fig 6.1D).**

2. **TREM2 directly binds DAMPs/PAMPs for phagocytosis**

While the primary role of TREM2 may not be phagocytosis, there have been reports of TREM2-mediated phagocytosis of a direct ligand, including phagocytosis of apoptotic neurons that express a TREM2 ligand (12, 17, 22), and bacteria (23) likely through recognition of anionic bacterial components (24). These examples did not require TREM2 stimulation by antibodies or separate ligands. Instead, cross-linking by bacterial carbohydrates or apoptotic membrane-exposed ligands activate TREM2 signaling, resulting in microtubule mobilization and phagocytosis **(Fig 6.1 E).**

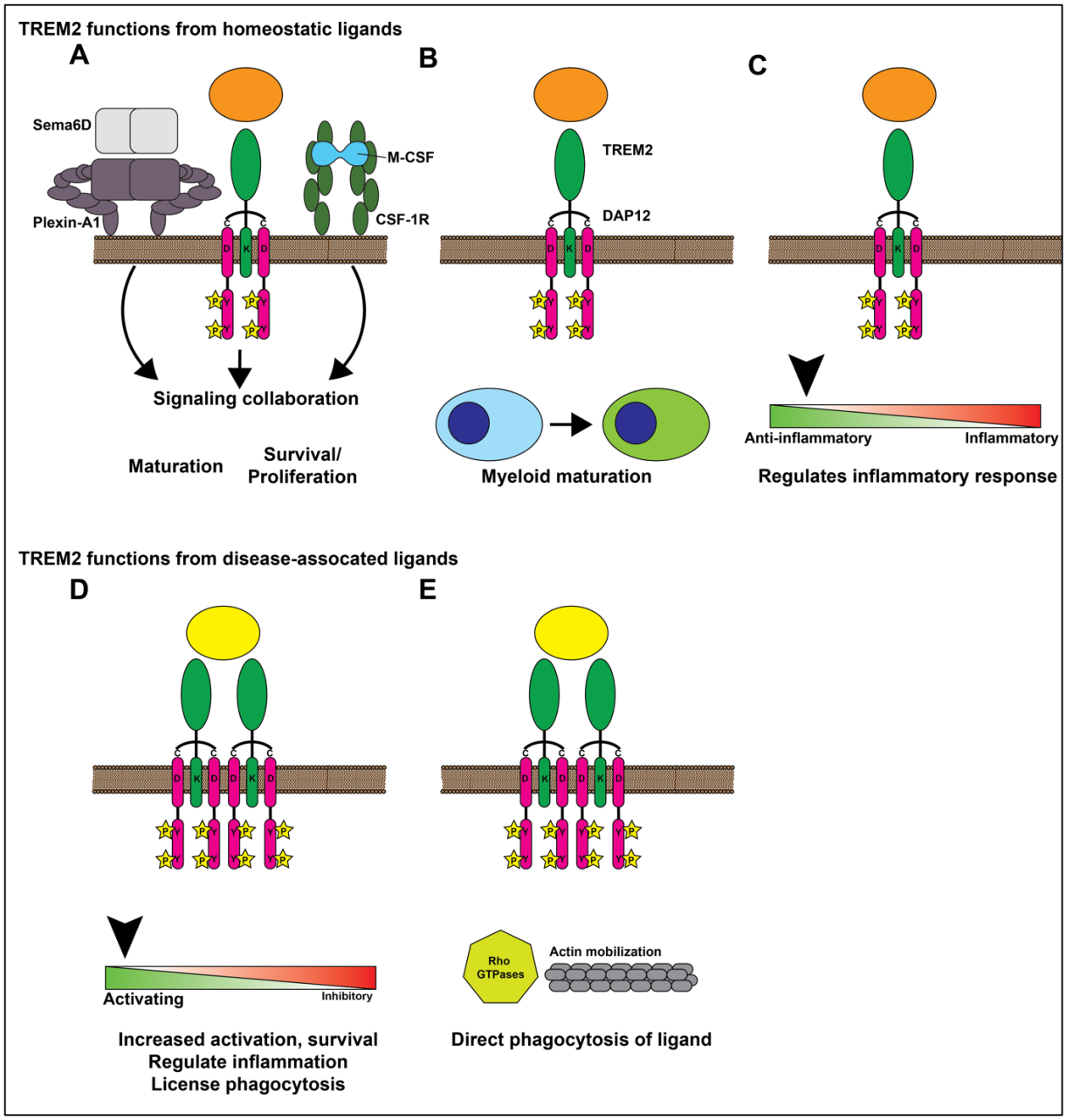

Figure 6.1. Possible roles for TREM2 resulting from different ligands. A-C) During normal conditions, TREM2 signaling from endogenous ligands permits a number of functions. **A)** TREM2 is a co-receptor or co-stimulatory molecule for signaling pathways involved in myeloid maturation, proliferation, and survival. **B)** TREM2 signals (perhaps independently of co-receptors) are important for maturation. **C)** TREM2 regulates inflammatory responses by influencing TLR and other activating networks to maintain homeostasis. D-E) TREM2 recognizes additional ligands associated with disease. **D)** These signals may increase activation and survival so that myeloid cells can respond in a context-dependent manner. **E)** TREM2 can induce phagocytosis of certain ligands, such as bacteria. **Figure 6.1 is modified from Kober and Brett 2017, submitted.**

6.2 Contributions from this study

The goal of this study was to determine the structure of TREM2, elucidate how disease-linked residues altered its structure and function, and to understand how TREM2 might engage with ligands. Genetic studies had identified key residues, and *in vitro* and *in vivo* studies identified a role for TREM2 signaling in cell survival and various activities. However, a structure-based model for TREM2 that connected TREM2-ligand interactions with the different observed functions was missing. This study addressed that knowledge gap and contributed to the understanding of TREM2 in five main areas:

1. **Determined the WT TREM2 structure**

The structure of WT hTREM2 was determined using protein expressed natively in mammalian cells. This protein was purified and crystallized using methods developed during this study. TREM2 is the only TREM family protein so far that has required mammalian expression to crystallize, suggesting post-translational modifications such as glycosylations are important for stability and should be carefully considered in future studies.

2. **Showed the NHD variants are misfolded, while the AD-risk variants are intact**

The structure revealed the location of residues linked to disease. The NHD-causative variants are buried in the protein core. These mutations cause protein misfolding and impair the expression of folded protein. However, these proteins may still reach the cell-surface in an unfolded state. In contrast, the AD-linked variants do not grossly alter structure or stability and are robustly detected by conformation-sensitive antibodies. However, there are subtle, measurable effects, particularly for the R47H variant. This variant uniquely has an altered CD signature, which could indicate a conformational change.

3. **Showed TREM2 binds a cell-surface proteoglycan-dependent ligand**

Despite reports that the R47H variant has impaired signaling in response to phospholipids (13, 15), I was not able to convincingly identify loss of phospholipid binding by disease variants. Indeed, direct binding to liposomes confirmed that R47H can bind phospholipids with similar kinetics as WT. Additionally, a separate study found TREM2 did not stain apoptotic Jurkat cells presenting PS on their outer membrane (25). Together, these findings show that while phospholipids may be part of a stimulatory complex recognized by TREM2, they are insufficient to be the complete TREM2 ligand and do not explain the effect of AD variants. Instead, the surface variants were found to alter binding to a cell surface ligand that was ablated with proteases or heparinases. WT TREM2 can directly bind heparin, and preliminary experiments showed that depleting GAG sulfates impaired signaling and altered surface localization, suggesting this ligand acts with TREM2 *in cis,* perhaps as a tonic ligand or to mediate signaling.

4. Disease variants map a functional ligand-binding surface

R47 and R62 are part of a basic patch that is involved in the recognition of anionic proteoglycans and other ligands such as ApoE and Aβ. T96K, another surface variant with unclear disease risk extends this basic surface. This surface is not observed on the other TREM family proteins and is unique to TREM2. Structure-guided mutations to this surface also resulted in loss of binding, confirming that it is a functional surface used to recognize ligands.

5. TREM2 binds ApoE and Aβ

TREM2 binds to ApoE and this interaction does not require ApoE lipidation. Full-affinity binding does require the hinge region of ApoE, and this is the first time this region has been

shown to be involved in a protein-protein interaction. The AD-risk residue R47H and basic patch mutations disrupt binding. TREM2 also binds Aβ and binding is impaired by the R47H variant. These findings suggest a physiological role for TREM2 in interacting with these important AD proteins.

These results explain how mutations within the same domain produce different diseases. The proposed effect of disease variants on TREM2 function is shown in **Figure 6.2**. AD variants have reduced function through decreased ligand binding, but are folded and likely retain some basal level function. These variants are typically heterozygotes. The NHD variants result in complete loss of function and produce a fatal disease when homozygous. These variants are extremely rare, however, it would be consistent with this model that heterozygote NHD variants increase AD risk.

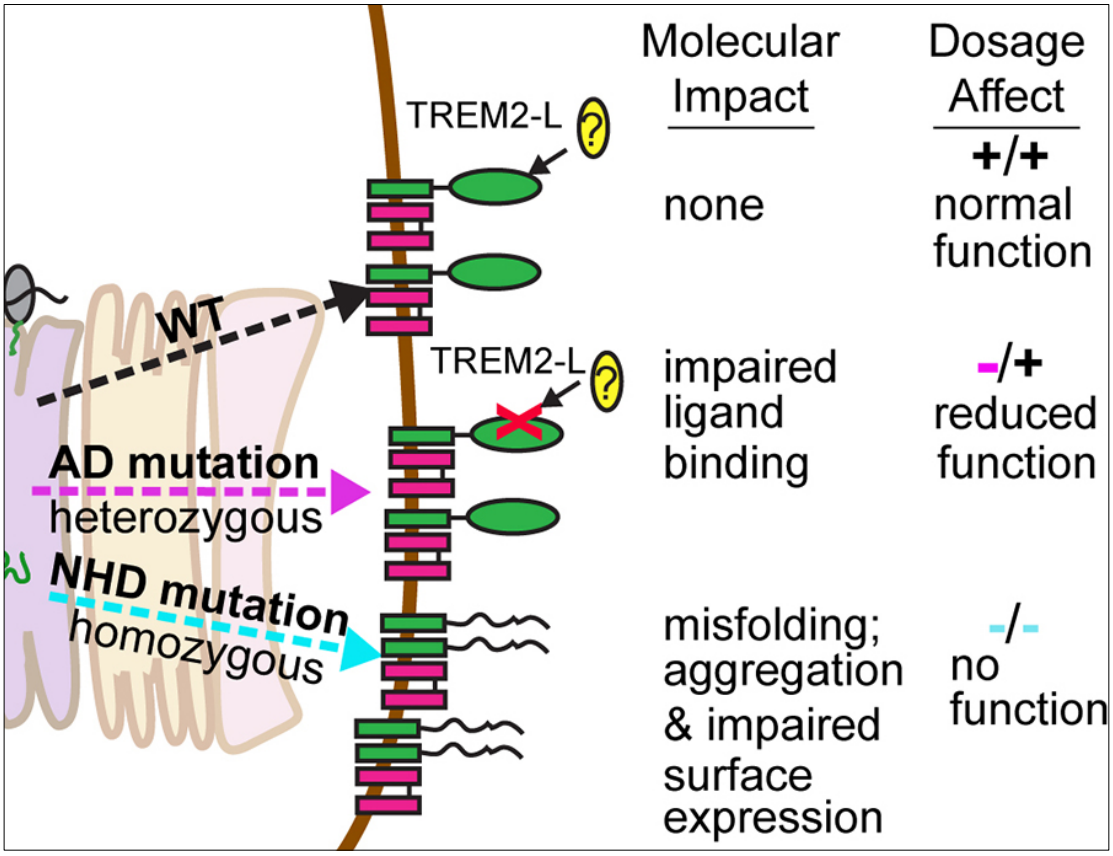

Figure 6.2 Proposed model for impact of disease mutations on TREM2 function. WT protein is surface expressed and engages with its ligand for signaling. AD variants, which are typically heterozygous, result in decreased signaling through impaired ligand recognition. NHD variants have been identified in homozygous cases and result in complete loss of function.

Figure 6.2 is modified from Kober et al, 2016 (26)

6.3 Proposed model for TREM2 function

The data produced in this study suggest that TREM2 interacts with heparan sulfate proteoglycans on the surface of myeloid cells. During resting conditions, these may represent a tonic ligand to control inflammation or maintain homeostasis. Additionally, GAGs may be required to orient, position, or cluster TREM2 on the surface to engage with activating ligands. These ligands may be phospholipids, ApoE, Aβ, or some as-of-yet unknown ligand. These ligands could interact with TREM2 separately from GAGs (as may be the case with phospholipids) or could compete with GAGs through a hand-off mechanism. In this scenario, the AD-disease mutations would result in loss of function because they would have decreased interactions with GAGs and perhaps additionally decreased interactions with stimulating ligands. Indeed, it may not be necessary for the variants to have complete loss of binding. A partial deficiency in binding to GAGs, phospholipids, or ApoE ect… would be compounded at each stage so that the end result is loss of signaling, as was observed for the R47H variant responding to plated phospholipids (15). This putative mechanism is depicted in **Fig 6.3.** Such a pathway would not be without precedent. GAG-protein interactions have been implicated in signaling with TLR (27), chemokine (28), and acetylcholine receptors (29). It is also possible that HS proteoglycans mediate attachment of sTREM2 to interact with a proteinaceous receptor on the cell surface or after HS-mediated internalization.

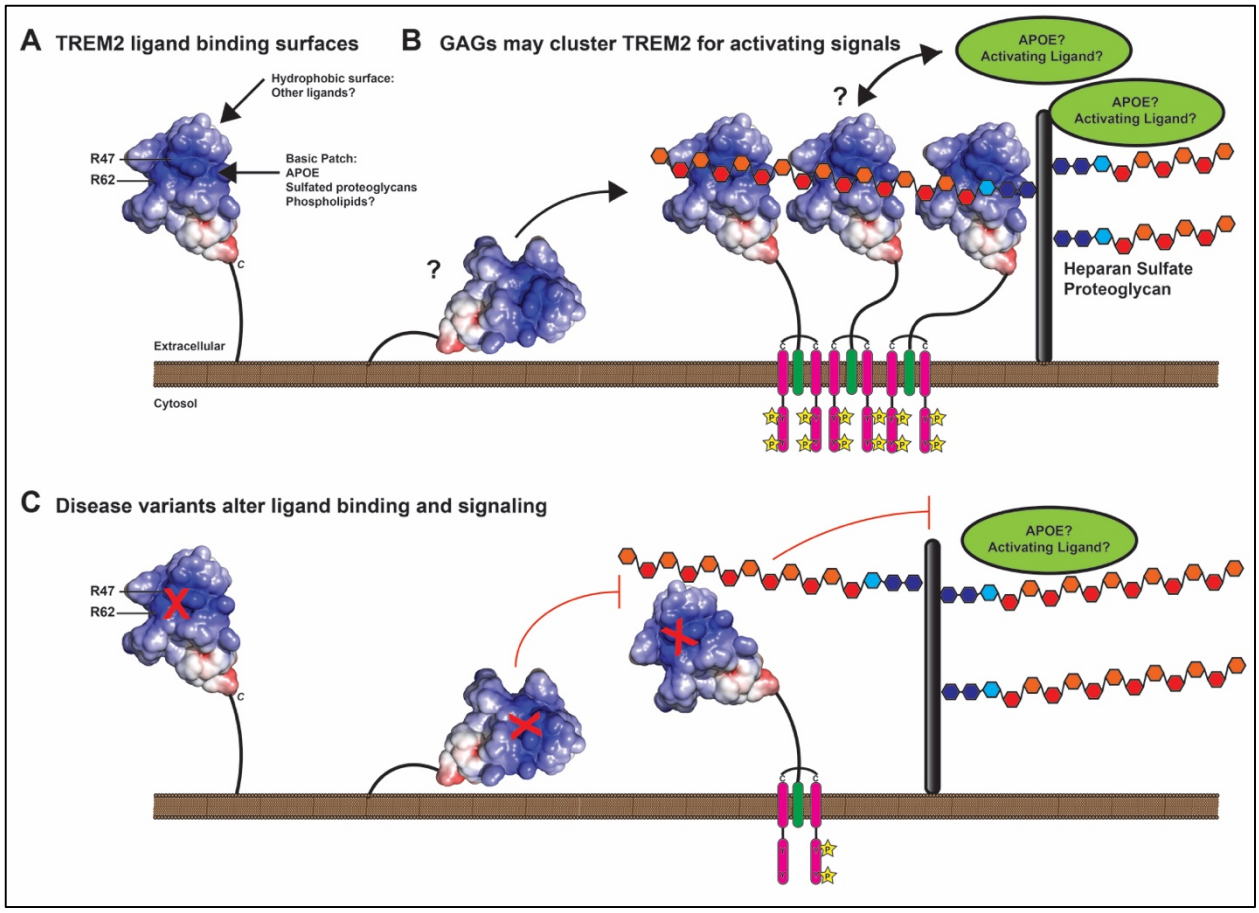

Figure 6.3. Model for TREM2 signal by WT and variant proteins. A) TREM2 has a pronounced basic patch, and the disease variants R47 and R62 are part of this surface. TREM2 also has separate surfaces that are potentially involved in ligand binding, such as a hydrophobic surface above the basic patch. Note that residues involved in recognition and binding of specific phospholipids in other Ig domain proteins are not present in TREM2. **B)** Role of GAGs in TREM2 signaling. Heparan sulfate proteoglycans interact with TREM2, likely in cis on TREM2-expressing cells. These may function to orient and cluster TREM2 to receive activating signals such as phospholipids or APOE. **C)** The R47H and R62H variant have reduced binding to cell-surface proteoglycans and have reduced signaling to phospholipids and lipoparticles. The decreased affinity for GAG may impair the ability of these variants to recognize and/or signal in response to these ligands.

Figure 6.3 taken from Kober and Brett 2017, manuscript in prep.

6.4 Future directions

1. How do TREM2 and ApoE interact?

I cloned, expressed, and purified a number of ApoE truncation constructs (**Fig 5.3**). These constructs will be tested in BLI experiments to determine which portions are essential for ApoE3 and ApoE4 to bind TREM2. Co-purification and co-crystallization trials will be attempted to obtain a high-resolution picture of the interaction. In lieu of a crystal structure, a SAXS envelope may be attainable. I have performed preliminary SAXS analysis of TREM2, and SAXS studies of lipidated ApoE have been reported previously (30), so this complex should be amenable to this type of analysis. BLI analysis will be done to verify residues implicated in binding by crystallography or SAXS. Additionally, I have developed and characterized novel anti-TREM2 mAbs that may be useful in co-crystallization and epitope mapping. The data here show that lipidation is not necessary for the ApoE-TREM2 interaction, but it will be important to conduct signaling assays to test whether lipidation is required to stimulate TREM2 signaling.

2. How does TREM2 interact with phospholipids?

In these experiments, TREM2 basic patch mutations did not appear to alter phospholipid binding. However, phospholipids are a potent stimulator of TREM2 signaling (13, 15). Determining how TREM2 interacts with phospholipids will be vital towards understanding TREM2 function. As discussed in Chapter 2, TREM2 has a hydrophobic surface that harbored unexplained density in the crystal structure. This density is likely NDSB-201, which may be acting as a surrogate for an endogenous lipid. **Fig 6.4** shows the hydrophobic patch with the contributing residues labeled. These residues have been individually mutated to Asp in the full-

length protein for signaling studies, and the Ig domains are being subcloned into pHLSEC vectors for lipid binding studies.

3. How do GAGs contribute to TREM2 signaling?

GAGs appear to be necessary for ERK activation, but this finding needs to be reproduced in CHO cells that don't express GAGs to control for off-target chemical effects. Additionally, signaling studies with phospholipids, ApoE, and Aβ should be conducted in the presence or absence of GAGs to see whether these ligands induce TREM signaling and whether GAGs are involved in these pathways.

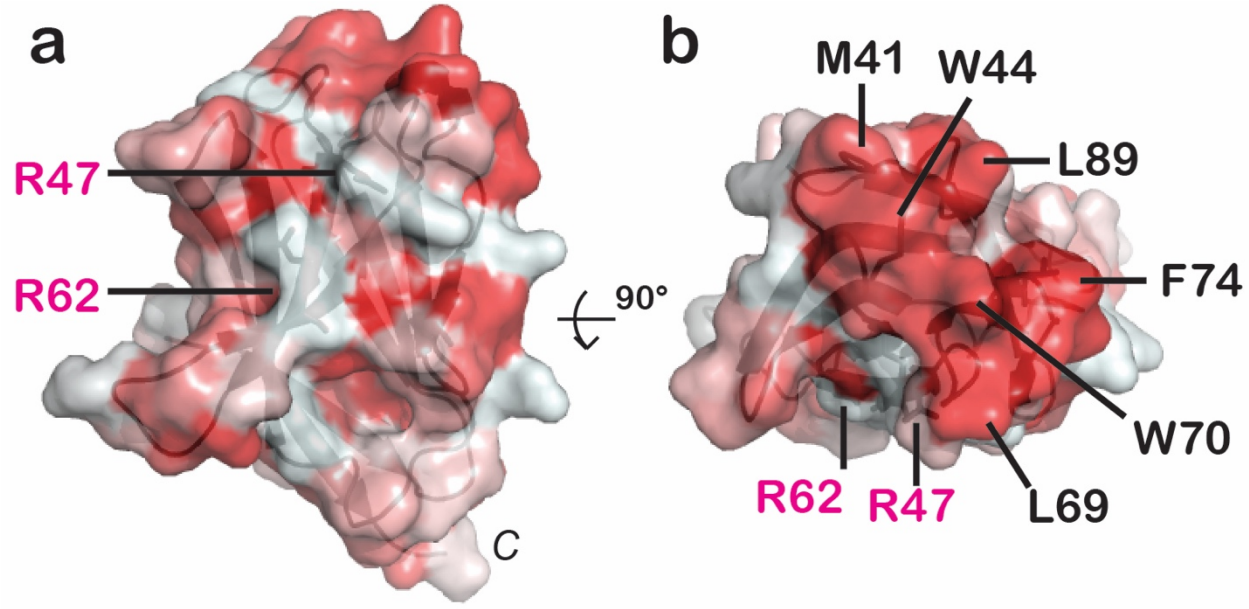

Figure 6.4. TREM2 hydrophobic patch. TREM2 hydrophobic surface plotted using color_h pymol script where red = hydrophobic. **a)** TREM2 side view as in **Figure 4.7** with R47 and R62 marked for orientation. **b)** top view, showing hydrophobic patch with contributing residues labeled.

Figure 6.4 is modified from Kober et al, 2016 (26)

4. What is the sTREM2 receptor?

Soluble TREM2 has been shown to inhibit apoptosis in microglia (31) and macrophages (32). The intracellular pathways were different, as survival was associated with PI3K/Akt signaling in microglia (31) and ERK signaling in macrophages (32). Whether there are two different receptors or the differences are due to cell origin or experimental conditions remains to be determined. Interestingly, the work in macrophages showed that sTREM2 was internalized and detectable on permeabilized but not intact macrophages, suggesting sTREM2 may interact with an intracellular receptor. Therefore, GAG interactions could mediate internalization for interaction with the unknown receptor. What is clear is that phospholipids or GAGs alone are not the complete signaling receptor for sTREM2, and future work will need to identify this receptor.

In an initial experiment, I used SEC-purified mTREM2 to stimulate RAW264.7 and BV2 cells (mouse macrophage and microglia). BV2 cells were a kind gift from Celeste Karch. I exposed the cells to 0.5 μM sTREM2 for 30 or 5 minutes and then collected the cells and immunoblotted for activated ERK and AKT as described above (pAKT and AKT antibodies were from Cell Signaling). Phosphor-ERK activation was observed in both RAW and BV2 cells at 30 minutes, but not 5 minutes (**Fig 6.5**). Boiling the TREM2 protein before application greatly reduced signaling (not shown). This was a control for LPS contamination. A small amount of signaling was detected with the boiled protein; this could indicate contamination or that some of the protein refolded after cooling, as was observed in CD experiments. In both sTREM2 reports, which used lower concentrations, boiling the protein abrogated the survival effect (31, 32). In contrast to the microglia report, I did not detect AKT activation in either cell line, although overall AKT detection was low. This suggests that ERK may be a proximal response to sTREM2 and AKT is more distal. This initial observation needs to be extended, but it confirms that the

TREM2 Ig domain is a potent signaling factor in addition to the role of TREM2 as a signaling receptor.

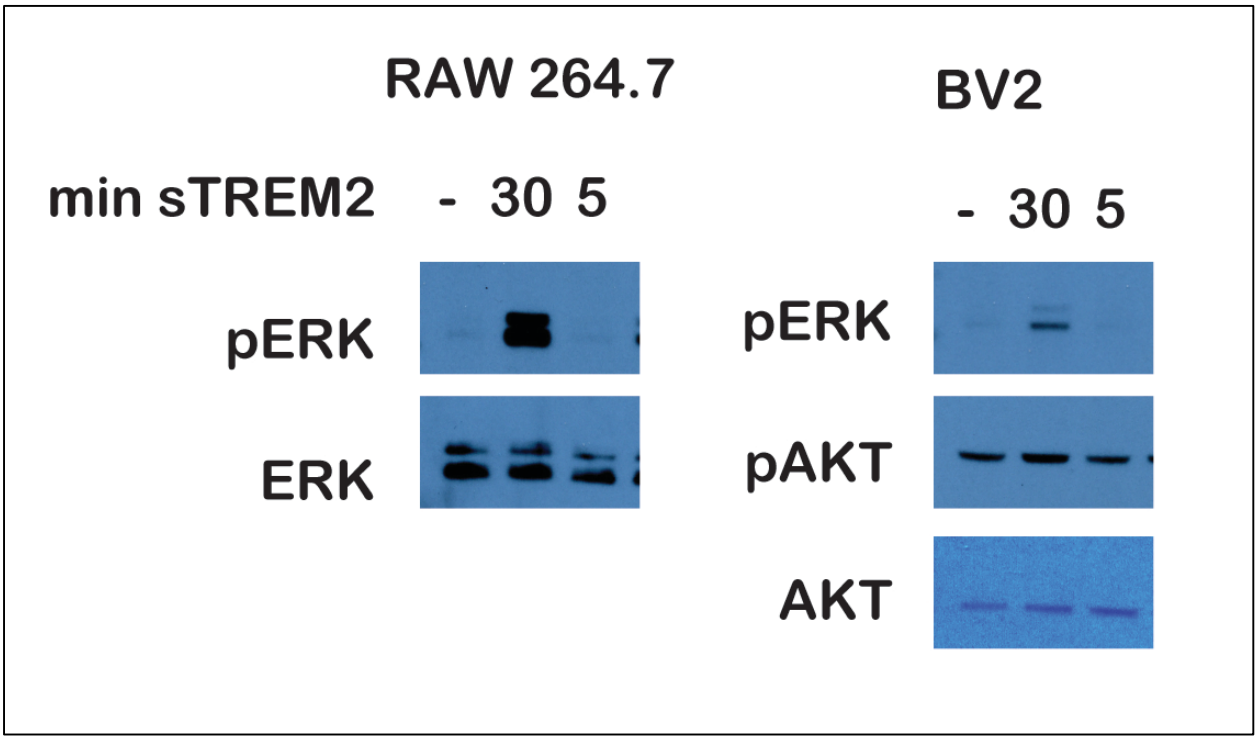

Figure 6.5. Soluble mTREM2 stimulates ERK signaling. Raw264.7 (left) and BV2 (right) cells were stimulated with 0.5 μM mTREM2 purified by SEC. Cells were harvested and lysed in PBS with 1% Triton X-100. Immunoblots were run for the indicated antigens. Phosphor-ERK, but not p-AKT was readily detected after 30 min exposure to mTREM2.

6.5 Translational implications of this work

This work is the first structural characterization of TREM2 and disease-associated variants, and there are several areas where these findings are of value in the pursuit of molecular therapies targeting or restoring TREM2 function.

1. **The structure could be used as a basis for *in situ* small-molecule docking.**

Small molecules could be screened *in situ* for potential interactions. Alternatively, high-throughput libraries could be screened for TREM2 activity (i.e. reporter cell signaling) and then the structure could be used to predict binding sites and suggest rational approaches to optimizing binding and selectivity. Candidate molecules could be further studied by co-crystallization with TREM2 to confirm binding modes. Currently, there are no well-validated TREM2 agonists or antagonist, so molecules performing either function would be useful as a research tool as well as therapeutically.

2. **Cell-surface expression data suggests the NHD variants are not cleared by ERAD and could be targeted molecular chaperones.**

In contrast to previous reports (33, 34), my expression system showed cell-surface expression of NHD variants by flow cytometry and confocal microscopy. Additionally, these Ig domains, while misfolded, were still secreted and detectable in solution. While this may be an artifact of overexpression, these findings should be investigated with human NHD samples by using antibodies that recognize the misfolded proteins. The detection of cell-surface protein shows that these proteins may survive clearance by ERAD and be amenable to folding

chaperones that restore function. This approach has been successfully used to target other misfolded proteins (e.g. Lumacaftor in cystic fibrosis)

3. **Basic patch variants could be targeted to restore binding.**

In contrast to the NHD variants, R47H and R62H do not grossly impair protein folding or stability. Instead, these variants negatively impact binding to ligands such as ApoE and cell-surface GAGs. Therapeutics could be designed either to rescue binding to these ligands or to directly stimulate the variant protein.

4. **Enhancing the TREM2-GAG-Ligand interactions.**

The disease-risk basic patch variants - R47H in particular - disrupt binding to cell-surface proteoglycans and soluble ligands such as ApoE. This suggests these interactions are important during disease and therefore molecules that enhance these interactions may be broadly therapeutic, and could potentially be used to increase microglia survival and activity during AD or other neurodegenerative disease in TREM2-WT patients.

5. **Soluble TREM2 as a therapeutic protein.**

With the Holtzman lab, we showed that soluble TREM2 inhibits macrophage apoptosis through ERK signaling and is a survival signal (32). These general findings were recently reproduced in primary microglia, although in that report the phenotype depended on AKT signaling (31). In this paradigm, sTREM2 may have therapeutic potential. Indeed, the T96K gain-of-binding variant should be tested to see if it has enhanced protective effects. Understanding this TREM2-receptor interaction could also suggest ways to enhance binding.

6.6 References:

1. Colonna M, Wang Y. TREM2 variants: new keys to decipher Alzheimer disease pathogenesis. Nat Rev Neurosci. 2016;17(4):201-7. doi: 10.1038/nrn.2016.7. PubMed PMID: 26911435.
2. Zheng H, Jia L, Liu CC, Rong Z, Zhong L, Yang L, Chen XF, Fryer JD, Wang X, Zhang YW, Xu H, Bu G. TREM2 Promotes Microglial Survival by Activating Wnt/beta-Catenin Pathway. J Neurosci. 2017;37(7):1772-84. doi: 10.1523/JNEUROSCI.2459-16.2017. PubMed PMID: 28077724.
3. Otero K, Shinohara M, Zhao H, Cella M, Gilfillan S, Colucci A, Faccio R, Ross FP, Teitelbaum SL, Takayanagi H, Colonna M. TREM2 and beta-catenin regulate bone homeostasis by controlling the rate of osteoclastogenesis. J Immunol. 2012;188(6):2612-21. doi: 10.4049/jimmunol.1102836. PubMed PMID: 22312126; PMCID: PMC3732181.
4. Zou W, Reeve JL, Liu Y, Teitelbaum SL, Ross FP. DAP12 couples c-Fms activation to the osteoclast cytoskeleton by recruitment of Syk. Mol Cell. 2008;31(3):422-31. doi: 10.1016/j.molcel.2008.06.023. PubMed PMID: 18691974; PMCID: PMC2584874.
5. Cella M, Buonsanti C, Strader C, Kondo T, Salmaggi A, Colonna M. Impaired differentiation of osteoclasts in TREM-2-deficient individuals. J Exp Med. 2003;198(4):645-51. doi: 10.1084/jem.20022220. PubMed PMID: 12913093; PMCID: PMC2194167.
6. Paloneva J, Mandelin J, Kiialainen A, Bohling T, Prudlo J, Hakola P, Haltia M, Konttinen YT, Peltonen L. DAP12/TREM2 deficiency results in impaired osteoclast differentiation and osteoporotic features. J Exp Med. 2003;198(4):669-75. doi: 10.1084/jem.20030027. PubMed PMID: 12925681; PMCID: PMC2194176.
7. Takegahara N, Takamatsu H, Toyofuku T, Tsujimura T, Okuno T, Yukawa K, Mizui M, Yamamoto M, Prasad DV, Suzuki K, Ishii M, Terai K, Moriya M, Nakatsuji Y, Sakoda S, Sato S, Akira S, Takeda K, Inui M, Takai T, Ikawa M, Okabe M, Kumanogoh A, Kikutani H. Plexin-A1 and its interaction with DAP12 in immune responses and bone homeostasis. Nat Cell Biol. 2006;8(6):615-22. doi: 10.1038/ncb1416. PubMed PMID: 16715077.
8. Bakker ABH, Hoek RM, Cerwenka A, Blom B, Lucian L, McNeil T, Murray R, Phillips JH, Sedgwick JD, Lanier LL. DAP12-deficient mice fail to develop autoimmunity due to impaired antigen priming. Immunity. 2000;13(3):345-53. doi: Doi 10.1016/S1074-7613(00)00034-0. PubMed PMID: WOS:000089616400007.
9. Hamerman JA, Jarjoura JR, Humphrey MB, Nakamura MC, Seaman WE, Lanier LL. Cutting edge: inhibition of TLR and FcR responses in macrophages by triggering receptor expressed on myeloid cells (TREM)-2 and DAP12. J Immunol. 2006;177(4):2051-5. PubMed PMID: 16887962.
10. Turnbull IR, Gilfillan S, Cella M, Aoshi T, Miller M, Piccio L, Hernandez M, Colonna M. Cutting edge: TREM-2 attenuates macrophage activation. J Immunol. 2006;177(6):3520-4. PubMed PMID: 16951310.
11. Kanekiyo T, Xu H, Bu G. ApoE and Abeta in Alzheimer's disease: accidental encounters or partners? Neuron. 2014;81(4):740-54. doi: 10.1016/j.neuron.2014.01.045. PubMed PMID: 24559670; PMCID: PMC3983361.
12. Hsieh CL, Koike M, Spusta SC, Niemi EC, Yenari M, Nakamura MC, Seaman WE. A role for TREM2 ligands in the phagocytosis of apoptotic neuronal cells by microglia. J Neurochem. 2009;109(4):1144-56. doi: 10.1111/j.1471-4159.2009.06042.x. PubMed PMID: 19302484; PMCID: PMC3087597.

13. Poliani PL, Wang Y, Fontana E, Robinette ML, Yamanishi Y, Gilfillan S, Colonna M. TREM2 sustains microglial expansion during aging and response to demyelination. J Clin Invest. 2015;125(5):2161-70. doi: 10.1172/JCI77983. PubMed PMID: 25893602; PMCID: PMC4463196.
14. Kawabori M, Kacimi R, Kauppinen T, Calosing C, Kim JY, Hsieh CL. Triggering receptor expressed on myeloid cells 2 (TREM2) deficiency attenuates phagocytic activities of microglia and exacerbates ischemic damage in experimental stroke. J Neurosci. 2015;35. doi: 10.1523/jneurosci.2620-14.2015.
15. Wang Y, Cella M, Mallinson K, Ulrich JD, Young KL, Robinette ML, Gilfillan S, Krishnan GM, Sudhakar S, Zinselmeyer BH, Holtzman DM, Cirrito JR, Colonna M. TREM2 lipid sensing sustains the microglial response in an Alzheimer's disease model. Cell. 2015;160(6):1061-71. doi: 10.1016/j.cell.2015.01.049. PubMed PMID: 25728668; PMCID: PMC4477963.
16. Xiang X, Werner G, Bohrmann B, Liesz A, Mazaheri F, Capell A, Feederle R, Knuesel I, Kleinberger G, Haass C. TREM2 deficiency reduces the efficacy of immunotherapeutic amyloid clearance. EMBO Mol Med. 2016;8(9):992-1004. doi: 10.15252/emmm.201606370. PubMed PMID: 27402340; PMCID: PMC5009806.
17. Takahashi K, Rochford CD, Neumann H. Clearance of apoptotic neurons without inflammation by microglial triggering receptor expressed on myeloid cells-2. J Exp Med. 2005;201(4):647-57. doi: 10.1084/jem.20041611. PubMed PMID: 15728241; PMCID: PMC2213053.
18. Yuan P, Condello C, Keene CD, Wang Y, Bird TD, Paul SM, Luo W, Colonna M, Baddeley D, Grutzendler J. TREM2 Haplodeficiency in Mice and Humans Impairs the Microglia Barrier Function Leading to Decreased Amyloid Compaction and Severe Axonal Dystrophy. Neuron. 2016;90(4):724-39. doi: 10.1016/j.neuron.2016.05.003. PubMed PMID: 27196974; PMCID: PMC4898967.
19. Ulrich JD, Finn MB, Wang Y, Shen A, Mahan TE, Jiang H, Stewart FR, Piccio L, Colonna M, Holtzmann DM. Altered microglial repsonse to AB plaques in APPPS1-21 mice heterozygous for TREM2. Molecular Neurodegeneration. 2014;9(20).
20. Wang Y, Ulland TK, Ulrich JD, Song W, Tzaferis JA, Hole JT, Yuan P, Mahan TE, Shi Y, Gilfillan S, Cella M, Grutzendler J, DeMattos RB, Cirrito JR, Holtzman DM, Colonna M. TREM2-mediated early microglial response limits diffusion and toxicity of amyloid plaques. J Exp Med. 2016;213(5):667-75. doi: 10.1084/jem.20151948. PubMed PMID: 27091843; PMCID: PMC4854736.
21. Ulrich JD, Holtzman DM. TREM2 Function in Alzheimer's Disease and Neurodegeneration. ACS Chem Neurosci. 2016;7(4):420-7. doi: 10.1021/acschemneuro.5b00313. PubMed PMID: 26854967.
22. Stefano L, Racchetti G, Bianco F, Passini N, Gupta RS, Panina Bordignon P, Meldolesi J. The surface-exposed chaperone, Hsp60, is an agonist of the microglial TREM2 receptor. J Neurochem. 2009;110(1):284-94. doi: 10.1111/j.1471-4159.2009.06130.x. PubMed PMID: 19457124.
23. N'Diaye EN, Branda CS, Branda SS, Nevarez L, Colonna M, Lowell C, Hamerman JA, Seaman WE. TREM-2 (triggering receptor expressed on myeloid cells 2) is a phagocytic receptor for bacteria. J Cell Biol. 2009;184(2):215-23. doi: 10.1083/jcb.200808080. PubMed PMID: 19171755; PMCID: PMC2654305.

24. Daws MR, Sullam PM, Niemi EC, Chen TT, Tchao NK, Seaman WE. Pattern recognition by TREM-2: binding of anionic ligands. J Immunol. 2003;171(2):594-9. PubMed PMID: 12847223.
25. Bailey CC, DeVaux LB, Farzan M. The Triggering Receptor Expressed on Myeloid Cells 2 Binds Apolipoprotein E. J Biol Chem. 2015;290(43):26033-42. doi: 10.1074/jbc.M115.677286. PubMed PMID: 26374897; PMCID: PMC4646256.
26. Kober DL, Alexander-Brett JM, Karch CM, Cruchaga C, Colonna M, Holtzman MJ, Brett TJ. Neurodegenerative disease mutations in TREM2 reveal a functional surface and distinct loss-of-function mechanisms. Elife. 2016;5:e20391. doi: 10.7554/eLife.20391. PubMed PMID: 27995897; PMCID: PMC5173322.
27. O'Callaghan P, Li JP, Lannfelt L, Lindahl U, Zhang X. Microglial Heparan Sulfate Proteoglycans Facilitate the Cluster-of-Differentiation 14 (CD14)/Toll-like Receptor 4 (TLR4)-Dependent Inflammatory Response. J Biol Chem. 2015;290(24):14904-14. doi: 10.1074/jbc.M114.634337. PubMed PMID: 25869127; PMCID: PMC4463438.
28. Murphy JW, Cho Y, Sachpatzidis A, Fan C, Hodsdon ME, Lolis E. Structural and functional basis of CXCL12 (stromal cell-derived factor-1 alpha) binding to heparin. J Biol Chem. 2007;282(13):10018-27. doi: 10.1074/jbc.M608796200. PubMed PMID: 17264079; PMCID: PMC3684283.
29. McDonnell KM, Grow WA. Reduced glycosaminoglycan sulfation diminishes the agrin signal transduction pathway. Dev Neurosci. 2004;26(1):1-10. doi: 10.1159/000080706. PubMed PMID: 15509893.
30. Peters-Libeu CA, Newhouse Y, Hall SC, Witkowska HE, Weisgraber KH. Apolipoprotein E*dipalmitoylphosphatidylcholine particles are ellipsoidal in solution. J Lipid Res. 2007;48(5):1035-44. doi: 10.1194/jlr.M600545-JLR200. PubMed PMID: 17308333.
31. Zhong L, Chen XF, Wang T, Wang Z, Liao C, Wang Z, Huang R, Wang D, Li X, Wu L, Jia L, Zheng H, Painter M, Atagi Y, Liu CC, Zhang YW, Fryer JD, Xu H, Bu G. Soluble TREM2 induces inflammatory responses and enhances microglial survival. J Exp Med. 2017. doi: 10.1084/jem.20160844. PubMed PMID: 28209725.
32. Wu K, Byers DE, Jin X, Agapov E, Alexander-Brett J, Patel AC, Cella M, Gilfilan S, Colonna M, Kober DL, Brett TJ, Holtzman MJ. TREM-2 promotes macrophage survival and lung disease after respiratory viral infection. J Exp Med. 2015;212(5):681-97. doi: 10.1084/jem.20141732. PubMed PMID: 25897174; PMCID: PMC4419356.
33. Kleinberger G, Yamanishi Y, Suarez-Calvet M, Czirr E, Lohmann E, Cuyvers E, Struyfs H, Pettkus N, Wenninger-Weinzierl A, Mazaheri F, Tahirovic S, Lleo A, Alcolea D, Fortea J, Willem M, Lammich S, Molinuevo JL, Sanchez-Valle R, Antonell A, Ramirez A, Heneka MT, Sleegers K, van der Zee J, Martin JJ, Engelborghs S, Demirtas-Tatlidede A, Zetterberg H, Van Broeckhoven C, Gurvit H, Wyss-Coray T, Hardy J, Colonna M, Haass C. TREM2 mutations implicated in neurodegeneration impair cell surface transport and phagocytosis. Sci Transl Med. 2014;6(243):243ra86. doi: 10.1126/scitranslmed.3009093. PubMed PMID: 24990881.
34. Park JS, Ji IJ, An HJ, Kang MJ, Kang SW, Kim DH, Yoon SY. Disease-Associated Mutations of TREM2 Alter the Processing of N-Linked Oligosaccharides in the Golgi Apparatus. Traffic. 2015;16(5):510-8. doi: 10.1111/tra.12264. PubMed PMID: 25615530.

Appendix

Protein Expression and Purification 96 (2014) 32–38

Contents lists available at ScienceDirect

Protein Expression and Purification

journal homepage: www.elsevier.com/locate/yprep

Preparation, crystallization, and preliminary crystallographic analysis of wild-type and mutant human TREM-2 ectodomains linked to neurodegenerative and inflammatory diseases

Daniel L. Kober [a,b], Kelsey M. Wanhainen [b], Britney M. Johnson [c], David T. Randolph [b], Michael J. Holtzman [b,e,f], Tom J. Brett [b,d,e,f,*]

[a] Molecular Microbiology and Microbial Pathogenesis Program, Washington University School of Medicine, St. Louis, MO 63110, United States
[b] Department of Internal Medicine, Washington University School of Medicine, St. Louis, MO 63110, United States
[c] Biochemistry Program, Washington University School of Medicine, St. Louis, MO 63110, United States
[d] Biochemistry and Molecular Biophysics, Washington University School of Medicine, St. Louis, MO 63110, United States
[e] Cell Biology and Physiology, Washington University School of Medicine, St. Louis, MO 63110, United States
[f] Drug Discovery Program in Pulmonary and Critical Care Medicine, Washington University School of Medicine, St. Louis, MO 63110, United States

ARTICLE INFO

Article history:
Received 18 December 2013
and in revised form 28 January 2014
Available online 7 February 2014

Keywords:
Innate immunity
Inflammation
Receptor
Crystallography
Neurodegenerative disease
Alzheimer's disease
Parkinson's disease

ABSTRACT

TREM-2 (triggering receptor expressed on myeloid cells-2) is an innate immune receptor expressed on dendritic cells, macrophages, osteoclasts, and microglia. Recent genetic studies have reported the occurrence of point mutations in TREM-2 that correlate with a dramatically increased risk for the development of neurodegenerative diseases, including Alzheimer's disease, frontotemporal dementia, and Parkinson's disease. Structural and biophysical studies of wild-type and mutant TREM-2 ectodomains are required to understand the functional consequences of these mutations. In order to facilitate these studies, we undertook the production and crystallization of these proteins. Here we demonstrate that, unlike many single Ig domain proteins, TREM-2 could not be readily refolded from bacterially-expressed inclusion bodies. Instead, we developed a mammalian-cell based expression system for the successful production of wild-type and mutant TREM-2 proteins in milligram quantities and a single-chromatography-step purification scheme that produced diffraction-quality crystals. These crystals diffract to a resolution of 3.3 Å and produce data sufficient for structure determination. We describe herein the procedures to produce wild-type and mutant human TREM-2 Ig domains in sufficient quantities for structural and biophysical studies. Such studies are crucial to understand the functional consequences of TREM-2 point mutations linked to the development of neurodegenerative diseases and, ultimately, to develop patient-specific molecular therapies to treat them.

Introduction

The molecular mechanisms contributing to age-related neurodegenerative disease pathogenesis are not well understood. Genetic studies released within the last year have identified specific mutations in *TREM2* that are linked to a significantly increased risk for the development of late-onset Alzheimer's Disease ([1]AD) [1,2]. The greatest risk is associated with the point mutant R47H, and is roughly equivalent to that associated with mutations in *APOE4*, currently the strongest known risk factor for late-onset AD [3]. This mutation has now been found in cohorts from Iceland [2], USA, Germany, Netherlands, Norway [1], Spain [4], and France [5]. Further, this mutation has recently been identified as a determinant in Parkinson's disease (PD) patients [6,7]. Additional variants including D87N and T96K have been linked to AD development [1] and two other point mutations in TREM-2 (Y38C and T66M) have been linked to the development of frontotemporal dementia (FTD) [8–11]. These findings highlight a crucial homeostatic role for *TREM2* in maintaining neuronal health and represent the first molecular link between innate inflammatory signaling and neurodegenerative diseases [12]. However, it is currently unknown how these mutations affect TREM-2 function and thereby contribute to neurodegenerative disease pathogenesis.

* Corresponding author. Address: Campus Box 8052, 660 S. Euclid, St. Louis, MO 63110, United States. Tel.: +1 (314) 747 0018; fax: +1 (314) 362 8987.
E-mail address: tbrett@wustl.edu (T.J. Brett).

[1] *Abbreviations used:* TREM-2, triggering receptor expressed on myeloid cells-2; AD, Alzheimer's disease; PD, Parkinson's disease; FTD, frontotemporal dementia; NHD, Nasu-Hakola disease; WT, wild-type; TLT-1, TREM-like transcript 1.

http://dx.doi.org/10.1016/j.pep.2014.01.015
1046-5928/

The *TREM2* gene encodes the protein triggering receptor expressed on myeloid cells 2 (TREM-2). TREM-2 is an innate immune receptor expressed on dendritic cells, macrophages, osteoclasts, and microglia [13]. The protein has a minimal intracellular sequence and therefore traffics and signals through association with the adaptor protein DAP12 [14]. The ectodomain consists of a single Ig fold anchored to a transmembrane domain via a short stalk. The major role of the Ig domain is presumed to be ligand engagement, though the endogenous signaling ligand(s) of TREM-2 are uncertain. Several different types of ligands have been suggested, including various anionic bacterial carbohydrates [15], apoptotic cell membrane components [16], the immune receptor Plexin-A1 [17], and the chaperone Hsp60 [18]. A proper understanding of the function of TREM-2 has been constrained by a lack of structural information and the elusive nature of TREM-2 ligands.

A crucial role for TREM-2 in neuronal health was first suggested through association with neurodegenerative Nasu-Hakola disease (NHD) [19]. The major mutations associated with NHD produce premature termination of TREM-2 protein and are also phenocopied by deletion of DAP12. In contrast, all of the point mutations associated with AD, PD, and FTD are located within the Ig domain, suggesting these mutations alter function of full-length TREM-2.

Proper understanding of how the newly identified point mutations of TREM-2 could modulate function and contribute to disease requires not only functional studies but also structural and biophysical comparisons of wild-type (WT) and mutant TREM-2 ectodomains. In order to facilitate this approach, we developed a mammalian cell-based expression and purification system to address the difficulties with generating TREM-2 protein suitable for structural and biophysical studies. Indeed, we were able to identify experimental conditions that produce crystals of human TREM-2 that diffract to 3.3 Å resolution and can be phased by molecular replacement. The studies outlined here provide a methodological framework for understanding the molecular basis of TREM-2 mutations and their contribution to the development of neurodegenerative diseases.

Materials and methods

Expression constructs

For expression in *Escherichia coli*, the Ig domains of human TREM-2 (NBCI ref NP_061838; amino acids 19–134; MW_{calc}[with tag] = 14387 Da; pI_{calc} = 8.5) and mouse TREM-2 (NCBI ref NP_112544; amino acids 19–136; MW_{calc}[with tag] = 14440 Da; pI_{calc} = 8.4) were amplified using PCR and cloned into pET23b as tagless constructs using standard molecular biology techniques. Full-length human *TREM-2* in pMX-3p plasmid (a gift from Marco Colonna) and mouse *Trem-2* cDNA were used as PCR templates, respectively. Mammalian cell expression constructs of human TREM-2 wild-type, R47H mutant, and mouse TREM-2 Ig domains were produced similarly by cloning into the pHLSEC vector [20], which contains an optimized signal sequence and C-terminal 6-histidine tag for purification. All constructs were confirmed by sequencing.

Expression and purification of TREM-2 inclusion bodies in E. coli

Human and mouse TREM-2 Ig domains in pET23b were transformed into Rosetta2 (DE3) cells (Novagen) for expression. Cultures were grown to $O.D._{600}$ = 1.0, induced with 0.5 mM IPTG, and expressed with shaking at 37 °C for 4 h. Cells were then harvested by centrifugation and lysed in buffer containing 50 mM Tris pH 8.0, 12.5% sucrose, 50 mM NaCl, 0.5 mM EDTA, 0.5% Trition X-100, and 10 mM DTT supplemented with lysozyme (0.5 mg/mL) and DNAse. The inclusion bodies were harvested by centrifugation and washed 3 times in buffer containing 50 mM Tris pH 8.0, 100 mM NaCl, 1 mM EDTA, 1 mM DTT and 0.5% Triton X-100. A final wash without Triton X-100 was performed and the purified inclusion bodies were solubilized in 6 M guanidine hydrochloride containing 20 mM β-ME and 50 mM Tris pH 8.0.

Refolding trials for human and mouse TREM-2 Ig domains

Initial refoldings were attempted by rapid dilution of the solubilized inclusion bodies into a buffer containing 100 mM Tris pH 8.5, 400 mM arginine, 2 mM EDTA, 5 mM reduced glutathione, and 0.5 mM oxidized glutathione, as similar conditions had previously been used to refold human and mouse TREM-1 [21–23], human TREM-like transcript 1 (TLT-1) [24], human immune receptor expressed on myeloid cells (IREM-1) [25], and human NK cell receptor NKp44 [26]. Solutions were initially clear upon addition of protein, but after about 1 h the protein would precipitate. Subsequent workup revealed no properly folded soluble protein. Therefore we performed screening of refolding conditions. A refolding screen was developed based on the QuickFold Protein

Table 1
Refolding screen conditions.

	Buffer	Salt	Cation/Chelator	Guanidine	Stabilizing agent(s)	Additives	Detergent	1 mM DTT	1 mM GSH/ 0.1 mM GSSH
1	MES pH 6.0	9.6 mM NaCl, 0.4 mM KCl	2 mM $MgCl_2$, 2 mM $CaCl_2$	0.75 M			0.5% Triton X-100	•	
2	MES pH 6.0	9.6 mM NaCl, 0.4 mM KCl	2 mM $MgCl_2$, 2 mM $CaCl_2$		0.5 M L-Arginine	0.05% PEG 3,350			•
3	MES pH 6.0	9.6 mM NaCl, 0.4 mM KCl	1 mM EDTA	0.75 M	0.4 M Sucrose	0.05% PEG 3,350	0.5% Triton X-100	•	
4	MES pH 6.0	240 mM NaCl, 10 mM KCl	2 mM $MgCl_2$, 2 mM $CaCl_2$		0.5 M L-Arginine		0.5% Triton X-100		•
5	MES pH 6.0	240 mM NaCl, 10 mM KCl	1 mM EDTA	0.75 M	0.4 M Sucrose			•	
6	MES pH 6.0	240 mM NaCl, 10 mM KCl	1 mM EDTA		0.4 M Sucrose 0.5 M L-Arginine	0.05% PEG 3,350	0.5% Triton X-100		•
7	MES pH 6.0	240 mM NaCl, 10 mM KCl	2 mM $MgCl_2$, 2 mM $CaCl_2$	0.75 M		0.05% PEG 3,350		•	
8	Tris pH 8.5	9.6 mM NaCl, 0.4 mM KCl	2 mM $MgCl_2$, 2 mM $CaCl_2$		0.4 M Sucrose	0.05% PEG 3,350	0.5% Triton X-100		•
9	Tris pH 8.5	9.6 mM NaCl, 0.4 mM KCl	1 mM EDTA	0.75 M	0.5 M L-Arginine	0.05% PEG 3,350		•	
10	Tris pH 8.5	9.6 mM NaCl, 0.4 mM KCl	2 mM $MgCl_2$, 2 mM $CaCl_2$	0.75 M	0.4 M Sucrose 0.5 M L-Arginine				•
11	Tris pH 8.5	9.6 mM NaCl, 0.4 mM KCl	1 mM EDTA				0.5% Triton X-100	•	
12	Tris pH 8.5	240 mM NaCl, 10 mM KCl	1 mM EDTA			0.05% PEG 3,350			•
13	Tris pH 8.5	240 mM NaCl, 10 mM KCl	1 mM EDTA	0.75 M	0.5 M L-Arginine		0.5% Triton X-100	•	
14	Tris pH 8.5	240 mM NaCl, 10 mM KCl	2 mM $MgCl_2$, 2 mM $CaCl_2$	0.75 M	0.4 M Sucrose 0.5 M L-Arginine	0.05% PEG 3,350	0.5% Triton X-100		•
15	Tris pH 8.5	240 mM NaCl, 10 mM KCl	2 mM $MgCl_2$, 2 mM $CaCl_2$		0.4 M Sucrose			•	

Refolding Kit (Athena Enzyme Systems) (Table 1). For this screen, 50 μL of each solubilized TREM-2 inclusion body (at 2 mg/mL) was added to 950 μL of each refolding condition, rocked overnight at 4 °C, and then centrifuged at high speed to pellet insoluble protein. The presence of soluble protein in the supernatant was assessed by SDS–PAGE.

Expression and purification of TREM-2 Ig domains from mammalian cells

Wild-type human and mouse TREM-2 Ig domain and human R47H mutant were expressed in mammalian cells by large-scale transient transfection. Briefly, plasmid DNA (1 μg/mL final concentration) was diluted in Opti-MEM (Gibco) and mixed 1:2 with 25 kDa branched polyethyleneamine chemically modified with trimethylene carbonate (termed PEI-TMC25) [27] (2 μg/mL final concentration) and allowed to form micellar complexes for 30 min. Transfection was achieved by adding these mixtures to FreeStyle 293F cells (Invitrogen) at a ratio of 1 μg DNA: 1×10^6 cells. Cells were allowed to grow in serum-free 293 FreeStyle media (Invitrogen) with shaking in vented flasks at 37 °C and 8% CO_2. The TREM-2 Ig domain has two conserved N-glycosylation sites (Fig. 1a). To facilitate removal of N-linked glycans, kifunensine (Sigma; 1 μg/mL), an inhibitor of α-mannosidase I, was added to the culture to inhibit maturation of N-linked glycans and leave them as high-mannose glycans that can be removed with EndoH [28]. Culture supernatants were collected at 72 and 144 h post-transfection, modified by addition of 50 mM phosphate, 10 mM Tris pH 8.5, 300 mM NaCl, and 10 mM imidazole, and then purified using NiNTA-affinity chromatography. Proteins were washed on column using the same buffer containing 20 mM imidazole and eluted in 250 mM imidazole. After elution, EndoHf (NEB), a fusion protein of EndoH and maltose binding protein, was used to deglycosylate TREM2 to homogeneity. This reaction cleaves the high-mannose glycan leaving a single glucose attached to the asparagine and was carried out by addition of 50 mM sodium citrate pH 5.5 and approximately 2000 units of EndoHf per mg of TREM-2 Ig domain. Reactions were incubated overnight at 25 °C. EndoHf was then removed by incubation with amylose resin for 1 h at 4 °C, followed by pelleting of the resin by centrifugation and harvesting of the supernatant. The deglycosylated TREM-2 Ig domains were then exchanged into buffer containing 20 mM Hepes pH 7.5 and 150 mM NaCl with a concentrator (Vivaspin, Sartorius) for use in experiments. The resulting proteins were >90% pure as assessed by SDS–PAGE.

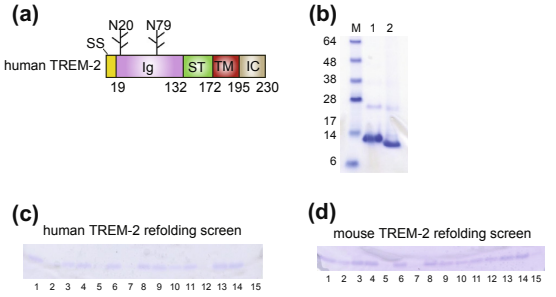

Fig. 1. Production of human and mouse TREM-2 ectodomain inclusion bodies in *E. coli* and refolding screening. (a) Schematic representation of human TREM-2 protein. Conserved N-linked glycosylation sites are shown as branched trees. Structural features are labeled as follows: SS = signal sequence; Ig = immunoglobulin domain; ST = stalk; TM = transmembrane; IC = intracellular region. (b) SDS–PAGE analysis of human (lane 1) and mouse (lane 2) TREM-2 solubilized inclusion bodies (M = molecular weight marker). Proteins in 6 M guanidine were diluted at a ratio of 1:50 into SDS–PAGE loading buffer (to prevent precipitation of guanidine by SDS). Final protein concentration in the loading buffer was 1 mg/ml and approximately 15 μg of protein were loaded on each lane of the gel. (c) SDS–PAGE analysis of refolding screen outcome for human TREM-2 and (d) mouse TREM-2 Ig domains. The lane numbers correlate to the refolding screen conditions in Table 1.

Table 2
Crystallographic data and initial molecular replacement statistics.

Space group	$P6_422$
X-ray data collection statistics	
Unit Cell (Å)	$a = 125.76$ $b = 125.76$ $c = 183.66$
X-ray source	APS, ID-19
Wavelength (Å)	0.979180
Resolution (Å)	50.00–3.30 (3.42–3.30)[a]
R_{sym} (%)	0.133 (0.920)
Completeness (%)	99.9 (100)
Redundancy	13.6 (14.1)
I/σ (I)	21.8 (3.0)
Molecular replacement statistics	
Probe PDB ID	1U9K
No. molecules/ASU	2
Program	PHASER
TFZ	13.8
Rigid body R_{work}	0.3909
Rigid body R_{free}	0.4602

[a] Values in parenthesis are for the highest-resolution shell.

Crystallization, data collection, and initial crystallographic analysis

Human and mouse TREM-2 Ig domains at 10 mg/mL were screened for crystallization by hanging drop vapor diffusion. Initial hits were only obtained for human TREM-2 Ig domain. Optimal crystals were obtained when protein solution was mixed 1:1 with well solution containing 100 mM Tris pH 7.1, 2.1 M NaCl, 200 mM $MgCl_2$, 200 mM NDSB-201. Crystals appeared over the course of 2–5 days and had approximate dimensions of 300 × 300 × 50 μm.

For data collection, crystals were cryopreserved in reservoir solution containing 25% ethylene glycol and flash-frozen in a nitrogen stream at 100 K. A native data set was collected at a wavelength of 1.0007 Å with 5 s exposure times and 1° oscillations per image at beamline ID19 (Advanced Photon Source, Argonne). Data were processed with HKL-2000 [29]. Scaling and analysis of systematic absences revealed the space group to be either $P6_122$ of $P6_422$. Molecular replacement was carried out in PHASER [30] using various similar single Ig domain probes including human TREM-1 (PDB ID: 1SMO) [22], mouse TREM-1 (1U9K) [21], human NKp44 (1HKF) [26], human TLT-1 (2FRG) [24], human IREM-1 (2NMS) [25], mouse CNRF35-like molecule 1 (CLM-1) (1ZOX), and ensembles of these structures. The best rotational and translational *Z* scores were obtained with mouse TREM-1 (1U9K). The translational search revealed the correct space group to be $P6_422$. Two copies of the probe were placed in the asymmetric unit (ASU). Data collection and molecular replacement statistics are provided in Table 2. Patterson and self-rotation function were calculated with GLRF [31] using a 25 Å radius of integration.

Western blot analysis

Recombinant human TREM-2 Ig domain proteins were analyzed on Western blot using an antibody directed against the C-terminal 6-histidine tag (HRP conjugated rabbit α-6-His antibody, Bethyl Labs, A190–114A). The antibody was used at a 1:5000 dilution in binding buffer (PBS containing 0.1% TWEEN-20 and 0.5% powered milk). Blocking, binding, and washing steps were carried

out in a SNAP i.d. system (Millipore) according to product recommendations.

Results and discussion

TREM-2 Ig domain refolding screen

Initial experiments were directed at obtaining the large amounts of purified protein that are required for structural and biophysical studies. Structure predictions estimate that the TREM-2 ectodomain consists of a single immunoglobulin (Ig) domain followed by an approximately 40 amino acid unstructured stalk (Fig 1a). Most of the mutations linked to increased risk of neurodegenerative diseases lie in the Ig domain [12], which is most likely to be involved in ligand engagement for signaling. A number of Ig domains from TREM family receptors have previously been crystallized, including human TREM-1 [22,23], mouse TREM-1 [21], human TLT-1 [24], human IREM-1 [25], mouse CLM-1, and human NKp44 [26]. Each of the proteins for these studies was produced by bacterial expression of insoluble inclusion bodies and refolding. Thus, we initiated our structural studies of the TREM-2 Ig domain by attempting to refold both the human and mouse TREM-2 Ig domains from bacterially expressed inclusion bodies. Although the inclusion body preparations were very homogeneous (Fig 1b), we were unable to refold these proteins by rapid dilution into a buffer similar to that used for other family members (100 mM Tris pH 8.5, 400 mM arginine, 2 mM EDTA, 5 mM reduced glutathione, and 0.5 mM oxidized glutathione). The protein would initially be soluble, but after about one hour, heavy precipitation was observed in the refolding buffer. We then attempted to screen numerous potential refolding conditions (Table 1). This screening produced a number of potential conditions (Fig 1c). A number of potential hits, including conditions #4 and #14, were expanded to large-scale refoldings in 500 mL of refolding buffer. However, these conditions produced similar results (heavy precipitation after 1 h) when scaled-up. In addition, given that NDSB-201 increased solubility and crystal size for the mammalian cell-produced protein, we attempted large-scale refolding in buffers incorporating that reagent as the solubilizer (50 mM Hepes pH 7.5, 0.4 –1.0 M NDSB-201, 150 mM NaCl, 5 mM EDTA, 5 mM reduced glutathione, and 0.5 mM oxidized glutathione). This attempt gave similar unsuccessful results. Some possible interpretations of these observations could be a requirement for post-translational modification that is unable to occur in *E. coli*, the need of chaperones for proper folding, or instability due to absence of a ligand.

Production and purification of TREM-2 from mammalian cells

To circumvent the protein production problems found in the bacterial system, we next pursued expression and purification of natively folded and secreted protein from mammalian cells. We previously incorporated a large-scale transient transfection system using mammalian cells in suspension to produce secreted proteins [32]. The advantages of this transient transfection system are: expression constructs can be quickly optimized as there is no requirement to produce expression viruses or stably expressing cell lines; the 293 Freestyle cells are readily transfected and can be grown to high densities (up to around 4×10^6/ml); and the cells can be cultured in serum-free media, simplifying purification from media supernatants (Fig 2a). Using this system, we transfected 293 Freestyle cells at a density of 1×10^6/ml with expression plasmids encoding mouse TREM-2 Ig domain, human WT TREM-2 Ig domain, and human TREM-2 Ig domain R47H variant. To inhibit glycan maturation, kifunensine was added to the culture medium at the time of transfection. This treatment allows for removal of the resulting high-mannose glycans by post-purification addition of Endo Hf, which is advantageous for crystallization. Media supernatants were harvested 72-h post-transfection and adjusted to pH 8.5 with phosphate/Tris, 300 mM NaCl, and 10 mM imidazole for efficient retrieval of the 6-histidine-tagged proteins using Ni–NTA superflow resin. Bound proteins were eluted from the column in a buffer consisting of 50 mM phosphate pH 8.0, 300 NaCl, and 250 mM imidazole. The eluted proteins ran at approximately 28 kDa on SDS–PAGE and displayed laddering due to inhomogeneous glycosylation (calculated monomeric weight is approximately 14 kDa) (Fig. 2b). The eluted proteins were then adjusted

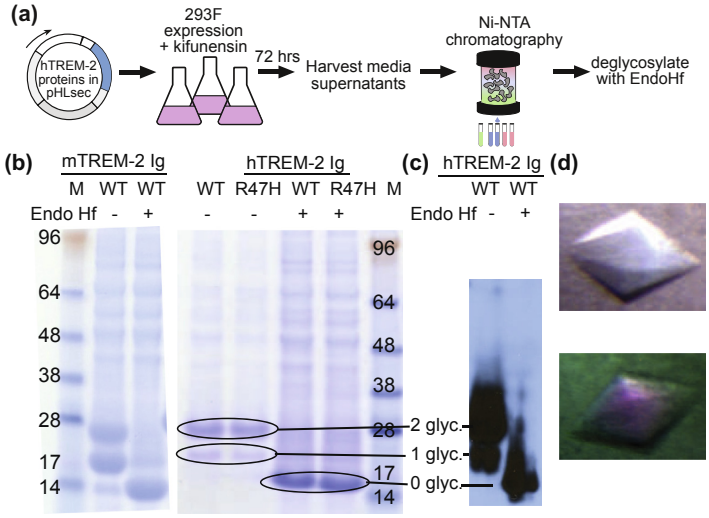

Fig. 2. Expression, purification, and crystallization of mammalian expressed TREM-2 Ig domains. (a) Schematic of protein production and purification from mammalian cells. (b) SDS–PAGE analysis of purified TREM-2 Ig domains before (−) and after (+) endoHf treatment. Proteins were diluted in SDS–PAGE loading buffer to a concentration of 1 mg/ml, and 15 μg of protein were loaded on each lane of the gel. (c) α-6-His Western blot of WT TREM-2 Ig domain before (−) and after (+) endoHf treatment. Bands corresponding to TREM-2 Ig domain modified with 2, 1, of 0 glycans are highlighted. (d) Hexagonal crystals of human TREM-2 WT Ig domain grown in 100 mM Tris pH 7.0–7.2, 2.0 M NaCl, 200 mM $MgCl_2$, 200 mM NDSB-201.

to acidic pH (50 mM sodium citrate pH 5.5) and treated with Endo Hf overnight at 25 °C. The deglycosylated proteins collapsed to a single band of about 15 kDa on SDS–PAGE (Fig 2b) and this was confirmed by Western blot for the C-terminal 6-histidine tag (Fig 2c). Typical yield was 5–10 mg of pure TREM-2 Ig domains per liter of culture medium.

Crystallization of the human TREM-2 Ig domain

Both human and mouse WT TREM-2 Ig domains were exchanged into a buffer consisting of 20 mM Hepes pH 7.5 and 150 mM NaCl and concentrated to 10 mg/mL prior to crystallization screening. Crystallization screening was carried using a Mosquito crystallization robot (TTP Labtech, UK). Screening was carried out by hanging drop vapor diffusion with crystallization drops containing 150 nL protein solution plus 150 nL precipitant solution. The most promising hits were obtained with the human TREM-2 Ig domain. The best initial condition produced multiple small hexagonal crystals per drop and consisted of 100 mM Bis-Tris pH 7.0, 2.0 M NaCl, 200 mM $MgCl_2$. Crystallization conditions were optimized by fine varying of buffer pH and NaCl concentration, and the addition of additives (96 condition Additive Screen, Hampton Research, CA, USA). The best additives produced only a few large crystals per drop and consisted of sulfobetaines (NDSB-201 and NDSB-211) and divalent cations ($CsCl_2$ and $BaCl_2$).

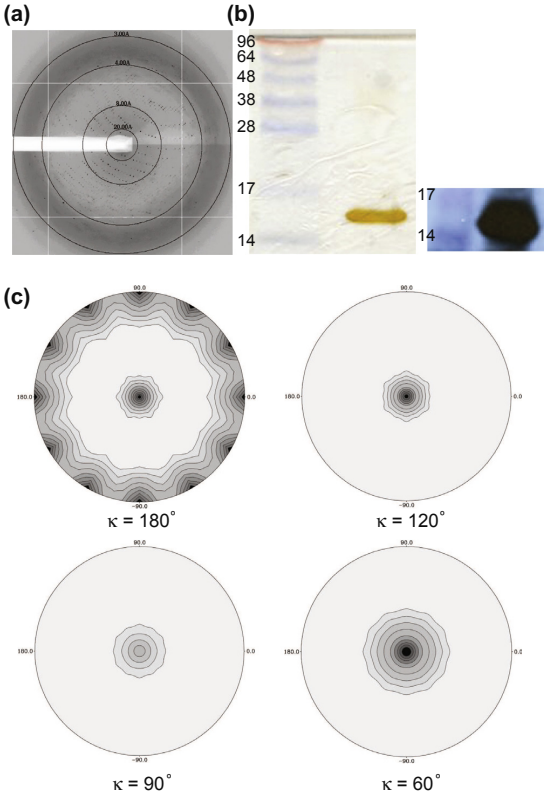

Fig. 3. Preliminary diffraction data from human TREM-2 WT Ig domain crystals (a) representative oscillation diffraction image from human TREM-2 WT Ig domain crystals (b) left: Silver-stained SDS–PAGE of human TREM-2 Ig WT crystals; Right: α-6-His Western blot of the TREM-2 Ig WT crystals (c) Patterson self-rotation function kappa sections from the 3.3 Å resolution data set.

The final optimized conditions for the best crystals consisted of 100 mM Tris pH 7.0–7.2, 2.0–2.2 M NaCl, 200 mM $MgCl_2$, and 200 mM NDSB-201 with crystallizations drops setup in a 1:1 protein:precipitant ratio. Large hexagonal crystals appeared after 2–3 days, reaching maximum dimensions of around 300 × 300 × 50 μM after 3–5 days (Fig. 2d).

Preliminary crystallographic data

Initial diffraction data was collected at the Advanced Photon Source, Argonne National Lab, beamline ID-19. Crystals of most of the previously analyzed TREM family members produced diffraction beyond 2.0 Å resolution. In contrast, the best crystals of human TREM-2 purified from mammalian cells diffracted to a resolution of 3.3 Å (Fig 3a). This decreased resolution is partially because the protein crystallizes in a large unit cell (Table 2). Even given the high symmetry space group ($P6_422$), six to seven TREM-2 Ig domains would be required per ASU for the crystals to have a solvent content near the commonly observed average of about 50%. However, molecular replacement using numerous suitable probes was only able to locate two molecules in the ASU, for a solvent content of 83%. This result suggested that a co-purified protein enriched in the crystallization process might have co-crystallized with the human TREM-2 Ig domain. In order to determine if this was the case, we extracted single crystals from crystallization drops, washed the crystals, dissolved them in SDS loading buffer, and finally analyzed the crystal contents by silver-stained SDS PAGE. This analysis revealed that the only protein in the crystals was human TREM-2 Ig domain and was confirmed by Western blot for the C-terminal 6-histidine tag (Fig 3b). Furthermore, analysis of the Patterson self-rotation function revealed only peaks consistent with the crystallographic symmetry on the $\kappa = 60°$, 120°, and 180° sections [33], and a unique peak on the $\kappa = 90°$ section (Fig 3c), indicative of twofold non-crystallographic symmetry, and thus consistent with the observation of two TREM-2 Ig domains in the ASU. Thus, the limited resolution observed from this crystal form of human TREM-2 Ig domain is mainly due to the large unit cell (limiting the number of unit cells per diffracting volume) and high solvent content. However, the data are sufficient to solve the structure to 3.3 Å resolution using molecular replacement.

Conclusions

TREM-2 is an innate immune receptor that is implicated in regulating inflammatory responses as well as acute and chronic inflammatory diseases [34]. In this capacity it has been suggested to contribute to and/or represent a biomarker for a number of diseases including multiple sclerosis [35,36], stroke [37], inflammatory bowel disease [38], and chronic inflammatory lung disease [39]. Recent genetics studies have uncovered point mutations in the TREM-2 Ig domain that correlate with a significantly increased risk for the development of neurodegenerative diseases such as AD, FTD, and PD. To begin to understand the influence of TREM-2 polymorphisms on TREM-2 function will require structural and biophysical studies of TREM-2 protein. These types of studies require generous amounts of purified protein and production of protein crystals that diffract to a resolution reasonable for structure determination. Single Ig domains often readily refold from bacterial inclusion bodies, however, we were unable to identify conditions under which the TREM-2 Ig domain would refold. There may be a functional basis for this observation, such as the lack of a stabilizing binding partner, post-translational modification, or folding chaperone. Nonetheless, we abandoned this strategy in favor of developing a mammalian cell-based expression system.

Using this system, we were able to produce both WT and mutant TREM-2 Ig domains in sufficient quantities for structural and biophysical studies. This protein readily crystallizes and these crystals produce diffraction data sufficient for structure determination at 3.3 Å. It is worth noting that we were able to perform a one-step purification to obtain these crystals, which are homogeneous by gel analysis and by preliminary LC/MS analysis of solvent extractions from the purified protein (data not shown). This is significant as further purification steps can often lead to losses in protein yield that then prohibit or limit the number of crystallization trials that can be attempted in order to identify crystallization conditions. Thus, this study is hallmark example of minimal purification that produces crystals sufficient for structure determination. In our future efforts, we will attempt to manipulate these crystals to diffract to higher resolution. High solvent content crystals such as the ones reported here usually respond well to dehydration [40,41], desiccation [42], or annealing [43–45]. The current results provide a basis for structural and biophysical studies of the TREM-2 variants associated with neurodegenerative diseases, which will be required to understand the functional consequences of these point mutations. Ultimately, these studies of TREM-2 structure and function have the potential to lead to the development of patient-specific treatments for neurodegenerative and related inflammatory diseases.

Acknowledgments

We thank Marco Colonna for the kind gift of the human TREM-2 WT construct in pMX-3P plasmid. We thank Artie Romero for synthesizing PEI-TMC25. We thank Zeynep Yurtsever and Jennifer Alexander-Brett for critical reading of the manuscript. This work was supported in part by funding from NIH R01-HL119813 (T.J.B) and U19-AI070489 (M.J.H.). Results were derived from work performed at Argonne National Laboratory, which is operated by U. Chicago Argonne, LLC, for the U.S. DOE, Office of Biological and Environmental Research (DE-AC02-06CH11357). The molecular replacement model is available upon request.

References

[1] R. Guerreiro, A. Wojtas, J. Bras, M. Carrasquillo, E. Rogaeva, E. Majounie, C. Cruchaga, C. Sassi, J.S. Kauwe, S. Younkin, L. Hazrati, J. Collinge, J. Pocock, T. Lashley, J. Williams, J.C. Lambert, P. Amouyel, A. Goate, R. Rademakers, K. Morgan, J. Powell, P. St George-Hyslop, A. Singleton, J. Hardy, TREM2 variants in Alzheimer's disease, N. Engl. J. Med. 368 (2013) 117–127.

[2] T. Jonsson, H. Stefansson, S. Steinberg, I. Jonsdottir, P.V. Jonsson, J. Snaedal, S. Bjornsson, J. Huttenlocher, A.I. Levey, J.J. Lah, D. Rujescu, H. Hampel, I. Giegling, O.A. Andreassen, K. Engedal, I. Ulstein, S. Djurovic, C. Ibrahim-Verbaas, A. Hofman, M.A. Ikram, C.M. van Duijn, U. Thorsteinsdottir, A. Kong, K. Stefansson, Variant of TREM2 associated with the risk of Alzheimer's disease, N. Engl. J. Med. 368 (2013) 107–116.

[3] A.M. Saunders, W.J. Strittmatter, D. Schmechel, P.H. George-Hyslop, M.A. Pericak-Vance, S.H. Joo, B.L. Rosi, J.F. Gusella, D.R. Crapper-MacLachlan, M.J. Alberts, et al., Association of apolipoprotein E allele epsilon 4 with late-onset familial and sporadic Alzheimer's disease, Neurology 43 (1993) 1467–1472.

[4] B.A. Benitez, B. Cooper, P. Pastor, S.C. Jin, E. Lorenzo, S. Cervantes, C. Cruchaga, TREM2 is associated with the risk of Alzheimer's disease in Spanish population, Neurobiol. Aging 34 (1711) (2013) e1715–e1717.

[5] C. Pottier, D. Wallon, S. Rousseau, A. Rovelet-Lecrux, A.C. Richard, A. Rollin-Sillaire, T. Frebourg, D. Campion, D. Hannequin, TREM2 R47H variant as a risk factor for early-onset Alzheimer's disease, J. Alzheimers Dis. 35 (2013) 45–49.

[6] B.A. Benitez, C. Cruchaga, TREM2 and neurodegenerative disease, N. Engl. J. Med. 369 (2013) 1567–1568.

[7] S. Rayaprolu, B. Mullen, M. Baker, T. Lynch, E. Finger, W.W. Seeley, K.J. Hatanpaa, C. Lomen-Hoerth, A. Kertesz, E.H. Bigio, C. Lippa, K.A. Josephs, D.S. Knopman, C.L. White 3rd, R. Caselli, I.R. Mackenzie, B.L. Miller, M. Boczarska-Jedynak, G. Opala, A. Krygowska-Wajs, M. Barcikowska, S.G. Younkin, R.C. Petersen, N. Ertekin-Taner, R.J. Uitti, J.F. Meschia, K.B. Boylan, B.F. Boeve, N.R. Graff-Radford, Z.K. Wszolek, D.W. Dickson, R. Rademakers, O.A. Ross, TREM2 in neurodegeneration: evidence for association of the p. R47H variant with frontotemporal dementia and Parkinson's disease, Mol. Neurodegener. 8 (2013) 19.

[8] R.J. Guerreiro, E. Lohmann, J.M. Bras, J.R. Gibbs, J.D. Rohrer, N. Gurunlian, B. Dursun, B. Bilgic, H. Hanagasi, H. Gurvit, M. Emre, A. Singleton, J. Hardy, Using exome sequencing to reveal mutations in TREM2 presenting as a frontotemporal dementia-like syndrome without bone involvement, JAMA. Neurol. 70 (2013) 78–84.

[9] R. Guerreiro, B. Bilgic, G. Guven, J. Bras, J. Rohrer, E. Lohmann, H. Hanagasi, H. Gurvit, M. Emre, A novel compound heterozygous mutation in TREM2 found in a Turkish frontotemporal dementia-like family, Neurobiol. Aging 34 (2890) (2013) e2891–2895.

[10] B. Borroni, F. Ferrari, D. Galimberti, B. Nacmias, C. Barone, S. Bagnoli, C. Fenoglio, I. Piaceri, S. Archetti, C. Bonvicini, M. Gennarelli, M. Turla, E. Scarpini, S. Sorbi, A. Padovani, Heterozygous TREM2 mutations in frontotemporal dementia, Neurobiol. Aging (2013).

[11] E. Cuyvers, K. Bettens, S. Philtjens, T. Van Langenhove, I. Gijselinck, J. van der Zee, S. Engelborghs, M. Vandenbulcke, J. Van Dongen, N. Geerts, G. Maes, M. Mattheijssens, K. Peeters, P. Cras, R. Vandenberghe, P.P. De Deyn, C. Van Broeckhoven, M. Cruts, K. Sleegers, Investigating the role of rare heterozygous TREM2 variants in Alzheimer's disease and frontotemporal dementia, Neurobiol. Aging 35 (726) (2014) e711–e729.

[12] T.E. Golde, W.J. Streit, P. Chakrabarty, Alzheimer's disease risk alleles in TREM2 illuminate innate immunity in Alzheimer's disease, Alzheimers Res. Ther. 5 (2013) 24.

[13] J.W. Ford, D.W. McVicar, TREM and TREM-like receptors in inflammation and disease, Curr. Opin. Immunol. 21 (2009) 38–46.

[14] A. Bouchon, C. Hernandez-Munain, M. Cella, M. Colonna, A DAP12-mediated pathway regulates expression of CC chemokine receptor 7 and maturation of human dendritic cells, J. Exp. Med. 194 (2001) 1111–1122.

[15] E.N. N'Diaye, C.S. Branda, S.S. Branda, L. Nevarez, M. Colonna, C. Lowell, J.A. Hamerman, W.E. Seaman, TREM-2 (triggering receptor expressed on myeloid cells 2) is a phagocytic receptor for bacteria, J. Cell. Biol. 184 (2009) 215–223.

[16] C.L. Hsieh, M. Koike, S.C. Spusta, E.C. Niemi, M. Yenari, M.C. Nakamura, W.E. Seaman, A role for TREM2 ligands in the phagocytosis of apoptotic neuronal cells by microglia, J. Neurochem. 109 (2009) 1144–1156.

[17] N. Takegahara, H. Takamatsu, T. Toyofuku, T. Tsujimura, T. Okuno, K. Yukawa, M. Mizui, M. Yamamoto, D.V. Prasad, K. Suzuki, M. Ishii, K. Terai, M. Moriya, Y. Nakatsuji, S. Sakoda, S. Sato, S. Akira, K. Takeda, M. Inui, T. Takai, M. Ikawa, M. Okabe, A. Kumanogoh, H. Kikutani, Plexin-A1 and its interaction with DAP12 in immune responses and bone homeostasis, Nat. Cell Biol. 8 (2006) 615–622.

[18] L. Stefano, G. Racchetti, F. Bianco, N. Passini, R.S. Gupta, P. Panina Bordignon, J. Meldolesi, The surface-exposed chaperone, Hsp60, is an agonist of the microglial TREM2 receptor, J. Neurochem. 110 (2009) 284–294.

[19] J. Paloneva, T. Manninen, G. Christman, K. Hovanes, J. Mandelin, R. Adolfsson, M. Bianchin, T. Bird, R. Miranda, A. Salmaggi, L. Tranebjaerg, Y. Konttinen, L. Peltonen, Mutations in two genes encoding different subunits of a receptor signaling complex result in an identical disease phenotype, Am. J. Hum. Genet. 71 (2002) 656–662.

[20] A.R. Aricescu, W. Lu, E.Y. Jones, A time- and cost-efficient system for high-level protein production in mammalian cells, Acta Crystallogr. D Biol. Crystallogr. 62 (2006) 1243–1250.

[21] M.S. Kelker, E.W. Debler, I.A. Wilson, Crystal structure of mouse triggering receptor expressed on myeloid cells 1 (TREM-1) at 1.76 A, J. Mol. Biol. 344 (2004) 1175–1181.

[22] M.S. Kelker, T.R. Foss, W. Peti, L. Teyton, J.W. Kelly, K. Wuthrich, I.A. Wilson, Crystal structure of human triggering receptor expressed on myeloid cells 1 (TREM-1) at 1.47 A, J. Mol. Biol. 342 (2004) 1237–1248.

[23] S. Radaev, M. Kattah, B. Rostro, M. Colonna, P.D. Sun, Crystal structure of the human myeloid cell activating receptor TREM-1, Structure 11 (2003) 1527–1535.

[24] J.L. Gattis, A.V. Washington, M.M. Chisholm, L. Quigley, A. Szyk, D.W. McVicar, J. Lubkowski, The structure of the extracellular domain of triggering receptor expressed on myeloid cells like transcript-1 and evidence for a naturally occurring soluble fragment, J. Biol. Chem. 281 (2006) 13396–13403.

[25] J.A. Marquez, E. Galfre, F. Dupeux, D. Flot, O. Moran, N. Dimasi, The crystal structure of the extracellular domain of the inhibitor receptor expressed on myeloid cells IREM-1, J. Mol. Biol. 367 (2007) 310–318.

[26] C. Cantoni, M. Ponassi, R. Biassoni, R. Conte, A. Spallarossa, A. Moretta, L. Moretta, M. Bolognesi, D. Bordo, The three-dimensional structure of the human NK cell receptor NKp44, a triggering partner in natural cytotoxicity, Structure 11 (2003) 725–734.

[27] C. Yang, W. Cheng, P.Y. Teo, A.C. Engler, D.J. Coady, J.L. Hedrick, Y.Y. Yang, Mitigated cytotoxicity and tremendously enhanced gene transfection efficiency of PEI through facile one-step carbamate modification, Adv. Healthcare Mater. 2 (2013) 1304–1308.

[28] V.T. Chang, M. Crispin, A.R. Aricescu, D.J. Harvey, J.E. Nettleship, J.A. Fennelly, C. Yu, K.S. Boles, E.J. Evans, D.I. Stuart, R.A. Dwek, E.Y. Jones, R.J. Owens, S.J. Davis, Glycoprotein structural genomics: solving the glycosylation problem, Structure 15 (2007) 267–273.

[29] Z. Otwinowski, W. Minor, Processing of X-ray diffraction data collected in oscillation mode, Methods Enzymol. 276 (1997) 307–326.

[30] A.J. McCoy, R.W. Grosse-Kunstleve, P.D. Adams, M.D. Winn, L.C. Storoni, R.J. Read, Phaser crystallographic software, J. Appl. Crystallogr. 40 (2007) 658–674.

[31] L. Tong, M.G. Rossmann, Rotation function calculations with GLRF program, Methods Enzymol. 276 (1997) 594–611.

[32] Z. Yurtsever, M. Sala-Rabanal, D.T. Randolph, S.M. Scheaffer, W.T. Roswit, Y.G. Alevy, A.C. Patel, R.F. Heier, A.G. Romero, C.G. Nichols, M.J. Holtzman, T.J. Brett, Self-cleavage of human CLCA1 protein by a novel internal metalloprotease domain controls calcium-activated chloride channel activation, J. Biol. Chem. 287 (2012) 42138–42149.

[33] M.R. Sawaya, Characterizing a crystal from an initial native dataset, Methods Mol. Biol. 364 (2007) 95–120.
[34] A. Paradowska-Gorycka, M. Jurkowska, Structure, expression pattern and biological activity of molecular complex TREM-2/DAP12, Hum. Immunol. 74 (2013) 730–737.
[35] L. Piccio, C. Buonsanti, M. Cella, I. Tassi, R.E. Schmidt, C. Fenoglio, J. Rinker 2nd, R.T. Naismith, P. Panina-Bordignon, N. Passini, D. Galimberti, E. Scarpini, M. Colonna, A.H. Cross, Identification of soluble TREM-2 in the cerebrospinal fluid and its association with multiple sclerosis and CNS inflammation, Brain 131 (2008) 3081–3091.
[36] K. Takahashi, M. Prinz, M. Stagi, O. Chechneva, H. Neumann, TREM2-transduced myeloid precursors mediate nervous tissue debris clearance and facilitate recovery in an animal model of multiple sclerosis, PLoS Med. 4 (2007) e124.
[37] M.W. Sieber, N. Jaenisch, M. Brehm, M. Guenther, B. Linnartz-Gerlach, H. Neumann, O.W. Witte, C. Frahm, Attenuated inflammatory response in triggering receptor expressed on myeloid cells 2 (TREM2) knock-out mice following stroke, PLoS One 8 (2013) e52982.
[38] C. Correale, M. Genua, S. Vetrano, E. Mazzini, C. Martinoli, A. Spinelli, V. Arena, L. Peyrin-Biroulet, F. Caprioli, N. Passini, P. Panina-Bordignon, A. Repici, A. Malesci, S. Rutella, M. Rescigno, S. Danese, Bacterial sensor triggering receptor expressed on myeloid cells-2 regulates the mucosal inflammatory response, Gastroenterology 144 (2013) 346–356.e3.
[39] S. Poliska, E. Csanky, A. Szanto, I. Szatmari, B. Mesko, L. Szeles, B. Dezso, B. Scholtz, J. Podani, I. Kilty, L. Takacs, L. Nagy, Chronic obstructive pulmonary disease-specific gene expression signatures of alveolar macrophages as well as peripheral blood monocytes overlap and correlate with lung function, Respiration 81 (2011) 499–510.
[40] B. Heras, M.A. Edeling, K.A. Byriel, A. Jones, S. Raina, J.L. Martin, Dehydration converts DsbG crystal diffraction from low to high resolution, Structure 11 (2003) 139–145.
[41] B. Heras, J.L. Martin, Post-crystallization treatments for improving diffraction quality of protein crystals, Acta Crystallogr. D Biol. Crystallogr. 61 (2005) 1173–1180.
[42] C. Abergel, Spectacular improvement of X-ray diffraction through fast desiccation of protein crystals, Acta Crystallogr. D Biol. Crystallogr. 60 (2004) 1413–1416.
[43] J.M. Harp, B.L. Hanson, D.E. Timm, G.J. Bunick, Macromolecular crystal annealing: evaluation of techniques and variables, Acta Crystallogr. D Biol. Crystallogr. 55 (1999) 1329–1334.
[44] J.M. Harp, D.E. Timm, G.J. Bunick, Macromolecular crystal annealing: overcoming increased mosaicity associated with cryocrystallography, Acta Crystallogr. D Biol. Crystallogr. 54 (1998) 622–628.
[45] J.I. Yeh, W.G. Hol, A flash-annealing technique to improve diffraction limits and lower mosaicity in crystals of glycerol kinase, Acta Crystallogr. D Biol. Crystallogr. 54 (1998) 479–480.

Video Article

Efficient Mammalian Cell Expression and Single-step Purification of Extracellular Glycoproteins for Crystallization

Daniel L. Kober*[1,2,3], Zeynep Yurtsever*[2,3,4,5], Thomas J. Brett[2,3,5,6,7]

[1]Molecular Microbiology and Microbial Pathogenesis Program, Washington University School of Medicine

[2]Department of Internal Medicine, Washington University School of Medicine

[3]Drug Discovery Program in Pulmonary and Critical Care Medicine, Washington University School of Medicine

[4]Biochemistry Program, Washington University School of Medicine

[5]Center for the Investigation of Membrane Excitability Diseases, Washington University School of Medicine

[6]Department of Biochemistry and Molecular Biophysics, Washington University School of Medicine

[7]Department of Cell Biology and Physiology, Washington University School of Medicine

*These authors contributed equally

Correspondence to: Thomas J. Brett at TBRETT@dom.wustl.edu

URL: http://www.jove.com/video/53445
DOI: doi:10.3791/53445

Keywords: Biochemistry, Issue 106, mammalian protein expression, nickel affinity chromatography, glycosylation, macromolecular crystallography

Date Published: 12/23/2015

Citation: Kober, D.L., Yurtsever, Z., Brett, T.J. Efficient Mammalian Cell Expression and Single-step Purification of Extracellular Glycoproteins for Crystallization. *J. Vis. Exp.* (106), e53445, doi:10.3791/53445 (2015).

Abstract

Production of secreted mammalian proteins for structural and biophysical studies can be challenging, time intensive, and costly. Here described is a time and cost efficient protocol for secreted protein expression in mammalian cells and one step purification using nickel affinity chromatography. The system is based on large scale transient transfection of mammalian cells in suspension, which greatly decreases the time to produce protein, as it eliminates steps, such as developing expression viruses or generating stable expressing cell lines. This protocol utilizes cheap transfection agents, which can be easily made by simple chemical modification, or moderately priced transfection agents, which increase yield through increased transfection efficiency and decreased cytotoxicity. Careful monitoring and maintaining of media glucose levels increases protein yield. Controlling the maturation of native glycans at the expression step increases the final yield of properly folded and functional mammalian proteins, which are ideal properties to pursue X-ray crystallography. In some cases, single step purification produces protein of sufficient purity for crystallization, which is demonstrated here as an example case.

Video Link

The video component of this article can be found at http://www.jove.com/video/53445/

Introduction

Understanding protein structure at an atomic level is key to uncovering the molecular basis of biological pathways and diseases. X-ray protein crystallography is the most widely used/applicable method for determining macromolecular structures. The main challenge of this method is obtaining sufficient amounts of properly folded, pure protein. This becomes an issue particularly when working with secreted mammalian proteins, which undergo specific post-translational modifications.

Bacterially-expressed proteins are the primary source of crystallized proteins deposited in the Protein Data Bank[1]. Bacterial expression systems are largely preferred because they are fast, inexpensive and typically produce high yields of protein. However, extracellular domains of mammalian proteins expressed in bacteria are often not properly folded, in which case refolding and extensive purification steps are required for obtaining homogeneously folded protein. Additionally, many mammalian proteins require post-translational glycosylation to achieve proper folding[2]. Although expression and glycosylation in yeast or insect cells can overcome the folding problem, post-translational modifications, including glycosylation, differ significantly from those of mammalian cells[3], yielding proteins with incorrect or non-homogeneous modifications.

Mammalian cells express all the required molecular machinery to ensure proper post-translational modifications and folding; however, these expression systems are not typically preferred by most labs, due to limited yields and high costs of reagents and consumables. Polyethyleneimine (PEI), a standard transfection reagent is relatively cheap but imposes considerable cytotoxicity and low transfection efficiency, resulting in increased costs in cell media, DNA, and culturing equipment. Many alternatives to PEI are prohibitively expensive. We address these issues by describing a combination of improved cell culture tools and chemically modified PEI for the quick and relatively inexpensive method for the expression of secreted mammalian proteins, followed by single-step purification. This robust method gives sufficient yields for functional and biochemical studies[4], and in some cases, results in protein amenable to crystallization without further purification.

This protocol describes several techniques to maximize expression and yield for secreted mammalian proteins in human embryonic kidney (HEK) 293F cells grown in suspension. Transfection efficiency (and cost), protein production and purification are all greatly enhanced by following this protocol. PEI modified by the addition of carbamates through a single-step ring-opening reaction (PEI-TMC-25, synthesis and properties described in detail in ref [5]) greatly improves transfection efficiency, reduces the cytotoxicity from cationic membrane disruption and accordingly reduces experiment costs. Furthermore, cell viability and protein expression are greatly improved with the addition of culture supplements to supply glucose and vitamins. Importantly for the production of glycosylated proteins, treatment with kifunensine, a non-toxic chemical inhibitor of Mannosidase I, produces proteins with defined, immature glycans, which can be removed by the endoglycosidase EndoHf to yield proteins with a single N-acetylglucosamine in place of a full-length N-linked glycan[6]. Finally, the secretion of proteins into a serum-free, chemically defined medium allows rapid and facile purification for structural and biochemical studies. Single-step nickel-nitrilotriacetic acid (Ni-NTA) resin purification removes the majority of contaminating species in the supernatant and, in some cases, can yield protein of sufficient purity for crystallization.

Protocol

1. Production of Milligram Quantities of Plasmid DNA for Large-scale Transient Transfection

1. Clone the protein of interest into a high copy number mammalian expression vector using restriction site cloning, or other appropriate technique.
    1. For optimal results, use pHLsec [7] vector, which has a built-in C-terminal 6His-tag, a strong promoter Kozak sequence and an optimized secretion signal.
2. Transform the plasmid onto competent cells.
    1. Add 20 µl of competent E. coli cells onto 1 µg of plasmid DNA and incubate on ice for 30 min.
    2. Heat shock cells at 42 °C for 35 sec, then incubate on ice for 2 min.
    3. Add 300 µl of microbial growth medium (SOC) and incubate at 37 °C for 45 mins, shaking at 220 rpm.
    4. Plate cells on agar plate with appropriate antibiotic selection.
        1. Use 100 µg/ml carbenicillin if the plasmid is in the pHLsec vector.
3. Culture colonies in 250 ml of Luria Broth (LB) Media supplemented with 100 µg/ml antibiotic (carbenicillin) O/N at 37 °C, shaking at 220 rpm.
4. Purify DNA from culture using Hi-Speed Plasmid Maxi Kit according to manufacturer's protocol.
    1. Elute DNA in buffer EB (10 mM Tris-Cl, pH 8.5), instead of buffer TE.
    2. Aliquot the purified plasmid at amount needed for transfection and store at -20 °C.

2. Large-scale Culture and Transient Transfection of 293F Cells

1. Supplement 1 L 293F media with 10 ml of glutamine and 5 ml Pen/Strep (both 100x). Store at 4 °C. 5 ml Pen/Strep is a sufficient strength in serum-free conditions and the reduced antibiotic concentration improves cell viability during transfection, which improves protein yields.
2. Culture 293F cells in 300 ml media in 1 L polycarbonate baffled Erlenmeyer flasks with vented caps at 37 °C with 8% CO_2, while shaking in a standard tissue culture incubator.
3. Dilute cells to 5 x 10^5/ml density one day before transfection.
4. On the day of transfection, supplement culture medium by adding 10% volume of 2% w/v Cell Boost in 293F media.
    1. Measure glucose concentration using a glucose monitor according to the manufacturer's instructions and use supplements as needed to achieve a glucose concentration of 500 mg/dL.
5. Add kifunensine (1 µg/ml final concentration) at this step to control protein glycosylation.
6. Calculate volume of DNA required for 1 µg plasmid per 1 x 10^6 cells. Under sterile conditions, dilute DNA in 5 ml serum-free medium.
7. Calculate volume of transfection reagent required for 1 µg plasmid per 2 µl transfection reagent. Under sterile conditions, dilute transfection reagent (PEI-TMC-25) in 5 ml serum-free medium.
8. Add transfection reagent into DNA solution in 1 ml increments, mixing gently. Incubate for 30 min at RT for reagent-DNA complexes to form. Then add the solution onto the cells in a drop-wise fashion.
9. Allow transfected cells to express protein for 72-96 hr. Supplement with ~10% volume Cell Boost Media daily, or as necessary to keep glucose reading 400-600 mg/dl.

3. Purification

1. Decant culture into a centrifuge flask, centrifuge for 20 min at 1,300 x g to pellet cells and then collect the supernatant. If necessary, spin a second time and/or use 0.22 µm filter to clarify supernatant.
2. Add 10% volume 10x Ni-NTA binding buffer (1.5 M NaCl, 0.5 M K_2HPO_4, 0.1 M Tris pH 8.5, 50 mM imidazole).
3. Prepare a gravity column by adding 2 ml of Ni-NTA slurry in a column and equilibrating with 10 column volumes (CV) of 1x binding buffer. If possible, do all column steps in a 4 °C room. Alternatively, chill protein and all buffers on ice before column step, and keep protein and collected flow-through on ice.
   Note: Ni-NTA slurry is 50% resin by volume and the manufacture's stated binding capacity is 50 mg/ml. Ni-NTA beads can be re-charged for multiple uses
4. Flow the supernatant over the resin and collect flow-through. Repeat this step.

5. Wash with 10 CV of wash buffer (300 mM NaCl, 50 mM K_2HPO_4, 20 mM imidazole pH 8).
6. Elute the protein in 5 CV of elution buffer (300 mM NaCl, 50 mM K_2HPO_4, 250 mM imidazole pH 8).
7. If deglycosylation is required:
    1. For a final volume of 0.5 ml, concentrate eluate to 0.43 ml using a centrifugation concentrator. If precipitates form, pellet any debris by centrifugation at 16,000 x g and 4 °C.
    2. Add 50 µl of 500 mM Na-Citrate pH 5.5.
    3. Add 20 µl of EndoHf (1 x 10^6 U/ml). Incubate at RT for 2 hr.
    Note: The enzyme works optimally at 37 °C, which may cause the concentrated protein to aggregate. Extend the RT incubation, if deglycosylation, assessed by SDS-PAGE or immunoblotting, is incomplete. The enzyme does not have activity at 4 °C.
    4. To remove EndoHf: Wash Amylose Resin 3x in phosphate buffered saline (PBS) or final storage buffer. Incubate protein with resin for 1 hr at 4 °C. Spin 5 min at 1,000 x g to pellet beads and collect the supernatant.
    5. Concentrate protein using appropriate molecular weight cutoff centrifugation filter and buffer exchange into storage buffer (150 mM NaCl and 20 mM HEPES pH 7.5).

Representative Results

Herein follows the results of this expression system applied to a secreted 13 kDa immunoglobin (Ig) domain from the human protein triggering receptor expressed on myeloid cells 2 (hTREM2, residues 19-132). TREM2 is a type I transmembrane protein containing a single extracellular Ig domain that has two disulfide bonds and two N-linked glycosylation sites. Unlike many other Ig domain proteins[8], TREM2 was not amenable to refolding from bacterial inclusion bodies[9]. Subsequent mutagenesis confirmed N-linked glycans are required for proper expression and folding. To facilitate structural and functional studies, TREM2 was introduced into the pHLsec vector with a C-terminal 6His-tag[7] using standard molecular biology techniques. Transient expression in HEK293F cells treated with kifunensine yielded protein that was purified by Ni-NTA chromatography (**Figure 1B, lane 2**) and the sample was then deglycosylated to produce natively folded, homogenous protein (**Figure 1B, lane 3**). 293F expression of TREM2 produced 5-10 mg/L (5-10µg/million transfected cells). After buffer exchanging into the storage buffer, this protein was crystallized (**Figure 1C**). Despite the final purity of about 80%, these crystals reliably reproduced, diffracted, and were shown by silver-stain to only contain TREM2 protein (**Figure 1D**). This observation suggests the biochemical homogeneity of the protein (*i.e.,* folding and post-translational modifications) can, in some cases, be more critical than overall purity for crystallization success.

In addition to crystallization, this system offers a robust tool for structural and functional studies. It is exploited to produce natively glycosylated protein and achieve >95% purity by size-exclusion chromatography (**Figure 1E, F**). This additional purification step, which shows the solution behavior of the protein, is also an ideal way to monitor protein quality. The purified protein should elute at a volume corresponding to its molecular weight and should be the most abundant species in the sample. Abnormally large amounts of aggregated protein may indicate unstable protein and provide clues to optimize protein production and purification. Furthermore, this final purified protein is superior for use in quantitative biophysical experiments such as circular dichroism spectroscopy, thermal stability, and investigating protein-ligand interactions. Lastly, controlling the extent of glycosylation provides a robust tool to study glycan-dependent functions.

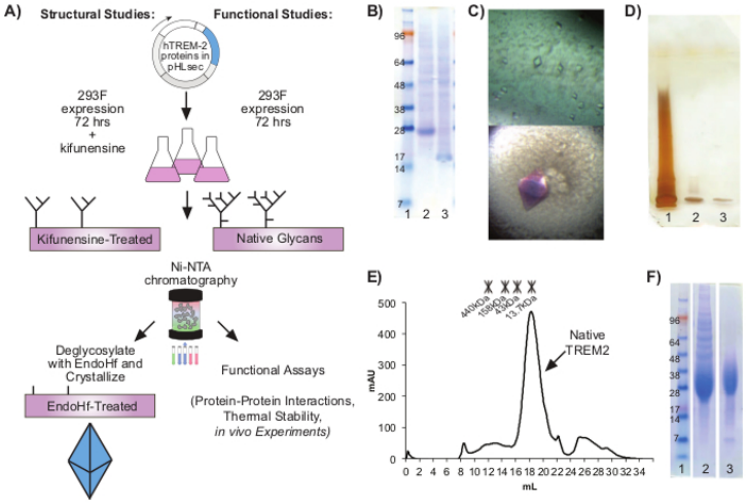

Figure 1. Mammalian Expression System: (**A**) Scheme for mammalian expression of proteins with controlled or native glycosylation in HEK 293F cells. (**B**) SDS-PAGE of NiNTA-purified hTREM2 expressed under kifunensine shown before (lane 2) and after (lane 3) deglycosylation with EndoHf. (**C**) Crystals produced from NiNTA-purified and deglycosylated protein. (**D**) Silver stain of crystallization input (lane 1) and harvested crystals (lanes 2 and 3) reveals crystals only contain TREM2. (**E**) Further purification of TREM2 was achieved using size-exclusion chromatography of NiNTA-purified TREM2 produced in 293F cells without Kifunensine. Asterisks (*) indicate elution volumes of molecular weight standards. Proteins eluted in TBS using an analytical S200 column (GE). (**F**) SDS-PAGE analysis of size exclusion-purified TREM2: input protein (lane 2) and folded peak (lane 3). Note how full, heterogeneous glycans run at a higher apparent molecular weight with a broad smear by SDS-PAGE. Please click here to view a larger version of this figure.

Discussion

HEK 293F cells offer robust production of proteins requiring post-translational modifications. This system allows rapid and scalable expression of natively folded proteins containing disulfides, glycosylation, and phosphorylation that would otherwise be absent using more routine expression tools. In addition, this system can be used for the expression and purification of multi-protein complexes simply by co-transfection of multiple plasmids. Besides TREM2, this system has been extensively used for functional studies with other proteins of interest in the lab[10,11]. Mammalian cells also offer endotoxin-free protein expression optimal for *in vivo* experiments or for production of natively folded antigens to generate conformation-dependent antibodies.

Optimal cell viability and transfection conditions are the most crucial for efficient protein production. For better cell viability, low-passage cell cultures are boosted with cell culture supplements and the antibiotic concentration in the growth media is reduced. The modified PEI-TMC-25 has suitable transection efficiency with most proteins; however, there are other options available at moderate price that offer increased transfection efficiency and reduced cytotoxicity. Hype 5 (Oz Bioscience) increases yields compared to PEI or other reagents, at a considerably reduced cost compared to more expensive transfection reagents, such as 293fectin. The reagent type and DNA: reagent ratios can be optimized for individual expressions and the needs of the desired experiment.

The method described here has several advantages over other methods of protein production. Mammalian cells offer native chaperone folding and post-translational modifications unavailable to bacteria and yeast. The reduced time for plasmid construction and preparation, along the use of media, the pH of which can be directly modified, make it superior to baculovirus-based production in insect cells; and finally, the serum-free media offers facile scaling (higher cell density) and purification not attainable to adherent 293T cells. The chief limitation of this system is only the time and scale the individual researcher is able to commit to protein expression.

Included below are troubleshooting options for the most common issues encountered.

Troubleshooting

If there is low protein expression, avoid passaging 293F cells longer than 2-3 months. Prolonged passaging results in decreased cell health reflected in slower doubling times and significantly reduced protein expression. Cell growth should be monitored daily and cultures no longer doubling daily should be discarded. Cell viability can be improved by using culture supplements while passaging cells. Monitor glucose to ensure a culture concentration of 400-600 mg/dl Cell density should not exceed 2 million/ml and cell viability should be ≥98% by trypan blue exclusion. Dilute dense cells to 0.5 million/ml and allow to double O/N before transfection. Optimize transfection using different ratios of transfection reagent: DNA (within the range of 1 µg DNA: 1.5-6 µl reagent). This can be done using 2 ml cultures in a 6-well plate and the output measured by immunoblotting. Doing 12 hr time points can indicate if the protein is being expressed and degraded rapidly; check the cell lysate if protein is not observed in the supernatant fraction. Misfolded proteins, which fail to be secreted, will still be apparent in the cell lysate by immunoblotting.

If Ni-NTA retention is low, *i.e.,* protein remains in flow-through after column binding, use fresh resin. Increasing pH of sample to 8.5 will result in stronger binding to the resin, although this will also increase non-specific binding. Concentrating the sample and batch binding to resin O/N

at 4 °C before Ni-NTA purification may result in ~5x increase in recovered protein. If the 6His-tag is inaccessible due to tertiary structure of the protein, try cloning it on the other terminus. Alternatively, use Cobalt resin, which has a higher affinity for His residues.

If the protein aggregates and/or precipitates during purification, increase solubility by adding 10% glycerol into the Ni-NTA wash and elution buffers. Run the nickel affinity columns at RT instead of 4 °C. Use differential scanning fluorimetry[12] to screen for pH and salt/additives that increase stability of the protein in solution.

Disclosures

The authors declare that they have no competing financial interests.

Acknowledgements

This work was supported by NIH R01-HL119813 (to T.J.B.), American Lung Association RG-196051 (to T.J.B.), a CIMED Pilot and Feasibility grant (to T.J.B.), American Heart Association Predoctoral Fellowships 14PRE19970008 (to Z.Y.) and 15PRE22110004 (to D.L.K.).

References

1. Meyer, S. *et al.* Multi-host expression system for recombinant production of challenging proteins. *PLoS One.* **8**, e68674 (2013).
2. Chang, V. T. *et al.* Glycoprotein structural genomics: solving the glycosylation problem. *Structure.* **15**, 267-273 (2007).
3. Rich, J. R., & Withers, S. G. Emerging methods for the production of homogeneous human glycoproteins. *Nat Chem Biol.* **5**, 206-215 (2009).
4. Wu, K. *et al.* TREM-2 promotes macrophage survival and lung disease after respiratory viral infection. *J Exp Med.* **212**, 681-697 (2015).
5. Yang, C. *et al.* Mitigated cytotoxicity and tremendously enhanced gene transfection efficiency of PEI through facile one-step carbamate modification. *Adv Healthc Mater.* **2**, 1304-1308 (2013).
6. Elbein, A. D. Glycosidase inhibitors: inhibitors of N-linked oligosaccharide processing. *FASEB J.* **5**, 3055-3063 (1991).
7. Aricescu, A. R., Lu, W., & Jones, E. Y. A time- and cost-efficient system for high-level protein production in mammalian cells. *Acta Crystallogr D Biol Crystallogr.* **62**, 1243-1250 (2006).
8. Kelker, M. S., Debler, E. W., & Wilson, I. A. Crystal structure of mouse triggering receptor expressed on myeloid cells 1 (TREM-1) at 1.76 A. *J Mol Biol.* **344**, 1175-1181 (2004).
9. Kober, D. L. *et al.* Preparation, crystallization, and preliminary crystallographic analysis of wild-type and mutant human TREM-2 ectodomains linked to neurodegenerative and inflammatory diseases. *Protein Expr Purif.* **96**, 32-38 (2014).
10. Yurtsever, Z. *et al.* Self-cleavage of human CLCA1 protein by a novel internal metalloprotease domain controls calcium-activated chloride channel activation. *J Biol Chem.* **287**, 42138-42149 (2012).
11. Sala-Rabanal, M., Yurtsever, Z., Nichols, C. G., & Brett, T. J. Secreted CLCA1 modulates TMEM16A to activate Ca-dependent chloride currents in human cells. *Elife.* **4** (2015).
12. Niesen, F. H., Berglund, H., & Vedadi, M. The use of differential scanning fluorimetry to detect ligand interactions that promote protein stability. *Nat Protoc.* **2**, 2212-2221 (2007).

eLIFE elifesciences.org

RESEARCH ARTICLE

Neurodegenerative disease mutations in TREM2 reveal a functional surface and distinct loss-of-function mechanisms

Daniel L Kober[1,2], Jennifer M Alexander-Brett[2], Celeste M Karch[3], Carlos Cruchaga[3], Marco Colonna[4], Michael J Holtzman[2,5,6], Thomas J Brett[2]*

[1]Molecular Microbiology and Microbial Pathogenesis Program, Washington University School of Medicine, St. Louis, United States; [2]Division of Pulmonary and Critical Care Medicine, Department of Internal Medicine, Washington University School of Medicine, St. Louis, United States; [3]Department of Psychiatry, Washington University School of Medicine, St. Louis, United States; [4]Department of Pathology and Immunology, Washington University School of Medicine, St. Louis, United States; [5]Department of Cell Biology and Physiology, Washington University School of Medicine, St. Louis, United States; [6]Department of Biochemistry and Molecular Biophysics, Washington University School of Medicine, St. Louis, United States

Abstract Genetic variations in the myeloid immune receptor TREM2 are linked to several neurodegenerative diseases. To determine how TREM2 variants contribute to these diseases, we performed structural and functional studies of wild-type and variant proteins. Our 3.1 Å TREM2 crystal structure revealed that mutations found in Nasu-Hakola disease are buried whereas Alzheimer's disease risk variants are found on the surface, suggesting that these mutations have distinct effects on TREM2 function. Biophysical and cellular methods indicate that Nasu-Hakola mutations impact protein stability and decrease folded TREM2 surface expression, whereas Alzheimer's risk variants impact binding to a TREM2 ligand. Additionally, the Alzheimer's risk variants appear to epitope map a functional surface on TREM2 that is unique within the larger TREM family. These findings provide a guide to structural and functional differences among genetic variants of TREM2, indicating that therapies targeting the TREM2 pathway should be tailored to these genetic and functional differences with patient-specific medicine approaches for neurodegenerative disorders.
DOI: 10.7554/eLife.20391.001

***For correspondence:** tbrett@wustl.edu

Competing interests: The authors declare that no competing interests exist.

Funding: See page 20

Received: 05 August 2016
Accepted: 28 November 2016

Reviewing editor: Axel T Brunger, Stanford University Medical Center, United States

Introduction

The precise molecular determinants and mechanisms underlying neurodegenerative diseases remain uncertain, but recent large-scale genetic sequencing projects have uncovered new candidates associated with these diseases. For example, whole genome and whole exome sequencing has identified point mutations in the gene encoding the protein TREM2 (triggering receptor expressed on myeloid cells 2) that correlate with a significantly increased risk of developing Alzheimer's disease (AD) (***Guerreiro et al., 2013b***; ***Jonsson et al., 2013***). In particular, the TREM2 R47H variant is associated with a risk that is similar to that associated with *APOE4*, previously the only well-established risk factor for late-onset AD. This mutation correlates with increased cerebrospinal fluid (CSF) tau levels, a well-established risk factor for AD (***Cruchaga et al., 2013***), and subsequent studies have identified this mutation in patients who have frontal temporal dementia (FTD), Parkinson's disease (PD) (***Rayaprolu et al., 2013***), and sporadic amyotrophic lateral sclerosis (ALS) (***Cady et al., 2014***). A

eLife digest Alzheimer's disease is a neurodegenerative disease and the most common cause of dementia – characterized by memory loss and difficulties with thinking, problem solving and language – in the elderly. Individuals with rare mutations in the gene that encodes a protein called TREM2 have a substantial risk of developing Alzheimer's disease in their mid-60s. A different set of mutations in the gene for TREM2cancause a more severe degenerative brain disease known as Nasu-Hakola disease in much younger people.

Proteins are made up of chains of building blocks called amino acids that need to fold into specific three-dimensional shapes to allow the protein to work properly. TREM2 is a signaling protein that is found on the surface of immune cells in the brain. Mutations causing Alzheimer's and Nasu-Hakola disease result in the production of mutant TREM2 proteins that differ from the normal protein by only a single amino acid. It is not clear how different mutations affecting the same protein can give rise to two distinct neurodegenerative diseases.

To address this question, Kober et al. used a range of techniques to study normal and mutant TREM2 proteins. First, a technique called X-ray crystallography – which makes it possible to construct three-dimensional models of proteins – revealed that the mutations responsible for Nasu-Hakola disease are buried deep within the core of the folded TREM2 protein. On the other hand, mutations associated with Alzheimer's disease lie on the surface of the protein.

Further experiments examined how these mutations alter the properties of TREM2, revealing that mutations linked to Nasu-Hakola disease affect the ability of TREM2 to fold correctly and how stable its final shape is. This results in fewer TREM2 proteins being present on the surface of immune cells. In contrast, mutations associated with Alzheimer's disease make it harder for TREM2 to bind to molecules known as glycosaminoglycans. The Alzheimer's mutations affect a specific part of TREM2 that is not found in other closely related proteins.

The findings of Kober et al. suggest that TREM2 binding to glycosaminoglycans is likely to be important in preventing Alzheimer's disease. The next step following on from this work is to find out exactly how these interactions affect immune cells, which may aid the development of new therapies for this disease.

DOI: 10.7554/eLife.20391.002

recent study of more than 1,600 late-onset AD (LOAD) and cognitively normal brains revealed that microglia-specific networks, including those containing TREM2, are those most significantly dysregulated in LOAD (***Zhang et al., 2013***). Thus, even in the absence of rare variants in *TREM2* that increase AD risk, *TREM2*-containing pathways play a significant role in disease. Recent studies in AD mouse models that are deficient in *TREM2* confirm that loss of TREM2 function contributes to classic AD pathology and demonstrates a crucial role for TREM2 in central nervous system (CNS) biology (***Jay et al., 2015***; ***Wang et al., 2015***; ***Ulrich et al., 2014***). *TREM2*-deficient AD mice display fewer activated microglia, and the absence of *TREM2* prevents microglia proliferation and promotes microglia apoptosis, which was correlated with increased accumulation of Aβ plaques (***Wang et al., 2015***; ***Jay et al., 2015***). Microglia in *TREM2*-deficient AD mice displayed less activation and did not engulf Aβ plaques. This impacts the density of Aβ plaques and promotes diffuse Aβ structures, which in turn are more neurotoxic, and contributes to the accumulation of classic AD pathology (***Wang et al., 2016***; ***Yuan et al., 2016***). These findings highlight a crucial role for *TREM2* in maintaining CNS homeostasis. Therefore,understanding how these risk variants affect TREM2 function and contribute to the pathogenesis of neurodegenerative diseases is vital to the development of therapies targeting these devastating conditions.

TREM2 is an innate immune receptor expressed on dendritic cells (DCs), resident macrophages such as osteoclasts and microglia, infiltrating (***Jay et al., 2015***) and inflammatory (***Wu et al., 2015***) macrophages, and CSF monocytes (***Colonna and Wang, 2016***). It is a type one receptor protein consisting of an extracellular V-type Ig domain, a short stalk, a transmembrane domain that associates with the adaptor protein DAP12 for signaling, and a cytoplasmic tail (***Figure 1a***) (***Colonna, 2003***). TREM2 has historically been shown to play an anti-inflammatory role *in vitro* by antagonizing the production of inflammatory cytokines from bone-marrow-derived macrophages

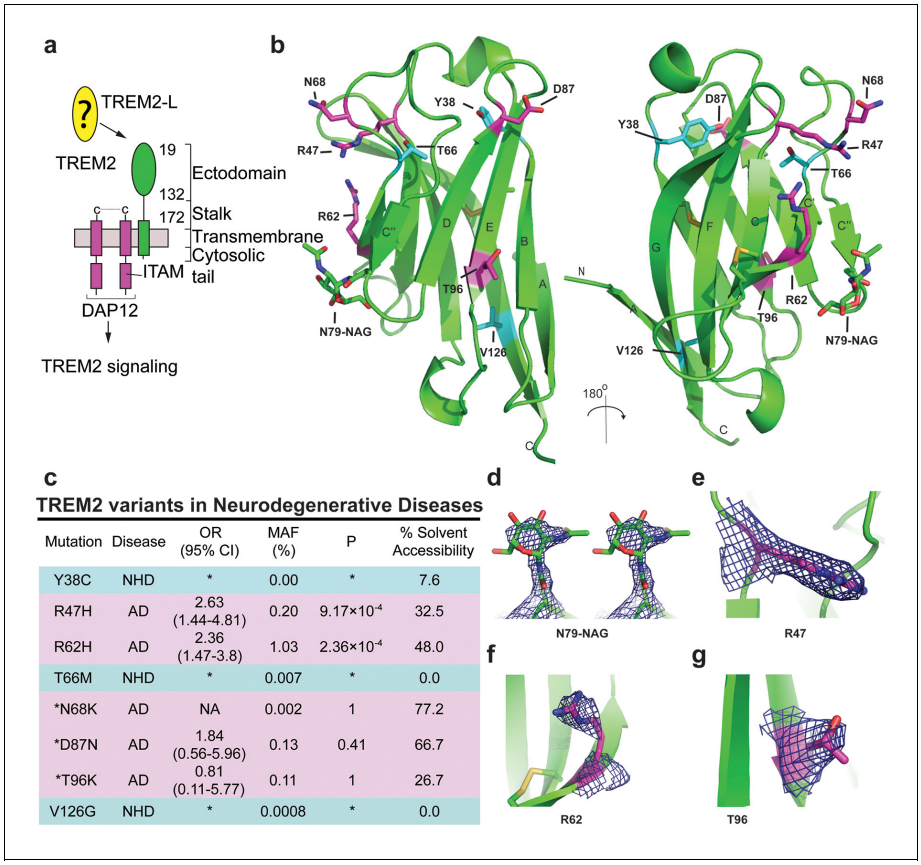

Figure 1. Crystal structure of the human TREM2 ectodomain. (**a**) Schematic of TREM2 cell-surface association with adapter protein DAP12, which contains an Immuno Tyrosine Activation Motif (ITAM). Engagement of TREM2-L by the ectodomain of TREM2 induces signaling. Domain boundaries are indicated. (**b**) TREM2 ectodomain in two orientations with disease-linked residues shown as sticks. The positions of AD risk variants are shown in magenta, whereas Nasu-Hakola disease (NHD) mutations are shown in cyan. The N-acetylglucosamine (NAG) is shown as green sticks. (**c**) Table of TREM2 disease-linked mutations, associated disease, and calculated solvent accessible surface exposure for the side-chain (calculated using Naccess), along with statistical correlations to AD (OR = odds ratio; MAF = mean allele frequency) (from ***Jin et al., 2014***). Table is highlighted with same color scheme as ***Figure 1b***. Validated AD risk variants (R47H and R62H) are not marked. Potential AD risk variants are denoted with an asterisk. (**d**) Side-by-side stereo view of difference electron density (2mFo-DFc contoured at 2σ) for the N79-NAG. (**e–g**) Difference electron density (2mFo-DFc contoured at 2σ) for the surface-exposed AD-associated mutation positions (**e**) R47, (**f**) R62 and (**g**) T96.

DOI: 10.7554/eLife.20391.003

The following figure supplements are available for figure 1:

Figure supplement 1. Analysis of TREM2 glycosylation, comparison of TREM2 monomers in the crystal structure, and SA-omit maps of AD-linked residues.

DOI: 10.7554/eLife.20391.004

Figure supplement 2. Packing neighbors for the TREM2 AD risk variant R47 and the TREM2 NHD mutants Y38, T66, and V126.

DOI: 10.7554/eLife.20391.005

(BMDMs) and dendritic cells (BMDDCs) in response to FcR (***Hamerman et al., 2006***) and Tlr signaling (***Turnbull et al., 2006***; ***Ito and Hamerman, 2012***). Likewise, TREM2 participates in phagocytosis of apoptotic cells in cultured microglia and reduces the production of inflammatory cytokines (***Takahashi et al., 2005***). However, TREM2-expressing macrophages can also promote inflammatory disease in the brain (***Jay et al., 2015***) and lung (***Wu et al., 2015***). The identity of a physiologic TREM2 ligand (TREM2-L) remains uncertain, although several classes of molecules have been

proposed, including bacterial carbohydrates (**Daws et al., 2003**; **Quan et al., 2008**), sulfoglycolipids (**Phongsisay et al., 2015**), nucleic acids (**Kawabori et al., 2015**), phospholipids (**Cannon et al., 2012**; **Wang et al., 2015**) and proteins (**Stefano et al., 2009**; **Takegahara et al., 2006**; **Yoon et al., 2012**; **Atagi et al., 2015**; **Bailey et al., 2015**). Additionally, previous studies have identified cells that express a TREM2-L, including astrocytes (**Daws et al., 2003**), DCs (**Ito and Hamerman, 2012**), BMDMs (**Hamerman et al., 2006**), neurons and apoptotic cells (**Hsieh et al., 2009**). This growing body of literature underscores the case for immune deregulation, specifically involving TREM2-associated pathways in neurodegenerative and inflammatory diseases (**Golde et al., 2013**).

Intriguingly, genetic variations in TREM2 are associated with two distinct groups of neurodegenerative diseases. Homozygous mutations including early-stop codons (**Paloneva et al., 2003**; **Soragna et al., 2003**), splice site mutations (**Numasawa et al., 2011**; **Chouery et al., 2008**), the coding stalk mutations D134G and K186N (**Paloneva et al., 2002**), and the coding ectodomain mutations Y38C, T66M, and V126G (**Guerreiro et al., 2013a**, **2013c**; **Le Ber et al., 2014**) cause either NHD, characterized by early-onset dementia, demyelination, and bone cyst lipoma (**Paloneva et al., 2002**; **Colonna, 2003**), or a frontotemporal dementia variant with severe loss of brain matter but lacking the bone manifestations. By contrast, *TREM2* mutations associated with AD contribute to disease risk as heterozygous variants. In addition to R47H, the coding mutation R62H is associated with increased risk of AD in independent studies (**Jin et al., 2014**; **Ridge et al., 2016**). These two variants have the strongest risk link to AD. N68K and D87N have also been identified in AD patients, but because these mutations are very rare, their risk remains uncertain (**Guerreiro et al., 2013b**; **Jonsson et al., 2013**). In addition, the mutation T96K has been linked to a decreased risk of AD, but this mutation is also too rare to allow verification of this observation (**Jin et al., 2014**). This curious segregation of disease phenotypes by distinct mutations occurring within the same protein suggest that these mutations should have divergent effects on the structure and function of TREM2.

In order to understand the molecular basis of how different mutations within TREM2 can lead to distinct neurodegenerative diseases, we performed structural, biophysical, and functional studies of wild-type (WT) and mutant TREM2 proteins. To facilitate these studies, we developed a novel mammalian expression system to produce the natively folded and glycosylated TREM2 ectodomains in milligram quantities (**Kober et al., 2014**, **2015**). We determined the crystal structure of the TREM2 ectodomain at 3.1 Å resolution and found that the disease-linked mutations exhibit distinct structural patterns, suggesting that they would impact TREM2 function through alternate mechanisms. To investigate this hypothesis, we carried out extensive biophysical, cellular, and functional assays. We found that NHD-causing mutations impact TREM2 protein folding and stability, whereas AD risk variants decrease binding to the cellular TREM2-ligand (TREM2-L). Furthermore, these AD-linked mutations appear to epitope map a disease-relevant functional surface on TREM2 that facilitates binding to cell-surface TREM2-L. These findings demonstrate two distinct loss-of-function mechanisms for TREM2, illuminate a disease-relevant functional surface on TREM2, and pave the way for the development of patient-specific molecular therapies for the treatment of distinct neurodegenerative diseases.

Results

Structure of the hTREM2 ectodomain

We previously reported the crystallization of the WT human TREM2 ectodomain (amino acids 19–134) purified from a mammalian cell expression system (**Kober et al., 2014**). These crystals diffracted to 3.1 Å (**Table 1** and **Table 2**). The TREM2 ectodomain is a V-type Ig domain containing two disulfide bonds, the canonical Ig disulfide between residues C36 and C110 (βB–βF) and an additional linkage between C51 and C60 (βC-βC') (**Figure 1b**). A single N-acetylglucosamine (NAG) glycan that remains after Endo Hf treatment (**Figure 1—figure supplement 1a**) is clearly visible in the electron density at residue N79 (**Figure 1d** and **Figure 1—figure supplement 1g**). The nine β-strands characteristic of proteins within this Ig domain class are present, and two short α-helix passages are observed spanning β-sheets B–C and E–F. The asymmetric unit (ASU) contains two monomers of hTREM2 in a parallel arrangement, but the limited buried surface area (~400 $Å^2$) and chemical nature of the interface suggest that this dimer would not exist in solution (**Figure 1—figure**

Table 1. Determination of resolution cut-off by evaluation of meaningful data.
To evaluate the functional resolution of data past 3.3 Å, data were scaled to 3.0 Å resolution. Data were successively truncated at 0.1 Å intervals from 3.4 Å to 3.0 Å and the initial 3.3 Å solution was used to initiate molecular replacement, rigid body refinement and XYZ refinement in PHENIX without manual refinements. After refinement at the higher resolution, the resulting model was used to calculate R and R_{free} values at the immediate lower resolution. If this resulted in a better model, as judged by R_{free}, the higher resolution data are useful for improving the model. Data at resolutions that improved the model are highlighted in green while data at resolutions that worsened the model are highlighted in red.

		Refine at:			
		3.3	3.2	3.1	3.0
Calculate at:	3.3	26.26/31.66	25.30/31.47		
	3.2		26.75/31.88	26.79/31.80	
	3.1			27.71/32.47	27.64/32.87
	3.0				28.30/32.52

DOI: 10.7554/eLife.20391.006

supplement 1b). Furthermore, these two monomers are quite similar (Cα RMSD of 0.65 Å, ***Figure 1—figure supplement 1c***), therefore, our analysis of hTREM2 described henceforth will refer to chain A.

Table 2. Data collection and refinement statistics.

	Human TREM2 ectodomain
Data collection	
Space group	P 6_4 2 2
Cell dimensions	
a, *b*, *c* (Å)	125.76, 125.76, 183.70
α, β, γ (°)	90, 90, 120
Resolution (Å)	50.00–3.10 (3.21–3.10)*
R_{sym}	0.11 (1.00)
Mean I / σI	21.0 (1.76)
Completeness (%)	99.88 (99.75)
Redundancy	12.9 (13.4)
Refinement	
Resolution (Å)	50.00–3.10
No. reflections	16,285
R_{work} / R_{free}	0.2605/0.2736
No. atoms	1,784
Protein	1,756
Carbohydrate	28
B-factors	93.48
Protein	92.39
Carbohydrate	162.1
R.m.s. deviations	
Bond lengths (Å)	0.006
Bond angles (°)	1.18

*Values in parentheses are for highest-resolution shell.
DOI: 10.7554/eLife.20391.007

We analyzed the structure to map the location of disease-linked point mutations and noticed an intriguing pattern. The side chains of mutations causing NHD (Y38, T66 and V126) are all buried within the core of the Ig fold, whereas the side chains of verified AD risk variants (R47H and R62H) and possible AD risk variants (N68K, D87N and T96K) all lie on the protein surface (***Figure 1b***). Quantification using solvent-accessible surface calculations verified this qualitative observation (***Figure 1c***). Using structural analysis, we can hypothesize how the buried NHD mutations could negatively impact protein folding. Y38 is adjacent to C36, which forms an intramolecular disulfide with C110, so the Y38C mutation most likely disrupts correct disulfide formation (***Figure 1—figure supplement 2b***). T66 immediately follows the C' β-sheet and is tightly packed inside the core of the protein, with the side chain hydroxyl engaging the backbone amide of K48 (***Figure 1—figure supplement 2c***). The T66M mutation would sterically disrupt this packing and probably destabilize the protein. V126 is located on β-sheet G; it is entirely buried and contributes to a hydrophobic core of the buried residues F24, D104, A105, and Y108. Removal of the side chain by the V126G mutation would disrupt this packing and probably destabilize this hydrophobic core (***Figure 1—figure supplement 2d***). In addition, sequence analysis reveals that Y38 and V126 are conserved within the TREM family, implying that they are probably required to preserve the common fold within this family of receptors (Figure 5c). The T66 residue is less conserved in the TREM family, but is highly conserved in TREM2 proteins across species.

In stark contrast to the NHD mutants, all of the residues implicated in the development of AD are surface exposed (***Figure 1b,c,e–g***) and engage in very few structure-stabilizing contacts. R47, the residue with the strongest link to AD as the R47H variant, is at the end of the loop preceding β-sheet C. It is well-ordered in the structure with the side chain lying parallel along the surface of the protein, and the side-chain amines engage the carbonyl oxygen of T66 (***Figure 1e***, ***Figure 1—figure supplement 2d***, and ***Figure 1—figure supplement 2a***). R62, another strong AD risk factor as the R62H variant, comes after the loop marked by the C51-C60 disulfide bond (***Figure 1f*** and ***Figure 1—figure supplement 2e***). Its side chain faces outward and makes no polar contacts. N68 is also surface exposed and its side chain makes no obvious polar contacts within the molecule. D87 is at the end of β-strand D; its side chain extends from the protein surface and the side-chain carboxyl engages the backbone amide of G90. This interaction probably stabilizes the βD-E loop. T96 is on the end of β-strand E and its side chain points away from the surface and engages the side chain of Q33 (***Figure 1g*** and ***Figure 1—figure supplement 2f***). On the basis of this structural analysis of neurodegenerative disease mutations in TREM2, we hypothesized that NHD mutants (which are buried) would affect protein folding and stability and thus decrease their surface expression, whereas AD risk variants (which lie on the protein surface) would not affect surface expression and instead probably impact ligand binding.

Impact of TREM2 variants on folding and surface expression

To begin to test tour hypothesis, we expressed each TREM2 ectodomain variant and analyzed their secretion and solution properties using size exclusion chromatography. WT hTREM2 ectodomain consistently eluted as a monomer (***Figure 2a and b***), in accordance with our crystallographic analysis. The verified (R47H and R62H) and possible (N68K, D87N and T96K) AD-risk variants all elute at the same volume as WT TREM2 (***Figure 2—figure supplement 1g–l***), suggesting that these mutations do not drastically alter the folding or oligomerization of TREM2 in solution. Furthermore, all of the TREM2 AD risk variant ectodomains migrated as monomers in the absence of reducing agent (***Figure 2b***). By contrast, although the buried NHD mutants Y38C, T66M, and V126G were secreted, they elute much earlier, consistent with aggregation and misfolding of these proteins (***Figure 2—figure supplement 1m–o***). Consistent with this observation, SDS-PAGE analysis of TREM2 NHD mutants in the absence of reducing agent showed that these ectodomains were largely produced as covalent dimers or trimers, indicating that misfolding of these mutants promoted the formation of aberrant intermolecular disulfide bonds (***Figure 2c***).

Given that our structural analysis suggested that the TREM2 NHD mutants should be misfolded, we were surprised to observe that these ectodomains bypassed cellular quality control and were secreted. We therefore devised an assay using flow cytometry to investigate whether these point mutants in full-length TREM2 impair cell surface expression. DAP12 was co-expressed with FLAG-tagged WT or mutant TREM2 full-length proteins and surface expression was measured either by an anti-FLAG antibody or by anti-TREM2 sera raised against our secreted, folded protein. Whole-cell

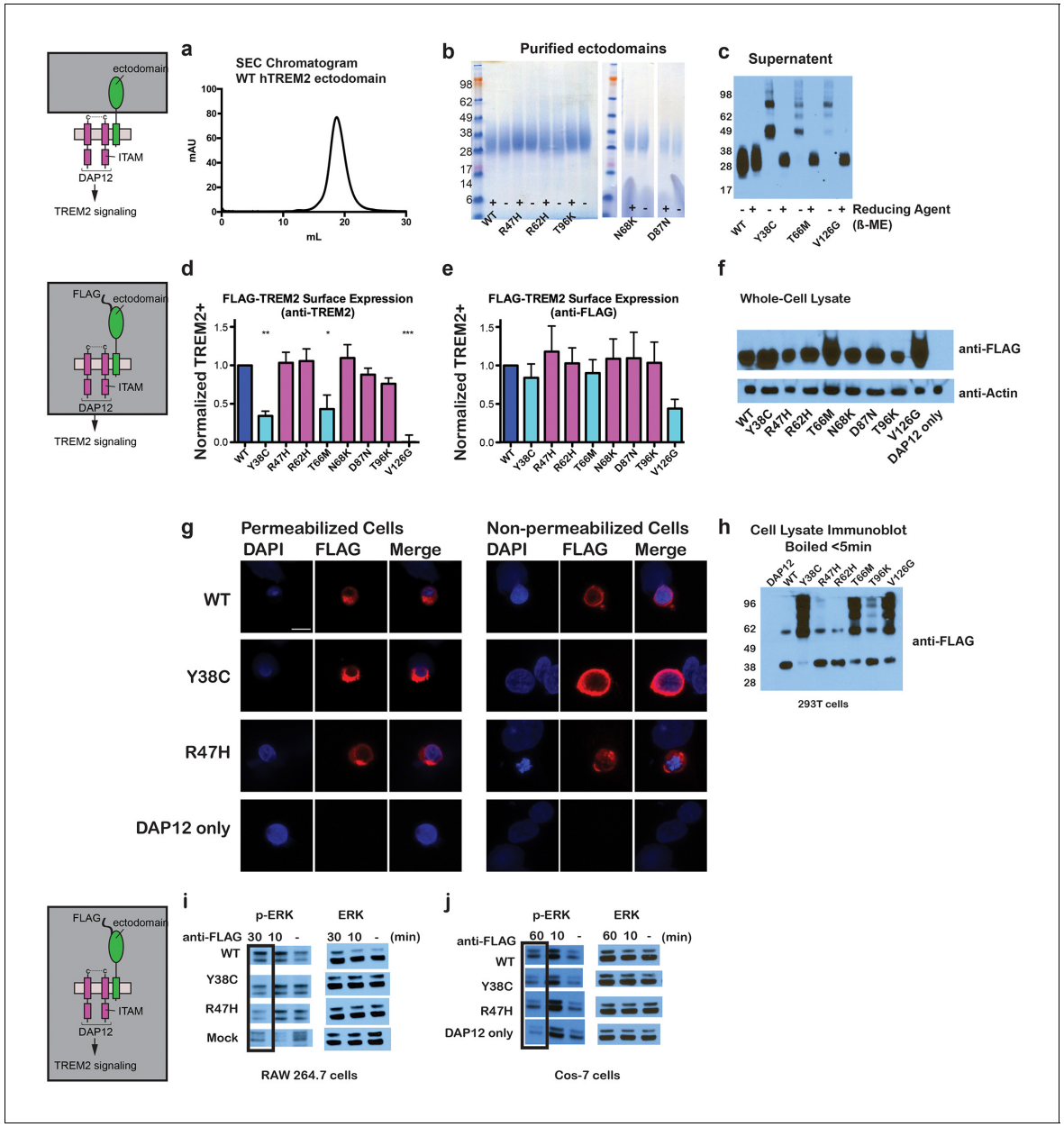

Figure 2. Chromatographic and surface expression analysis of WT and variant TREM2. The schematic depicts the domain of TREM2 used in the experiments shown in (**a–c**). (**a**) Gel filtration chromatography profile (Superdex 200 10/300 GL) of purified WT human TREM2 ectodomain showing a single monomeric peak. (**b**) SDS-PAGE analysis of purified TREM2 AD risk variants prepared with (+) and without (-) reducing agent (β-mercaptoethanol). (**c**) Western blot analysis of TREM2 NHD mutants secreted from transfected 293F cells prepared with (+) and without (-) reducing agent (β-mercaptoethanol). The NHD mutants Y38C, T66M, and V126G all migrate as higher MW oligomers under non-reduced conditions, indicating that they are misfolded and linked by aberrant intermolecular disulfide bonds. Purified WT TREM2 is shown for comparison. Representative of more than three independent expressions. The second schematic depicts FLAG TREM2 used in the experiments shown in (**d–h**). (**d–e**) Surface expression of WT and variant TREM2 in 293F cells assayed by flow cytometry. Full-length FLAG-WT or mutant TREM2 were co-transfected with mDAP12 into 293F cells. Surface expression was measured by either (**d**) a polyclonal serum or (**e**) an anti-FLAG antibody. Normalized TREM2 indicates the normalized

Figure 2 continued on next page

Figure 2 continued

fraction of cells staining positive over DAP12-only background. Data are from four (**d**) or five (**e**) independent experiments. Bars are color-coded in the same way as the residues in ***Figure 1b*** (cyan = NHD mutant; magenta = AD risk variant). Error bars are SEM. Significance was determined by ANOVA with Bonferroni post-test correction. (*p<0.05, **p<0.01, and ***p<0.001). (**f**) Western blot analysis of whole-cell lysates of 293F cells used in (**d**) and (**e**) showing expression levels of WT, NHD mutant (Y38C, T66M and V126G), and AD risk variant (R47H, R62H, N68K, D87N and T96K) TREM2. Note that the NHD mutants are more highly expressed than the AD risk variants. (**g**) Confocal microscopy of 293F cells co-transfected with DAP12 and FLAG-TREM2. Cells were fixed and either permeabilized (left) or non-permeabilized (right) and stained with anti-FLAG antibody (red). (**h**) FLAG-TREM2 full-length constructs were co-transfected with DAP12 into 293T cells and expression analyzed by anti-FLAG immunoblot. Samples were prepared by suspending cells in reducing SDS loading buffer and boiling for no more than 5 min. We observe SDS-resistant aggregate bands for the NHD variants, which were largely absent in WT and AD risk variants. The T96K variant shows some light aggregation, consistent with the slight shift (~5˚C) in denaturation temperature for that variant (***Figure 3***). Schematic depicts FLAG TREM2 signaling assay employed in the experiments shown in (**i–j**). (**i**) TREM2 signaling analyzed by phosphor-ERK1/2 and ERK1/2 immunoblot in RAW264.7 macrophage cells transfected with WT or variant FLAG-TREM2. (RAW264.7 cells express endogenous DAP12.) 24 hr post-transfection, cells were stimulated with anti-FLAG antibody (1:100) for the indicated length of time. ERK/pERK content was assessed by immunoblot. In these cells, we observe pERK at 10 min post-stimulation. However, only WT sustained signaling 30 min post-stimulation. (**j**) TREM2 signaling analyzed in Cos-7 cells as in (**c**). Cos-7 cells were co-transfected with DAP12 and TREM2. In these cells, there is a non-specific antibody response at 10 min. However, as in the RAW264.7 cells, we observe sustained WT signaling at the later time point which is diminished in R47H and Y38C variants.

DOI: 10.7554/eLife.20391.008

The following figure supplements are available for figure 2:

Figure supplement 1. Analysis of WT and variant TREM2 ectodomains by size exclusion chromatography.

DOI: 10.7554/eLife.20391.009

Figure supplement 2. hTREM2 surface expression probed using a commercial antibody.

DOI: 10.7554/eLife.20391.010

expression levels of the TREM2 NHD mutants were slightly higher than those of WT or AD risk variant TREM2 (***Figure 2f***). However, as predicted by our structural analysis, anti-TREM2 staining was decreased for the NHD mutants Y38C, T66M, and V126G, but not for the AD risk variants R47H, R62H, N68K, D87N, and T96K (***Figure 2d***). Similar observations were made using a commercial anti-TREM2 antibody (R&D, ***Figure 2—figure supplement 2***). By contrast, the anti-FLAG antibody showed surface expression for all TREM2 mutants (***Figure 2e***). We next examined cells expressing TREM2 WT, NHD mutant Y38C, and AD risk variant R47H by immuofluorescence confocal microscopy in the presence or absence of permeabilization. We found that the surface expression pattern in non-permeabilized cells was similar for all cell types, whereas in permeabilized cells, the NHD mutant Y38C displayed diffuse intracellular accumulation, in comparison to WT and R47H which displayed a distinct punctate staining pattern (***Figure 2g***). Taken together, these results suggest that NHD mutant proteins do retain some level of surface expression; but the protein is misfolded or aggregated and thus is not recognized by conformation-specific TREM2 antibodies. Consistent with these observations, we found significant amounts of SDS-resistant aggregates by anti-FLAG immunoblotting when expressing the full-length TREM2 NHD mutants in 293T cells (***Figure 2h***). Finally, we evaluated how these different classes of mutations impact TREM2 signaling by crosslinking the different versions of FLAG-TREM2 using anti-FLAG antibody. Consistent with our observation of FLAG-TREM2 on the cell surface for all the variant proteins, we found that while both the Y38C and R47H variants have some signaling potential, as assessed by phosphorylated-ERK blotting in RAW264.7 and Cos-7 cells, neither of these variants sustains signaling as efficiently as WT TREM2 (***Figure 2i,j***). The loss of sustained signaling by the disease variants may suggest that these mutant proteins have aberrant folding kinetics (and thus are replenished more slowly at the surface than WT proteins) or cannot bind co-factors that may be required to sustain signaling. Altogether, these experiments demonstrate that the buried residue changes linked to NHD cause misfolding and aggregation, with variable impact on surface expression, as would be suggested by our structural analysis.

AD variants slightly impact TREM2 stability and structure

We next sought to evaluate whether the AD-linked surface mutations affect protein structure or stability using sensitive solution techniques. First, we used circular dichroism (CD) spectroscopy to analyze whether AD-linked variants induced large conformational changes in the TREM2 ectodomain. For these experiments, we chose to analyze the R47H and R62H mutations, as they represent the

most significant TREM2 risk factors identified to date, as well as the T96K mutation, which is a sporadically occurring mutation that is not significantly associated with AD. In order to evaluate whether the point mutations induced conformational changes, we collected CD spectra on the proteins, analyzed for large changes, and compared the ratio in minima at 214 nm (due to β sheets) to minima at 233 nm (due to tryptophans), which are characteristic features of the CD spectra for Ig folds (***Sikkink and Ramirez-Alvarado, 2008***). We found that R62H and T96K displayed CD spectra similar to WT proteins while, surprisingly, R47H showed a subtle, yet statistically significant difference in the 214 nm/233 nm ratio (***Figure 3a and b***). Thus the R47H mutation in TREM2 seems to induce a small, but measurable, conformational change, whereas the R62H and T96K mutations do not induce any structural changes detectable by CD.

We next investigated the impact of these mutations on thermal stability using differential scanning fluorimetry (DSF) (***Niesen et al., 2007***). Each surface variant produced slightly lower denaturation temperatures, with R47H and R62H marginally reduced when compared to WT proteins and T96K having the lowest denaturation temperatures (***Figure 3c***). As a control, the same experiments were carried out in the presence of 1 mM DTT, which induced the expected shift to lower denaturation temperatures by disrupting the disulfide bonds. We also used thermal denaturation CD to assess the thermal stability of these proteins. By obtaining full CD scans at 5°C increments, we observed that TREM2 has a denaturation transition at 225 nm, consistent with other Ig domains (***Sikkink and Ramirez-Alvarado, 2008***), and this wavelength was monitored in subsequent denaturation experiments (***Figure 3—figure supplement 1a***). WT TREM2 and all the TREM2 variants tested

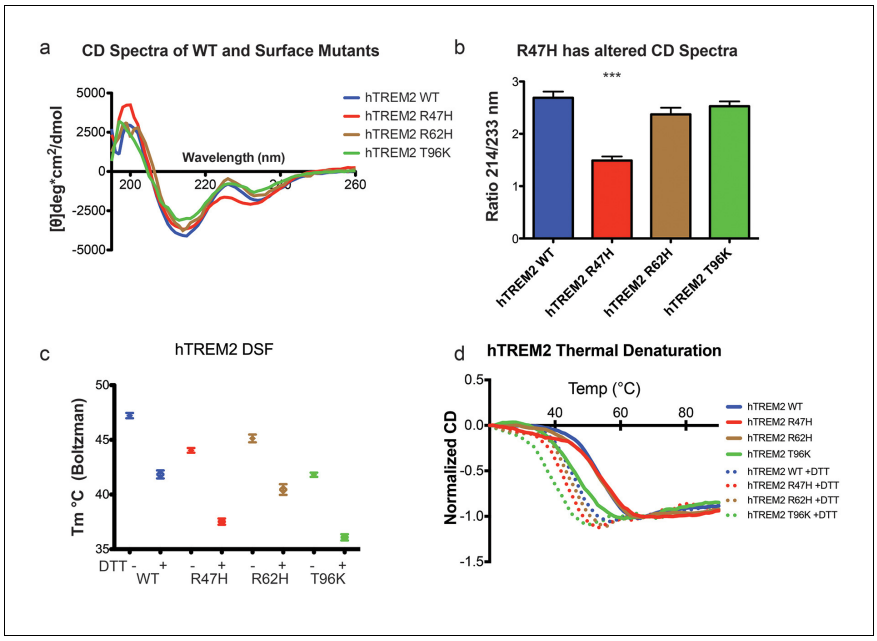

Figure 3. Structure and stability analysis by CD and DSF of human WT and AD-linked surface variant TREM2 ectodomains. (**a**) CD spectra of human WT TREM2 (blue) and R47H (red), R62H (brown), and T96K (green) variants. (**b**) Ratio of CD minima at 214 nm and 233 nm reveals that R47H has an altered CD spectrum. Minima ratios were measured on five (WT and R47H) or three (R62H and T96K) independent protein preparations, respectively. (**c**) Thermal melt temperatures measured by DSF. (**d**) WT and variant TREM2 thermal denaturation measured by CD at 225 nm while increasing the temperature from 20°C to 90°C with or without 1 mM DTT.

DOI: 10.7554/eLife.20391.011

The following figure supplement is available for figure 3:

Figure supplement 1. Structure and stability analysis by CD and DSF of human WT and AD-linked surface variant TREM2 ectodomains.

DOI: 10.7554/eLife.20391.012

showed reversible thermal denaturation as they reacquired their native spectra rapidly after cooling from 90˚C to 20˚C, but their ability to refold was ablated in the presence of DTT (not shown). In contrast to DSF measurements, thermal denaturation by CD did not show a difference between WT, R47H, and R62H proteins; however, the T96K variant has a pronounced shift towards lower denaturation temperature (***Figure 3d***). In the presence of DTT, all proteins had lower denaturation temperatures (***Figure 3d***). We further assayed stability using chemical denaturation by titration of guanidine-HCl (GuHCl) in CD experiments. The R47H and R62H proteins melt at slightly lower GuHCl concentrations than the WT protein, while the T96K variant unfolds at lower GuHCl concentrations than R47H and R62H, consistent with the thermal melt experiments (***Figure 3—figure supplement 1b***). Thus, as predicted by our structural analysis, the AD-risk surface variants do not induce large conformational changes in TREM2, nor do they dramatically impact protein stability, but they can induce subtle changes in both parameters.

TREM2 AD risk variants impact binding to TREM2-L

Our structural analysis suggested that AD risk variants might impact function by altering ligand binding due to the surface presentation of the mutated residues. Recently, TREM2 was shown to signal following stimulation of reporter cells by plated phospholipids, and the R47H mutation resulted in loss of signaling (***Wang et al., 2015***). To test the direct binding of TREM2 to phospholipids in a cell-free system, we used purified protein in solid-state ELISA and liposome sedimentation assays. Consistent with the results of previous work (***Cannon et al., 2012***), we detected TREM2 binding to phospholipids by both ELISA and liposome sedimentation. However, we did not observe differences in phospholipid discrimination or in direct lipid binding between WT and AD variant TREM2 ectodomains (***Figure 4—figure supplement 1a–c***). We therefore investigated binding to a cell surface ligand (TREM2-L). Although no endogenous protein ligand for TREM2 has yet been identified, several cell types have been reported to express a ligand on the basis of staining with a TREM2-Fc fusion construct (***Ito and Hamerman, 2012***; ***Hamerman et al., 2006***; ***Daws et al., 2003***; ***Hsieh et al., 2009***; ***Stefano et al., 2009***). In order to evaluate the effect of AD-linked mutations on TREM2 binding to TREM2-L, we constructed a novel TREM2 protein cell-binding reagent containing a site-specific BirA-biotinylation sequence on the C-terminus of TREM2, which could then be complexed with PE-labeled streptavidin to create a tetrameric cell-staining reagent (***Figure 4a***). In initial experiments, we found that both human and mouse TREM2/SA-PE tetramers were able to bind Neuro2A (N2A) and THP-1 cells (***Figure 4b–d,f,g*** and ***Figure 4—figure supplement 2a,c***). To validate the specificity of our reagent, we cultured THP-1 cells with various immune stimuli and found that overnight treatment with PMA/ionomycin dramatically decreased binding of TREM2/SA-PE tetramers to THP-1 cells (***Figure 4b and c***), while the myeloid cell marker CD45 remained unchanged (not shown). Other stimuli tested (overnight exposure to IL-13, Poly I:C, LPS, or M-CSF) did not alter staining (***Figure 4—figure supplement 2a***). PMA/ionomycin treatment is the first identified stimulus that ablates TREM2 staining, and this confirms that TREM2 recognizes a specific cell-surface ligand.

We next sought to interrogate the endogenous target recognized by TREM2 on the cell surface, and found that TREM2 binding is sensitive to proteinase treatment of cells prior to incubation with our staining reagent (***Figure 4d*** and ***Figure 4—figure supplement 2b***). Treatment with proteinase K abolished binding while the more specific proteases chymotrypsin and elastase had an intermediate effect. Proteinase K treatment did not affect cell viability, which was >99% by 7-aminoactinomycin D (7-AAD) staining (***Figure 4—figure supplement 2f***). This demonstrates that TREM2-L contains a protein component. In addition, given the high pI of TREM2, and the frequent reports of anionic potential ligands for TREM2, we reasoned that proteoglycans containing highly sulfated glycosaminoglycans (GAGs) may facilitate cell-surface binding. We tested binding to wild-type CHO-K1 cells, which express heparan and chondroitin sulfates, and to CHO-745 cells, which are deficient in GAG maturation and surface expression (***Esko et al., 1985***). In this experiment, GAG-dependent cell binding of the TREM2 tetramer was observed (***Figure 4e***). Next, we used heparinases (which also cleave heparan sulfates) and chondroitinase ABC to ask whether TREM2 selectively binds either type of GAG. In CHO (***Figure 4e***), THP-1 (***Figure 4f***) and N2A (***Figure 4g***) cells, treatment with heparinases had a pronounced effect on cell surface binding while chondroitinase only slightly diminished binding, together implicating GAGs, specifically heparin sulfate, as a major component of the cell surface TREM2-L.

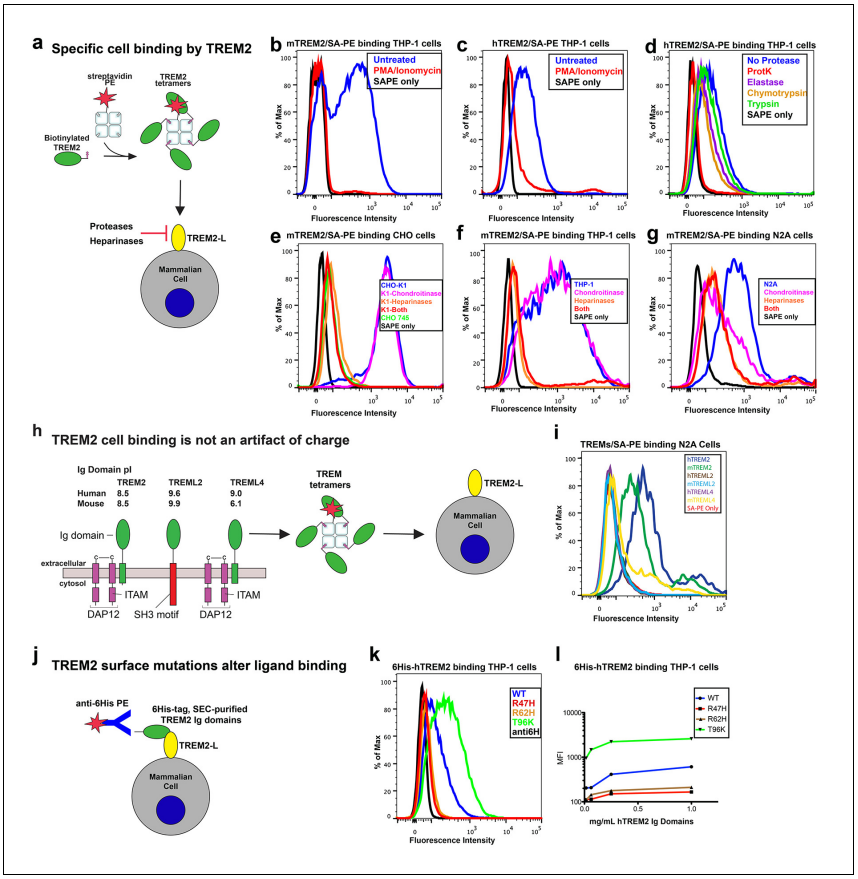

Figure 4. AD risk variants in TREM2 alter binding to cell surface TREM2-L. (**a**) Schematic outlining the flow cytometry experiments in (**b–g**). TREM2 ectodomains were specifically biotinylated at the C-terminus and probed for binding to TREM2-L on the surface cells, which was reduced by pre-treating cells with proteinases or heparinases. (**b–c**) Flow cytometry analysis of either (**b**) mTREM2/SA-PE tetramer or (**c**) hTREM2/SA-PE tetramer staining of THP-1 cells ± PMA/ionomycin treatment. (**d**) Flow cytometry analysis of hTREM2/SA-PE tetramer staining of THP-1 cells pretreated by various proteases. (**e**) mTREM2 staining of CHO-745 (GAGless) and CHO-K1 cells. CHO-K1 cells were treated with a cocktail of heparinases, chondroitinase ABC, or both. (**f–g**) mTREM2 staining of (**f**) THP-1 and (**g**) N2A cells treated with heparinases, chondroitinases, or both. (**h**) Schematic outline of control cell-binding experiments with the TREM-like proteins TREML2 and TREML4. On the left is a schematic of receptor versions of TREM2, TREML2, and TREML4, along with calculated pI values for the respective ectodomains. (**i**) Tetramer staining of TREM family ectodomains to N2A cells. (**j**) Schematic outlining monomeric TREM2-6His cell-staining experiments. Cells were stained with monomeric TREM2-6H and detected using PE-labeled anti-6H antibody. (**k**) Representative plot of THP-1 staining by hTREM2-6H analyzed by flow cytometry. (**l**) MFI of anti-6His staining of SEC-purified hTREM2 WT and variant ectodomains pre-incubated with THP-1 cells at the indicated concentrations. All data are representative of at least two independent experiments.

DOI: 10.7554/eLife.20391.013

The following figure supplements are available for figure 4:

Figure supplement 1. TREM2 lipid binding as assessed by phospholipid ELISA and liposome sedimentation.

DOI: 10.7554/eLife.20391.014

Figure supplement 2. TREM2 binding to mammalian cells.

DOI: 10.7554/eLife.20391.015

Next, we tested the impact of TREM2 AD risk variants on TREM2-L binding in three different formats. For these experiments, we chose to compare WT TREM2, the validated TREM2 AD risk variants (R47H and R62H), and the possibly protective AD risk variant (T96K). We utilized anti-6H detection of purified monomeric hTREM2 ectodomains bound to THP-1 cells (***Figure 4j,k, and l***), tetramer staining of WT and variant mTREM2 binding to N2A and THP-1 cells (***Figure 4—figure supplement 2c,d***), and competition assays in which SEC-purified monomers competed with SA-PE-labeled WT tetramers (***Figure 4—figure supplement 2e***). Consistent with our hypothesis, the AD-linked variant R47H displayed markedly diminished binding to N2A and THP-1 cells. In stark contrast, the potentially AD-protective T96K variant significantly increased binding. The R62H variant reduced binding as measured in the anti-6H format, but the reduction in binding was less dramatic when measured by competition or tetramer staining, suggesting an intermediate decrease in affinity. Thus, as suggested by our structural analysis, the AD risk variant R47H TREM2 negatively impacts binding to cell surface TREM2-L, whereas the variant T96K results in increased cellular binding. These data, together with our direct phospholipid binding experiments, suggest that TREM2 AD-risk variants retain phospholipid binding, and instead impact binding to cell surface GAGs. As the R47H risk variant is able to bind phospholipids directly, but does not signal in cellular assays of TREM2 signaling triggered by plated phospholipids (***Wang et al., 2015***), we suggest that TREM2 interaction with GAGs in cis is likely required to orient or cluster TREM2 to mediate signaling upon stimulation by phospholipids. Alternatively, phospholipids may function to orient TREM2 on the cell surface for proper presentation to GAGs and/or additional as of yet undefined protein surface receptors.

AD risk variants map a unique functional surface on TREM2

Our cell surface TREM2-L binding experiments categorized the naturally occurring TREM2 mutations as loss-of-binding (R47H and R62H) and enhancement-of-binding (T96K) compared to WT, and showed that these mutations influence TREM2 interactions with cell surface GAGs. We returned to analysis of our crystal structure in order to interpret these observations. Upon mapping the electrostatic surface of hTREM2, we noticed a large basic surface that was not present on the surface of other TREM family receptors for which coordinates are available (mTREM1, PDB 1 U9K, [***Kelker et al., 2004a***]; hTREM1, PDB 1SMO, [***Kelker et al., 2004b***]; and TLT-1, PDB 2FRG [***Gattis et al., 2006***]) (***Figure 5a,b and d–f***). Furthermore, sequence analysis shows that the residues constituting this basic patch are highly conserved within TREM2, but not within the rest of the TREM family, suggesting that this interface has evolved specifically toward a role in TREM2 function (***Figure 5c***). To demonstrate this, we prepared staining tetramers for other TREM-like family members with similar overall high pI values calculated for the ectodomain (***Figure 4h***). Consistent with our hypothesis, TREM2 ectodomain tetramers bound to N2A cells, while tetramers of ectodomains from TREM-like 2 (TREML2) and TREM-like 4 (TREML4) did not (***Figure 4i***). This cluster of residues contains most of the AD-linked surface mutations (including R47H and R62H). Additionally, the T96K mutation is located adjacent to this basic patch and would therefore extend it, providing a structural explanation for the gain of function observed with this variant (***Figure 5b***). To test whether additional basic residues located within this surface influence TREM2-L binding, we selected two other basic residues that are conserved only in TREM2 (R76 and R77), and assayed the ability of these variants to bind TREM2-L using our flow cytometry assay. We found that both a R76D and a R77D mutation decreased binding to TREM2-L on THP-1 cells in a manner similar to the validated AD risk variants (R47H and R62H) (***Figure 5g***). Together, the data indicate that this surface represents a conserved functional interface on TREM2 that participates in cell-surface ligand binding and that this surface is unique to TREM2 within the TREM family.

Discussion

Here we elucidate how distinct point mutations in *TREM2* give rise to different neurodegenerative diseases via two separate loss-of-function mechanisms. Our studies indicate, as presaged by our crystal structure, that NHD-linked mutant residues are buried and impact protein folding and stability, while AD-linked variant residues are on the protein surface and do not diminish the stability or surface expression of the molecule but instead impact ligand engagement (***Figure 6a***). Several variants have been reported for TREM2, but some are very rare, so it is not clear whether they associate

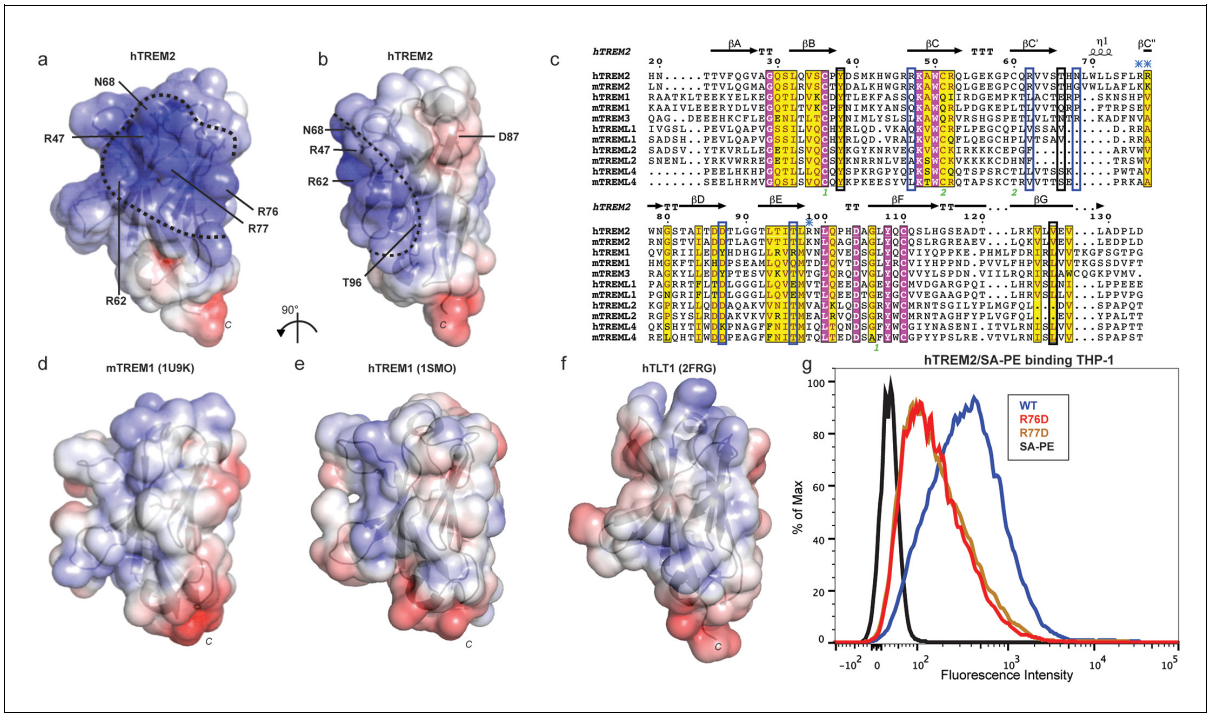

Figure 5. AD risk variants reveal a functional surface on TREM2. (**a**) Electrostatic surface of hTREM2 and (**b**) hTREM2 rotated 90˚. The extended basic patch on hTREM2 is outlined with a dashed line. (**c**) Structure-based sequence alignment of human (h) and mouse (m) TREM family members. Secondary structure assigned using the DSSP server. Invariant residues are shown in magenta and conserved residues are shown in yellow. Disulfide bonds are numbered in green. NHD residues are highlighted with black boxes and AD residues in blue boxes. Basic patch residues are labeled with blue asterisks. (**d**) mTREM-1 (1 U9K), (**e**) hTREM-1 (1SMO), and (**f**) hTLT-1 (2FRG) aligned with hTREM2 as in (**a**). Electrostatic potential was plotted on the solvent-accessible surface using the AMBER force field and the PDB2PQR server within the APBS Pymol plugin. Scale is −6.0 kT/e (blue) to +6 kT/e (red). (**g**) Flow cytometry analysis of WT, R76D, and R77D hTREM2/SA-PE binding to TREM2-L on THP-1 cells. Representative of two independent experiments.

DOI: 10.7554/eLife.20391.016

with AD risk. The structure-based studies presented here provide a framework with which one could make predictions as to the variant's impact on function. Our observation of detectable misfolded cell-surface TREM2 NHD mutant proteins was surprising, given that one would expect that the cellular quality-control machinery should degrade misfolded proteins and prevent their surface expression. In addition, previous reports noted decreased surface expression for these mutants (***Park et al., 2015***; ***Kleinberger et al., 2014***). Here, we used an approach that probes surface expression using both non-conformational (anti-FLAG) and conformational (anti-hTREM2) antibodies. We found that both the NHD-associated and AD-linked mutant proteins reach the cell surface, however the NHD-associated TREM2 mutants are probably not functional as they are either misfolded or aggregated, and thus are not recognized by the conformational-dependent antibodies. These results are supported by our analysis of the solution behavior of theTREM2 ectodomains of these mutant proteins. An alternative explanation could be that the FLAG tag or overexpression drives the surface expression of these mutated proteins; but we do not think that is the case since we found that the TREM2 ectodomains carrying these mutations (which contain a different tag that is on the opposite terminus) were also secreted. These findings are of potential therapeutic value, as the discovery of molecular chaperones that rescue the folding of and restore function to these mutants could be pursued for patient-specific NHD treatments.

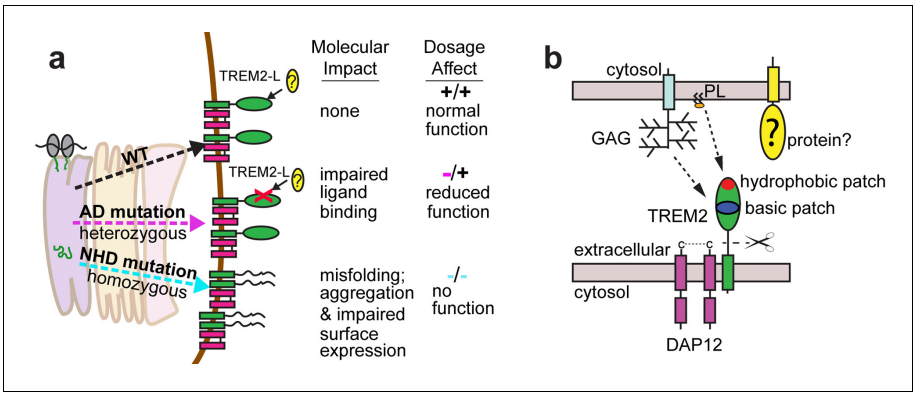

Figure 6. Models developed from the current data. (**a**) Current model for the role of TREM2 ectodomain point mutations in neurodegenerative diseases. WT TREM2 is surface expressed in complex with DAP12 and engages TREM2-L normally. AD risk variants do not impair surface expression, but do impair ligand binding. They occur heterozygously, so this would lead to overall reduced TREM2 function in individuals carrying these risk variants. NHD mutations cause misfolding, which leads to aggregation and impaired surface expression. These mutations occur homozygously, leading to no TREM2 function in individuals carrying these mutations. (**b**) Current model for the engagement of possible TREM2 ligands investigated here. Membrane-bound or soluble TREM2 (sTREM2) produced by proteolytic cleavage likely engages GAGs via the basic patch and engages phospholipids (PL) via the hydrophobic patch. In addition, there is a protein component of TREM2-L.

DOI: 10.7554/eLife.20391.017

The following figure supplement is available for figure 6:

Figure supplement 1. hTREM2 has an extended hydrophobic surface.

DOI: 10.7554/eLife.20391.018

In contrast to the buried NHD mutant proteins, the AD risk variants lie on the surface of the protein and do not severely impact the protein folding or stability of TREM2. However, it should be noted that the R47H mutation does induce a subtle change in secondary structure detectable by CD. The AD mutations probably alter TREM2 function by impairing ligand binding. Recent studies in AD mouse models that are deficient in *TREM2* confirm that loss of TREM2 function contributes to classic AD pathology and suggest a crucial role for TREM2 in microglia function (***Jay et al., 2015***; ***Wang et al., 2015***; ***Ulrich et al., 2014***). *TREM2*-deficient AD mice display fewer activated microglia, and the absence of *TREM2* prevents microglia proliferation and promotes microglia apoptosis, which is correlated with increased accumulation of Aβ plaques (***Wang et al., 2015***; ***Jay et al., 2015***). Microglia in *TREM2*-deficient AD mice display less activation and do not engulf Aβ plaques, which reduces the density of Aβ plaques and promotes diffuse Aβ structures, which, in turn, are more neurotoxic and contribute to the accumulation of classic AD pathology (***Wang et al., 2016***; ***Yuan et al., 2016***). These models suggest a crucial role for TREM2 in microglia biology and in the turnover of Aβ. On the basis of the conserved nature of AD-linked basic surface residues and our analysis of cell-surface ligand binding for multiple cell lines, we favor the concept that AD risk variants lead to impaired binding of TREM2-L, which in turn perturbs microglia function.

With this in mind, we investigated how AD risk variants in TREM2 affect binding to previously identified and newly hypothesized ligands based on the analysis of ourcrystal structure. The many diverse ligands reported for TREM2 may in fact suggest that TREM2 is capable of recognizing multiple ligands and that under different conditions, their respective affinities might tune signaling accordingly. For example, low-affinity ligands may induce a tonic inhibitory signal while ligation of a high-affinity ligand could result in an activating response. Indeed, anionic bacterial carbohydrates (***Daws et al., 2003***), phospholipids (***Wang et al., 2015***), myelin lipids (***Poliani et al., 2015***), and even purified DNA (***Kawabori et al., 2015***) all activate TREM2 reporter cell lines. This is not surprising in light of our crystal structure, which reveals an extended basic patch on the surface of TREM2 that would be capable of forming electrostatic interactions with these anionic ligands. In contrast to highly selective phospholipid binding by other Ig domains (***Kobayashi et al., 2007***; ***Miyanishi et al., 2007***; ***Santiago et al., 2007***; ***Simhadri et al., 2012***), purified TREM2 shows only

broad discrimination for anionic (PA, PG, PI, PS) over more neutral (PC, PE) lipids (***Figure 4—figure supplement 1a,b and c***). Structurally, Ig domains with selective lipid binding feature a canonical FG loop motif that contains large hydrophobic residues, absent in TREM2, which mediate membrane insertion and acyl chain binding (***Tietjen et al., 2014***) (***Figure 4—figure supplement 1d,e***). Moreover, while TREM2 does share a conserved aspartic acid residue from this motif, which chelates a required Ca^{2+} ion for the TIM and CD300a proteins, TREM2-lipid binding is not sensitive to EDTA, unlike TIM and CD300 (***Figure 4—figure supplement 1e and f***). Thus, while we do observe direct binding of TREM2 to phospholipids, it does not appear that TREM2 binds phospholipids with high selectivity or using the same binding mode as other phospholipid-binding Ig domains. By contrast, it should be noted that there is a long and narrow hydrophobic patch on the end of TREM2 most distal from the plasma membrane (***Figure 6—figure supplement 1***) that is the most likely lipid-binding surface. Interestingly this patch is adjacent to the basic patch, which could mediate interaction with anionic phospholipid head groups (***Figure 6b***). These hypotheses will need to be tested in future studies using sensitive binding assays (such as surface plasmon resonance) and crystallographic studies of TREM2-phospholipid recognition. In contrast to recent studies employing reporter cells expressing TREM2 R47H (***Wang et al., 2015***), we did not observe any large differences in binding to phospholipids for any of the validated TREM2 AD risk variants. In light of our experimental observations, we believe this is best explained by the hypothesis that another interaction (such as TREM2 binding to GAGs, which we show here is impacted by these AD risk variants) is required to mediate phospholipid signaling; thus in the context of cellular experiments, TREM2 R47H shows diminished signaling, while in direct lipid-binding assays it performs in the same way as WT TREM2. This is potentially supported by a recent report that TREM2 binds to isolated PS, but does not bind apoptotic Jurkat T cells, which present PS on their cell surface but may also be deficient in GAGs (***Bailey et al., 2015***). The results presented here suggest that the point mutations in *TREM2* participate in neurodegenerative disease pathogenesis through distinct molecular mechanisms.

We found that the validated AD risk variants in TREM2 impact binding to a cell-surface ligand (TREM2-L). This ligand does appear to contain a protein component, as pre-treatment of cells with proteases decreases or prevents the binding of TREM2 to these cells. This interaction also appears to be highly GAG-mediated, as TREM2 cell-staining tetramers do not bind CHO 745 cells, which do not express GAGs. This interaction seems most dependent on heparan sulfate, as treatment with heparin sulfatases remove much of the observed binding. As the AD risk variants most notably impact binding to TREM2-L, we reason that this interaction is involved in the pathogenesis of AD. In support of this, we find that the mutations R47H and perhaps R62H deleteriously impact TREM2-L recognition. By contrast, T96K appears to be a potential gain-of-function mutation in our binding experiments. Interestingly, this mutation appears at a much higher frequency than R47H and R62H, and in some studies it has been reported to be enriched in European-American AD cases compared to controls; overall it is associated with a decreased odds ratio for the development of late-onset AD (***Figure 1c***), again suggesting the TREM2-L binding function is coupled to AD risk. Altogether, the structural and functional analysis of these variants illuminates a surface epitope that is specific to TREM2, that is not conserved among the other members of the TREM family, and that mediates binding to a cell-surface ligand. Additional point mutations localized to that surface also resulted in loss of binding, supporting this functional role. Our results suggest that this ligand may have a specific protein component in addition to GAGs. On that note, while this manuscript was in preparation, it was reported that TREM2 binds lipid-loaded ApoE and that this interaction facilitates uptake of Aβ loaded into lipoparticles by microglia (***Yeh et al., 2016***). This report also suggests that TREM2 AD risk variants decrease binding to ApoE, but binding affinities were not quantitated. However, we do not suspect that ApoE is the protein component of cell surface TREM2-L because it is a soluble rather than a surface-bound protein. Our study demonstrates that TREM2 can specifically bind GAGs, utilizing the basic patch; other TREM-like proteins with the same overall calculated pI, but lacking the basic patch residues, do not bind GAGs. We also demonstrate that TREM2 AD risk variants affect binding to GAGs. Future studies will need to focus on how TREM2 binding to GAGs and ApoE are coordinated and how they impact TREM2 function in microglia.

Our results illustrate two distinct paths to loss-of-function in TREM2, so how might these different mechanisms result in either AD or NHD? In attempting to explain this, it is important to take into account genetics-based dosage affects (***Figure 6a***). In NHD, the mutations are homozygous and the TREM2 is either deleted or misfolded, leading to a complete loss of function, and more serious and

early-onset neurodegenerative disease. In AD, the mutations are heterozygous and impair function (but do not completely abolish it), leading to less severe and late onset neurodegenerative disease. Under this hypothesis, it should be possible that a heterozygous NHD mutant would give increased risk for AD. Consistent with this, there have been reports of rare AD cases containing heterozygous NHD variants, including Q33X, Y38C, and T66M (**Guerreiro et al., 2013b**). In addition, TREM2 may function not only as a receptor but also as a signaling molecule as it can be cleaved. We have recently shown that the soluble TREM2 may be a survival signal in bone-marrow macrophages (**Wu et al., 2015**). Interestingly, we have observed that the absence of *TREM2* in an AD mouse model prevents microglia proliferation and promotes microglia apoptosis, suggesting that soluble TREM2 could play a similar role in the CNS (**Wang et al., 2015**). Accordingly, soluble TREM2 can be detected in the CNS, and we have shown that some AD risk variants, but not the NHD mutant proteins are readily detected in the CSF of patients (**Piccio et al., 2016**). Because the AD risk variant proteins are expressed and stable enough to be soluble factors, they may retain some signaling ability and prevent more serious diseases. These hypotheses will require animal knock-in studies for full evaluation. Therefore, a comprehensive analysis of all TREM2 variants will be essential to understanding TREM2 function in both neurodegenerative diseases and other inflammatory diseases, and to design targeted therapies accordingly.

Materials and methods

Expression constructs

Full-length wild-type (WT) human *TREM2* as well as R47H, N68K, D87N, and T96K mutants in pMX-3p plasmid and mouse *Trem2* cDNA were used as PCR templates. Mammalian cell expression constructs of human TREM2 wild-type, R47H, D87N, T96K and mouse TREM2 ectodomains were produced as previously described (**Kober et al., 2014**, **2015**) by subcloning from these templates into the pHLsec vector, which contains an optimized signal sequence and a C-terminal 6-histidine tag for purification. Similarly, primers were designed to amplify the full-length human *TREM2* gene with an N-terminal FLAG peptide. Additional mutants (human Y38C, R62H, T66M, R76D, R77D; mouse R47H, R62H, and T96K) were generated in the pHsec constructs using either the QuikChange Lightning Site-Direct Mutagenesis Kit (Agilent. Santa Clara, CA) or the Q5 Mutagenesis Kit (NEB) (primer sequences in **Table 3**). WT and mutant human and mouse TREM2 constructs containing site-specific biotinylation sites were generated by *EcoRI-KpnI* restriction digest of the pHLsec inserts followed by ligation into the pHLAvitag3 vector, which encodes a C-terminal BirA biotin ligase biotinylation sequence followed by a 6-histidine tag. All constructs were verified by sequencing.

Crystallization, structure determination, and analysis

The WT human TREM2 ectodomain was expressed in Freestyle 293F cells in the presence of 1 µg mL^{-1} kifunensine, deglycosylated with EndoHf, and purified for crystallization in a single-step using Ni-NTA resin as previously described (**Kober et al., 2014**). Protein was concentrated to 10 mg ml^{-1} in buffer containing 20 mM HEPES pH 7.4 and 150 mM NaCl. Crystals were grown by hanging drop vapor diffusion by mixing 1:1 with well solution containing 100 mM HEPES 7.0, 2.1 M NaCl, 0.2 M $MgCl_2$ and 0.2 M NDSB-201. Crystals were cryoprotected in mother liquor containing 20% ethylene glycol and flash frozen under a nitrogen stream at −160°C.

Data were collected at the Advanced Photon Source, beamline 19-ID (Argonne National Lab, Chicago). A molecular replacement solution was found with PHASER using mouse TREM-1 ectodomain (1 U9K) (**Kelker et al., 2004a**) as the probe, locating two molecules in the asymmetric unit (ASU). Data were initially scaled and processed at 3.3 Å using HKL2000 (**Otwinowski and Minor, 1997**). The initial model was substantially improved by iterative rounds of manual rebuilding in COOT (**Emsley et al., 2010**) and refinement using Phenix (**Adams et al., 2010**). Next, resolution was extended using the method described by Karplus and Diederichs (**Karplus and Diederichs, 2012**) (**Table 1**). The 3.3 Å model was used as a molecular replacement probe on data scaled to 3.4 Å and 3.3 Å, and subsequently subjected to automated refinement in Phenix without manual intervention. The 3.3 Å solution was then used to calculate Rfree and Rwork at 3.4 Å. Rfree was lower at 3.4 Å using the model refined at 3.3 Å compared to the model refined at 3.4 Å, providing evidence that 3.3 Å data improved the model. Similarly, data were again extended to 3.2 Å and finally 3.1 Å. Data

Table 3. Primers used in this study.

hTREM2 ectodomain	GAAACCGGTCACAACACCACAGTGTTCCAGGGC CGGGGTACCCAGGGGGTCTGCCAGCACCTCCAC
hTREM2 Y38C*	CTGCAGGTGTCTTGCCCCTGTGACTCCATGAAGCACT AGTGCTTCATGGAGTCACAGGGGCAAGACACTTGCAG
hTREM2 T66M*	TGCCAGCGTGTGGTCAGCATGCACAACTTGTGGCTGC GCAGCCACAAGTTGTGCATGCTGACCACACGCTGGCA
hTREM2 V126G*	TCAGGAAGGTCCTGGGGGAGGTGCTGGCAGA TCTGCCAGCACCTCCCCCAGGACCTTCCTGA
hTREM2 R62H+	CCCAGTCCAGCATGTGGTCAGCA CCCTTCTCTCCCAGCTGGC
hTREM2 R76D+	GTCCTTCCTGGACAGGTGGAATGGG AGCAGCCACAAGTTGTGC
hTREM2 R77D+	CTTCCTGAGGGACTGGAATGGGAGCACAG GACAGCAGCCACAAGTTG
FLAG-hTREM2	GAAACCGGTGATTATAAAGATGATGATGATAAACACAACACCACAGTGTTCCAGGGC CGGGGTACCTCACGTGTCTCTCAGCCCTGGCAG
mTREM2 ectodomain	GAAACCGGTCTCAACACCACGGTGCT CGGGGTACCTTGGTCATCTAGAGGGT
mTREM2 R62H+	CCCATGCCAGCATGTGGTGAGCA CCCTCCTCACCCAGCTGC
mTREM2 R47H*	AAGCACTGGGGGAGACACAAGGCCTGGTGTCGG CCGACACCAGGCCTTGTGTCTCCCCCAGTGCTT
mTREM2 T96K*	CTTGCTGGAACCGTCACCATCAAGCTGAAGAACCTCCAAGCCGGT ACCGGCTTGGAGGTTCTTCAGCTTGATGGTGACGGTTCCAGCAAG
mDAP12	CCGGAATTCGCCACCATGGGGGCTCTGGAGCCCTCCTGG CGGGGTACCTCATCTGTAATATTGCCTCTGTGT

All primers 5′–3′ with the coding direction primer listed first

*Designed for Quikchange Lightning Mutagenesis

+Designed for NEB Q5 mutagenesis

DOI: 10.7554/eLife.20391.019

past 3.1 Å did not improve the model as determined by an increased Rfree calculated at 3.1 Å using the model refined on 3.0 Å data. Final model refinement occurred by iterative building and refinement in Phenix. NCS and secondary structure restraints were used during refinement, and TLS refinement of B-factors was applied in later rounds. The structure is complete with only one N-terminal residue and four C-terminal residues not visible in the electron density (***Figure 1b***). Ramachandran statistics are 97.7% favored, 0% outliers, 2.3% allowed. Molprobity score was 1.66 (100th percentile) and clashscore was 9.62 (96th percentile) for the final model.

Calculations on the final model were performed using Naccess (***Hubbard and Thornton, 1993***) to measure the solvent accessibility of side chains and HBPLUS (***McDonald and Thornton, 1994***) to identify hydrogen bonds. LigPlot+ (***Laskowski and Swindells, 2011***) was used to analyze side-chain contacts. For structure-based alignment, amino acid sequences were aligned using Clustal Omega (***Sievers et al., 2011***) and residue conservation scored by ESPript (***Robert and Gouet, 2014***). All crystallographic and analysis software used were compiled and distributed by the SBGrid resource (***Morin et al., 2013***) and diffraction images were archived with the SB Data Grid (***Meyer et al., 2016***).

Cell culture

For protein expression, Freestyle 293F cells were cultured at 8% CO_2 in serum-free 293Freestyle media supplemented with Glutamax and penicillin/streptomycin (Pen/Strep, Gibco by ThermoFisher, Waltham, MA). Human monocyte THP-1 cells were cultured at 5% CO_2 in RPMI media supplemented with 10% Fetal Bovine Serum (FBS), 10 mM HEPES, 50 µM β-mercaptoethanol, L-glutamine and penicillin/streptomycin (Pen/Strep). Mouse neuroblast N2A cells were cultured at 5% CO_2 in MEM

supplemented with 10% FBS, L-glutamine and Pen/Strep. CHO cells were cultured at 5% CO_2 in Ham's F12 supplemented with 10% FBS, L-glutamine and Pen/Strep.

Protein expression and purification

Protein expression for biophysical and functional studies was performed as described previously (***Kober et al., 2014***). In brief, plasmid DNA was complexed at a ratio of 1:2 (µg/µg) with PEI-TMC25 to transfect Freestyle 293F suspension cells cultured in serum-free 293 Freestyle Media. One µg of plasmid DNA was used per 1×10^6 cells. Transfected cells were allowed to express protein for 72–96 hr. Supernatants were collected and protein was purified using Ni-NTA chromatography. The eluted protein was then further purified by gel filtration chromatography using an analytical s200 size-exclusion column (GE) run in a buffer containing 20 mM Tris pH 8.5 and 150 mM NaCl.

Surface expression studies

Full-length FLAG-tagged hTREM2 WT or mutant genes in pHL vectors were co-transfected with mDAP12 in pcDNA3.1 vector into 293F cells using 293fectin. After 24 hr, cells were harvested and washed into FACs buffer (1% BSA in PBS). FLAG epitope expression was detected using a FITC-conjugated M2 anti-FLAG antibody (1:50, Sigma-Aldrich. St. Louis, MO), and folded TREM2 surface expression was detected by staining with anti-TREM2 primary polysera (1:1000, hamster) followed by PE-anti-hamster secondary (1:200 eBioscience). Background was defined by cells transfected with mouse DAP12 only.

WT and mutant TREM2 cell-surface ligand binding studies

Production of fluorescently labeled TREM2 tetramers

For analysis of cell binding by flow cytometry, pHLAvitag3 constructs of WT and mutant human and mouse TREM2 ectodomains were transfected into Freestyle 293F cells and proteins were purified by Ni-NTA chromatography. The eluted proteins were exchanged into buffer containing 100 mM Tris-HCl pH 7.5, 200 mM K-glutamate, and 5 mM MgCl2, concentrated to 400 µL, and then enzymatic biotinylation was carried out by addition of 40 mM bicine pH 8.3, 8 mM $Mg(OAc)_2$, 8 mM ATP, 0.1 mM biotin and 20 µL *Escherichia coli* BirA biotin ligase (1 mg/mL). Biotinylation proceeded for 12 hr at 4°C. Excess biotin was removed using Zeba desalting spin columns (Thermo Scientific) and biotinylation was confirmed by western blot with Extravidin-HRP (Sigma). The biotinylated TREM2 was pre-incubated with SA-PE at a 4:1 molar ratio for 15 min at 25°C to produce fluorescently labeled tetramers (TREM2/SA-PE). Biotinylated TREM2 was complexed with phycoerythrin-conjugated streptavidin (SA-PE) at a 4:1 molar ratio on ice for 1 hr in 1% FBS prior to staining cells.

Cell staining

Prior to staining, N2A and CHO cells were lifted following brief exposure to trypsin/EDTA (other cells grow in suspension). Cells (4×10^5 cells/ sample) were stained using tetramers at 1:100 dilution in PBS containing 1% FCS (FACS buffer) at 4°C. Cells were either stained with SA-PE alone (1:100) or with TREM2/SA-PE (1:100). Cells were incubated for 1 hr on ice then washed three times with FACS buffer, and then analyzed for binding by flow cytometry using a BD FACScan. Analysis was performed using FlowJo (Tree Star).

Chemical stimulation

For each condition, 1 x 10^6 THP-1 cells were stimulated overnight at the indicated concentration. Poly IC (1 µg mL^{-1}), LPS (1 µg mL^{-1}), PMA+ionomycin (20 ng μL^{-1} and 500 ng mL^{-1}, respectively), M-CSF (20 ng μL^{-1}), and IL-13 (50 ng mL^{-1}). Cells were collected and washed in FACs buffer before staining.

Protease treatment

Cells were washed in ice-cold PBS and then incubated with indicated proteases (50 µg mL^{-1}) on ice for 30 min. Proteolysis was quenched by washing cells four times in FACs buffer containing PMSF. Cells were stained with SAPE-TREM2 in FACs buffer containing PMSF and HALT protease inhibitors. Cell viability was verified by 7-AAD staining (BD Biosciences. San Jose, CA) according to the manufacturer's directions.

6-His staining of THP-1 cells

WT and mutant human TREM2 ectodomains were purified by SEC as in ***Figure 2—figure supplement 1***. The monomeric peak was collected, concentrated and buffer-exchanged into PBS by centrifugation. Protein concentration was quantitated in triplicate using the Micro BCA kit (Thermo Scientific) according to the manufacturer's instructions. THP-1 cells were washed into FACS buffer and incubated with purified proteins for 1 hr, washed twice, and then incubated in FACS media with Fc-block followed by anti-6His-PE (Miltenyi Biotec. Germany) for 30 min before a final wash and flow cytometry analysis. 20,000 cells were counted for each measurement.

Proteoglycan digestion assay

Chondroitinase ABC and Heparinases I, II, and III were purchased from Sigma-Aldrich. Digestion of cell-surface sulfated glycans was carried out as follows: cells were washed into PBS with 0.1% BSA and incubated with enzymes at 0.1 U mL^{-1} for 1 hr at 37°C while shaking before being washed three times with cold FACS buffer.

Thermostability of TREM2 variants by DSF

Thermal stability was assessed by differential scanning fluorimetry (DSF) on protein purified by SEC. The Protein Thermal Shift kit (Applied Biosystems) was used according to the manufacturer's instructions. Briefly, protein was concentrated to 0.5 mg mL^{-1} after buffer exchange into PBS. 5 µl of reaction buffer and 2.5 µl 8x fluorescent dye were added to 12.5 µL protein on ice. Melt-curve experiments were performed using Fast7500 qPCR machine (ABI) starting at 25°C and with continuous 1% ramp to 95°C (roughly 1°C min^{-1}). The data were analyzed using Protein Thermal Shift software.

Thermal and chemical stability of TREM2 variants by CD

Circular dichroism spectroscopy (CD) measurements were performed using a JASCO J-815 spectropolarimeter equipped with a Peltier temperature controller. Thermal denaturation experiments were carried out in 10 mM phosphate (pH 7.0) and 150 mM NaF. For native and GuHCl-denaturation scans, a 1 mm path length cuvette was used and the protein concentration was 30 µM. For denaturation experiments, a 1 cm path length cuvette was used and the protein concentration was 3 µM. For reducing conditions, the buffer contained 1 mM DTT. Ellipticity was measured at 225 nm in 1°C steps from 20°C to 90°C at a rate of 1°C min^{-1} and melt-curve data were smoothed using JASCO software. For chemical stability experiments, purified human ectodomains were incubated with GuHCl (Fluka 50933) at room temperature for at least 1 hr before measuring CD. Repeat measurements at later time points confirmed that equilibrium had been achieved.

Solid-Phase lipid ELISA

Lipid ELISA experiments were carried out essentially as described by ***Kobayashi et al., (2007)***. In brief, phospholipids were dissolved in methanol or methanol:chloroform as needed and diluted to 5 µg mL^{-1} in methanol. 100 µL was added to ELISA plates and allowed to air-dry. Wells were blocked with 3% BSA in PBS. Biotinylated WT or mutant TREM2 in 3% BSA-PBS were incubated overnight at 4°C. Plates were washed three times in PBS + 0.05% Tween 20. Biotinylated TREM2 was detected by streptavidin-HRP (R and D) in 1% BSA-PBS for 2 hr at RT before final wash and developing with TMB Microwell Peroxidase Substrate (KPL. Gaithersburg, MD). Absorbance was measured at 450 nm on a Gemini Plus plate reader (Molecular Devices. Sunnyvale, CA).

Immunoflourescent confocal microscopy

HEK293T cells were co-transfected with full-length FLAG-TREM2 and DAP12 for 24 hr before replating on glass slides. Cells were washed 2x with PBS, then fixed with 4% paraformaldehyde (PFA) in PBS for 5 min. Cells were then washed and blocked with animal-free blocker (Vector Laboratories. Burlingame, CA) for 1 hr at RT. For permeabilized cells, 0.1% triton x-100 was added to the blocking buffer and subsequent steps. Anti-FLAG antibody (M2, Sigma) was added at 1:1000 overnight at 4°C. Cells were then washed twice, and anti-mouse secondary Alexa Fluor 555 conjugate (Life Technologies) was added at 1:200 for 1 hr. Cells were washed a final time and then mounted in VECTASHIELD H-1200 Mounting Medium with DAPI (Vector Laboratories). Confocal

microscopy was carried out using a Zeiss LSM 510 META Confocal Laser Scanning Microscope (Carl Zeiss Microscopy, Thornwood, NY) at 400x magnification. The images were acquired with LSM 4.2 software.

Liposome sedimentation assays

Liposomes consisted of a base of 35:35:10 PtdCholine, PtdEthanolamine, and cholesterol with an additional 20% wt/wt of candidate phospholipids. Phospholipids were purchased from Sigma or Avanti dissolved in chloroform. Lipids were mixed in solvent-washed glass vials and solvent was evaporated under nitrogen stream. Lipids were resuspended in PBS, warmed at 37°C for 15 min followed by three freeze-thaw cycles on liquid N_2 and 37°C H_2O. For the sedimentation assay, 10 µg TREM2 proteins quantified by BCA were mixed with 100 µg liposomes and incubated for 1 hr at room temperature. Liposomes were sedimented by centrifugation at 16,800 x *g* at 4°C. The supernatant was removed and the pellet resuspended in SDS buffer for 6His immunoblot analysis.

Statistics

All statistics were calculated using GraphPad Prism5.

Acknowledgements

This work was supported in part by funding from NIH R01-HL119813 (TJB), Knight Alzheimer's Disease Research Center pilot grant P50-AG005681-30.1 (TJB), Alzheimer's Association Research Grant AARG-16-441560 (TJB), K08-HL121168 (JAB), Burroughs-Wellcome Fund Career Award for Medical Scientists (JAB), NIH K01-AG046374 (CMK), R01-AG044546 (CC), R01-AG051485 (MC), R01-HL120153 (MJH), R01-HL121791 (MJH), T32-GM007067 (DLK), and American Heart Association Predoctoral Fellowship PRE22110004 (DLK). Results were derived from work performed at Argonne National Laboratory (ANL) Structural Biology Center. ANL is operated by University of Chicago Argonne, LLC, for the U.S. DOE, Office of Biological and Environmental Research (DE-AC02-06CH11357).

Additional information

Funding

Funder	Grant reference number	Author
American Heart Association	Predoctoral Fellowship PRE22110004	Daniel L Kober
National Institute of General Medical Sciences	T32-GM007067	Daniel L Kober
National Heart, Lung, and Blood Institute	K08-HL121168	Jennifer M Alexander-Brett
Burroughs Wellcome Fund	Career Award for Medical Scientists	Jennifer M Alexander-Brett
National Institute on Aging	K01-AG046374	Celeste M Karch
National Institute on Aging	R01-AG044546	Carlos Cruchaga
National Institute on Aging	R01-AG051485	Marco Colonna
National Heart, Lung, and Blood Institute	R01-HL120153	Michael J Holtzman
National Heart, Lung, and Blood Institute	R01-HL121791	Michael J Holtzman
National Heart, Lung, and Blood Institute	R01-HL119813	Thomas J Brett
National Institute on Aging	P50-AG005681-30.1	Thomas J Brett
Knight Alzheimer's Disease Research Center	Pilot grant P50-AG005681-30.1	Thomas J Brett

Alzheimer's Association	AARG-16-441560	Thomas J Brett

The funders had no role in study design, data collection and interpretation, or the decision to submit the work for publication.

Author contributions

DLK, TJB, Conception and design, Acquisition of data, Analysis and interpretation of data, Drafting or revising the article, Contributed unpublished essential data or reagents; JMA-B, Conception and design, Analysis and interpretation of data, Drafting or revising the article; CMK, Conception and design, Drafting or revising the article; CC, Analysis and interpretation of data, Drafting or revising the article, Contributed unpublished essential data or reagents; MC, MJH, Drafting or revising the article, Contributed unpublished essential data or reagents

Author ORCIDs

Celeste M Karch, http://orcid.org/0000-0002-6854-5547
Thomas J Brett, http://orcid.org/0000-0002-6871-6676

References

Adams PD, Afonine PV, Bunkóczi G, Chen VB, Davis IW, Echols N, Headd JJ, Hung LW, Kapral GJ, Grosse-Kunstleve RW, McCoy AJ, Moriarty NW, Oeffner R, Read RJ, Richardson DC, Richardson JS, Terwilliger TC, Zwart PH. 2010. PHENIX: a comprehensive Python-based system for macromolecular structure solution. *Acta Crystallographica. Section D, Biological Crystallography* **66**:213–221. doi: 10.1107/S0907444909052925, PMID: 20124702

Atagi Y, Liu CC, Painter MM, Chen XF, Verbeeck C, Zheng H, Li X, Rademakers R, Kang SS, Xu H, Younkin S, Das P, Fryer JD, Bu G. 2015. Apolipoprotein E Is a Ligand for Triggering Receptor Expressed on Myeloid Cells 2 (TREM2). *The Journal of Biological Chemistry* **290**:26043–26050. doi: 10.1074/jbc.M115.679043, PMID: 26374899

Bailey CC, DeVaux LB, Farzan M. 2015. The Triggering Receptor Expressed on Myeloid Cells 2 Binds Apolipoprotein E. *The Journal of Biological Chemistry* **290**:26033–26042. doi: 10.1074/jbc.M115.677286, PMID: 26374897

Cady J, Koval ED, Benitez BA, Zaidman C, Jockel-Balsarotti J, Allred P, Baloh RH, Ravits J, Simpson E, Appel SH, Pestronk A, Goate AM, Miller TM, Cruchaga C, Harms MB. 2014. TREM2 variant p.R47H as a risk factor for sporadic amyotrophic lateral sclerosis. *JAMA Neurology* **71**:449–453. doi: 10.1001/jamaneurol.2013.6237, PMID: 24535663

Cannon JP, O'Driscoll M, Litman GW. 2012. Specific lipid recognition is a general feature of CD300 and TREM molecules. *Immunogenetics* **64**:39–47. doi: 10.1007/s00251-011-0562-4, PMID: 21800138

Chouery E, Delague V, Bergougnoux A, Koussa S, Serre JL, Mégarbané A. 2008. Mutations in TREM2 lead to pure early-onset dementia without bone cysts. *Human Mutation* **29**:E194–E204. doi: 10.1002/humu.20836, PMID: 18546367

Colonna M. 2003. DAP12 signaling: from immune cells to bone modeling and brain myelination. *Journal of Clinical Investigation* **111**:313–314. doi: 10.1172/JCI17745

Colonna M, Wang Y. 2016. TREM2 variants: new keys to decipher Alzheimer disease pathogenesis. *Nature Reviews. Neuroscience* **17**:201–207. doi: 10.1038/nrn.2016.7, PMID: 26911435

Cruchaga C, Kauwe JS, Harari O, Jin SC, Cai Y, Karch CM, Benitez BA, Jeng AT, Skorupa T, Carrell D, Bertelsen S, Bailey M, McKean D, Shulman JM, De Jager PL, Chibnik L, Bennett DA, Arnold SE, Harold D, Sims R, et al. 2013. GWAS of cerebrospinal fluid tau levels identifies risk variants for Alzheimer's disease. *Neuron* **78**:256–268. doi: 10.1016/j.neuron.2013.02.026, PMID: 23562540

Daws MR, Sullam PM, Niemi EC, Chen TT, Tchao NK, Seaman WE. 2003. Pattern recognition by TREM-2: binding of anionic ligands. *Journal of Immunology* **171**:594–599. doi: 10.4049/jimmunol.171.2.594, PMID: 12847223

Emsley P, Lohkamp B, Scott WG, Cowtan K. 2010. Features and development of Coot. *Acta Crystallographica. Section D, Biological Crystallography* **66**:486–501. doi: 10.1107/S0907444910007493, PMID: 20383002

Esko JD, Stewart TE, Taylor WH. 1985. Animal cell mutants defective in glycosaminoglycan biosynthesis. *PNAS* **82**:3197–3201. doi: 10.1073/pnas.82.10.3197, PMID: 3858816

Gattis JL, Washington AV, Chisholm MM, Quigley L, Szyk A, McVicar DW, Lubkowski J. 2006. The structure of the extracellular domain of triggering receptor expressed on myeloid cells like transcript-1 and evidence for a naturally occurring soluble fragment. *The Journal of Biological Chemistry* **281**:13396–13403. doi: 10.1074/jbc.M600489200, PMID: 16505478

Golde TE, Streit WJ, Chakrabarty P. 2013. 'sAlzheimer. *Alzheimer's Research & Therapy* **5**:24. doi: 10.1186/alzrt178, PMID: 23692967

Guerreiro R, Bilgic B, Guven G, Brás J, Rohrer J, Lohmann E, Hanagasi H, Gurvit H, Emre M. 2013a. A novel compound heterozygous mutation in TREM2 found in a Turkish frontotemporal dementia-like family. *Neurobiology of Aging* **34**:2890.e1–282890. doi: 10.1016/j.neurobiolaging.2013.06.005

Guerreiro R, Wojtas A, Bras J, Carrasquillo M, Rogaeva E, Majounie E, Cruchaga C, Sassi C, Kauwe JS, Younkin S, Hazrati L, Collinge J, Pocock J, Lashley T, Williams J, Lambert JC, Amouyel P, Goate A, Rademakers R, Morgan K, et al. 2013b. 'sTREM2 variants in Alzheimer. *New England Journal of Medicine* **368**:117–127. doi: 10.1056/NEJMoa1211851, PMID: 23150934

Guerreiro RJ, Lohmann E, Brás JM, Gibbs JR, Rohrer JD, Gurunlian N, Dursun B, Bilgic B, Hanagasi H, Gurvit H, Emre M, Singleton A, Hardy J. 2013c. Using exome sequencing to reveal mutations in TREM2 presenting as a frontotemporal dementia-like syndrome without bone involvement. *JAMA Neurology* **70**:78–84. doi: 10.1001/jamaneurol.2013.579, PMID: 23318515

Hamerman JA, Jarjoura JR, Humphrey MB, Nakamura MC, Seaman WE, Lanier LL. 2006. Cutting edge: inhibition of TLR and FcR responses in macrophages by triggering receptor expressed on myeloid cells (TREM)-2 and DAP12. *Journal of Immunology* **177**:2051–2055. doi: 10.4049/jimmunol.177.4.2051, PMID: 16887962

Hsieh CL, Koike M, Spusta SC, Niemi EC, Yenari M, Nakamura MC, Seaman WE. 2009. A role for TREM2 ligands in the phagocytosis of apoptotic neuronal cells by microglia. *Journal of Neurochemistry* **109**:1144–1156. doi: 10.1111/j.1471-4159.2009.06042.x, PMID: 19302484

Hubbard S, Thornton J. 1993. *NACCESS, Computer Program*. University College London: Department of Biochemistry Molecular Biology.

Ito H, Hamerman JA. 2012. TREM-2, triggering receptor expressed on myeloid cell-2, negatively regulates TLR responses in dendritic cells. *European Journal of Immunology* **42**:176–185. doi: 10.1002/eji.201141679, PMID: 21958852

Jay TR, Miller CM, Cheng PJ, Graham LC, Bemiller S, Broihier ML, Xu G, Margevicius D, Karlo JC, Sousa GL, Cotleur AC, Butovsky O, Bekris L, Staugaitis SM, Leverenz JB, Pimplikar SW, Landreth GE, Howell GR, Ransohoff RM, Lamb BT. 2015. TREM2 deficiency eliminates TREM2+ inflammatory macrophages and ameliorates pathology in Alzheimer's disease mouse models. *The Journal of Experimental Medicine* **212**:287–295. doi: 10.1084/jem.20142322, PMID: 25732305

Jin SC, Benitez BA, Karch CM, Cooper B, Skorupa T, Carrell D, Norton JB, Hsu S, Harari O, Cai Y, Bertelsen S, Goate AM, Cruchaga C. 2014. 'sCoding variants in TREM2 increase risk for Alzheimer. *Human Molecular Genetics* **23**:5838–5846. doi: 10.1093/hmg/ddu277, PMID: 24899047

Jonsson T, Stefansson H, Steinberg S, Jonsdottir I, Jonsson PV, Snaedal J, Bjornsson S, Huttenlocher J, Levey AI, Lah JJ, Rujescu D, Hampel H, Giegling I, Andreassen OA, Engedal K, Ulstein I, Djurovic S, Ibrahim-Verbaas C, Hofman A, Ikram MA, et al. 2013. 'sVariant of TREM2 associated with the risk of Alzheimer. *New England Journal of Medicine* **368**:107–116. doi: 10.1056/NEJMoa1211103, PMID: 23150908

Karplus PA, Diederichs K. 2012. Linking crystallographic model and data quality. *Science* **336**:1030–1033. doi: 10.1126/science.1218231, PMID: 22628654

Kawabori M, Kacimi R, Kauppinen T, Calosing C, Kim JY, Hsieh CL, Nakamura MC, Yenari MA. 2015. Triggering receptor expressed on myeloid cells 2 (TREM2) deficiency attenuates phagocytic activities of microglia and exacerbates ischemic damage in experimental stroke. *Journal of Neuroscience* **35**:3384–3396. doi: 10.1523/JNEUROSCI.2620-14.2015, PMID: 25716838

Kelker MS, Debler EW, Wilson IA. 2004a. Crystal structure of mouse triggering receptor expressed on myeloid cell 1 (TREM-1) at 1.76 A. *Journal of Molecular Biology* **344**:1175–1181. doi: 10.1016/j.jmb.2004.10.079, PMID: 15544810

Kelker MS, Foss TR, Peti W, Teyton L, Kelly JW, Wüthrich K, Wilson IA. 2004b. Crystal structure of human triggering receptor expressed on myeloid cells 1 (TREM-1) at 1.47 A. *Journal of Molecular Biology* **342**:1237–1248. doi: 10.1016/j.jmb.2004.07.089, PMID: 15351648

Kleinberger G, Yamanishi Y, Suárez-Calvet M, Czirr E, Lohmann E, Cuyvers E, Struyfs H, Pettkus N, Wenninger-Weinzierl A, Mazaheri F, Tahirovic S, Lleó A, Alcolea D, Fortea J, Willem M, Lammich S, Molinuevo JL, Sánchez-Valle R, Antonell A, Ramirez A, et al. 2014. TREM2 mutations implicated in neurodegeneration impair cell surface transport and phagocytosis. *Science Translational Medicine* **6**:243ra86. doi: 10.1126/scitranslmed. 3009093, PMID: 24990881

Kobayashi N, Karisola P, Peña-Cruz V, Dorfman DM, Jinushi M, Umetsu SE, Butte MJ, Nagumo H, Chernova I, Zhu B, Sharpe AH, Ito S, Dranoff G, Kaplan GG, Casasnovas JM, Umetsu DT, Dekruyff RH, Freeman GJ. 2007. TIM-1 and TIM-4 glycoproteins bind phosphatidylserine and mediate uptake of apoptotic cells. *Immunity* **27**: 927–940. doi: 10.1016/j.immuni.2007.11.011, PMID: 18082433

Kober DL, Wanhainen KM, Johnson BM, Randolph DT, Holtzman MJ, Brett TJ. 2014. Preparation, crystallization, and preliminary crystallographic analysis of wild-type and mutant human TREM-2 ectodomains linked to neurodegenerative and inflammatory diseases. *Protein Expression and Purification* **96**:32–38. doi: 10.1016/j. pep.2014.01.015, PMID: 24508568

Kober DL, Yurtsever Z, Brett TJ. 2015. Efficient mammalian cell expression and Single-step purification of extracellular glycoproteins for crystallization. *Journal of Visualized Experiments* **106**:e53445. doi: 10.3791/53445

Laskowski RA, Swindells MB. 2011. LigPlot+: multiple ligand-protein interaction diagrams for drug discovery. *Journal of Chemical Information and Modeling* **51**:2778–2786. doi: 10.1021/ci200227u, PMID: 21919503

Le Bret T, De Septenville A, Guerreiro R, Bras J, Camuzat A, Caroppo P, Lattante S, Couarch P, Kabashi E, Bouya-Ahmed K, Dubois B, Brice A. 2014. Homozygous TREM2 mutation in a family with atypical frontotemporal dementia. *Neurobiology of Aging* **35**:2419.e23–2412.e25. doi: 10.1016/j.neurobiolaging.2014.04.010

McDonald IK, Thornton JM. 1994. Satisfying hydrogen bonding potential in proteins. *Journal of Molecular Biology* **238**:777–793. doi: 10.1006/jmbi.1994.1334, PMID: 8182748

Meyer PA, Socias S, Key J, Ransey E, Tjon EC, Buschiazzo A, Lei M, Botka C, Withrow J, Neau D, Rajashankar K, Anderson KS, Baxter RH, Blacklow SC, Boggon TJ, Bonvin AM, Borek D, Brett TJ, Caflisch A, Chang CI, et al. 2016. Data publication with the structural biology data grid supports live analysis. *Nature Communications* **7**: 10882. doi: 10.1038/ncomms10882, PMID: 26947396

Miyanishi M, Tada K, Koike M, Uchiyama Y, Kitamura T, Nagata S. 2007. Identification of Tim4 as a phosphatidylserine receptor. *Nature* **450**:435–439. doi: 10.1038/nature06307, PMID: 17960135

Morin A, Eisenbraun B, Key J, Sanschagrin PC, Timony MA, Ottaviano M, Sliz P. 2013. Collaboration gets the most out of software. *eLife* **2**:e01456. doi: 10.7554/eLife.01456, PMID: 24040512

Niesen FH, Berglund H, Vedadi M. 2007. The use of differential scanning fluorimetry to detect ligand interactions that promote protein stability. *Nature Protocols* **2**:2212–2221. doi: 10.1038/nprot.2007.321, PMID: 17853878

Numasawa Y, Yamaura C, Ishihara S, Shintani S, Yamazaki M, Tabunoki H, Satoh JI. 2011. Nasu-Hakola disease with a splicing mutation of TREM2 in a Japanese family. *European Journal of Neurology* **18**:1179–1183. doi: 10.1111/j.1468-1331.2010.03311.x, PMID: 21834902

Otwinowski Z, Minor W. 1997. *Processing of X-Ray Diffraction Data Collected in Oscillation Mode*. New York: Academic Press.

Paloneva J, Mandelin J, Kiialainen A, Bohling T, Prudlo J, Hakola P, Haltia M, Konttinen YT, Peltonen L. 2003. DAP12/TREM2 deficiency results in impaired osteoclast differentiation and osteoporotic features. *The Journal of Experimental Medicine* **198**:669–675. doi: 10.1084/jem.20030027, PMID: 12925681

Paloneva J, Manninen T, Christman G, Hovanes K, Mandelin J, Adolfsson R, Bianchin M, Bird T, Miranda R, Salmaggi A, Tranebjaerg L, Konttinen Y, Peltonen L. 2002. Mutations in two genes encoding different subunits of a receptor signaling complex result in an identical disease phenotype. *American Journal of Human Genetics* **71**:656–662. doi: 10.1086/342259, PMID: 12080485

Park JS, Ji IJ, An HJ, Kang MJ, Kang SW, Kim DH, Yoon SY. 2015. Disease-Associated Mutations of TREM2 Alter the Processing of N-Linked Oligosaccharides in the Golgi Apparatus. *Traffic* **16**:510–518. doi: 10.1111/tra.12264, PMID: 25615530

Phongsisay V, Iizasa E, Hara H, Yamasaki S. 2015. 3-O-sulfo-β-D-galactose moiety of endogenous sulfoglycolipids is a potential ligand for immunoglobulin-like receptor LMIR5. *Molecular Immunology* **63**:595–599. doi: 10.1016/j.molimm.2014.07.023, PMID: 25172093

Piccio L, Deming Y, Del-Águila JL, Ghezzi L, Holtzman DM, Fagan AM, Fenoglio C, Galimberti D, Borroni B, Cruchaga C. 2016. Cerebrospinal fluid soluble TREM2 is higher in Alzheimer disease and associated with mutation status. *Acta Neuropathologica* **131**:925–933. doi: 10.1007/s00401-016-1533-5, PMID: 26754641

Poliani PL, Wang Y, Fontana E, Robinette ML, Yamanishi Y, Gilfillan S, Colonna M. 2015. TREM2 sustains microglial expansion during aging and response to demyelination. *The Journal of Clinical Investigation* **125**: 2161–2170. doi: 10.1172/JCI77983, PMID: 25893602

Quan DN, Cooper MD, Potter JL, Roberts MH, Cheng H, Jarvis GA. 2008. TREM-2 binds to lipooligosaccharides of Neisseria gonorrhoeae and is expressed on reproductive tract epithelial cells. *Mucosal Immunology* **1**:229–238. doi: 10.1038/mi.2008.1, PMID: 19079182

Rayaprolu S, Mullen B, Baker M, Lynch T, Finger E, Seeley WW, Hatanpaa KJ, Lomen-Hoerth C, Kertesz A, Bigio EH, Lippa C, Josephs KA, Knopman DS, White CL, Caselli R, Mackenzie IR, Miller BL, Boczarska-Jedynak M, Opala G, Krygowska-Wajs A, et al. 2013. TREM2 in neurodegeneration: evidence for association of the p.R47H variant with frontotemporal dementia and Parkinson's disease. *Molecular Neurodegeneration* **8**:19. doi: 10.1186/1750-1326-8-19, PMID: 23800361

Ridge PG, Hoyt KB, Boehme K, Mukherjee S, Crane PK, Haines JL, Mayeux R, Farrer LA, Pericak-Vance MA, Schellenberg GD, Kauwe JSK. 2016. Assessment of the genetic variance of late-onset alzheimer's disease. *Neurobiology of Aging* **41**:200.e13–200.e20. doi: 10.1016/j.neurobiolaging.2016.02.024

Robert X, Gouet P. 2014. Deciphering key features in protein structures with the new ENDscript server. *Nucleic Acids Research* **42**:W320–W324. doi: 10.1093/nar/gku316, PMID: 24753421

Santiago C, Ballesteros A, Martínez-Muñoz L, Mellado M, Kaplan GG, Freeman GJ, Casasnovas JM. 2007. Structures of T cell immunoglobulin mucin protein 4 show a metal-Ion-dependent ligand binding site where phosphatidylserine binds. *Immunity* **27**:941–951. doi: 10.1016/j.immuni.2007.11.008, PMID: 18083575

Sievers F, Wilm A, Dineen D, Gibson TJ, Karplus K, Li W, Lopez R, McWilliam H, Remmert M, Söding J, Thompson JD, Higgins DG. 2011. Fast, scalable generation of high-quality protein multiple sequence alignments using Clustal Omega. *Molecular Systems Biology* **7**:539. doi: 10.1038/msb.2011.75, PMID: 21988835

Sikkink LA, Ramirez-Alvarado M. 2008. Salts enhance both protein stability and amyloid formation of an immunoglobulin light chain. *Biophysical Chemistry* **135**:25–31. doi: 10.1016/j.bpc.2008.02.019, PMID: 18395318

Simhadri VR, Andersen JF, Calvo E, Choi SC, Coligan JE, Borrego F. 2012. Human CD300a binds to phosphatidylethanolamine and phosphatidylserine, and modulates the phagocytosis of dead cells. *Blood* **119**: 2799–2809. doi: 10.1182/blood-2011-08-372425, PMID: 22302738

Soragna D, Papi L, Ratti MT, Sestini R, Tupler R, Montalbetti L. 2003. An italian family affected by Nasu-Hakola disease with a novel genetic mutation in the TREM2 gene. *Journal of Neurology, Neurosurgery & Psychiatry* **74**:825–826. doi: 10.1136/jnnp.74.6.825-a, PMID: 12754369

Stefano L, Racchetti G, Bianco F, Passini N, Gupta RS, Panina Bordignon P, Meldolesi J. 2009. The surface-exposed chaperone, Hsp60, is an agonist of the microglial TREM2 receptor. *Journal of Neurochemistry* **110**: 284–294. doi: 10.1111/j.1471-4159.2009.06130.x, PMID: 19457124

Takahashi K, Rochford CD, Neumann H. 2005. Clearance of apoptotic neurons without inflammation by microglial triggering receptor expressed on myeloid cells-2. *The Journal of Experimental Medicine* **201**:647–657. doi: 10.1084/jem.20041611, PMID: 15728241

Takegahara N, Takamatsu H, Toyofuku T, Tsujimura T, Okuno T, Yukawa K, Mizui M, Yamamoto M, Prasad DV, Suzuki K, Ishii M, Terai K, Moriya M, Nakatsuji Y, Sakoda S, Sato S, Akira S, Takeda K, Inui M, Takai T, et al. 2006. Plexin-A1 and its interaction with DAP12 in immune responses and bone homeostasis. *Nature Cell Biology* **8**:615–622. doi: 10.1038/ncb1416, PMID: 16715077

Tietjen GT, Gong Z, Chen CH, Vargas E, Crooks JE, Cao KD, Heffern CT, Henderson JM, Meron M, Lin B, Roux B, Schlossman ML, Steck TL, Lee KY, Adams EJ. 2014. Molecular mechanism for differential recognition of membrane phosphatidylserine by the immune regulatory receptor Tim4. *PNAS* **111**:E1463–E1472. doi: 10.1073/pnas.1320174111, PMID: 24706780

Turnbull IR, Gilfillan S, Cella M, Aoshi T, Miller M, Piccio L, Hernandez M, Colonna M. 2006. Cutting edge: TREM-2 attenuates macrophage activation. *Journal of Immunology* **177**:3520–3524. doi: 10.4049/jimmunol.177.6.3520, PMID: 16951310

Ulrich JD, Finn MB, Wang Y, Shen A, Mahan TE, Jiang H, Stewart FR, Piccio L, Colonna M, Holtzman DM. 2014. Altered microglial response to Aβ plaques in APPPS1-21 mice heterozygous for TREM2. *Molecular Neurodegeneration* **9**:20. doi: 10.1186/1750-1326-9-20, PMID: 24893973

Wang Y, Cella M, Mallinson K, Ulrich JD, Young KL, Robinette ML, Gilfillan S, Krishnan GM, Sudhakar S, Zinselmeyer BH, Holtzman DM, Cirrito JR, Colonna M. 2015. 'sTREM2 lipid sensing sustains the microglial response in an Alzheimer. *Cell* **160**:1061–1071. doi: 10.1016/j.cell.2015.01.049, PMID: 25728668

Wang Y, Ulland TK, Ulrich JD, Song W, Tzaferis JA, Hole JT, Yuan P, Mahan TE, Shi Y, Gilfillan S, Cella M, Grutzendler J, DeMattos RB, Cirrito JR, Holtzman DM, Colonna M. 2016. TREM2-mediated early microglial response limits diffusion and toxicity of amyloid plaques. *The Journal of Experimental Medicine* **213**:667–675. doi: 10.1084/jem.20151948, PMID: 27091843

Wu K, Byers DE, Jin X, Agapov E, Alexander-Brett J, Patel AC, Cella M, Gilfilan S, Colonna M, Kober DL, Brett TJ, Holtzman MJ. 2015. TREM-2 promotes macrophage survival and lung disease after respiratory viral infection. *The Journal of Experimental Medicine* **212**:681–697. doi: 10.1084/jem.20141732, PMID: 25897174

Yeh FL, Wang Y, Tom I, Gonzalez LC, Sheng M. 2016. TREM2 binds to apolipoproteins, including APOE and CLU/APOJ, and thereby facilitates uptake of amyloid-beta by microglia. *Neuron* **91**:328–340. doi: 10.1016/j.neuron.2016.06.015, PMID: 27477018

Yoon SH, Lee YD, Ha J, Lee Y, Kim HH. 2012. TLT-1s, alternative transcripts of triggering receptor expressed on myeloid cell-like transcript-1 (TLT-1), Inhibits the triggering receptor expressed on myeloid cell-2 (TREM-2)-mediated signaling pathway during osteoclastogenesis. *The Journal of Biological Chemistry* **287**:29620–29626. doi: 10.1074/jbc.M112.351239, PMID: 22761415

Yuan P, Condello C, Keene CD, Wang Y, Bird TD, Paul SM, Luo W, Colonna M, Baddeley D, Grutzendler J. 2016. TREM2 haplodeficiency in mice and humans impairs the microglia barrier function leading to decreased amyloid compaction and severe axonal dystrophy. *Neuron* **90**:724–739. doi: 10.1016/j.neuron.2016.05.003, PMID: 27196974

Zhang B, Gaiteri C, Bodea LG, Wang Z, McElwee J, Podtelezhnikov AA, Zhang C, Xie T, Tran L, Dobrin R, Fluder E, Clurman B, Melquist S, Narayanan M, Suver C, Shah H, Mahajan M, Gillis T, Mysore J, MacDonald ME, et al. 2013. Integrated systems approach identifies genetic nodes and networks in late-onset Alzheimer's disease. *Cell* **153**:707–720. doi: 10.1016/j.cell.2013.03.030, PMID: 23622250

TREM2-ligand interactions in health and disease

Daniel L. Kober[1,2] and Tom J. Brett[2,3,4]
1- Molecular Microbiology and Microbial Pathogenesis Program,
2- Division of Pulmonary and Critical Care Medicine, Department of Internal Medicine
3- Department of Cell Biology and Physiology
4- Department of Biochemistry and Molecular Biophysics[4] ,Washington University School of Medicine, St. Louis, Missouri 63110

Correspondence to: Tom J. Brett, PhD., Campus Box 8052, 660 S. Euclid, St. Louis, MO 63110.
Phone: (314) 747-0018; Fax: (314) 362-8987; Email: (tbrett@wustl.edu)

Abstract

The protein Triggering receptor expressed on myeloid cells-2 (TREM2) is an immunomodulatory receptor with a central role in myeloid cell activation and survival. In recent years, the importance of TREM2 has been highlighted by the identification of coding variants that increase risk for Alzheimer's disease and other neurodegenerative diseases. Animal studies have further shown the importance of TREM2 in neurodegenerative and other inflammatory disease models including chronic obstructive pulmonary disease, multiple sclerosis, and stroke. A mechanistic understanding of TREM2 function remains elusive, however, due in part to the absence of conclusive information regarding the identity of endogenous TREM2 ligands. While many TREM2 ligands have been proposed, their physiological role and mechanism of engagement remains to be determined. In this review, we highlight the suggested roles of TREM2 in these diseases, recent advances in our understanding of TREM2, and discuss potential TREM2-ligand interactions and their potential roles in signaling during health and disease. We develop a model based on the TREM2 structure to explain how different TREM2 ligands might interact with the receptor and how disease-risk variants may alter ligand interactions. Finally, we propose future experimental directions to establish the role and importance of these different interactions on TREM2 function.

Introduction

Triggering receptor expression on myeloid cells-2 (TREM2) is an extracellular innate immune receptor expressed on myeloid lineage cells such as dendritic cells (DC) and resident tissue macrophages (including osteoclasts and microglia). The receptor consists of an extracellular V-type immunoglobulin (Ig) domain followed by a short stalk (ectodomain = 19-172 a.a.) leading to a single transmembrane helix which interacts with DNAX-activation protein 12 (DAP12, also known as TYROBP) to mediate downstream signaling. TREM2 terminates with a short cytosolic tail (195-230 a.a.) lacking known signaling or trafficking motifs [1]. In addition to the membrane-bound form, soluble TREM2 ectodomains (sTREM2) can be generated by proteolytic processing [2] or by alternative splicing [3]. The importance of TREM2 is highlighted by genetic studies linking TREM2 variants to various neurodegenerative diseases, including Alzheimer's disease (AD) [4, 5]. TREM2 has been implicated in a wide array of functions including cell maturation, survival, proliferation, activation, phagocytosis, and the regulation of inflammation [1]. Accompanying this diverse set of functions is an even longer list of potential TREM2 ligands. Indeed, since its discovery, the identification of bona fide endogenous TREM2 ligands has proven elusive, although there is an emerging pattern of ligands that are anionic and/or lipidic in nature. It is unclear if the TREM2 ligand is among the suggested ligands or whether TREM2 is simply a highly promiscuous receptor that can engage a wide array of ligands. The goals of this review are to: 1) highlight functions for TREM2 evident from animal studies of homeostasis and disease; 2) identify facets of TREM2 signaling that may be influenced by different ligands; 3) discuss the evidence for the various TREM2 ligands; and 4) suggest where and how different ligands may be involved in TREM2 function. We develop the model that distinct ligands may mediate different components of TREM2 signaling and that a complex of ligands interacting with various portions of TREM2 may be required to assemble a productive signaling complex.

1. TREM2 in disease

TREM2 variants are risk factors for neurodegenerative diseases

The importance of TREM2 in neuronal health was first demonstrated by genetic studies that identified *TREM2* variants in families with Nasu-Hakola disease (NHD, also known as Polycystic lipomembranous osteodysplasia with sclerosing leukoencephalopathy, or PLOSL) a fatal disease characterized by presenile dementia and bone cysts [6-8]. NHD patients are homozygous for loss-of-function *DAP12* or *TREM2* variants. In some cases, *TREM2* mutant carriers present a fronto-temporal lobar form of dementia lacking the bone phenotype. The *TREM2* variants include splice site [7, 9] early stop sites [7, 10-12], and coding ectodomain mutations [7, 8, 13-15]. These mutations are all believed to produce nonfunctional proteins. More recently, separate coding variants in the Ig domain of TREM2 were linked to an increase risk for late onset AD (LOAD) [4, 5]. The link between *TREM2* variants and LOAD, particularly the R47H and R62H variants, is now well-established [3, 16-18]. *TREM2* AD risk variants are rare, but carry roughly the same risk as a copy of the apolipoprotein E4 (*APOE4*) allele and clearly link the innate immune system to neurodegenerative disease [19]. Beyond AD, *TREM2* variants have been linked to other neurodegenerative diseases, including Parkinson's disease [20, 21] and sporadic amyotrophic lateral sclerosis (ALS) [22], and fronto-temporal dementia [23, 24], though these non-AD associations have not been as widely reproduced [16]. The association of distinct variants with different diseases is born out on the protein level. Structural, biophysical, and cellular studies have shown the NHD coding mutants are misfolded with immature glycosylation patterns while the AD variants are properly folded and have mature glycosylation patterns but likely impact ligand binding [25, 26]. Slightly altered glycosylation patterns have been observed for the R47H variant [27, 28], but it is unclear if these have functional ramifications. Finally, a study examined the levels of sTREM2 in human variant

carriers and found reduced levels of protein with NHD variants but normal or perhaps even elevated detection of AD variants, showing a functional divergence in protein stability with the different variants [29].

Animal models and human studies of CNS disease indicate a crucial role for TREM2 in microglia function

Most studies of TREM2 in neurodegenerative diseases have used mouse models of AD. We will highlight key findings from those models and draw connections between the AD phenotypes and those observed in other neurodegenerative models such as stroke and MS to identify functions TREM2 may be contributing to during disease (Table 1).

Animal model studies by several groups have consistently found *Trem2* expression in the CNS restricted to microglia and increasing with age and disease progression [4, 30-33]. Within the normal human brain, *TREM2* is expressed most highly in white matter, with transcripts detected in all major areas [34]. Pathway analysis identified the TREM2 co-receptor DAP12 as a key regulator of expression changes in LOAD [35]. Although there have been reports of TREM2 detection on non-myeloid/microglial cells in the CNS [4, 36], these cases have largely used immunostaining methods to identify neuronal expression of TREM2, which may identify sTREM2 produced by microglia that is released and bound to neurons which express a TREM2 ligand [26, 37-39]. RNA expression analyses have confirmed *Trem2* is expressed selectively on microglia in the brain [40, 41], and parabiosis experiments show these microglia are most likely resident microglia and not infiltrating monocytes [42], although this is still controversial [43]. Within human AD brain, laser microdissection showed *Trem2* is highly expressed on plaque-associated microglia [44], and high resolution microscopy techniques showed that TREM2 protein is concentrated on microglia processes that are in contact with amyloid beta (Aβ) plaques [45]. Thus, *TREM2* is expressed in the brain and its expression

increases both with aging and in response to disease. Moreover, during AD, TREM2 is present on microglia at sites of Aβ deposition. Consistent with its expression on microglia, studies using *Trem2*-deficient mouse models of AD have shown a role for TREM2 in microglial survival and activation (Table 1).

Impacts of TREM2 function on Amyloid beta pathology

The amyloid cascade hypothesis posits that Aβ is the cause of AD, whether directly by mediating neurotoxicity or indirectly by triggering other neurotoxic events, such as tau aggregation [46]. It is based on the observation that autosomal dominant mutations causative for AD are found in proteins responsible for the production and maturation of the Aβ peptide. Common animal models of AD are genetically engineered to carry these mutant proteins and/or overexpress Aβ. To date, all AD studies involving *Trem2* knockout mice have utilized such models. However, the Aβ phenotypes have been inconsistent in these studies. Some studies using *Trem2*$^{-/-}$ mice found no change in the overall plaque load [42, 47], while further studies found increased [30, 43] or even decreased burden [31, 43]. Some of these differences are perhaps explained by the timing of data collection [43], although they could suggest Aβ clearance is not the only role for TREM2.

While there have been mixed results on the accumulation of Aβ, all *Trem2*$^{-/-}$ studies have shown decreased clustering of myeloid or microglial cells around plaques, suggesting a defect in microgliosis, or microglia activation [30, 31, 42, 43, 45, 47]. These studies have also found that *Trem2*$^{-/-}$ mice have fewer microglia and increased microglia apoptosis. Importantly, samples from human R47H carriers recapitulate the microglia- Aβ plaque phenotype observed in *Trem2* haploinsufficient mice, with fewer microglia clustering around the plaques, and the plaques displaying a diffuse morphology, which is more toxic to neurons [45]. Therefore, although TREM2 may not have a dramatic effect on the overall Aβ content of the diseased brain, it

strongly affects the ability of microglia to respond to and contain the plaques. In support of a role for TREM2 in microgliosis, a recent study found that production of sTREM2 is increased prior to the onset of symptoms but after initial markers of Aβ accumulation and neuronal injury [48]. This sTREM2 continues to increase until after the onset of symptoms and highlights the role for TREM2 in microgliosis at a critical point for the response to accumulating damage from disease.

TREM2 in models of Tau pathology

Besides Aβ, intracellular tangles of hyperphosphorylated tau proteins are the other major pathological component of AD [49]. While no studies using *Trem2*$^{-/-}$ mice have been published in tau models, Jiang and colleagues have conducted studies altering TREM2 expression *in vivo* by lentiviral overexpression (under a Cd11b promoter) or shRNA knockdown [50, 51] in the P301S tau transgenic model. These studies found that TREM2 reduces inflammation, decreases tau kinase activity, and improves cognitive function. Future studies should utilize *Trem2* knockout and mutant *Trem2* knock-in models on this background to confirm the role of TREM2 in tau-mediated neuropathies (if any).

TREM2 in other neurodegenerative diseases

Similar to what has been observed in AD models, *Trem2*-deficient mouse models of aging, prion pathogenesis and the cuprizone model of multiple sclerosis (MS) demonstrated fewer activated microglia in the course of the disease [52-54]. In MS models, there was less myelin clearance by microglia [52, 53] although there was no obvious deficiency in myelin uptake *in vitro*. Instead, *Trem2* deficiency was associated with decreased expression of lipid metabolism enzymes and a failure to degrade myelin debris [52, 53]. These findings suggest a more general defect in activation [52-54]. Other studies examining the role of TREM2 in stroke have found increased expression following ischemic attack [39, 55, 56]. As in the other cases,

these studies found that *Trem2* deficiency decreased inflammation, impaired microglial activation, and resulted in a failure of microglia to cluster at scar tissue [39, 55].

Summary TREM2 in neurodegenerative diseases

The consensus from the neurodegenerative disease studies is that TREM2 is important for enabling the response of myeloid cells (primarily microglia in the CNS) to disease. Mice lacking TREM2 have fewer microglia, and these microglia fail to activate and respond to damage during disease. These observations suggest a general deficit in microgliosis. Additionally, sTREM2 in CSF seems to be a general feature of inflammatory neurodegenerative disease. Soluble TREM2 was first identified in the CSF of MS patients and neuroinflammatory patients [57], and has since been identified in a number of AD cohorts [58-61].

Non-CNS diseases – the role of TREM2 in COPD, gut injury, and infection

Because of the genetic link between TREM2 and neurodegenerative diseases, the majority of TREM2 research in recent years has focused on its role in the CNS. However, TREM2 has important roles outside the CNS, particularly in models where the activation and phenotype of myeloid/macrophage cells is pivotal to disease development. In a model of virus-induced chronic obstructive pulmonary disease (COPD), TREM2 is required for survival and proliferation of alternatively activated (M2) macrophages [62]. Unlike the healthy microglial response in AD, these macrophages promote a COPD-like disease. However, the role of TREM2 in preventing macrophage apoptosis and permitting macrophage proliferation bears a striking similarity to the TREM2 phenotype in CNS diseases (where TREM2 contributes to microglia survival and proliferation). This study also identified a potential role for sTREM2 as a signaling molecule, as application of recombinant sTREM2 prevented macrophage apoptosis following M-CSF withdrawal.

In a gut injury model, TREM2 also promoted an M2 macrophage phenotype, which was important for promoting wound healing [63]. TREM2-expressing macrophages infiltrated the

wound area, inhibited the expression of inflammatory cytokines, and promoted the expression of Th2 cytokines IL-4 and IL-13. However, in a chemical injury model of inflammatory bowel disorder (IBD), TREM2 promoted an inflammatory phenotype that was detrimental to healing [64]. The differences in these studies may be due to the environment. In the biopsy injury model, the first step in healing was for epithelial cells to form a layer over the wound, which the authors hypothesized would reduce exposure to bacteria and therefore reduce strong TLR signals that are known to down-regulate TREM2 [63]. The healing response may be different in the chemical model, and the interaction between TREM2 and TLR pathways may result in the increased inflammation observed in that model [64].

While the initial characterizations of NHD patients with DAP12 and TREM2 mutants did not report immune deficiencies [7, 65], the role of TREM2 in infections has been studied in various models of bacterial infection. In general, these models are more acute than those discussed above, and therefore may highlight different roles for TREM2 in the innate response to bacteria. These studies have mostly found TREM2 to be phagocytic and anti-inflammatory, although there are some exceptions (Table 1). Cellular studies have shown that TREM2 regulates the response to bacteria, in two examples by promoting killing of bacteria through production of reactive oxygen species (ROS) [66, 67] – even against bacteria that were not directly detected by TREM2 [66]. The role of TREM2 may vary with different pathogens, as it did not promote killing of *B. abortus*, [68] a pathogen that specializes in invading and surviving in macrophages.

Conclusions from disease models of TREM2

Recent years have seen substantial progress in identifying an important role for TREM2 in animal models of disease. Studies using *Trem2*-deficient mice highlight its role in sustaining the microglial response to disease. However, important questions remain about what precise function TREM2 is performing, how different ligands may stimulate these functions, and how

disease variants or mutations affect function. Mechanistically, there are several possibilities for TREM2 functions, and the answers to these questions depend upon understanding the interaction between TREM2, its signaling mechanisms, and its ligands.

2. TREM2 Signaling

DAP12 mediates intracellular signaling of TREM2 and other receptors

DAP12 is the co-receptor for TREM2 and a number of other single-pass transmembrane receptors. DAP12 contains an Immuno-Tyrosine Activation Motif (ITAM, consensus sequence: YxxI/Lx(6–12)YxxI/L). Broadly, TREM2 signaling through DAP12 results in ITAM phosphorylation which leads to Ca^{2+} mobilization, ERK (MAPK) phosphorylation, and actin remodeling. However, TREM2 also negatively regulates TLR signaling and has roles in signaling pathways for other receptors [69]. Here we review the TREM2 signaling pathway and highlight areas where TREM2 signaling may have influence outside of the canonical "activation" pathway.

DAP12 associates with receptors through transmembrane interactions

DAP12 forms a disulfide-bonded homodimer with two intermolecular disulfide bonds contained within in a short ectodomain (14 residues in human aa 28-41 [70], 16 in mouse aa 28-43 [71]). Within the transmembrane domain, an electronegative Asp from each DAP12 monomer forms a 2:1 interaction with a Lys from the receptor. A Thr four residues below the Asp is also involved in the electrostatic network [72-74]. The interaction with the receptor is important to shield the polar residues from the lipophilic membrane environment and to allow trafficking to the cell surface (reviewed in [75]). While it is established that DAP12 requires complexing with a receptor for trafficking to the cell surface, there have been multiple reports of TREM2 surface expression in *Dap12* and *Dap12/Dap10*-deficient cells [62, 76, 77]. Other

DAP12-coupled receptors require DAP12 for surface expression [77], so it is possible that DAP12 could traffic to the surface with another receptor and engage TREM2 there.

The DAP12 signaling pathway

The standard DAP12-receptor signaling pathway was delineated using Ly49D as a model DAP12-coupled receptor on NK cells [78]. Ly49D ligation results in ITAM phosphorylation by Src kinases. The two phosphorylated Tyr residues in the ITAM create a binding site for the SH2 domain of the kinase Syk. Activation of Syk leads to the phosphorylation of ERK1/2, PLCγ1, and Cbl. These same features were observed with TREM2. Stimulation with an anti-TREM2 antibody produced calcium flux and ERK phosphorylation while monovalent stimulation by anti-TREM2 Fab did not result in calcium flux [79]. Functionally, TREM2 stimulation prolonged DC survival following withdrawal of GM-CSF and IL-4. TREM2 has also been implicated in actin mobilization [10, 80]. Monocytes from TREM2-null NHD patients had defective actin rearrangement following RANKL/MCSF stimulation. These initial studies linked TREM2 to the hallmark ITAM signaling events: Ca^{2+} mobilization, ERK phosphorylation, and actin remodeling (Fig. 1A). Further studies extended the TREM2 signaling pathway, and began to identify nuances that are key to fully understanding TREM2 function.

Although DAP12 is the primary adaptor for TREM2, DAP10 can also interact with DAP12-TREM2 complex, possibly through the formation of DAP12-DAP10 heterodimers [81]. DAP10 contains a "YINM" motif that can recruit PI3K. Accordingly, DAP10 was required for effective activation of PI3K, Grb2, and therefore Akt and ERK signaling. However, calcium mobilization was surprisingly unchanged in $DAP10^{-/-}$ bone marrow-derived macrophages (BMDMs) [81]. Beyond DAP12, signaling cascades in hematopoietic cells that begin with ITAM phosphorylation use scaffolding proteins to recruit downstream effector proteins such as Grb2, Cbl, PI3K, and Vav. Two such proteins are the Linkers for the Activation of T and B cells (LAT and LAB; LAB is also known as LAT2 and NTAL) [82]. While they share most functions, a key

difference is that LAT stimulates calcium mobilization more efficiently than LAB. DAP12 can signal using either LAT or LAB, however TREM2 signaling through DAP12 utilizes LAB in osteoclasts and BMDMs [83].

TREM2-DAP12 signaling is inhibited by phosphatases and ubiquitin ligases

Once activated, how is TREM2 signaling terminated? Following TREM2 stimulation by anti-TREM2 antibodies, the phosphatidylinositol phosphatase SHIP-1 binds the phosphorylated membrane-proximal tyrosine, pY65, within the ITAM motif of DAP12 to inhibit DAP12 signaling and TREM2-dependent osteoclast multinucleation [81]. This tyrosine is part of a "closet ITIM" sequence which was previously hypothesized to mediate inhibitory signals (SPYQEL, canonical ITIM is S/I/V/LxYxxI/V/L) [84]. Furthermore, as noted above, the E3 ubiquitin ligase Cbl is recruited to LAB and forms a complex with LAB and PI3K [83] to target Src and Syk for ubiquitination and degradation [85]. This activity requires LAB, as *LAB*$^{-/-}$ cells have increased Syk activation but decreased ERK activation [83]. Therefore, DAP12 signaling directly leads to its own inhibition by the recruitment of these two molecules. Finally, TREM-like transcript 1, (TREML1, also TLT-1), an ITIM-containing member of the TREM family is expressed in bone tissue [86] and associates with the tyrosine phosphatase SHP-1 upon phosphorylation. A short alternatively-spliced transcript lacking much of the ectodomain (TREML1s) is also expressed in osteoclast precursors and macrophages. TREML1s co-IPs with TREM2, SHP-1, and SHIP-1 and decreases ERK, Akt, and calcium signals following RANKL stimulation [87]. Therefore, TREML1 (or TREML1s) may inhibit TREM2 signaling (Fig. 1B).

TREM2 regulates inflammation through tonic signaling

In contrast with TREM1, which signals through DAP12 to amplify TLR responses [88], TREM2 inhibits inflammatory cytokine production following TLR stimulation in cultured BMDMs and DCs [89-91]. TREM2-dependent modulation of cytokine production did not require

exogenous stimulation of TREM2, suggesting TREM2 could be recognizing endogenous ligands to produce an inhibitory signal. There is precedence for inhibitory ITAM signaling in a similar system [92]. In this example, IgA binds its receptor FcαRI, which signals through the ITAM-containing co-receptor FcRγ to produce either inhibitory (SHP-1 recruiting) or activating ITAM signals based on whether IgA is monomeric or aggregated by antigens. The transient monomeric interaction produces inefficient ITAM phosphorylation, leading the recruitment of the inhibitory tyrosine phosphatase SHP-1. This IgA-FcαRI-FcRγ system is analogous to ligand-TREM2-DAP12 and previous commentaries have suggested monovalent or low-affinity TREM2 ligands induce tonic signals that are less activating and anti-inflammatory through such a mechanism [93-95] (Fig. 1C). However, the endogenous, inhibitory TREM2 ligand has not been identified. Along these lines, it was recently observed that expression of DAP12 with a C-terminal fragment of TREM2, which lacks the ectodomain but contains the DAP12-interacting transmembrane domain, is sufficient to inhibit cytokine production following LPS stimulation [96]. The C-terminal fragment may occupy DAP12 similarly to TREM2 with a monovalent ligand.

Soluble TREM2 (sTREM2) as a signaling molecule

The TREM2 receptor signals through DAP12. However, release of the soluble TREM2 ectodomain (sTREM2) via proteolysis is well-documented [2, 25]. The production of soluble TREM ectodomains appears to be a general feature of the family as soluble forms of TREM1 [97] and TREML1 [98] have also been reported. While sTREM1 is thought to be a decoy receptor [99], current evidence suggests sTREM2 is a signaling molecule. In the first study of sTREM2 function, application of sTREM2 (residues 19-136) to cultured BMDMs resulted in ERK and MAPK14 activation that persisted several hours and prevented apoptosis following M-CSF withdrawal [62]. A similar phenotype was recently observed using microglia [100], although the signaling mechanism differed (Fig. 1D**)**. In the macrophage study, sTREM2 did not detectably increase pAKT, while in microglia, the anti-apoptotic effect was blocked with PI3K inhibitors and

was mediated by AKT inhibition of GSK3-β to increase β-catenin. Soluble TREM2 also increased transcription of inflammatory cytokines in microglia through NF-kB activation [100], a pathway that was not previously reported to be activated by cellular TREM2 signaling [79]. It is interesting that only some functions associated with receptor TREM2, such as survival but not proliferation have been recapitulated with sTREM2, which suggests discrete roles for TREM2 both as a cellular receptor and soluble signaling molecule.

TREM2 regulates TLR signaling using inhibitory adaptors

TREM2 also uses adaptor proteins to influence the inflammatory environment. *LAB*$^{-/-}$ macrophages display increased ERK phosphorylation following TLR stimulation [83]. It could be that TREM2 signaling through LAB restricts ERK or other signaling molecules needed for TLR signaling, or that LAB-dependent Cbl-mediated ubiquitination reduces the level of kinases needed to activate TLR pathways [82]. Another pathway for inhibiting TLR signals is the recruitment of the anti-inflammatory adaptor protein DOK3 to DAP12 following TLR stimulation with LPS. Following LPS stimulation, DOK3 becomes phosphorylated, associates with DAP12, and interacts with Grb2 and Sos1 to inhibit the TLR response. In this system, SHIP-1 was not required to inhibit TLR signals, demonstrating that the inhibition of ITAM signaling by SHIP-1 is separate from the inhibition of TLR signaling by DAP12 [101] (Fig. 2A).

The role of TREM2 and DAP12 in co-stimulatory signaling

Plexin-A1 is expressed in a number of tissues including DCs and osteoclasts and is a receptor for two separate Semaphorin proteins. When expressed on osteoclast precursors, Plexin-A1 constitutively interacts with Neuropilin-1 (Nrp1) to mediate Semaphorin-3A (Sema3A) signaling, which prevents osteoclast maturation [102]. However, when osteoclast precursors are stimulated with RANKL, Nrp1 is downregulated and Plexin-A1 can be bound by Sema6D to drive osteoclast maturation [103]. Unexpectedly, this Sema6D signaling required TREM2 and DAP12 [104]. When *Plexin-A1*$^{-/-}$ mice were first characterized, they were discovered to have an

osteopetrotic phenotype with decreased osteoclast counts as well as deficits in activation of T cells by DCs, similar to what had been reported for DAP12$^{-/-}$ mice [105, 106]. Takegahara et al. found that stimulation of BMDCs with a soluble form of Sema6D resulted in DAP12 phosphorylation and also found an interaction between TREM2 and Plexin-A1 using co-IP and intracellular FRET. DAP12 and Plexin-A1 did not co-IP without TREM2, suggesting TREM2 connects DAP12 to Plexin-A1 signaling [104]. This Plexin-A1/TREM2 interaction is specific for Sema6D signaling, because the Nrp1-Plexin-A1 interaction displaces TREM2 in co-IP experiments [102, 107] (Fig. 2B).

TREM2 is also involved in M-CSF-mediated survival and proliferation in macrophages and osteoclast precursors. M-CSF signals through its receptor CSF-1R to activate β-catenin through phosphorylation of β-catenin by calmodulin-dependent kinases downstream of DAP12 in a TREM2-dependent mechanism [108, 109]. In *Trem2*$^{-/-}$ mice, the β-catenin deficit in osteoclast precursors reduces proliferation and prematurely accelerates osteoclast maturation. The increase in osteoclasts produces an osteopenic phenotype in the *Trem2*$^{-/-}$ mice, similar to NHD patients [108]. How are TREM2 and DAP12 activated by M-CSF signaling? A separate study showed M-CSF stimulation resulted in DAP12 phosphorylation by Src kinases activated by CSF-1R [110]. This mechanism suggests these receptor pairs are in close physical proximity; however, a direct interaction between TREM2 and CSF-1R has not been reported (Fig. 2C). Very recently, a study using mouse microglia confirmed a role for TREM2 in Wnt/β-catenin signaling in these cells. *Trem2*$^{-/-}$ microglia had suppressed β-catenin signaling and suffered G1/S cell cycle arrest [111], as predicted from the studies in osteoclast precursors. This results in fewer microglia and impaired microgliosis.

3. TREM2 Ligands.

TREM2 binds anionic bacterial ligands

Bacteria and poly-anionic molecules were the first potential ligands identified for TREM2 [112]. TREM2 interacted with Gram-positive and Gram-negative bacteria in direct binding and signaling studies. In another study, CHO cells transfected with a chimeric TREM2-DAP12 construct became competant to phagocytose bacteria [113]. Phagocytosis was dependent on Syk activation and the activity of the Rho GTPases Rac and Cdc42. Additional studies confirmed TREM2 can bind *E. coli*, but not Salmonella [66]. TREM2 also interacts with an unknown ligand in *C. jejuni*, a gram-negative bacteria which is a causative agent for food poisening [114].

The study by Daws *et al.* also found that anionic bacterial carbohydrates, particularly dextran sulfate, LPS, and LTA, but not chondroitin sulfate (CS), could block TREM2 binding to bacteria. Dextran sulfate could also activate TREM2 reporter cell lines similarly to *E. coli* [112]. Another study found that TREM2 can directly bind lipooligosaccharides (LOS) from *N. gonococcus.* Enzymatic removal of the acyl chains reduced binding, suggesting the lipidic acyl chains mediate binding to TREM2. SPR experiments were used to quantify the interaction ($K_d \approx$ 350 nM) [115].

TREM2 binds myeloid and non-myeloid mammalian cells

Because myeloid cells have TREM2-dependent phenotypes when cultured without other cell types, it was hypothesized they would express a TREM2 ligand. Indeed, TREM2 can bind primary macrophages [89] and DCs [91]. With DCs, stimulation with LPS, CpG DNA, or Zymosan did not alter staining levels. However, TREM2 staining of THP-1 monocytes was shown to be ablated when cells were pre-treated with PMA+ionomycin [26], the first time a cellular TREM2 ligand was shown to be regulated in viable cells. These findings suggest a ligand that interacts with TREM2 in *cis*, perhaps to provide tonic signals or to function as a co-receptor with TREM2 to recognize ligands in *trans* from extracellular stimuli. Importantly, the

AD-risk mutations R47H and R62H had decreased binding to this cell-surface ligand, while a T96K variant had enhanced binding. This last variant has unclear disease risk, but may be protective. If these mutations affect binding to a cis ligand required for signaling, it will be important to experimentally distinguish deficits in ligand binding from signaling.

Given the role of TREM2 in CNS homeostasis, several studies have also investigated the potential for a direct interaction between TREM2 on microglia and the other cells of the CNS, namely astrocytes and neurons. The first report of TREM2 ligands used Fc-TREM2 proteins to bind a variety of astrocyte lines [112]. Binding could be blocked by competition with LPS or LTA, showing a role for anionic recognition in the cell-surface TREM2 ligand. Other groups have also shown TREM2 binds primary cultured rat astrocytes [116], and astrocytes can activate TREM2 reporter cells [117]. In addition to astrocytes, cytochemistry and reporter cell activation demonstrated the presence of a TREM2 ligand on cultured neurons [37], and flow cytometry experiments confirmed Neuro2A cells express a TREM2-specific ligand, as other TREM family proteins (TREML2 and TREML4) had minimal binding [26].

In addition to binding viable neurons, Fc-TREM2 staining of Neuro2A and other cell lines increased when the cells were apoptotic [37] and TREM2 staining of neurons was increased following iscemic attack [39]. Apoptotic neurons [37] and thymocytes [30] have also been shown to stimulate TREM2 signaling, suggesting a common ligand on apoptotic cells. It is unclear whether this increased binding to apoptotic cells is from increased exposure of one ligand or nascent exposure of an additional ligand. Functionally, downregulating *Trem2* by shRNA in BV2 microglial cells reduced phagocytosis of apoptotic neurons, and transfecting CHO cells with TREM2 made the cells competant to phagocytose apoptotic cells [37]. Altogether, these studies have identified TREM2 interactions with mammalian cells that do and do not express TREM2.

TREM2 binds anionic ligands on mammalian cells

TREM2 has been shown to bind a number of anionic molecules from mammalian cells. Cannon *et al.* performed the first demonstration of TREM2 proteins binding to phospholipids.

Solid-state lipid ELISAs using a variety of plated phospholipids showed TREM2 binding was strongest with phosphatidylethanolamine (PE), phosphatidylserine (PS), and cardiolipin (CL), while phosphatidylcholine (PC) or sphingomyelin (SM) displayed greatly diminished binding [118]. Two other groups have obtained similar results showing strong binding to anionic lipids such as phosphatidic acid (PA) and PS using dot blots [119] or ELISA and liposome sedimentation [26]. Unlike assays with CD300 or [118, 120] or TIM [121, 122] family proteins, additon of calcium or magnesium did not enhance TREM2 binding, suggesting a different mode of recognition [26, 118]. The TREM2 crystal structure also showed that TREM2 does not contain structural features associated with selective phospholipid binding by other Ig domains [26].

Studies using TREM2 reporter cells also support the concept of phospholipids as TREM2 ligands. Plated sulfatide, PC, and SM all strongly stimulated mTREM2 [53] and similar results were obtained with hTREM2 [30]. However, the recognition profile is different than what has been observed in direct binding assays, where PC has minimal binding and anionic moieties have higher binding [26, 118, 119]. The R47H variant had minimal signaling to lipids other than PC and SM [30]. In a followup study with other TREM2 variants, R62H behaved similarly to R47H, while D87N and T96K increased signaling in response to PS and Sulfatide, but not PC [123]. These findings further support the hypothesis that TREM2 variants alter ligand binding and, hence, signaling.

While TREM2 certainly binds phospholipids in the context of solid-state ELISA and liposome assays, and phospholipids can stimulate signaling in reporter cells, they are unlikely to represent the complete TREM2 ligand. In one study, apoptotic Jurkat cells (which expose PS on the cell surface) did not bind Fc-TREM2 [119]. This suggests that phospholipids are not sufficient for TREM2-cell binding and may need co-presentation with other molecules. Second, while results in our lab showed TREM2 binding to phospholipids by ELISA and liposome sedimentation, the disease variants R47H, R62H, and T96K did not grossly alter phospholipid

binding [26]. Therefore, it will be important to understand how multiple interactions may influence TREM2 to recognize ligands and facilitate signaling.

In addition to phospholipids, nucleic acids released by damaged cells are a possible TREM2 ligand. TREM2 can IP nucleotides from the supernatant of ischemic brains and purified DNA activated TREM2 reporter cells [39]. Given the common anionic theme for TREM2 ligands, it would not be surprising that nucleotides released from damaged cells in the brain could stimulate TREM2.

Finally, by using enzymes that selectively cleave either heparan sulfates (HS) or CS, it was shown that TREM2 binds cell-surface proteoglycans and these are a major component of the cell-surface ligand [26]. Staining to THP-1 and Neuro2A cells was largely ablated by pre-treating the cells with heparan sulfatases, but not chondroitinase. This selectivity for HS over CS is consistent with the earlier studies showing heparin (but not CS) could block TREM2 binding to bacteria [112]. In addition, proteoglycan binding would explain why TREM2 can bind such a wide range of cells. The AD disease risk variants lose binding to these cells while the T96K variant gained binding, suggesting proteoglycans are an important TREM2 ligand. Future work will be needed to address whether HS is a tonic or activating ligand, whether it is required for presenting another ligand, or whether it is necessary to orient TREM2 to signal upon ligation of an activating ligand such as phospholipids.

TREM2 binds cellular mammalian proteins

Beyond the anionic biomolecules, TREM2 has been linked to other mammalian proteins. Pulldown experiments of surface-biotinylated neurons identified the cytosolic chaperone protein HSP60 [116]. ELISA assays demonstrated a direct interaction between these proteins with a low micromolar affinity. While it is counter-intuitive for an intracellular chaperone to mediate extracellular signals, there is a body of research characterizing the role of various heat-shock chaperones as alarmins for the innate immune system [124].

Additionally, as discussed above, the receptor Plexin-A1 interacts with TREM2 as part of a signaling complex. These proteins were co-immunoprecipitated and the interaction was ablated by deleting certain domains in Plexin-A1 [104]. In addition to Plexin-A1, TREML1s co-IPs with TREM2. The structural basis for these interactions are not known, and they may be indirect through association with signaling complexes [87].

TREM2 binds lipoproteins

In 2015, two groups independently identified a direct interaction between TREM2 and apolipoproteins, including ApoE. APOE and APOA were identified in protein bands precipitated from CSF by TREM2 [119] and interaction was verified by co-IP, ELISA, and dot blots [119, 125]. Both groups found that TREM2 binds all ApoE isoforms, lipidated and non-lipidated, and that the R47H variant reduced binding to ApoE. A separate study used a protein microarray to identify ligands for TREM2 from a library of extracellular and secreted proteins and investigated potential hits with bio-layer interferometry (BLI) [126]. TREM2 bound apolipoproteins, including APOA, APOB, APOE, CLU, and LDL. In contrast to the other reports, non-lipidated proteins had reduced binding as assessed by the response amplitude. The kinetics of these responses were not quantified, so it is unclear if the differences are reduced affinity or because the lower molecular weight non-lipidated proteins produce a smaller signal by BLI. The R47H, R62H, and D87N variants had reduced signal compared to WT. Functionally, ectopic expression of *TREM2* in 293T cells enabled phagocytosis of APOE and Aβ that was bound to APOE [126]. Finally, in a study with reporter cells, TREM2 signaled in response to LDL and HDL [123]. However, in contrast with the BLI data, the D87N had about three-fold increase in signaling.

The link between APOE and TREM2 connects these two key AD-risk proteins. The risk associated with *TREM2* variants is comparable with the *APOE4* allele. Other evidence suggested TREM2 and APOE could have overlapping areas of function. TREM2 has been linked to lipid metabolism: *Trem2* transgenic mice gain more weight on a high fat diet [127], and expression analysis connected *Trem2* to lipid metabolic pathways [29, 53]. Furthermore, APOE

interacts with Aβ, lipids, and heparan sulfates [128], and is important for microglial functions including phagocytosis, inflammation, and cell health [129, 130]. Lipoproteins are highly abundant in serum, and the presence and role of lipoproteins will need to be considered in cellular experiments with TREM2.

4. TREM2 function and model for ligand engagement.

To conclude, we summarize the reported TREM2 functions and try to arrange them through the context of various ligands. The reported ligands for TREM2 are broad and include ligands that could be thought to represent steady-state tonic stimuli or disease-specific stimuli. Therefore, the functions of TREM2 signaling could range from specific responses such as phagocytosis, cell activation, or collaboration with other signaling pathways to maintain cell survival and proliferation (Fig. 3). These possibilities are not mutually exclusive; on the contrary, it may be useful to conceptualize the different ligands as either tonic, homeostatic signals or damage-associated signals which produce different kinds or strengths of stimuli in order to accomplish the wide variety of functions reported for TREM2.

TREM2 functions from endogenous signals maintain myeloid cell homeostasis, regulate inflammation, and enable phagocytosis.

During development and homeostatic conditions, TREM2 is important for myeloid cell survival, proliferation, and maturation. TREM2 signals ensure myeloid cells remain ready and competent to respond to damage and disease.

1. **TREM2 responds to tonic stimuli as a receptor and/or co-receptor for myeloid survival and maturation**

This is an attractive, but still undefined mechanism where TREM2 signaling sustains myeloid cell survival and proliferation in order that the myeloid cells can respond to other stimuli in a condition-specific manner. One possible mechanism is a role for TREM2 in β-catenin activation

[111], which probably involves interactions with M-CSF signals [108]. Another possibility is TREM2 is not engaging an activating ligand, but is preferentially associating with DAP12 to localize it at the cell surface where it can be phosphorylated by Src or other kinases activated by CSF-1 or other survival pathways **(**Fig. 3A).

2. **TREM2 signals are important for myeloid cell maturation**

Studies using human monocytes from NHD patients with mutations in TREM2 observed decreased capacity to mature into osteoclasts and DCs [10, 80]. Similar to collaboration with M-CSF, TREM2 connects Plexin-A1 to DAP12 for osteoclastogenesis [104]. Therefore, TREM2 plays a role in the ability of myeloid cells to mature following stimulation by cytokines **(**Fig. 3B**).**

3. **TREM2 responds to tonic stimuli to regulate inflammation**

TREM2 and DAP12 reduce inflammatory TLR signals [89, 90] in cultured BMDMs. This role did not require stimulation with an exogenous ligand, suggesting it is mediated by a ligand on the BMDMs or perhaps from the culture media. This function likely also involves co-regulation of adaptor proteins that dampen TLR signaling (Fig. 3C).

Which ligands could be important for these functions? Many of these *in vitro* results did not require antibody stimulation of TREM2, suggesting a ligand present on the myeloid cells or readily available in culture. Phospholipids, proteoglycans, or lipoproteins make attractive candidates as these ligands would be ubiquitous. For example, APOE is highly abundant in serum and CSF, with concentrations in the µg/mL range [131]. However, because these ligands are so ubiquitous, understanding how signaling could be regulated is a challenge.

TREM2 functions during disease

In addition to its role as a tonic receptor, TREM2 recognizes a variety of ligands associated with damage, disease, and infection. These ligands may mimic tonic stimuli or instead may produce an activating signal above the tonic threshold.

1. **TREM2 responds to damage stimuli to drive survival and activation of myeloid cells.**

During disease, TREM2 responds to DAMPs such as ligands exposed on apoptotic membranes, myelin lipids, DNA exposed by necrotic cells, ligands presented by Aβ plaques, or perhaps lipoparticles enriched in apoptotic phospholipids. TREM2 stimulation by these ligands could be important for TREM2 function under the additional stress from damage. In this scenario, TREM2 signaling licenses the response to pathogens and other damage. This cellular activation program can take a number of forms, including sustaining cell survival, regulating cytokine production, and/or permitting phagocytosis by other receptor pathways. For example, TREM2 was required for full phagocytic capacity of antibody-Aβ complexes (which are recognized by FcR for phagocytosis), showing TREM2 enables the phagocytic functions of other receptors [132]. TREM2 inhibits inflammatory cytokine production in cultured microglia following exposure to apoptotic neurons [133], and *Trem2*-deficient and haploinsufficient microglia have impaired microgliosis and don't properly respond to plaques [30, 42, 45, 47, 134] (Fig. 3D).

2. TREM2 directly binds DAMPs/PAMPs for phagocytosis

While the primary role of TREM2 may not be phagocytosis, there have been reports of TREM2-mediated phagocytosis of a direct ligand, including phagocytosis of apoptotic neurons that express a TREM2 ligand [37, 116, 133], and bacteria [113] likely through recognition of anionic bacterial components [112]. These examples did not require TREM2 stimulation by antibodies or separate ligands. Instead, cross-linking by bacterial carbohydrates or apoptotic membrane-exposed ligands activate TREM2 signaling, resulting in microtubule mobilization and phagocytosis (Fig. 3E).

Phagocytosis is a good example for how different types of TREM2 signaling and ligands may induce different functions. Studies generally ascribe a pro-phagocytic role for TREM2. For example, some studies have shown ectopic expression of TREM2 is sufficient to promote phagocytosis in non-myeloid cells [25, 113]. However a most interesting study from Knapp and

colleagues demonstrated *Trem2* deficiency had opposite effects on phagocytosis by bone marrow and alveolar macrophages [135]. In the context of neurodegenerative disease, it has often been assumed that TREM2 has a major role in phagocytosis of debris. However, given that studies have observed increased [30], unchanged [136], and decreased [31] levels of Aβ plaque levels in *Trem2*-deficient mice, phagocytosis may not be the principal role of TREM2 in AD. Indeed, despite the defect in microgliosis and an apparent role for the plaques in stimulating TREM2 [45], *Trem2*-haploinsufficient mice did not have a phagocytic deficit. *Trem2* deficient microglia display impaired phagocytosis, but this may be an indirect result of even more severe deficits in microglia activation [42, 45]. Another study noted that phagocytosis of Aβ is increased in *Trem2*-transduced microglia isolated from 7-month-old, but not 18-month-old APPswe/PS1dE9 mice [137], suggesting that TREM2 itself is not sufficient for phagocytosis if other factors lost with age are not present.

The TREM2 crystal structure provides insights into ligand engagement

The human TREM2 Ig domain crystal structure provides some clues as to how TREM2 may interact with various ligands. TREM2 has a pronounced basic patch on its surface that is involved in the recognition of cell-surface proteoglycans and is most likely important in the recognition of additional anionic ligands [26]. The major AD-risk variants (R47H, R62H) are contained in this surface and additional mutations that increase the basic surface (T96K) increase binding to ligands while other R to D mutations in the basic surface decrease cellular binding. Therefore, this surface is involved in recognition of cell-surface proteoglycans. Furthermore, this surface is not observed on TREM1 or the other TREM family crystal structures. Also noteworthy is that circular dichroism spectroscopy studies revealed a subtle conformation change for the R47H variant, but not the R62H or T96K variant. The portion of the CD spectra altered is associated with tryptophan residues within Ig folds. Therefore, it is possible that the R47H variant specifically disrupts another part of the protein structure whereas

the other residues likely only impact the basic patch. There is also a hydrophobic surface on the protein that may be involved with recognizing lipidous ligands. In particular, cell-surface proteoglycans on myeloid cells may act in *cis* as a tonic ligand for TREM2 while simultaneously orienting or clustering the protein to receive activating signals from other ligands. These signals may be induced through interactions with other surfaces on TREM2 or may result by "hand-off" from GAGs to a higher-affinity ligand that recognizes the basic surface (Fig. 4). There are several precedents for receptor-GAG interactions mediating immune signaling, such as CD14-TLR4 [138], CXCL12 chemokine [139], and acetylcholine receptors [140]. To answer these questions, experiments must be performed with the different TREM2 ligands to dissect their effect on the different modules of TREM2 signaling and interplay with other pathways. Epitope-mapping experiments will be needed to confirm binding sites between TREM2 and ligands to understand overlap in TREM2 ligands and also to understand how different ligands interact with TREM2 to result in inhibitory or activating signals. Given that different TREM2 variants produce different results on protein structure and function [25, 26, 28], it will be also important to conduct studies using knock-in models of the mutant proteins. Finally, it is important to consider the role of sTREM2 in disease and to identify its signaling receptors.

Future perspectives: Outstanding questions regarding TREM2

1. Is there a role for TREM2 in regulating C1q and complement expression in microglia? TREM2 was reported to inhibit expression of C1q in alveolar macrophages [141] and C1q is expressed by microglia during development and improperly during AD to prune neuronal synapses [142].
2. Is surplus TREM2 signaling harmful? The T96K variant has been shown in two studies to have increased ligand binding or signaling [26, 123], but this variant has not been robustly linked to disease. If gain-of-function TREM2 variants are indeed disease-risk, it would mean therapies that stimulate TREM2 must be carefully assessed.

3. When is TREM2 function most critical during disease and when could TREM2 agonists or antagonists have the most benefit? TREM2 deficiency is reported to have opposing effects on Aβ levels and disease pathology during early and late disease [43].
4. What is the role of sTREM2 in AD, and can it be exploited therapeutically? A decoy function would make stimulation of transmembrane TREM2 more difficult. However, if sTREM2 has a beneficial function as a signaling molecule, recombinant sTREM2 could be considered as a therapeutic.
5. How do culturing conditions influence the interpretation of cellular assays? TREM2 is likely to be highly influenced by cell density, health of neighboring cells, and perhaps most importantly, the concentration and activity of lipoparticles.

Acknowledgements

This work was supported in part by funding from NIH R01-HL119813 (T.J.B), Knight Alzheimer's Disease Research Center pilot grant P50-AG005681-30.1 (T.J.B.), Alzheimer's Association Research Grant AARG-16-441560 (T.J.B.), NIH T32-GM007067 (D.L.K.), and American Heart Association Predoctoral Fellowships 15PRE22110004 and 17PRE32780001 (D.L.K.).

Keywords:

Alzheimer's disease

Inflammation

Immune Signaling

Neurodegeneration

Microglia

Abbreviations used:

Aβ, amyloid beta; AD, Alzheimer's disease; Akt, Protein kinase B; ALS, amyotrophic lateral sclerosis; APOE, Apolipoprotein E; BLI, BioLayer Interferometry; BMDM, Bone marrow-derived macrophage; CL, cardiolipin; COPD, chronic obstructive pulmonary disease; CS, Chondroitin sulfate; CSF-1R, Colony stimulating factor 1 receptor; DAG, diacylglycerol; DAP12, DNAX-activation protein 12; DC, Dendritic cell; ELISA, Enzyme-linked immunosorbent assay; ERK, extracellular singal-related kinase; FRET, Förster resonance energy transfer; GM-CSF, Granulocyte macrophage colony-stimulating factor; Grb2, Growth factor receptor-bound protein 2; GSK3-β, Glycogen synthase kinase 3; HDL, high-density lipoprotein; HS, Heparan sulfate; IBD, inflammatory bowel disorder; Ig, immunoglobulin; IL-4, interleukin 4; IP, immunoprecipitate; ITAM, Immuno-Tyrosine Activation Motif; ITIM, Immuno-Tyrosine Inhibitor Motif; LAB, Linker for the activation of B cells; LAT, Linker for the activation of T cells; LDL, low-density lipoprotein; LMIR5, Leukocyte mono-immunoglobulin (Ig)–like receptor-5 (Also CD300b); LOAD, late-onset Alzheimer's disease; LOS, Lipooligosaccharides; LPS, Lipopolysaccharide; LTA, Lipoteichoic acid; M-CSF, macrophage colony-stimulating factor; MAPK, Mitogen-activated protein kinase MS, multiple sclerosis; NF-kB, Nuclear factor kappa B; NHD, Nasu-Hakola Disease; Nrp1, Neuropilin-1; PA, phosphatidic acid; PC, phosphatidylcholine; PE, phosphatidylethanolamine; PI3K, phosphoinositide 3-kinase; PIP3, phosphatidylinositol-3,4,5-trisphosphate; PLCγ1, phospholipase C γ; PMA, phorbol 12-myristate 13-acetate; PS, phosphatidylserine; RANKL, Receptor activator of nuclear factor kappa-B ligand; ROS, reactive oxygen species; Sema3A, Semaphorin-3A; Sema6D, Semaphorin-6D; SHIP-1, phosphatidylinositol phosphatase; SHP-1, Protein tyrosine phosphatase; SM, sphingomyelin; SOS, son of sevenless, SPR, surface plasmon resonance; sTREM2, soluble TREM2; TIM, T cell Ig mucin; TLR, Toll-like receptor; TREM2, Triggering receptor expressed on myeloid cells-2; TREML, Triggering receptor expressed on myeloid cells like.

Table 1 – Summary of TREM2 links to human disease and animal models of disease

Disease	Observation or model	Phenotype	Possible role of TREM2	Reference:
Neurodegenerative disease				
Nasu-Hakola Disease	NHD patient	TREM2 mutations co-segregate with NHD	TREM2 mutations cause NHD	[7]
	Osteoclast maturation from PBMCs	Monocytes from NHD TREM2 carriers have impaired osteoclast differentiation.	TREM2 involved in myeloid maturation	[10, 80]
	Osteopenic mice	Reduced proliferation of osteoclast precursors, accelerated osteoclast maturation and apoptosis.	Myeloid proliferation and survival	[108]
Alzheimer's disease Genetic links	Sequencing & GWAS studies	First two studies to identify a link between TREM2 variants and AD	R47H is a risk variant. Others possible.	[4, 5]
		TREM2 R47H correlated with CSF tau and p-tau	R47H is an AD risk variant	[18]
		R47H did not fully explain TREM2 disease risk	R62H is an AD risk variant	[3]
Alzheimer's disease Aβ Models	APPPS1 mice	Decreased number and size of plaque-associated microglia in *Trem2* heterozygotes. No change in total Aβ.	Microgliosis	[47]
	5XFAD mice	*Trem2*$^{-/-}$ mice have Increased Aβ and impaired microglial response at 8mo. Decreased microglial survival.	Microglia survival, microgliosis. Protective in Aβ	[30]
	5XFAD, APPPS1 mice	5XFAD *Trem2*$^{-/-}$ mice have fewer microglia (8mo) and less plaque clustering (4,8mo), producing diffuse plaque morphology and increased neuronal pathology. No change in total Aβ.	Microgliosis, microglial proliferaction. Protective in Aβ	[42]
	APPPS1 mice	*Trem2*$^{-/-}$ mice have reduced Aβ plaque burden at 4mo. Decreased plaque clustering of Iba1+ cells.	Plaque response. Possible role in proliferation, survival, and/or trafficking Detrimental in Aβ	[31]
	5XFAD, CRND8, PS/APP Human R47H carrier samples	TREM2 is required for microglial barrier function around Aβ plaques. Human R47H carriers mirror *Trem2* haploinsufficient mice.	Microgliosis and protective plaque response	[45]
	APPPS1 mice	TREM2 increases amyloid burden early, but reduces Aβ burden late in disease.	Microglial/myeloid proliferation, inflammation, and plaque response	[43]
	APPswe/PS1dE9 mice	*In vivo* overexpression reduced plaque load and inflammation.	Anti-inflammatory, Phagocytosis of Aβ	[32]

	APPswe/PS1dE9 mice	Overexpressing *Trem2* in old mice (18mo) had no effect on AD pathology.	Age-restricted protective role	[137]
Alzheimer's disease	P301S mice	*Trem2* overexpression ameliorated tau pathology.	Protective, anti-inflammatory	[50]
Tau models	P301S mice	Lentiviral knockdown increased tau pathology.	Protective, anti-inflammatory	[51]
Multiple Sclerosis	Cuprizone	TREM2 sustains microglia during aging and cuprizone challenge. Reduces myelin debris.	Microglial survival and proliferation during aging myelin response	[53]
	Cuprizone	*Trem2*$^{-/-}$ mice have increased myelin debris, decreased microglial proliferation and activation.	Microgliosis and proliferation	[52]
	EAE	Antibody blockade of TREM2 signaling exacerbates symptoms.	Beneficial in MS	[117]
	EAE	EAE symptoms were reduced by *Trem2*-transduced macrophages.	Anti-inflammatory, protective	[143]
Prion Pathogenesis	Prion infection	No effect on prion pathogenesis, but reduced microglial activation.	Microgliosis and proliferation	[54]
Cardiovascular disease				
Stroke	Experimental Ischemia	*Trem2*$^{-/-}$ mice had increased infarction, decreased microglia activation, and fewer phagocytic microglia.	Microgliosis and phagocytosis Protective following stoke	[39]
	Experimental Ischemia	*Trem2*$^{-/-}$ mice have fewer microglia at glial scars and decreased microglial activation. No change in scar size.	Microgliosis	[55]
Chronic pulmonary disease				
Viral-induced COPD	SeV-induced chronic airway disease	*Trem2*$^{-/-}$ mice have reduced macrophage expansion which reduced chronic disease. IL-13 stimulation produces sTREM2 which prevents macrophage apoptosis.	Survival and proliferation. sTREM2 prevents macrophage apoptosis, allowing conversion to alternatively activated macrophages, which promote airway disease	[62]
Wound Healing				
Colon injury	Chemical colon injury	*Trem2*$^{-/-}$ mice had reduced inflammation and wound damage.	Inflammatory, bacterial killing.	[64]
	Biopsy injury	TREM2 required for wound healing and promotes M2 phenotype	Promote anti-inflammatory M2 phenotype	[63]
Infection				
Animal infection	*E. coli* endotoximia.	TREM2 was protective in sepsis infection.	Phagocytic, anti-inflammatory	[144]
	LPS and *E. coli* endotoximia.	Trem2$^{-/-}$ mice had increased early inflammation and faster resolution.	Phagocytic. Anti-inflammatory.	[145]

	P. aeruginosa	TREM2 activated PI3K/Akt pathway to control inflammation.	Anti-inflammatory	[146]
	S. pneumoniae	TREM2 decreased C1q expression in alveolar macrophages and TREM2 was detrimental to survival in intranasal challenge.	Anti-phagocytotic, pro-inflammatory in AMs. Opposite results in BMDMs	[141]
In vitro cellular infection	*P. aeruginosa*	TREM2 increased ROS production through Akt/PI3K pathway. No change in phagocytosis.	Bacterial killing	[67]
	S. Typhimurium	TREM2/DAP12 required for ROS response following Salmonella infection.	Bacterial killing	[66]
	B. abortus	TREM2 inhibited NO production and increased bacterial load.	Promotes bacterial growth	[68]

Table 2. Reported TREM2 ligands

Ligand	Techniques	Variants	Ref
Bacteria/bacterial components			
Whole Bacteria	CS, P, FC, RC, CB, E		[66, 112, 113]
C. jejuni lysate	E, RC		[114]
N. gonococcus lipooligosaccharides	E, SPR, RC		[115]
Anionic Bacterial Carbohydrates	CB		[112]
Cholora toxin B	E, RC		[147]
Mammalian Cells			
THP-1 monocytes	FC		[26]
BMDMs	FC		[89]
BMDCs	FC		[91]
Astrocytes	RC, CS		[112, 116, 117]
Neuronal Cells	CS, RC, FC		[26, 37, 39, 116]
Apoptotic cells	FC, RC, P		[30, 37]
Anionic molecules			
Phospholipids & Sulfolipids	E, DB, RC, LB	R47H, R62H ↓ D87N, T96K ↑	[26, 30, 53, 118, 119, 123, 148]
DNA	IP, RC		[39]
Sulfated proteoglycans	FC		[26]
Mammalian proteins			
HSP60	E, CS.		[116]
Plexin-A1	FRET, IP		[104]
TREML1 (short transcript)	IP		[87]
Apolipoproteins (A,B,E,J)	DB, P, IP, E, BLI, PM	R47H ↓[119, 125] R47H, R62H, D87N↓[126]	[119, 125, 126]
Lipoparticles	BLI, RC, PM	R47H, R62H ↓ D87N↑↓, T96K ↑	[123, 126]
Negative results			
Certain Mammalian Cells	CS		[112]
Apoptotic Jurkat cells	FC		[119]

Key: E = ELISA, RC = reporter cell, FC = flow cytometry P = phagocytosis/cellular uptake, IP = Co-immunoprecipitation, CB = 5 competitive binding, CS = cell staining, LB = liposome binding, BLI = biolayer interferometry, PM = protein microarray, SPR = 6 surface plasmon resonance.

Figure Legends

Figure 1. TREM2 signaling mechanisms.

A) Canonical TREM2 signaling occurs following cross-linking of TREM2. Src phosphorylates the DAP12 ITAM. This recruits and activates Syk. Syk activity leads the phosphorylation and activation of downstream effectors including PI3K, PLCγ, LAB or LAT, Cbl, Grb2, and Vav. DAP10 also recruits PI3K. The end result of these pathways is Akt activation, calcium flux, ERK/MAPK activity, and actin mobilization. **B)** TREM2 signaling is inhibited through multiple mechanisms. TREML1 associates with TREM2 signaling complexes and recruits SHP-1 through its ITIM. The scaffolding protein LAB recruits the E3 ubiquitin ligase Cbl, which downregulates Src and Syk. Incomplete DAP12 phosphorylation results in a "hidden ITIM" which can recruit SHIP-1. **C)** The most prevalent model for multifaceted TREM2 signaling is activating vs tonic receptor engagement by multivalent, high-affinity ligands vs low affinity, monovalent ligands. D) Soluble TREM2 is produced by proteolytic cleavage and may have signaling functions separate from transmembrane TREM2.

Figure 2. Role for TREM2 in regulating other signal pathways.

A) TREM2 inhibits TLR responses through the recruitment of DOK3 to the DAP12 ITAM at the plasma membrane and potentially by sequestering signaling intermediates such as ERK or creating a less activating environment with scaffolding proteins such as LAB. (Structures PDBs: TREM2 5ELI [26] and 3FXI [149] - signaling complex of TLR4 (dark and light red), MD2 (cyans) complexed with LPS). **B)** TREM2 is required for the Plexin-A1 response to Sema6D. Two molecules of Plexin-A1 dimerize upon binding to a dimer of Sema6D. The Ig-like domains of Plexin-A1 colored in magenta were required for the interaction with TREM2. Structure PDBs: TREM2 5ELI, Plexin-A4 dimer 5L5K [150] - (Blue and cyan with magenta highlights) superimposed on Sema6D (greens, 3OKY, [151]). **C)** TREM2 signaling is required for β-catenin

activation during M-CSF/CSF-1R signaling. (Structure PDB:4WRM [152] - CSF-1R orange and M-CSF cyan with signaling dimer shown in lighter shading).

Figure 3. Possible roles for TREM2 resulting from different ligands.

A-C) During normal conditions, TREM2 signaling from endogenous ligands permits a number of functions. **A)** TREM2 is a co-receptor or co-stimulatory molecule for signaling pathways involved in myeloid maturation, proliferation, and survival. **B)** TREM2 signals (perhaps independently of co-receptors) are important for maturation. **C)** TREM2 regulates inflammatory responses by influencing TLR and other activating networks to maintain homeostasis. D-E) TREM2 recognizes additional ligands associated with disease. **D)** These signals may increase activation and survival so that myeloid cells can respond in a context-dependent manner. **E)** TREM2 can induce phagocytosis of certain ligands, such as bacteria.

Figure 4. Model for TREM2 signal by WT and variant proteins.

A) TREM2 has a pronounced basic patch, and the disease variants R47 and R62 are part of this surface. TREM2 also has separate surfaces that are potentially involved in ligand binding, such as a hydrophobic surface above the basic patch. Note that residues involved in recognition and binding of specific phospholipids in other Ig domain proteins are not present in TREM2. **B)** Role of GAGs in TREM2 signaling. Heparan sulfate proteoglycans interact with TREM2, likely in cis on TREM2-expressing cells. These may function to orient and cluster TREM2 to receive activating signals such as phospholipids or APOE. **C)** The R47H and R62H variant have reduced binding to cell-surface proteoglycans and have reduced signaling to phospholipids and lipoparticles. The decreased affinity for GAG may impair the ability of these variants to recognize and/or signal in response to these ligands.

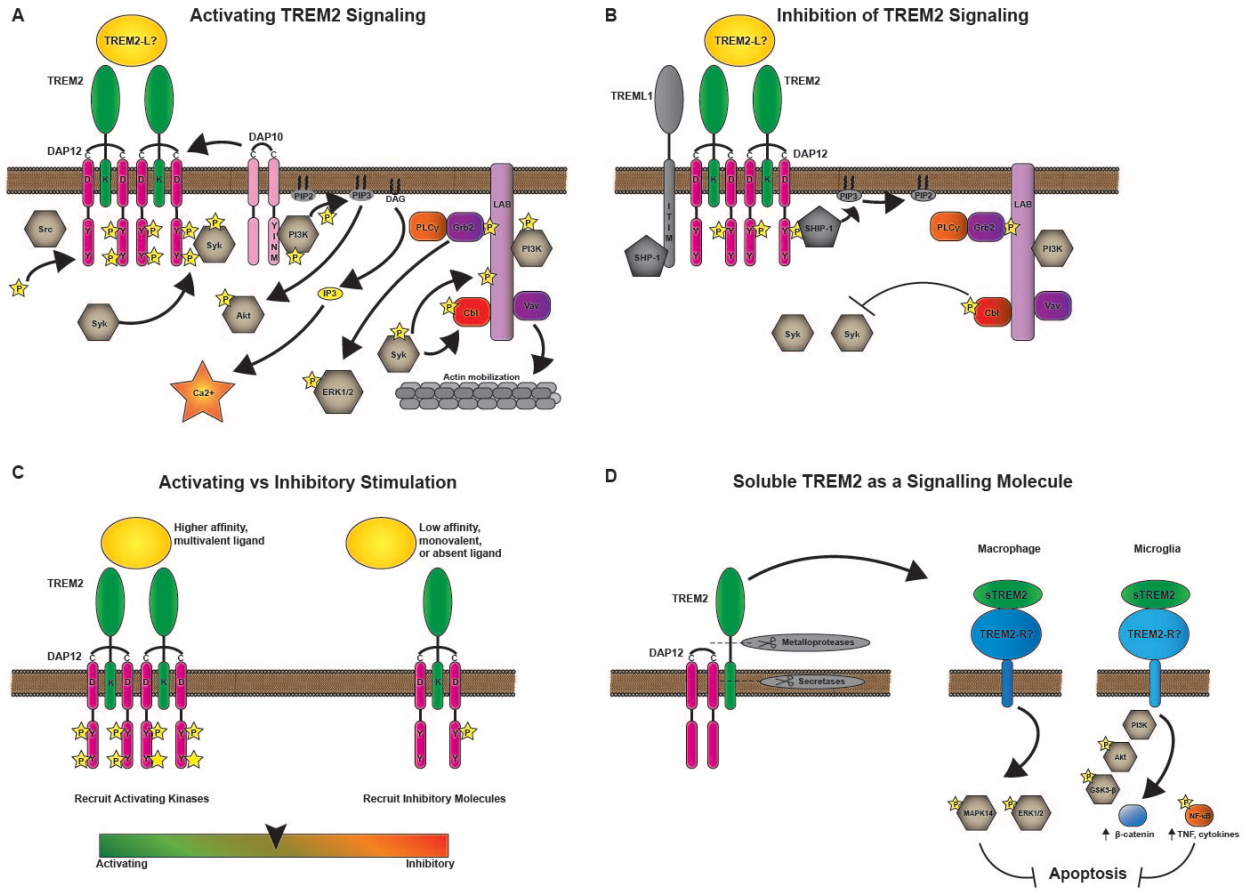

Figure 1. Kober and Brett

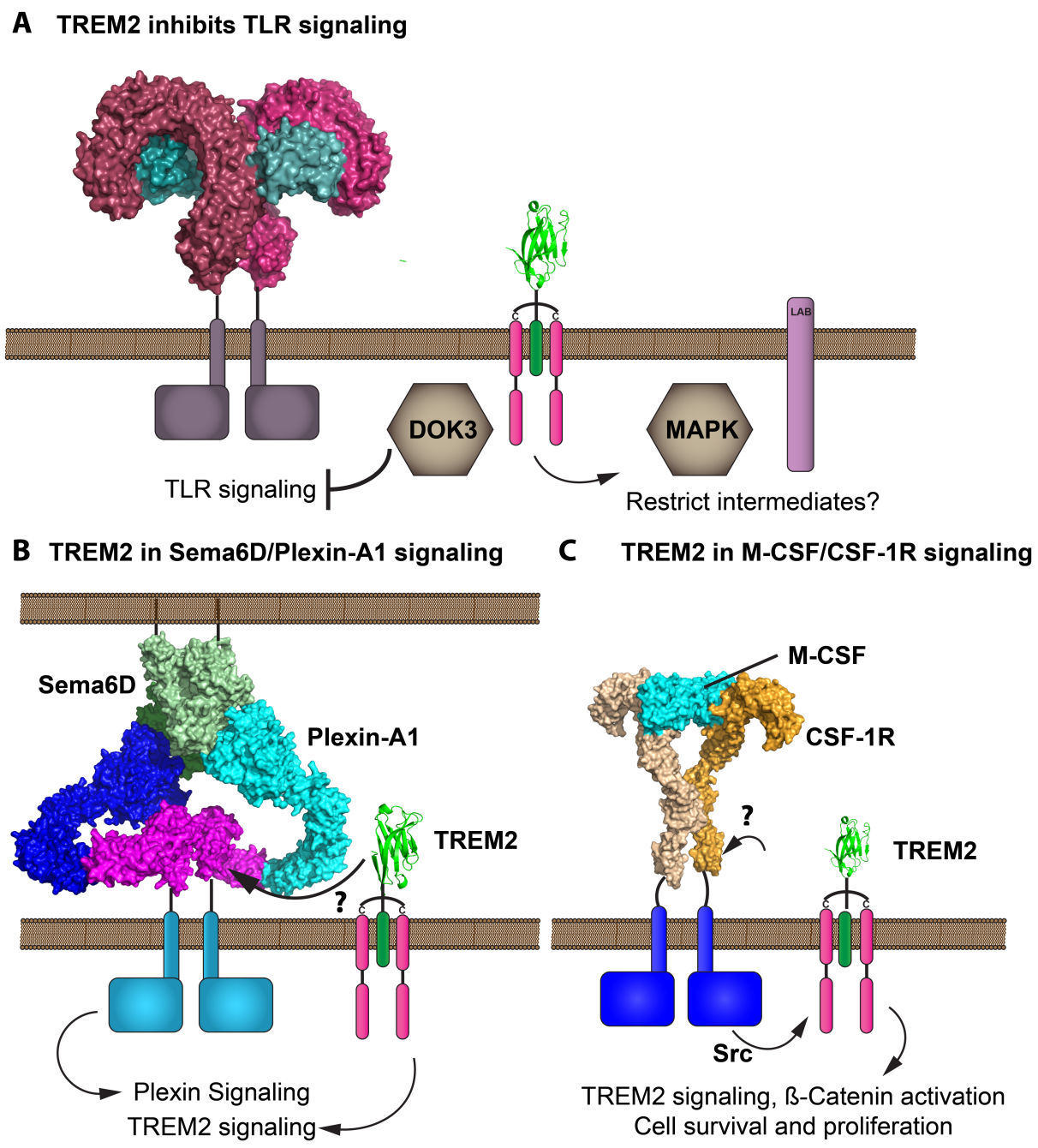

Figure 2 Kober and Brett

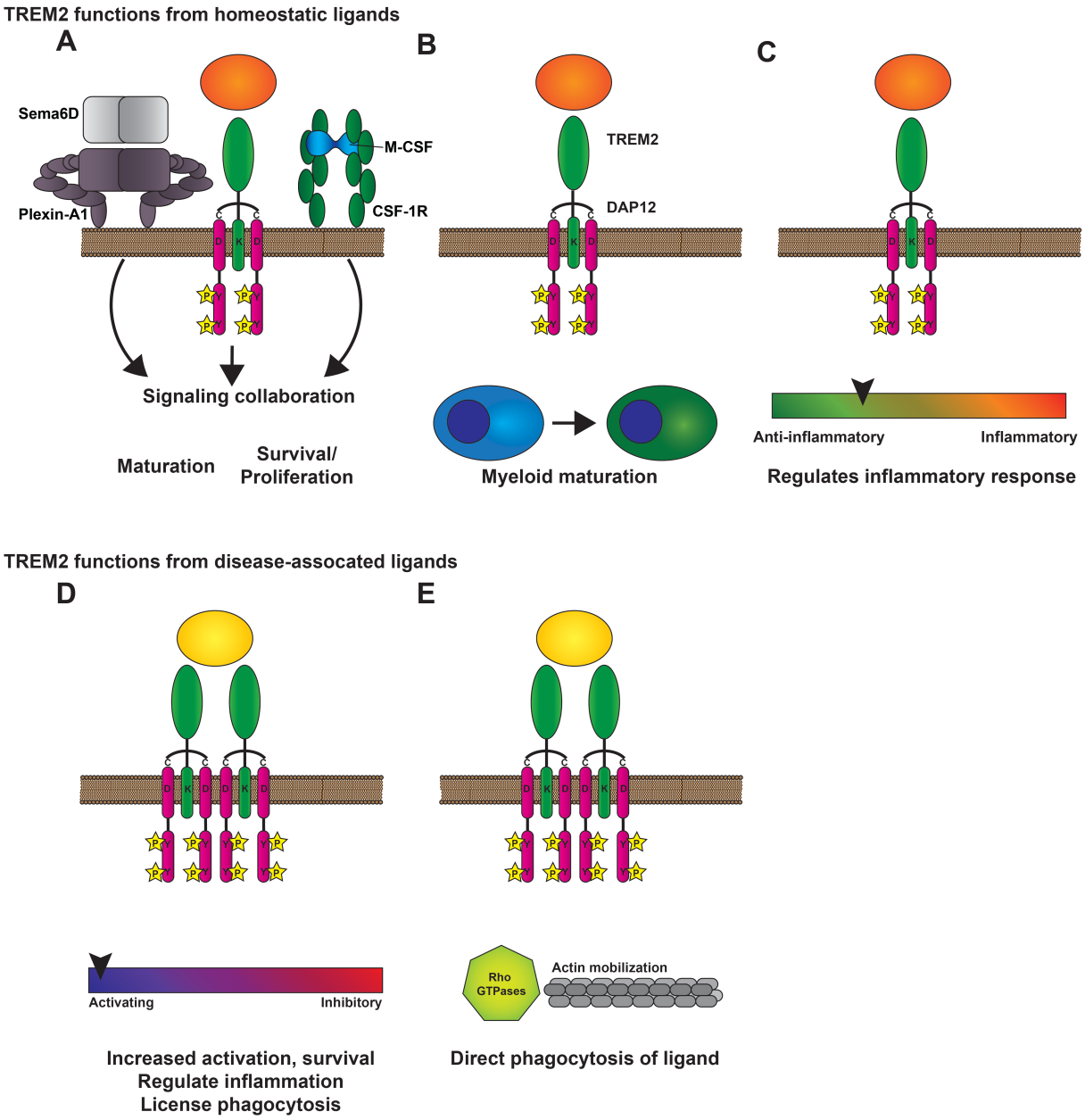

Figure 3 Kober and Brett

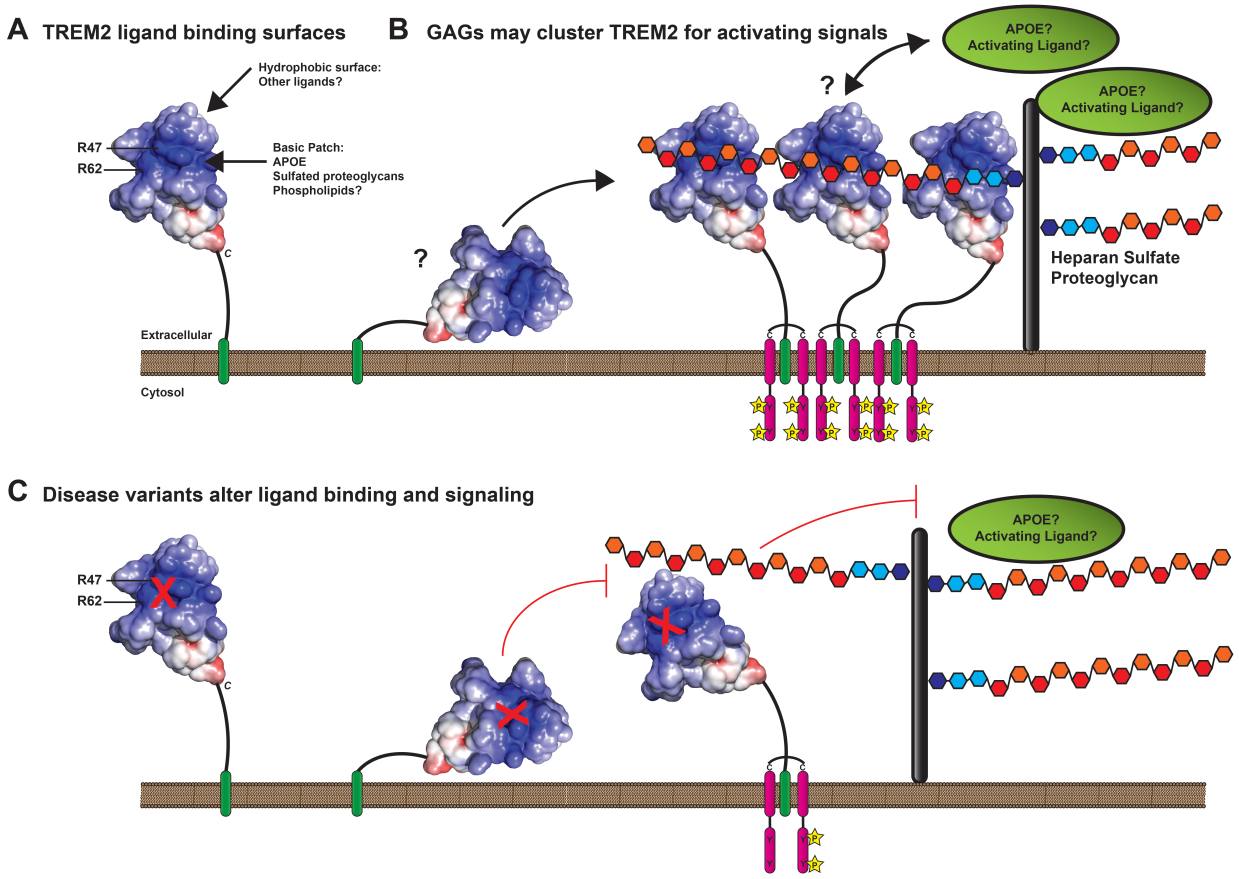

1

2 **Figure 4 Kober and Brett**

References:

[1] Colonna M, Wang Y. TREM2 variants: new keys to decipher Alzheimer disease pathogenesis, Nat Rev Neurosci. 17 (2016) 201-207.
[2] Wunderlich P, Glebov K, Kemmerling N, Tien NT, Neumann H, Walter J. Sequential proteolytic processing of the triggering receptor expressed on myeloid cells-2 (TREM2) protein by ectodomain shedding and gamma-secretase-dependent intramembranous cleavage, J Biol Chem. 288 (2013) 33027-33036.
[3] Jin SC, Benitez BA, Karch CM, Cooper B, Skorupa T, Carrell D, et al. Coding variants in TREM2 increase risk for Alzheimer's disease, Hum Mol Genet. 23 (2014) 5838-5846.
[4] Guerreiro R, Wojtas A, Bras J, Carrasquillo M, Rogaeva E, Majounie E, et al. TREM2 variants in Alzheimer's disease, N Engl J Med. 368 (2013) 117-127.
[5] Jonsson T, Stefansson H, Steinberg S, Jonsdottir I, Jonsson PV, Snaedal J, et al. Variant of TREM2 associated with the risk of Alzheimer's disease, N Engl J Med. 368 (2013) 107-116.
[6] Paloneva Bm J, Autti T, Raininko R, Partanen J, Salonen O, Puranen M, et al. CNS manifestations of Nasu-Hakola disease: A frontal dementia with bone cysts, Neurology. 56 2001) 1552-1558.
[7] Paloneva J, Manninen T, Christman G, Hovanes K, Mandelin J, Adolfsson R, et al. Mutations in two genes encoding different subunits of a receptor signaling complex result in an identical disease phenotype, Am J Hum Genet. 71 (2002) 656-662.
[8] Klunemann HH, Ridha BH, Magy L, Wherrett JR, Hemelsoet DM, Keen RW, et al. The genetic causes of basal ganglia calcification, dementia, and bone cysts: DAP12 and TREM2, Neurology. 64 (2005) 1502-1507.
[9] Chouery E, Delague V, Bergougnoux A, Koussa S, Serre JL, Megarbane A. Mutations in TREM2 lead to pure early-onset dementia without bone cysts, Human mutation. 29 (2008) E194-204.
[10] Paloneva J, Mandelin J, Kiialainen A, Bohling T, Prudlo J, Hakola P, et al. DAP12/TREM2 deficiency results in impaired osteoclast differentiation and osteoporotic features, J Exp Med. 198 (2003) 669-675.
[11] Soragna D, Papi L, Ratti MT, Sestini R, Tupler R, Montalbetti L. An Italian family affected by Nasu-Hakola disease with a novel genetic mutation in the TREM2 gene, J Neurol Neurosurg Psychiatry. 74 (2003) 825-826.
[12] Giraldo M, Lopera F, Siniard AL, Corneveaux JJ, Schrauwen I, Carvajal J, et al. Variants in triggering receptor expressed on myeloid cells 2 are associated with both behavioral variant frontotemporal lobar degeneration and Alzheimer's disease, Neurobiol Aging. 34 (2013) 2077 e2011-2078.
[13] Guerreiro R, Bilgic B, Guven G, Bras J, Rohrer J, Lohmann E, et al. Novel compound heterozygous mutation in TREM2 found in a Turkish frontotemporal dementia-like family, Neurobiol Aging. 34 (2013) 2890 e2891-2895.
[14] Guerreiro RJ, Lohmann E, Bras JM, Gibbs JR, Rohrer JD, Gurunlian N, et al. Using exome sequencing to reveal mutations in TREM2 presenting as a frontotemporal dementia-like syndrome without bone involvement, JAMA Neurol. 70 (2013) 78-84.

[15] Le Ber I, De Septenville A, Guerreiro R, Bras J, Camuzat A, Caroppo P, et al. Homozygous TREM2 mutation in a family with atypical frontotemporal dementia, Neurobiol Aging. 35 (2014) 2419 e2423-2415.
[16] Lill CM, Rengmark A, Pihlstrom L, Fogh I, Shatunov A, Sleiman PM, et al. The role of TREM2 R47H as a risk factor for Alzheimer's disease, frontotemporal lobar degeneration, amyotrophic lateral sclerosis, and Parkinson's disease, Alzheimer's & dementia : the journal of the Alzheimer's Association. 11 (2015) 1407-1416.
[17] Jin SC, Carrasquillo MM, Benitez BA, Skorupa T, Carrell D, Patel D, et al. TREM2 is associated with increased risk for Alzheimer's disease in African Americans, Mol Neurodegener. 10 (2015) 19.
[18] Cruchaga C, Kauwe JSK, Harari O, Jin SC, Cai Y, Karch CM, et al. GWAS of cerebrospinal fluid tau levels identifies risk variants for Alzheimer's disease, Neuron. 78 (2013) 256-268.
[19] Golde TE, Streit WJ, Chakrabarty P. Alzheimer's disease risk alleles in TREM2 illuminate innate immunity in Alzheimer's disease, Alzheimers Res Ther. 5 (2013) 24.
[20] Rayaprolu S, Mullen B, Baker M, Lynch T, Finger E, Seeley WW, et al. TREM2 in neurodegeneration: evidence for association of the p.R47H variant with frontotemporal dementia and Parkinson's disease, Mol Neurodegener. 8 (2013) 19.
[21] Liu G, Liu Y, Jiang Q, Jiang Y, Feng R, Zhang L, et al. Convergent Genetic and Expression Datasets Highlight TREM2 in Parkinson's Disease Susceptibility, Mol Neurobiol. 53 (2016) 4931-4938.
[22] Cady J, Koval ED, Benitez BA, Zaidman C, Jockel-Balsarotti J, Allred P, et al. TREM2 Variant p.R47H as a Risk Factor for Sporadic Amyotrophic Lateral Sclerosis, JAMA neurology. 71 (2014) 449-453.
[23] Borroni B, Ferrari F, Galimberti D, Nacmias B, Barone C, Bagnoli S, et al. Heterozygous TREM2 mutations in frontotemporal dementia, Neurobiol Aging. 35 (2014) 934 e937-910.
[24] Cuyvers E, Bettens K, Philtjens S, Van Langenhove T, Gijselinck I, van der Zee J, et al. Investigating the role of rare heterozygous TREM2 variants in Alzheimer's disease and frontotemporal dementia, Neurobiol Aging. 35 (2014) 726 e711-729.
[25] Kleinberger G, Yamanishi Y, Suarez-Calvet M, Czirr E, Lohmann E, Cuyvers E, et al. TREM2 mutations implicated in neurodegeneration impair cell surface transport and phagocytosis, Sci Transl Med. 6 (2014) 243ra286.
[26] Kober DL, Alexander-Brett JM, Karch CM, Cruchaga C, Colonna M, Holtzman MJ, et al. Neurodegenerative disease mutations in TREM2 reveal a functional surface and distinct loss-of-function mechanisms, Elife. 5 (2016) e20391.
[27] Park JS, Ji IJ, Kim DH, An HJ, Yoon SY. The Alzheimer's Disease-Associated R47H Variant of TREM2 Has an Altered Glycosylation Pattern and Protein Stability, Front Neurosci. 10 (2016) 618.
[28] Park JS, Ji IJ, An HJ, Kang MJ, Kang SW, Kim DH, et al. Disease-Associated Mutations of TREM2 Alter the Processing of N-Linked Oligosaccharides in the Golgi Apparatus, Traffic. 16 (2015) 510-518.
[29] Piccio L, Deming Y, Del-Aguila JL, Ghezzi L, Holtzman DM, Fagan AM, et al. Cerebrospinal fluid soluble TREM2 is higher in Alzheimer disease and associated with mutation status, Acta Neuropathol. 131 (2016) 925-933.

[30] Wang Y, Cella M, Mallinson K, Ulrich JD, Young KL, Robinette ML, et al. TREM2 lipid sensing sustains the microglial response in an Alzheimer's disease model, Cell. 160 (2015) 1061-1071.
[31] Jay TR, Miller CM, Cheng PJ, Graham LC, Bemiller S, Broihier ML, et al. TREM2 deficiency eliminates TREM2+ inflammatory macrophages and ameliorates pathology in Alzheimer's disease mouse models, J Exp Med. 212 (2015) 287-295.
[32] Jiang T, Tan L, Zhu XC, Zhang QQ, Cao L, Tan MS, et al. Upregulation of TREM2 ameliorates neuropathology and rescues spatial cognitive impairment in a transgenic mouse model of Alzheimer's disease, Neuropsychopharmacology. 39 (2014) 2949-2962.
[33] Jiang T, Yu JT, Zhu XC, Tan MS, Gu LZ, Zhang YD, et al. Triggering receptor expressed on myeloid cells 2 knockdown exacerbates aging-related neuroinflammation and cognitive deficiency in senescence-accelerated mouse prone 8 mice, Neurobiol Aging. 35 (2014) 1243-1251.
[34] Forabosco P, Ramasamy A, Trabzuni D, Walker R, Smith C, Bras J, et al. Insights into TREM2 biology by network analysis of human brain gene expression data, Neurobiol Aging. 34 (2013) 2699-2714.
[35] Zhang B, Gaiteri C, Bodea LG, Wang Z, McElwee J, Podtelezhnikov AA, et al. Integrated systems approach identifies genetic nodes and networks in late-onset Alzheimer's disease, Cell. 153 (2013) 707-720.
[36] Sessa G, Podini P, Mariani M, Meroni A, Spreafico R, Sinigaglia F, et al. Distribution and signaling of TREM2/DAP12, the receptor system mutated in human polycystic lipomembraneous osteodysplasia with sclerosing leukoencephalopathy dementia, Eur J Neurosci. 20 (2004) 2617-2628.
[37] Hsieh CL, Koike M, Spusta SC, Niemi EC, Yenari M, Nakamura MC, et al. A role for TREM2 ligands in the phagocytosis of apoptotic neuronal cells by microglia, J Neurochem. 109 (2009) 1144-1156.
[38] Stefano L, Racchetti G, Bianco F, Passini N, Gupta RS, Panina Bordignon P, et al. The surface-exposed chaperone, Hsp60, is an agonist of the microglial TREM2 receptor, Journal of neurochemistry. 110 (2009) 284-294.
[39] Kawabori M, Kacimi R, Kauppinen T, Calosing C, Kim JY, Hsieh CL, et al. Triggering receptor expressed on myeloid cells 2 (TREM2) deficiency attenuates phagocytic activities of microglia and exacerbates ischemic damage in experimental stroke, J Neurosci. 35 (2015) 3384-3396.
[40] Hickman SE, Kingery ND, Ohsumi TK, Borowsky ML, Wang LC, Means TK, et al. The microglial sensome revealed by direct RNA sequencing, Nature neuroscience. 16 (2013) 1896-1905.
[41] Butovsky O, Jedrychowski MP, Moore CS, Cialic R, Lanser AJ, Gabriely G, et al. Identification of a unique TGF-beta-dependent molecular and functional signature in microglia, Nature neuroscience. 17 (2014) 131-143.
[42] Wang Y, Ulland TK, Ulrich JD, Song W, Tzaferis JA, Hole JT, et al. TREM2-mediated early microglial response limits diffusion and toxicity of amyloid plaques, J Exp Med. 213 (2016) 667-675.
[43] Jay TR, Hirsch AM, Broihier ML, Miller CM, Neilson LE, Ransohoff RM, et al. Disease progression-dependent effects of TREM2 deficiency in a mouse model of Alzheimer's disease, The Journal of Neuroscience. (2016).

[44] Frank S, Burbach GJ, Bonin M, Walter M, Streit W, Bechmann I, et al. TREM2 is upregulated in amyloid plaque-associated microglia in aged APP23 transgenic mice, Glia. 56 (2008) 1438-

[45] Yuan P, Condello C, Keene CD, Wang Y, Bird TD, Paul SM, et al. TREM2 Haplodeficiency in Mice and Humans Impairs the Microglia Barrier Function Leading to Decreased Amyloid Compaction and Severe Axonal Dystrophy, Neuron. 90 (2016) 724-739.
[46] Musiek ES, Holtzman DM. Three dimensions of the amyloid hypothesis: time, space and 'wingmen', Nature neuroscience. 18 (2015) 800-806.
[47] Ulrich JD, Finn MB, Wang Y, Shen A, Mahan TE, Jiang H, et al. Altered microglial repsonse to AB plaques in APPPS1-21 mice heterozygous for TREM2, Molecular Neurodegeneration. 9

[48] Suarez-Calvet M, Araque Caballero MA, Kleinberger G, Bateman RJ, Fagan AM, Morris JC, et al. Early changes in CSF sTREM2 in dominantly inherited Alzheimer's disease occur after amyloid deposition and neuronal injury, Sci Transl Med. 8 (2016) 369ra178.
[49] Pimplikar SW. Neuroinflammation in Alzheimer's disease: from pathogenesis to a therapeutic target, J Clin Immunol. 34 Suppl 1 (2014) S64-69.
[50] Jiang T, Zhang YD, Chen Q, Gao Q, Zhu XC, Zhou JS, et al. TREM2 modifies microglial phenotype and provides neuroprotection in P301S tau transgenic mice, Neuropharmacology. 105 (2016) 196-206.
[51] Jiang T, Tan L, Zhu XC, Zhou JS, Cao L, Tan MS, et al. Silencing of TREM2 exacerbates tau pathology, neurodegenerative changes, and spatial learning deficits in P301S tau transgenic Neurobiol Aging. 36 (2015) 3176-3186.
[52] Cantoni C, Bollman B, Licastro D, Xie M, Mikesell R, Schmidt R, et al. TREM2 regulates microglial cell activation in response to demyelination in vivo, Acta Neuropathol. 129 (2015)

[53] Poliani PL, Wang Y, Fontana E, Robinette ML, Yamanishi Y, Gilfillan S, et al. TREM2 sustains microglial expansion during aging and response to demyelination, J Clin Invest. 125 (2015) 2170.
[54] Zhu C, Herrmann US, Li B, Abakumova I, Moos R, Schwarz P, et al. Triggering receptor expressed on myeloid cells-2 is involved in prion-induced microglial activation but does not contribute to prion pathogenesis in mouse brains, Neurobiol Aging. 36 (2015) 1994-2003.
[55] Sieber MW, Jaenisch N, Brehm M, Guenther M, Linnartz-Gerlach B, Neumann H, et al. Attenuated inflammatory response in triggering receptor expressed on myeloid cells 2 (TREM2) knock-out mice following stroke, PLoS One. 8 (2013) e52982.
[56] Kawabori M, Hokari M, Zheng Z, Kim JY, Calosing C, Hsieh CL, et al. Triggering Receptor Expressed on Myeloid Cells-2 Correlates to Hypothermic Neuroprotection in Ischemic Stroke, Ther Hypothermia Temp Manag. 3 (2013) 189-198.
[57] Piccio L, Buonsanti C, Cella M, Tassi I, Schmidt RE, Fenoglio C, et al. Identification of soluble TREM-2 in the cerebrospinal fluid and its association with multiple sclerosis and CNS inflammation, Brain. 131 (2008) 3081-3091.
[58] Heslegrave A, Heywood W, Paterson R, Magdalinou N, Svensson J, Johansson P, et al. Increased cerebrospinal fluid soluble TREM2 concentration in Alzheimer's disease, Mol Neurodegener. 11 (2016) 3.

[59] Suarez-Calvet M, Kleinberger G, Araque Caballero MA, Brendel M, Rominger A, Alcolea D, et al. sTREM2 cerebrospinal fluid levels are a potential biomarker for microglia activity in early-stage Alzheimer's disease and associate with neuronal injury markers, EMBO Mol Med. 8 (2016) 466-476.
[60] Henjum K, Almdahl IS, Arskog V, Minthon L, Hansson O, Fladby T, et al. Cerebrospinal fluid soluble TREM2 in aging and Alzheimer's disease, Alzheimers Res Ther. 8 (2016) 17.
[61] Gispert JD, Suarez-Calvet M, Monte GC, Tucholka A, Falcon C, Rojas S, et al. Cerebrospinal fluid sTREM2 levels are associated with gray matter volume increases and reduced diffusivity in early Alzheimer's disease, Alzheimer's & dementia : the journal of the Alzheimer's Association. 12 (2016) 1259-1272.
[62] Wu K, Byers DE, Jin X, Agapov E, Alexander-Brett J, Patel AC, et al. TREM-2 promotes macrophage survival and lung disease after respiratory viral infection, J Exp Med. 212 (2015) 681-697.
[63] Seno H, Miyoshi H, Brown SL, Geske MJ, Colonna M, Stappenbeck TS. Efficient colonic mucosal wound repair requires Trem2 signaling, Proc Natl Acad Sci U S A. 106 (2009) 256-261.
[64] Correale C, Genua M, Vetrano S, Mazzini E, Martinoli C, Spinelli A, et al. Bacterial sensor triggering receptor expressed on myeloid cells-2 regulates the mucosal inflammatory response, Gastroenterology. 144 (2013) 346-356 e343.
[65] Paloneva J, Kestila M, Wu J, Salminen A, Bohling T, Ruotsalainen V, et al. Loss-of-function mutations in TYROBP (DAP12) result in a presenile dementia with bone cysts, Nat Genet. 25 (2000) 357-361.
[66] Charles JF, Humphrey MB, Zhao X, Quarles E, Nakamura MC, Aderem A, et al. The innate immune response to Salmonella enterica serovar Typhimurium by macrophages is dependent on TREM2-DAP12, Infect Immun. 76 (2008) 2439-2447.
[67] Zhu M, Li D, Wu Y, Huang X, Wu M. TREM-2 promotes macrophage-mediated eradication of Pseudomonas aeruginosa via a PI3K/Akt pathway, Scand J Immunol. 79 (2014) 187-196.
[68] Wei P, Lu Q, Cui G, Guan Z, Yang L, Sun C, et al. The role of TREM-2 in internalization and intracellular survival of Brucella abortus in murine macrophages, Vet Immunol Immunopathol. 163 (2015) 194-201.
[69] Ford JW, McVicar DW. TREM and TREM-like receptors in inflammation and disease, Curr Opin Immunol. 21 (2009) 38-46.
[70] Lanier LL, Corliss BC, Wu J, Leong C, Phillips JH. Immunoreceptor DAP12 bearing a tyrosine-based activation motif is involved in activating NK cells, Nature. 391 (1998) 703-707.
[71] Tomasello E, Olcese L, Vely F, Geourgeon C, Blery M, Moqrich A, et al. Gene structure, expression pattern, and biological activity of mouse killer cell activating receptor-associated protein (KARAP)/DAP-12, Journal of Biological Chemistry. 273 (1998) 34115-34119.
[72] Call ME, Wucherpfennig KW, Chou JJ. The structural basis for intramembrane assembly of an activating immunoreceptor complex, Nat Immunol. 11 (2010) 1023-1029.
[73] Wei P, Zheng BK, Guo PR, Kawakami T, Luo SZ. The association of polar residues in the DAP12 homodimer: TOXCAT and molecular dynamics simulation studies, Biophys J. 104 (2013) 1435-1444.
[74] Cheng X, Im W. NMR observable-based structure refinement of DAP12-NKG2C activating immunoreceptor complex in explicit membranes, Biophys J. 102 (2012) L27-29.

[75] Call ME, Wucherpfennig KW. Common themes in the assembly and architecture of activating immune receptors, Nat Rev Immunol. 7 (2007) 841-850.
[76] Humphrey MB, Daws MR, Spusta SC, Niemi EC, Torchia JA, Lanier LL, et al. TREM2, a DAP12-associated receptor, regulates osteoclast differentiation and function, J Bone Miner Res. 21 (2006) 237-245.
[77] Inui M, Kikuchi Y, Aoki N, Endo S, Maeda T, Sugahara-Tobinai A, et al. Signal adaptor DAP10 associates with MDL-1 and triggers osteoclastogenesis in cooperation with DAP12, Proc Natl Acad Sci U S A. 106 (2009) 4816-4821.
[78] McVicar DW, Taylor LS, Gosselin P, Willette-Brown J, Mikhael AI, Geahlen RL, et al. DAP12-mediated signal transduction in natural killer cells. A dominant role for the Syk protein-tyrosine kinase, J Biol Chem. 273 (1998) 32934-32942.
[79] Bouchon A, Hernandez-Munain C, Cella M, Colonna M. A DAP12-mediated pathway regulates expression of CC chemokine receptor 7 and maturation of human dendritic cells, J Exp Med. 194 (2001) 1111-1122.
[80] Cella M, Buonsanti C, Strader C, Kondo T, Salmaggi A, Colonna M. Impaired differentiation of osteoclasts in TREM-2-deficient individuals, J Exp Med. 198 (2003) 645-651.
[81] Peng Q, Malhotra S, Torchia JA, Kerr WG, Coggeshall KM, Humphrey MB. TREM2- and DAP12-dependent activation of PI3K requires DAP10 and is inhibited by SHIP1, Sci Signal. 3 (2010) ra38.
[82] Orr SJ, McVicar DW. LAB/NTAL/Lat2: a force to be reckoned with in all leukocytes?, J Leukoc Biol. 89 (2011) 11-19.
[83] Whittaker GC, Orr SJ, Quigley L, Hughes L, Francischetti IM, Zhang W, et al. The linker for activation of B cells (LAB)/non-T cell activation linker (NTAL) regulates triggering receptor expressed on myeloid cells (TREM)-2 signaling and macrophage inflammatory responses independently of the linker for activation of T cells, J Biol Chem. 285 (2010) 2976-2985.
[84] Barrow AD, Trowsdale J. You say ITAM and I say ITIM, let's call the whole thing off: the ambiguity of immunoreceptor signalling, Eur J Immunol. 36 (2006) 1646-1653.
[85] Rao N, Dodge I, Band H. The Cbl family of ubiquitin ligases: critical negative regulators of tyrosine kinase signaling in the immune system, J Leukoc Biol. 71 (2002) 753-763.
[86] Washington AV, Quigley L, McVicar DW. Initial characterization of TREM-like transcript (TLT)-1: a putative inhibitory receptor within the TREM cluster, Blood. 100 (2002) 3822-3824.
[87] Yoon SH, Lee YD, Ha J, Lee Y, Kim HH. TLT-1s, alternative transcripts of triggering receptor expressed on myeloid cell-like transcript-1 (TLT-1), Inhibits the triggering receptor expressed on myeloid cell-2 (TREM-2)-mediated signaling pathway during osteoclastogenesis, J Biol Chem. 287 (2012) 29620-29626.
[88] Colonna M. TREMs in the immune system and beyond, Nat Rev Immunol. 3 (2003) 445-453.
[89] Hamerman JA, Jarjoura JR, Humphrey MB, Nakamura MC, Seaman WE, Lanier LL. Cutting edge: inhibition of TLR and FcR responses in macrophages by triggering receptor expressed on myeloid cells (TREM)-2 and DAP12, J Immunol. 177 (2006) 2051-2055.
[90] Turnbull IR, Gilfillan S, Cella M, Aoshi T, Miller M, Piccio L, et al. Cutting edge: TREM-2 attenuates macrophage activation, J Immunol. 177 (2006) 3520-3524.
[91] Ito H, Hamerman JA. TREM-2, triggering receptor expressed on myeloid cell-2, negatively regulates TLR responses in dendritic cells, Eur J Immunol. 42 (2012) 176-185.

[92] Pasquier B, Launay P, Kanamaru Y, Moura IC, Pfirsch S, Ruffie C, et al. Identification of FcalphaRI as an inhibitory receptor that controls inflammation: dual role of FcRgamma ITAM, Immunity. 22 (2005) 31-42.
[93] Hamerman JA, Lanier LL. Inhibition of immune responses by ITAM-bearing receptors, Sci STKE. 2006 (2006) re1.
[94] Xing J, Titus AR, Humphrey MB. The TREM2-DAP12 signaling pathway in Nasu-Hakola disease: a molecular genetics perspective, Res Rep Biochem. 5 (2015) 89-100.
[95] Turnbull IR, Colonna M. Activating and inhibitory functions of DAP12, Nat Rev Immunol. 7 (2007) 155-161.
[96] Zhong L, Chen XF, Zhang ZL, Wang Z, Shi XZ, Xu K, et al. DAP12 Stabilizes the C-terminal Fragment of the Triggering Receptor Expressed on Myeloid Cells-2 (TREM2) and Protects against LPS-induced Pro-inflammatory Response, J Biol Chem. 290 (2015) 15866-15877.
[97] Gomez-Pina V, Soares-Schanoski A, Rodriguez-Rojas A, Del Fresno C, Garcia F, Vallejo-Cremades MT, et al. Metalloproteinases shed TREM-1 ectodomain from lipopolysaccharide-stimulated human monocytes, J Immunol. 179 (2007) 4065-4073.
[98] Gattis JL, Washington AV, Chisholm MM, Quigley L, Szyk A, McVicar DW, et al. The structure of the extracellular domain of triggering receptor expressed on myeloid cells like transcript-1 and evidence for a naturally occurring soluble fragment, J Biol Chem. 281 (2006) 13396-13403.
[99] Haselmayer P, Grosse-Hovest L, von Landenberg P, Schild H, Radsak MP. TREM-1 ligand expression on platelets enhances neutrophil activation, Blood. 110 (2007) 1029-1035.
[100] Zhong L, Chen XF, Wang T, Wang Z, Liao C, Wang Z, et al. Soluble TREM2 induces inflammatory responses and enhances microglial survival, J Exp Med. (2017).
[101] Peng Q, Long CL, Malhotra S, Humphrey MB. A physical interaction between the adaptor proteins DOK3 and DAP12 is required to inhibit lipopolysaccharide signaling in macrophages, Sci Signal. 6 (2013) ra72.
[102] Hayashi M, Nakashima T, Taniguchi M, Kodama T, Kumanogoh A, Takayanagi H. Osteoprotection by semaphorin 3A, Nature. 485 (2012) 69-74.
[103] Kumanogoh A, Kikutani H. Immunological functions of the neuropilins and plexins as receptors for semaphorins, Nature Reviews Immunology. 13 (2013) 802-814.
[104] Takegahara N, Takamatsu H, Toyofuku T, Tsujimura T, Okuno T, Yukawa K, et al. Plexin-A1 and its interaction with DAP12 in immune responses and bone homeostasis, Nat Cell Biol. 8 (2006) 615-622.
[105] Bakker ABH, Hoek RM, Cerwenka A, Blom B, Lucian L, McNeil T, et al. DAP12-deficient mice fail to develop autoimmunity due to impaired antigen priming, Immunity. 13 (2000) 345-353.
[106] Mocsai A, Humphrey MB, Van Ziffle JA, Hu Y, Burghardt A, Spusta SC, et al. The immunomodulatory adapter proteins DAP12 and Fc receptor gamma-chain (FcRgamma) regulate development of functional osteoclasts through the Syk tyrosine kinase, Proc Natl Acad Sci U S A. 101 (2004) 6158-6163.
[107] Zhang Y, Su J, Wu S, Teng Y, Yin Z, Guo Y, et al. DDR2 (discoidin domain receptor 2) suppresses osteoclastogenesis and is a potential therapeutic target in osteoporosis, Sci Signal. 8 (2015) ra31.

[108] Otero K, Shinohara M, Zhao H, Cella M, Gilfillan S, Colucci A, et al. TREM2 and beta-catenin regulate bone homeostasis by controlling the rate of osteoclastogenesis, J Immunol. 188 (2012) 2612-2621.
[109] Otero K, Turnbull IR, Poliani PL, Vermi W, Cerutti E, Aoshi T, et al. Macrophage colony-stimulating factor induces the proliferation and survival of macrophages via a pathway involving DAP12 and beta-catenin, Nat Immunol. 10 (2009) 734-743.
[110] Zou W, Reeve JL, Liu Y, Teitelbaum SL, Ross FP. DAP12 couples c-Fms activation to the osteoclast cytoskeleton by recruitment of Syk, Mol Cell. 31 (2008) 422-431.
[111] Zheng H, Jia L, Liu CC, Rong Z, Zhong L, Yang L, et al. TREM2 Promotes Microglial Survival by Activating Wnt/beta-Catenin Pathway, J Neurosci. 37 (2017) 1772-1784.
[112] Daws MR, Sullam PM, Niemi EC, Chen TT, Tchao NK, Seaman WE. Pattern recognition by TREM-2: binding of anionic ligands, J Immunol. 171 (2003) 594-599.
[113] N'Diaye EN, Branda CS, Branda SS, Nevarez L, Colonna M, Lowell C, et al. TREM-2 (triggering receptor expressed on myeloid cells 2) is a phagocytic receptor for bacteria, J Cell Biol. 184 (2009) 215-223.
[114] Phongsisay V. Campylobacter jejuni targets immunoglobulin-like receptor LMIR5, Mol Immunol. 63 (2015) 574-578.
[115] Quan DN, Cooper MD, Potter JL, Roberts MH, Cheng H, Jarvis GA. TREM-2 binds to lipooligosaccharides of Neisseria gonorrhoeae and is expressed on reproductive tract epithelial cells, Mucosal Immunology. 1 (2008) 229-238.
[116] Stefano L, Racchetti G, Bianco F, Passini N, Gupta RS, Panina Bordignon P, et al. The surface-exposed chaperone, Hsp60, is an agonist of the microglial TREM2 receptor, J Neurochem. 110 (2009) 284-294.
[117] Piccio L, Buonsanti C, Mariani M, Cella M, Gilfillan S, Cross AH, et al. Blockade of TREM-2 exacerbates experimental autoimmune encephalomyelitis, Eur J Immunol. 37 (2007) 1290-1301.
[118] Cannon JP, O'Driscoll M, Litman GW. Specific lipid recognition is a general feature of CD300 and TREM molecules, Immunogenetics. 64 (2012) 39-47.
[119] Bailey CC, DeVaux LB, Farzan M. The Triggering Receptor Expressed on Myeloid Cells 2 Binds Apolipoprotein E, J Biol Chem. 290 (2015) 26033-26042.
[120] Simhadri VR, Andersen JF, Calvo E, Choi SC, Coligan JE, Borrego F. Human CD300a binds to phosphatidylethanolamine and phosphatidylserine, and modulates the phagocytosis of dead cells, Blood. 119 (2012) 2799-2809.
[121] Kobayashi N, Karisola P, Pena-Cruz V, Dorfman DM, Jinushi M, Umetsu SE, et al. TIM-1 and TIM-4 glycoproteins bind phosphatidylserine and mediate uptake of apoptotic cells, Immunity. 27 (2007) 927-940.
[122] Tietjen GT, Gong Z, Chen CH, Vargas E, Crooks JE, Cao KD, et al. Molecular mechanism for differential recognition of membrane phosphatidylserine by the immune regulatory receptor Tim4, Proc Natl Acad Sci U S A. 111 (2014) E1463-1472.
[123] Song W, Hooli B, Mullin K, Jin SC, Cella M, Ulland TK, et al. Alzheimer's disease-associated TREM2 variants exhibit either decreased or increased ligand-dependent activation, Alzheimer's & dementia : the journal of the Alzheimer's Association. (2016).
[124] Giuliano JS, Jr., Lahni PM, Wong HR, Wheeler DS. Pediatric Sepsis - Part V: Extracellular Heat Shock Proteins: Alarmins for the Host Immune System, Open Inflamm J. 4 (2011) 49-60.

[125] Atagi Y, Liu CC, Painter MM, Chen XF, Verbeeck C, Zheng H, et al. Apolipoprotein E Is a Ligand for Triggering Receptor Expressed on Myeloid Cells 2 (TREM2), J Biol Chem. 290 (2015) 26043-26050.
[126] Yeh FL, Wang Y, Tom I, Gonzalez LC, Sheng M. TREM2 Binds to Apolipoproteins, Including APOE and CLU/APOJ, and Thereby Facilitates Uptake of Amyloid-Beta by Microglia, Neuron. 91 (2016) 328-340.
[127] Park M, Yi JW, Kim EM, Yoon IJ, Lee EH, Lee HY, et al. Triggering receptor expressed on myeloid cells 2 (TREM2) promotes adipogenesis and diet-induced obesity, Diabetes. 64 (2015) 117-127.
[128] Frieden C. ApoE: the role of conserved residues in defining function, Protein Sci. 24 (2015) 138-144.
[129] Mahley RW, Weisgraber KH, Huang Y. Apolipoprotein E: structure determines function, from atherosclerosis to Alzheimer's disease to AIDS, J Lipid Res. 50 Suppl (2009) S183-188.
[130] Terwel D, Steffensen KR, Verghese PB, Kummer MP, Gustafsson JA, Holtzman DM, et al. Critical role of astroglial apolipoprotein E and liver X receptor-alpha expression for microglial Abeta phagocytosis, J Neurosci. 31 (2011) 7049-7059.
[131] Kanekiyo T, Xu H, Bu G. ApoE and Abeta in Alzheimer's disease: accidental encounters or partners?, Neuron. 81 (2014) 740-754.
[132] Xiang X, Werner G, Bohrmann B, Liesz A, Mazaheri F, Capell A, et al. TREM2 deficiency reduces the efficacy of immunotherapeutic amyloid clearance, EMBO Mol Med. 8 (2016) 992-1004.
[133] Takahashi K, Rochford CD, Neumann H. Clearance of apoptotic neurons without inflammation by microglial triggering receptor expressed on myeloid cells-2, J Exp Med. 201 (2005) 647-657.
[134] Ulrich JD, Holtzman DM. TREM2 Function in Alzheimer's Disease and Neurodegeneration, ACS Chem Neurosci. 7 (2016) 420-427.
[135] Sharif O, Gawish R, Warszawska JM, Martins R, Lakovits K, Hladik A, et al. The Triggering Receptor Expressed on Myeloid Cells 2 Inhibits Complement Component 1q Effector Mechanisms and Exerts Detrimental Effects during Pneumococcal Pneumonia, PLOS Pathogens. 10 (2014) e1004167.
[136] Ulrich JD, Finn MB, Wang Y, Shen A, Mahan TE, Jiang H. Altered microglial response to Abeta plaques in APPPS1-21 mice heterozygous for TREM2, Mol Neurodegener. 9 (2014).
[137] Jiang T, Wan Y, Zhang YD, Zhou JS, Gao Q, Zhu XC, et al. TREM2 Overexpression has No Improvement on Neuropathology and Cognitive Impairment in Aging APPswe/PS1dE9 Mice, Mol Neurobiol. 54 (2017) 855-865.
[138] O'Callaghan P, Li JP, Lannfelt L, Lindahl U, Zhang X. Microglial Heparan Sulfate Proteoglycans Facilitate the Cluster-of-Differentiation 14 (CD14)/Toll-like Receptor 4 (TLR4)-Dependent Inflammatory Response, J Biol Chem. 290 (2015) 14904-14914.
[139] Murphy JW, Cho Y, Sachpatzidis A, Fan C, Hodsdon ME, Lolis E. Structural and functional basis of CXCL12 (stromal cell-derived factor-1 alpha) binding to heparin, J Biol Chem. 282 (2007) 10018-10027.
[140] McDonnell KM, Grow WA. Reduced glycosaminoglycan sulfation diminishes the agrin signal transduction pathway, Dev Neurosci. 26 (2004) 1-10.

[141] Sharif O, Gawish R, Warszawska JM, Martins R, Lakovits K, Hladik A, et al. The triggering receptor expressed on myeloid cells 2 inhibits complement component 1q effector mechanisms and exerts detrimental effects during pneumococcal pneumonia, PLoS Pathog. 10 (2014) e1004167.
[142] Hong S, Beja-Glasser VF, Nfonoyim BM, Frouin A, Li S, Ramakrishnan S, et al. Complement and microglia mediate early synapse loss in Alzheimer mouse models, Science. 352 (2016) 712-716.
[143] Takahashi K, Prinz M, Stagi M, Chechneva O, Neumann H. TREM2-transduced myeloid precursors mediate nervous tissue debris clearance and facilitate recovery in an animal model of multiple sclerosis, PLoS Med. 4 (2007) e124.
[144] Chen Q, Zhang K, Jin Y, Zhu T, Cheng B, Shu Q, et al. Triggering receptor expressed on myeloid cells-2 protects against polymicrobial sepsis by enhancing bacterial clearance, Am J Respir Crit Care Med. 188 (2013) 201-212.
[145] Gawish R, Martins R, Bohm B, Wimberger T, Sharif O, Lakovits K, et al. Triggering receptor expressed on myeloid cells-2 fine-tunes inflammatory responses in murine Gram-negative sepsis, FASEB J. 29 (2015) 1247-1257.
[146] Sun M, Zhu M, Chen K, Nie X, Deng Q, Hazlett LD, et al. TREM-2 Promotes Host Resistance Against Pseudomonas aeruginosa Infection by Suppressing Corneal Inflammation via a PI3K/Akt Signaling PathwayTREM-2 in Corneal Inflammation, Investigative Ophthalmology & Visual Science. 54 (2013) 3451-3462.
[147] Phongsisay V, Iizasa E, Hara H, Yoshida H. Evidence for TLR4 and FcRgamma-CARD9 activation by cholera toxin B subunit and its direct bindings to TREM2 and LMIR5 receptors, Mol Immunol. 66 (2015) 463-471.
[148] Phongsisay V, Iizasa E, Hara H, Yamasaki S. 3-O-sulfo-beta-D-galactose moiety of endogenous sulfoglycolipids is a potential ligand for immunoglobulin-like receptor LMIR5, Mol Immunol. 63 (2015) 595-599.
[149] Park BS, Song DH, Kim HM, Choi BS, Lee H, Lee JO. The structural basis of lipopolysaccharide recognition by the TLR4-MD-2 complex, Nature. 458 (2009) 1191-1195.
[150] Kong Y, Janssen BJ, Malinauskas T, Vangoor VR, Coles CH, Kaufmann R, et al. Structural Basis for Plexin Activation and Regulation, Neuron. 91 (2016) 548-560.
[151] Janssen BJ, Robinson RA, Perez-Branguli F, Bell CH, Mitchell KJ, Siebold C, et al. Structural basis of semaphorin-plexin signalling, Nature. 467 (2010) 1118-1122.
[152] Felix J, De Munck S, Verstraete K, Meuris L, Callewaert N, Elegheert J, et al. Structure and Assembly Mechanism of the Signaling Complex Mediated by Human CSF-1, Structure. 23 (2015) 1621-1631.

Molecular Bases of Disease:

Microfibril-associated Glycoprotein 2 (MAGP2) Loss of Function Has Pleiotropic Effects *in Vivo*

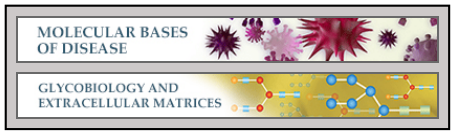

Michelle D. Combs, Russell H. Knutsen, Thomas J. Broekelmann, Holly M. Toennies, Thomas J. Brett, Chantel A. Miller, Daniel L. Kober, Clarissa S. Craft, Jeffrey J. Atkinson, J. Michael Shipley, Barbara C. Trask and Robert P. Mecham

J. Biol. Chem. 2013, 288:28869-28880.
doi: 10.1074/jbc.M113.497727 originally published online August 20, 2013

THE JOURNAL OF BIOLOGICAL CHEMISTRY VOL. 288, NO. 40, pp. 28869–28880, October 4, 2013

Microfibril-associated Glycoprotein 2 (MAGP2) Loss of Function Has Pleiotropic Effects *in Vivo*[*] [S]

Received for publication, June 27, 2013, and in revised form, August 6, 2013 Published, JBC Papers in Press, August 20, 2013, DOI 10.1074/jbc.M113.497727

Michelle D. Combs[‡], Russell H. Knutsen[‡], Thomas J. Broekelmann[‡], Holly M. Toennies[§], Thomas J. Brett[‡§¶], Chantel A. Miller[§], Daniel L. Kober[§‖], Clarissa S. Craft[‡], Jeffrey J. Atkinson[§], J. Michael Shipley[§], Barbara C. Trask[**], and Robert P. Mecham[‡§1]

From the [‡]Department of Cell Biology and Physiology, [§]Division of Pulmonary and Critical Care Medicine, [¶]Department of Biochemistry, and [‖]Molecular Biology and Microbial Pathogenesis Program, Washington University School of Medicine, Saint Louis, Missouri 63110, and the [**]Department of Zoology, Weber State University, Ogden, Utah 84408

Background: The function of MAGP2 was studied by inactivating its gene (*Mfap5*$^{-/-}$) in mice.
Results: *Mfap5*$^{-/-}$ mice have a neutrophil deficiency and other phenotypes that are different from MAGP1- and fibrillin-deficient animals.
Conclusion: MAGP2 has functional roles in hematopoiesis and in vessel wall maintenance.
Significance: Characterization of MAGP2 function is crucial to the identification and treatment of microfibril-related disease.

Microfibril-associated glycoprotein (MAGP) 1 and 2 are evolutionarily related but structurally divergent proteins that are components of microfibrils of the extracellular matrix. Using mice with a targeted inactivation of *Mfap5*, the gene for MAGP2 protein, we demonstrate that MAGPs have shared as well as unique functions *in vivo*. *Mfap5*$^{-/-}$ mice appear grossly normal, are fertile, and have no reduction in life span. Cardiopulmonary development is typical. The animals are normotensive and have vascular compliance comparable with age-matched wild-type mice, which is indicative of normal, functional elastic fibers. Loss of MAGP2 alone does not significantly alter bone mass or architecture, and loss of MAGP2 in tandem with loss of MAGP1 does not exacerbate MAGP1-dependent osteopenia. MAGP2-deficient mice are neutropenic, which contrasts with monocytopenia described in MAGP1-deficient animals. This suggests that MAGP1 and MAGP2 have discrete functions in hematopoiesis. In the cardiovascular system, MAGP1;MAGP2 double knockout mice (*Mfap2*$^{-/-}$;*Mfap5*$^{-/-}$) show age-dependent aortic dilation. These findings indicate that MAGPs have shared primary functions in maintaining large vessel integrity. In solid phase binding assays, MAGP2 binds active TGFβ1, TGFβ2, and BMP2. Together, these data demonstrate that loss of MAGP2 expression *in vivo* has pleiotropic effects potentially related to the ability of MAGP2 to regulate growth factors or participate in cell signaling.

The ECM[2] is a complex biopolymer that provides strength to tissues and plays instructive roles in organogenesis and tissue homeostasis (1). An abundant component of the ECM is the microfibril, which imparts limited elasticity to tissues, acts as a template for elastin deposition, and is a regulator of signaling events. Microfibrils are 10- to 12-nm fibers built upon a backbone of fibrillin and decorated with function-modifying accessory proteins that include growth factor complexes, fibulins, emilins, and MAGPs (2, 3). Mutations in the genes for microfibril components have varied systemic effects that are not always apparent with *in vitro* experimentation (3–5). The complexity of microfibril structure necessitates *in vivo* manipulation of proteins for an accurate understanding of microfibril function and identification of microfibril-related disease.

MAGP1 (the protein product of the *microfibrillar-associated protein 2* (*Mfap2*) gene) and MAGP2 (the protein product of the *Mfap5* gene and also known as MP-25) are a two-member family of small microfibril-associated proteins ~31 kDa and 25 kDa in size, respectively (6, 7). Both proteins are found only in vertebrates, and phylogenetic studies suggest that MAGP2 arose from MAGP1 through gene duplication early in vertebrate evolution (8). The two MAGPs share a functional C-terminal matrix-binding domain that is characterized by conserved cysteine residues (9, 10). MAGP2 has a conserved proprotein convertase cleavage site within this domain that makes MAGP2 a substrate for multiple proprotein convertase family members (11). Also unique to MAGP2 is an RGD integrin-binding motif located at the N terminus.

Amino acid sequences in the N-terminal regions of MAGP1 and MAGP2 are dissimilar, but both are enriched in acidic amino acids. MAGP1 contains two consensus sequences for *O*- but not *N*-glycosylation (12), whereas MAGP2 contains five conserved, predicted *O*-linked glycosylation sequences. Functional studies with MAGP1 show that the acidic N terminus contains a growth factor interaction motif capable of binding active TGFβ and bone morphogenic protein (BMP) (13).

* This work was supported, in whole or in part, by National Institutes of Health Grants HL53325, HL74138, and HL105314 (to R. P. M.), National Institutes of Health Developmental Cardiology and Pulmonary Training Grant T32 HL007873 (to M. D. C.), and National Institutes of Health Grant P30-AR057235 (to the Musculoskeletal and Morphology Cores).
[S] This article contains supplemental Figs. S1–S3 and Table S1.
[1] To whom correspondence should be addressed: Dept. of Cell Biology and Physiology, Box 8228, 660 S. Euclid, Saint Louis, MO 63110. E-mail: bmecham@wustl.edu.
[2] The abbreviations used are: ECM, extracellular matrix; MAGP, microfibril-associated glycoprotein; BMP, bone morphogenic protein; DKO, MAGP1/2 double knockout; 2KO, MAGP2 knockout; 1KO, MAGP1 knockout; μCT, microcomputed tomography; BLI, biolayer interferometry; Neo, neomycin resistance cassette; gDNA, genomic DNA.

MAGP1 is associated with all microfibrils except those directly adjacent to the plasma membrane of aortic endothelial cells and those at the junction of the zonule of the eye (14–16). Although MAGP2 has been localized to both elastin-associated microfibrils and elastin-free microfibrils in a number of tissues, the protein exhibits patterns of tissue localization and developmental expression that are more restricted than those of MAGP1 (7, 17). The association of MAGP1 and MAGP2 with other microfibrillar proteins is covalent, requiring reducing agents for their extraction (18).

Genetic deletion of extracellular MAGP1 in mice results in an array of phenotypes, including a bleeding diathesis, obesity, and osteopenia (13, 19, 20). MAGP1-deficient animals also have a pronounced deficiency in circulating and tissue monocytes. Here we report the generation and initial characterization of mice with null alleles of the MAGP2 gene (*Mfap5*) and both MAGP1 and MAGP2 ($Mfap2^{-/-};Mfap5^{-/-}$) (DKO) genes. We find that $Mfap5^{-/-}$ (2KO) phenotypes are non-overlapping with mice lacking MAGP1 (1KO). However, the absence of both MAGPs causes changes in large vessel architecture. Biochemical studies show that MAGP2 protein binds active TGFβ1, TGFβ2, and BMP2. Taken together, these data show that MAGP2 has unique, MAGP1-independent functions in hematopoiesis and that MAGPs have redundant functions in large vessels.

EXPERIMENTAL PROCEDURES

Generation and Breeding of MAGP2-deficient and MAGP1-MAGP2-deficient Mice—Homologous recombination was used to insert a gene-targeting cassette containing the coding sequence for neomycin resistance into the exon 9 region of the *Mfap5* gene in murine ES cells. G418-resistant ES cell colonies were screened by Southern blot analysis, and ES cell clones, positive for recombination, were injected into C57Bl/6 blastocysts. Chimeric mice were bred for germ line transmission. Genotype analysis was performed on genomic DNA isolated from tail tissue using primers listed in supplemental Table 1. Generation of mice deficient in both MAGP1 and MAGP2 was achieved by breeding MAGP2 mutant mice with previously generated animals deficient in MAGP1 (13). Mice used for these studies were maintained on a mixed-strain background, and wild-type controls were generated from the same parental stock as MAGP-deficient animals. Animals were housed in a pathogen-free facility, and the Washington University Animal Studies Committee approved all procedures.

Genomic DNA Isolation and Sequencing—Genomic DNA isolated from adult mouse tail tissue was used with primers listed in supplemental Table 1 to confirm the location and orientation of the targeting construct within the *Mfap5* gene locus. For all sequencing reactions, bands were extracted from agarose gel, and PCR products were isolated using a QIAquick gel extraction kit according to the protocol of the manufacturer (Qiagen Inc., Valencia, CA). Amplicons were then ligated into the pGEM-T vector using the rapid DNA ligation kit according to the protocol of the manufacturer (Roche Diagnostics, Mannheim, Germany) and introduced into DH5α *Escherichia coli* (Promega Corp., Madison, WI). The growth medium was inoculated with ampicillin-resistant, color-selected colonies, and plasmid products were isolated using QIAprep Spin Miniprep kits according to the instructions of the manufacturer (Qiagen). The Protein and Nucleic Acid Chemistry Laboratory (Washington University, Saint Louis, MO) performed DNA sequencing. All DNA alignments were performed using DNASTAR Lasergene 9 software.

Total RNA Isolation and in Situ Hybridization—Total RNA was isolated from adult mouse lung, kidney, and heart using TRIzol reagent, and reverse transcription cDNA amplification was performed using 1 μg of RNA and SuperScript III first-strand synthesis system with oligo(dT) according to the specifications of the manufacturer (Invitrogen). Complement DNA was amplified using primers listed in supplemental Table 1. Ethidium bromide gels for nonsense-mediated decay studies were imaged with the ChemiDoc MP system and Image Lab version 4.0 software using identical exposure and filter settings (Bio-Rad). For sequencing, PCR band excision and sequencing were performed according to methods detailed previously. RNA probe generation and *in situ* hybridization for *Mfap5*, *Mfap2*, and collagen1α1 (*Col1a1*) was performed as described previously using mRNA isolated from adult mouse heart and primers listed in supplemental Table 1 (21–23). RNA probes were 806 bp in length for *Mfap5*, 802 bp for *Mfap2*, and 846 bp for *Col1a1*.

Antibodies, Western Blotting, and Immunohistochemistry—Rabbit polyclonal antibodies against mouse MAGP2 (24) and MAGP1 (13) have been described previously. For Western blot analysis of serially extracted mouse tissue lysates, adult mouse lung was homogenized in 990 μl of PBS (pH7.4) and 10 μl of protease inhibitor mixture (catalog no. P8340, Sigma Aldrich, Saint Louis, MO) and extracted 24 h at 4 °C. The samples were pelleted by centrifugation at 16,000 $\times$ *g* or 20 min at 4 °C. The liquid portion of the sample was removed for Western blotting, and the pellet was resuspended in 1 M NaCl and protease inhibitors and extracted for 24 h. The process was repeated using 8 M urea, PBS, and 20 mM DTT (seen in Fig. 5*C*,D), and 8 M urea + DTT. Western blotting was performed using standard procedures. Samples were run on 7.5% or 12% SDS-PAGE gels and transferred to nitrocellulose membranes. Ponceau S stain was applied for 5 min and removed using 0.1 M NaOH. All blocking steps were performed with blocking buffer containing 5% casein, 0.1% coldwater fish skin gelatin, and 0.01% Tween 20 in TBS. Primary antibodies were applied overnight at 4 °C at a dilution of 1:10,000 for MAGP2 (in 5% BSA) or 1:1000 for MAGP1 (in 5% BSA). Secondary antibodies were applied at 1:4000 in casein block and incubated for 1 h at room temperature. ECL reagents were used for detection of horseradish peroxidase, and chemiluminescence was read using the ChemiDoc MP system and Image Lab version 4.0 software (GE Healthcare). Immunohistochemistry for paraffin sections was performed using the ultrasensitive ABC peroxidase rabbit IgG staining kit (Fisher Scientific, Pittsburgh, PA) according to the instructions of the manufacturer, with the following modifications for MAGP2 detection. After peroxidase quenching, the sections were washed in 0.1% BSA in TBS. Hyaluronidase digestion solution (1 mg/ml hyaluronidase in 0.1 M sodium acetate buffer (pH5.5) containing 0.85% NaCl) was applied, and the sections were incubated in a humid chamber for 30 min at

37 °C. The sections were washed in BSA/TBS three times for 5 min. A guanidine/DTT solution was applied to the sections for 15 min. The sections were washed with BSA/TBS three times for 5 min before incubation with iodoacetamide solution for 15 min. The sections underwent a final BSA/TBS wash before application of ultra-sensitive staining kit block solution. Primary anti-MAGP2 antibody was diluted 1:8000 in blocking solution and applied to the sections overnight at 4 °C. Secondary antibody solution was made using 2.25 μl/ml of secondary antibody. Horseradish peroxidase reactivity was visualized using the metal enhanced DAB substrate kit (Fisher). Imaging was performed on a Zeiss Axioskop using identical exposure and filter settings. Image processing was performed using Adobe Photoshop CS5 software.

Flow Cytometry—Monoclonal antibodies used for flow cytometry were as follows: phycoerythrin-conjugated hamster anti-mouse CD3e (BD Biosciences), FITC rat anti-mouse CD335 (NKp46, eBioscience, San Diego, CA), FITC rat anti-mouse Ly-6G (eBioscience), phycoerythrin rat anti-mouse CD115 (eBioscience), allophycocyanin rat F4/80 (Abcam, Cambridge, MA). Phycoerythrin hamster IgG1, FITC rat IgG2a, FITC rat IgG2b, phycoerythrin rat IgG2a control, and allophycocyanin rat IgG2b isotype controls were utilized according to the suggestions of the manufacturer. Mice were killed by CO_2 narcosis, and the chest and abdominal cavity were exposed to reveal the heart, dorsal aorta, and spleen. Whole blood was collected from the dorsal aorta in a heparinized syringe. Red cells were lysed with NH_4Cl buffer for 10 min at room temperature and washed twice with FACs buffer (1× PBS and 2% FBS). After blocking with mouse Fc Block (BD Biosciences) for 20 min, 2×10^5 cells were incubated with antigen-specific or isotype control antibodies for 30 min at 4 °C. Cells were washed twice with FACs buffer and fixed with 4% paraformaldehyde for 15 min, washed twice, and stored overnight. Spleens were removed, and splenocytes were isolated after passage through a 70-μm nylon mesh filter. Lysis, blocking, incubation, and fixation were identical to the white blood cell treatment above. Cells were sorted on a FACSCalibur machine (BD Biosciences) with Cell-Quest software (BD Biosciences). The percentage of positive cells for each cell type was determined by gating on isotype control, nonspecific labeling (percentage of positive cells within gate < 5% for control), followed by subtraction of background percentage from antibody-specific results. A minimum of 10^5 live cell events were recorded for each analysis. Experiments were performed with at least five animals of each genotype ($n \geq 5$), and experiments were repeated at least two times with mice 2 and 6 months of age.

Microcomputed Tomography (μCT)—Microcomputed tomography analysis of left tibias from 6-month-old mice was performed as described previously (19), with the exception that the tibias were not frozen. The tibias were embedded in 2% agarose and scanned using a Scanco μCT 40 (Scanco Medical AG, Zurich, Switzerland). For trabecular bone measurements, the growth plate was excluded and 30 × 16-μm sections were contoured. For cortical bone, the sections were analyzed just above the tibiofibular junction, and three sections per tibia were analyzed. Contouring and analysis were performed by the Washington University Musculoskeletal Research Facility using Scanco MicroCT software. Identical contouring and analysis parameters were used for all tibias. The tibias from at least five male mice of each genotype ($n \geq 5$) were used for analysis.

Blood Pressure and Mechanical Properties of Ascending Aorta and Left Carotid Artery—Six-month-old male mice were weighed and then anesthetized using 1.5% isoflurane, keeping the body temperature constant. A solid-state catheter was inserted into the right common carotid artery, isoflurane was reduced to 0.5%, and blood pressure measurements were recorded (25, 26). The hearts were excised and weighed, and the aortas and left carotid arteries were removed for mechanical testing as reported previously (25). At least 12 male mice of each genotype ($n \geq 12$) were used for analysis.

Recombinant MAGP2 and MAGP1 Proteins and Biolayer Interferometry (BLI)—The coding sequence for mouse MAGP2 protein, excluding the N-terminal signal sequence, was cloned into pET23b as a tagless construct. This plasmid was transformed into Rosetta 2(DE3) *E. coli* cells for protein expression. MAGP2 proteins were purified from inclusion bodies, followed by oxidative refolding as described previously (27). Recombinant His_6-tagged MAGP1, used for Western blotting, was expressed and isolated as described previously for this protein (13).

Native MAGP2 protein was expressed in mammalian cells and purified as follows. Full-length mature-form MAGP2, without the endogenous signal sequence, was cloned into the pHL-Avitag3 vector (28) containing an optimized signal sequence at the N terminus as well as a BirA biotin ligase recognition sequence and hexahistidine (His_6) tag at the C terminus. Protein was expressed by large-scale transient transfection of FreeStyle 293F cells cultured in serum-free Freestyle 293 medium (Life Tech.). Culture supernatants were collected 72 h post-transfection, and protein was purified to homogeneity using nickel affinity chromatography. Purity was assessed by SDS-PAGE. Site-specific biotinylation of the C-terminal tags were carried out using *E. coli* BirA biotin ligase.

All surface plasmon resonance binding was performed on a Reichert SR7000 surface plasmon resonance system. To bind MAGP2 protein to the carboxymethyl dextran (CM-5) chip, the chip was preactivated with a mixture of 200 mM 1-ethyl-3(3-dimethylaminopropyl)carbodiimide hydrochloride and 50 mM *N*-hydroxysuccinimide, and then 100 μl MAGP2 was diluted in 5 mM acetate buffer (pH 4.5) and injected with a flow rate of 10 μl/min at a concentration of 20 μM. This resulted in ~1300 resonance units of MAGP2 protein coupled to the chip. Excess reactive sites on the chip were then quenched with a 70-μl injection of 0.5 M ethanolamine (pH 8). To measure MAGP2 binding to active TGFβ1, carrier-free active human TGFβ1 (R&D Systems, Minneapolis, MN) was diluted in surface plasmon resonance running buffer (10 mM HEPES, 150 mM NaCl, 0.05% Triton X-100 (pH 7.4)) and injected for 100 s at a flow rate of 50 μl/min. The dissociation was monitored for 300 s. The chip was recycled with 0.2 M glycine (pH 2.3) before subsequent injections. The concentrations of TGFβ1 injected were 100, 50, 50, 25, 25, and 12.5 nM. Background subtraction and calculation of the dissociation constant for individual curves

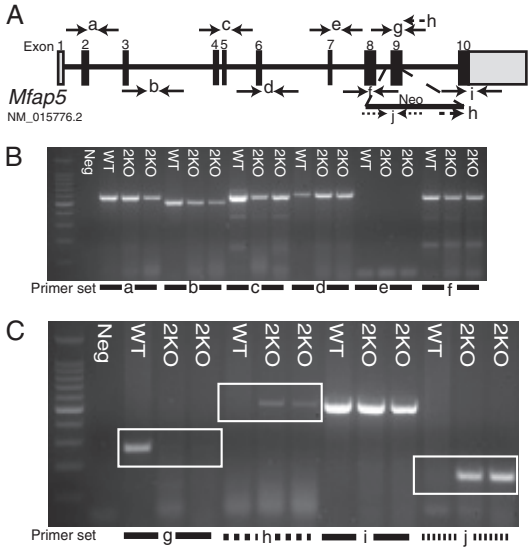

FIGURE 1. **Schematic of Mfap5 gene targeting.** *A*, schematic of the *Mfap5* gene with *numbered bars* representing exons (*gray*, non-coding; *black*, coding). A gene-targeting cassette containing the coding sequence for neomycin resistance was introduced by homologous recombination into the murine *Mfap5* gene. *Lettered arrows* represent primer pairs used for PCR. *B* and *C*, gDNA from one WT and two 2KO mice was subjected to PCR. *Lettered lines* refer to primer pairs indicated in *A*. A PCR amplicon is produced from the WT and not the 2KO template because of the presence of the targeting construct (*boxed region*, *C*, *g*). Primers to the targeting construct and *Mfap5* sequence produce a PCR product from the 2KO and not the WT gDNA template (*boxed region*, *C*, *h*). PCR primers to Neo produce a product only from 2KO gDNA (*boxed region*, *C*, *j*).

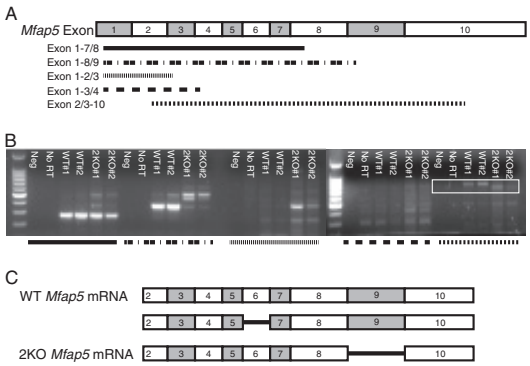

FIGURE 2. **Exon 9 is spliced out of the targeted Mfap5 transcript.** A naturally occurring Mfap5 splice variant lacking exon 6 also occurs. *A*, illustration of the *Mfap5* mRNA transcript, with *shaded rectangles* representing exons. PCR primer pairs directed against an exon and an exon/intron junction are labeled, and the amplicon is depicted by *shaded lines*. *B*, RT-PCR was performed using the mRNA template from two WT and two 2KO mice. No reverse transcriptase (*No RT*) and no cDNA template (*Neg*) controls were included in the PCR reactions. *Shaded lines* refer to primer pairs illustrated in *A*. PCR products using exon 2/3–10 primers (*boxed region*) were larger for the WT template than for the 2KO template. *C*, schematic representation of *Mfap5* mRNA transcripts from WT and 2KO mice. Shown are schematics demonstrating a full-length transcript as well as a naturally occurring splice variant lacking exon 6 from WT mice. All *Mfap5* mRNA transcripts amplified from 2KO mice lack exon 9.

was calculated using Scrubber2 software (Center for Biolmolecular Interaction Analysis, University of Utah).

The Octet system for Biolayer interferometry (Pall Life Sciences, Ann Arbor, MI) was also used to assess MAGP2 binding to active TGFβ1 as well as TGFβ2 and BMP2. Streptavidin-coated biosensors from ForteBio were used to capture biotinylated MAGP2 onto the surface of the sensor. After reaching base line, sensors were moved to the association step containing 1000, 500, 250, 125, 62.5, 31.3, 15.6, and 7.8 nM active mouse TGFβ1, TGFβ2, or BMP2 for 300 s and then dissociated for 300 s. A buffer-only reference was subtracted from all curves. The running buffer consisted of 10 mM HEPES (pH 7.4), 150 mM NaCl, 3.4 mM EDTA, 1% BSA, 0.01% azide, 0.05% Tween, and 0.005% Triton X-100. Affinities were estimated from global kinetic analysis.

Statistical Analysis—Statistical significance was determined by Student's *t* test. Data are reported as a mean ± S.D.

RESULTS

MAGP2 Gene Targeting—Homologous recombination was used to disrupt the MAGP2 gene (*Mfap5*) by replacing exon 9 with a neomycin resistance cassette (Neo), causing a downstream frameshift. Our attempts to target exon 1 and the upstream promoter sequence were unsuccessful. Exon 9 encodes the matrix-binding domain. If expressed, the mutant protein lacking this domain would be incapable of binding to fibrillin and, hence, would be a functional null.

PCR primers flanking each exon from 2–10, as well as within the Neo cassette itself, were used to walk along the targeted *Mfap5* gene and confirm localization of the Neo cassette to exon 9. Genomic DNA (gDNA) isolated from WT and *Mfap5*$^{-/-}$ mice yielded identical amplicons using primers flanking exons 2–8 of the *Mfap5* gene (Fig. 1, *A* and *B*, and supplemental Table 1). An exon 9 amplicon was generated from WT but not 2KO genomic DNA, and a forward primer to the Neo sequence and a reverse primer at exon 9 produced an amplicon from 2KO and not WT gDNA (Fig. 1, *A* and *C*). These PCR bands were gel-extracted and sequenced, confirming that the Neo sequence was introduced at exon 9 of the *Mfap5* gene (supplemental Fig. S1).

To generate DKO animals, 2KO mice were bred with 1KO mice generated in a previous study (13). Fig. 4*B* confirms the genotype of the DKO animals. The exon 9 forward primer, Neo primer, and reverse exon 9 primer described above were used for *Mfap5* genotyping reactions (Figs. 1 and 4*B*).

The Mfap5-targeted Allele (2Δ9) Is Transcribed, but the Mutant mRNA Is Degraded—RT-PCR amplification was used to determine whether mRNA is transcribed from the mutated *Mfap5* gene in 2KO mice. PCR products representing the *Mfap5* exon 2–10 sequence were amplified from both WT and 2KO cDNA. However, the 2KO amplicon is 74 bp smaller than the WT product (Fig. 2, *A* and *B*). DNA sequencing revealed that the 2KO product is a transcript with exon 9 and the Neo cassette spliced out (2Δ9) (supplemental Fig. S2 and Fig. 2*C*). This sequence does not occur as a natural splice variant, although we did identify a naturally occurring WT transcript

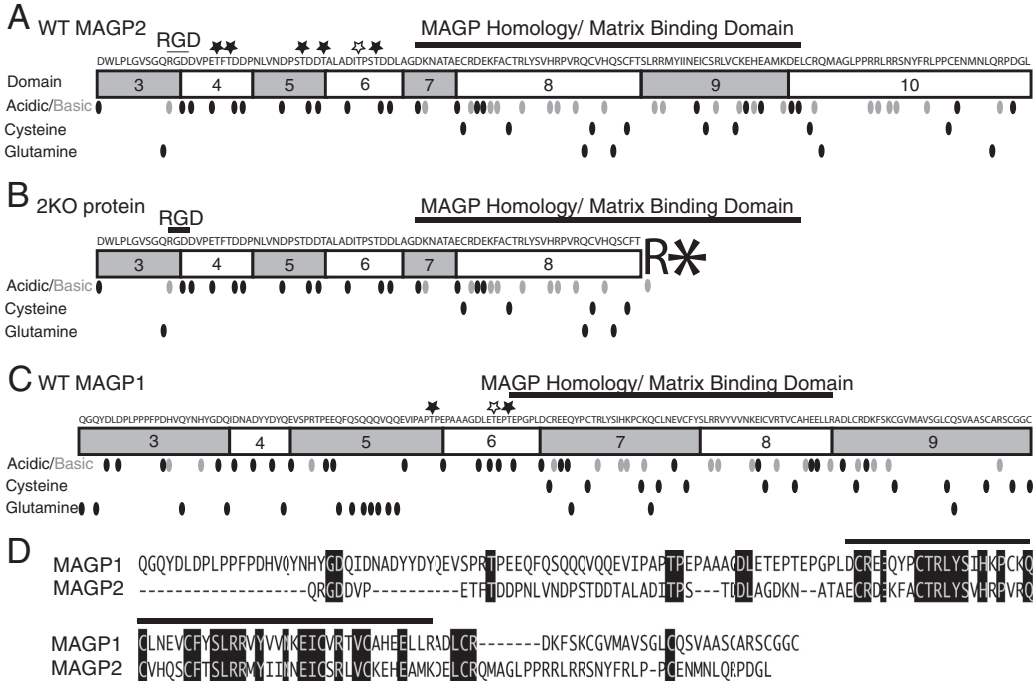

FIGURE 3. **Comparison of MAGP1 and MAGP2 sequences and predicted protein transcripts from WT and MAGP2-KO genes.** The amino acid sequences of MAGP1 and MAGP2 are listed, with *shaded rectangles* representing protein domains. Known functional regions are labeled. Amino acids are represented by *dots* to denote their position in the protein sequence. *Black*, acidic; *gray*, basic; *black*, cysteine; *black*, glutamine. Threonine residues predicted to undergo *O*-linked glycosylation are marked (⋆). *Black*, conserved from opossum to human; *white*, not conserved among species. *A*, MAGP2 protein translated from the WT mRNA sequence. *B*, predicted MAGP2 protein translated from the 2KO mRNA sequence. Splicing out exon 9 creates a frameshift that introduces an arginine followed by a premature stop (*asterisk*) codon after exon 8. *C*, illustration of mature MAGP1 protein. *D*, comparison of mature MAGP1 and MAGP2 protein sequences. Amino acids conserved between proteins are shaded *black*. The MAGP homology/matrix binding domain is represented by a *black line* over the protein sequences.

lacking exon 6 in one of four WT animals tested (supplemental Fig. S3 and Fig. 2*C*).

Because of a frameshift at the atypical exon 8–10 splice junction, there is a serine-to-arginine substitution and then a premature stop codon after domain 8 of the 2Δ9 transcript when translated (Fig. 3, *A* and *B*). Premature termination codons that occur upstream of an exon-exon junction frequently elicit nonsense-mediated decay, a RNA surveillance mechanism that degrades mutant transcripts (29). To determine whether nonsense-mediated decay affects the stability of the 2Δ9 transcript, RT-PCR was used to amplify 2Δ9 or WT mRNA isolated from the heart, lung, and kidney. After 27 cycles of PCR, there were only trace amounts of 2Δ9 PCR product compared with an abundant WT message in all three tissues (Fig. 4). These results indicate that little 2Δ9 mRNA escapes nonsense-mediated decay in 2KO animals. Similar results were found for MAGP1-MAGP2 double knockout animals (Fig. 4).

An antibody to MAGP2 was used to confirm loss of MAGP2 protein expression in 2KO and DKO animals. This antibody reacts specifically with MAGP2 protein and does not recognize MAGP1 (Fig. 5*A*). Immunohistochemistry on mouse aorta sections shows MAGP2 labeling in the intimal layer as well as throughout the adventitia (Fig. 5*B*). This expression pattern agrees with previous reports for MAGP2 expression in fetal calf aortic tissue and supports the specificity of the MAGP2 antibody (7). MAGP2-reactive bands are present in Western blot analyses using sequentially extracted lung tissue from WT mice, whereas 2KO and DKO lung tissue lacks MAGP2 protein (Fig. 5*C*). Also, WT and 2KO mouse lungs are positive for MAGP1, whereas DKO mice lack this protein (Fig. 5*D*). Taken together, these data demonstrate that the gene targeting strategy was successful in preventing MAGP2 protein expression in 2KO and DKO animals and that DKO animals lack both MAGP2 and MAGP1.

MAGP2 Deficiency Results in Decreased Levels of Circulating Neutrophils but Normal Monocyte Counts—2KO and DKO mice are viable and fertile with no gross abnormalities in appearance or behavior. This contrasts with 1KO mice, which have complex phenotypes, including hematopoietic defects, obesity, and abnormal bone homeostasis (13, 19, 20). To investigate whether 2KO mice have defects in hematopoiesis, antibody labeling and flow cytometry were used to assess the complement of hematopoietic cells in the peripheral blood circulation or in spleen tissue. An average of 3330 ± 672 white cells/ml of blood were collected. There was no statistical difference in total white blood cells per mouse among genotypes.

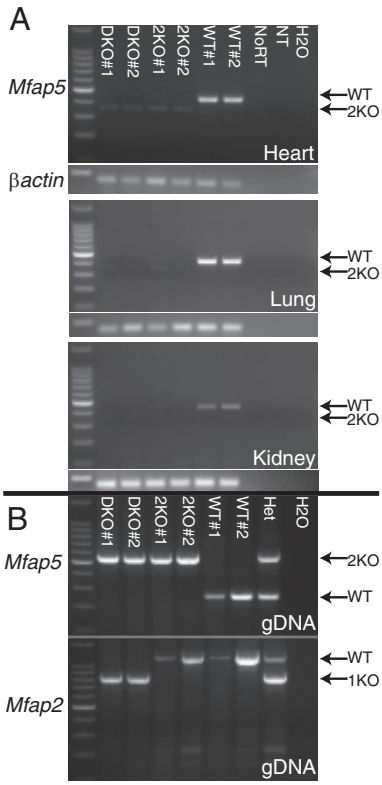

FIGURE 4. **Absence of MAGP2Δ9 mRNA confirms functional knockout of MAGP2.** A, polyadenylated mRNA from the heart, lung, and kidney of two DKO, 2KO, and WT animals each was reverse-transcribed and subjected to 27 rounds of PCR amplification with primers specific for the *Mfap5* message. *Arrows* indicate WT and 2Δ9 amplicons (2KO). Reactions with primers to *β-actin* were run in tandem as a loading control. *B*, PCR genotyping of genomic DNA from animals used in the assay. WT, 2KO, and 1KO amplicons are indicated by *arrows*. *NoRT*, no reverse transcriptase control; *NT*, no template for reverse transcription control; H_2O, no template for PCR control.

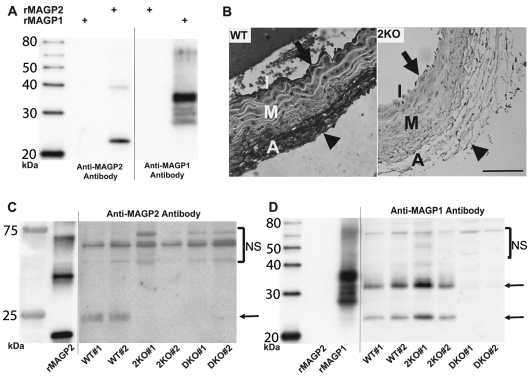

FIGURE 5. **2KO and DKO mice lack MAGP2 protein.** *A*, Western blot analyses showing that anti-MAGP2 and anti-MAGP1 antibodies are specific for their respective recombinant murine proteins (rMAGP2 and rMAGP1). *B*, immunohistochemistry on WT and 2KO sections demonstrates MAGP2 reactivity at the intima (*arrow*) and adventitia (*arrowhead*) of WT mouse aorta. No MAGP2 reactivity is seen in the 2KO aorta section. *Scale bar* = 100 μm. *C*, Western blotting of sequentially extracted (20 mM DTT fraction) mouse whole lung lysates with anti-MAGP2 antibody demonstrating the absence of MAGP2 protein in 2KO and DKO animal tissue. Two animals of each genotype were used, and an *arrow* indicates the MAGP2 protein band. Mammalian MAGP2 from tissue lysate runs as a larger protein than bacterially expressed rMAGP2 because of posttranslational modifications. *D*, Western blotting of sequentially extracted mouse whole lung lysates with anti-MAGP1 antibody demonstrating the absence of MAGP1 protein in DKO animals only. Two animals of each genotype were used, and *arrows* indicate MAGP1 protein bands. The major rMAGP1 band runs as a larger protein because of the His_6 tag. Tissue lysates were run with bacterially expressed rMAGP2 or His_6-tagged rMAGP1 and shown on the same blot. However, the recombinant protein section of the blot is shown at a shorter exposure interval, as indicated by a *black line*. Bands above the indicated MAGP proteins represent nonspecific antibody reactivity (*NS*). *I* = intima; *M* = media; *A* = adventitia.

Using GR1 positivity as an antibody marker, our results show that WT mice have neutrophil counts of 12.5% and 8.8% of total peripheral blood and spleen cells, respectively. Similarly, 1KO mice have neutrophil counts of 13.4% of total peripheral blood (data not shown). In contrast, 2KO mice have significantly decreased neutrophils (5.6% blood and 5.1% spleen) compared with age-matched WT controls (Fig. 6). Likewise, DKO mice also exhibit neutropenia, with 6.4% of total cells in peripheral blood and 5.7% in the spleen. These findings indicate that loss of MAGP2 causes a neutrophil deficiency in 2KO mice that is not seen in 1KO animals and is not altered by loss of MAGP1 in DKO animals.

We have shown that mice deficient in MAGP1 are monocytopenic with fewer circulating monocytes and fewer tissue macrophages.[3] 2KO mice, in contrast, have CD115+ monocyte numbers comparable with WT controls (4.5% *versus* 4.4% blood and 0.7% *versus* 0.8% spleen, respectively) (Fig. 6). DKO animals have reduced monocytes as a fraction of peripheral blood (3.6% blood and 0.7% spleen), as would be expected for 1KO animals. F4/80 antibody reactivity was used as a marker for macrophages in spleen tissue. 2KO and DKO mice had macrophage numbers comparable with WT controls. These data show that loss of MAGP2 does not impact monocyte number alone or in conjunction with loss of MAGP1. This demonstrates that both 1KO and 2KO mice have unique alterations in the myeloid cell lineage.

CD3 reactivity was used to assess lymphocytes in WT, 2KO, and DKO mice. All three genotypes have equivalent lymphocyte numbers as a percentage of peripheral blood (Fig. 6). Similar results were shown for 1KO animals.[3] Taken together, these data show that loss of MAGP2 causes neutropenia *in vivo* and demonstrate that this hematopoietic defect is MAGP1-independent. Further, loss of MAGP2 on a 1KO background does not impact the monocytopenia phenotype observed in 1KO animals. Thus, MAGP1 and MAGP2 have discrete functions in hematopoiesis.

Loss of MAGP2 Alone Does Not Significantly Alter Bone Mass or Architecture—Mice lacking MAGP1 are osteopenic by 6 months of age, with a high incidence of spontaneous fractures (13, 20). Spontaneous fractures are not observed in 2KO or DKO mice, and the skeleton appears grossly normal. μCT of left tibias in 6-month-old 2KO mice shows trabecular and cor-

[3] R. P. Mecham, unpublished results.

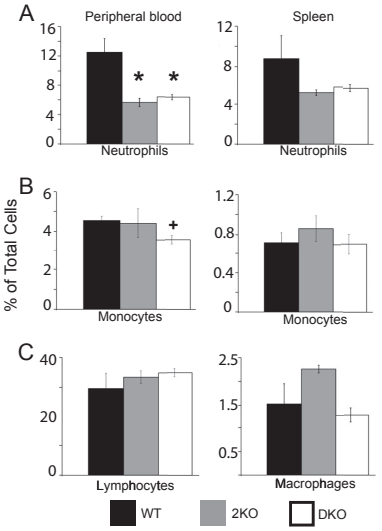

FIGURE 6. **2KO mice are neutropenic.** Flow cytometry was performed on peripheral blood and spleen cells collected from WT, 2KO, and DKO mice. *A*, GR1-positive neutrophil numbers were assessed, demonstrating that 2KO and DKO mice are significantly neutropenic. *B*, DKO animals have significantly fewer CD115-positive monocytes as a fraction of peripheral blood. *C*, histogram showing CD3-positive lymphocytes as a fraction of whole blood. *D*, histogram showing F4/80-positive macrophages as a fraction of total spleen cells. *, $p \leq 0.01$; +, $p \leq 0.02$. All data are independent of mouse age.

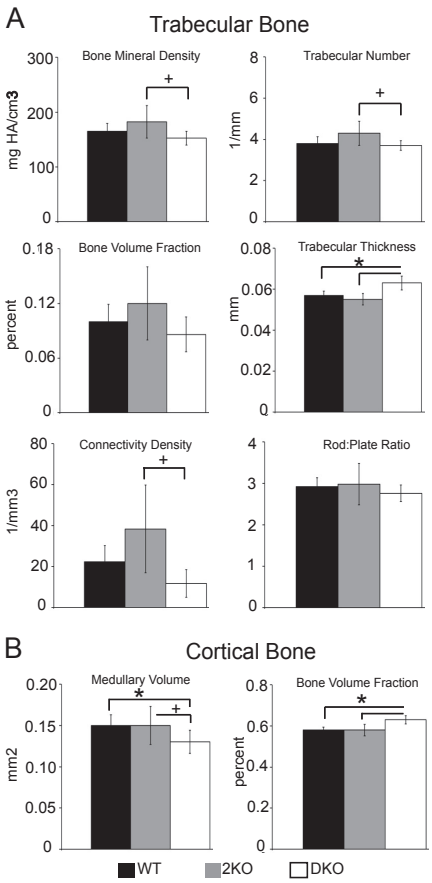

FIGURE 7. **Bone density and architecture are not significantly affected by loss of MAGP2.** μCT assessment of left tibias from 6-month-old WT, 2KO, and DKO mice. *A*, measurements of trabecular bone indicate no significant changes in 2KO trabecular bone compared with the WT. *B*, measurements of cortical bone indicate no changes in 2KO bone compared with the WT. A smaller marrow cavity (medullary area), associated with loss of MAGP1, persists in DKO mice, and this increases bone volume fraction in these animals. $n = 5$ (WT), 7 (2KO), and 5 (DKO) mice. *HA*, hydroxyapatite. *, $p \leq 0.01$; +, $p < 0.05$.

tical bone to be comparable in all aspects with age-matched WT controls (Fig. 7). Further, loss of MAGP2 on a 1KO background (DKO) does not exacerbate changes in bone mass and architecture associated with MAGP1 loss of function (Fig. 7). It is interesting to note that DKO mice share the abnormal cortical bone morphology of 1KO mice characterized by a smaller marrow cavity, or medullary area, than WT or 2KO mice and, therefore, have an increased bone volume fraction (Fig. 7*B*). These data demonstrate that loss of MAGP2 by itself has a minimal effect on bone character and suggest that, unlike MAGP1, MAGP2 has little or no role in normal bone homeostasis.

MAGP1 and MAGP2 Double-null (DKO) Mice Have a Larger Aorta at Physiological Pressures—In vitro studies suggest MAGP2 expression may be necessary for normal elastic fiber assembly (30). This idea is supported by the expression pattern of MAGP2 in elastin-rich structures such as the aorta, aortic root, atrialis of the mitral valve, bronchioles of the lung, large vessels of the heart, lung, and kidney, as well as skin (Figs. 8 and 5*B*) (7). Previous work determined that 1KO mice are normotensive with normal aortic and left carotid pressure outer diameter curves at 14 weeks of age (13). The cardiopulmonary system in 2KO, 1KO, and DKO mice appears grossly normal. These mice are normotensive with systolic, diastolic, and mean blood pressures comparable with age-matched WT animals (Fig. 9*A*). However, compliance studies show that the diameter of the ascending aorta in 6-month-old DKO mice is significantly increased compared with WT controls, 1KO, and 2KO mice at physiologic pressures of 75–125 millimeters of mercury (Fig. 9*B*). Pressure measurements of the outer diameter taken at 4 months of age indicate that the ascending aorta outer diameter is not significantly different from the WT at this time point (data not shown). These data show that, in DKO animals, the loss of MAGP1 and MAGP2 have a combinatorial effect in increasing the aorta outer diameter at physiologic pressures and that this change in tissue architecture becomes apparent with increasing age.

To determine whether changes in the outer diameter of aortic vessels could be explained by changes in heart size, heart weight to body weight ratios were calculated and found to be comparable among all genotypes (Fig. 9, *C* and *D*). Taken together, these data demonstrate that loss of both MAGP1 and MAGP2 expression increases aortic vessel diameter *in vivo*. These changes are age-dependent and not secondary to

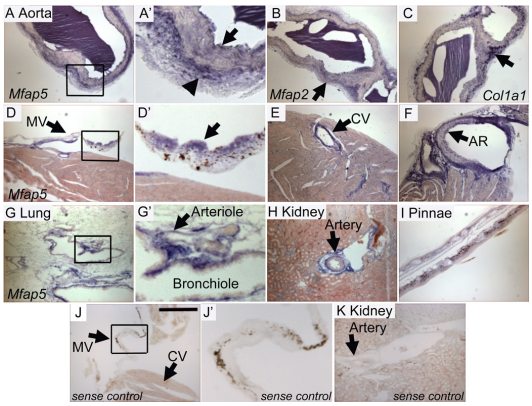

FIGURE 8. ***Mfap5* mRNA is expressed by cells of the aorta, mitral valve, coronary vessels, kidney, lung, and pinnae.** *In situ* hybridization to detect *Mfap5* (*A* and *D–I*), *Mfap2* (*B*), and *Col1a1* (*C*), expression was performed on 14-μm sections from 4-month-old wild-type mice. *A* and *A′*, *arrows* demonstrate digoxigenin-labeled mRNA (*blue*) localized to the intima (*arrow*) and adventitia (*arrowhead*) of the aorta. *A′* is a magnification of the boxed region in *A*. *B*, *Mfap2* mRNA is expressed throughout the aorta (*arrow*). *C*, *Col1a1* mRNA is heavily expressed in the aortic adventitia (*arrow*). *D* and *D′*, *Mfap5* is expressed in the atrialis of the mitral valve (*MV*, *arrow*). *E*, *Mfap5* mRNA is found in the coronary vessel (*CV*, *arrow*). *F*, significant *Mfap5* expression is localized to the aortic root (*AR*, *arrow*). *G* and *G′*, large airways and arterioles (*G′*, *arrow*) are positive for *Mfap5* expression. *H*, large vessels of the kidney express *Mfap5* (*arrow*). *J*, *J′*, and *K*, no nonspecific reactivity is detected in *Mfap5* sense control sections. *Scale bar* = 300 μm. Micrographs were taken using identical camera settings and image processing.

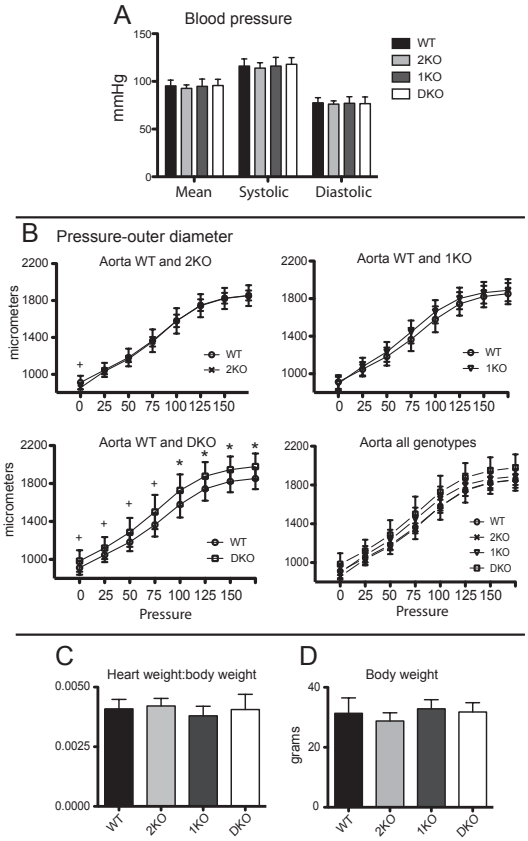

FIGURE 9. **The outer diameter of aortic vessels is increased at physiological pressures in DKO mice.** *A*, histogram of mean blood pressure measurements. *B*, pressure myography performed on aortae from 6-month-old male mice. A significant increase in aortic outer diameter at physiologic pressures is seen in DKO animals. *C*, graph indicating mean body weight of mice at the time of sacrifice. *D*, graph depicting mean heart weight to body weight ratios. *, $p \leq 0.01$; +, $p = 0.02$.

changes in body size, composition, or heart size. This suggests that MAGP1 and MAGP2 have shared primary functions in maintaining large vessel integrity.

MAGP2 Protein Binds Active TGFβ and BMP Growth Factors—MAGP1 has an acidic TGFβ-binding domain located in the N terminus of the protein, and loss of MAGP1 increases TGFβ signaling in multiple tissues (13, 19, 31). Although the amino-terminal sequences are different in MAGP1 and MAGP2, both regions are highly acidic (Fig. 3, *A*, *C*, and *D*), suggesting that MAGP2 may have the ability to bind TGFβ family ligands (8). Surface plasmon resonance and BLI were performed with immobilized MAGP2 and active TGFβ1, TGFβ2, or BMP2 in solution. TGFβ1, TGFβ2, and BMP2 bound reversibly to MAGP2 (Fig. 10, *A–C*). Steady-state analysis of BMP2 binding to bacterially expressed and refolded or native mammalian cell-secreted MAGP2 showed similar kinetics. The equilibrium dissociation constant (K_D) for BMP2 binding of refolded, bacterially expressed MAGP2 is 210 nM, whereas the K_D for binding to mammalian MAGP2 is 190 nM. These data demonstrate that MAGP2 binds active TGFβ superfamily members and suggests that these interactions may have biological relevance.

DISCUSSION

MAGP2 is a protein component of fibrillin-containing microfibrils where it partners with MAGP1 and other microfibril-associated proteins to define microfibril function (18). Mutations in fibrillin lead to Marfan syndrome, characterized by long bone overgrowth and abnormalities in the cardiovascular and pulmonary systems (3). It is interesting that none of those changes are evident in MAGP2-deficient mice. MAGP2 deficiency also shows little overlap with phenotypes found in mice lacking MAGP1, which supports unique functions for the individual proteins and agrees with the more limited distribution of MAGP2 compared with MAGP1.

Microfibrils serve to regulate growth factor availability, particularly the activity of TGFβ, BMP, and Notch family members (32–34). Because these growth factors are produced by and signal to many cell types, signaling must be tightly regulated. The fibrillins sequester the TGFβ large latent complex in the ECM, where it can be activated when needed. Mutations in fibrillin lead to elevated active TGFβ levels, which accounts for the phenotypes associated with Marfan syndrome. The role of MAGPs in growth factor signaling may be more complex in that they may function to sequester ligands from, or present them to, signaling receptors in a tissue-specific manner (33, 34).

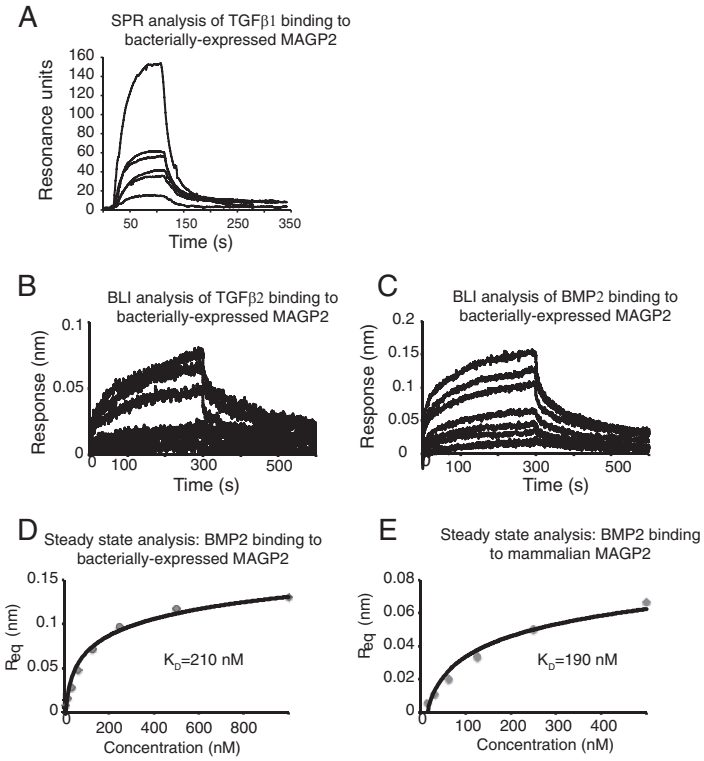

FIGURE 10. **MAGP2 binds active growth factor cytokines.** *A*, surface plasmon resonance was used to monitor real-time binding of immobilized, bacterially expressed, and refolded murine MAGP2 to active human TGFβ1 at concentrations of 100, 50, 50, 25, 25, and 12.5 nM. *B*, BLI was used to monitor real-time binding of immobilized murine MAGP2 to murine TGFβ2 at concentrations of 1000, 500, 250, 125, 62.5, 31.3, 15.6, and 7.8 nM. *C*, BLI was used to monitor real-time binding of immobilized refolded murine MAGP2 to murine BMP2 at concentrations of 1000, 500, 250, 125, 62.5, 31.3, 15.6, and 7.8 nM. *D*, equilibrium analysis of refolded MAGP2 binding BMP2 as measured by BLI. *E*, equilibrium analysis of natively secreted MAGP2 binding BMP2 as measured by BLI. Response units at equilibrium (R_{eq}) values from BLI data are plotted against cytokine concentration with a non-linear fit superimposed.

MAGP1 binds TGFβs, BMPs, and Notch receptors and ligands (13, 33). Much like the classical fibrillinopathies, MAGP1 loss of function leads to increased TGFβ signaling and subsequent disease in some tissues (4, 13, 19, 20). Like MAGP1, MAGP2 also binds TGFβ superfamily members as well as Notch receptors and ligands. This suggests that MAGP2 may regulate these growth factors *in vivo*. Interestingly, proper levels of Notch signaling are required for definitive hematopoiesis, whereas TGFβ and BMP are master regulators of hematopoietic stem cell quiescence and osteoblastic niche size, respectively (35–37). TGFβ signaling can differentially affect most hematopoietic stem cell types according to signal strength, signal localization, and differentiation state of the target cell (36). Thus, misregulation of Notch, TGFβ, or BMP signaling because of loss of MAGPs is consistent with alterations in cells of the myeloid lineage. Both MAGP1 and MAGP2 are expressed in trabecular bone, consistent with a potential role for these proteins in hematopoiesis (16). Differences in MAGP1 and MAGP2 expression patterns and growth factor binding affinities may explain the neutropenia in 2KO mice and monocytopenia in 1KO animals. Interestingly, loss of MAGP2 function does not modify the monocytopenia seen in MAGP1-deficient mice because DKO animals exhibit both neutropenia and reduced monocyte cell numbers.

In addition to influencing cells within the bone marrow, TGFβ/BMP signaling coordinates bone anabolism (via osteoblast activation) with bone catabolism (via differentiation of osteoclasts from hematopoietic stem cell precursors) (38–41). MAGP1-deficient mice develop osteopenia with age because of increased osteoclast number (20). A study of these animals revealed increased circulating levels of the osteoclast differentiation factor receptor activator of NFκB ligand (RANKL) (19). Treatment of cultured MAGP1-deficient osteoblasts with TGFβ neutralizing antibodies reduced RANKL production by these cells to base-line levels, suggesting increased TGFβ signaling because of loss of MAGP1 function as the primary defect in bone homeostasis. The studies detailed here indicate that, unlike MAGP1, loss of MAGP2 function does not negatively affect bone mineral density. Furthermore, DKO mice do not develop spontaneous fractures and lack severe osteopenia associated with MAGP1 deficiency. This suggests that loss of MAGP2 in tandem with loss of MAGP1 restores bone mineral density.

MAGP2 Loss of Function Has Pleiotropic Effects in Vivo

An explanation for why loss of MAGP2 is protective against bone loss may lie in the ability of MAGP2 to manipulate Notch signaling. MAGP1 and MAGP2 both have the ability to bind Notch1, Jagged1, Jagged2, and Delta1 (33). Both proteins mediate ectodomain shedding of Notch1 and activate the Notch intracellular domain. MAGP2, however, has the added ability to activate Notch signaling through release of Jagged1 from the cell surface (42). The activated Notch intracellular domain inhibits osteoclast differentiation both from hematopoietic precursors and from preosteoclasts (43). Jagged1/Notch intracellular domain signaling also impedes osteoclast formation by inhibiting RANKL expression in mature osteoblasts (43). Inhibition of Notch signaling in the context of bone formation increases osteoblast differentiation, thereby increasing bone formation (43). The studies detailed here indicate that loss of MAGP2 alone has a slight net anabolic effect on bone mass. Thus, changes in Notch signaling associated with MAGP2 deficiency may provide a mechanistic explanation for why MAGP1-induced increases in osteoclastogenesis are not as prominent in DKO animals.

Previous work demonstrates that fibrillin-1 deficiency leads to increased aortic diameter pressure curves, hypotension, fragmentation of elastin, and changes in aortic compliance that becomes apparent with age (44, 45). Our findings also show increases in aortic diameter pressure curves in 6-month-old MAGP DKO mice but not in the single knockouts. As with the fibrillinopathies, changes in large vessel architecture and function in DKO animals may occur because of several contributing factors. Firstly, changes in MAGP expression may cause developmental changes in ECM architecture that become more apparent with age. This idea is supported by studies in zebrafish, where loss of MAGP1 causes distension and loss of vessel integrity in cranial and caudal blood vessels during development (46, 47). Secondly, ECM remodeling and homeostasis may be altered by loss of MAGPs. Increased TGFβ signaling in aortic tissue occurs with loss of growth factor binding by microfibril proteins (3, 44, 48). This leads to extensive pathological remodeling, loss of vessel integrity, and, ultimately, aortic dissection in mice and humans *in vivo* (3, 48, 49). Loss of MAGP results in a similar, albeit blunted pattern of pathologic remodeling, leading to loss of vessel integrity but not aortic dissection. Because MAGPs are highly expressed in large vessels and bind active TGFβ ligands, it is possible that loss of MAGPs causes small changes in TGFβ signaling that, over time, produce a fibrillinopathy-like phenotype in large vessels (7, 13).

An Arg-Gly-Asp (RGD)-containing sequence in fibrillin-1, when applied to cells, was found to increase the expression of matrix metalloproteinases 1 and 3 (50). Increased proteolytic activity by matrix metalloproteinases is a characteristic feature of fibrillinopathies such as Marfan syndrome (51). MAGP2 also contains an RGD sequence that binds $\alpha v\beta 3$ integrins, although the function of this domain in MAGP2 is not understood (52). Because RGD-containing sequences can be important regulators of proteolytic activity, cell adhesion, and growth factor presentation to cells, one must consider mutations in fibrillins or MAGPs that impair MAGP-fibrillin interaction as potentially important. As stated previously, MAGPs covalently bind fibrillins on the microfibril. Disease-causing mutations in fibrillin-1 in mice are associated with increases in MAGP2 expression *in vivo*, suggesting a regulatory link between these microfibrillar proteins (24, 53, 54). Increased gene expression and/or mutations in MAGPs or fibrillins may result in unbound MAGPs in the ECM with unknown effects on growth factor signaling and matrix metalloproteinases expression. When taken together, these data demonstrate that loss of MAGPs shares pathological features of fibrillinopathies and raise the question as to how much of the pathology attributed to loss of fibrillin function is directly linked to loss of MAGP-fibrillin interaction and subsequent MAGP-dependent ECM changes.

Interestingly, MAGP2 expression is negatively correlated with patient survival from advanced-stage ovarian cancer (55). Mok *et al.* (55) suggest that MAGP2-dependent changes in cancer cell biology may be conferred via multiple mechanisms. The authors correlate MAGP2-mediated $\alpha v\beta 3$ integrin interaction with chemotherapy resistance and cell survival (55). Also integral to tumor survival is development of a blood supply through angiogenesis. MAGP2 negatively regulates Notch signaling in endothelial tip cells and promotes angiogenic sprouting, potentially providing another mechanism for MAGP2-mediated tumor growth and survival (34). Previous studies demonstrate a high metastatic potential in human melanoma cell clones with expression of peanut agglutinin-reactive glycosylation on MAGP1 and MAGP2 (56). Analysis of MAGP proteins with the NetOGlyc server demonstrates two highly conserved and one non-conserved predicted *O*-linked glycosylation site in the N terminus of MAGP1 (12). MAGP2 has five highly conserved and one non-conserved *O*-linked carbohydrate site, all within the amino-terminal portion of the molecule (Fig. 3*B*). Additional glycosylation domains on MAGP2 suggest evolutionary acquisition of unique protein-protein interactions. It is currently known that protein glycosylation patterns change in the context of cancer, with the net effect of altering cell signaling and nutrient availability (57, 58). Moreover, MAGP2 physically interacts with active TGFβs, BMPs, and Notch receptors and ligands. It is not difficult to imagine that MAGP2 expression may allow transformed cells to harness several powerful mechanisms to promote tumor growth, metastasis, and chemotherapy resistance. Research directed at uncovering the molecular mechanisms by which MAGP2 promotes tumor growth and metastasis is clinically important.

These studies demonstrate that MAGP2 plays a role in the biology of the hematopoietic and vascular systems and suggest that MAGP2 is capable of regulating growth factor bioavailability. Work by other authors also links MAGP2 expression status to cancer outcome (34). Clearly, further understanding of MAGP2 function not only increases our understanding of ECM biology but has the potential to significantly impact human health.

Acknowledgments—We thank Megan Curtis and Chris Ciliberto for technical assistance, Fernando Segade for helpful discussion, Terese Hall for administrative support, and the Washington University Musculoskeletal and Morphology Cores for assistance with specimen analysis.

REFERENCES

1. Mecham, R. P. (2011) *The Extracellular Matrix. An Overview.* Springer-Verlag, Berlin
2. Jensen, S. A., Robertson, I. B., and Handford, P. A. (2012) Dissecting the fibrillin microfibril. Structural insights into organization and function. *Structure* **20,** 215–225
3. Kielty, C. M. (2006) Elastic fibres in health and disease. *Expert Rev. Mol. Med.* **8,** 1–23
4. Ramirez, F., and Sakai, L. Y. (2010) Biogenesis and function of fibrillin assemblies. *Cell Tissue Res.* **339,** 71–82
5. Yanagisawa, H., and Davis, E. C. (2010) Unraveling the mechanism of elastic fiber assembly. The roles of short fibulins. *Int. J. Biochem. Cell Biol.* **42,** 1084–1093
6. Gibson, M. A., Hughes, J. L., Fanning, J. C., and Cleary, E. G. (1986) The major antigen of elastin-associated microfibrils is a 31-kDa glycoprotein. *J. Biol. Chem.* **261,** 11429–11436
7. Gibson, M. A., Finnis, M. L., Kumaratilake, J. S., and Cleary, E. G. (1998) Microfibril-associated glycoprotein-2 (MAGP-2) is specifically associated with fibrillin-containing microfibrils but exhibits more restricted patterns of tissue localization and developmental expression than its structural relative MAGP-1. *J. Histochem. Cytochem.* **46,** 871–886
8. Segade, F. (2009) Functional evolution of the microfibril-associated glycoproteins. *Gene* **439,** 43–54
9. Segade, F., Trask, B. C., Broekelmann, T. J., Pierce, R. A., and Mecham, R. P. (2002) Identification of a matrix-binding domain in MAGP1 and MAGP2 and intracellular localization of alternative splice forms. *J. Biol. Chem.* **277,** 11050–11057
10. Hatzinikolas, G., and Gibson, M. A. (1998) The exon structure of the human MAGP-2 gene. *J. Biol. Chem.* **273,** 29309–29314
11. Donovan, L. J., Cha, S. E., Yale, A. R., Dreikorn, S., and Miyamoto, A. (2013) Identification of a functional proprotein convertase cleavage site in microfibril-associated glycoprotein 2. *Matrix Biol.* **32,** 117–122
12. Trask, B. C., Broekelmann, T., Ritty, T. M., Trask, T. M., Tisdale, C., and Mecham, R. P. (2001) Post-translational modifications of microfibril associated glycoprotein-1 (MAGP-1). *Biochemistry* **40,** 4372–4380
13. Weinbaum, J. S., Broekelmann, T. J., Pierce, R. A., Werneck, C. C., Segade, F., Craft, C. S., Knutsen, R. H., and Mecham, R. P. (2008) Deficiency in microfibril-associated glycoprotein-1 leads to complex phenotypes in multiple organ systems. *J. Biol. Chem.* **283,** 25533–25543
14. Davis, E. C. (1994) Immunolocalization of microfibril and microfibril-associated proteins in the subendothelial matrix of the developing mouse aorta. *J. Cell Sci.* **107,** 727–736
15. Henderson, M., Polewski, R., Fanning, J. C., and Gibson, M. A. (1996) Microfibril-associated glycoprotein-1 (MAGP-1) is specifically located on the beads of the beaded-filament structure of fibrillin-containing microfibrils as visualized by the rotary shadowing technique. *J. Histochem. Cytochem.* **44,** 1389–1397
16. Kumaratilake, J. S., Gibson, M. A., Fanning, J. C., and Cleary, E. G. (1989) The tissue distribution of microfibrils reacting with a monospecific antibody to MAGP, the major glycoprotein antigen of elastin-associated microfibrils. *Eur. J. Cell Biol.* **50,** 117–127
17. Visel, A., Thaller, C., and Eichele, G. (2004) GenePaint.org. An atlas of gene expression patterns in the mouse embryo. *Nucleic Acids Res.* **32,** D552–556
18. Gibson, M. A., Hatzinikolas, G., Kumaratilake, J. S., Sandberg, L. B., Nicholl, J. K., Sutherland, G. R., and Cleary, E. G. (1996) Further characterization of proteins associated with elastic fiber microfibrils including the molecular cloning of MAGP-2 (MP25). *J. Biol. Chem.* **271,** 1096–1103
19. Craft, C. S., Broekelmann, T. J., Zou, W., Chappel, J. C., Teitelbaum, S. L., and Mecham, R. P. (2012) Oophorectomy-induced bone loss is attenuated in MAGP1-deficient mice. *J. Cell. Biochem.* **113,** 93–99
20. Craft, C. S., Zou, W., Watkins, M., Grimston, S., Brodt, M. D., Broekelmann, T. J., Weinbaum, J. S., Teitelbaum, S. L., Pierce, R. A., Civitelli, R., Silva, M. J., and Mecham, R. P. (2010) Microfibril-associated glycoprotein-1, an extracellular matrix regulator of bone remodeling. *J. Biol. Chem.* **285,** 23858–23867
21. Ehrman, L. A., and Yutzey, K. E. (1999) Lack of regulation in the heart forming region of avian embryos. *Dev. Biol.* **207,** 163–175
22. Lincoln, J., Alfieri, C. M., and Yutzey, K. E. (2006) BMP and FGF regulatory pathways control cell lineage diversification of heart valve precursor cells. *Dev. Biol.* **292,** 292–302
23. Shelton, E. L., and Yutzey, K. E. (2007) Tbx20 regulation of endocardial cushion cell proliferation and extracellular matrix gene expression. *Dev. Biol.* **302,** 376–388
24. Lemaire, R., Farina, G., Kissin, E., Shipley, J. M., Bona, C., Korn, J. H., and Lafyatis, R. (2004) Mutant fibrillin 1 from tight skin mice increases extracellular matrix incorporation of microfibril-associated glycoprotein 2 and type I collagen. *Arthritis Rheum.* **50,** 915–926
25. Faury, G., Pezet, M., Knutsen, R. H., Boyle, W. A., Heximer, S. P., McLean, S. E., Minkes, R. K., Blumer, K. J., Kovacs, A., Kelly, D. P., Li, D. Y., Starcher, B., and Mecham, R. P. (2003) Developmental adaptation of the mouse cardiovascular system to elastin haploinsufficiency. *J. Clin. Invest.* **112,** 1419–1428
26. Wagenseil, J. E., Nerurkar, N. L., Knutsen, R. H., Okamoto, R. J., Li, D. Y., and Mecham, R. P. (2005) Effects of elastin haploinsufficiency on the mechanical behavior of mouse arteries. *Am. J. Physiol. Heart Circ. Physiol.* **289,** H1209–1217
27. Swiecki, M., Scheaffer, S. M., Allaire, M., Fremont, D. H., Colonna, M., and Brett, T. J. (2011) Structural and biophysical analysis of BST-2/tetherin ectodomains reveals an evolutionary conserved design to inhibit virus release. *J. Biol. Chem.* **286,** 2987–2997
28. Aricescu, A. R., Lu, W., and Jones, E. Y. (2006) A time- and cost-efficient system for high-level protein production in mammalian cells. *Acta Crystallogr. D. Biol. Crystallogr.* **62,** 1243–1250
29. Maquat, L. E. (2004) Nonsense-mediated mRNA decay. Splicing, translation and mRNP dynamics. *Nat. Rev. Mol. Cell Biol.* **5,** 89–99
30. Lemaire, R., Bayle, J., Mecham, R. P., and Lafyatis, R. (2007) Microfibril-associated MAGP-2 stimulates elastic fiber assembly. *J. Biol. Chem.* **282,** 800–808
31. Massam-Wu, T., Chiu, M., Choudhury, R., Chaudhry, S. S., Baldwin, A. K., McGovern, A., Baldock, C., Shuttleworth, C. A., and Kielty, C. M. (2010) Assembly of fibrillin microfibrils governs extracellular deposition of latent TGF β. *J. Cell Sci.* **123,** 3006–3018
32. Ramirez, F., Sakai, L. Y., Rifkin, D. B., and Dietz, H. C. (2007) Extracellular microfibrils in development and disease. *Cell Mol. Life Sci.* **64,** 2437–2446
33. Miyamoto, A., Lau, R., Hein, P. W., Shipley, J. M., and Weinmaster, G. (2006) Microfibrillar proteins MAGP-1 and MAGP-2 induce Notch1 extracellular domain dissociation and receptor activation. *J. Biol. Chem.* **281,** 10089–10097
34. Albig, A. R., Becenti, D. J., Roy, T. G., and Schiemann, W. P. (2008) Microfibril-associate glycoprotein-2 (MAGP-2) promotes angiogenic cell sprouting by blocking notch signaling in endothelial cells. *Microvasc. Res.* **76,** 7–14
35. Bigas, A., and Espinosa, L. (2012) Hematopoietic stem cells. To be or Notch to be. *Blood* **119,** 3226–3235
36. Blank, U., and Karlsson, S. (2011) The role of Smad signaling in hematopoiesis and translational hematology. *Leukemia* **25,** 1379–1388
37. Munger, J. S., and Sheppard, D. (2011) Cross talk among TGF-β signaling pathways, integrins, and the extracellular matrix. *Cold Spring Harb. Perspect. Biol.* **3,** a005017
38. Chen, G., Deng, C., and Li, Y. P. (2012) TGF-β and BMP signaling in osteoblast differentiation and bone formation. *Int. J. Biol. Sci.* **8,** 272–288
39. Nistala, H., Lee-Arteaga, S., Carta, L., Cook, J. R., Smaldone, S., Siciliano, G., Rifkin, A. N., Dietz, H. C., Rifkin, D. B., and Ramirez, F. (2010) Differential effects of alendronate and losartan therapy on osteopenia and aortic aneurysm in mice with severe Marfan syndrome. *Hum. Mol. Genet.* **19,** 4790–4798
40. Nistala, H., Lee-Arteaga, S., Smaldone, S., Siciliano, G., Carta, L., Ono, R. N., Sengle, G., Arteaga-Solis, E., Levasseur, R., Ducy, P., Sakai, L. Y., Karsenty, G., and Ramirez, F. (2010) Fibrillin-1 and -2 differentially modulate endogenous TGF-β and BMP bioavailability during bone formation. *J. Cell Biol.* **190,** 1107–1121
41. Nistala, H., Lee-Arteaga, S., Smaldone, S., Siciliano, G., and Ramirez, F. (2010) Extracellular microfibrils control osteoblast-supported osteoclastogenesis by restricting TGFβ stimulation of RANKL production. *J. Biol.*

Chem. **285,** 34126–34133
42. Nehring, L. C., Miyamoto, A., Hein, P. W., Weinmaster, G., and Shipley, J. M. (2005) The extracellular matrix protein MAGP-2 interacts with Jagged1 and induces its shedding from the cell surface. *J. Biol. Chem.* **280,** 20349–20355
43. Mead, T. J., and Yutzey, K. E. (2012) Notch signaling and the developing skeleton. *Adv. Exp. Med. Biol.* **727,** 114–130
44. Mariko, B., Pezet, M., Escoubet, B., Bouillot, S., Andrieu, J. P., Starcher, B., Quaglino, D., Jacob, M. P., Huber, P., Ramirez, F., and Faury, G. (2011) Fibrillin-1 genetic deficiency leads to pathological ageing of arteries in mice. *J. Pathol.* **224,** 33–44
45. Carta, L., Wagenseil, J. E., Knutsen, R. H., Mariko, B., Faury, G., Davis, E. C., Starcher, B., Mecham, R. P., and Ramirez, F. (2009) Discrete contributions of elastic fiber components to arterial development and mechanical compliance. *Arterioscler. Thromb. Vasc. Biol.* **29,** 2083–2089
46. Alvarez, Y., Cederlund, M. L., Cottell, D. C., Bill, B. R., Ekker, S. C., Torres-Vazquez, J., Weinstein, B. M., Hyde, D. R., Vihtelic, T. S., and Kennedy, B. N. (2007) Genetic determinants of hyaloid and retinal vasculature in zebrafish. *BMC Dev. Biol.* **7,** 114
47. Chen, E., Larson, J. D., and Ekker, S. C. (2006) Functional analysis of zebrafish microfibril-associated glycoprotein-1 (Magp1) *in vivo* reveals roles for microfibrils in vascular development and function. *Blood* **107,** 4364–4374
48. Habashi, J. P., Judge, D. P., Holm, T. M., Cohn, R. D., Loeys, B. L., Cooper, T. K., Myers, L., Klein, E. C., Liu, G., Calvi, C., Podowski, M., Neptune, E. R., Halushka, M. K., Bedja, D., Gabrielson, K., Rifkin, D. B., Carta, L., Ramirez, F., Huso, D. L., and Dietz, H. C. (2006) Losartan, an AT1 antagonist, prevents aortic aneurysm in a mouse model of Marfan syndrome. *Science* **312,** 117–121
49. Ramirez, F., and Dietz, H. C. (2004) Therapy insight. Aortic aneurysm and dissection in Marfan's syndrome. *Nat. Clin. Pract. Cardiovasc. Med.* **1,** 31–36
50. Booms, P., Pregla, R., Ney, A., Barthel, F., Reinhardt, D. P., Pletschacher, A., Mundlos, S., and Robinson, P. N. (2005) RGD-containing fibrillin-1 fragments upregulate matrix metalloproteinase expression in cell culture. A potential factor in the pathogenesis of the Marfan syndrome. *Hum. Genet.* **116,** 51–61
51. Xiong, W., Meisinger, T., Knispel, R., Worth, J. M., and Baxter, B. T. (2012) MMP-2 regulates Erk1/2 phosphorylation and aortic dilatation in Marfan syndrome. *Circ. Res.* **110,** e92-e101
52. Gibson, M. A., Leavesley, D. I., and Ashman, L. K. (1999) Microfibril-associated glycoprotein-2 specifically interacts with a range of bovine and human cell types via $\alpha V\beta 3$ integrin. *J. Biol. Chem.* **274,** 13060–13065
53. Ito, S., Bartolák-Suki, E., Shipley, J. M., Parameswaran, H., Majumdar, A., and Suki, B. (2006) Early emphysema in the tight skin and pallid mice. Roles of microfibril-associated glycoproteins, collagen, and mechanical forces. *Am. J. Respir. Cell Mol. Biol.* **34,** 688–694
54. Lemaire, R., Korn, J. H., Shipley, J. M., and Lafyatis, R. (2005) Increased expression of type I collagen induced by microfibril-associated glycoprotein 2. Novel mechanistic insights into the molecular basis of dermal fibrosis in scleroderma. *Arthritis Rheum.* **52,** 1812–1823
55. Mok, S. C., Bonome, T., Vathipadiekal, V., Bell, A., Johnson, M. E., Wong, K. K., Park, D. C., Hao, K., Yip, D. K., Donninger, H., Ozbun, L., Samimi, G., Brady, J., Randonovich, M., Pise-Masison, C. A., Barrett, J. C., Wong, W. H., Welch, W. R., Berkowitz, R. S., and Birrer, M. J. (2009) A gene signature predictive for outcome in advanced ovarian cancer identifies a survival factor. Microfibril-associated glycoprotein 2. *Cancer Cell* **16,** 521–532
56. Zebda, N., Bailly, M., Brown, S., Doré, J. F., and Berthier-Vergnes, O. (1994) Expression of PNA-binding sites on specific glycoproteins by human melanoma cells is associated with a high metastatic potential. *J. Cell. Biochem.* **54,** 161–173
57. Hanover, J. A., Krause, M. W., and Love, D. C. (2012) Bittersweet memories. Linking metabolism to epigenetics through *O*-GlcNAcylation. *Nat. Rev. Mol. Cell Biol.* **13,** 312–321
58. Hart, G. W., Slawson, C., Ramirez-Correa, G., and Lagerlof, O. (2011) Cross talk between *O*-GlcNAcylation and phosphorylation. Roles in signaling, transcription, and chronic disease. *Annu. Rev. Biochem.* **80,** 825–858

TREM-2 promotes macrophage survival and lung disease after respiratory viral infection

Kangyun Wu,[1] Derek E. Byers,[1] Xiaohua Jin,[1] Eugene Agapov,[1] Jennifer Alexander-Brett,[1] Anand C. Patel,[1,2] Marina Cella,[3] Susan Gilfilan,[3] Marco Colonna,[3] Daniel L. Kober,[1] Tom J. Brett,[1,4,5] and Michael J. Holtzman[1,5]

[1]Pulmonary and Critical Care Medicine, Department of Medicine, [2]Department of Pediatrics, [3]Department of Pathology and Immunology, [4]Department of Biochemistry and Biophysics, and [5]Department of Cell Biology, Washington University School of Medicine, St. Louis, MO 63110

Viral infections and type 2 immune responses are thought to be critical for the development of chronic respiratory disease, but the link between these events needs to be better defined. Here, we study a mouse model in which infection with a mouse parainfluenza virus known as Sendai virus (SeV) leads to long-term activation of innate immune cells that drive IL-13–dependent lung disease. We find that chronic postviral disease (signified by formation of excess airway mucus and accumulation of M2-differentiating lung macrophages) requires macrophage expression of triggering receptor expressed on myeloid cells-2 (TREM-2). Analysis of mechanism shows that viral replication increases lung macrophage levels of intracellular and cell surface TREM-2, and this action prevents macrophage apoptosis that would otherwise occur during the acute illness (5–12 d after inoculation). However, the largest increases in TREM-2 levels are found as the soluble form (sTREM-2) long after clearance of infection (49 d after inoculation). At this time, IL-13 and the adapter protein DAP12 promote TREM-2 cleavage to sTREM-2 that is unexpectedly active in preventing macrophage apoptosis. The results thereby define an unprecedented mechanism for a feed-forward expansion of lung macrophages (with IL-13 production and consequent M2 differentiation) that further explains how acute infection leads to chronic inflammatory disease.

CORRESPONDENCE
Michael J. Holtzman:
holtzmanm@wustl.edu

Abbreviations used: APEC, airway progenitor epithelial cell; Arg1, arginase 1; Chi3l3, chitinase 3–like-3; COPD, chronic obstructive pulmonary disease; DAP12, DNAX activation protein of 12 kD; dpi, days post-inoculation; EpCAM, epithelial cell adhesion molecule; ERK, extracellular signal-regulated kinase; FSC, forward scatter; iNKT cell, invariant NK T cell; MUC5AC, mucin 5AC; Op, osteopetrotic; PKR, protein kinase R; SeV, Sendai virus; SSC, side scatter; sTREM-2, soluble TREM 2; TREM, triggering receptor expressed on myeloid cells.

A critical step toward improved diagnosis and treatment of chronic inflammatory diseases depends on defining the immune mechanisms for the persistent accumulation of activated immune cells in the target tissue. In the case of the lung, clinical evidence suggests that acute infection with a respiratory virus might lead to chronic lung diseases such as asthma and COPD (Holtzman, 2012). To determine precisely how acute infection causes chronic lung disease, we developed a high-fidelity mouse model of this process. In this model, mouse parainfluenza virus (also known as Sendai virus, SeV) is substituted for the related human pathogen to achieve more efficient viral replication and thereby produce the severe acute illness and subsequent chronic respiratory disease that is typical of the pathology found in humans (Walter et al., 2002). Using this model system, we determined that postviral lung disease depends on airway progenitor epithelial cell (APEC) production of IL-33 to drive invariant NK T cells (iNKT cells) and lung macrophages toward IL-13 production (Kim et al., 2008; Byers et al., 2013). The result is IL-13–dependent inflammation (signified by type 2 activation and accumulation of lung macrophages) and airway mucus production (signified by *MUC5AC* mucin gene expression). This innate epithelial to immune cell loop also appears relevant to human disease because increased numbers of IL-33–expressing APECs are found in association with an IL-13 gene expression signature (including increased MUC5AC mRNA and protein) in the lungs of humans with severe chronic obstructive pulmonary disease (COPD; Kim et al., 2008; Agapov et al., 2009; Alevy et al., 2012; Byers et al., 2013).

In our previous work, we recognized that the APEC population was capable of self-renewal

The Rockefeller University Press $30.00
J. Exp. Med. 2015 Vol. 212 No. 5 681–697
www.jem.org/cgi/doi/10.1084/jem.20141732

The Journal of Experimental Medicine

and inducible release of IL-33 to sustain ongoing activation of the innate immune system (Holtzman et al., 2014). However, the existing data did not explain the selective activation of the lung macrophage population and the special dominance of type 2 (M2) macrophages as a downstream part of the disease process. In the present study, we therefore aimed to better understand how the lung macrophage component of this disease process is triggered by acute infection and then is manifest for months. We reasoned that triggering receptor expressed on myeloid cells 2 (TREM-2) might contribute to this process because M2 polarization is associated with TREM-2 expression in isolated macrophages (Turnbull et al., 2006). In pursuing this possibility, we found that the soluble form of TREM-2 (sTREM-2) was linked to the development of chronic postviral lung disease and was active in promoting macrophage survival. The data stand in contrast to the conventional view that cleavage of cell surface TREM-2 to sTREM-2 results in an inactive end product. The results thereby provide for a previously unrecognized control over macrophage survival and a consequent type 2 immune response that can serve both as a pathogenic mechanism and as a therapeutic target and accompanying biomarker for chronic inflammatory disease.

RESULTS

Macrophage control of postviral disease

To further define the role of macrophages in our postviral mouse model of chronic lung disease (Walter et al., 2002), we first assessed the impact of a new strategy for macrophage deficiency. We previously showed that mice that were treated with clodronate or mice that were homozygous for the *op* mutation in the *Csf1* gene (*Csf1*$^{op/op}$) led to marked macrophage depletion and blockade of postviral lung disease, but both pharmacologic and genetic approaches to depletion led to mice that were also more susceptible to viral infection (Tyner et al., 2005; Kim et al., 2008). In the present case, we started with *Csf1*$^{op/opT}$ (*op/opT*) mice, which carry an osteocalcin-driven *Csf1* transgene (*T*) that rescues the osteopetrotic, but not the macrophage defect, in *op/op* mice (Abboud et al., 2002). We then used these mice to generate heterozygous *Csf1*$^{wt/opT}$ (*wt/opT*) mice with a subtler defect in macrophage level and perhaps function. Of note, we still found that the increase in lung levels of tissue monocytes (SSC^{low}Ly6G^{-}F4/80^{+}CD11b^{+}) and interstitial macrophages (SSC^{high}CD11c^{-}Ly6G^{-}Siglec-F^{-}F4/80^{+}CD11b^{+}) that occurs in WT (*wt/wt*) mice at 5 d post-inoculation (dpi) with Sendai virus (SeV) was significantly attenuated in *wt/opT* mice (Fig. 1 A and Fig. S1). We observed no increase (and instead found a significant decrease) in alveolar macrophages (SSC^{high}CD11c^{+}Ly6G^{-}Siglec-F^{+}F4/80^{+}CD11b^{-}) in *wt/wt* and *wt/opT* mice at 5 dpi, reflecting a predominant effect of Csf1 deficiency on tissue monocytes and interstitial macrophages during acute infection. Despite these differences in lung monocyte–macrophage levels, we found the same degree of acute illness (0–12 dpi) as signified by essentially identical body weight changes, viral titers, and pattern of tissue inflammation in *wt/wt* and *wt/opT* mice (not depicted).

In contrast to the similarities in acute illness in *wt/wt* and *wt/opT* mice, we found marked differences in the development of chronic lung disease that develops after clearance of infectious virus and is fully manifest at 49 dpi (Walter et al., 2002; Kim et al., 2008; Byers et al., 2013). Under these chronic conditions, we observed that the increases in each lung monocyte–macrophage population at 49 dpi in *wt/wt* mice were all markedly attenuated in *wt/opT* mice (Fig. 1 B). Tissue monocytes, which were the most abundant monocyte–macrophage population in the lung, exhibited no increase in *wt/opT* mice at 49 dpi. In concert with the decreased lung monocyte–macrophage levels in *wt/opT* mice, we also found that induction of IL-13 expression and mucous cell metaplasia in *wt/wt* mice was markedly inhibited in *wt/opT* mice at 49 dpi (Fig. 1 C). Similarly, the postviral increases in lung levels of *Il13* mRNA and downstream *Muc5ac* mRNA and type 2 macrophage (M2) markers *Arg1* and *Chitinase 3–like-3 (Chi3l3)* mRNA in *wt/wt* mice were completely blocked in *wt/opT* mice at 49 dpi (Fig. 1 D). These findings are consistent with our previous work showing that lung macrophages are critical for IL-13 production, and in turn, that IL-13 is required to drive mucus production and M2 differentiation in our postviral mouse model of lung disease (Tyner et al., 2006; Kim et al., 2008; Byers et al., 2013). The results also provide a basis for next determining what factors might regulate the expansion of disease-producing lung macrophages under these conditions.

TREM-2 control of postviral disease

Based on the association of TREM-2 with M2 differentiation (Turnbull et al., 2006), we investigated the role of TREM-2 in macrophage-dependent postviral lung disease. In that context, we found that the development of this type of lung disease was associated with increased lung *Trem2* (but not other *Trem*) mRNA levels based on gene expression microarray and real-time qPCR assay (Fig. 2, A and B; and Table S1). Moreover, the development of postviral lung disease at 49 dpi in WT mice was markedly attenuated in *Trem2*$^{-/-}$ mice. Thus, *Trem2*$^{-/-}$ mice showed marked decreases in lung inflammation and airway mucus production based on tissue staining (Fig. 2 C) as well as significantly decreased lung levels of the key cytokine *Il13* mRNA, the predominant mucin *Muc5ac* mRNA, and the M2 markers *Arg1* and *Chi3l3* mRNA based on real-time qPCR assay (Fig. 2 D). *Dap12*$^{-/-}$ mice exhibited a similar inhibition of postviral disease (Fig. 2, C and D), consistent with the association of TREM-2 and DAP12 phenotype in other systems (Bouchon et al., 2000; Kaifu et al., 2003; Turnbull et al., 2006). In contrast, *Trem1/3*$^{-/-}$ mice manifested no significant difference in the development of chronic postviral disease (Fig. 2, C and D), perhaps divergent from the pro-inflammatory role of TREM-1 in other disease models (Bouchon et al., 2001a; Schenk et al., 2007; Klesney-Tait et al., 2013).

The distinct nature of TREM-2 actions in postviral lung disease prompted a further examination of mechanism. We

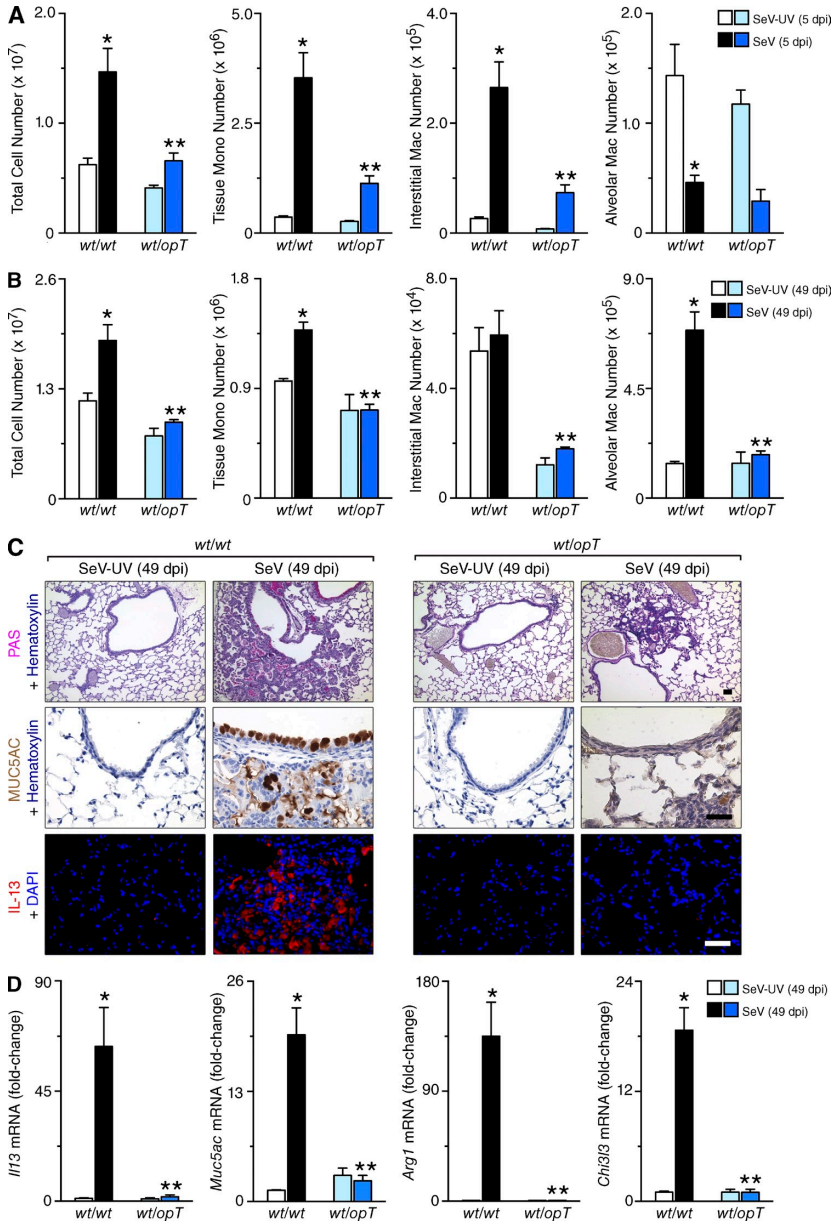

Figure 1. Effect of macrophage deficiency on postviral lung disease. (A) Lung levels of total cells, tissue monocytes (tissue monos), interstitial macrophages (interstitial macs), and alveolar macrophages (alveolar macs) for *wt/wt* and *wt/opT* mice at 5 dpi with SeV or UV-inactivated SeV (SeV-UV) determined by flow cytometry staining with fluorescent bead-based quantitation. (B) For conditions in (A), corresponding values for 49 dpi. (C) Representative photomicrographs of lung sections stained with PAS plus hematoxylin, immunostained for MUC5AC and counterstained with hematoxylin, or immunostained for IL-13 and counterstained with DAPI. Bars, 200 µm. (D) Lung levels of *Il13*, *Muc5ac*, *Arg1*, and *Chi3l3* mRNA in *wt/wt* and *wt/opT* mice at 49 dpi with SeV or SeV-UV. For A, B, and D, * represents a significant increase from SeV-UV, and ** represents a significant decrease from corresponding *wt/wt* control value. All experimental data were verified in at least three independent experiments.

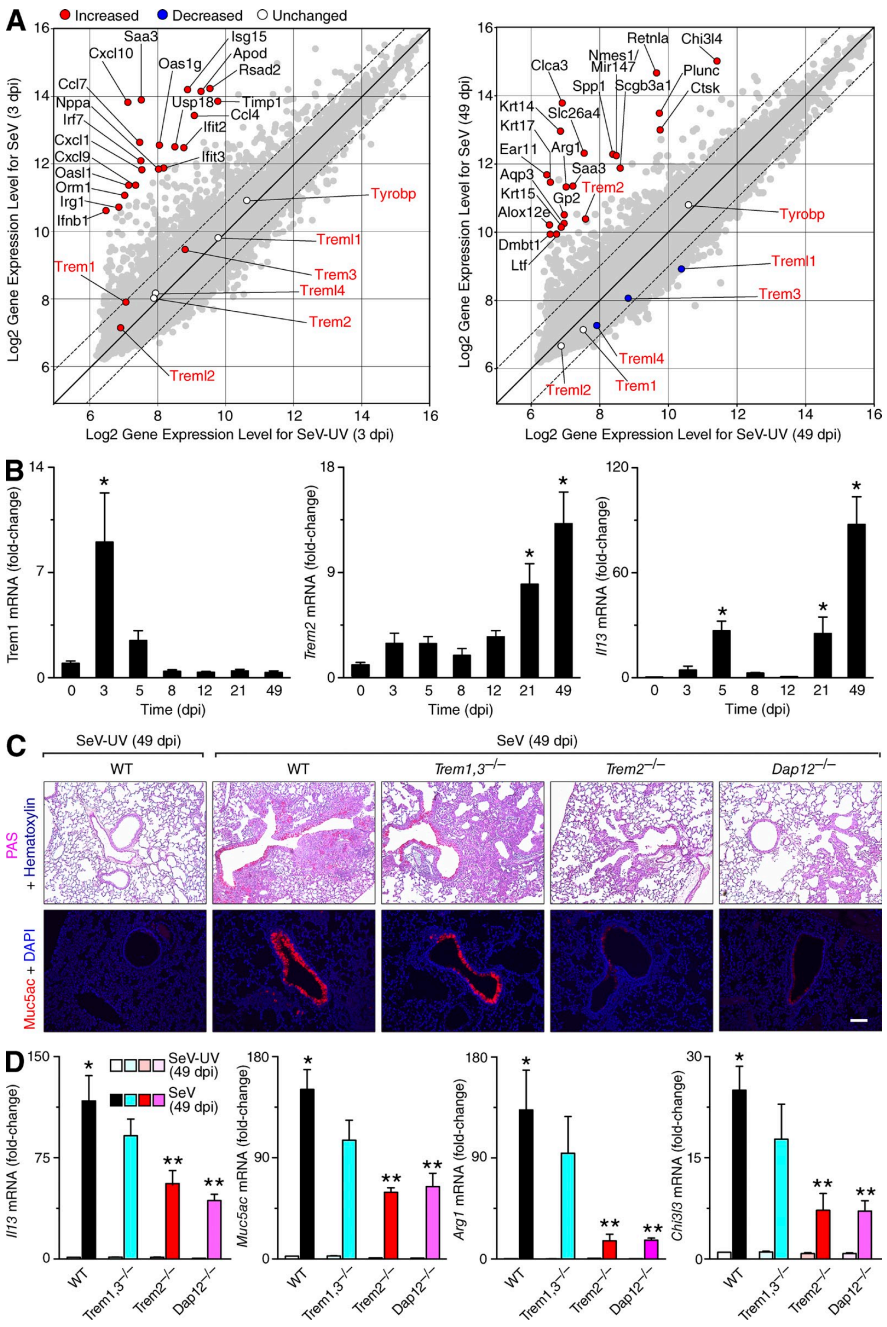

Figure 2. Induction and function of *Trem2* gene expression during postviral lung disease. (A) Gene expression microarray analysis of mRNA from lungs of mice at 3 and 49 dpi with SeV (10^5 pfu) or SeV-UV. Scatter plot depicts $\log_2$ normalized gene expression. Each symbol represents the expression value for an individual gene with the top 20 differentially expressed genes colored red and annotated in black, and others colored gray. Genes encoding *Trem* family members and *Dap12* are colored red if significantly increased, blue if decreased, or white if unchanged, and are annotated in red. (B) Lung levels of *Trem1*, *Trem2*, and *Il13* mRNA at indicated dpi with SeV. * represents a significant increase from (–) SeV control value. Values at 0 dpi were no different than those for SeV-UV 0–49 dpi. (C) Representative photomicrographs of PAS and Muc5ac staining of lung sections from WT, *Trem2*$^{-/-}$,

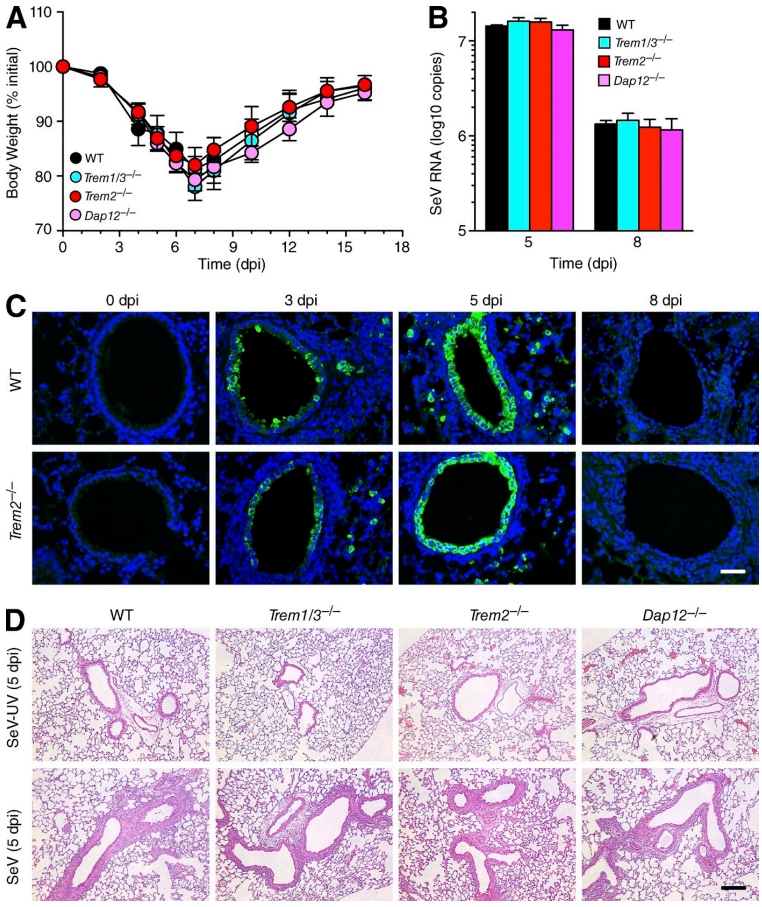

Figure 3. Similarity of acute illness after viral infection in WT and knockout mice. (A) Body weights in WT, *Trem2*$^{-/-}$, *Dap12*$^{-/-}$, and *Trem1/3*$^{-/-}$ mice at the indicated dpi. (B) Viral titers assessed by real-time qPCR assay for SeV N gene RNA in lungs of indicated mouse strains at 5 and 8 dpi. For A and B, values represent mean ± SEM for 4–7 mice. (C) Representative photomicrographs SeV immunostaining in lung sections from WT and *Trem2*$^{-/-}$ mice at 0–8 dpi. (D) Representative photomicrographs of hematoxylin and eosin staining of lung sections from indicated mouse strains at 5 dpi. Each section contains an area of bronchiolitis with inflammatory cells surrounding an airway and adjacent blood vessel. Bar, 200 µm. All experimental data were verified in at least three independent experiments.

first established that there was no significant difference in acute illness among *Trem2*$^{-/-}$, *Dap12*$^{-/-}$, and *Trem1/3*$^{-/-}$ mice as signified by similarities in body weight change, viral titer and tissue distribution, and pattern of tissue inflammation (Fig. 3, A–D). Therefore, we returned to our interest in the role of TREM-2 in modifying long-term macrophage function. We first found that TREM-2 expression at 49 dpi was specific to lung tissue macrophages based on co-localization with macrophage markers F4/80 and Mac-3 in tissue immunostaining (Fig. 4 A). Similarly, TREM-2 expression was found in lung macrophages (CD45^{+}F4/80^{+}) and not stromal cells, e.g., epithelial cells (CD45^{-}EpCAM^{+}), based on flow cytometry staining (unpublished data).

As demonstrated previously (Kim et al., 2008), we also found a marked expansion of IL-13^{+} lung macrophages in WT mice at 49 dpi (Fig. 4 B). Here, we show that this expansion is markedly down-regulated in *Trem2*$^{-/-}$ mice based on tissue immunostaining (Fig. 4 B). In addition, FACS-based separation of lung macrophage populations revealed that tissue monocytes and interstitial macrophages exhibited a marked increase in *Il13*, *Arg1*, and *Chi3l3* mRNA levels with the development of postviral disease at 49 dpi in WT mice, and this postviral induction was markedly attenuated in *Trem2*$^{-/-}$ mice (Fig. 4 C). In contrast, alveolar macrophages showed no induction of *Il13* mRNA but nonetheless still manifested a slight increase in *Arg1* mRNA and a marked increase in *Chi3l3* mRNA at 49 dpi in WT mice. The observed levels of *Il13*, *Arg1*, and *Chi3l3* mRNA in alveolar macrophages from WT mice were nearly identical to those in *Trem2*$^{-/-}$ mice (Fig. 4 C). This subset profile might again reflect a predominant

Dap12$^{-/-}$, and *Trem1/3*$^{-/-}$ mice at SeV p.i. day 49. Bar, 200 µm. (D) Corresponding lung levels of *Il13*, *Muc5ac*, *Arg1*, and *Chi3l3* mRNA for conditions in (A). * represents a significant increase from SeV-UV mice and ** a significant decrease from corresponding WT control mice. All experimental data were verified in at least three independent experiments.

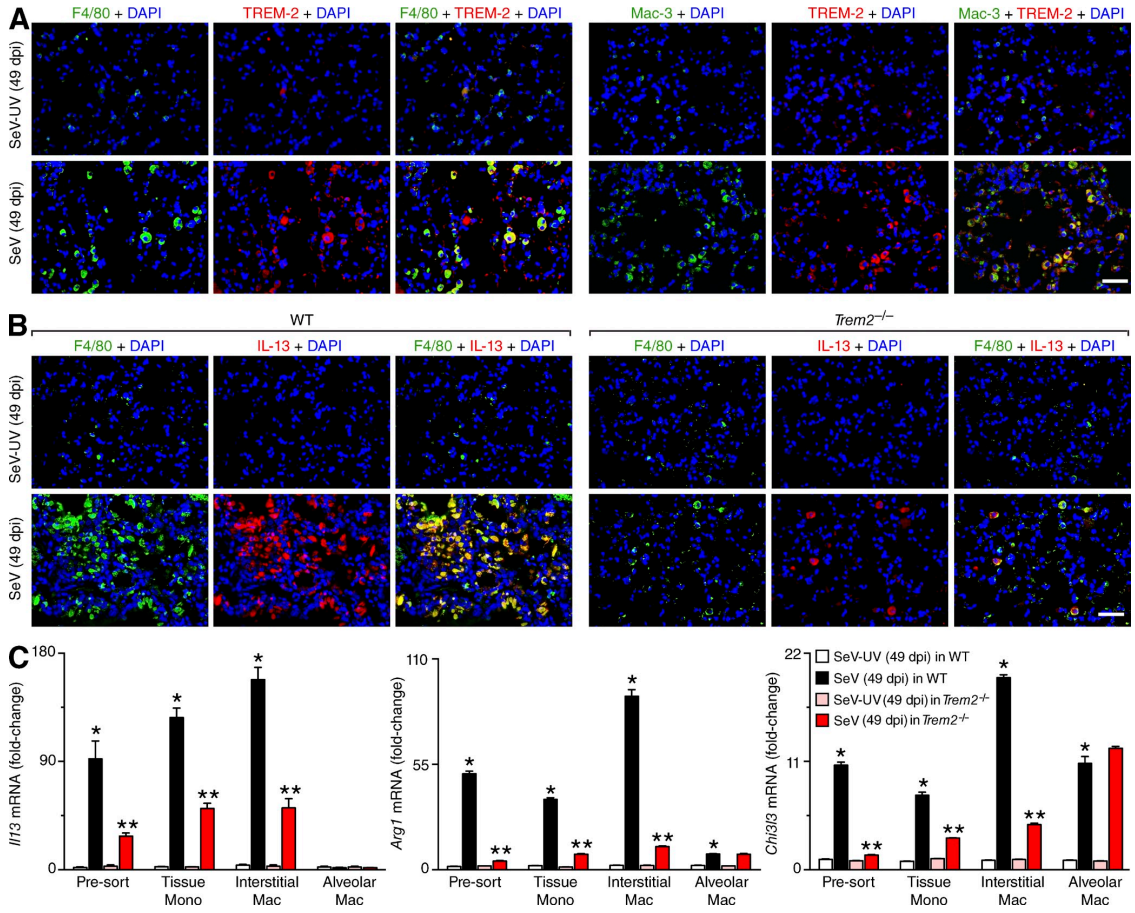

Figure 4. Induction and function of TREM-2 in lung macrophages during postviral lung disease. (A) Representative photomicrographs of TREM-2 plus F4/80 or Mac-3 immunostaining of lung sections from WT mice at 49 dpi with SeV or SeV-UV. Bar, 200 µm. (B) Representative photomicrographs of F4/80 plus IL-13 immunostaining of lung sections from WT and *Trem2*$^{-/-}$ mice at 49 dpi with SeV-UV or SeV. Bar, 200 µm. (C) Levels of *Il13*, *Arg1*, and *Chi3l3* mRNA in FACS-purified tissue monos, interstitial macs, and alveolar macs from WT and *Trem2*$^{-/-}$ mice at 49 dpi with SeV or SeV-UV. Each value represents mean ± SEM for five mice and is representative of three experiments. * represents a significant increase from corresponding SeV-UV in WT value, and ** represents a significant decrease from corresponding SeV in WT value. All experimental data were verified in at least three independent experiments.

effect of TREM-2 deficiency on tissue monocytes and interstitial macrophages. Given the predominance of the tissue monocyte population, these findings were consistent with the decrease in whole lung levels of *Il13*, *Arg1*, and *Chi3l3* mRNA found in *Trem2*$^{-/-}$ mice.

Cell surface TREM-2 expression and function

We next assessed the regulation of TREM-2 expression and function under the current paradigm that TREM-2 expressed on the cell surface works in coordination with its adapter protein DAP12 to signal for macrophage activation (Turnbull et al., 2006). In the present model, cell surface expression of TREM-2 on lung macrophages was detected on tissue monocytes and interstitial macrophages but not alveolar macrophages (Fig. 5 A). Moreover, flow cytometry staining for TREM-2 was found exclusively on CD11b^{+}CD11c^{-} lung cells at 5 dpi (Fig. S2), which is consistent with localization to tissue monocytes and interstitial macrophages and not to alveolar macrophages or dendritic cells. Postviral induction of cell surface TREM-2 was found only at 2–8 dpi (Fig. 5, A and B) and was therefore similar to induction for lung levels of SeV, suggesting that SeV replication might increase cell surface TREM-2 on macrophages. To follow up this possibility, we studied BMDMs infected with GFP-labeled SeV and showed an increase in cell surface staining for TREM-2 that correlated closely with viral titer (Fig. 5, C and D). Moreover, SeV infection caused a dose-dependent increase in cell surface TREM-2 levels on BMDMs that was reproduced using poly(IC) treatment,

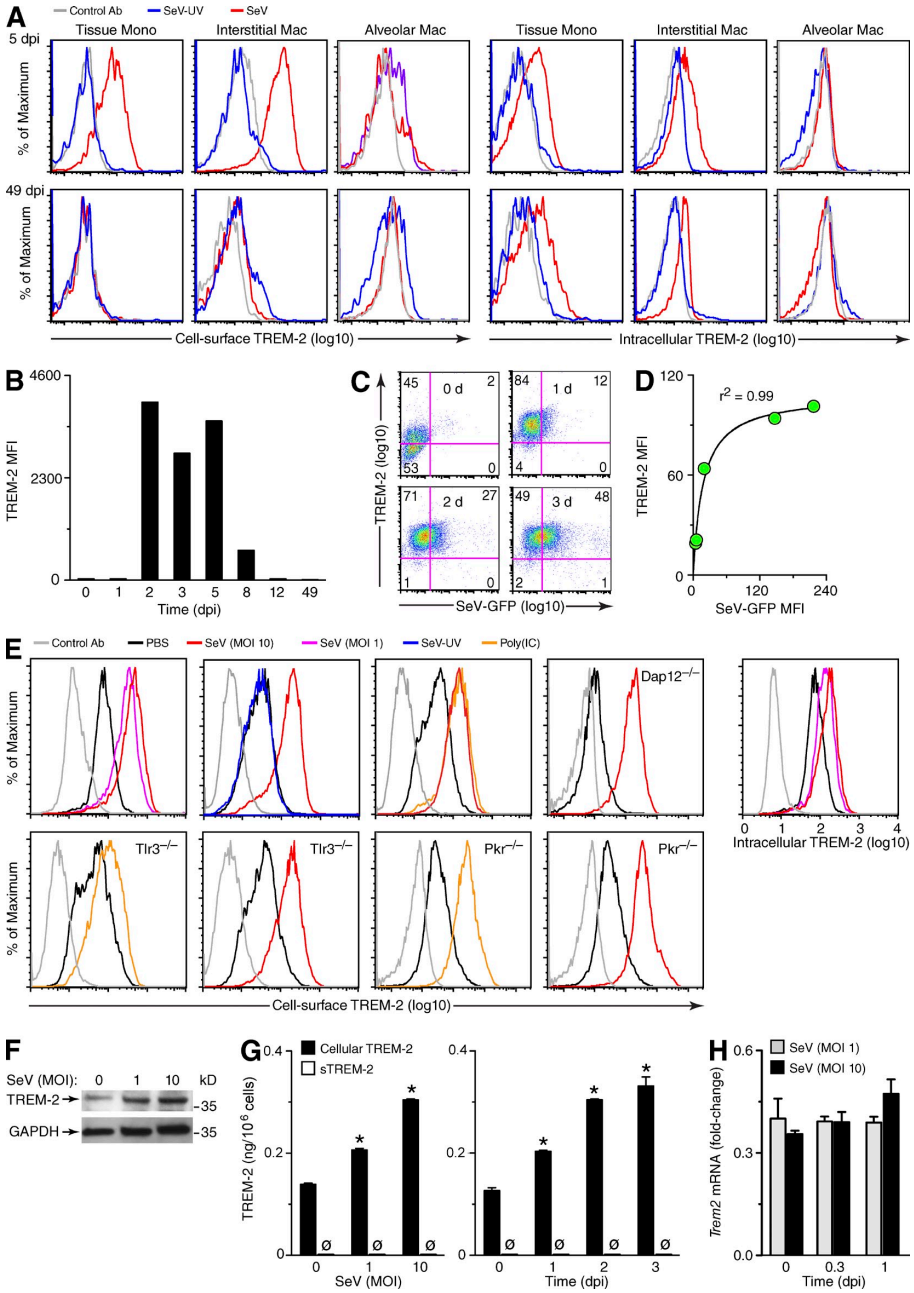

Figure 5. Regulation of cell surface and intracellular TREM-2 levels during viral replication and postviral lung disease. (A) Representative histograms from FACS analysis of TREM-2 immunostaining for tissue monos, interstitial macs, and alveolar macs from lungs of mice at 5 or 49 dpi with SeV-UV or SeV. (B) Corresponding MFI values for cell surface TREM-2 levels on tissue monos at the indicated dpi based on analysis conditions in A. (C) Representative cytograms from flow cytometry analysis of cell surface TREM-2 immunostaining for BMDMs at 0–3 dpi with GFP-expressing SeV (SeV-GFP). (D) Corresponding MFI values for cell surface TREM-2 and SeV-GFP for conditions in C. (E) Representative histograms for flow cytometry analysis of cell surface and intracellular TREM-2 immunostaining for BMDMs with indicated conditions. (F) Western blotting of TREM-2 in BMDMs at 2 dpi with SeV (MOI 0–10). (G) ELISA of cellular TREM-2 and sTREM-2 in BMDMs at 2 dpi with SeV for indicated MOI or with SeV at MOI 10 for 0–3 dpi. * represents a significant increase from corresponding control at MOI 0 and 0 dpi and Ø represents an undetectable level of sTREM-2. (H) *Trem2* mRNA level in BMDMs with SeV at MOI 1 and 10 for 0–1 dpi. All experimental data verified in at least three independent experiments.

and this increase was unaffected by DAP12, TLR3, or PKR deficiency (Fig. 5 E). In addition to the increase in surface TREM-2 levels, we also found that SeV infection caused a smaller but sustained increase in intracellular levels of TREM-2 in BM-derived macrophages (BMDMs) unaccompanied by any detectable production of sTREM-2 or any increases in *Trem2* mRNA (Fig. 5, F–H). A similar increase in intracellular TREM-2 level was found in vivo at 5 and 49 dpi. Together, the results suggest that SeV promotes an increase in surface TREM-2 levels based on increased TREM-2 formation and either transport to or retention at the cell surface with relatively little if any TREM-2 cleavage from the cell surface.

The relatively transient increase in cell surface TREM-2 levels suggested an acute effect on macrophage function after viral infection. Consistent with this idea, we found that the increase in the number of tissue monocytes (and interstitial macrophages but not neutrophils) at 5 dpi in WT mice was attenuated in *Trem2*$^{-/-}$ mice (Fig. 6 A and not depicted). This attenuation was not accompanied by decreases in monocyte chemokine production based on lung levels of *Ccl2* and *Cx3cl1* mRNA at 3–5 dpi (Fig. 6 B) or decreases in monocyte influx into the lung based on tracking CD45.2 transferred monocytes by flow cytometry at 5 dpi (Fig. 6 C). However, we did detect increased macrophage apoptosis in *Trem2*$^{-/-}$ mice compared with WT mice based on immunostaining for active caspase-3 and Mac-3 at 5–12 dpi (Fig. 6, D and E), suggesting a role for TREM-2 in specifically promoting macrophage survival after viral infection. Cells that were active caspase-3^{+} were not also SeV^{+} (Fig. 6 F), suggesting that TREM-2 antiapoptotic actions were independent of viral cytopathic effect. In addition, the timing of apoptosis corresponded to a relative decrease in *Csf1* mRNA and CSF-1 protein levels in the lung (Fig. 6, G and H), consistent with the link between CSF-1 and macrophage survival via DAP12 signaling (Otero et al., 2009). Moreover, we detected no defect in CSF-1 production in *Trem2*$^{-/-}$ mice suggesting that the CSF-1 survival signal required downstream activation of TREM-2 to prevent apoptosis. Indeed, we found a marked increase in apoptosis with CSF-1 withdrawal in BMDMs from *Trem2*$^{-/-}$ mice compared with WT control mice based on propidium iodide staining, Annexin V staining, and active Caspase-3 immunoblotting (Fig. 6, I–K). We detected a slight increase in apoptosis in BMDMs from *Trem2*$^{-/-}$ mice even in cultures with CSF-1, but this effect was also attributable to CSF-1 withdrawal because CSF-1 was added only once at the start of the 2-d culture period and was therefore being consumed and depleted from the culture medium. This condition therefore represents a partial degree of CSF-1 withdrawal and a consequent loss of the CSF-1 to TREM-2 survival signal in *Trem2*$^{-/-}$ cells. Together, our results suggested that cell surface TREM-2 might preserve macrophage survival and promote macrophage accumulation after viral infection and thereby lead to long-term macrophage-dependent disease. However, the relatively transient effect of TREM-2 during acute infection also raised the possibility that TREM-2 had additional effects at later time points that influenced long-term disease outcome.

sTREM-2 expression and function

To pursue the possible chronic actions of TREM-2 in the postviral model, we first determined whether there was long-term production of TREM-2 protein in the lung in this model. Indeed, we found a marked increase in lung levels of TREM-2 at 49 dpi compared with baseline or to the relatively small increase found at 5 dpi (Fig. 7 A). Given the absence of detectable cell surface TREM-2 at 49 dpi and the relatively small increase in intracellular TREM-2 at either 5 or 49 dpi (Fig. 5 A), this late increase in TREM-2 levels at 49 dpi was likely a marker of sTREM-2 formation in the diseased lung. Since IL-13 production was also markedly increased at 49 dpi, we questioned whether IL-13 might promote TREM-2 cleavage at the cell surface and consequent formation of sTREM-2. In support of this possibility, we found that IL-13 administration caused a time-dependent loss of cell surface levels of TREM-2 in BMDMs (Fig. 7 B). The effect of IL-13 was specific for the IL-13 receptor since the same effect was found for IL-4 (that also activates this receptor) but was not detectable for other type 2 cytokines (IL-5 and IL-9; Fig. 7 C). Treatment with IL-13 also resulted in a time-dependent increase in cellular TREM-2 levels in BMDMs, as expected for M2 differentiation, but caused an even greater increase in sTREM-2 levels released from BMDMs (Fig. 7 D). The increases in cellular TREM-2, especially the even greater increases in sTREM-2 production, were attenuated in BMDMs from *Dap12*$^{-/-}$ mice (Fig. 7 D). Moreover, the expected increase in sTREM-2 levels was not found during postviral disease in *Dap12*$^{-/-}$ mice (Fig. 7 E). Together, these findings indicated that both IL-13 and DAP12 were contributing to sTREM-2 formation and any consequent function of sTREM-2 in chronic postviral disease.

To pursue a possible role for sTREM-2 in postviral disease, we analyzed the effect of recombinant sTREM-2 (amino acids 19–136) on macrophage function. Immunostaining of BMDMs incubated with sTREM-2 showed that the protein was localized to the cell cytoplasm and not the cell surface and was thereby accessible to intracellular proteins (Fig. 8 A). In that context, we found that sTREM-2 administration to BMDMs caused a significant increase in *Arg1* mRNA levels (as a sign of M2 differentiation), but the increase was not preserved for other M2 markers (e.g., *Chi3l3* mRNA) and was not nearly as effective as IL-13 for driving these responses (Fig. 8 B). Thus, the direct effect of sTREM-2 on M2 differentiation was relatively small and was therefore unlikely to contribute to biological function or postviral disease. However, in the process of conducting these experiments, we recognized that sTREM-2 treatment of BMDMs resulted in marked protection against the usual progression to cell death in this culture system, and this protective effect resulted in expanded numbers of BMDMs from both WT and *Trem2*$^{-/-}$ mice (Fig. 8 C). Similarly, sTREM-2 treatment caused a dose-dependent expansion of BMDMs from WT, *Trem2*$^{-/-}$, and *Dap12*$^{-/-}$ mice (Fig. 8 D). Here again,

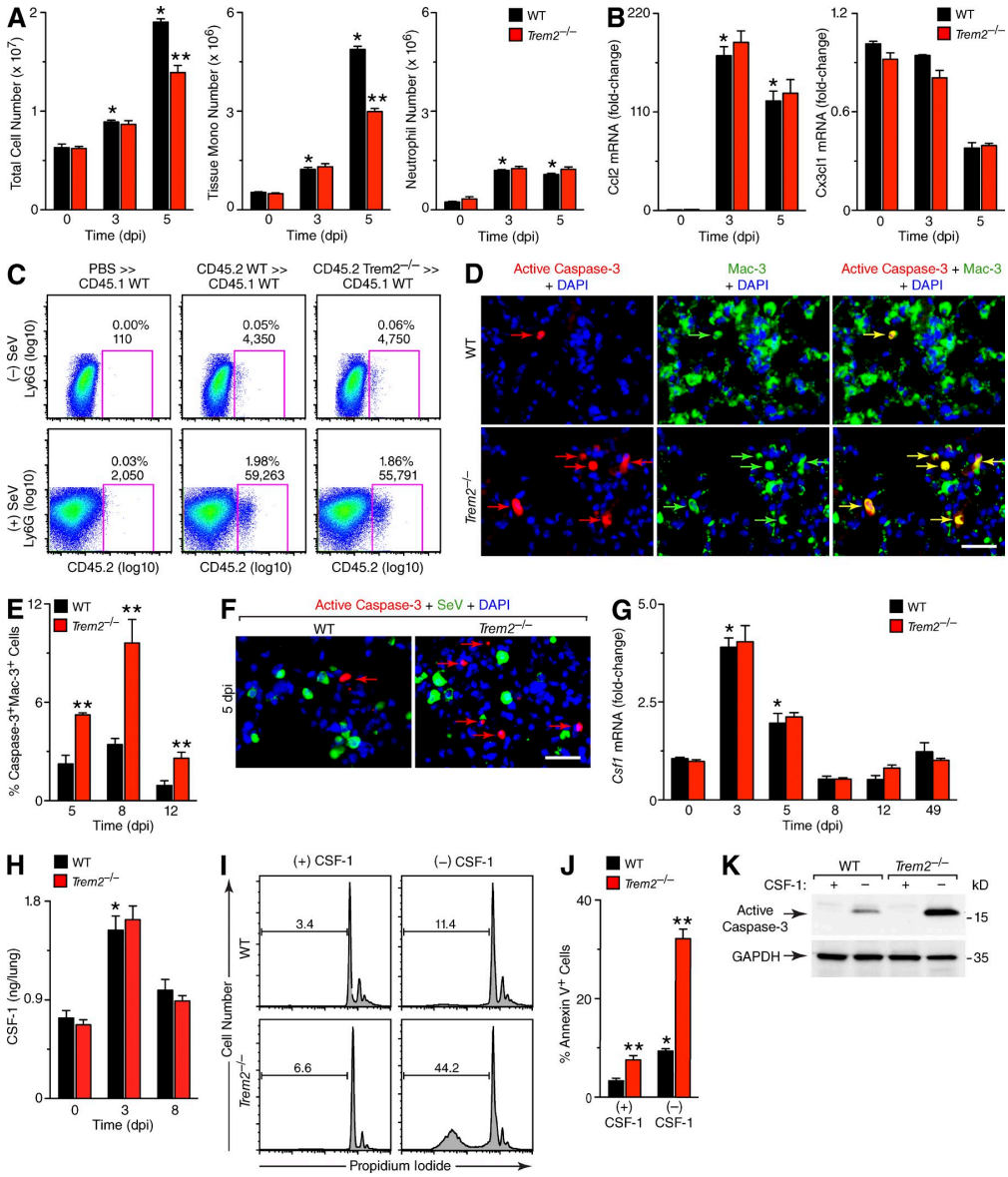

Figure 6. Effect of cellular TREM-2 on macrophage apoptosis during acute viral infection. (A) Flow cytometry analysis of lung levels of total cells, tissue monos, and neutrophils ($SSC^{high}Ly6G^{+}$) for WT and *Trem2*$^{-/-}$ mice at 0–5 dpi with SeV. (B) *Ccl2* and *Cx3cl1* mRNA levels in WT and *Trem2*$^{-/-}$ mice at 0–5 dpi. For A and B, values represent mean ± SEM for 5 mice, and * represents a significant increase from 0 dpi and ** a significant decrease from corresponding WT mice. (C) Representative cytograms for flow cytometry analysis of levels of $CD45.2^{+}$ tissue monos in WT and *Trem2*$^{-/-}$ mice at 3 dpi after CD45.2 WT and *Trem2*$^{-/-}$ BMDMs were introduced into CD45.1 WT mice at 0 dpi. (D) Representative photomicrographs of active caspase-3 and Mac-3 immunostaining of lung sections from WT and *Trem2*$^{-/-}$ mice at 8 dpi. Arrows indicate cells with double-positive immunostaining. Bar, 200 µm. (E) Quantification of analysis in (D). Values represent mean ± SEM for 12 randomly selected fields of lung sections from 3 mice, and ** represents a significant increase from corresponding WT mice. (F) Representative photomicrographs of active caspase-3 and SeV immunostaining of lung sections from WT and *Trem2*$^{-/-}$ mice at 5 dpi. Arrows indicate cells with active caspase-3^{+} immunostaining. Bar, 200 µm. (G) Lung levels of *Csf1* mRNA for WT and *Trem2*$^{-/-}$ mice at indicated dpi. (H) Corresponding lung levels of CSF-1 for conditions in (G). For G and H, values represent mean ± SEM for 5 mice, and * represents a significant increase from 0 dpi. (I) Flow cytometry analysis of propidium iodide staining of BMDMs from WT and *Trem2*$^{-/-}$ mice cultured with or without CSF-1 for 1 d. (J) Levels of Annexin V immunostaining in PI^{-} cells for culture conditions in (I). Values represent mean ± SEM for 6 randomly selected fields of replicate wells, and * represents a significant increase from (+) CSF-1, and ** a significant increase from corresponding WT mice. (K) Western blot levels of active caspase-3 for culture conditions in I. All experimental data were verified in at least three independent experiments.

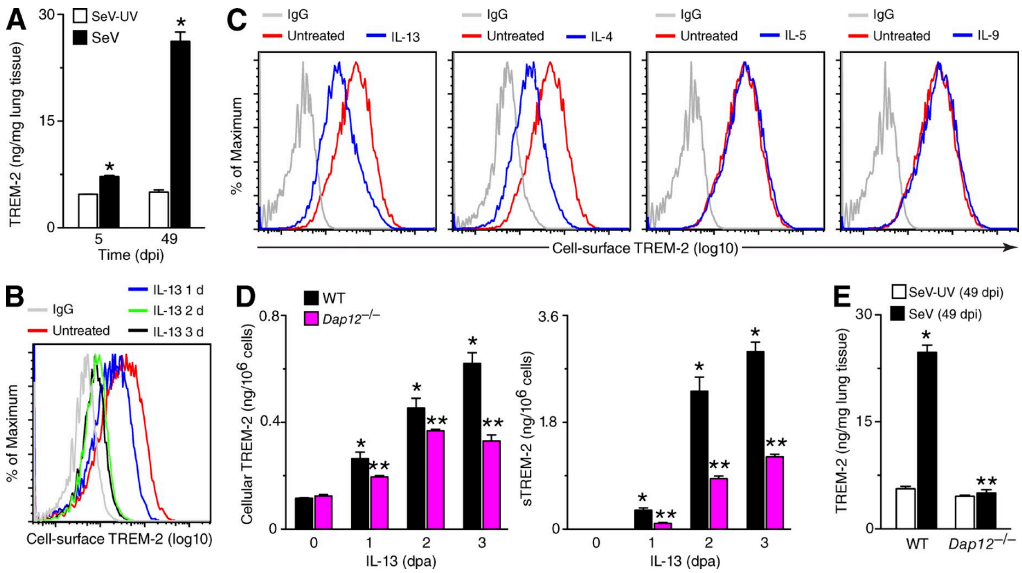

Figure 7. Effect of IL-13 on production of sTREM-2. (A) Lung levels of TREM-2 determined by ELISA at 5 or 49 dpi with SeV or SeV-UV. Values represent mean ± SEM for 5 mice, and * represents a significant increase from corresponding SeV-UV mice. (B) Representative histograms from flow cytometry analysis of cell surface TREM-2 on BMDMs treated with or without IL-13 (20 ng/ml) or IgG control for 1–3 d. (C) Representative histograms from flow cytometry analysis of cell surface TREM-2 on BMDMs treated with or without IL-13, IL-4, IL-5, or IL-9 (20 ng/ml) or IgG control for 1 d. (D) Levels of cellular and sTREM-2 in BMDMs obtained from WT and *Dap12*$^{-/-}$ mice and cultured with IL-13 for 1–3 d post-administration (dpa) as in B. Values represent mean ± SEM for 3 replicate wells, and * represents a significant increase from 0 dpa and ** a significant decrease from corresponding WT cells. (E) Lung levels of TREM-2 in WT and *Dap12*$^{-/-}$ mice at 49 dpi. Values represent mean ± SEM for 5 mice, and * represents a significant increase from SeV-UV and ** a significant decrease from corresponding WT mice. All experimental data were verified in at least three independent experiments.

the baseline numbers of BMDMs were increased in WT mice compared with *Trem2*$^{-/-}$, and *Dap12*$^{-/-}$ mice under these culture conditions, but this difference was corrected in response to sTREM-2 treatment (Fig. 8 D). The protective effect was specific for active sTREM-2 because it was lost with heat inactivation (Fig. 8 E). Flow cytometry analysis with propidium iodide staining indicated that sTREM-2 administration resulted in attenuation of apoptosis due to CSF-1 withdrawal in BMDMs from WT mice, as well as *Trem2*$^{-/-}$ and *Dap12*$^{-/-}$ mice (Fig. 8 F). As expected, the level of apoptosis with CSF-1 withdrawal in BMDMs from WT mice was markedly increased in *Trem2*$^{-/-}$ and *Dap12*$^{-/-}$ mice, but this effect was also fully preventable and dose-dependent with sTREM-2 administration (Fig. 8 F). Treatment with sTREM-2 also reversed the increase in activate caspase-3 levels that develops with CSF-1 withdrawal, confirming an effect on apoptosis (Fig. 8 G). In contrast, sTREM-2 had no effect on cellular proliferation based on BrdU incorporation (Fig. 8 H), as expected for cell cultures deprived of CSF-1 stimulation. This result is also consistent with the absence of significant cell proliferation in the lung in vivo when disease becomes manifest (Tyner et al., 2006). Together, these findings support a role for sTREM-2 in protection against macrophage apoptosis under low CSF-1 conditions, and thereby explained the increased levels of apoptosis under these conditions in *Trem2*$^{-/-}$ and *Dap12*$^{-/-}$ macrophages that are unable to generate sTREM-2.

Given the difficulties in monitoring apoptosis in vivo (e.g., we detected no active caspase-3 tissue staining at 49 dpi; unpublished data) we sought additional markers of sTREM-2 action during postviral lung disease. In that regard, we were able to establish that sTREM-2 treatment resulted in a time-dependent and selective increase in molecular pathways connected to cell survival and proliferation, e.g., ERK1/2 and MAPK14 phosphorylation but not AKT phosphorylation or BCL-2 induction (Fig. 9 A). The effect of sTREM-2 on phospho-ERK1/2 and phospho-MAPK formation was more pronounced in BMDMs from *Trem2*$^{-/-}$ mice compared with WT mice (Fig. 9 A), consistent with the enhanced effect of sTREM-2 on viability of BMDMs from *Trem-2*$^{-/-}$ compared with WT mice based on fold-change (Fig. 8 D). In translating these findings to the postviral model in vivo, we found that phospho-ERK1/2 immunostaining was markedly increased and co-localized to lung macrophages at 49 dpi compared with 5 dpi or SeV-UV control conditions in WT mice (Fig. 9 B). Moreover, the increase in phospho-ERK1/2 immunostaining was not detected at 49 dpi in *Trem2*$^{-/-}$ mice (Fig. 9 B). These results were consistent with increases in the numbers of total

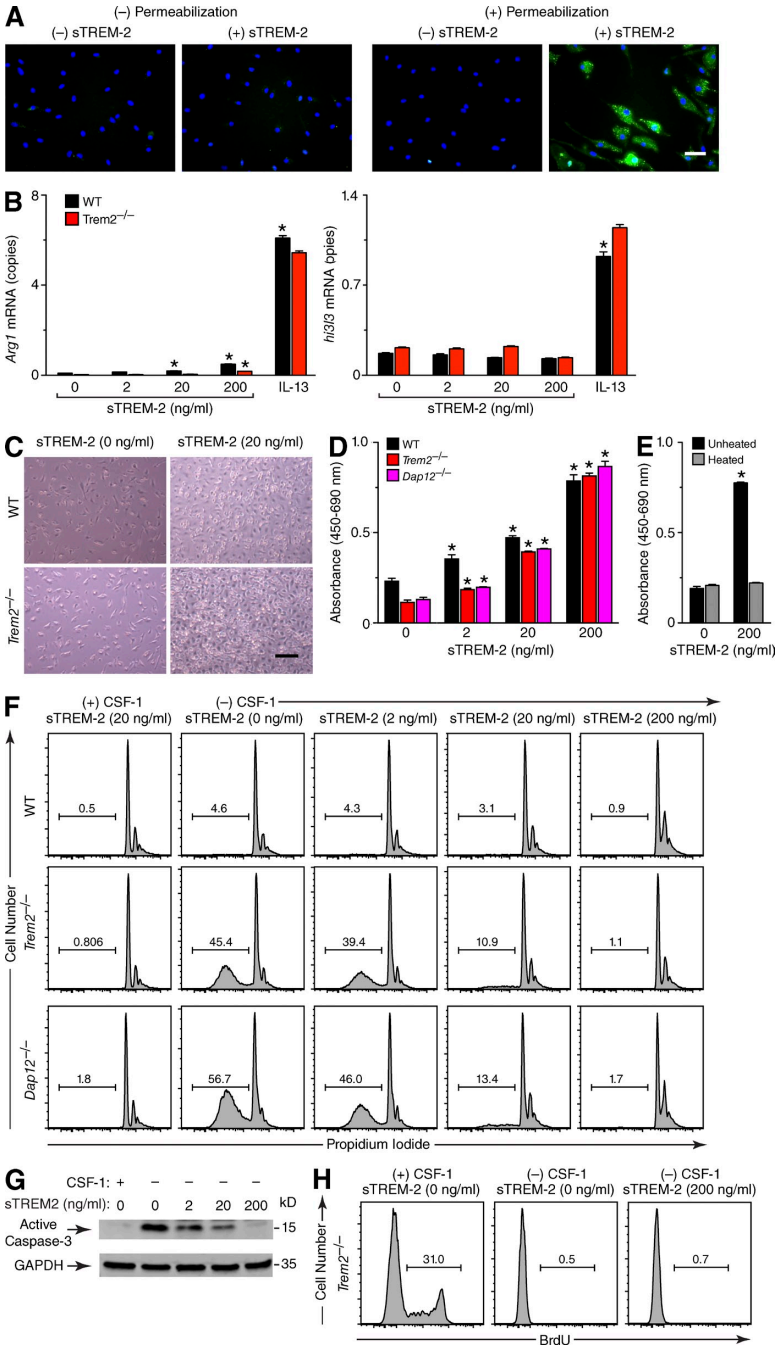

Figure 8. Effect of sTREM-2 on macrophage apoptosis. (A) Representative photomicrographs of immunostaining for recombinant sTREM-2 after incubation with BMDMs for 30 min with and without cell permeabilization with saponin. Bar, 100 µm. (B) Levels of *Arg1* and *Chi3l3* mRNA in BMDMs obtained from *Trem2*$^{-/-}$ and WT mice and then cultured with sTREM-2 (0–200 ng/ml) or IL-13 (20 ng/ml) for 1 d. Values represent mean ± SEM for 3 replicate wells, and * represents a significant increase from no treatment control (0 ng/ml). (C) Representative photomicrographs of sTREM-2–treated BMDMs cultured in 15% L-cell conditioned medium for 7 d. Bar = 200 µm. (D) XTT assay for BMDMs obtained from WT, *Trem2*$^{-/-}$, and *Dap12*$^{-/-}$ mice and then cultured with sTREM-2 (0–200 ng/ml) for 2 d after CSF-1 withdrawal. Values represent mean ± SEM for 3 replicate wells, and * represents a significant increase from corresponding untreated control cells. (E) XTT assay of BMDMs from WT mice cultured with native (unheated) or denatured (heated) sTREM-2 (0–200 ng/ml) with culture conditions in D. * represents a significant increase from corresponding untreated control cells. (F) Flow cytometry analysis of propidium iodide staining of BMDMs obtained from WT, *Trem2*$^{-/-}$, and *Dap12*$^{-/-}$ mice and cultured with sTREM-2 (0–200 ng/ml) with or without CSF-1 for 1 d. (G) Western blot levels of active caspase-3 for culture conditions in F. (H) Flow cytometry analysis of BrdU-labeling of BMDMs from *Trem2*$^{-/-}$ mice for culture conditions in F. All experimental data were verified in at least three independent experiments.

immune cells and macrophages in the lung at 49 dpi in WT mice, as well as marked inhibition of this cellular response at 49 dpi in *Trem2*$^{-/-}$ mice (Fig. 9 C). Together, these findings provide for a crucial regulatory role of TREM-2 in a feed-forward pathway that expands the M2 macrophage population and thereby promotes IL-13–dependent chronic lung disease.

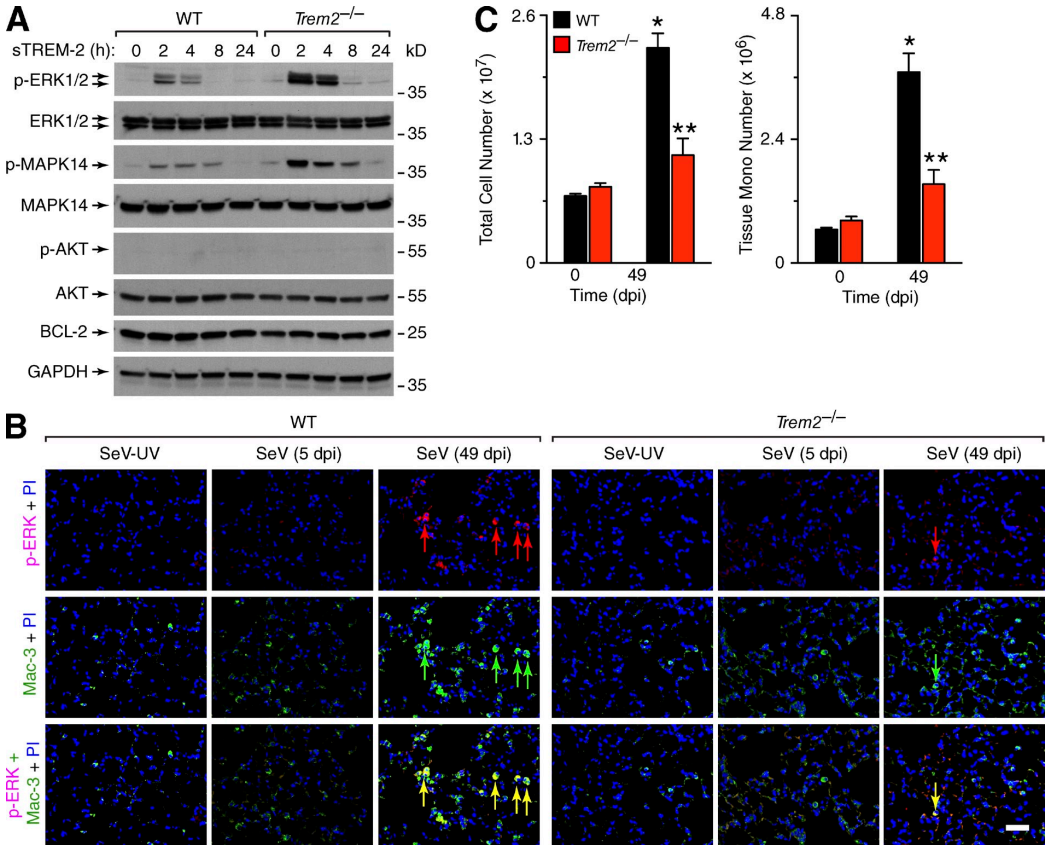

Figure 9. Effect of TREM-2 deficiency on apoptosis signaling pathway. (A) Western blot levels of indicated cell survival proteins in BMDMs cultured from WT and Trem22/2 mice after treatment with mouse sTREM-2 (200 ng/ml) for 0–24 h. (B) Representative photomicrographs of phospho-ERK1/2 (p-ERK) and Mac-3 immunostaining with DAPI counterstaining of lung sections from WT and Trem22/2 mice at 5 or 49 dpi with SeV or SeV-UV. Arrows indicate cells with double-positive immunostaining. Bar, 200 µm. (C) Flow cytometry analysis of lung levels of total cells and tissue monos for WT and Trem22/2 mice at 0 and 49 dpi. Values represent mean ± SEM for 5 mice, and * represents a significant increase from 0 dpi and ** a significant decrease from corresponding WT mice. Values at 0 dpi were no different than those for SeV-UV (49 dpi). All experimental data were verified in at least three independent experiments.

DISCUSSION

This report identifies TREM-2 as a key component of an innate immune pathway for the pathogenesis of chronic lung disease. We use a postviral mouse model of this type of disease to show that: (1) during acute illness, viral replication increases lung macrophage levels of intracellular and cell surface TREM-2, and this action mediates a CSF-1–dependent cell survival signal that prevents macrophage apoptosis; (2) during chronic postviral disease, IL-13 and DAP12 signals promote increased expression and cleavage of TREM-2 from the cell surface to form sTREM-2 at increased levels in the lung; and (3) sTREM-2 is not inactive as previously thought, but is instead capable of promoting macrophage survival via antiapoptotic signals such as ERK1/2 activation. Together, these events allow for TREM-2 to participate in a feed forward mechanism to amplify the accumulation of macrophages in the lung. In the context of our previous work, the increased number of macrophages would be available to interact with iNKT cells and drive further IL-13 production thereby resulting in IL-13–dependent differentiation of the macrophage population toward an M2 pattern of gene expression (including *Arg1* and *Chi3l3*) and differentiation of an airway progenitor epithelial cell (APEC) niche to airway mucous cells (AMCs) as signatures of chronic lung disease (as diagrammed in Fig. 10). The scheme is consistent with our observation that TREM-2–deficient mice are markedly protected from the development of chronic lung disease as a long-term consequence of viral infection.

The role of TREM-2 in chronic disease described in this study provides for at least four major and unexpected insights. First, TREM-2 signaling was often portrayed as antiinflammatory and reparative, whereas increased TREM-1 signals

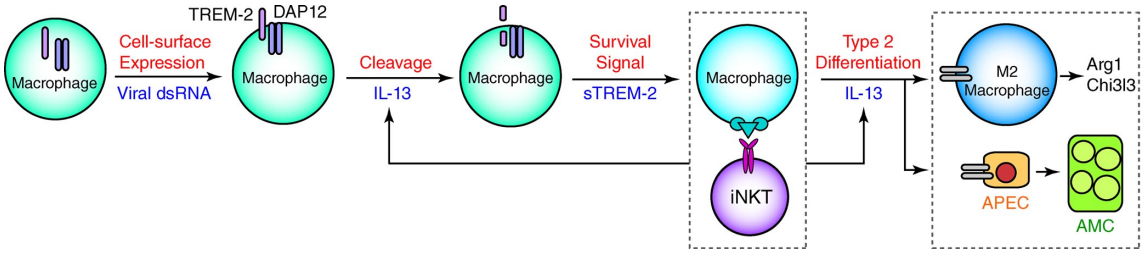

Figure 10. Scheme for regulation and function of TREM-2 in chronic postviral lung disease. Major steps include: (1) early activation of lung macrophages in which viral replication increases TREM-2 at the cell surface; (2) cleavage of TREM-2 from the cell surface to form sTREM-2 in a process that is up-regulated by IL-13 and DAP12; (3) sTREM-2 actions to prevent apoptosis in association with increased ERK1/2 activation and thereby allow for amplified macrophage interaction with iNKT cells and consequent IL-13 production; and (4) IL-13–dependent differentiation of the macrophage population toward an M2 pattern of gene expression (including Arg1 and Chi3l3) and differentiation of an airway progenitor epithelial cell (APEC) niche to airway mucous cells (AMCs) as signatures of chronic lung disease.

were thought to be proinflammatory and destructive in models of intestinal and CNS disease (Schenk et al., 2007; Takahashi et al., 2007; Seno et al., 2009). This view is consistent with studies showing that engagement of TREM-1 promotes secretion of proinflammatory cytokines (including IL-6 and TNF) and increases the inflammatory responses downstream of TLR and NLR engagement (Bouchon et al., 2000, 2001a; Bleharski et al., 2003; Netea et al., 2006; Fortin et al., 2007; Schenk et al., 2007). Meanwhile, similar approaches showed that TREM-2 activation generally antagonized activation signals for inflammation (Daws et al., 2001; Colonna, 2003; Hamerman et al., 2006; Turnbull et al., 2006). In contrast, the present results provide for a paradigm in which TREM-2 activation promotes the development of chronic inflammatory disease. This model is consistent with reports for up-regulation of M2 gene expression (including *TREM2*) in macrophages isolated from cigarette smokers with and without COPD (Shaykhiev et al., 2009; Koth et al., 2010). However, these previous studies as well as others that assess association with disease cannot determine cause and effect actions of TREM signaling in the development of disease. Moreover, the present application of new tools to separately study both TREM-1 and TREM-2 deficiency in vivo and in vitro in the same model system was critical to dissect any differences in TREM family member function.

A second unexpected aspect of the present findings is the biological activity of sTREM-2. In fact, we initially approached the issue of TREM-2 activity as being a function of TREM-2 localization to the cell surface, where it could presumably bind to an as yet poorly defined ligand, and in association with DAP12, initiate a signaling pathway for cell survival (Otero et al., 2009). Indeed, we were able to secure evidence for this mechanism in the setting of acute infection, wherein viral replication increases TREM-2 on the surface of infected macrophages. However, this relatively transient effect on macrophage survival did not appear to explain the long-term effect of TREM-2 on postviral lung disease. We therefore pursued evidence that the greatest increases in TREM-2 lung levels were found long after clearance of infectious virus and were manifest as marked increases in sTREM-2 that had been cleaved from the cell surface. These circumstances led to the unexpected function of sTREM-2 as a potent antiapoptotic factor for macrophages. Our data suggests that sTREM-2 acts as an intracellular messenger to trigger the activation of kinases (e.g., ERK1/2) that promote cell survival. However, additional work will need to define the precise molecular pathway downstream of sTREM-2 actions, including those proposed for TREM-2–DAP12 signaling for cell survival (Otero et al., 2009, 2012). Meanwhile, however, our results may also help to explain the proposed benefit of sTREM-2 cleavage in neurodegenerative disease, where decreased sTREM-2 cleavage caused by mutation may be associated with impaired macrophage (i.e., microglial) function in the CNS (Kleinberger et al., 2014).

A third unanticipated result of our study was the potent role of DAP12 and IL-13 in regulating TREM-2 cleavage and sTREM-2 formation. Similar to signaling function of cell surface TREM-2, the formation of sTREM-2 and any consequent downstream action of sTREM-2 was still dependent on DAP12. This new connection between sTREM-2 and DAP12 could help explain how distinct TREM signals are transduced into different downstream effects on cell behavior. Thus, both TREM-1 and TREM-2 on the cell surface are proposed to signal via DAP12, and this adaptor has only a single immunoreceptor tyrosine-based activation motif (ITAM) for subsequent signal transduction. It has been proposed that the avidity of TREM (or other receptor) interaction with DAP12 might dictate a positive versus negative signal from this ITAM to the downstream kinase (Turnbull and Colonna, 2007). In the present experiments, we find that TREM-2 function is linked to DAP12 by a protein maturation process that appears distinct from TREM-1–DAP12 and TREM-2–DAP12 signaling. Similarly, IL-13 also contributed to the TREM-2 cleavage process in what appears to be a novel role for IL-13. In both cases, additional work is needed to define the molecular mechanism for TREM-2 cleavage. This type of

insight could provide a useful target for antiinflammatory therapy by inhibiting cleavage and a consequent excess of sTREM-2 formation.

A fourth issue that is distinct for our results relates to the view of M2 macrophages and macrophage subsets in mediating inflammatory disease. For example, other disease models such as allergen challenge concentrate on blocking the macrophage response to IL-13 and conclude that there is no role for M2 macrophages in the disease process (Nieuwenhuizen et al., 2012). In contrast, our model focuses on the role of macrophages in IL-13 production as the fundamental step in producing disease, so it is this step that needs to be targeted for disruption. Notably, however, allergen-challenge models may depend on recruited monocytes but not resident alveolar macrophages for the development of lung disease (Zasłona et al., 2014). Similarly, we found differences in tissue monocyte and interstitial macrophage versus alveolar macrophage characteristics (e.g., level of *Il13* mRNA induction and sensitivity to TREM-2 regulation) during the development of postviral disease. These results also support the paradigm of inflammatory monocyte recruitment and subsequent differentiation into disease-producing macrophages and provide a basis for assessing these events in situ with reporter labeling and intravital imaging in the future.

Our study focused on the role of TREM-2 in macrophage function based on evidence that macrophages are key to the development of postviral disease. However, we recognize that myeloid (conventional) DCs may contribute to postviral disease at least in the first few weeks after viral inoculation (Grayson et al., 2007) and may express TREM-2 at least in vitro (Bouchon et al., 2001b; Ito and Hamerman, 2012). We found TREM-2 expression on $CD11b^+CD11c^-$ cells (i.e., monocytes and macrophages) and not on $CD11b^+CD11c^+$ cells (i.e., DCs) at 5 dpi with virus using FACS, but we cannot yet exclude expression on DCs at 49 dpi given the low levels of cellular expression of TREM-2 and the low numbers of DCs at this later time point. Thus, further studies with different technologies will be needed to determine any role for DC-expressed TREM-2 after viral infection.

In sum, we have defined a novel role for TREM-2 in the development of chronic lung disease using a postviral mouse model of this process. Our previous work led to a new consideration of the role of innate immune activation of macrophages in this type of disease. However, there was little subsequent progress toward further understanding and thereby specifically blocking the macrophage component of postviral disease in experimental models or humans. Herein, we describe an unanticipated mechanism whereby TREM-2 allows for macrophages to accumulate in the lung and thereby amplify disease-promoting IL-13 production. In this setting, TREM-2 appears to affect the chronic disease process without influencing acute viral illness, thereby creating an opportunity to inhibit excessive TREM-2 action without compromising host defense. The findings thereby provide an opportunity to downregulate the type 2 immune response and prevent the development of this type of immune-mediated disease by interrupting sTREM-2 formation or action. Initial studies already suggest an increase in TREM-2 expression in concert with excess levels of airway mucus and M2 macrophages in human lung disease (Byers and Holtzman, 2011; Byers et al. 2013. International Meeting of the American Thoracic Society. Abstr. A141.). The present findings justify further validation of these observations in humans with chronic lung disease and additional work to correct any abnormalities in TREM-2 action in this type of disease and other diseases that implicate a role for TREM-2 in regulating macrophage survival.

MATERIALS AND METHODS

Mice. WT C57BL/6J mice were obtained from The Jackson Laboratory. The *op/opT* mice were generated as described previously (Abboud et al., 2002) and were provided by N. Ghosh-Choudhury (University of Texas, San Antonio). These mice were crossed to WT mice to generate heterozygous *wt/opT* mice and littermate *wt/wt* control mice. $Dap12^{-/-}$ mice were provided by T. Takai (Tohoku University, Sendai, Japan). $Trem2^{-/-}$ mice were generated as described previously (Turnbull et al., 2006). $Trem1/3^{-/-}$ mice were generated as described previously and were backcrossed to C57BL/6 mice until >99% of the loci were derived from this strain. $Tlr3^{-/-}$ mice were generated as described previously (Alexopoulou et al., 2001). $Pkr^{-/-}$ mice were generated as described previously (Yang et al., 1995) and rederived from frozen embryos obtained from M. White and H. Virgin IV (Washington University, St. Louis, MO). All mice were maintained on a C57BL/6 genetic background and were used in protocols approved by Animal Studies Committee of Washington University School of Medicine in accordance with National Institutes of Health guidelines.

Viral inoculation and monitoring. Mice were inoculated with SeV (10^5 pfu), an equivalent amount of UV-inactivated SeV (SeV-UV), or PBS as described previously (Kim et al., 2008). SeV-UV and PBS inoculations gave identical results, and therefore are treated interchangeably as controls. Viral titers for stock solutions and lung infections were monitored by plaque-forming and real-time PCR assays as described previously (Kim et al., 2008).

Analysis of mRNA. For gene expression microarrays, RNA was isolated and analyzed using Illumina Mouse-WG6 v2 BeadChips (Illumina) as described previously (Byers et al., 2013). Visualization and plotting was performed using DecisionSite for Functional Genomics (TIBCO Spotfire). Microarray data were deposited in the National Center for Biotechnology Information (NCBI) Gene Expression Omnibus (GEO) under series accession nos. GSE49603 and GSE61437. For real-time qPCR assays, RNA was purified from lung homogenate using TRIzol (Invitrogen) and was converted to cDNA using the High-Capacity cDNA Archive kit (Applied Biosystems). Target mRNA was quantified by real-time PCR assay using specific fluorogenic probes and primer sets and the Fast Universal PCR Master Mix system (Applied Biosystems). Primer-probe sets for mouse *Ccl2* (*Mcp-1*; Mm00441242_m1), *Cx3cr1l* (Mm00436454_m1), *Trem1* (Mm00451738_m1), *Trem2* (Mm00451744_m1), *Chi3l3* (Mm00657889_mH), *Arg1* (Mm00475988_m1), and *Dap12* (Mm00449152_m1) were obtained from Applied Biosystems. The forward and reverse primers and probes for mouse *Il13* were 5′-GGTGCCAAGATCTGTGTCTC-3′, 5′-CCACACTCCATACCATGCTG-3′, and 5′-AAGACCAGACTCCCCTGTGCAAC-3′; for *Muc5ac* were 5′-TACCACTCCCTGCTTCTGCAGCGTGTCA-3′, 5′-ATAGTAACAGTGGCCATCAAGGTCTGTCT-3′, and 5′-TATACCCCTTGGGATCCATCATCTACA-3′; for *Csf1* were 5′-CTTCATGCCAGATTGCCTTTG-3′, 5′-CGCATGGTCTCATCTATTATGTCT-3′, 5′-CAGCTGGATGATCCTGTTTGCTACCT-3′; and for mouse *Gapdh* were 5′-AAGGTGAAGGTCGGAGTCA-3′, 5′-CATGTAAACCATGTAGTTGAGGT-3′, and 5′-CGGATTTGGTCGTATTGGGCGC-3′. All

probes were designed to span introns and did not react with genomic DNA. Samples were assayed on the 7500 Fast Real-Time PCR System and analyzed using the 7500 Fast System Software (Applied Biosystems). Levels of specific gene expression were normalized to *Gapdh* mRNA levels.

Western blotting. For TREM-2 expression, BMDMs were seeded in 6-well tissue culture plates and were infected with SeV at MOI 1 and 10 for 48 h. For caspase-3 expression, BMDMs were seeded in 6-well tissue culture plates and were cultured in the presence or absence of L cell-conditioned medium for 16 h. Cells were lysed and boiled in reducing SDS-PAGE sample buffer containing 100 mM Tris, pH 6.8, 4% SDS, 5% β-mercaptoethanol, 20% glycerol and 0.2% bromophenol blue. Lysates was subjected to 4–15% gradient gel electrophoresis (Bio-Rad Laboratories) and transferred to PVDF membrane (Millipore) in 10% methanol, 25 mM Tris and 192 mM glycine, pH 8.3. Anti-Caspase-3 Ab was from Cell Signaling Technology. Rat anti–mouse TREM-2 mAb (clone 178.9.4) was generated as described previously (Turnbull et al., 2006). Antibody binding was detected using the enhanced chemiluminescence (ECL) system (GE Healthcare). Molecular weight standards were run on each blot to validate that each of the indicated bands corresponded to the appropriate molecular weight.

Recombinant protein expression and purification. The mouse TREM-2 Ig domain (amino acid residues 19–136) tagged with 6X His (sTREM-2-his) was expressed, secreted, and purified from mammalian cell culture as previously described (Kober et al., 2014). Precautions were taken to prevent introduction of endotoxin either by using either new, sterile plasticware or by soaking glassware overnight in 0.5 M NaOH. The final purified protein was exchanged in PBS using a microconcentrator (Sartorius). For heat inactivation, sTREM-2-his was boiled at 100°C for 1 h.

Microscopy. Tissues were fixed with 10% formalin, embedded in paraffin, cut into 5-µm sections, and adhered to charged slides. Sections were deparaffinized in Citrosolv (Fisherbrand), hydrated, and in the case of immunofluorescence microscopy, treated with heat-activated antigen unmasking solution (Vector Laboratories). Immunostaining of mouse tissue was performed using anti-MUC5AC mAb (Thermo Fisher Scientific; clone 45M1), anti–Mac-3 mAb (BD; clone M3/84), anti–Caspase-3 mAb (clone 5A1E; Cell Signaling Technology), anti–mouse TREM-2 (R&D Systems), anti–mouse F4/80 mAb (clone CI:A3-1; Abcam), anti–mouse phospho-ERK1/2 (clone D13.14.4E, Cell Signaling Technology), anti–mouse IL-13 mAb (R&D Systems), and anti-SeV antibody (SPAFAS, Inc.). Antibody binding was visualized using Alexa Fluor 488 or 594 fluorochromes (Invitrogen). Slides were counterstained with DAPI-containing mounting media (Vector Laboratories).

For sTREM-2 immunostaining, BMDMs were seeded into 2-well chamber slide (Nalge Nunc International) at 2×10^5 cell per well. For surface sTREM-2 immunostaining, BMDMs were incubated with sTREM2-his (10 µg/ml) for 30 min on ice and then washed four times with chilled PBS and incubated with mouse anti-6X His tag antibody (Abcam; clone His. H8) followed by Alexa Fluor 488–conjugated anti–mouse IgG (Invitrogen) and fixation with 4% PFA. For intracellular sTREM-2 immunostaining, cells were incubated with sTREM-2-his for 30 min at 37°C, washed with PBS, fixed with 4% PFA, and then permeabilized with 0.2% Saponin, 2% BSA in PBS for 30 min before incubation with anti-6X His tag antibody and Alexa Fluor 488–conjugated anti–mouse IgG. All microscopy was performed using an Olympus BX51 microscope and a Retiga-2000R camera system (QImaging).

Flow cytometry and FACS. Single-cell lung suspensions were made from minced lung tissue subjected to collagenase (Liberase Blendzyme III; Roche), hyaluronidase (Sigma-Aldrich), and DNase I (grade II; Roche) digestion for 45 min at 37°C and then treated with ACK buffer to remove red blood cells. Cell percentages were unchanged if lungs were perfused before digestion (suggesting that intravascular cells did not contribute significantly to the analysis), so unperfused lungs were used for all experiments. Staining of surface markers was performed using FcR blockade and fluorochrome-conjugated mAb at 4°C. We used the following antibodies: rat anti-mCD11b (clone M1/70; eBioscience), anti-Ly6C (clone al-21; BD), anti-Ly6G (clone 1a8; BD), anti-mouse F4/80 (clone BM8; eBioscience), anti-mouse TREM-1 (clone 174031; R&D Systems), anti-m/hTREM-2 (clone 237920; R&D Systems), anti–mouse CD11c (clone HL3; BD), anti–mouse CD45.2 (clone 104; eBioscience), and anti–mouse Siglec-F (clone E50-2440; BD). We used flow cytometry and FACS to identify and purify specific cell populations in mouse lungs using the following gates: tissue monocytes as $SSC^{low}Ly6G^{-}F4/80^{+}CD11b^{+}$, interstitial macrophages as $SSC^{high}CD11c^{-}Ly6G^{-}Siglec\text{-}F^{-}F4/80^{+}CD11b^{+}$, alveolar macrophages as $SSC^{high}CD11c^{+}Ly6G^{-}Siglec\text{-}F^{+}F4/80^{+}CD11b^{-}$, and neutrophil gate as $SSC^{high}Ly6G^{+}$ (Fig. S1). Analysis was performed using Moflo (DAKO-Cytomation) and FlowJo software (Tree Star). Cells were counted using flow cytometry and fluorescent counting beads (CountBright; Life Technologies).

Cell culture. Bone marrow cells were flushed from femurs and differentiated in 150 × 15 mm Petri dishes in DMEM medium containing 0.29 g/liter L-glutamine, 1 mM sodium pyruvate, 10% FBS, and 30% L929 fibroblast-conditioned medium as a source of CSF-1. At day 6 or indicated times, BMDMs were resuspended by incubation in 1 mM EDTA in PBS for 10 min on ice, washed twice with PBS and plated into tissue culture plates. In some experiments, BMDMs were incubated with poly(IC) (Sigma-Aldrich) or mouse IL-13 (R&D Systems). For cell viability assays, BMDMs were seeded into 96-well tissue culture plates at 5×10^4 cells per well and were assessed for viability using the Cell Proliferation kit (XTT) from Roche. For cell proliferation assays, BMDMs were seeded into 6-well tissue culture plates, labeled for 18 h with BrdU (10 µM), and then assessed using flow cytometry with the FITC BrdU Flow kit (BD).

Apoptosis assays. For propidium iodide (PI) assay, BMDMs were cultured in L cell–conditioned medium for 5 d and deprived of CSF-1 for 1 d to induce apoptosis (Otero et al., 2009). Cells were detached using EDTA (1 mM) in PBS, washed, fixed with 70% ethanol, and incubated with PI (50 µg/ml) and RNase (40 µg/ml) for 1 h. Samples were analyzed for DNA content using a FACScan (BD). For Annexin V assay, BMDMs were differentiated in L cell–conditioned medium for 5 d, detached with EDTA, seeded onto the poly-D-Lysine-coated coverslips (BD) placed in a 24-well plate, and cultured in medium without CSF-1 for 1 d. PI and Annexin V immunostaining was performed according to the manufacture's protocol (Invitrogen). Annexin V–positive, PI-negative staining cells were quantified using microscopy, and values were expressed as the percentage of apoptotic cells (Annexin V positive, PI negative) relative to the total number of cells in 6 randomly selected fields of the two wells.

Monocyte influx. For analysis of monocyte influx into the lung, BMMs were purified from CD45.2 WT and *Trem2*$^{-/-}$ mice using negative selection with the EasySep Mouse Monocyte Enrichment kit (StemCell Technologies). Purified monocytes were then introduced into CD45.1 WT mice (3×10^6 cells per mouse via tail vein injection) at 0 dpi with SeV, and the number of $CD45.2^{+}$ cells in the lung was determined 3 or 5 d later using FACS and fluorescent counting beads.

ELISA. For lung tissue samples, lung tissue was minced and then homogenized in PBS containing protease inhibitor cocktail (cOmplete; Roche) using a rotor-type homogenizer (Tissue-Tearor; Biospec Products). For cell supernatant and lysate samples, BMDM (2×10^6 cells in 2 ml of complete DMEM containing 15% L cell–conditioned medium) were seeded into 12-well tissue plates, treated with or without IL-13 (20 ng/ml) or SeV (MOI 1 and 10). Cell supernatants were collected, and cells were washed twice with chilled PBS and then lysed in radio-immunoprecipitation assay (RIPA) buffer (Sigma-Aldrich) containing protease inhibitors. Levels of CSF-1 were determined using a Duoset ELISA kit (R&D Systems) and levels of cellular TREM-2 and sTREM-2 with a TREM-2 ELISA kit (Antibodies-online.com).

Statistical analyses. For experiments in mice and cell culture, all experiments were repeated a minimum of three times, and representative values are presented. PCR data were presented as mean ± SEM and was analyzed using an unpaired Student's *t* test. If variances were unequal, Welch's correction was applied. For all analyses, $P < 0.05$ were considered significant. For SeV-GFP versus TREM-2 expression, nonlinear curve fit was performed using a simple hyperbolic function where $Y = B_{max} \times X/(K_d + X)$.

Online supplemental material. Fig. S1 shows the flow cytometry scheme for analysis of lung macrophages. Fig. S2 shows a scheme for FACS analysis of cell surface and intracellular TREM-2 immunostaining. Table S1 shows microarray gene expression values for Fig. 2 A, including values for all TREM family members. Online supplemental material is available at http://www.jem.org/cgi/content/full/jem.20141732/DC1.

We thank the Alvin J. Siteman Cancer Center at Washington University School of Medicine and Barnes-Jewish Hospital for the use of the High Speed Cell Sorter Core. We also appreciate valuable scientific and technical input from Loralyn Benoit, Darlene Stewart, and Theresa Tolley.

This work was supported by grants from the National Institutes of Health (OD and NIAID grants AADCRC U19-AI07048 and NHLBI grants T32-HL-007317, P50-HL-084922, P01-HL-029594, R01-HL-073159, and R01-HL-121791) and the Martin Schaeffer Fund.

The authors declare no competing financial interests.

Submitted: 7 September 2014
Accepted: 20 March 2015

REFERENCES

Abboud, S.L., K. Woodruff, C. Liu, V. Shen, and N. Ghosh-Choudhury. 2002. Rescue of the osteopetrotic defect in op/op mice by osteoblast-specific targeting of soluble colony-stimulating factor-1. *Endocrinology*. 143:1942–1949. http://dx.doi.org/10.1210/endo.143.5.8775

Agapov, E., J.T. Battaile, R. Tidwell, R. Hachem, G.A. Patterson, R.A. Pierce, J.J. Atkinson, and M.J. Holtzman. 2009. Macrophage chitinase 1 stratifies chronic obstructive lung disease. *Am. J. Respir. Cell Mol. Biol.* 41:379–384. http://dx.doi.org/10.1165/2009-0122R

Alevy, Y.G., A.C. Patel, A.G. Romero, D.A. Patel, J. Tucker, W.T. Roswit, C.A. Miller, R.F. Heier, D.E. Byers, T.J. Brett, and M.J. Holtzman. 2012. IL-13-induced airway mucus production is attenuated by MAPK13 inhibition. *J. Clin. Invest.* 122:4555–4568. http://dx.doi.org/10.1172/JCI64896

Alexopoulou, L., A.C. Holt, R. Medzhitov, and R.A. Flavell. 2001. Recognition of double-stranded RNA and activation of NF-kappaB by Toll-like receptor 3. *Nature*. 413:732–738. http://dx.doi.org/10.1038/35099560

Bleharski, J.R., V. Kiessler, C. Buonsanti, P.A. Sieling, S. Stenger, M. Colonna, and R.L. Modlin. 2003. A role for triggering receptor expressed on myeloid cells-1 in host defense during the early-induced and adaptive phases of the immune response. *J. Immunol.* 170:3812–3818. http://dx.doi.org/10.4049/jimmunol.170.7.3812

Bouchon, A., J. Dietrich, and M. Colonna. 2000. Cutting edge: inflammatory responses can be triggered by TREM-1, a novel receptor expressed on neutrophils and monocytes. *J. Immunol.* 164:4991–4995. http://dx.doi.org/10.4049/jimmunol.164.10.4991

Bouchon, A., F. Facchetti, M.A. Weigand, and M. Colonna. 2001a. TREM-1 amplifies inflammation and is a crucial mediator of septic shock. *Nature*. 410:1103–1107. http://dx.doi.org/10.1038/35074114

Bouchon, A., C. Hernández-Munain, M. Cella, and M. Colonna. 2001b. A DAP12-mediated pathway regulates expression of CC chemokine receptor 7 and maturation of human dendritic cells. *J. Exp. Med.* 194:1111–1122. http://dx.doi.org/10.1084/jem.194.8.1111

Byers, D.E., and M.J. Holtzman. 2011. Alternatively activated macrophages and airway disease. *Chest*. 140:768–774. http://dx.doi.org/10.1378/chest.10-2132

Byers, D.E., J. Alexander-Brett, A.C. Patel, E. Agapov, G. Dang-Vu, X. Jin, K. Wu, Y. You, Y. Alevy, J.-P. Girard, et al. 2013. Long-term IL-33-producing epithelial progenitor cells in chronic obstructive lung disease. *J. Clin. Invest.* 123:3967–3982. http://dx.doi.org/10.1172/JCI65570

Colonna, M. 2003. TREMs in the immune system and beyond. *Nat. Rev. Immunol.* 3:445–453. http://dx.doi.org/10.1038/nri1106

Daws, M.R., L.L. Lanier, W.E. Seaman, and J.C. Ryan. 2001. Cloning and characterization of a novel mouse myeloid DAP12-associated receptor family. *Eur. J. Immunol.* 31:783–791. http://dx.doi.org/10.1002/1521-4141(200103)31:3<783::AID-IMMU783>3.0.CO;2-U

Fortin, C.F., O. Lesur, and T. Fulop Jr. 2007. Effects of TREM-1 activation in human neutrophils: activation of signaling pathways, recruitment into lipid rafts and association with TLR4. *Int. Immunol.* 19:41–50. http://dx.doi.org/10.1093/intimm/dxl119

Grayson, M.H., D. Cheung, M.M. Rohlfing, R. Kitchens, D.E. Spiegel, J. Tucker, J.T. Battaile, Y. Alevy, L. Yan, E. Agapov, et al. 2007. Induction of high-affinity IgE receptor on lung dendritic cells during viral infection leads to mucous cell metaplasia. *J. Exp. Med.* 204:2759–2769. http://dx.doi.org/10.1084/jem.20070360

Hamerman, J.A., J.R. Jarjoura, M.B. Humphrey, M.C. Nakamura, W.E. Seaman, and L.L. Lanier. 2006. Cutting edge: inhibition of TLR and FcR responses in macrophages by triggering receptor expressed on myeloid cells (TREM)-2 and DAP12. *J. Immunol.* 177:2051–2055. http://dx.doi.org/10.4049/jimmunol.177.4.2051

Holtzman, M.J. 2012. Asthma as a chronic disease of the innate and adaptive immune systems responding to viruses and allergens. *J. Clin. Invest.* 122:2741–2748. http://dx.doi.org/10.1172/JCI60325

Holtzman, M.J., D.E. Byers, J. Alexander-Brett, and X. Wang. 2014. The role of airway epithelial cells and innate immune cells in chronic respiratory disease. *Nat. Rev. Immunol.* 14:686–698. http://dx.doi.org/10.1038/nri3739

Ito, H., and J.A. Hamerman. 2012. TREM-2, triggering receptor expressed on myeloid cell-2, negatively regulates TLR responses in dendritic cells. *Eur. J. Immunol.* 42:176–185. http://dx.doi.org/10.1002/eji.201141679

Kaifu, T., J. Nakahara, M. Inui, K. Mishima, T. Momiyama, M. Kaji, A. Sugahara, H. Koito, A. Ujike-Asai, A. Nakamura, et al. 2003. Osteopetrosis and thalamic hypomyelinosis with synaptic degeneration in DAP12-deficient mice. *J. Clin. Invest.* 111:323–332. http://dx.doi.org/10.1172/JCI16923

Kim, E.Y., J.T. Battaile, A.C. Patel, Y. You, E. Agapov, M.H. Grayson, L.A. Benoit, D.E. Byers, Y. Alevy, J. Tucker, et al. 2008. Persistent activation of an innate immune response translates respiratory viral infection into chronic lung disease. *Nat. Med.* 14:633–640. http://dx.doi.org/10.1038/nm1770

Kleinberger, G., Y. Yamanishi, M. Suárez-Calvet, E. Czirr, E. Lohmann, E. Cuyvers, H. Struyfs, N. Pettkus, A. Wenninger-Weinzierl, F. Mazaheri, et al. 2014. TREM2 mutations implicated in neurodegeneration impair cell surface transport and phagocytosis. *Sci. Transl. Med.* 6:243ra86. http://dx.doi.org/10.1126/scitranslmed.3009093

Klesney-Tait, J., K. Keck, X. Li, S. Gilfillan, K. Otero, S. Baruah, D.K. Meyerholz, S.M. Varga, C.J. Knudson, T.O. Moninger, et al. 2013. Transepithelial migration of neutrophils into the lung requires TREM-1. *J. Clin. Invest.* 123:138–149. http://dx.doi.org/10.1172/JCI64181

Kober, D.L., K.M. Wanhainen, B.M. Johnson, D.T. Randolph, M.J. Holtzman, and T.J. Brett. 2014. Preparation, crystallization, and preliminary crystallographic analysis of wild-type and mutant human TREM-2 ectodomains linked to neurodegenerative and inflammatory diseases. *Protein Expr. Purif.* 96:32–38. http://dx.doi.org/10.1016/j.pep.2014.01.015

Koth, L.L., C.J. Cambier, A. Ellwanger, M. Solon, L. Hou, L.L. Lanier, C.L. Abram, J.A. Hamerman, and P.G. Woodruff. 2010. DAP12 is required for macrophage recruitment to the lung in response to cigarette smoke and chemotaxis toward CCL2. *J. Immunol.* 184:6522–6528. http://dx.doi.org/10.4049/jimmunol.0901171

Netea, M.G., T. Azam, G. Ferwerda, S.E. Girardin, S.H. Kim, and C.A. Dinarello. 2006. Triggering receptor expressed on myeloid cells-1 (TREM-1) amplifies the signals induced by the NACHT-LRR (NLR) pattern recognition receptors. *J. Leukoc. Biol.* 80:1454–1461. http://dx.doi.org/10.1189/jlb.1205758

Nieuwenhuizen, N.E., F. Kirstein, J. Jayakumar, B. Emedi, R. Hurdayal, W.G.C. Horsnell, A.L. Lopata, and F. Brombacher. 2012. Allergic airway disease is unaffected by the absence of IL-4Rα-dependent alternatively

activated macrophages. *J. Allergy Clin. Immunol.* 130:743–750: e8. http://dx.doi.org/10.1016/j.jaci.2012.03.011

Otero, K., I.R. Turnbull, P.L. Poliani, W. Vermi, E. Cerutti, T. Aoshi, I. Tassi, T. Takai, S.L. Stanley, M. Miller, et al. 2009. Macrophage colony-stimulating factor induces the proliferation and survival of macrophages via a pathway involving DAP12 and beta-catenin. *Nat. Immunol.* 10:734–743. http://dx.doi.org/10.1038/ni.1744

Otero, K., M. Shinohara, H. Zhao, M. Cella, S. Gilfillan, A. Colucci, R. Faccio, F.P. Ross, S.L. Teitelbaum, H. Takayanagi, and M. Colonna. 2012. TREM2 and β-catenin regulate bone homeostasis by controlling the rate of osteoclastogenesis. *J. Immunol.* 188:2612–2621. http://dx.doi.org/10.4049/jimmunol.1102836

Schenk, M., A. Bouchon, F. Seibold, and C. Mueller. 2007. TREM-1–expressing intestinal macrophages crucially amplify chronic inflammation in experimental colitis and inflammatory bowel diseases. *J. Clin. Invest.* 117:3097–3106. http://dx.doi.org/10.1172/JCI30602

Seno, H., H. Miyoshi, S.L. Brown, M.J. Geske, M. Colonna, and T.S. Stappenbeck. 2009. Efficient colonic mucosal wound repair requires Trem2 signaling. *Proc. Natl. Acad. Sci. USA.* 106:256–261. http://dx.doi.org/10.1073/pnas.0803343106

Shaykhiev, R., A. Krause, J. Salit, Y. Strulovici-Barel, B.G. Harvey, T.P. O'Connor, and R.G. Crystal. 2009. Smoking-dependent reprogramming of alveolar macrophage polarization: implication for pathogenesis of chronic obstructive pulmonary disease. *J. Immunol.* 183:2867–2883. http://dx.doi.org/10.4049/jimmunol.0900473

Takahashi, K., M. Prinz, M. Stagi, O. Chechneva, and H. Neumann. 2007. TREM2-transduced myeloid precursors mediate nervous tissue debris clearance and facilitate recovery in an animal model of multiple sclerosis. *PLoS Med.* 4:e124. http://dx.doi.org/10.1371/journal.pmed.0040124

Turnbull, I.R., and M. Colonna. 2007. Activating and inhibitory functions of DAP12. *Nat. Rev. Immunol.* 7:155–161. http://dx.doi.org/10.1038/nri2014

Turnbull, I.R., S. Gilfillan, M. Cella, T. Aoshi, M. Miller, L. Piccio, M. Hernandez, and M. Colonna. 2006. Cutting edge: TREM-2 attenuates macrophage activation. *J. Immunol.* 177:3520–3524. http://dx.doi.org/10.4049/jimmunol.177.6.3520

Tyner, J.W., O. Uchida, N. Kajiwara, E.Y. Kim, A.C. Patel, M.P. O'Sullivan, M.J. Walter, R.A. Schwendener, D.N. Cook, T.M. Danoff, and M.J. Holtzman. 2005. CCL5-CCR5 interaction provides antiapoptotic signals for macrophage survival during viral infection. *Nat. Med.* 11:1180–1187. http://dx.doi.org/10.1038/nm1303

Tyner, J.W., E.Y. Kim, K. Ide, M.R. Pelletier, W.T. Roswit, J.D. Morton, J.T. Battaile, A.C. Patel, G.A. Patterson, M. Castro, et al. 2006. Blocking airway mucous cell metaplasia by inhibiting EGFR antiapoptosis and IL-13 transdifferentiation signals. *J. Clin. Invest.* 116:309–321. http://dx.doi.org/10.1172/JCI25167

Walter, M.J., J.D. Morton, N. Kajiwara, E. Agapov, and M.J. Holtzman. 2002. Viral induction of a chronic asthma phenotype and genetic segregation from the acute response. *J. Clin. Invest.* 110:165–175. http://dx.doi.org/10.1172/JCI0214345

Yang, Y.L., L.F.L. Reis, J. Pavlovic, A. Aguzzi, R. Schäfer, A. Kumar, B.R. Williams, M. Aguet, and C. Weissmann. 1995. Deficient signaling in mice devoid of double-stranded RNA-dependent protein kinase. *EMBO J.* 14:6095–6106.

Zasłona, Z., S. Przybranowski, C. Wilke, N. van Rooijen, S. Teitz-Tennenbaum, J.J. Osterholzer, J.E. Wilkinson, B.B. Moore, and M. Peters-Golden. 2014. Resident alveolar macrophages suppress, whereas recruited monocytes promote, allergic lung inflammation in murine models of asthma. *J. Immunol.* 193:4245–4253. http://dx.doi.org/10.4049/jimmunol.1400580

Biochimica et Biophysica Acta 1860 (2016) 2335–2344

Contents lists available at ScienceDirect

Biochimica et Biophysica Acta

journal homepage: www.elsevier.com/locate/bbagen

First comprehensive structural and biophysical analysis of MAPK13 inhibitors targeting DFG-in and DFG-out binding modes

Zeynep Yurtsever [a,b,c], Dhara A. Patel [a], Daniel L. Kober [a,d], Alvin Su [a], Chantel A. Miller [a], Arthur G. Romero [a], Michael J. Holtzman [a,e], Tom J. Brett [a,c,e,f,*]

[a] Division of Pulmonary and Critical Care Medicine, Department of Medicine, Washington University School of Medicine, St. Louis, MO 63110, United States
[b] Biochemistry Program, Washington University School of Medicine, St. Louis, MO 63110, United States
[c] Center for the Investigation of Membrane Excitability Diseases, Washington University School of Medicine, St. Louis, MO 63110, United States
[d] Microbiology Program, Washington University School of Medicine, St. Louis, MO 63110, United States
[e] Department of Cell Biology and Physiology, Washington University School of Medicine, St. Louis, MO 63110, United States
[f] Department of Biochemistry and Molecular Biophysics, Washington University School of Medicine, St. Louis, MO 63110, United States

ARTICLE INFO

Article history:
Received 13 April 2016
Received in revised form 13 June 2016
Accepted 26 June 2016
Available online 29 June 2016

Keywords:
p38 kinase
Structure-based drug design
Chronic inflammatory lung disease
Kinase inhibitor
Inhibitor half-lives
Differential scanning fluorimetry

ABSTRACT

Background: P38 MAP kinases are centrally involved in mediating extracellular signaling in various diseases. While much attention has previously been focused on the ubiquitously expressed family member MAPK14 (p38α), recent studies indicate that family members such as MAPK13 (p38δ) display a more selective cellular and tissue expression and might therefore represent a specific kinase to target in certain diseases.
Methods: To facilitate the design of potent and specific inhibitors, we present here the structural, biophysical, and functional characterization of two new MAPK13-inhibitor complexes, as well as the first comprehensive structural, biophysical, and functional analysis of MAPK13 complexes with four different inhibitor compounds of greatly varying potency.
Results: These inhibitors display IC_{50} values either in the nanomolar range or micromolar range (>800-fold range). The nanomolar inhibitors exhibit much longer ligand-enzyme complex half-lives compared to the micromolar inhibitors as measured by biolayer interferometry. Crystal structures of the MAPK13 inhibitor complexes reveal that the nanomolar inhibitors engage MAPK13 in the DFG-out binding mode, while the micromolar inhibitors are in the DFG-in mode. Detailed structural and computational docking analyses suggest that this difference in binding mode engagement is driven by conformational restraints imposed by the chemical structure of the inhibitors, and may be fortified by an additional hydrogen bond to MAPK13 in the nanomolar inhibitors.
Conclusions: These studies provide a structural basis for understanding the differences in potency exhibited by these inhibitors.
General significance: They also provide the groundwork for future studies to improve specificity, potency, pharmacodynamics, and pharmacokinetic properties.

1. Introduction

The mitogen activated protein kinase (MAPK) p38α (MAPK14) is the founding and most studied member of the p38 MAPK family. MAPK14 is ubiquitously expressed and centrally involved in pro-inflammatory signaling; it has thus been the focus of numerous drug-development projects for several diseases involving chronic inflammation, including rheumatoid arthritis and inflammatory bowel disease [1–4]. Recent breakthroughs in structure-based drug design have resulted in highly specific and potent inhibitors to MAPK14 [5–7], but there are remaining concerns as to the practicality of targeting this enzyme, since knockout of this gene in mice results in embryonic lethality [8–10], and efforts to develop MAPK14 inhibitors have ended in failed drug trials, usually due to toxicity [11]. In contrast to MAPK14, other members of the p38 MAPK family display restricted tissue and cellular expression, and therefore may represent viable targets for specific diseases. Along these lines, MAPK11 (p38β) is highly similar to MAPK14 (75% sequence identity), whereas MAPK12 (p38γ) and MAPK13 (p38δ) are more sequence diverse (62% and 61% identical to MAPK14, respectively). Also, the MAPK12/MAPK13 double knockout mouse displays no detrimental phenotypes, only reduced innate inflammatory responses induced by lipopolysaccharide (LPS) [12].

MAPK13 has recently emerged as a disease-specific p38 MAPK drug target. Compared to MAPK14, MAPK13 displays more tissue-specific

* Corresponding author at: Campus Box 8052, 660 S. Euclid, St. Louis, MO 63110, United States.
E-mail address: tbrett@wustl.edu (T.J. Brett).

http://dx.doi.org/10.1016/j.bbagen.2016.06.023
0304-4165/

expression patterns, and therefore contributes to more restricted functions [13,14]. This restricted expression pattern suggests that this kinase may be targeted in specific biological pathways. For example, MAPK13 regulates insulin secretion and survival of pancreatic β-cells, and MAPK13-deficient mice are protected against insulin resistance induced by a high-fat diet and oxidative stress-mediated β-cell failure, suggesting a role in diabetes [15]. MAPK13 is also pivotal in neutrophil chemotaxis pathways, where it contributes to acute respiratory distress syndrome (ARDS) [16]. In addition, studies in knockout mice indicate that MAPK13 contributes to pathways activated in chronic inflammatory conditions [12], is centrally involved in tumorogenesis in both colitis-associated colon cancer [17] and squamous cell carcinoma models [18], and is crucial for development of arthritis in certain models [19]. Finally, MAPK13 activation is required for IL-13-dependent airway mucus overproduction which is a characteristic feature of chronic inflammatory lung disease [20].

Given the role of MAPK13 in chronic lung disease (and possibly other diseases), we initiated the first structure-based drug project to develop inhibitors targeting MAPK13 [20]. This work also presented the first structures of MAPK13 complexes with inhibitors, and for any p38 MAPK family member other than MAPK14. As noted above, MAPK14 has been the subject of intense structure-based drug design efforts, and numerous structural and biophysical studies of MAPK14-inhibitor complexes have been reported (>170 structures in the PDB as of October 2015). Thus, much is known about the structural requirements for MAPK14 inhibition [21]. To develop a more complete understanding of the structural basis for activation of MAPK13, we developed methods to produce both unphosphorylated (inactive) and dually-phosphorylated (active) MAPK13 in quantities for structural and biophysical studies and used these proteins to study complexes with inhibitors for the purposes of targeting this kinase through structure-based drug design [20,22]. Here we present a complete functional, biophysical, and structural characterization of two new MAPK13-inhibitor complexes, new biophysical data on two previously reported complexes, and the first comprehensive analysis of MAPK13 in complex with all four structurally characterized inhibitors, which display greatly varying potency. These studies reveal the structural basis for differences in potency for this set of inhibitors.

2. Materials and methods

2.1. Materials

All inhibitors were synthesized at Washington University as described previously [20].

2.2. Expression constructs

Full-length human MAPK13 is 365 amino acids and contains several basic residues at the C-terminus. For crystallization, a slightly truncated MAPK13 construct (1–352) was designed and cloned into pET28a as a N-terminal 6-His-tagged construct using the *Nde*I and *Xho*I restriction endonuclease sites. A full-length human MAPK13 construct was prepared similarly to produce protein for enzyme inhibition and biophysical studies [20]. The construct was confirmed by sequencing. A pET28a construct of N-terminal-6-His-tagged lambda-phosphatase was a kind gift from Dima Klenchin (University of Wisconsin, Madison, WI).

2.3. Protein expression and purification

Constructs were transformed into Rosetta2 (DE3) *Escherichia coli* (Stratagene) and colonies were grown on a plate with kanamycin selection (50 μg/ml). Cultures for protein expression were grown in Luria broth (LB) media using chloramphenicol (40 μg/ml) and kanamycin (50 μg/ml) selection. Both the MAPK13 crystallization construct (1–352) and full-length protein (1–365) were expressed and purified in a similar manner, as outlined here. Protein expression was induced at 30 °C by addition of 0.5 mM isopropyl β-D-1-thiogalactopyranoside (IPTG) and each 1 L of media was enriched with 10 ml of saturated glucose solution during protein expression. Protein expression was carried out at 30 °C for 4 h.

Cell pellets were harvested by centrifugation and suspended in lysis buffer suitable for nickel-nitrilotriacetic acid (Ni-NTA) gravity chromatography (50 mM K_2HPO_4 pH 8.0, 300 mM NaCl, 10 mM imidazole, 10% glycerol, 10 mM 2-mercaptoethanol). Cells were lysed by addition of 0.5 mg/ml lysozyme and DNAse I followed by sonication. Clarified lysate was passed over Ni-NTA superflow resin (Qiagen), which was then washed with lysis buffer containing 20 mM imidazole and then proteins were eluted with 250 mM imidazole. The protein was further purified by gel filtration chromatography (Superdex 200) in a buffer consisting of 20 mM HEPES pH 7.5, 150 mM NaCl, 0.001% NaN_3, 5 mM dithiotreitol (DTT), and 10% glycerol. The protein eluted as a single peak correlating to a monomeric molecular weight [22]. This peak was harvested and then dephosphorylated *in vitro* by addition of lambda phosphatase (0.1 mg/ml) and 5 mM $MnCl_2$ at room temperature for 30 min, which was then quenched with 5 mM EDTA. This treatment was not very efficient and only increased the amount of dephosphorylated MAPK13 by about 10% [22]. Following dialysis against a buffer consisting of 20 mM Tris pH 8.0, 10 mM NaCl, 1 mM DTT, and 10% glycerol (buffer A) at 4 °C overnight, the protein was then subjected to anion exchange chromatography using a MonoQ column (GE Lifesciences). Protein was injected onto the column using buffer A and then eluted off using a gradient from 0 to 60% of buffer B (20 mM Tris pH 8.0, 1 M NaCl, 1 mM DTT, and 10% glycerol) over 40 column volumes. This resulted in separation of unphosphorylated and phosphorylated MAPK13 [22]. The unphosphorylated MAPK13 peak was harvested and used for structural studies with inhibitors. Full-length MAPK13 for enzyme inhibition and biophysical assays was expressed and purified similarly.

2.4. Preparation of MAPK13-inhibitor co-crystals

Crystals of non-phosphorylated MAPK13 were obtained by mixing protein solution (at 10 mg/ml) with reservoir solution (50 mM ammonium tartrate, 18% PEG 3350) in a 4:1 (protein: reservoir) ratio, similar to as previously described by us [20]. Co-crystal complexes with inhibitor compounds 58 and 117 were prepared by soaking, similar to our previous work. Inhibitor compound stocks were prepared in DMSO at 100 mM and then added to crystal-containing drops at 1:10 volume, for a final inhibitor concentration of 10 mM in the drop. Crystals were allowed to soak for 10 min to 4 h before cryoprotection in mother liquor supplemented with 25% ethylene glycol, followed by flash-freezing at −160 °C in a chilled nitrogen stream.

2.5. Data collection, reduction and structure determination

X-ray diffraction data were collected at either the Advanced Photon Source (beamline 19-ID) or the Advanced Light Source (beamline 4.2.2). Data were indexed and processed with HKL2000 [23]. The phase problem was solved by isostructural replacement using the apo form of MAPK13 (PDB ID: 4YNO) [20] in an initial round of rigid body refinement. Compounds were clearly visible in $F_O - F_C$ difference maps following rigid body refinement (see Fig. 3). Model rebuilding and compound fitting to electron density maps was performed manually using Coot [24] and refinement was carried out in PHENIX [25]. Structural analysis of MAPK13-inhibitor contacts was performed in LigPlot + [26]. All molecular graphics figures were produced using PyMOL [27]. All crystallographic software were obtained and maintained by the SBGrid distribution [28]. Diffraction images were deposited with the Structural Biology Data Grid [29]. Data collection and refinement statistics are summarized in Table 1.

Table 1
Crystallographic statistics for MAPK13 complexes with inhibitor compounds.

Compound	58	117
Data collection statistics		
Space group	$P2_12_12_1$	$P2_12_12_1$
Unit cell (Å)	a = 61.0	a = 61.3
	b = 70.2	b = 69.7
	c = 92.9	c = 93.1
Source	ALS 4.2.2	APS 19-ID
Wavelength (Å)	1.0000	0.9790
Resolution (Å)	50.0–2.60 (2.69-)	50.0–2.00 (2.07-)
R_{sym} (%)	9.1 (50.8)	5.5 (36.9)
Completeness (%)	88.5 (100)	81.2 (87.8)
Redundancy	7.0 (7.3)	4.6 (4.4)
I/σ (I)	20.6 (3.6)	21.6 (2.5)
Refinement statistics		
R_{work} (%)	21.8	20.0
R_{free} (%)	27.3	24.1
Amino acid residues (#)	340	340
Waters (#)	23	213
RMSD bond length (Å)/angles (°)	0.003/0.667	0.004/0.904
Wilson B ($Å^2$)	48.4	31.3
Ave B. protein	52.2	37.0
Ave. B inhibitor	40.5	31.3
Ave. B water	48.1	42.7
Ramachandran		
%Favored	87.4	95.3
%Allowed	12.0	4.4
%Outliers	0.6	0.3
Poor rotamers (no./%)	12/3.99%	5/1.6%
Clashscore (score/percentile)	6.72/99th	6.10/95th
Molprobity (score/percentile)	2.16/94th	1.83/85th
Luzzati error	0.35	0.24
PDB ID	5EKN	5EKO

Values in parenthesis are for the highest-resolution shell.

2.6. Differential scanning fluorimetry

Melting temperature of MAPK13 and MAPK14 was measured in the presence of inhibitors (58, 61, 117, 124) using a Protein Thermal Shift Dye Kit (Life Technologies, CA) according to manufacturer's specifications. This assay used both the unphosphorylated and the phosphorylated forms of MAPK13 and unphosphorylated MAPK14 at a final concentration of 0.15 mg/ml in the reaction mixture. A titration experiment was carried out first to demonstrate specificity and establish dynamic range. Based on this, single point experiments were carried out on all kinases using a final inhibitor concentration of 25 μM. Each condition was replicated five times. The experiment was carried out on a 7500 Fast Real-Time PCR System (Life Technologies, CA) using the melt curve template. The initial incubation step at 25 °C was modified to be 30 min to ensure complex formation between the inhibitors and the proteins. Data were analyzed using Protein Thermal Shift Software v1.1 (Life Technologies). Additional statistical analysis was carried out in Prism v5.0c. Results are summarized in Fig. 6 and Table 3 and presented as mean ± S.E.M. Replicate experiments were carried out using three different protein preps on different days to obtain mean ± S.E.M.

2.7. MAPK13 inhibition assay

Compounds were assayed for inhibition of MAPK13 kinase activity using an immobilized metal affinity polarization (IMAP) as previously described [20]. Briefly, the assay contained activated (phosphorylated) MAPK13, a FITC-labeled substrate, and the test compound. Experiments were carried out at concentrations in the linear phase of the rate kinetics. Assay reactions contained 0–100 μM test compound, 5–35 nM (EC_{80}) activated MAPK13, 3 μM ($K_{m,app}$) ATP, and 100 nM FITC-labeled EGFR peptide substrate (FITC-KRELVERLTPSGEAPNQALLR-NH_2). The IC_{50} values for each compound were determined from the compound concentration versus fluorescence polarization (mP) plot using nonlinear curve fitting.

2.8. Inhibitor binding kinetics measured by biolayer interferometry

Kinetics of MAPK13 binding to small molecules was assessed using bio-layer interferometry with an Octet (ForteBio, Menlo Park, CA) as described previously [20]. MAPK13 was randomly biotinylated *in vitro* using EZ-link NHS-PEG4-Biotin (Thermo Scientific) at a 1:2 molar ratio (protein: reagent). Super-streptavidin-coated biosensors from ForteBio were used to capture biotinylated MAPK13 onto the surface of the sensor. After reaching baseline, sensors were moved to association step for 300 s and then dissociation for 300 s. Curves were corrected by a double-referencing technique using both biotin-coated pins dipped into the experimental wells and a buffer-only reference. The binding buffer consisted of 20 mM HEPES pH 7.5, 150 mM NaCl, 0.005% Tween 20, and 5% DMSO.

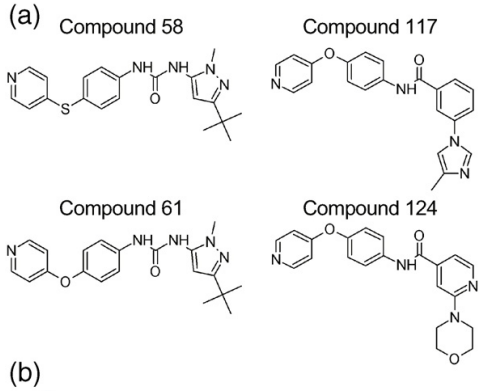

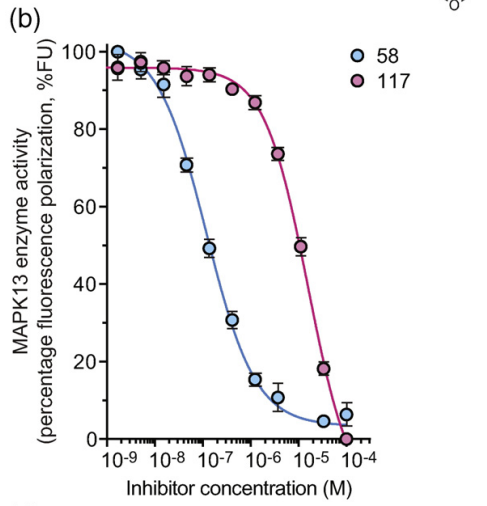

(c)

Compound	IC_{50}(nM)	95% Confidence	R^2
58	117	87-165	0.99
61*	620	530-724	0.99
117	15785	12530-19885	0.99
124*	98747	28862-337855	0.90

Fig. 1. Schematic of MAPK13 inhibitors and their IC_{50} values. (a) Schematic of MAPK13 inhibitor compounds characterized in this manuscript. (b) Data and curve fit used to determine IC_{50} values for compounds 58 and 117. Values represent mean and error bars are SEM. (c) IC_{50} values, 95% confidence range, and coefficients of determination (R^2). * denotes values were previously reported [20].

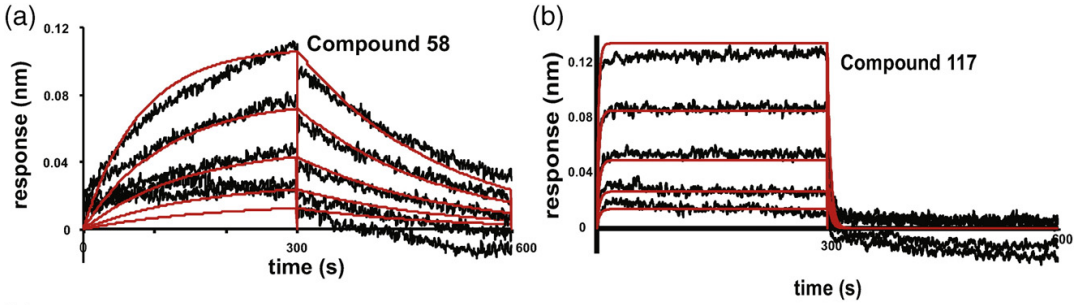

(c)

Compound	$t_{1/2}$(sec)	Binding Mode
58	137	DFG-out
61*	111	DFG-out
117	3	DFG-in
124*	1	DFG-in

Fig. 2. Biolayer interferometry analysis of MAPK13 binding to inhibitors. (a–b) Biolayer interferometry sensorgrams for (a) compound 58 and (b) compound 117. Processed data are shown as black lines with global kinetic fits overlaid as red lines. (c) Table of MAPK13-inhibitor complex half-lives derived from the global kinetic fits of $k_{association}$ and $k_{dissociation}$ ($t_{1/2} = \ln 2/k_{dissociation}$). * denotes values were previously reported [20].

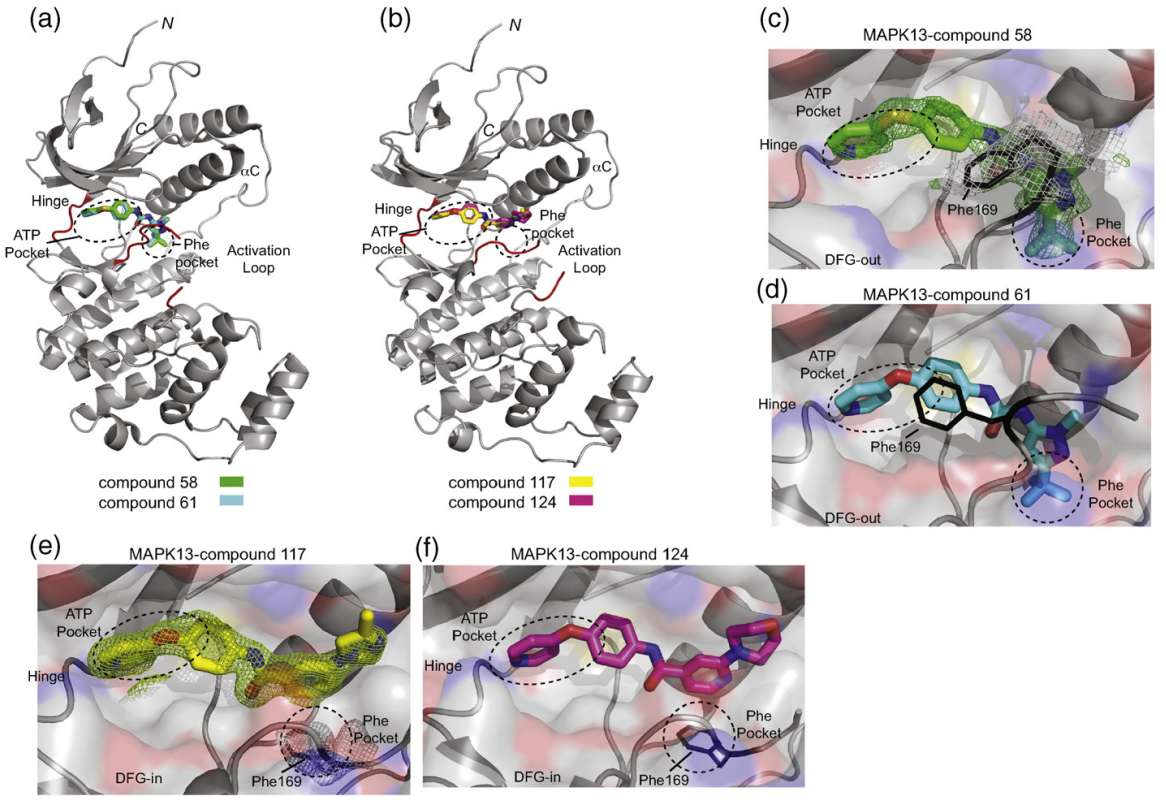

Fig. 3. Structures of MAPK13 complexes with inhibitors. (a) Ribbon diagram of MAPK13 (grey) with DFG-out inhibitors 58 and 61. Hinge and activation loop are both colored red. (b) Ribbon diagram of MAPK13 (grey) with DFG-in inhibitors 117 and 124. Hinge and activation loop are both colored red. (c) Crystal structure of compound 58 (green) in complex with MAPK13 in DFG-out mode. Omit *Fo – Fc* electron density contoured at 3.0 σ is shown for the compound and *2Fo – Fc* electron density contoured at 2.0 σ is shown for Phe169. (d) Our previously reported crystal structure of compound 61 (cyan) in complex with MAPK13 in DFG-out mode for comparison (4EYJ). (e) Crystal structure of compound 117 (yellow) in complex with MAPK13 in DFG-in mode. Omit *Fo – Fc* electron density contoured at 3.0 σ is shown for the compound and *2Fo – Fc* electron density contoured at 2.0 σ is shown for Phe169. (f) Our previously reported crystal structure of compound 124 (magenta) in complex with MAPK13 in DFG-in mode for comparison (4EYM). The dynamic positioning of Phe169 of the DFG motif is shown in all complexes.

Table 2
Backbone torsion angles that define the conformation of the MAPK13 DFG motif.

Compound	DFG conformation	Leu 167		Asp 168		Phe 169	
		φ (°)	ψ (°)	φ (°)	ψ (°)	φ (°)	ψ (°)
58	DFG-out	−124.5	170.8	−154.0	150.4		
61	DFG-out	−119.6	169.4	−144.7	93.6	−66.0	−22.9
117	DFG-in	−107.8	156.4	62.5	37.1	−82.5	150.0
124	DFG-in	−111.3	160.9	55.5	39.7	−81.9	162.6

MAPK13-inhibitor complex half-lives were calculated from dissociation constants determined from global kinetic analysis ($t_{1/2} = \ln 2/k_{dissociation}$).

2.9. Computational docking

In silico docking studies were carried out in GLIDE from the Schrodinger Suite [30,31]. All inhibitors were treated as ligands and prepared from their SMILES strings using LigPrep without changing ionization states. Protein coordinates were imported from pdb files and processed using the Protein Preparation Wizard (PDB ID 4MP9 for MAPK13 DFG-out; 4MP5 for MAPK13 DFG-in; 1KV2 for MAPK14 DFG-out; 1P38 for MAPK14 DFG-in). A rigid grid of 36 Å was generated centered on the DFG residues. Ligands were docked flexibly into the grid in Standard Precision (SP) mode. After the docking simulation was completed, the protein was overlapped with the coordinates from the co-crystal structures. RMSD between the docked coordinates and the crystal coordinates for the inhibitor was calculated using a command-line script, rmsd.py (available from http://www.schrodinger.com/scriptcenter/14). Results are summarized in Table 4.

3. Results and discussion

3.1. A series of inhibitors with greatly varied potencies for MAPK13

Here we report the steady-state, biophysical, and structural evaluation of a set of MAPK13 inhibitors. The inhibitor design was inspired by analyzing potent MAPK14-inhibitor complex structures, superposing on our unphosphorylated (apo) MAPK13 structure, and realizing smaller substituents in the ATP-binding pocket would be required for optimal binding [20]. Specifically, we focused on BIRB-796, which binds to MAPK14 in DFG-out mode and exhibits an IC_{50} of 4 nM, and inhibits other p38 isoforms, but at much lower potencies (IC_{50} = 520 nM for MAPK13) [32]. Superposition of BIRB-796 into MAPK13 indicated it could sterically clash with the gatekeeper residue, so we designed inhibitors with smaller substituents at this position that we hypothesized would bind in DFG-out mode [20]. We began by determining the IC_{50} values in a steady-state enzyme inhibition assay. These values for 1-(3-*tert*-butyl-1-methyl-1H-pryzol-5-yl)-3-[4-(pyridin-4-yloxy)phenyl]urea (compound 61) and 2-(morpholin-4-yl)-*N*-[4-(pyridin-4-yloxy)phenyl] pyridine-4-carboxamide (compound 124) were reported previously [20]. Here we determine the IC_{50} values for 1-(3-*tert*-butyl-1-

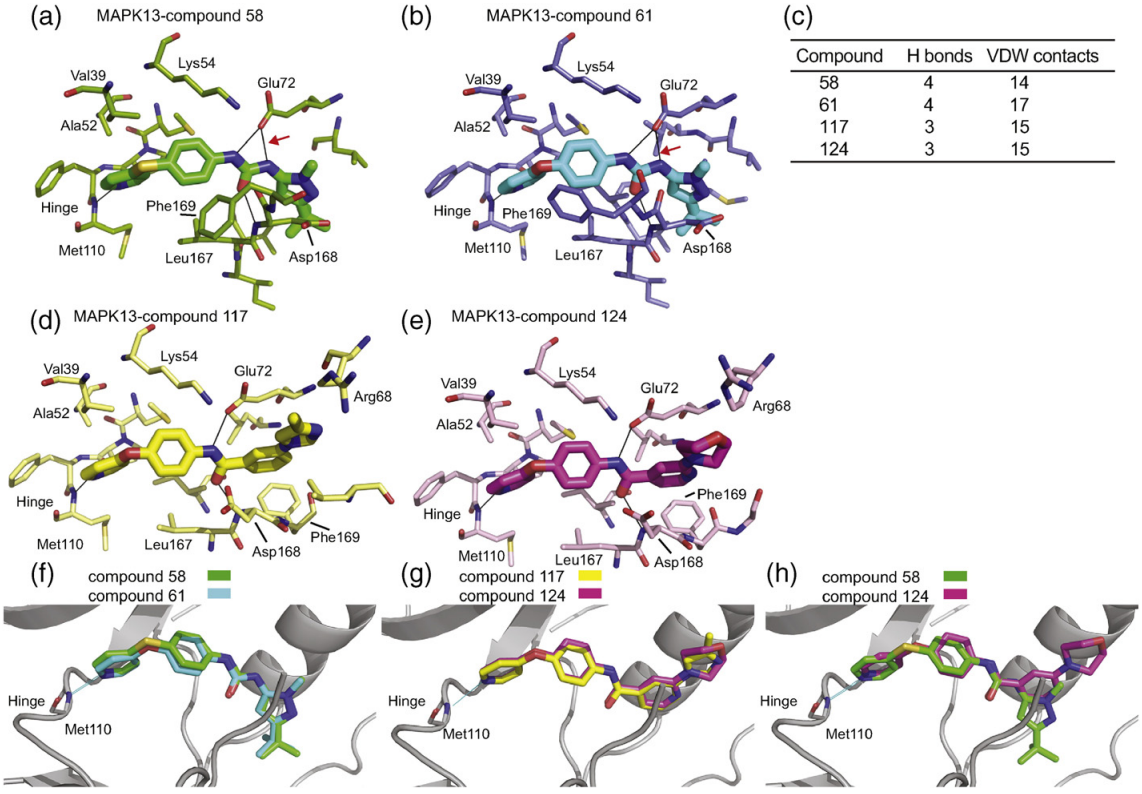

Fig. 4. MAPK13 binding pockets for inhibitor compounds. Binding pockets for (a) compound 58, (b) compound 61, (d) compound 117, and (e) compound 124. All residues that make van der Waals or polar contacts are shown. Hydrogen bonds are shown as thin black lines. One hydrogen bond that is unique to compounds 58 and 61 as compared to 117 and 124 is highlighted with the red arrow. (c) Table of polar and non-polar contacts each compound makes with MAPK13. (f–h) Overlay comparison showing hinge interactions with the pyridinyl rings of (f) compounds 58 and 61, (g) compounds 117 and 124, and (h) compounds 58 and 124. Note in (h) that there is a displacement of 0.5 Å for the pyridinyl nitrogen in comparing 58 and 124.

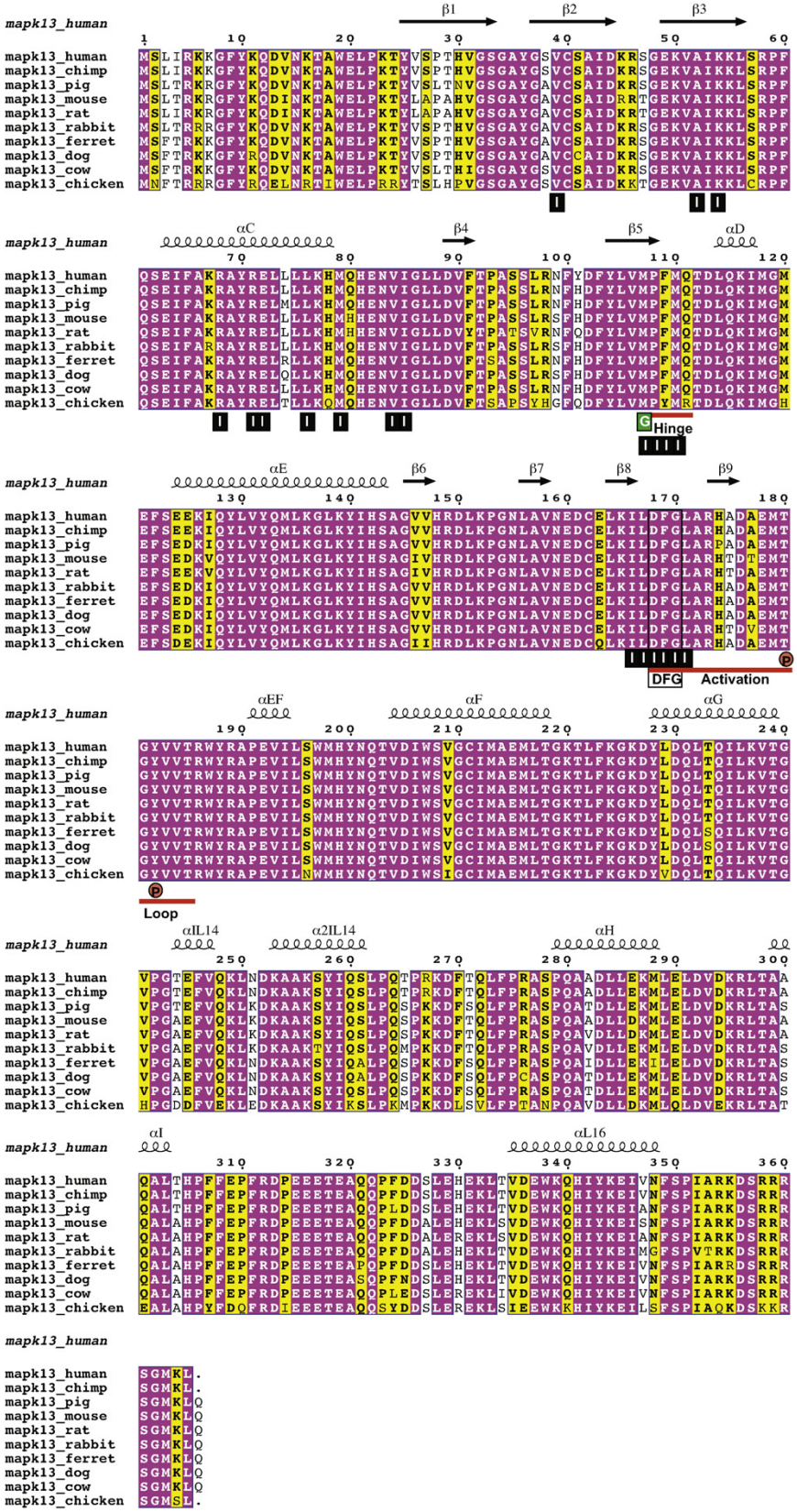
mapk13_human
β1
β2
β3
mapk13_human MSLIRKKGFYKQDVNKTAWELPKTYVSPTHVGSGAYGSVCSAIDKRSGEKVAIKKLSRPF
mapk13_chimp MSLIRKKGFYKQDVNKTAWELPKTYVSPTHVGSGAYGSVCSAIDKRSGEKVAIKKLSRPF
mapk13_pig MSLTRKRGFYKQDVNKTAWELPKTYVSLTNVGSGAYGAVCSAIDKRSGEKVAIKKLSRPF
mapk13_mouse MSLTRKRGFYKQDINKTAWELPKTYLAPAHVGSGAYGAVCSAIDRRTGEKVAIKKLSRPF
mapk13_rat MSLIRKRGFYKQDINKTAWELPKTYLAPAHVGSGAYGAVCSAIDKRTGEKVAIKKLSRPF
mapk13_rabbit MSLTRRRGFYKQDVNKTAWELPKTYVSPTHVGSGAYGAVCSAIDKRSGEKVAIKKLSRPF
mapk13_ferret MSFTRKKGFYKQDVNKTAWELPKTYVSPTHVGSGAYGAVCSAIDKRSGEKVAIKKLSRPF
mapk13_dog MSFTRKKGFYRQDVNKTAWELPKTYVSPTHVGSGAYGAVCCAIDKRSGEKVAIKKLSRPF
mapk13_cow MSFTRKKGFYKQDVNKTAWELPKTYVSLTHIGSGAYGSVCSAIDKRSGEKVAIKKLSRPF
mapk13_chicken MNFTRRRGFYRQELNRTIWELPRRYTSLHPVGSGAYGSVCSAIDKKTGEKVAIKKLCRPF
αC
β4
β5
αD
mapk13_human QSEIFAKRAYRELLLLKHMQHENVIGLLDVFTPASSLRNFYDFYLVMPFMQTDLQKIMGM
mapk13_chimp QSEIFAKRAYRELLLLKHMQHENVIGLLDVFTPASSLRNFHDFYLVMPFMQTDLQKIMGM
mapk13_pig QSEIFAKRAYRELMLLKHMQHENVIGLLDVFTPASSLRNFHDFYLVMPFMQTDLQKIMGM
mapk13_mouse QSEIFAKRAYRELLLLKHMHHENVIGLLDVFTPASSLRSFHDFYLVMPFMQTDLQKIMGM
mapk13_rat QSEIFAKRAYRELLLLKHMHHENVIGLLDVYTPATSVRNFQDFYLVMPFMQTDLQKIMGM
mapk13_rabbit QSEIFARRAYRELLLLKHMQHENVIGLLDVFTPASSLRSFHDFYLVMPFMQTDLQKIMGM
mapk13_ferret QSEIFAKRAYRELRLLKHMQHENVIGLLDVFTSASSLRNFHDFYLVMPFMQTDLQKIMGM
mapk13_dog QSEIFAKRAYRELQLLKHMQHENVIGLLDVFTPASSLRSFHDFYLVMPFMQTDLQKIMGM
mapk13_cow QSEIFAKRAYRELLLLKHMQHENVIGLLDVFTPASSLRNFHDFYLVMPFMQTDLQKIMGM
mapk13_chicken QSEIFAKRAYRELTLLKQMQHENVIGLLDVFTSAPSYHGFQDFYLVMPYMRTDLQKIMGH
Hinge
αE
β6
β7
β8
β9
mapk13_human EFSEEKIQYLVYQMLKGLKYIHSAGVVHRDLKPGNLAVNEDCELKILDFGLARHADAEMT
mapk13_chimp EFSEEKIQYLVYQMLKGLKYIHSAGVVHRDLKPGNLAVNEDCELKILDFGLARHADAEMT
mapk13_pig EFSEDKIQYLVYQMLKGLKYIHSAGVVHRDLKPGNLAVNEDCELKILDFGLARPADAEMT
mapk13_mouse EFSEDKVQYLVYQMLKGLKYIHSAGIVHRDLKPGNLAVNEDCELKILDFGLARHTDTEMT
mapk13_rat EFSEEKVQYLVYQMLKGLKYIHSAGIVHRDLKPGNLAVNEDCELKILDFGLARHTDAEMT
mapk13_rabbit EFSEDKIQYLVYQMLKGLKYIHSAGVVHRDLKPGNLAVNEDCELKILDFGLARHADAEMT
mapk13_ferret EFSEDKIQYLVYQMLKGLKYIHSAGVVHRDLKPGNLAVNEDCELKILDFGLARHADAEMT
mapk13_dog EFSEDKIQYLVYQMLKGLKYIHSAGVVHRDLKPGNLAVNEDCELKILDFGLARHADAEMT
mapk13_cow EFSEDKIQYLVYQMLKGLKYIHSAGVVHRDLKPGNLAVNEDCELKILDFGLARHTDVEMT
mapk13_chicken EFSDEKIQYLVYQMLKGLKYIHSAGIIHRDLKPGNLAVNEDCQLKILDFGLARHADAEMT
DFG
Activation
αEF
αF
αG
mapk13_human GYVVTRWYRAPEVILSWMHYNQTVDIWSVGCIMAEMLTGKTLFKGKDYLDQLTQILKVTG
mapk13_chimp GYVVTRWYRAPEVILSWMHYNQTVDIWSVGCIMAEMLTGKTLFKGKDYLDQLTQILKVTG
mapk13_pig GYVVTRWYRAPEVILSWMHYNQTVDIWSVGCIMAEMLTGKTLFKGKDYLDQLTQILKVTG
mapk13_mouse GYVVTRWYRAPEVILSWMHYNQTVDIWSVGCIMAEMLTGKTLFKGKDYLDQLTQILKVTG
mapk13_rat GYVVTRWYRAPEVILSWMHYNQTVDIWSVGCIMAEMLTGKTLFKGKDYLDQLTQILKVTG
mapk13_rabbit GYVVTRWYRAPEVILSWMHYNQTVDIWSVGCIMAEMLTGKTLFKGKDYLDQLTQILKVTG
mapk13_ferret GYVVTRWYRAPEVILSWMHYNQTVDIWSVGCIMAEMLTGKTLFKGKDYLDQLSQILKVTG
mapk13_dog GYVVTRWYRAPEVILSWMHYNQTVDIWSVGCIMAEMLTGKTLFKGKDYLDQLSQILKVTG
mapk13_cow GYVVTRWYRAPEVILSWMHYNQTVDIWSVGCIMAEMLTGKTLFKGKDYLDQLTQILKVTG
mapk13_chicken GYVVTRWYRAPEVILNWMHYNQTVDIWSIGCIMAEMLTGKTLFKGKDYVDQLTQILKVTG
Loop
αIL14
α2IL14
αH
mapk13_human VPGTEFVQKLNDKAAKSYIQSLPQTPRKDFTQLFPRASPQAADLLEKMLELDVDKRLTAA
mapk13_chimp VPGTEFVQKLNDKAAKSYIQSLPQTPRKDFTQLFPRASPQAADLLEKMLELDVDKRLTAA
mapk13_pig VPGTEFVQKLKDKAAKSYIQSLPQSPKKDFSQLFPRASPQATDLLEKMLELDVDKRLTAS
mapk13_mouse VPGAEFVQKLKDKAAKSYIQSLPQSPKKDFTQLFPRASPQAADLLDKMLELDVDKRLTAA
mapk13_rat VPGAEFVQKLKDKAAKSYIQSLPQSPKKDFTQLFPRASPQAVDLLDKMLELDVDKRLTAA
mapk13_rabbit VPGAEFVQKLKDKAAKTYIQSLPQMPKKDFTQLFPRASPQAVDLLEKMLELDVDKRLTAS
mapk13_ferret VPGAEFVQKLNDKAAKSYIQALPQSPKKDFSQLFPRASPQAIDLLEKILELDVDKRLTAS
mapk13_dog VPGAEFVQKLNDKAAKSYIQALPQSPKKDFSQLFPCASPQATDLLEKMLELDVDKRLTAS
mapk13_cow VPGAEFVQKLNDKAAKSYIQSLPQSPKKDFSQLFPRASPQATDLLEKMLELDVDKRLTAS
mapk13_chicken HPGDDFVEKLEDKAAKSYIKSLPKMPKKDLSVLFPTANPQAVDLLDKMLQLDVEKRLTAT
αI
αL16
mapk13_human QALTHPFFEPFRDPEEETEAQQPFDDSLEHEKLTVDEWKQHIYKEIVNFSPIARKDSRRR
mapk13_chimp QALTHPFFEPFRDPEEETEAQQPFDDSLEHEKLTVDEWKQHIYKEIVNFSPIARKDSRRR
mapk13_pig QALTHPFFEPFRDPEEETEAQQPLDDSLEHEKLTVDEWKQHIYKEIANFSPIARKDSRRR
mapk13_mouse QALAHPFFEPFRDPEEETEAQQPFDDALEHEKLSVDEWKQHIYKEISNFSPIARKDSRRR
mapk13_rat QALAHPFFEPFRDPEEETEAQQPFDDALEREKLSVDEWKQHIYKEIANFSPIARKDSRRR
mapk13_rabbit QALAHPFFEPFRDPEEETEAQQPFDDALEHEKLTVDEWKQHIYKEIMGFSPVTRKDSRRR
mapk13_ferret QALAHPFFEPFRDPEEETEAPQPFDDSLEHEKLTVDEWKQHIYKEIVNFSPIARRDSRRR
mapk13_dog QALAHPFFEPFRDPEEETEASQPFNDSLEHEKLTVDEWKQHIYKEIVNFSPIARKDSRRR
mapk13_cow QALAHPFFEPFRDPEEETEAQQPLEDSLERKLIVDEWKQHIYKEIVNFSPIARKDSRRR
mapk13_chicken EALAHPYFDQFRDIEEETEAQQSYDDSLERKLSIEEWKKHIYKEILSFSPIAQKDSKKR
mapk13_human
mapk13_human SGMKL.
mapk13_chimp SGMKL.
mapk13_pig SGMKLQ
mapk13_mouse SGMKLQ
mapk13_rat SGMKLQ
mapk13_rabbit SGMKLQ
mapk13_ferret SGMKLQ
mapk13_dog SGMKLQ
mapk13_cow SGMKLQ
mapk13_chicken SGMSL.

methyl-1H-pyrazol-5-yl)-3-[4-(pyridin-4-ylsulfanyl)phenyl]urea (compound 58) and 3-(4-methyl-1H-imidazol-1-yl)-*N*-[4-(pyridin-4-xyloxy) phenyl] benzamide (compound 117) (Fig. 1a). Surprisingly, the IC_{50} values varied over a wide range; while compounds 58 and 61 displayed IC_{50} values in the nanomolar range, compounds 117 and 124 displayed IC_{50} values in the micromolar range, over 800-fold less potent (Fig. 1b and c).

3.2. Kinetic and binding analysis of inhibitors with MAPK13

Inhibitor binding kinetics has become an important drug design criteria. In particular, slow dissociation rates have been associated with improved inhibitor activities due to prolonged target engagement *in vivo* [33]. To understand whether inhibitor binding kinetics correlated with potency, we analyzed this property using biolayer interferometry (BLI), in a manner similar to that for compounds 61 and 124 reported previously [20]. In these assays, biotinylated MAPK13 was immobilized on the streptavidin-coated BLI pin and association and dissociation kinetics were analyzed. The two compounds that displayed IC_{50} values in the nanomolar range displayed slower association and dissociation rates with around 100-fold longer complex half-lives ($t_{1/2}$ = 111 to 137 s) as compared to inhibitor compounds with micromolar IC_{50} values ($t_{1/2}$ = 1 to 3 s) (Fig. 2a–c). These kinetic constants are of similar magnitude as those for MAPK14 complexes with inhibitors measured by surface plasmon resonance (SPR) [34]. We hypothesized that this difference could correlate with different binding modes or binding pockets utilized by the inhibitors.

3.3. MAPK13 inhibitors display two different binding modes

In order to elucidate how our novel inhibitors bound to MAPK13, we determined the X-ray crystal structures of the complexes (Table 1). We had noticed during our structural analysis of the inactive (MAPK13) and dually-phosphorylated active (MAPK13/pTpY) forms of the protein [22] that a significant portion of the activation loop (residues 173–180), which is ordered in the dual-phosphorylated protein, is not visible in our high resolution electron density maps of the unphosphorylated form. We therefore reasoned that we should be able to obtain inhibitor complexes with MAPK13 *via* soaking inhibitors into crystals of the unphosphorylated form, and indeed we were able to demonstrate the validity of this method previously with the crystal structures of MAPK13 in complex with compounds 61 (PDB ID: 4EYJ) and 124 (4EYM). We observed a strong difference electron density for the two new compounds using this method (Fig. 3c & e). We found that the compounds displaying nanomolar IC_{50} values all bound similarly and occupied the ATP binding pocket, as well as an adjacent pocket usually occupied by Phe169 (of the DFG motif), displacing it from this pocket (Fig. 3a, c–d, and Table 2). This mode of binding has been termed as "DFG-out" and was first observed in the complexes of c-Abl with Gleevac [35] and MAPK14 with BIRB-796 [36]. In contrast, compounds displaying micromolar IC_{50} values bound in a similar manner, but did not displace Phe169 from the pocket (Fig. 3b, e, f), binding to MAPK13 in what is known as "DFG-in" mode (Table 2). Thus, in the case of the MAPK13 inhibitors presented here, it appears that binding mode creates a marked difference in potency. However, it should be noted that highly potent inhibitors that bind to MAPK14 in DFG-in mode have been identified (*e.g.*, skepinone-L [5] and SB203580 [37]), so binding mode does not always dictate efficacy.

3.4. Analysis of binding pocket interactions of inhibitors in complex with MAPK13

To understand the structural basis for the observed binding modes exhibited by the different MAPK13-inhibitor complexes, we performed a comprehensive analysis of the binding pockets occupied by each inhibitor. The inhibitors analyzed here have similar designs, consisting of a heterocyclic ring that interacts with the hinge region of MAPK13, a central aromatic that occupies the ATP-binding site, and a bulky (mostly hydrophobic) group, with these units spanned with by various polar linkers (Fig. 1a). The binding pockets were very similar, with similar numbers of van Der Waals contacts and hydrogen bonds to MAPK13. We found that, compared to the micromolar inhibitors, the nanomolar inhibitors engaged in one additional hydrogen bond with MAPK13 (3 versus 4) (Fig. 4c). All inhibitors engaged in hydrogen bonds with the backbone amide nitrogens of Met110 (in the hinge) and Asp168 (in the DFG motif) (Fig. 4a, b, d, e). The main difference was seen in interactions involving the side-chain carboxylic acid of Glu72. This side-chain engages in a hydrogen bond with the linker between central aromatic and bulky hydrophobic groups in these inhibitors. The nanomolar inhibitors all contain urea linkers whereas the micromolar inhibitors both contain amide linkers. The second hydrogen bond made possible with the urea linkages (red arrow, Fig. 4a, b) assists to lock the bulky hydrophobic groups in relative conformations that require the moieties to bind to the Phe pocket, thus making these inhibitors selective for the DFG-out conformation of the kinase. In addition, the extra atom in the urea versus amide linkage likely assists in optimal positioning of terminal hydrophobic groups to access the allosteric Phe169 pocket. Analysis of the hinge hydrogen bond with the pyridine moieties found in each of these inhibitors showed that in the DFG-in inhibitors (compounds 58 and 61) this hydrogen bond is about 2.5 Å (Fig. 4f, h), whereas this distance is about 3.0 Å in the DFG-out inhibitors (117 and 124) (Fig. 4g, h). Thus it appears that the shorter linkage (amide versus urea) also impacts inhibitor potency by lowering the strength of the hinge hydrogen bond interaction in an attempt to optimally bind the hydrophobic pockets on the opposite end of the molecule. Therefore, it appears from analysis of these compounds in complex with MAPK13 that not only does the urea linkage provide additional hydrogen bonding ability with MAPK13, it also assists in providing optimal spacing of large ring groups to optimally bind to respective pockets, including the allosteric Phe169 pocket. However, it should be noted that biphenyl amide inhibitors similar to compounds 117 and 124 have previously been observed to bind to both DFG-in and DFG-out conformations of MAPK14 and bind in similar modes to those observed in our MAPK13 structures [34], thus the inclusion of such groups does not dictate that these inhibitors can only bind in DFG-in modes.

3.5. Sequence comparison of inhibitor binding pockets in mammalian MAPK13 proteins

Given that numerous animal systems are used for *in vitro* studies, we carried out analysis of MAPK13 sequences from higher mammals to examine whether there were any gross differences in the MAPK13 binding pockets for the inhibitors characterized here. The MAPK13 sequences for the species analyzed here averaged >90% identity (Fig. 5). Of the numerous residues lining the binding pocket for the inhibitors, only one displayed a very conservative variation. Residue Phe109 (in the hinge region) is a Tyr in chicken MAPK13 (Fig. 5). Structure-based analysis of the inhibitor binding pocket sequence conservation would suggest

Fig. 5. Sequence alignment of MAPK13 from relevant disease model mammals. Invariant and conserved residues are highlighted with magenta and yellow backgrounds, respectively. Secondary structure of human MAPK13 is shown above the alignment. The hinge region, DFG motif, gatekeeper (G), dual phosphorylation site (P), and activation loop are shown. Residues that form the binding pockets for inhibitor compounds are marked (black I). Figure was generated using *ESPript3.0* [43].

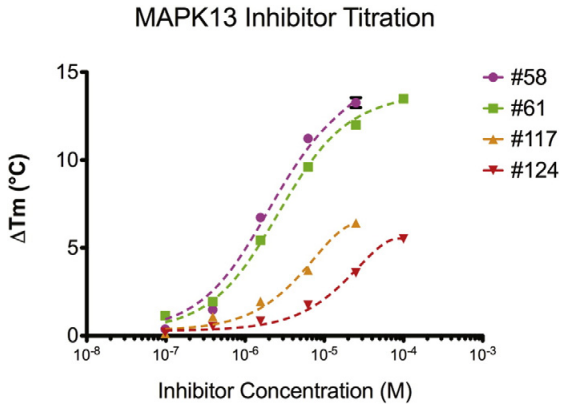

Fig. 6. Changes in MAPK13 melting temperatures (ΔT_m) induced by binding inhibitors as measured by DSF. Titration of inhibitors is shown while MAPK13 concentration was held at 0.15 mg/ml. The point at each concentration is an average of three replicate experiments conducted with different protein preps. Error bars are SEM. Curve fitting done in PRISM 5 using the one site total binding equation for nonlinear regression. Calculated Kd's listed in Table 3.

that the inhibitors analyzed here should bind similarly to MAPK13 proteins in common animal models.

3.6. Thermodynamic stability of MAPK13 complexes with inhibitors

Previous studies have demonstrated the use of differential scanning fluorimetry as a method for identifying potential kinase inhibitors based on the enhanced thermal stability upon complexation [38,39]. A general observation has been that more potent kinase inhibitors lend greater thermal stability to the protein [40]. We decided to analyze our diverse potency inhibitors using this method. We carried out experiments with both the inactive (unphosphorylated) MAPK13 and active (dually-phosphorylated) MAPK13/pTpY, as well as with MAPK14. First, we carried out a titration on MAPK13 to establish a dynamic range for the inhibitors (Fig. 6). Based on this result, we carried out subsequent experiments with 25 μM inhibitor. The differences in melting temperatures using the two forms of MAPK13 were similar, indicating that the inhibitors effectively bound both forms of the protein (Table 3). The melting point shifts were about a degree higher for MAPK13/pTpY, likely due to the fact that this form is stabilized by contacts involving the phosphorylated activation loop, [22] which would be dislodged by the DFG-out inhibitors. We found that the micromolar inhibitors (compounds 117 and 124) induced small increases in melting temperatures of MAPK13 (1–2 °C). In contrast, the nanomolar inhibitors all induced large shifts in melting temperatures of MAPK13 (7–8 °C). In addition, we found that our inhibitors induced larger T_m shifts in MAPK13 than MAPK14 (by a difference of 2–3 °C). For comparison, we also ran the DSF experiments with the potent MAPK14 inhibitor BIRB-796, which is optimized for MAPK14 (IC_{50} [MAPK14] = 4 nM; IC_{50} [MAPK13] = 520 nM) [32]. We found that the melting point shifts corresponded with the known differences in potencies (DTm [MAPK14] = 13.7 °C; [MAPK13] = 5.9 °C). Taken together, these results suggest our best inhibitors characterized here display slight selectivity for MAPK13 versus MAPK14, which should improve with optimization. Thus, the inhibitors which displayed the greatest potency and longest complex half-lives induced the greatest shift in thermal stability, indicating that this could be a robust screening method to presage inhibitor potency for MAPK13, and selectivity versus MAPK14.

Table 3
Inhibitor-induced thermal stability shifts measured by differential scanning fluorimetry (DSF).

Compound	ΔT_m-MAPK13 (°C)[a]	ΔT_m-MAPK13/pTpY (°C)[a]	ΔT_m-MAPK14 (°C)[a]	K_d (μM)[b]
58	8.1 ± 0.3	9.0 ± 0.4	5.2 ± 0.3	1.9 ± 0.3
61	7.2 ± 0.3	7.8 ± 0.4	5.1 ± 0.3	2.6 ± 0.5
117	1.8 ± 0.4	2.0 ± 0.5	−1.4 ± 0.4	N.D.[c]
124	1.1 ± 0.3	1.2 ± 0.5	−0.8 ± 0.3	N.D.
BIRB-796	5.9 ± 0.2		13.7 ± 0.3	

[a] ΔT_m are reported at inhibitor concentrations of 25 μM and kinase concentrations at 2.5 μM.
[b] Derived from titrations shown in Fig. 6.
[c] Not determined.

3.7. Computational analysis of inhibitor complexes

We carried out computational docking studies to gain further insight into why subsets of inhibitors bind to the DFG-in conformation versus the DFG-out conformation of MAPK13. In these calculations, the inhibitors were introduced as SMILES strings (with no predefined conformation) and were flexible during docking. The inhibitors were docked to MAPK13 coordinates in both the DFG-in and DFG-out mode. For compounds 58 and 61, which bind in the DFG-out mode, the calculations reproduced the crystal structures extremely accurately when docked to the MAPK13 DFG-out coordinates (Table 4). However, they showed high variation and poor docking scores when docked to MAPK13 in DFG-in coordinates. In contrast, for compounds 117 and 124, which bind in DFG-in mode, the calculations accurately reproduced the crystal structure coordinates for the inhibitors regardless of whether MAPK13 was in DFG-in or DFG-out mode (Table 4). In other words, regardless of whether or not the Phe pocket was available for inhibitor moiety binding, the DFG-in inhibitors preferred to bind to the same pockets as observed in the crystal structure. These calculations indicate that this set of inhibitor structures can be predicted fairly accurately using GLIDE, and imply that part of the selective driving force is goodness of fit to the available pockets and the inherent structure preferred by inhibitor. To analyze this further, we carried out the same calculation using MAPK14 in both DFG-in and DFG-out mode as the receptor for these inhibitors. With the MAPK14 structures, we obtained similar results as with MAPK13, and the simulations reproduced inhibitors binding configurations observed in the MAPK13 co-crystal structures. Thus, regardless of the receiver kinase, the inhibitors take on configurations observed in the crystal structures, indicating that the major driving forces for this set of inhibitors is chemically-encoded structural constraints of the compound and shape complementarity to available pockets.

4. Conclusions

Here we present the functional, biophysical, and structural characterization of two new inhibitor complexes with MAPK13, as well as the first comprehensive functional, biophysical, and structural analysis of all four of our inhibitor complexes, including the first use of thermodynamic and computational methods to study these complexes. These represent the only four MAPK13 inhibitor complexes structurally characterized to date, and are thus extremely valuable to drug design efforts that target this emerging molecular target. The inhibitors examined here displayed widely varying potencies, with IC_{50} values in either the nanomolar range, or, >800-fold less potent, in the micromolar range. These potencies correlated well with small-molecule binding kinetics measured by BLI. The nanomolar-potency inhibitors displayed complex half-lives about 100 times longer than those of the micromolar inhibitors. It should be noted that the half-lives measured here using BLI are comparable to those of MAPK14-inhibitor interactions measured by the comparable flow-based method of SPR [34]. Co-crystal structures of MAPK13 in complex with each of the four inhibitors revealed that the high potency inhibitors all bound to the kinase in DFG-out configuration, whereas the lower potency inhibitors both bound in DFG-in

Table 4
GLIDE *in silico* docking results compared to co-crystal structures.

Compound	58		61		117		124	
	Score[a]	RMSD[b]	Score	RMSD	Score	RMSD	Score	RMSD
MAPK13 DFG-out	−9.91	1.26	−8.88	1.23	−8.85	1.42	−8.24	1.62
MAPK13 DFG-in	−5.34	10.15	−5.21	9.99	−9.81	1.07	−6.14	2.00
MAPK14 DFG-out	−9.25	1.34	−8.70	1.10	−7.96	1.92	−4.20	12.71
MAPK14 DFG-in	−4.10	11.92	−4.16	12.25	−5.26	9.71	−8.15	3.57

[a] Glide Score in kcal/mol.
[b] RMSD of compound heavy atom positions compared to crystal structure (Å).

configuration. This is worth noting, since high potency inhibitors can be developed for either mode, for example skepinone-L [5] and SB203580 [37] are highly potent MAPK14 inhibitors that bind in DFG-in mode. Slow inhibitor dissociation rates have emerged as an important parameter for sustained efficacy of kinase inhibitors. In general, slower kinetics have been observed for inhibitors binding to the DFG-out mode of kinases, possibly due to kinetic constraints caused by the necessary structural reconfiguration [36,41]. However, the structural mechanisms that influence inhibitor binding kinetics are poorly understood, thus comprehensive structural and kinetic studies such as those presented here are quite valuable in creating these correlations. It can be noted that the structures for the inhibitor complexes were derived by soaking inhibitors into already formed crystals, and thus, may not be reflective of solution structure. However, given the correlation between the solid state observation of binding modes and the solution state biophysical data (binding thermodynamics, kinetics, and IC_{50} values) and computational predictions, we believe this is highly unlikely.

Detailed analysis of the binding pockets for the inhibitors revealed that all inhibitors, regardless of potency, interacted with MAPK13 in a very similar fashion, forming hydrogen bonds with the same residues in all four structures. The high potency inhibitors all engaged in one additional hydrogen bond, but computational docking and chemical reasoning indicate that this is mostly driven by the preferred lowest energy configuration of the inhibitor, which is intrinsic to its structure, and the goodness of fit of that conformation to the available pockets. It is worth noting that one of the development points of the GLIDE software has been to predict accurate kinase complexes with inhibitors [42]. The complexes with MAPK13 characterized here were readily predicted and suggest that this software approach could be used effectively for *in silico* screening to identify new chemical families with the potential to bind MAPK13.

DSF has been shown previously to be an effective method for screening for potential binders and inhibitors of kinases, and the thermal melting shifts usually correlate well with affinity [40]. We found this to be the case with the set of inhibitors here, with the thermal shifts also correlating with binding mode (DFG-in versus DFG-out). These thermal shifts appear to correlate with binding affinities of the inhibitors, as observed in our titration experiments. These experiments do suggest, however, that this method could be utilized effectively to identify new inhibitors for MAPK13 by screening and to prioritize ranking based on magnitude of melting point stabilization. These experiments also suggest this method could be used to screen for inhibitors that selectively target MAPK13 versus MAPK14. The inhibitors analyzed here have not been optimized yet for potency or selectivity, yet they do display some preference for binding MAPK13 in our DSF experiments. Combining our structural studies of inhibitor binding done here with sequence comparison of MAP13 versus MAPK14 [22], the most sequence divergent area that contacts the inhibitors is in the hinge region, thus this will be focus of our future iterations of inhibitor design.

Recent studies of disease models in MAPK13 knockout mice and cellular studies have highlighted the importance that signaling pathways relying on MAPK13 may contribute to several diseases, including certain types of asthma, arthritis, cancer, and diabetes [15,17–20]. Altogether, the functional, structural, and biophysical characterizations presented here provide the first comprehensive analysis of this type for inhibitor complexes with MAPK13, elucidating the structural basis for their mechanism of action, thus providing a knowledge base for the structure-based development of potent, and eventually specific, inhibitors.

Conflict of interest statement

The authors declare no competing financial interests.

Transparency Document

The transparency document associated with this article can be found, in online version.

Acknowledgements

This work was supported in part by funding from NIH R01-HL119813 (T.J.B), CADET P50-HL107183, CADET II UH2-HL123429 (M.J.H.), American Heart Association Predoctoral Fellowships PRE19970008 (Z.Y.) and PRE22110004 (D.L.K.), and a pre-doctoral training grant T32-GM007067 (D.L.K.). Results were derived from work performed at Argonne National Laboratory (ANL) Structural Biology Center and the Advanced Light Source, Berkeley CA (ALS). ANL is operated by U. Chicago Argonne, LLC, for the U.S. DOE, Office Biological and Environmental Research (DE-AC02-06CH11357). ALS is supported by the Office of Basic Energy Sciences of the U.S. DOE (DE-AC02-05CH11231).

PDB References: mitogen-activated protein kinase 13, complex with compound 58 (PDB ID: 5EKN); complex with compound 117 (PDB ID: 5EKO).

References

[1] Y.J. Feng, Y.Y. Li, The role of p38 mitogen-activated protein kinase in the pathogenesis of inflammatory bowel disease, J. Dig. Dis. 12 (2011) 327–332.
[2] G.L. Schieven, The p38alpha kinase plays a central role in inflammation, Curr. Top. Med. Chem. 9 (2009) 1038–1048.
[3] S. Muller, S. Knapp, Targeting kinases for the treatment of inflammatory diseases, Expert Opin. Drug Discovery 5 (2010) 867–881.
[4] M.J. Schnieders, T.S. Kaoud, C. Yan, K.N. Dalby, P. Ren, Computational insights for the discovery of non-ATP competitive inhibitors of MAP kinases, Curr. Pharm. Des. 18 (2012) 1173–1185.
[5] S.C. Koeberle, J. Romir, S. Fischer, A. Koeberle, V. Schattel, W. Albrecht, C. Grutter, O. Werz, D. Rauh, T. Stehle, S.A. Laufer, Skepinone-L is a selective p38 mitogen-activated protein kinase inhibitor, Nat. Chem. Biol. 8 (2012) 141–143.
[6] R. Azevedo, M. van Zeeland, H. Raaijmakers, B. Kazemier, J. de Vlieg, A. Oubrie, X-ray structure of p38alpha bound to TAK-715: comparison with three classic inhibitors, Acta Crystallogr. D Biol. Crystallogr. 68 (2012) 1041–1050.
[7] D.S. Millan, M.E. Bunnage, J.L. Burrows, K.J. Butcher, P.G. Dodd, T.J. Evans, D.A. Fairman, S.J. Hughes, I.C. Kilty, A. Lemaitre, R.A. Lewthwaite, A. Mahnke, J.P. Mathias, J. Philip, R.T. Smith, M.H. Stefaniak, M. Yeadon, C. Phillips, Design and synthesis of inhaled p38 inhibitors for the treatment of chronic obstructive pulmonary disease, J. Med. Chem. 54 (2011) 7797–7814.
[8] R.H. Adams, A. Porras, G. Alonso, M. Jones, K. Vintersten, S. Panelli, A. Valladares, L. Perez, R. Klein, A.R. Nebreda, Essential role of p38alpha MAP kinase in placental but not embryonic cardiovascular development, Mol. Cell 6 (2000) 109–116.
[9] J.S. Mudgett, J. Ding, L. Guh-Siesel, N.A. Chartrain, L. Yang, S. Gopal, M.M. Shen, Essential role for p38alpha mitogen-activated protein kinase in placental angiogenesis, Proc. Natl. Acad. Sci. U. S. A. 97 (2000) 10454–10459.

[10] K. Tamura, T. Sudo, U. Senftleben, A.M. Dadak, R. Johnson, M. Karin, Requirement for p38alpha in erythropoietin expression: a role for stress kinases in erythropoiesis, Cell 102 (2000) 221–231.
[11] D.M. Goldstein, T. Gabriel, Pathway to the clinic: inhibition of P38 MAP kinase. A review of ten chemotypes selected for development, Curr. Top. Med. Chem. 5 (2005) 1017–1029.
[12] A. Risco, C. del Fresno, A. Mambol, D. Alsina-Beauchamp, K.F. MacKenzie, H.T. Yang, D.F. Barber, C. Morcelle, J.S. Arthur, S.C. Ley, C. Ardavin, A. Cuenda, p38gamma and p38delta kinases regulate the Toll-like receptor 4 (TLR4)-induced cytokine production by controlling ERK1/2 protein kinase pathway activation, Proc. Natl. Acad. Sci. U. S. A. 109 (2012) 11200–11205.
[13] A. Risco, A. Cuenda, New insights into the p38gamma and p38delta MAPK pathways, J. Signal. Transduct. 2012 (2012) 520289.
[14] C. O'Callaghan, L.J. Fanning, O.P. Barry, p38delta MAPK: emerging roles of a neglected isoform, Int. J. Cell. Biol. 2014 (2014) 272689.
[15] G. Sumara, I. Formentini, S. Collins, I. Sumara, R. Windak, B. Bodenmiller, R. Ramracheya, D. Caille, H. Jiang, K.A. Platt, P. Meda, R. Aebersold, P. Rorsman, R. Ricci, Regulation of PKD by the MAPK p38delta in insulin secretion and glucose homeostasis, Cell 136 (2009) 235–248.
[16] A. Ittner, H. Block, C.A. Reichel, M. Varjosalo, H. Gehart, G. Sumara, M. Gstaiger, F. Krombach, A. Zarbock, R. Ricci, Regulation of PTEN activity by p38delta-PKD1 signaling in neutrophils confers inflammatory responses in the lung, J. Exp. Med. 209 (2012) 2229–2246.
[17] P. Del Reino, D. Alsina-Beauchamp, A. Escos, M.I. Cerezo-Guisado, A. Risco, N. Aparicio, R. Zur, M. Fernandez-Estevez, E. Collantes, J. Montans, A. Cuenda, Pro-oncogenic role of alternative p38 mitogen-activated protein kinases p38gamma and p38delta, linking inflammation and cancer in colitis-associated colon cancer, Cancer Res. (2014).
[18] R. Zur, L. Garcia-Ibanez, A. Nunez-Buiza, N. Aparicio, G. Liappas, A. Escos, A. Risco, A. Page, C. Saiz-Ladera, D. Alsina-Beauchamp, J. Montans, J.M. Paramio, A. Cuenda, Combined deletion of p38gamma and p38delta reduces skin inflammation and protects from carcinogenesis, Oncotarget 6 (2015) 12920–12935.
[19] G. Criado, A. Risco, D. Alsina-Beauchamp, M.J. Perez-Lorenzo, A. Escos, A. Cuenda, Alternative p38 MAPKs are essential for collagen-induced arthritis, Arthritis Rheum. 66 (2014) 1208–1217.
[20] Y.G. Alevy, A.C. Patel, A.G. Romero, D.A. Patel, J. Tucker, W.T. Roswit, C.A. Miller, R.F. Heier, D.E. Byers, T.J. Brett, M.J. Holtzman, IL-13-induced airway mucus production is attenuated by MAPK13 inhibition, J. Clin. Invest. 122 (2012) 4555–4568.
[21] M.R. Lee, C. Dominguez, MAP kinase p38 inhibitors: clinical results and an intimate look at their interactions with p38alpha protein, Curr. Med. Chem. 12 (2005) 2979–2994.
[22] Z. Yurtsever, S.M. Scheaffer, A.G. Romero, M.J. Holtzman, T.J. Brett, The crystal structure of phosphorylated MAPK13 reveals common structural features and differences in p38 MAPK family activation, Acta Crystallogr. D Biol. Crystallogr. 71 (2015) 790–799.
[23] Z. Otwinowski, W. Minor, Processing of X-ray diffraction data collected in oscillation mode, Methods Enzymol. 276 (1997) 307–326.
[24] P. Emsley, K. Cowtan, Coot: model-building tools for molecular graphics, Acta Crystallogr. D Biol. Crystallogr. 60 (2004) 2126–2132.
[25] P.D. Adams, R.W. Grosse-Kunstleve, L.W. Hung, T.R. Ioerger, A.J. McCoy, N.W. Moriarty, R.J. Read, J.C. Sacchettini, N.K. Sauter, T.C. Terwilliger, PHENIX: building new software for automated crystallographic structure determination, Acta Crystallogr. D Biol. Crystallogr. 58 (2002) 1948–1954.
[26] R.A. Laskowski, M.B. Swindells, LigPlot+: multiple ligand-protein interaction diagrams for drug discovery, J. Chem. Inf. Model. 51 (2011) 2778–2786.
[27] L.L.C. Schrodinger, The PyMOL Molecular Graphics System, Version 1.3r1(in) 2010.
[28] A. Morin, B. Eisenbraun, J. Key, P.C. Sanschagrin, M.A. Timony, M. Ottaviano, P. Sliz, Collaboration gets the most out of software, Elife 2 (2013), e01456.
[29] P.A. Meyer, S. Socias, J. Key, E. Ransey, E.C. Tjon, A. Buschiazzo, M. Lei, C. Botka, J. Withrow, D. Neau, K. Rajashankar, K.S. Anderson, R.H. Baxter, S.C. Blacklow, T.J. Boggon, A.M. Bonvin, D. Borek, T.J. Brett, A. Caflisch, C.I. Chang, W.J. Chazin, K.D. Corbett, M.S. Cosgrove, S. Crosson, S. Dhe-Paganon, E. Di Cera, C.L. Drennan, M.J. Eck, B.F. Eichman, Q.R. Fan, A.R. Ferre-D'Amare, J.C. Fromme, K.C. Garcia, R. Gaudet, P. Gong, S.C. Harrison, E.E. Heldwein, Z. Jia, R.J. Keenan, A.C. Kruse, M. Kvansakul, J.S. McLellan, Y. Modis, Y. Nam, Z. Otwinowski, E.F. Pai, P.J. Pereira, C. Petosa, C.S. Raman, T.A. Rapoport, A. Roll-Mecak, M.K. Rosen, G. Rudenko, J. Schlessinger, T.U. Schwartz, Y. Shamoo, H. Sondermann, Y.J. Tao, N.H. Tolia, O.V. Tsodikov, K.D. Westover, H. Wu, I. Foster, J.S. Fraser, F.R. Maia, T. Gonen, T. Kirchhausen, K. Diederichs, M. Crosas, P. Sliz, Data publication with the structural biology data grid supports live analysis, Nat. Commun. 7 (2016) 10882.
[30] T.A. Halgren, R.B. Murphy, R.A. Friesner, H.S. Beard, L.L. Frye, W.T. Pollard, J.L. Banks, Glide: a new approach for rapid, accurate docking and scoring. 2. Enrichment factors in database screening, J. Med. Chem. 47 (2004) 1750–1759.
[31] R.A. Friesner, J.L. Banks, R.B. Murphy, T.A. Halgren, J.J. Klicic, D.T. Mainz, M.P. Repasky, E.H. Knoll, M. Shelley, J.K. Perry, D.E. Shaw, P. Francis, P.S. Shenkin, Glide: a new approach for rapid, accurate docking and scoring. 1. Method and assessment of docking accuracy, J. Med. Chem. 47 (2004) 1739–1749.
[32] Y. Kuma, G. Sabio, J. Bain, N. Shpiro, R. Marquez, A. Cuenda, BIRB796 inhibits all p38 MAPK isoforms in vitro and in vivo, J. Biol. Chem. 280 (2005) 19472–19479.
[33] E.R. Wood, A.T. Truesdale, O.B. McDonald, D. Yuan, A. Hassell, S.H. Dickerson, B. Ellis, C. Pennisi, E. Horne, K. Lackey, K.J. Alligood, D.W. Rusnak, T.M. Gilmer, L. Shewchuk, A unique structure for epidermal growth factor receptor bound to GW572016 (Lapatinib): relationships among protein conformation, inhibitor off-rate, and receptor activity in tumor cells, Cancer Res. 64 (2004) 6652–6659.
[34] R.M. Angell, T.D. Angell, P. Bamborough, M.J. Bamford, C.W. Chung, S.G. Cockerill, S.S. Flack, K.L. Jones, D.I. Laine, T. Longstaff, S. Ludbrook, R. Pearson, K.J. Smith, P.A. Smee, D.O. Somers, A.L. Walker, Biphenyl amide p38 kinase inhibitors 4: DFG-in and DFG-out binding modes, Bioorg. Med. Chem. Lett. 18 (2008) 4433–4437.
[35] T. Schindler, W. Bornmann, P. Pellicena, W.T. Miller, B. Clarkson, J. Kuriyan, Structural mechanism for STI-571 inhibition of abelson tyrosine kinase, Science 289 (2000) 1938–1942.
[36] C. Pargellis, L. Tong, L. Churchill, P.F. Cirillo, T. Gilmore, A.G. Graham, P.M. Grob, E.R. Hickey, N. Moss, S. Pav, J. Regan, Inhibition of p38 MAP kinase by utilizing a novel allosteric binding site, Nat. Struct. Biol. 9 (2002) 268–272.
[37] Z. Wang, B.J. Canagarajah, J.C. Boehm, S. Kassisa, M.H. Cobb, P.R. Young, S. Abdel-Meguid, J.L. Adams, E.J. Goldsmith, Structural basis of inhibitor selectivity in MAP kinases, Structure 6 (1998) 1117–1128.
[38] F.H. Niesen, H. Berglund, M. Vedadi, The use of differential scanning fluorimetry to detect ligand interactions that promote protein stability, Nat. Protoc. 2 (2007) 2212–2221.
[39] M. Vedadi, F.H. Niesen, A. Allali-Hassani, O.Y. Fedorov, P.J. Finerty Jr., G.A. Wasney, R. Yeung, C. Arrowsmith, L.J. Ball, H. Berglund, R. Hui, B.D. Marsden, P. Nordlund, M. Sundstrom, J. Weigelt, A.M. Edwards, Chemical screening methods to identify ligands that promote protein stability, protein crystallization, and structure determination, Proc. Natl. Acad. Sci. U. S. A. 103 (2006) 15835–15840.
[40] O. Fedorov, F.H. Niesen, S. Knapp, Kinase inhibitor selectivity profiling using differential scanning fluorimetry, Methods Mol. Biol. 795 (2012) 109–118.
[41] L.M. Gruenbaum, R. Schwartz, J.R. Woska Jr., R.P. DeLeon, G.W. Peet, T.C. Warren, A. Capolino, L. Mara, M.M. Morelock, A. Shrutkowski, J.W. Jones, C.A. Pargellis, Inhibition of pro-inflammatory cytokine production by the dual p38/JNK2 inhibitor BIRB796 correlates with the inhibition of p38 signaling, Biochem. Pharmacol. 77 (2009) 422–432.
[42] P.D. Lyne, M.L. Lamb, J.C. Saeh, Accurate prediction of the relative potencies of members of a series of kinase inhibitors using molecular docking and MM-GBSA scoring, J. Med. Chem. 49 (2006) 4805–4808.
[43] P. Gouet, X. Robert, E. Courcelle, ESPript/ENDscript: extracting and rendering sequence and 3D information from atomic structures of proteins, Nucleic Acids Res. 31 (2003) 3320–3323.

Daniel L. Kober

Work Address:
660 S. Euclid Avenue
P.O. Box 8052
St. Louis, MO 63110

Contact:
Email: daniellkober@gmail.com
Cell: 314-807-4258

LinkedIn profile: www.linkedin.com/in/daniellkober

Professional Profile

Structural biologist with a strong track record of multiple publications and presentations. Interested in the application of structural biology to problems relevant to human health and disease. I have extensive experience with the tools of structural biology including recombinant protein production using mammalian and bacterial expression systems, protein purification, X-ray crystallography, small-angle X-ray scattering, circular dichroism spectroscopy, and differential scanning fluorimetry. Additionally, I have diverse experience in studying protein-protein and protein-small molecule interactions using biolayer interferometry, flow cytometry, ELISA, liposome sedimentation, and thermal stability assays. Finally, I have experience with molecular biology tools including molecular cloning, confocal microscopy and cellular signaling.

Highlights

Received two nationally competitive pre-doctoral fellowships from American Heart Association for my Ph.D. dissertation project.

Education

Washington University in St. Louis PhD expected May 2017
Ph.D. in Molecular Microbiology and Microbial Pathogenesis GPA: 3.81

Evangel University May 2012
B.S. in Biology and Chemistry awarded Summa Cum Laude GPA: 3.96

Research Experience

Graduate Research Assistant, Washington University in St. Louis 2012-present
Division of Basic Biological Sciences
Advisor: Dr. Thomas J. Brett
Thesis project:
Structural, functional, and biophysical characterization of TREM2 disease variants

University of Missouri, Research Experience for Undergrads 2011
PI: Dr. Stefan Sarafianos
Project: Expression, Purification, and Characterization of SARS Coronovirus proteins

Teaching Experience

Graduate Teaching Assistant 2014
Washington University in St. Louis
Course: Molecular Microbiology and Pathogenesis
Coursemaster:. Dr. Joseph Vogel
Responsibilities: Journal club sessions, exam writing and grading.

Laboratory Teaching Assistant 2010-2012
Evangel University
Courses: Microbiology, Genetics, Organic Chemistry
Coursemasters: Dr. Glenner Richards, Dr. Fred Fortunato
Responsibilities: Preparing lab materials, teaching microbial and molecular techniques.

Publications

Kober DL and Brett TJ. *TREM2-ligand interactions in health and disease.* (In Press. J. Molecular Biology).

Kober DL, Alexander-Brett JM, Karch CM, Cruchaga C, Colonna M, Holtzman MJ, Brett TJ. *Neurodegenerative disease mutations in TREM2 reveal a functional surface and distinct loss-of-function mechanisms*. eLife 12/2016; 5. DOI:10.7554/eLife.20391

Yurtsever Z, Patel DA, **Kober DL**, Su A, Miller CA, Romero AG, Holtzman MJ, Brett TJ. *First comprehensive structural and biophysical analysis of MAPK13 inhibitors targeting DFG-in and DFG-out binding modes*. Biochimica et Biophysica Acta 06/2016; 1860(11). DOI:10.1016/j.bbagen.2016.06.023

Kober DL*, Yurtsever Z*, Brett TJ. *Efficient Mammalian Cell Expression and Single-step Purification of Extracellular Glycoproteins for Crystallization*. Journal of Visualized Experiments 12/2015; 2015(106). DOI:10.3791/53445 *Contributed equally

Wu K, Byers DE, Jin X, Agapov E, Alexander-Brett JM, Patel AC, Cella M, Gilfilan S, Colonna M, **Kober DL**, Brett TJ, Holtzman MJ. *TREM-2 promotes macrophage survival and lung disease after respiratory viral infection*. Journal of Experimental Medicine 04/2015; 212(5). DOI:10.1084/jem.20141732

Kober DL, Wanhainen KM, Johnson BM, Randolph DT, Holtzman MJ, Brett TJ. *Preparation, crystallization, and preliminary crystallographic analysis of wild-type and mutant human TREM-2 ectodomains linked to neurodegenerative and inflammatory diseases*. Protein Expression and Purification 04/2014; 96. DOI:10.1016/j.pep.2014.01.015

Combs MD, Knutsen RH, Broekelmann TJ, Toennies HM, Brett TJ, Miller CA, **Kober DL**, Craft CS, Atkinson JJ, Shipley JM, Trask BC, Mecham RP. *Microfibril-associated Glycoprotein 2 (MAGP2) Loss of Function Has Pleiotropic Effects in Vivo*. Journal of Biological Chemistry 08/2013; 288(40). DOI:10.1074/jbc.M113.497727

Abstracts

Kober DL, Alexander-Brett J, Cruchaga C, Colonna M, and Brett TJ. *Neurodegenerative disease mutations in TREM2 reveal a functional surface and two distinct loss-of-function mechanisms*. Poster Presentation, Gordon Research Conference Neuroimmune Communication in Health & Disease. January 2017. Ventura Beach, CA.

Kober DL, Brett TJ: *Structural Studies of TREM-2 Mutants Linked to Neurodegenerative Diseases*. Acta Crystallographica Section A: Foundations and Advances 08/2014; 70(a1). DOI:10.1107/S2053273314097514. Abstract for poster presentation, 23rd conference, International Union of Crystallography. September 2014. Montreal, Canada

Kober DL, Alexander-Brett J, and Brett TJ. *Neurodegenerative disease mutations in TREM-2 reveal functional surfaces and two distinct loss-of-function mechanisms*. Poster Presentation, Center for Neuroimmunology and Neuroinfectious Diseases Annual Symposium. October 2014, 2015, and 2016. Washington University in St. Louis. **** Awarded best graduate student poster (2014)***

Kober DL, Alexander-Brett J, and Brett TJ. *Neurodegenerative disease mutations in TREM2 reveal a functional surface and two distinct loss-of-function mechanisms*. Poster Presentation, Pulmonary Research Conference. April 2015 and 2016. Washington University in St. Louis.

Awards and Honors

2008-2012	Dean's list, Evangel University
2009-2012	Science and Technology Endowed Scholarship, Evangel University
2012	Outstanding Graduate in Chemistry, Evangel University
2012-2014	Cell Molecular Biology Interdepartmental Training Grant (5T32GM007067-39)
2014	NSF-GRF Fellowship Honorable Mention
2015-2016	American Heart Association Pre-doctoral fellowship (15PRE22110004)
2016-2018	American Heart Association Pre-doctoral fellowship (17PRE32780001)

Memberships

American Heart Association